THE UNIVERSITY
of EDINBURGH

GEOLOGICAL RISK AND RESERVOIR QUALITY IN HYDROCARBON EXPLORATION

Changyou Xia

Thesis submitted for the degree of Doctor of Philosophy

School of Geosciences

The University of Edinburgh

2018

Declaration

I declare that this thesis was composed by myself, that the work contained herein is my own except where explicitly stated otherwise in the text, and that this work has not been submitted for any other degree or professional qualification.

Changyou Xia

Lay summary

The record of well-drilling for oil exploration shows that only one in three exploration wells find the hoped-for oil resources. The other two wells out of three are unsuccessful exploration and will be subsequently abandoned. The first part of my PhD studies the reasons for the failure of unsuccessful wells, which are termed 'geological risks' in this thesis. The study in Chapter 2 and 3 collected data from 382 unsuccessful wells. The results show that the most common reasons of failure are the absence of the target oil reservoir, and that the reservoir is not porous enough for oil production. The study has also determined the probability of occurrence for the geological risks. For example, the chance of the target reservoir of an exploration well being absent is 19%. These quantitative risk data can aid in the risk assessment in future hydrocarbon exploration.

An oil reservoir usually needs to have at least 10% of porosity for oil production. The next part of this PhD thesis (Chapter 4 and 5) study what controls the porosity of an oil reservoir - why some reservoirs have high porosity (e.g. > 20%) and some reservoirs have little porosity (e.g. <10%). Petrographic data suggest that the amount of clays in a reservoir is the important factor in deciding the porosity. In addition, the data from a North Sea oilfield (Kessog Field) indicate that the oil itself may also help form high porosity in its host reservoir.

Some minerals in oil reservoirs would dissolve under the high-temperature and high-pressure conditions of the subsurface. An important question is where do the dissolved minerals go? If they move out of the oil reservoir, then the dissolution of minerals would create new porosity and increase the economic value of the reservoir. However, if the dissolved minerals create new minerals within the same reservoir, then this will not lead to a net porosity increase for the oil reservoir. Chapter 4 and Chapter 6 includes two projects studying this topic. The conclusion supports the second scenario: that mineral dissolution does not increase the porosity of an oil reservoir.

Abstract

In the next 20 years, the global demand for oil is forecast to grow by 0.7% every year, and the demand for natural gas will increase by 1.6% annually. But as we continue to produce oil and gas, the resources of our current oilfields are depleting. To meet the rising global energy demand, it is essential that we can keep discovering more petroleum resources in the future.

The primary aim of this PhD project is to deepen our understanding of hydrocarbon reservoirs and enhance our ability to explore. The first project looked at the geological risks in hydrocarbon exploration. It reviewed and statistically analysed the data of 382 unsuccessful boreholes in the UK offshore area. The results suggest that the most significant risk for an exploration well is encountering a thin or absent target reservoir. This risk happened to 27 ± 4% of the past unsuccessful wells. The following most common risks are low-porosity reservoirs (22 ± 4% of all cases) and the lack of a closed trap (23 ± 4%). The probability of a target reservoir having a leaky caprock is 5 ± 2%. The study has calculated the probability of occurrence of all the geological risks in exploration, and this risk data can be applied to predict the potential geological risks in future exploration.

One challenge in developing saline aquifers as CO_2 storage reservoirs is the lack of subsurface data, unless a well has been drilled. Drawing on the experience of hydrocarbon exploration, a potential CO_2 storage site identified on seismic profiles will be subject to many uncertainties, such as thin or low-porosity reservoirs, leaky seals, which are analogue to the geological risks of an undrilled hydrocarbon prospect. Since the workflow of locating CO_2 storage reservoirs is similar to the exploration for hydrocarbon reservoirs, the risk data of hydrocarbon exploration wells can be applied to infer the geological risks of the exploration wells for CO_2 storage reservoirs. Based on this assumption, the study of Chapter 3 estimated that the probability of a borehole encountering a reservoir suitable for CO_2 storage is c. 41–57% (90% confidence interval). For reservoirs with stratigraphic traps within the UKCS, the probability of success is slightly lower, at 39 ± 10% (90% confidence).

Chapter 4 studies the porosity and diagenetic process of the Middle Jurassic Pentland Formation in the North Sea. The analysis data come from 21 wells that drilled and cored the Pentland Formation. Petrographic data suggest the content of detrital illite is the most important factor affecting the porosity of the Pentland Sandstone - the porosities of the sandstones with more than 15% of illite (determined by point-count) are invariably low (< 10%). Quartz cement grows at an average rate of 2.3 %/km below the depth of 2km, and it is the main porosity occluding phase in the deep Pentland Sandstone. Petrographic data shows the clean, fine-grained sandstones contain the highest amount of quartz cement. Only 1-2 % of K-feldspar seems to have dissolved in the deep Pentland Sandstone (> 2 km), and petrographic data suggest that K-feldspar dissolution does not have any substantial influence on the sandstone porosity. There is no geochemical evidence for mass transfer between the sandstones and shales of the Pentland Formation.

Chapter 5 investigates the high porosity of the Pentland Sandstone in the Kessog Field, Central North Sea. The upper part of the Kessog reservoir displays an anomalously high porosity (c. 25 %, helium porosity) that is 10 % higher than the porosity of other Pentland sandstones at the same depth (c. 15 %, 4.1 - 4.4 km). Petrographic data show these high porosities are predominantly primary porosity. The effects of sedimentary facies, grain coats, secondary porosity and overpressure on the formation of the high porosity are considered to be negligible in this case. Early hydrocarbon emplacement is the only explanation for the high porosity. In addition to less quartz cement, the high-porosity sandstones also contain more K-feldspar and less kaolin than the medium-porosity sandstones of the same field. This indicates that early hydrocarbon emplacement has also inhibited the replacement of K-feldspar.

The last chapter studies the potential mass transfer of silica, aluminium, potassium, iron, magenesium and calcium at sandstone-shale contacts. The study samples include 18 groups of sandstones and shales that were collected from five oilfields in the North Sea. The interval space between the samples of each group varies from centimetres to meters. The research aim is to find evidence of mass transfer by studying the samples' variation of mineralogy and chemistry as a function of the distance to the nearest sandstone-shale contact. The sandstones are mostly turbidite sandstones, and the shales are Kimmeridge Clay shales. Petrographic, mineralogical and chemical data do not provide firm evidence for mass transfer within any group of

the samples. The result indicates that the scale of mobility of silica, aluminium, potassium, iron, magenesium and calcium in the subsurface may be below the scale of detection of the study method, i.e. < 5 cm.

Acknowledgements

I am grateful to my supervisors Mark Wilkinson and Stuart Haszeldine for dedicating so much of their time, energy and wisdom to my PhD study. China Scholarship Council is appreciated for funding this PhD work, and British Geological Survey is acknowledged for kindly providing the study rock samples. Many thanks go to the fellows of the Edinburgh Geoenergy Group. They have been very helpful for providing insightful discussions and comments for my project. I am indebted to Nicholas Odling, who spent much effort on helping with my X-ray analysis work. Thanks to Steve Hillier for providing me with a standard sample to determine the reliability of XRD results, and to the technical staff in the School of Geosciences, University of Edinburgh: Michael Hall, Nicola Cayzer, John Craven and Richard Hinton, for their kind assistance on experiments.

Many thanks to my good friends, without whom life would be dull during the last four years: Ali, Amelia, Angus, Berit, Emma, Flo, Johny and many others.

Table of Contents

Chapter 1

Introduction

1.1 Research aim

The 21st-century world has seen a boom in the renewable energy sector, however, scientific institutions have predicted that fossil fuels will continue to be the dominant source of energy worldwide for many decades. For instance, the International Energy Agency (EIA) predicts that the global demand for oil will increase by 0.7% per year and natural gas by 1.6% between 2015 and 2040 (Figure 1.1; EIA, 2017). The predictions of other credible sources, e.g. BP, ExxonMobil and Statoil (Figure 1.1), also yield similar conclusions that the global consumption of fossil fuels will rise steadily in the foreseeable future (BP, 2017; ExxonMobil, 2017; Statoil, 2017). A sufficient supply of energy is fundamental to ensure the stability and sustainable development of the global economy. It is essential that the world can maintain and expand oil supply in the following decades to keep pace with the rising energy demands.

Currently, many accessible hydrocarbon reserves are depleted, at least in some largest economic bodies, e.g. the European Union (EU) and China. Many analysts

have been warning that the ‘era of cheap oil’ is ending and that we will have to face the challenges of harder-to-extract oil. The frontiers of hydrocarbon exploration are shifting to areas of very deep water, very far away and very complex geology. This will inevitably drive up exploration risks and production costs, and further lead to high energy prices. As a result, the future global economy will be at risk of being damaged by expensive energy. To avoid the potential economic risk and handle the ever increasing complexity of hydrocarbon reservoirs, one solution is to increase our knowledge of hydrocarbon exploration and hydrocarbon reservoir through scientific research.

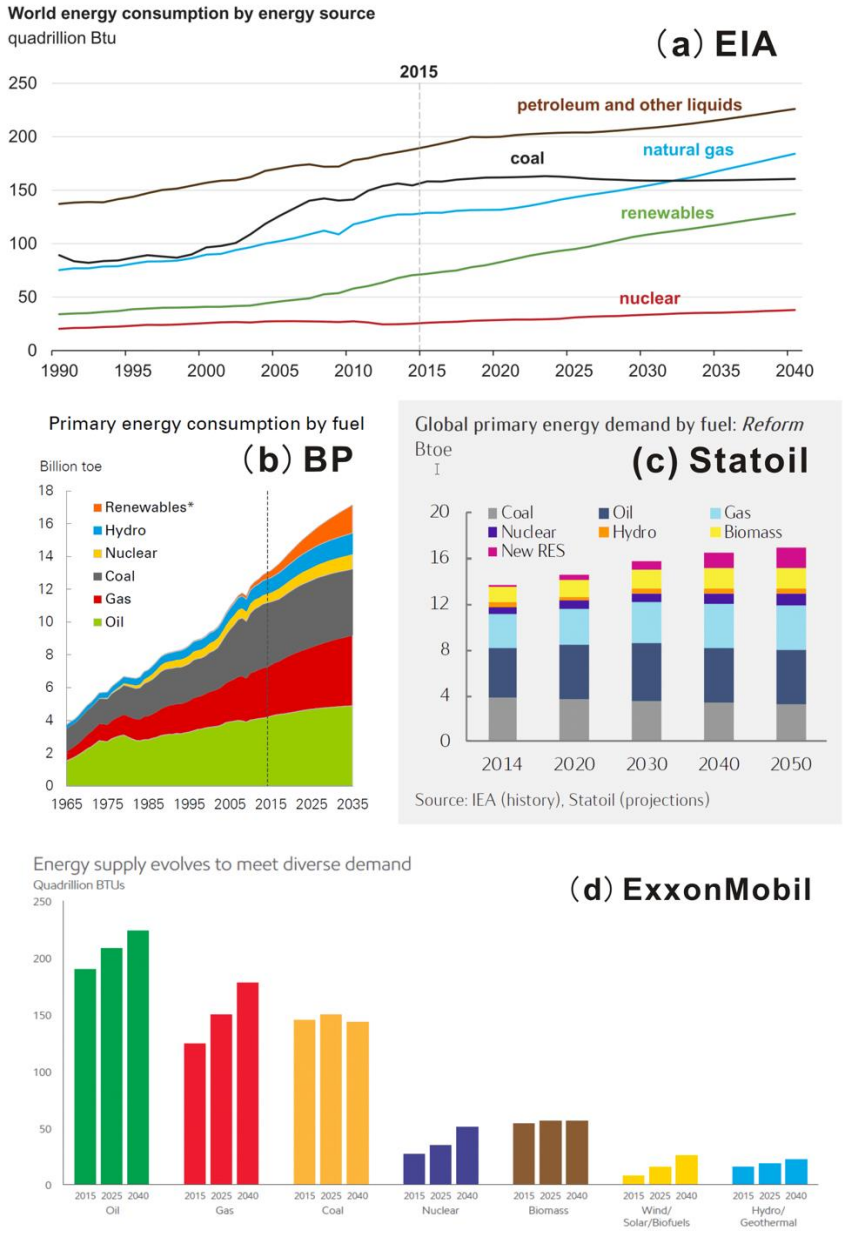

Figure 1.1 (a) International Energy Agency, (b) BP, (c) Statoil and (d) ExxonMobil predict that the global consumption of fossil fuels will continue to rise steadily in the next 20-35 years.

The initiative of this PhD project aims to enhance our skills in hydrocarbon exploration and oilfield management from two aspects. Firstly, it uses the information of unsuccessful exploration wells to study the geological risks that can potentially occur during exploration drilling. The aim is to learn from the lessons of past failures to improve future performance. Secondly, it examines the petrography, mineralogy and chemistry of reservoir rocks from several North Sea oilfields, to understand the factors that control the quality of these hydrocarbon reservoirs. The research outputs will be beneficial for improving our current method of reservoir quality prediction.

The title of this thesis is “Geological Risk and Reservoir Quality in Hydrocarbon Exploration”. At the beginning of this thesis, it is necessary to clearly define the meaning of two keywords in the tile - “geological risk” and “reservoir quality”. The definitions are:

(1) Geological risk: a geological factor or reason that can lead to the failure of a hydrocarbon exploration well.
(2) Reservoir quality: it is a term that generally represents the reserve and producibility of a hydrocarbon reservoir. The quality of a hydrocarbon reservoir can be affected by its size, porosity, permeability and connectivity. Among the factors, petroleum geologists are most concerned with porosity, as a high-porosity reservoir can generally deliver both sufficient storage space and effective flow network. In this thesis, a good quality hydrocarbon reservoir is normally referred to a high-porosity reservoir.

The work in Chapter 2 is focused on geological risks in hydrocarbon exploration. As finding oil gets more challenging, the prices may rise, and riskier exploration therefore becomes more rewarding. It is now more important than ever to gain a better understanding of the potential risks in exploration. For example, the North Sea oil industry has been calling for a systematic review of past unsuccessful exploration and drilling activities. The publication of “Moray Firth – Central North Sea Post Well Analyses” by the UK Oil & Gas Authority is one response to this call (Mathieu, 2015). The study of Chapter 2 has the same primary purpose, but takes a different approach from Mathieu (2015) to study the exploration risk. It uses the data from unsuccessful wells included in relinquishment reports, which oil companies hand into the government at the expiry of exploration licences. There are 382 unsuccessful wells in

total; all the wells are either dry or only encountered a small pool of hydrocarbons, due to some unexpected or underestimated geological risk. Based on this large database of unsuccessful wells, the study of Chapter 2 will estimate the probability of occurrence of the common geological risks in hydrocarbon exploration.

Chapter 3 is an application case study using the risk data in Chapter 2. Chapter 3 uses the probabilistic risk information to predict the geological risk of storing CO_2 in subsurface reservoirs. In the results, the data estimates that the rate of success of using subsurface structures as CO_2 storage reservoirs is c. 41–57% (90% confidence interval).

Chapter 4, 5 and 6 are related to the subject of sandstone diagenesis – the process through which loose sands on the earth surface become hard sandstones during burial. Sandstone diagenesis is a well-studied field, owing to a great deal of research support from the oil industry over the past few decades. But some key issues remain unaddressed, such as the origin of quartz cement, the effect of hydrocarbon emplacement on sandstone diagenesis, and the scale of mass transfer in intermediate-late diagenesis (50 – 200^{o}C). This PhD project attempts to provide solutions to the latter two problems. Chapter 4 starts with examining the diagenesis of the Middle Jurassic Pentland Formation in the North Sea. The rock formation is made of interbedded sandstones and shales, and is hence suitable for studying the potential chemical interactions between the two types of rocks in diagenesis. The study in Chapter 4 will compare the mineralogy and chemistry of the sandstones and shales buried at different depths, to document their evolution process with increasing depth. How much has K-feldspar been dissolved during the burial process of the Pentland sandstones? Where have the products of K-feldspar dissolution been re-distributed to? Could it be to the shales? Chapter 4 will try to answer these questions. It will test the hypothesis that in diagenesis, aluminium and potassium migrate from sandstones to shales, and silica migrates from shales to sandstones.

In the process of studying the Pentland Formation, some Pentland sandstones were noted to be anomalously porous in comparison to other sandstones at the same depth. At the same time, these high-porosity sandstones also show signs of high oil saturation, which leads to the speculation that the presence of hydrocarbons and the high porosity are correlated. In practice, there are many possible processes that may

lead to the formation of high-porosity sandstones at depth (Bloch et al., 2002; Taylor et al., 2010). Chapter 5 will use petrographic and mineralogical data to examine the role of hydrocarbon emplacement, as well as other potential mechanisms, in causing the high porosity in the Pentland sandstones. The hypothesis that the high porosity was preserved by early hydrocarbon emplacement in the reservoir will be tested. The importance of studying the formation of exceptional porosity in sandstones is obvious - it has the function of suggesting us where a high-porosity, high-value reservoir might be located in the immense subsurface.

The final part of this PhD project (Chapter 6) is focussed on the topic of mass transfer. The purpose is to determine the scale of movement of major elements, i.e. silica, aluminium and potassium, in sediments during diagenesis and the possibility of mass exchange between sandstones and shales. There has been a lot of speculation about this, for example: (1) potassium released from K-feldspar dissolution in sandstones may be added to neighbouring shales (Awwiller, 1993; Day-Stirrat et al., 2010); (2) organic acids and CO_2 produced in shales during the maturation of organic matter may migrate into sandstones, and dissolve local carbonate cement and K-feldspar, potentially creating new porosity (Lundegard and Land, 1986; Surdam et al., 1984); (3) silica might move from shales to sandstones to form quartz cement (Sullivan and McBride, 1991; Thyne, 2001). The likelihood and the scale of influence of these processes have been the most important issues in studies of clastic diagenesis for decades (Bjørlykke, 2011). Chapter 6 will use the petrographic data, mineralogical data and chemical data of sandstones and shales samples from five oilfields, to study the potential mass transfer processes in these sites. Will the sandstones near shale contain higher porosity or lower porosity than the sandstones more distant to shales? If there is a difference in porosity between sandstones on the scale of 10cm? 1m? Or 10m? The answers to these questions have an enormous impact on reservoir quality prediction, and in Chapter 6, they will be addressed.

1.2 Background literature - the constitution of a hydrocarbon reservoir

Five elements are needed for a subsurface rock to become oil-bearing: the source, migration, reservoir, seal and trap.

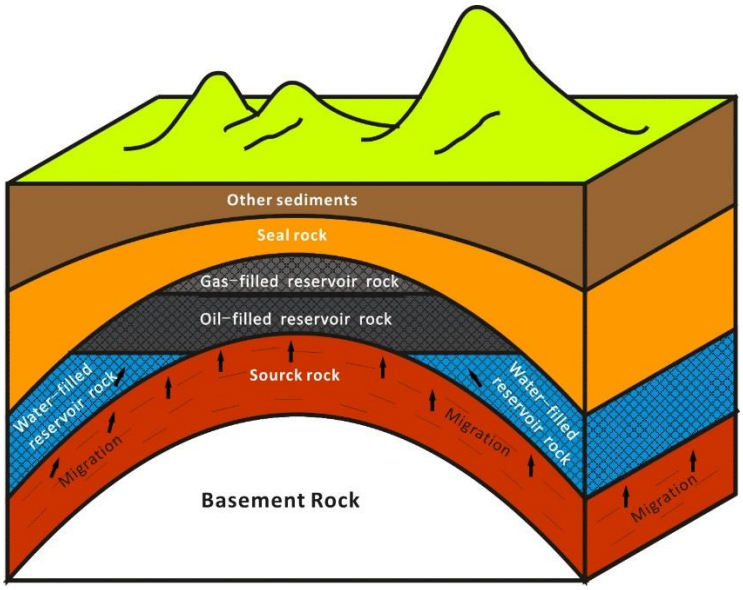

Figure 1.2 A schematic illustration of a subsurface hydrocarbon reservoir and the associated seal, source rock and hydrocarbon migration process (figure drawn by CorelDRAW). The black arrows represent the migration direction of hydrocarbons.

At great burial depth (2-4 km), where the temperature is much higher than at the earth surface (80 – 150 ^{o}C), organic matters in sedimentary rocks will be transformed into oil and gas (Bjørlykke, 2010). The rocks that are rich in organic matters (1-20 wt%) will become the source rocks for large hydrocarbon reservoirs (Gluyas and Swarbrick, 2003). The generation of petroleum within the source rocks causes a dramatic increase in fluid pressure, which expels the produced petroleum out of the source rocks. The petroleum then migrates in the subsurface, until it reaches and accumulates in a porous rock with large storage space (*the reservoir*). Since hydrocarbons are less dense than water, in a sedimentary basin where pores of rocks are often filled with water, hydrocarbons have the tendency to successively migrate upwards under the driving of buoyancy, until it is leaked at the Earth's surface.

Therefore, a reservoir rock containing hydrocarbons needs a layer of impermeable rocks (*the seal*) above that can prevent the upward leakage of hydrocarbon. Any type of rock that has sufficiently low permeability can be the seal rock (Downey, 1984). In addition, the seal rocks need to be present like a cap, i.e. in a concave-down form, that covers on the top of a reservoir. This geometric combination of reservoir and seal rocks is called a *trap* in petroleum geoscience.

The following five sections will respectively provide more detailed descriptions of the hydrocarbon source, migration, reservoir, seal and trap, and the presence of these elements in the North Sea hydrocarbon province where this study is focused.

1.2.1 The source

Source rocks are organic-rich sedimentary rocks that can produce petroleum when heated in the deep basin (Tissot, 1984). Black shales are the most common type of source rocks; coals and organic-rich marls and carbonates can also be potential source rocks (Klemme and Ulmishek, 1991). Temperature is the most important factor in deciding the maturation progress (petroleum generation) of source rocks. In the North Sea, for example, most of the oil is generated in the temperature range of 130-140^{o}C (Bjørlykke, 2010, p. 341), which corresponds to the depth of 3.5 - 4 km. Rock thickness, total organic carbon (TOC) content and type of organics (kerogen type) are the indexes deciding the oil-generation potential of a source rock. Rich source rocks typically contain > 5 wt% TOC (Gluyas and Swarbrick, 2003, p. 93). Type I and type II kerogens mainly produce oil, whereas type III kerogen produces gas (Pepper and Corvi, 1995).

In the UK offshore area, which is the study area of this PhD project, there are two main source rock units: the Upper Jurassic Kimmeridge Clay Formation (KCF) and the Carboniferous Coal Measures (Cornford, 1998).

The KCF is the main hydrocarbon source for the oilfields in the Central and Northern North Sea (Barnard and Bastow, 1991), as well as the Faroe-Shetland Basin (Bailey et al., 1987). The majority of the KCF is organic-rich, black shales that were deposited in a deep-sea environment (Richards et al., 1993). The organics in the KCF are dominated by oil-prone, marine type II kerogen (Isaksen, 2004). Total organic carbon

(TOC) of the KCF typically varies between 2 and 10 % (see summary in Cornford 2009, p.438) with an average of 5% (Gautier, 2005). The thickness of the KCF is in the range of 0.3 – 1.4 km (Richards et al., 1993). The oil generation of the KCF in the Central and Northern North Sea started during Cretaceous, in areas that had undergone the fastest and greatest subsidence; oil generation then became widespread during Eocene (Gautier, 2005; Spencer et al., 1999). As the process of burial continued, some highly matured KCF began to generate gas during the Neogene to Holocene periods (Gautier, 2005; Spencer et al., 1999).

The Carboniferous Coal Measures (CCM) are widely distributed across the Southern North Sea, and are the principal source rock for the Southern North Sea gas province. The CCM mainly consist of gas-prone coal seams and shales that were deposited in a coastal delta environment (Glennie, 1986). An intact CCM sequence, which has not been eroded during earlier inversion, varies from 1.0 km to 2.5 km in thickness (Cornford, 1998), of which about 3% are gas-producing coal seams (Lutz et al., 1975). The shales within the Coal Measures typically contain over 1% TOC (Cornford, 1998, p. 430) and the coals contain over 50% TOC (Isaksen et al., 1998). Maturation and gas generation of the Coal Measures began in the Carboniferous, but the generated gas was lost during subsequent regional uplift and erosion in the Variscan Orogeny (Cornford, 1998, p. 429). The timing of gas generation and migration associated with present-day gas fields are reported to be during Jurassic to the present day (Cornford, 1998, p. 429).

1.2.2 The migration

In the deep basin, the generation of oil and gas, as well as the compaction of sediments, leads to an increase in fluid pressure within the hydrocarbon source rocks (Osborne and Swarbrick, 1997). As a result, the generated hydrocarbons will be extruded from the source rocks due to fluid overpressure. After leaving source rocks, hydrocarbons migrate both vertically and laterally, driven by buoyancy and fluid pressure gradient, and deflected by lateral impermeable sedimentary beds, such as shales (Hindle, 1997). Prediction for the hydrocarbon migration route is important as it would point to the locations where hydrocarbons might be trapped. The estimation of migration route and the volume of migrated hydrocarbon can be achieved by basin and petroleum system modelling, which integrates stratigraphic, lithological,

geothermal and geochemical data to simulate the process of source rock maturation to hydrocarbon migration into a target trap (Burnham and Sweeney, 1991). Modelling the process of oil migration indicates the rate of migration can reach as high as 100km per one million years (Sylta et al., 1998). The maximum horizontal distance that hydrocarbon can migrate, however, is related to the structural style of sedimentary basins (Hindle, 1997). In a basin that is regularly cross-cut by sub-vertical faults or igneous rock intrusions, the maximum horizontal distance of oil migration may be limited to 50km from the source rock area (Hindle, 1997). In comparison, in a basin that is characterised by horizontally well-connected strata, the maximum migration distance may exceed 150km (Hindle, 1997). A review of the petroleum systems of the major oil-producing basins worldwide has revealed that the areas underlain by mature source rocks correspond to the areas where there is a high chance of sucess in finding petroleum resources (Demaison, 1984). The risk of having no oil charge for exploration prospects tends to increase with the distance to mature source rocks (Demaison, 1984).

1.2.3 The reservoir

A reservoir rock may be any rock that contains sufficient porosity to allow oil and gas to accumulate and be produced in economic quantities (Lapedes, 1978). This PhD study focuses sandstones, since the bulk of hydrocarbon resources of the North Sea, where the study data is from, are reserved within sandstone reservoirs. Sandstone is also an important type of hydrocarbon reservoir in the global context, where 60% of all petroleum reservoirs are found in sandstones; the remaining 40% are carbonate reservoirs (Bjørlykke and Jahren, 2010, p. 113).

The most important properties of sandstones as hydrocarbon reservoirs are porosity and permeability. Porosity denotes the fraction of void space within a solid rock. It determines the amount of petroleum that a certain volume of reservoir rock can reserve. Permeability measures how easily a fluid (e.g. oil, gas or water) can pass through a reservoir rock, reflecting the productivity of a reservoir.

An original, newly deposited sandstone near the earth surface typically contains 40-60% porosity (Pettijohn, 1975). In the following burial process, the porosity will rapidly reduce to 25-30% in the first several hundred meter of burial, due to mechanical

compaction. Then, the porosity continues to decrease at an average rate of about 2.5% per km, according to the statistics of sandstone reservoirs worldwide by Ehrenberg and Nadeau (2005). Between the depth of of 0-2 km, the porosity is mainly lost from the compaction due to the increasing weight of overburden sediments, and below 2 km, quartz cementation becomes the main porosity-reducing process (Worden and Burley, 2003). The progress of compaction is related to the physical weight of the overburden sediments (Lundegard, 1992), whereas the rate of quartz cement is thought to be controlled by temperature (Gluyas et al., 1993a). Reservoir permeability normally shows a positive correlation to the reservoir porosity, and a porous sandstone is often also highly permeable. The growth of illite, which is characterised by its special fibrous morphology, can significantly reduce sandstone permeability (Wilkinson et al., 2014a). The growth of illite could result from the dissolution of feldspars and micas, or the transformation of smectite and kaolin (Giles and de Boer, 1990).

Encountering a low-porosity and low-permeability target reservoir is a common problem in hydrocarbon exploration, which can lead to the failure of an exploration well. A low-porosity and low-permeability sandstone reservoir can be caused by a high degree of compaction due to a high content of clay minerals in the sandstone, or pervasive quartz or carbonate cementation (Lander and Walderhaug, 1999; Primmer et al., 1997). In addition, illite growth may also lead to a low-permeability sandstone (Pevear, 1999).

In addition to the risk of low reservoir quality, there are three other common categories of risks that may be related to hydrocarbon reservoirs during exploration: (1) no/poor reservoir development, (2) reservoir compartmentatlization and (3) high uncertainty concerning the lateral variation of reservoir quality. No/poor reservoir development can be caused by false interpretation of seismic data, which is the primary information used to map the subsurface. The phenomenon of reservoir compartmentalization is usually related to the presence of barriers to fluid flow that subdivides a petroleum reservoir into several independent fluid flow units (Jolley et al., 2010). The barriers can be sealed faults, cemented reservoir fractures, internal shale beds or highly-cemented layers (Smalley et al., 1994). Reservoir compartmentalization may reduce the volume of oil that is connected to production wells, thus lowers the value of a reservoir prospect. The issue of high uncertainty concerning the lateral variation of

reservoir quality occurs when a target reservoir is found to be very different from in the pre-drill reservoir model, even if the exploration well has discovered some hydrocarbon resources. The unexpected occurrence and the unfamiliarity with the new reservoir may greatly increase the exploration risk and reduce the confidence of future investment to develop the field, thus leading to the termination of an exploration project. More details and actual cases of the abovementioned geological risks concerning hydrocarbon reservoirs will be illustrated in Chapter 2.

1.2.4 The seal

The top seal of a reservoir must be a rock with competent thickness, continuity, ductility and capillary entry pressure (Downey, 1984); theoretically any lithology can form a top seal as long as it is provided with these attributes (Downey, 1984). The most common type of seal rock is mudstone, which consists of less than 0.0625 mm grain size carbonate and/or siliciclastic minerals (Grunau, 1987). Evaporites are another common type of seal rock owing to its high ductility and strong resistance against fracturing (Grunau, 1987). These two types of seal rocks are both common and important in the UK offshore area (Glennie, 1998; Underhill, 1998). In the Central and Northern North Sea, the top seals of most local oilfields are provided by the mudstones of the Upper Jurassic Kimmeridge Clay Formation (KCF). It is also the seal rock unit for the Kessog Field, which is the study field of Chapter 5, and for the Miller Field in Chapter 6. In comparison, the Upper Permian Zechstein evaporite is the main sealing rock unit for gas fields in the Southern North Sea.

When evaluating seal rocks, the main concern of geoscientists is on the weakest point of a seal rock, rather than the average performance (Downey, 1984). The sealing ability of a seal rock sample can be quantitatively measured in the laboratory (e.g. Schlömer and Krooss, 1997). However, extrapolating a sample, which is only a few cubic centimetres in scale, to the whole caprock that is sealing a large hydrocarbon reservoir is highly risky (Downey, 1984). For instance, the faulting, fracturing and facies variation within seal rocks, which may cause the seal to leak, are unlikely to be inferred by laboratory samples. In practice, the seismic method is often unable to detect these weaknesses as they are below the resolution of the technique. Hence, leaky seals might be a common geological risk encountered during exploration, as exploration techniques cannot effectively predict the overall sealing competency of a

seal rock. To better manage the risk of reservoir seals and make better decisions during exploration, it would be useful to study the probability that a leaky seal rock might present.

Another common type of seal for hydrocarbon reservoirs is fault. Faults can either be conduits or barriers to fluid flow, depending on the sealing ability of the fault plane (Smith, 1966). In an extensional tectonic setting as the North Sea, fault planes formed at shallow depth tend to be initially transmissible for fluids, and then gradually become sealed through deeper burial (Downey, 1984). There are a variety of parameters affecting whether a fault is sealed, such as the age, orientation, burial depth, displacement, the volume of the shale in the faulted rocks, and the juxtaposition of lithologies across the fault plane (Knott, 1993; Sperrevik et al., 2002; Yielding et al., 1997). When oil companies explore the subsurface of the North Sea, structures that were formed due to fault movement are often the primary exploration targets; many of the largest oilfields in the North Sea are bounded by one or several large faults, such as the Brent Field and Beryl Field (Karasek et al., 2003; Taylor et al., 2003). The sealing condition of a fault is an important matter to consider when assessing a potential exploration prospect. The study of Chapter 2 provides valuable information to this sphere, by using a large dataset of exploration wells to estimate the proportion of reservoir faults that are sealed in the North Sea area.

1.2.5 The trap

A trap, in petroleum geology, is a structure of rocks that can confine hydrocarbons and maintain hydrocarbon accumulation (McCarthy et al., 2011). Based on the formation mechanism, traps that are formed through the deformation of rocks (e.g. folding or faulting) are classified as structural traps (Kevin T. Biddle, 1994). Alternatively, the traps that are due to a variation in lithology, i.e. not by structural deformation, are classified as stratigraphic traps (Rittenhouse, 1972). Figure 1.3 displays a variety of trap styles that often appear as hydrocarbon exploration targets. The most typical type of stratigraphic trap is a pinch-out of a sandstone encompassed by shales (Figure 1.3). In some occasions, the top and lateral sides of a trap may be formed, respectively, by the elements of structural and stratigraphic traps (see Figure 1.3); these traps are named as structural-stratigraphic traps, or combination traps (Kevin T. Biddle, 1994). The importance of precise trap definition is self-explanatory:

geoscientists have to rely on this information to establish the volumetrics and hence the economic value of a potential prospect, and decide whether to drill or not. A trap evaluation should incorporate the prediction and description for the burial depth, height, edge and geometry of the trap.

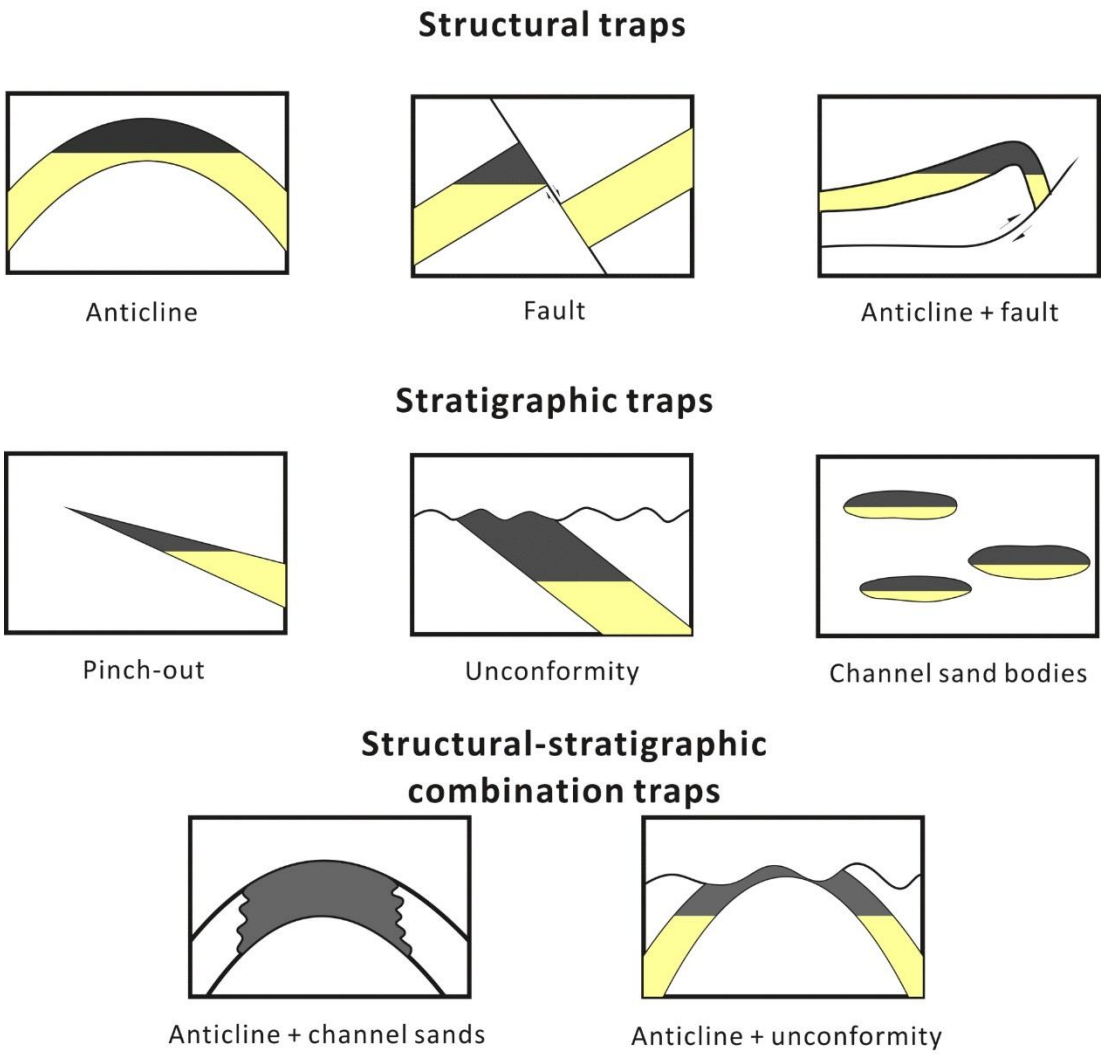

Figure 1.3 Common types of structural, stratigraphic and structural-stratigraphic combination traps (drawn by CorelDRAW). Grey colour represents hydrocarbon-filled reservoirs and yellow colour water-filled sandstone reservoirs.

Seismic imaging is the main method used to map a subsurface trap. A precise trap definition requires, firstly, good quality raw seismic data, and then, effective data processing and interpretation. The processing and interpretation of seismic data sometimes can be extremely challenging. It is a process of converting the time, which reflected seismic waves spend travelling in the subsurface, to depth information (Dix, 1955). This is difficult as the speed of acoustic waves, which is a function of rock type,

porosity and structure, is highly variable in the subsurface (Etris et al., 2001; Faust, 1951). For example, even the same rocks could exhibit different seismic velocity when they are within different geological structures, or at different depths. It is impossible to take into account all the individual variations in the seismic time-depth conversion process. As a result, the conversion is usually completed with great uncertainty; there are always discrepancies (errors) between the subsurface geological model suggested by the seismic method and the reality. Therefore, the interpretation of petroleum traps on seismic profiles is one of the most challenging aspects in hydrocarbon exploration.

1.3 Background literature - the main stratigraphic units of hydrocarbon reservoirs in the UK North Sea

The research objective of this PhD project covers reservoirs of various sedimentary environments and ages. This section is an introduction to the reservoir characteristics and hydrocarbon resources of the Palaeocene, Eocene, Cretaceous, Jurassic, Triassic, Permain and Carboniferous sediments in the North Sea region, which are involved in this study.

The Palaeocene and Eocene deep marine, turbidite fan deposits form prolific, prospective hydrocarbon reservoirs offshore the UK. Approximately 10% of the North Sea oil reverses are conserved within the Palaeocene reservoirs, and 3-5% are within Eocene reservoirs (Eriksen et al., 2003). The lateral distribution of deep-water sandstone bodies are restricted, but they can locally form thick, large sandstone stacks (Holloway and Knox, 1992). For instance, the thickness of the Maureen and Lista Formations (Palaeocene) could exceed 400m in some places (Holloway and Knox, 1992) . The largest oil field of the North Sea – the Forties Field, is a Palaeocene field (Eriksen et al., 2003). In this study, the Palaeocene and Eocene reservoirs are collectively referred to as the Paleogene reservoirs. In the Oligocene to Holocene successions above the Eocene sediments, there have been no significant discoveries to date that could be developed into oil and gas fields, despite some hydrocarbon shows having been reported (Fyfe et al., 2003).

Lower Cretaceous and Upper Jurassic deep-water sandstones also constitute some giant oil and gas fields, such as the Magnus (Shepherd, 1991), Britannia (Hill and Palfrey, 2003) and Claymore fields (Harker et al., 1991). Compared to the Paleogene counterparts, the Cretaceous and Jurassic turbidite sandstones are closer to the Upper Jurassic source rocks on the stratigraphic framework, which may facilitate the oil charge of these reservoirs. But they are buried deeper than the Paleogene turbidites and therefore are of relatively lower porosity and permeability (Garrett et al., 2000; Oakman, 2014). The oil-gas reserves data of the Cretaceous-Jurassic deep

water sandstone reservoirs are lacking in the literature. But in the study of Chapter 2, there is a surprisingly large number of wells (73 wells) targeted on these reservoirs, manifesting their great importance to the oil industry.

The Fulmar Formation includes all the Upper Jurassic shallow marine sandstones in the UK Central Graben (Richards et al., 1993). Approximately one-fifth of the study wells in Chapter 2 are targeted at this level, highlighting its significance to the North Sea oil industry. During the Late Jurassic, a global sea level rise caused a transgression in the Central North Sea, which at the time was occupied by coastal-plain or lagoonal environments, leading to the deposition of the Fulmar Formation as a prograding shoreface deposit (Gatliff et al., 1994; Haszeldine et al., 1999). The Fulmar Formation sandstones are light grey, feldspathic sandstones with a highly homogenous appearance (Howell et al., 1996; Stewart, 1986). Intensive bioturbation has destroyed nearly all the primary sedimentary structures in the formation (Howell et al., 1996). The thickness of the formation is highly variable, ranging from 5m to over 350m (Howell et al., 1996). Like many other shallow marine sandstones, concretionary carbonate cement is common in the Fulmar Formation, in some cases forming horizontal barriers for fluid flow (Hendry et al., 2000). The other principal diagenetic cement in the Fulmar Formation includes grain-coating microquartz, quartz overgrowth and illite (Wilkinson and Haszeldine, 2011).

The Triassic sediments are easily distinguishable from the overlying Jurassic rocks by the presence of red beds, suggesting the Triassic sediments were deposited an arid continental environment (Johnson et al., 1994). In the Central and Northern North Sea, coarse clastic sediments originating from alluvial and fluvial settings predominate in the Triassic strata (Fisher and Mudge, 1998). Whereas in the Southern North Sea, the sediments are more comprised of fine-grained sandstones and evaporites that are formed in a wider range of environments, such as sabkha and playa lakes. Triassic reservoirs are only of minor importance to the North Sea petroleum province (Eriksen et al., 2003). For instance, Triassic reservoirs only contain 0.02% of the oil resources in the Central and Northern North Sea area.

The Permian Rotliegend sandstones are the most important hydrocarbon reservoir in the Southern North Sea, storing about 80% of the gas resources of the basin (Gray, 2013). Most of the Rotliegend sands were deposited in a tropical desert environment

and a few in fluvial or sabkha environments (Johnson et al., 1994). Gas reservoirs in the Southern North Sea are mostly comprised of the aeolian dune sands within the Rotliegend Group (Glennie and Provan, 1990), and the gas is mainly sourced from the coals in the underlying Carboniferous strata. The top sealing mechanism of the Rotliegend reservoir is provided by the Permian Zechstein evaporites (Glennie, 1998, p. 140). One advantage of the Rotliegend Sandstone as a hydrocarbon reservoir is its wide distribution and exceptional thickness, which extends some 1500km from East England all the way to the Russia-Poland Border and locally can be up to 200-300 m thick (Glennie, 1998; Johnson et al., 1994).

Coals and source rocks for gas are abundant among the Carboniferous sequence of the North Sea (Besly, 1998). The best prospective reservoir potential in the Carboniferous strata falls within the channel sandstones of fluvial-deltaic sediments, particularly where the sandstones occur as multiple stacked units (Bailey et al., 1993). Similar to other fluvial-deltaic sediments, the Carboniferous sandstone reservoirs are constantly interbedded with siltstones, shales and coals. The Carboniferous rocks are the oldest main stratigraphic reservoir unit in the North Sea. Prolonged burial history, compaction, quartz and dolomite cement have reduced most of the primary porosity in the sandstones (Bailey et al., 1993; Leeder and Hardman, 1990). The visible porosity under the microscope is almost entirely secondary porosity, which is created from the dissolution of carbonate cement and detrital feldspars (Besly, 1998). Grain-size of the sandstones has a strong correlation with the reservoir performance, with the potential reservoirs occurring only in medium- to coarse-grained sandstones (Leeder and Hardman, 1990).

1.4 Research data and method

The research database of Chapter 2 and 3 is comprised of the information of 382 unsuccessful wells. The information includes the failure reason, hydrocarbon shows and target reservoir of these wells summarised from the exploration relinquishment reports of oil companies, which are published by the UK Oil and Gas Authority on its website. Table 1.1 lists the names of the wells and the numbers of the reports from which the information is collected. The principal analytical method is to compute the probability of occurrence of each geological risk, by dividing its frequency of occurrence by the total number of the wells.

Table 1.2 lists the studied rock samples in Chapter 4, 5 and 6, and the applied analytical techniques. The samples were collected from the Core Store of British Geological Survey at Keyworth, Nottingham.

The point-count method (Table 1.2) is for quantitatively determining the volume percentage of each mineral phase and porosity in a sandstone sample. It randomly selects 250-300 points on a sandstone thin-section under the optical microscope, discriminates the mineral (or porosity) at each point, and then statistically calculates the fraction of each mineral within the sandstone.

The measurement of grain-size for the sandstones is conducted by measuring the diameters of 100 quartz grains on the microphotograph of each sample. The mean size of the 100 quartz grains is measured on the 2D cross-section of quartz grains. To convert this 2D grain-size to the actual 3D grain-size of the spheres of quartz grains, the mean 2D size is multiplied by a factor of 1.273 (Kong et al., 2005)

The point-count method can only determine the mineralogy of sandstones; shale samples are too fine-grained for the observation under the optical microscope. X-ray diffraction (XRD), which is also capable of detecting the mineralogical composition of rock samples, has been applied to analysing both the sandstone and shale samples (Table 1.2).

One disadvantage of the XRD analysis of bulk rock samples is its low accuracy for clay mineral analysis. This is mostly owing to the inherent complexity of clay minerals, such as their highly variable crystal structure and chemical composition and their tendency to lay oriented in a powder sample for XRD analysis (Brindley, 1980). Therefore, in this study, the clay minerals of some samples have been separated from the bulk rocks for independent XRD analysis. This method can provide higher accuracy for measuring the relative abundance of each group of clay minerals (smectite, kaolin, chlorite and illite) in a sandstone or shale sample.

X-ray fluorescence (XRF) has been applied to quantify the amounts of major and trace chemical elements in the study samples (Table 1.2).

Secondary electron imaging under scanning electron microscopy (SEM) can reach a high resolution (5-20 nm), to observe the surface of particles in a wide range of natural and industrial materials, including sandstones and shales. In Chapter 6, this method is used for observing the morphology of quartz cement within 10 sandstone samples from the Kessog Field of the North Sea.

Table 1.1 A list of the unsuccessful wells in this study and the corresponding relinquishment reports where well information is collected

Report number	Well
P804	103/1-1
P804	103/1-2
P1479	110/13b-21
P099	110/14-1
P099	110/14c-6
P099	110/14d-8
P1547	110/3b-6a
P1477	110/8a-5
p1155	113/22-1
P1568	113/26b-3
P1255	12/14-2
P1301	12/17b-1
P1887	12/17b-1
P1723	12/20b-1
P1266	12/20b-1
P1268	12/21-3
P1082	13/17-1
P1083	13/22c-30
P1610	13/23a-7
P1404 & 1459	13/24a-2A
P1084	13/26a-2
P1084	13/26a-4
P1084	13/27a-4
P1460	13/30b-5
P1393	13/11-1
P1393	13/12-1
P1866	13/28-1
P253	14/14-1
P253	14/14a-3
P1461	14/17-1
P1461	14/17-2
P1462	14/18-1
P984	14/21a-1
P1294	14/23a-1
P1499	14/24-1
P1499	14/24a-5
P731	14/26b-5
P732	14/28-1
P732	14/28a-3A
P1089 &P1295	14/28a-5
P732	14/28b-2
P732	14/28b-4
P1463	14/30a-5
P250	15/17-19
P250	15/17-20
P1994	15/17-24&24Z
P250	15/17-25
P1994	15/17-25
P1994	15/17-26
P1870	15/21-50
P1651	15/21b-45
P1870	15/21d-54
P1559	15/23-3
P1465	15/23d-15
P1465	15/24a-9
P2065	15/26a-7Z
P1298 & P1770	15/26b-5
P1298 & P1770	15/26b-9
P1412, P1468 & P1492	15/28a-8
P1256	15/28c-9
P1412, P1468 & P1492	15/29b-4Z
P1292	15/11-3
P1501	16/03d-13
P1657	16/13a-3

Report number	Well
P477 & P1045	16/18b-5
P240	16/22-2
P1778	16/24a-1
P225	16/27a-8
P110 & P591	16/29-3
P110 & P591	16/29a-17
P1300	16/3a-4
P1214 & P1892	16/3a-4
P1214 & P1892	16/3a-4Z
P1300	16/3a-6
P1214 & P1892	16/3d-16
P1871	16/8c-13
P1682	2/10-1a
P1682	2/10-3
P1967	2/3-1
P1967	2/4-2
P1505	20/20-1
P1303	20/2b-10
P1100	20/4a-10
P1100	20/4a-10X
P1100	20/4a-10Y
P1100	20/4a-11
P1100	20/4a-8
P1100	20/4a-9
P1658	20/5b-12
P1658	20/5b-2
P1305	20/5b-2
P1305	20/5b-3
P1305	20/5c-4
P1047	20/7b-5
P1217	20/10-1
P272	20/7-1
P272	20/7-3
P1636	204/15-1
P1023	204/18-1
P1631	204/18b-2a
P1636	205/8-1
P1838	205/9-2
P1597	206/10-1
P1161	206/10a-1
P1161	206/5a-3
P1597	206/5a-3
P1454	208/11-1
P2001	21/10-F4
P743	21/11-C1
P743	21/11-C2
P743	21/11-C2Z
P1618	21/13a-3
P1414	21/13b-1
P1414	21/13b-2
P1618	21/13b-2
P1618	21/14a-4
P1618	21/14b-2
P1618	21/14b-3
P120	21/15a-7
P120	21/15a-8
P1109	21/15a-8
P743	21/16-1
P743	21/16-2
P743	21/16-3
P743	21/16-A1
P743	21/16-A1Z
P743	21/16-A3
P743	21/16-A5
P743	21/16a-A2
P743	21/16a-A4
P185	21/20a-5

Report number	Well
P1584	21/20b-3
P421	21/20b-4y
P185	21/20b-4Y
P185	21/20d-8
P1561	21/20d-8
P1562	21/21-1
P1625	21/24-4
P1619	21/27b-7
P1619	21/28-1
P1790	21/28b-7
P215	21/29b-4
P1563	21/29b-4
P215	21/29b-9
P1563	21/29b-9
P1048	21/6a-7
P1784	21/7b-4
P246	21/10-7
P246	21/10-9
P743	21/11-2
P743	21/11-4
P743	21/11-6
P743	21/11-7
P1218	21/4-1
P1785	21/8-3
P1571	210/24a-13
P1571	210/24a-5
P1571	210/29a-3
P1680	210/29c-5
P1487	211/2-1
P1067	211/22-2
P232 (part), P296 (part), P721, P2043 and P2059	211/23b-12
P232 (part), P296 (part), P721, P2043 and P2059	211/23b-12Z
P2075	211/24c-7
P1634	211/27e-13
P1487	211/7a-4
P212	211/8a-2
P1632	211/8c- 4z
P1632	211/8c-4
P1632	211/8c-5
P1603	213/23-1
P2020	214/17-1
P799	214/21a-2
P2020	214/26-1
P1196	217/15-1
P1418	22/11b-13
P077	22/12a-10
P077	22/12a-12
P1950	22/13b-3
P1420 & P1801	22/13b-9
P1114	22/14b-5
P089	22/15-2
P089	22/15-4
P1799	22/16-6
P1421	22/16a-2Z
P1421	22/16b-5
P1804	22/21-2
P1804	22/21-7
P233	22/22b-2Y
P233	22/22b-5
P1426	22/27a-1
P1804	22/27a-1
P1804	22/27a-2
P1426	22/28-1
P357	22/29-1
P012	22/29-2
P012	22/29-3
P012	22/29-6S2

Report number	Well
P012	22/29-7
P059	22/3a-1
P1722	22/4b-6
P1260	22/2-2
P1372	22/8-3
P1427	23/16d-7z
P1181	23/22B-6z
P1315	26/14-1
P1315	26/12-1
P1315	26/4-1
P1315	26/7-1
P1315	26/8-1
P1315	27/3-1
P2188	28/15-1
P2188	28/15-2
P1316	28/4a-2
P1316	28/4a-3
P1316	28/4b-1
P1627	28/6a-4
P012	29/3a-5
P1317	29/3b-4
P1317	29/4a-1
P1317	29/4a-2
P1317	29/4b-3
P1515	29/6a-3
P1627	29/6a-3
P1627	29/6a-8
P1813	29/9a-1
P1817	29/15-1
P1817	29/15-2
P1817	29/15-3
P012	29/7-1
P1628	29/7-1
P012	29/7-2
P1948	29/7-2
P012	29/7-3
P012	29/7-5
P1861	3/10b-1
P090	3/15a-15
P1754	3/18c-1
P239 & P118	3/19b-3
P239	3/1a-3
P1573	3/22a- 2
P1170	3/23-1
P1170	3/28c-5
P1608	3/11-1
P239	3/1-2
P1753	3/17-2
P1969	3/2-7
P1406	3/6-1
P185	30/12b-10
P185	30/12b-3
P1706	30/12b-7
P185	30/12b-7
P1435	30/25a-4
P006	30/8-2
P006	30/8-3
P1152	39/02c-5
P1591	39/2-4
P1856	41/10a-2Z
P1131	41/24a-1
P1131	41/24a-2
P1131	41/24a-3
P1131	41/25a-4
P1856	41/5-1
P1229	42/10b-2&2Z
P1327	42/14-2

Report number	Well
P1229	42/15a-2
P1229	42/15b-1
P1525	42/18-1
P1525	42/18-2
P1132	42/21-1
P1232	42/21-1
P1132	42/22-1
P1858	42/25-2
P001	42/29-8
P001	42/29a-10
P1335	43/13a-5
P1134 & P 1135 &P1136	43/13b-4
P1334	43/13b-4
P1134 & P 1135 &P1136	43/16-2
P1726	43/16-2
P1134 & P 1135 &P1136	43/17-2
P1726	43/17-2
P1134 & P 1135 &P1136	43/18-1
P1726	43/18a-2,2z & 2Y
P608	43/20b-2
P1527	43/2-1
P1667	43/21b-5z
P1339	43/23-1
P1729	43/23-1
P1729	43/23-2
P499	43/25a-2W
P1669	43/28-1
P1527	43/3-1
P1238	43/10-1
P1532	44/13-1
P1238	44/14-1
P1532	44/14-1
P1532	44/14-2
P2102	44/16-1 & 1Z
P2102	44/16-2
P1138	44/19-3
P1138	44/19-4
P2102	44/21b-8
P1184	44/26-4
P1672	44/26c-5 & -6
P517	44/27-1
P1345	44/28a-3
P1673	44/28a-6
P1898	44/2-1
P1238	44/7-1
P1238	44/8-1Z
P1746	48/11a-12
P1927	48/13b-8
P1247	48/16-1
P1444	48/17-1
P1349	48/1a-4
P130	48/20b-6
P467	48/22-1
P467	48/22-2
P467	48/23-2
P1012	48/23-2
P467	48/23a-4
P007	48/24-3
P007	48/24-5
P1595	48/2b-3
P1446	48/30-12
P1446	48/30-4
P1007	48/6-42
P1675	48/7-4
P1734	48/8b-2
P1595	48/3-4
P523	49/09a-8

Report number	Well
P1860	49/10-8
P033	49/16-15
P088	49/20a-8
P039	49/21-8A
P1544	49/22b-16
P025	49/22-N03
P1747	49/2-3
P1747	49/2-4&4Z
P1364	49/29-3
P1364	49/29-8
P1364	49/29-9
P1364	49/30-1
P1364	49/30-4
P1345	49/3-1
P1677	49/3-1
P1345	49/3-3
P1677	49/3-3
P1147	49/8c-4
P1150	50/16-1
P1251	53/04-2
P1251	53/04-4
P1251	53/04a-7
P1251	53/04a-8
P1367	53/07-1
P1367	53/07-2
P1367	53/08-1
P1367	53/09-1
P1252	53/15-1
P1252	53/18-1
P1252	53/19-1
P1250	53/3-1
P1250	53/3-5
P133	53/3a-7
P1250	53/3c-4
P1365	53/3d-10
P1450 & P1567	53/3d-10
P1252	54/11-1
P063	54/1a-5
P1847	6104/25-1
P2004	7/4-3
P1278	8/15-2A
P090	9/10b-1
P1980	9/10c-4
P1207, P1282 & P1946	9/11e-14
P1863	9/17-1a
P1863	9/17b-4
P1284	9/27a-4
P1285	9/28b-19a
P1281	9/5b-5 & 5A
P1980	9/9b-5
P1575	9/7-1
P1022	98/06-M18
P1605	NOR 6201/11-1 (a Norweigian North Sea well)
P1605	NOR 6201/11-2 (a Norweigian North Sea well)
P1252	P07-01 (a Dutch well)
P1252	P10-01 (a Dutch well)
P1252	P10-02 (a Dutch well)
P1252	P10-04 (a Dutch well)

Note: some wells in this table may correspond to two relinquishment reports - it means the information of the wells have given in both of the two reports.

Table 1.2 The rock samples in this PhD study and the applied research techniques

Chapter	Well number	Lithology	Driller's depth	True vertical depth (m)	Point-count	Grain-size	XRD	XRD-clays*	XRF- major†	XRF- trace§	SEM#
Chapter 4	15/17-P46	Sandstone	10414.00 ft	2389.30			√		√	√	
Chapter 4	15/17-P46	Sandstone	10416.00 ft	2389.90			√		√	√	
Chapter 4	15/17-P46	Sandstone	10419.00 ft	2390.90			√		√	√	
Chapter 4	15/17-P46	Sandstone	10421.50 ft	2391.60			√		√	√	
Chapter 4	15/17-P46	Sandstone	10429.00 ft	2393.90			√		√	√	
Chapter 4	15/17-P46	Shale	10386.00 ft	2380.8			√		√	√	
Chapter 4	15/17-P46	Shale	10388.00 ft	2381.4			√	√	√		
Chapter 4	15/17-P46	Shale	10390.00 ft	2382.0			√	√	√	√	
Chapter 4	16/17-19	Sandstone	14010 ft	4242.80			√		√	√	
Chapter 4	16/17-19	Sandstone	14031 ft	4249.20							
Chapter 4	16/17-19	Sandstone	14036 ft	4250.70			√		√	√	
Chapter 4	16/17-19	Sandstone	14039 ft	4251.70			√		√	√	
Chapter 4	16/17-19	Sandstone	14046 ft	4253.80					√	√	
Chapter 4	16/17-19	Sandstone	14070 ft	4261.10			√		√	√	
Chapter 4	16/17-19	Shale	14010.80 ft	4231.1			√		√	√	
Chapter 4	16/17-19	Shale	14016.80 ft	4244.8			√		√	√	
Chapter 4	16/17-19	Shale	14040.00 ft	4252.0			√		√	√	
Chapter 4	16/17-19	Shale	14044.00 ft	4253.2			√		√	√	
Chapter 4	16/17-19	Shale	14074.00 ft	4262.5			√	√	√	√	
Chapter 4	16/18-1	Sandstone	13262.75 ft	4018.10			√		√	√	
Chapter 4	16/18-1	Sandstone	13267.00 ft	4019.40			√		√	√	
Chapter 4	16/18-1	Sandstone	13274.75 ft	4021.80			√		√	√	
Chapter 4	16/18-1	Shale	13269.50 ft	4020.2					√	√	
Chapter 4	16/18-1	Shale	13279.00 ft	4023.1			√	√	√	√	
Chapter 4	16/18-1	Shale	13280.66 ft	4023.6					√	√	
Chapter 4	16/18-1	Shale	13282.20 ft	4024.0					√	√	
Chapter 4	16/18-1	Shale	13284.00 ft	4024.6			√		√	√	
Chapter 4	16/23-5	Sandstone	11533.0 ft	3490.00			√		√	√	
Chapter 4	16/23-5	Sandstone	11537.5 ft	3491.30			√		√	√	
Chapter 4	16/23-5	Sandstone	11539.5 ft	3491.90			√				

Chapter	Well number	Lithology	Driller's depth	True vertical depth (m)	Point-count	Grain-size	XRD	XRD-clays*	XRF- major†	XRF- trace§	SEM#
Chapter 4	16/23-5	Sandstone	11553.5 ft	3496.20			√		√	√	
Chapter 4	16/23-5	Shale	11547.7 ft	3494.4			√	√	√	√	
Chapter 4	16/23-5	Shale	11560.5 ft	3498.4			√	√	√	√	
Chapter 4	16/23-5	Shale	11566.5 ft	3500.2			√		√	√	
Chapter 4	16/23-5	Shale	11570.1 ft	3501.3			√		√	√	
Chapter 4	16/23-5	Shale	11577.0 ft	3503.4			√		√	√	
Chapter 4	16/28-3	Sandstone	3415.59 m	3381.59			√		√	√	
Chapter 4	16/28-3	Sandstone	3416.75 m	3382.75			√		√	√	
Chapter 4	16/28-3	Sandstone	3417.75 m	3383.75			√		√	√	
Chapter 4	16/28-3	Sandstone	3418.75 m	3384.75			√		√	√	
Chapter 4	16/28-3	Shale	3418.95 m	3385.0			√		√	√	
Chapter 4	16/28-3	Shale	3420.50 m	3386.5			√		√	√	
Chapter 4	16/28-3	Shale	3421.15 m	3387.2			√		√	√	
Chapter 4	16/28-3	Shale	3422.20 m	3388.2			√		√		
Chapter 4	16/28-3	Shale	3423.80 m	3389.8			√		√	√	
Chapter 4	21/13b-2	Siltstone	11999.00 ft	3631.40			√		√	√	
Chapter 4	21/13b-2	Siltstone	12001.50 ft	3632.10			√		√	√	
Chapter 4	21/13b-2	Siltstone	12010.75 ft	3635.00			√		√	√	
Chapter 4	21/13b-2	Siltstone	12033.00 ft	3641.80			√		√	√	
Chapter 4	21/13b-2	Siltstone	12053.00 ft	3647.80			√		√	√	
Chapter 4	21/13b-2	Shale	11623 ft	3542.7			√				
Chapter 4	21/13b-2	Shale	11626.3 ft	3543.7			√				
Chapter 4	21/13b-2	Shale	11630.4 ft	3544.9			√	√			
Chapter 4	21/13b-2	Shale	11632.5 ft	3545.6			√				
Chapter 4	22/25b-4S1	Shale	15800 ft	4788.4			√	√	√	√	
Chapter 4	22/29-1	Shale	15102.00 ft	4579.6			√	√	√	√	
Chapter 4	22/30c-G4	Sandstone	5893.50 m	5704.00			√		√	√	
Chapter 4	22/30c-G4	Sandstone	5897.18 m	5707.68			√		√	√	
Chapter 4	22/30c-G4	Sandstone	5904.90 m	5715.40			√		√		
Chapter 4	22/30c-G4	Sandstone	5909.30 m	5719.80					√	√	
Chapter 4	22/30c-G4	Sandstone	5928.95 m	5739.45			√		√	√	

Chapter	Well number	Lithology	Driller's depth	True vertical depth (m)	Point-count	Grain-size	XRD	XRD-clays*	XRF- major†	XRF- trace§	SEM#
Chapter 4	22/30c-G4	Sandstone	5932.80 m	5743.30			√		√	√	
Chapter 4	22/30c-G4	Sandstone	5937.52 m	5748.02			√		√	√	
Chapter 4	22/30c-G4	Sandstone	5945.95 m	5756.45			√		√	√	
Chapter 4	22/30c-G4	Sandstone	5952.75 m	5763.25			√		√	√	
Chapter 4	22/30c-G4	Sandstone	5957.95 m	5768.45			√		√	√	
Chapter 4	22/30a-16	Shale	18092.0 ft	5492.1			√		√	√	
Chapter 4	22/30a-16	Shale	18094.0 ft	5492.7			√	√	√	√	
Chapter 4	22/30a-16	Shale	18098.0 ft	5493.9			√	√	√	√	
Chapter 4	29/5a-5	Shale	14509.0 ft	4396.1			√				
Chapter 4	30/1c-5	Sandstone	4176.50 m	4150.50	√		√		√	√	
Chapter 4	30/1c-5	Sandstone	4177.30 m	4151.30	√		√		√		
Chapter 4	30/1c-5	Sandstone	4183.60 m	4157.60	√		√		√		
Chapter 4	30/1c-5	Sandstone	4185.00 m	4159.00	√		√		√		√
Chapter 4	30/1c-5	Sandstone	4185.90 m	4159.90	√		√		√		
Chapter 5	30/1c- 3	Sandstone	4433.84 m	4408.84	√						
Chapter 5	30/1c- 3	Sandstone	4434.90 m	4409.90	√						
Chapter 5	30/1c- 3	Sandstone	4435.55 m	4410.55	√						
Chapter 5	30/1c- 3	Sandstone	4439.86 m	4414.86	√						
Chapter 5	30/1c- 3	Sandstone	4440.87 m	4415.87	√						
Chapter 5	30/1c- 3	Sandstone	4441.91 m	4416.91	√						
Chapter 5	30/1c- 3	Sandstone	4443.72 m	4418.72	√						
Chapter 5	30/1c- 3	Sandstone	4447.60 m	4422.60	√						
Chapter 5	30/1c- 4	Sandstone	4316.52 m	4289.72	√						
Chapter 5	30/1c- 4	Sandstone	4319.23 m	4292.43	√						
Chapter 5	30/1c- 4	Sandstone	4322.10 m	4295.30	√						
Chapter 5	30/1c- 4	Sandstone	4323.30 m	4296.50	√						√
Chapter 5	30/1c- 4	Sandstone	4324.33 m	4297.53	√						
Chapter 5	30/1c- 4	Sandstone	4327.68 m	4300.88	√						√
Chapter 5	30/1c- 4	Sandstone	4327.75 m	4300.95	√						
Chapter 5	30/1c- 4	Sandstone	4328.47 m	4301.67	√						
Chapter 5	30/1c- 5	Sandstone	4177.10 m	4151.10	√						√

Chapter	Well number	Lithology	Driller's depth	True vertical depth (m)	Point-count	Grain-size	XRD	XRD-clays*	XRF- major†	XRF- trace§	SEM#
Chapter 5	30/1c- 5	Sandstone	4177.60 m	4151.60	√						√
Chapter 5	30/1c- 5	Sandstone	4183.32 m	4157.32	√						
Chapter 5	30/1c- 5	Sandstone	4184.00 m	4158.00	√						√
Chapter 5	30/1c- 5	Sandstone	4185.90 m	4159.90	√						
Chapter 5	30/1c- 6	Sandstone	4407.40 m	4381.50	√						
Chapter 5	30/1c- 6	Sandstone	4408.43 m	4382.53	√						
Chapter 5	30/1c- 6	Sandstone	4411.39 m	4385.49	√						
Chapter 5	30/1c- 6	Sandstone	4419.22 m	4393.32	√						
Chapter 5	30/1c- 6	Sandstone	4424.25 m	4398.35	√						√
Chapter 5	30/1c- 6	Sandstone	4417.15 m	4391.25	√						√
Chapter 5	30/1c- 9	Sandstone	4444.72 m	4400.42	√						
Chapter 5	30/1c- 9	Sandstone	4445.18 m	4400.88	√						
Chapter 5	30/1c- 9	Sandstone	4448.33 m	4404.03	√						
Chapter 5	30/1c- 9	Sandstone	4448.41 m	4404.11	√						√
Chapter 5	30/1c- 9	Sandstone	4448.95 m	4404.65	√						
Chapter 5	30/1c- 9	Sandstone	4450.65 m	4406.35	√						
Chapter 5	30/1c- 9	Sandstone	4451.25 m	4406.95	√						
Chapter 5	30/1c- 9	Sandstone	4455.46 m	4411.16	√						√
Chapter 6	16/8b-5	Sandstone	14180.6 ft				√		√		
Chapter 6	16/8b-5	Sandstone	14180.7 ft		√						
Chapter 6	16/8b-5	Sandstone	14194.0 ft				√		√		
Chapter 6	16/8b-5	Sandstone	14195.3 ft		√		√		√		
Chapter 6	16/8b-5	Sandstone	14168.8 ft				√		√		
Chapter 6	16/8b-5	Sandstone	14168.9 ft				√		√		
Chapter 6	16/8b-5	Sandstone	14169.0 ft				√		√		
Chapter 6	16/8b-5	Sandstone	14169.03 ft				√		√		
Chapter 6	16/8b-5	Sandstone	14169.07 ft				√		√		
Chapter 6	16/8b-5	Sandstone	14197.80 ft				√		√		
Chapter 6	16/8b-5	Sandstone	14197.87 ft				√		√		
Chapter 6	16/8b-5	Sandstone	14197.93 ft				√		√		
Chapter 6	16/8b-5	Sandstone	14198.00 ft				√		√		

Chapter	Well number	Lithology	Driller's depth	True vertical depth (m)	Point-count	Grain-size	XRD	XRD-clays*	XRF- major†	XRF- trace§	SEM#
Chapter 6	16/8b-5	Sandstone	14198.07 ft				√		√		
Chapter 6	16/8b-5	Sandstone	14198.13 ft				√		√		
Chapter 6	16/8b-A1	Sandstone	4751.9 m				√		√		
Chapter 6	16/8b-A1	Sandstone	4752.3 m				√		√		
Chapter 6	16/8b-A1	Sandstone	4753 m		√		√		√		
Chapter 6	16/8b-A1	Sandstone	4753.8 m		√		√		√		
Chapter 6	16/8b-A1	Sandstone	4754.6 m		√		√		√		
Chapter 6	16/8b-A1	Sandstone	4758 m		√		√		√		
Chapter 6	16/8b-A1	Sandstone	4750.94 m				√		√		
Chapter 6	16/8b-A1	Sandstone	4750.96 m				√		√		
Chapter 6	16/8b-A1	Sandstone	4750.98 m				√		√		
Chapter 6	16/8b-A1	Sandstone	4751.00 m				√		√		
Chapter 6	16/8b-A1	Sandstone	4751.02 m				√		√		
Chapter 6	16/8b-A1	Sandstone	4751.04 m				√		√		
Chapter 6	16/8b-A1	Shale	4750.30 m				√		√		
Chapter 6	16/8b-A1	Shale	4751.00 m				√		√		
Chapter 6	16/8b-A1	Shale	4751.05 m				√		√		
Chapter 6	16/8b-A1	Shale	4751.10 m				√		√		
Chapter 6	16/8b-A1	Shale	4751.20 m				√	√	√		
Chapter 6	16/17-19	Sandstone	13998.84 ft				√		√		
Chapter 6	16/17-19	Sandstone	13998.87 ft				√		√		
Chapter 6	16/17-19	Sandstone	13998.9 ft				√		√		
Chapter 6	16/17-19	Sandstone	13998.93 ft				√		√		
Chapter 6	16/17-19	Sandstone	13998.97 ft				√		√		
Chapter 6	16/17-19	Sandstone	13999.0 ft				√		√		
Chapter 6	16/17-19	Sandstone	13999.03 ft				√		√		
Chapter 6	16/17-19	Sandstone	13999.07 ft				√		√		
Chapter 6	16/17-19	Sandstone	13999.10 ft				√		√		
Chapter 6	16/17-19	Sandstone	13999.13 ft				√		√		
Chapter 6	16/17-19	Sandstone	14047.93 ft						√		
Chapter 6	16/17-19	Sandstone	14047.97 ft						√		

Chapter	Well number	Lithology	Driller's depth	True vertical depth (m)	Point-count	Grain-size	XRD	XRD-clays*	XRF- major†	XRF- trace§	SEM#
Chapter 6	16/17-19	Sandstone	14048.00 ft						√		
Chapter 6	16/17-19	Sandstone	14048.07 ft						√		
Chapter 6	16/17-19	Sandstone	14048.13 ft						√		
Chapter 6	16/17-19	Sandstone	14048.16 ft						√		
Chapter 6	16/17-19	Sandstone	14069.87 ft				√		√		
Chapter 6	16/17-19	Sandstone	14069.93 ft				√		√		
Chapter 6	16/17-19	Sandstone	14070.0 ft				√		√		
Chapter 6	16/17-19	Sandstone	14070.07 ft				√		√		
Chapter 6	16/17-19	Sandstone	14070.13 ft				√		√		
Chapter 6	16/17-19	Sandstone	14070.2 ft				√		√		
Chapter 6	21/1a-20	Sandstone	14063.2 ft		√		√		√		
Chapter 6	21/1a-20	Sandstone	14065.8 ft		√		√		√		
Chapter 6	21/1a-20	Sandstone	14068.3 ft				√		√		
Chapter 6	21/1a-20	Sandstone	14070.1 ft				√		√		
Chapter 6	21/1a-20	Sandstone	14071.0 ft		√		√		√		
Chapter 6	21/1a-20	Shale	14073.0 ft				√		√		
Chapter 6	21/1a-20	Shale	14074.4 ft				√		√		
Chapter 6	21/1a-20	Shale	14075.6 ft				√		√		
Chapter 6	21/1a-20	Shale	14085.6 ft				√		√		
Chapter 6	21/1a-20	Sandstone	14071.87 ft				√		√		
Chapter 6	21/1a-20	Sandstone	14071.89 ft		√						
Chapter 6	21/1a-20	Sandstone	14071.90 ft				√		√		
Chapter 6	21/1a-20	Sandstone	14071.93 ft				√		√		
Chapter 6	21/1a-20	Sandstone	14071.96 ft		√						
Chapter 6	21/1a-20	Sandstone	14072.0 ft				√		√		
Chapter 6	21/1a-20	Sandstone	14072.17 ft						√		
Chapter 6	21/1a-20	Sandstone	14072.13 ft				√		√		
Chapter 6	21/1a-20	Shale	14044.87 ft				√		√		
Chapter 6	21/1a-20	Shale	14044.90 ft						√		
Chapter 6	21/1a-20	Shale	14044.93 ft				√		√		
Chapter 6	21/1a-20	Shale	14045.0 ft				√	√	√		

Chapter	Well number	Lithology	Driller's depth	True vertical depth (m)	Point-count	Grain-size	XRD	XRD-clays*	XRF- major†	XRF- trace§	SEM#
Chapter 6	21/1a-20	Shale	14045.07 ft				√		√		
Chapter 6	21/1a-20	Shale	14045.13 ft				√		√		
Chapter 6	211/12a-18	Sandstone	2935.38 m		√				√		
Chapter 6	211/12a-18	Sandstone	2949.57 m		√				√		
Chapter 6	211/12a-18	Sandstone	2952.68 m		√				√		
Chapter 6	211/12a-18	Sandstone	2955.43 m		√						
Chapter 6	211/12a-18	Sandstone	2955.73 m						√		
Chapter 6	211/12a-18	Sandstone	2956.00 m		√				√		
Chapter 6	211/12a-18	Sandstone	2956.50 m						√		
Chapter 6	211/12a-18	Sandstone	2957.00 m						√		
Chapter 6	211/12a-18	Sandstone	2958.00 m						√		
Chapter 6	211/12a-18	Sandstone	2958.75 m						√		
Chapter 6	211/12a-18	Sandstone	2943.56 m						√		
Chapter 6	211/12a-18	Sandstone	2943.58 m						√		
Chapter 6	211/12a-18	Sandstone	2943.60 m						√		
Chapter 6	211/12a-18	Sandstone	2943.61 m						√		
Chapter 6	211/12a-18	Sandstone	2943.62 m						√		
Chapter 6	211/12a-18	Sandstone	2938.48 m						√		
Chapter 6	211/12a-18	Sandstone	2938.49 m						√		
Chapter 6	211/12a-18	Sandstone	2938.50 m						√		
Chapter 6	211/12a-18	Sandstone	2938.52 m						√		
Chapter 6	211/12a-18	Sandstone	2938.54 m						√		
Chapter 6	211/12a-18	Sandstone	2938.56 m						√		
Chapter 6	211/12a-18	Shale	2947.46 m						√		
Chapter 6	211/12a-18	Shale	2947.55 m						√		
Chapter 6	211/12a-18	Shale	2947.66 m						√		
Chapter 6	211/12a-18	Shale	2947.69 m						√		
Chapter 6	211/12a-18	Shale	2954.66 m						√		
Chapter 6	211/12a-18	Shale	2954.67 m						√		
Chapter 6	211/12a-18	Shale	2954.68 m						√		
Chapter 6	211/12a-18	Shale	2954.70 m					√	√		

Chapter	Well number	Lithology	Driller's depth	True vertical depth (m)	Point-count	Grain-size	XRD	XRD-clays*	XRF- major†	XRF- trace§	SEM#
Chapter 6	211/12a-18	Shale	2954.72 m						√		
Chapter 6	211/12a-18	Shale	2954.74 m						√		
Chapter 6	211/12a-18	Shale	2954.76 m						√		
Chapter 6	211/12a-18	Shale	2941.51 m						√		
Chapter 6	211/12a-18	Shale	2941.53 m						√		
Chapter 6	211/12a-18	Shale	2941.55 m						√		
Chapter 6	211/12a-18	Shale	2941.57 m						√		
Chapter 6	211/12a-18	Shale	2941.58 m						√		
Chapter 6	211/12a-18	Shale	2941.59 m						√		

Note: the samples in Chapter 6 are labelled with the driller's depth for clearer reference and comparison. Thus, the depth was not converted for true vertialcal depth.

*XRD-clays = X-ray diffraction analysis of clay mineral seperates

†XRF- major = X-ray fluorensence analysis of major chemical elements

§XRF- trace = X-ray fluorensence analysis of trace chemical elements

#SEM = observation using the electron imaging under scanning electron microscopy

Chapter 2

The Geological Risks of Drilling an Exploration Well on the UK Continental Shelf

ABSTRACT

In hydrocarbon exploration, many geological risks can cause an exploration well to be a failure, such as the absence of offshore source rocks, low reservoir porosity, leaky seals or unclosed traps. This study is aimed at assessing the significance and the probability of occurrence of each geological risk for the exploration wells on the UK Continental Shelf. The study data were collected from 382 unsuccessful wells that are documented in the relinquishment reports, which oil companies handed to the government at the expiry of an exploration license. The results show that within the unsuccessful wells, the most common geological risks are thin or absent reservoir (27 ± 4% of cases), low reservoir quality (22 ± 4%) and lack of trap (23 ± 4%). The risk of the target reservoir having no oil charge is also significant (14 ± 3%). The issue of leaky top-seal caprocks does not occur frequently (7 ± 2%); but for fault-seal and

stratigraphic traps, the chances of having leaky seals are much higher (24 ± 6%; 36 ± 14 %, respectively).

The major geological risk for exploration varies with different geological formations. Thin or absent reservoir is the most significant risk for turbidite reservoirs (34 ± 11%) and the Jurassic shallow marine sandstone reservoirs (49 ± 10%). For Triassic reservoirs, it is the incorrect prediction for trap geometry (26 ± 13%). For the Permian Rotliegend and Carboniferous reservoirs, the main risks are low reservoir porosity (35 ± 10% and 52 ± 12%).

2.1 Introduction

Offshore drilling is a highly risky and expensive business, for which a single well could cost tens of millions of US dollars (Kaiser, 2009). In the Central North Sea particularly, where a large number of hydrocarbon reserves are held within high-pressure, high-temperature reservoirs (Holm, 1998), drilling to reach the deep basin calls for special rigs, drilling fluids and experienced technicians, which would bring significant costs to exploration activity. Therefore, any method that is able to improve the success rate of an exploration well even by 1% would have a great economic significance. One effective method is to systematically summarise the unsuccessful exploration cases in the past and apply them as a supplement to aid risk assessment and decision-making in future exploration (Peel and Brooks, 2016).

The UK Department of Energy and Climate Change (DECC) has been continuously publishing relinquishment reports since 2008. These relinquishment reports are required by DECC from oil companies when an exploration license is given up or expired. In addition to stating the reasons for relinquishing an area, these reports also cover the exploration history and geological information of the area, such as seismic data acquired, wells drilled, target reservoirs and stratigraphy. Although not successful in finding commercial reservoirs, these failure cases are valuable as a broad guide to inform us of the potential exploration risk in different areas of the North Sea, especially when sufficient geological information is lacking.

This study presents an overview of 382 unsuccessful exploration or appraisal wells in the relinquishment reports that were released during 2008-2016. The focus is on the geological risks that caused the failures of the wells. The aim of this study is to generate a statistical dataset regarding the geological risks of drilling on the UK Continental Shelf. The broad categories of the risks include hydrocarbon charge, reservoir, trap, seal and hydrocarbon quality. The causes and the frequencies of occurrence for these five categories are given and discussed, and a variety of failure case studies described. Also presented are the implications for the geological risks of drilling wells for CO_2 storage in saline aquifer reservoirs, as there has been no study on record that has addressed this issue.

2.2 The definition of ‘success’, ‘chance of success’, ‘risk’, and ‘uncertainty’ in exploration

Hydrocarbon exploration is comprised of a progressive series of investment decisions as to whether to acquire further geological information or build new infrastructure (Otis and Schneidermann, 1997; Rose, 2001). As the process proceeds, different levels of success are achieved one after another until reaching the final stage of field development and production. ‘Technical success’ and ‘commercial success’ are two common broad levels of success assigned to an exploration well. When a well finds a measurable reserve of petroleum resources, it is usually determined as a technical success; when the finding is forecasted to be worthy of the money invested and can make a profit, it is a commercial success (Bush and Johnston, 1998, p. 129).

Determining the ‘chance of success’ parameter of a prospect before drilling is a norm in hydrocarbon exploration (Rose, 1999). However, the precise meaning of ‘chance of success’ lacks consistency across different individuals and groups. For instance, Rose (1992) introduced the term ‘chance of success’ to represent the probability that a well will produce a sustainable hydrocarbon flow. Otis & Schneidermann (1997) shared the prospect evaluation method from Chevron, in which a term ‘the probability of geological success’ (Pg), instead of ‘chance of success’, is used for denoting the probability that a well will achieve continuing hydrocarbon production. Here, ‘the probability of geological success’ and ‘chance of success’ have the same meaning, but are different terminologies taken by different individuals. However, Peel & Brooks (2015) presented a different definition for ‘chance of success’. In general, each exploration prospect before drilling has a geological model that details every geological element of the target, such as trap geometry, reservoir thickness, porosity and permeability range. The ‘chance of success’ defined by Peel & Brooks (2015) is the probability that the pre-drill geological model is correct, which does not equal to the criteria that a well will flow hydrocarbon to the surface. In other sources, the phrases such as the probability of success (POS), the geological probability of success (GPoS) or geologic chance of success (GCOS) may be used representing the ‘chance of success’. The variation in the meaning of ‘chance of success’ is essentially due to the varying meaning of ‘success’ in different groups. Every company has its own method to assess exploration risk. In order to avoid confusion or

misunderstanding, a high-quality estimation for the ‘chance of success’ of a potential prospect must clarify what the ‘success’ means, as to whether it means encountering ‘flowable hydrocarbons’ or ‘a considerable reserve of hydrocarbon’ (Ofstad et al., 2000b).

Despite the inconsistency in definition, the method of calculating ‘chance of success’ for exploration prospect is fundamentally the same, that is by multiplying together the probability of success of each geological component (Jahn et al., 2008, p. 366; Rose, 1992). The only significant difference between each method is the geological components they define. For example, some methods identified the geological components as that hydrocarbon charge, reservoir rock, seal closure, so that the ‘chance of success’ = p(charge) × p(reservoir) × p(seal closure) (Ofstad et al., 2000b). However, some other methods may use source, migration, sealed trap, reservoir and timing as the geological components (e.g. Jahn et al., 2008, p. 366). In all those methods, each of their geological components is equally important because the failure of any of them will result in the failure of the whole prospect (Rose, 1992).

The definition of risk among petroleum scientists is even more diverse than the term ‘chance of success’ (Ross, 2004). Some refer to risk for representing ‘chance of success’ whereas some others may use it to represent ‘chance of failure’ (Peel and Brooks, 2015). Rose (1987) and Megill (1979) defined risk as "an opportunity for loss", whereas Ross (2004) considered it as the probability that an event will happen. Jahn et al. (2008, p. 366) suggested that risk can be quantitatively defined by the loss in monetary terms multiplied by its probability of occurrence. Smalley et al. (2008) saw a risk as an event that would have an impact on exploration activity once it occurs, and meanwhile they also emphasized that a good risk description should contain three essential elements: the cause of the risk, the probability of occurrence of the risk and the consequence if it happens (Smalley et al., 2008). The risk concerned in this study is the geological risk, or one could say the geological threat, that can lead to the failure of an exploration or appraisal well. Following the suggestions of Smalley et al. (2008), the cause and probability of occurrence of each geological risk are also addressed and discussed. In addition to the geological risks, the other frequently-considered risks in hydrocarbon exploration include financial risks concerning the fluctuation of oil price, safety risks relating to the health of employees and environmental risks as an impact of the exploration activity (Chung, 1999).

Uncertainty is the degree by which a calculated or estimated value, or an expected situation may differ from the reality. Uncertainty can be numerically expressed by a range of probabilities that some condition may exist or occur, or an estimated parameter may lie (Rose, 1987; Smalley et al., 2008). The tightness of the probability range reflects the degree of uncertainty, and a broader range corresponds to a higher uncertainty (Peel & Brooks 2015). Nothing can be 100% certain in the subsurface, and therefore uncertainty always exists throughout the whole process of petroleum exploration (Rose 1987).

Recognising the difference between risk and uncertainty is important (Peel and Brooks, 2015). Uncertainty and risk do not exist in the real-world reservoirs, but in our knowledge, description and judgement concerning the reservoirs (Ma, 2011). In the process of exploration with a gradual accumulation of new information, both risk and uncertainty will change. With more information, uncertainty regarding the geology of the prospect will be decreased, whereas the risk can either increase or decrease (Peel and Brooks, 2015). For instance, with improved quality of seismic data, we will be more confident (less uncertain) about the trap geometry, but the risk about the reservoir volume can either increase or decrease depending on the new size of the reservoir compared to the old size assumed before.

2.3 Historical success rate of exploration wells

The first well on the UK Continental Shelf came in operation in 1964 (UK DECC, 2014). As of 2013, altogether 2445 hydrocarbon exploration wells had been drilled in the offshore area (UK DECC, 2014). In the same duration, 581 'significant hydrocarbon discoveries' were made (UK DECC, 2015), suggesting an overall technical success rate of 23.8% for UK offshore exploration wells. A well is deemed as of 'significant discovery' by DECC if it has achieved a flow rate of 1000 barrels of oil per day or 15 million cubic feet of gas during testing (UK DECC 2015). Among the unsuccessful wells, some may have been abandoned due to mechanical drilling problems, rather than the geological problems of reservoirs. Hence, the overall technical success rate of 23.8% is likely to be an underestimation.

Munns et al. (2005) analysed the records of 2150 exploration wells on the UK Continental Shelf drilled during 1964-2002, and concluded that the technical success rate is 31.5% (Figure 2.1). They also emphasised that within the more recent 82 wells completed during 1998-2002, 41 wells made significant discoveries, giving a technical success rate of 50% (Munns et al., 2005). More recently in 2015, UK DECC completed a Post Well Analysis Project, which studied 150 exploration and appraisal wells drilled during 2003-2013 in the Moray Firth and Central North Sea (Mathieu, 2015). The overall technical success of these exploration and appraisal wells is 40% as calculated by DECC (Mathieu, 2015). Summarizing the data above, it can be estimated that, with current technology and the understanding of North Sea geology, the general success rate of an exploration well in the North Sea is now around 40%. And in history, there was a significant increase in the rate from 30% to 40% in the 1990s, as Figure 2.1 illustrates.

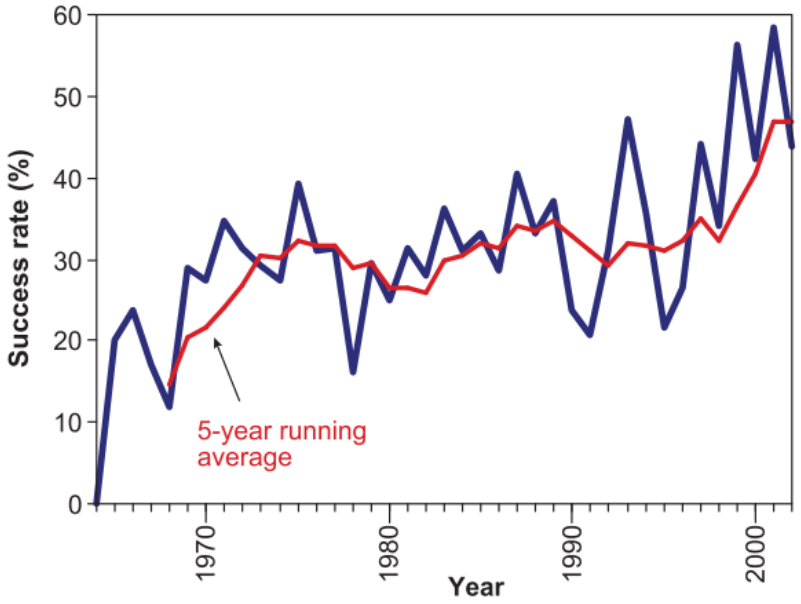

Figure 2.1 Technical success rate of the exploration wells on the UK Continental Shelf during 1964-2002 (Munns et al., 2005). The success rate increased considerably from around 30% to above 40% in the 1990s.

A similar success rate has been reported for the Norwegian Continental Shelf. The result of the 'Evaluation of Norwegian Wildcat Wells' project yielded a total technical success rate of 36% for 196 wells drilled during 1990-1997 (Ofstad et al., 2000a). The average estimated pre-drill success rate of those wells was 23%, compared with a final finding rate of 27% (Ofstad et al., 2000a). In addition, there are 9% of surprising findings that were not expected in the pre-drill prognosis (Ofstad et al., 2000a). The comparison between pre-drill estimation and post-drill results indicate that oil companies are slightly pessimistic but generally perform well in risk assessment and prospect evaluation (Ofstad et al., 2000b).

It is noteworthy that, for reservoirs of varying age and stratigraphic level, the exploration difficulty and success rate is different. According to the data of Brzozowska et al. (2003), the Middle Jurassic reservoirs, mostly the Brent Group sandstones in the Northern North Sea, has the most successful exploration history (success rate 37%, Figure 2.2). The next are Eocene and Palaeocene reservoirs, whose success rates are 36% and 35% respectively (Figure 2.2). Although the largest number of exploration wells in the North Sea region were targeted at the Upper Jurassic level, the success rate of the reservoirs is only about 27%. As for pre-Jurassic reservoirs, the success rates are significantly lower, generally less than 20%.

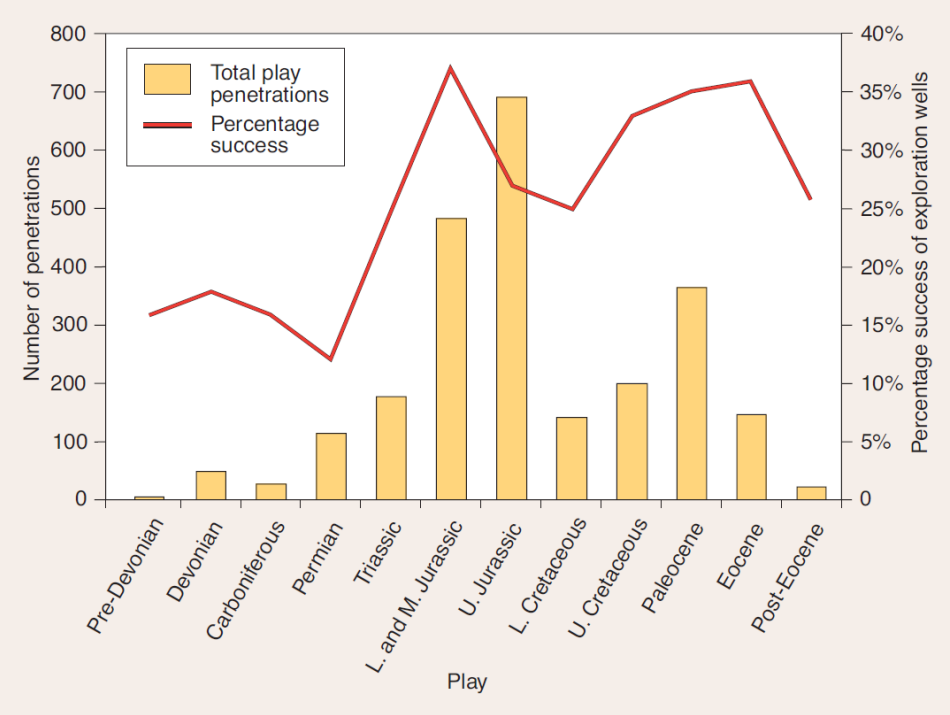

Figure 2.2 The exploration success rate of different age reservoirs in the Central and Northern North Sea (Brzozowska et al., 2003). The success rates of Pre-Devonian, Devonian and Carboniferous reservoirs are below 20%, but for reservoirs of other ages, the average success rates are around 30%. These well data do not include wells from the Southern North Sea or the Fareo-Shetland Basin.

2.4 Methodology

UK relinquishment reports can be found on the UK Oil and Gas Authority website (https://itportal.decc.gov.uk/web_files/relinqs/relinqs.htm). These reports are named after the numbers of the corresponding exploration licenses, e.g. P102, P1023. In the following text, the references to these reports are marked by these numbers of the reports. All the 651 reports on the website to date (until the year of 2016) have been analysed. From these relinquishment reports, seven pieces of important information about each unsuccessful well mentioned in the reports were collected. The information contains well number, failure reason, target formation, sedimentary facies, trap type, geographical location and hydrocarbon shows. Although efforts have been made to make sure the data of each well are as complete as possible, data gaps are inevitable as not all the reports have given detailed well information. Since this study focuses on geological aspect, wells that were unsuccessful due to technical issues during drilling were not considered.

The classification scheme for the failure reasons includes five main categories: source, reservoir, trap, seal and hydrocarbon quality (Table 2.1). This is a novel classification scheme that was built by myself to fit the risk data of this study.

Table 2.1 The classification scheme for the potential geological risk (failure reason) of exploration drilling in this study

Source	Migration route missed trap
	Migration event prior to trap formation
Reservoir	No/poor reservoir development
	Low-porosity and/or low-permeability
	Reservoir compartmentalization
	High uncertainty concerning the lateral variation of reservoir quality
Trap	Incorrect trap geometry and extent prediction
	Incorrect trap depth prediction
Seal	Failed caprock sealing
	Failed bottom/lateral lithological sealing
	Failed bounding-fault sealing
Hydrocarbon	Low hydrocarbon quality

A few wells have complicated failure reasons that are beyond the scope of Table 2.1. For instance, a low market oil price, a long distance to pre-existing production infrastructure, and excessive sea water depth, these factors may be combined to cause the failure of a well. The unsuccessful wells of this kind are not included in the analysis.

Table 2.2 illustrates the table used for data collection and analysis, to assess the significance of each geological risk. The following paragraphs will explain how each of the parameters in Table 2.2 is determined. I designed the risk assessment method in Equation 2.1 to Equation 2.4.

Frequency: In the data collection process, for every well, each significant geological risk that has caused the failure is counted as 1 unit. Many wells may have 2 to 3 failure reasons (Mathieu, 2015; Ofstad et al., 2000b). Only the critical risks that significantly degrade the prospectivity of a well were considered and counted. For example, if a well was unsuccessful due to both low reservoir permeability and a lack of hydrocarbon charge, each of the reasons is counted as 1 because both of them are "fatal". When a well has multiple reservoir targets, only the main target was counted. One common situation is that a well was found to be dry, but it cannot be decided whether this is due to a lack of charge or lack of reservoir seal. If this circumstance occurs, both the risks of hydrocarbon source and reservoir seal were counted as 0.5.

P_{occur}: This parameter refers to the probability of occurrence of a geological risk within UNSUCCESSFUL wells. It is calculated by Equation 2.1. In this chapter, the significance of each geological risk is expressed using the parameter of P_{occur} (the second column in Table 2.2). Since not all the unsuccessful wells are targeted on reservoirs that have fault seal or stratigraphic seal, P_{occur} for failed fault or stratigraphic seal is derived through dividing the frequency by the number of the unsuccessful wells that are targeted on fault-seal traps or stratigraphic traps.

Equation 2.1 P_{occur} = Frequency/Total number of the unsuccessful wells

Uncertainty: The probability distribution of each geological risk follows a binomial distribution pattern (Xia and Wilkinson, 2017). For each geological risk, the process drilling a well can be imagined as tossing a coin. Each coin toss has two results -

heads up or tails up. For each risk, a well also has only two results - occurrence of reserves or no occurrence. Using 'head up' to represent the occurrence of a risk, drilling 100 wells is like tossing a coin 100 times. If a risk occurred 80 times in the 100 wells, the distribution pattern can be seen as 80 times of 'head up' in 100 times of coin tossing. Understanding the pattern of probability distribution of the risk data is for formulating the equation to calculate the data's range of uncertainty. The uncertainty of a probability of binomial distribution can be resolved by Equation 2.2 (Wallis, 2013). This study utilises 90% confidence interval, and hence the z value applied in the equation is 1.645 (Wallis, 2013).

Equation 2.2 Uncertainty = 90% confidence interval of the percentage = $\boldsymbol{z} \times \frac{\sqrt{\mathbf{1}-\boldsymbol{p}}}{\sqrt{\boldsymbol{np}}}$, (p = probability; n = number of trials; z=1.645 for 90% confidence interval; Wallis, 2013).

P_{avoid}: the probability of a risk factor being avoided (for all wells). Equation 2.3 is the method for determining the value of P_{avoid}. In the calculation process, it needs to further take into account the general success rate of all wells. The current average success rate for exploration wells in the North Sea is around 40%, whereas the historic average rate is about 30% (see *Section 2.3*). The aim of the study is to review historic drilling data, and hence 30% is a more reasonable approximation. It is should be aware that P_{avoid} is more representative for the probability of a well in the past to avoid a geological risk. Nowadays, because oil companies now have better technology and richer exploration experience, we should be more confident to estimate and hence avoid a risk.

Equation 2.3 P_{avoid} = [1 - Frequency / (unsuccessful wells + successful wells)] × 100%
= [1 - Frequency × (1 - well success rate) / unsuccessful wells] × 100%

The uncertainty of P_{avoid} is calculated using the uncertainty value of the corresponding P_{occur} by:

Equation 2.4 Uncertainty (P_{avoid}) = Uncertainty (P_{occur}) × (100% - well success rate)

Although the overall success rate for all wells is assumed to be 30%, as Figure 2.2 shows, the overall success rate for the wells targeted on reservoirs of different ages varies, i.e. from 25 – 35%. Therefore, when estimating the P_{avoid} of the geological risks

of the reservoirs of a specific age or stratigraphic level, the corresponding success rate in Figure 2.2 was applied.

The trap type of the target prospect was here classified as either structural or stratigraphic traps (Table 2.3). The structural traps further include 4-way dip trap and fault-seal trap; stratigraphic traps includes pure stratigraphic traps and combined stratigraphic-structural traps (Table 2.3).

The geographic location that was covered includes the Central, Northern and Southern North Sea, and also with other smaller UK offshore hydrocarbon basins such as the Faeroe-Shetland Basin and the East Irish Sea. The boundary and area of the Central and Northern North Sea in this study follow the ones that utilized in the North Sea litho-stratigraphic atlas (Richards et al., 1993), in that the Central North Sea mainly includes the Moray Firth and the Central Graben, and the Northern North Sea comprises the East Shetland Basin and the Viking Graben.

The classification of hydrocarbon shows is based on the type of hydrocarbon and the degree of the shows observed during well test. Six categories have been applied, including Oil (clear), Oil (ambiguous), Gas (clear), Gas (ambiguous), Oil and Gas (clear) and water (Table 2.4). ‘Clear’ in this context means definite or high confidence. “Clear oil or/and gas shows” approximates to the meaning of ‘discoveries’ in exploration, and ambiguous oil or gas shows are low saturation gas- or oil-bearing cases. ‘Water’ means no trace of hydrocarbon was detected.

Table 2.2 An example of the statistical table applied in this study. The calculation method is in Equation 2.1 - Equation 2.4.

	Geological risks	Frequency	P_{occur} (%)	Uncertainty (%)	P_{avoid} (%)	Uncertainty (%)
Source	Migration route missed trap					
	Migration event prior to trap formation					
Reservoir	No/poor reservoir development					
	Low-porosity and/or low-permeability					
	Reservoir compartmentalization					
	High uncertainty concerning the lateral variation of reservoir quality					
Trap	Incorrect trap geometry and extent prediction					
	Incorrect trap depth prediction					
Seal	Failed caprock sealing					
	Failed bottom/lateral lithological sealing					
	Failed bounding-fault sealing					
Hydrocar-bon	Low hydrocarbon quality					

Table 2.3 Classification schemes of trap styles in this study

Trap categories	Sub-categories
Structural trap	4-way dip trap
	Fault-bounding trap
Stratigraphic trap	Pure stratigraphic trap
	Structural-stratigraphic trap

Table 2.4 Applied classification scheme for hydrocarbon shows in this study

Hydrocarbon shows type (degree)
Gas (clear)
Gas (ambiguous)
Oil (clear)
Oil (ambiguous)
Water
Both oil and gas shows (clear)

2.5 Results

In total, this work has collected the data of 382 wells from 651 relinquishment reports. Many of the exploration licences are relinquished after a regional seismic survey, with no confident drillable target and therefore no drilling. Also, many of the 382 wells were not drilled within the valid period of the licenses, but a long time ago presumably by previous owners of the licenses, since the exploration license of one area could have been held by different oil companies over time. The ages of the 382 wells are somewhat randomly distributed over a long period, since the 1970s – present.

One defect of the dataset of this study, however, is that not all the important information of the wells is available, or of sufficient detail. For example, there are 382 unsuccessful wells on the record, but only 348 wells have clear information as to why they were dry. In addition, many of the relinquishment reports only give terse information about the unsuccessful wells they include. This may lead to the failure reasons of some wells being simplified or misinterpreted in the data collection process.

The Excel spreadsheet which contains the whole statistical data of this study can be download from the online address: https://ars.els-cdn.com/content/image/1-s2.0-S1750583617300282-mmc1.xlsx.

2.5.1 Well type

Within the 382 wells, 374 of them have information regarding their well types. The result shows that 319 of the 374 wells (85.3%) are exploration wells, with the remaining 55 wells (14.7%) being appraisal wells (Table 2.5).

Some prospects discovered by one exploration well may have several subsequent appraisal wells. For example, the Dauntless Prospect mentioned in Report P743 and P883 has 5 appraisal wells, and another prospect, the Durward Prospect (in the same report), has 4 appraisal wells. The histories of these two prospects are briefly outlined in *Section 2.6.2(Poor/absence of reservoir development)*. The other unsuccessful discoveries, if they have been appraised, usually only have one appraisal well. All of these appraisal wells were plugged and abandoned together with their corresponding exploration wells due to negative appraisal results.

Table 2.5 Type and number of the unsuccessful wells reviewed in this study.

	Total Number	**Percentage**
Exploration Well	319	85.3%
Appraisal Well	55	14.7%
Total	374	100%

Note: 8 wells in this study lack the well type information and hence are not included in this table.

2.5.2 Well Location

The activity of hydrocarbon exploration in the UK offshore water has been the most intensive in the areas of the Central Graben and the Moray Firth, with 46.3% of the wells in the study being located in these areas (Table 2.6). The Southern North Sea and Northern North Sea are the next two most important areas, where contain 31.2% and 14.4% of the total wells, respectively (Table 2.6). The Faroe-Shetland Basin is a relatively new area for oil and gas exploration activity with the first oilfield, the Foinaven Field, just being discovered in 1992 (Lamers and Carmichael, 1999). Relinquished licenses and abandoned wells in the Faroe-Shetland Basin are also less common. Only 13 unsuccessful wells were recorded. The East Irish Sea has 8 unsuccessful wells, and other UK offshore basins altogether have only 10.

Table 2.6 Geographical distribution of the studied unsuccessful wells. Most of the wells are located in the Central and Southern North Sea.

	Total number of unsuccessful wells	**Percentage**
Central North Sea (includes the Moray Firth)	177	46.3%
Southern North Sea	119	31.2%
Northern North Sea	55	14.4%
Faroe-Shetland Basin	13	3.4%
East Irish Sea	8	2.1%
Others*	10	2.6%
Total	382	100.0%

* ‘others’ include the Celtic Sea, the Mid-North Sea High, the Forth Approaches Basin and the English Channel.

2.5.3 **Hydrocarbon shows**

349 wells have the information regarding the type of fluids they encountered (Table 2.7). Notably, 43.3% of the wells are water-bearing throughout with no sign of hydrocarbon presence. The relinquishment reports do not include any fluid saturation data, and the significance level of hydrocarbon shows was only inferred from the descriptions of drilling process or result in the reports. Therefore, the difference between clear and weak hydrocarbon shows is not quantitatively defined, but very much depends on my subjective judgement. Hence, the numbers in Table 2.7 have some degrees of uncertainty. It is, however, much easier to differentiate a water-bearing well from hydrocarbon-bearing wells, and thus, the number of unsuccessful dry wells (43.3%) is estimated with good confidence.

Table 2.7 The type and percentage of different hydrocarbon shows of the study wells. It is notable that 43% of the wells did not encounter hydrocarbon in the penetrated reservoirs (dry).

	Total number of the unsuccessful wells	**Percentage**
Gas shows (clear)	68	19.5%
Gas shows (ambiguous)	16	4.6%
Gas condensate shows (clear)	12	3.4%
Oil shows (clear)	83	23.8%
Oil shows (ambiguous)	10	2.9%
Both oil and gas shows (clear)	9	2.6%
Water (dry)	151	43.3%
Total	349	100%

2.5.4 **Stratigraphic target**

The Jurassic is the most attractive hydrocarbon reservoir level, with nearly half of the studied wells (44.7%) having Jurassic reservoirs as the drilling target (Table 2.8). The next most frequent targets are the Permian (18.5%), Carboniferous (11.9%) and Paleogene reservoirs (10.2%, Table 2.8). The Cretaceous chalk reservoirs, although important in the Norwegian and Danish North Sea, only contains small reserves on the UK side. Only 1% of the oil production from the North Sea chalk reservoirs is contributed by the chalk reservoirs in UK water, with the remaining 64% and 35% of the chalk reservoir production being in the Norwegian and Danish water, respectively (Eriksen et al., 2003). There are only 2 chalk wells in this study. Despite that 4.6 % of the wells in this study targeted at Cretaceous reservoirs, most of them were exploring for Cretaceous deep-water sandstone reservoirs, rather than the chalk.

Table 2.8 Stratigraphic targets of the study wells. Jurassic reservoirs are the most important reservoir horizons, with 44% of the wells being targeted at this level. Permian reservoirs are the second most common targets of exploration.

	Total Number of the unsuccessful wells	**Percentage**
Paleogene	36	10.2%
Cretaceous	16	4.6%
Jurassic	157	44.7%
Triassic	30	8.5%
Permian	65	18.5%
Carboniferous	42	11.9%
Devonian	5	1.4%
Total	351	100.0%

2.5.5 **Trap type**

The North Sea is comprised of several rift basins that are controlled by series of extensional faults (Glennie and Underhill, 1998). The majority of the studied unsuccessful wells (50.7%) were drilled into the structural traps bounded by these faults (Table 2.9). One third (32.4%) of the wells were drilled for 4-way-dip closures. Stratigraphic trap targets are much less common: the result shows that only 32 unsuccessful wells were targeted on pure stratigraphic traps and 14 are on structural-stratigraphic combination traps.

Table 2.9 The numbers of different trap styles targeted by the studied unsuccessful wells

Trap categories	Sub-categories	Total Number of the unsuccessful wells	Percentage
Structural trap	4-way dip trap	88	32.4%
	Fault-bounding trap	138	50.7%
Stratigraphic trap	Pure stratigraphic trap	32	11.8%
	Structural-stratigraphic trap	14	5.1%
	Total	272	100.0%

2.5.6 Significance of each geological risk

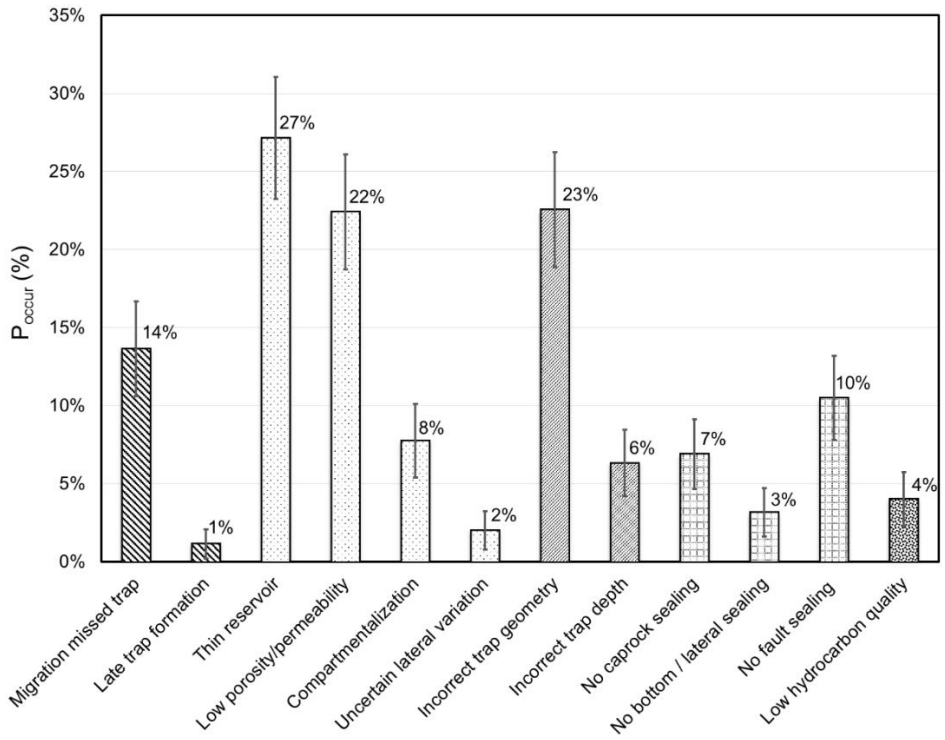

Figure 2.3 The probability of occurrence (P_{occur}%) of each geological risk for the studied UK offshore unsuccessful wells. Thin reservoir, low porosity/permeability and incorrect trap definition are the most significant risks for these exploration wells. P_{occur}% is calculated based upon the data of 348 wells among the 382 total studied wells whose information regarding their failure reasons is available. Raw data are in Table A 2. 1.

The statistical result indicates that the failures of most of the studied wells are related to reservoir problems. Significantly, 27 ± 4 % of the wells were abandoned because of the small thickness/absence of the target reservoirs; and 22 ± 4% were due to the low porosity/permeability problems of the target reservoirs (Figure 2.3). The issues of reservoir compartmentalization and high uncertainty with reservoir lateral continuation and extension may also happen sometimes, but are much less common. Altogether, in all the studied wells, there are 27 wells (8 ± 2%) encountered compartmentalized target reservoirs (8 ± 2%); and comparatively, only 7 (2 ± 1%) had target reservoirs that are highly uncertain with their lateral variations of reservoir quality (Figure 2.3).

The trap is the second most prominent main risk category (Figure 2.3). About one-fifth of the studied wells (23 ± 4%) had target traps that were not correctly interpreted in the pre-drill prognosis. 6 ± 2% of the wells did not reach their target at anticipated depth.

As for seal risks, unsuccessful fault sealing is the most frequent type of failure for reservoir seals (10 ± 3%), followed by failed caprock sealing (7 ± 2%), and then bottom/lateral lithological sealing (3 ± 1%).

When a target reservoir is found not charged, the reason is mostly interpreted to be that the hydrocarbon migration route has by-passed the reservoir. This issue has occurred to 14 ± 3% of the unsuccessful wells. Whereas the case that the migration occurred prior to trap formation is rare. Only the target reservoirs of 4 wells (1 ± 1%) seem to have met this problem.

The exploration geological risks of the Paleogene and Cretaceous-Jurassic deep-water sandstones, the Fulmar Formation sandstones and the Rotliegend sandstones are illustrated in Table A 2. 2 - Table A 2. 7.

2.5.7 Variation of geological risk among reservoirs of different ages and sedimentary facies

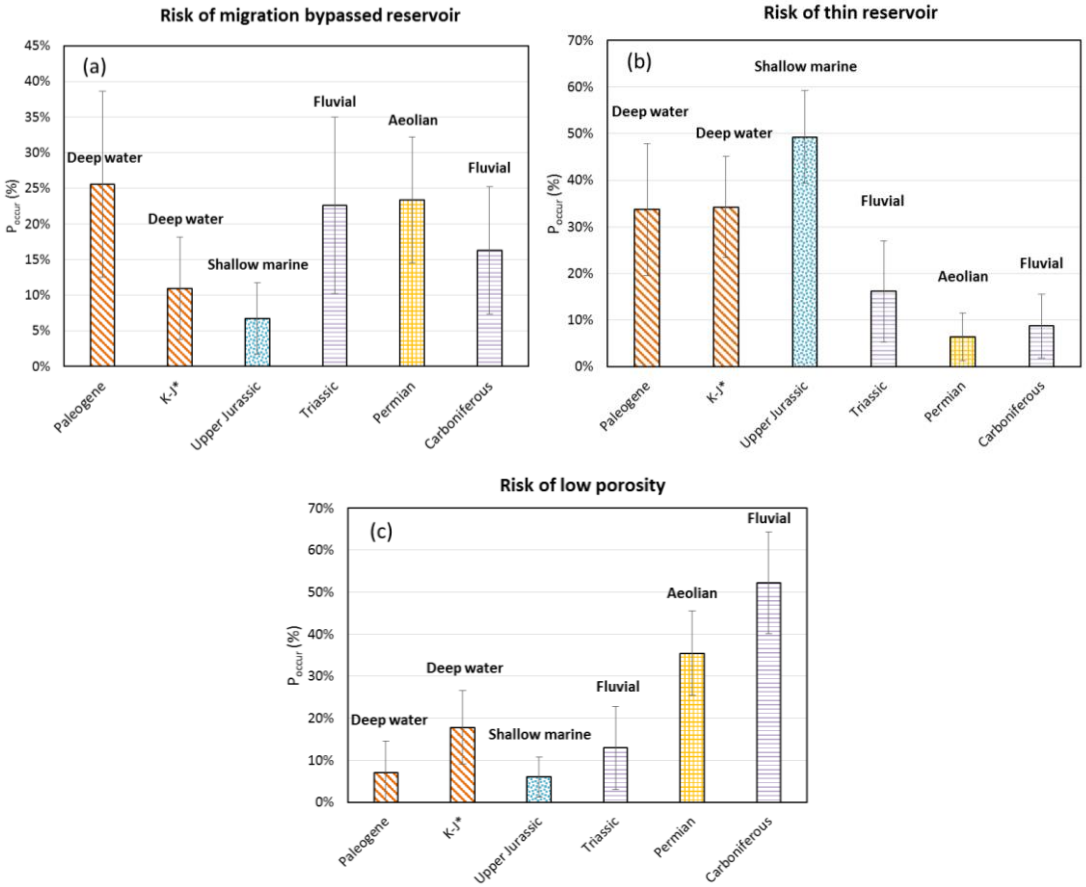

Figure 2.4 No oil charge, thin reservoir and low porosity were noted to vary significantly between different age reservoirs. (a) Risk of no oil charge for the upper Jurassic shallow-marine sandstones is 2-3 times lower than the other reservoirs; (b) Risk of encountering thin reservoirs is more significant in deep-water and shallow-marine sandstones than in fluvial and aeolian sandstones; (c) Risk of low-quality target reservoir increases with reservoir age.

In the studied wells, the cases where the target reservoirs are not charged occurred most frequently to the reservoirs of Paleogene (26 ± 13%), and then Triassic (23 ± 12 %) and Permian (26 ± 9%). The Cretaceous-Jurassic deep-water sandstones (11 ± 7%) and Upper Jurassic shallow-marine sandstones (7 ± 5%) are more likely to have been oil-filled (see later *Section 2.6.1* on 'oil charge risk').

The risk of encountering target sandstones that are much thinner than pre-drill prediction is the most significant in shallow-marine sandstone (49 ± 10%) and deep-

water sandstones (34 ± 14%; see later *Section 2.6.2* on 'risk of encountering thin reservoir'). Sandstones of terrestrial origin, i.e. the Permian aeolian sands (6 ± 5%) and the Triassic and Carboniferou fluvial sends (16 ± 9%; 9 ± 7%), appear to be more predictable in terms of reservoir presence.

The risk of low porosity generally increases with the age of the reservoir (Figure 2.4c). Carboniferous reservoirs (52 ± 12 %) and Permian reservoirs (35 ± 10 %) commonly have the low reservoir quality problem, whereas this risk of low porosity is less significant in the Triassic, Jurassic, Cretaceous and Paleogene reservoirs (Figure 2.4c). Shallow-marine sandstones is the sedimentary facies that form the best-quality reservoirs in the North Sea area (Figure 2.4c).

2.6 Discussion

2.6.1 Hydrocarbon source and migration

Estimating the volume and type of hydrocarbon accumulated in a prospective reservoir is one essential step in the assessment of exploration risk (Al-Hajeri et al., 2009), as the estimated size and reserve of a target reservoir, to a large extent, decides its economic potential and therefore influences the decision of drilling. On the UK Continental Shelf, the data show that 14 ± 3 % of the well failures were caused by the migration path bypassing the target trap, and 1 ± 1% by trap formation occurring later than the timing of migration (Figure 2.3). The P_{avoid} (probability of avoiding a risk) estimated for the risk of no hydrocarbon charge is 90 ± 2 % (Table A 2. 1), which means 9 in 10 exploration wells will drill through hydrocarbon-bearing rocks. This suggests that, in most cases, successful simulation of source rock maturation history and hydrocarbon migration fairways are not difficult to achieve, or perhaps that in a sedimentary basin with mature source rocks, a large proportion of available traps will be filled.

- **Migration influencing the stratigraphic distribution of hydrocarbon resources**

This section will discuss and demonstrate how the risk of hydrocarbon migration would vary from stratum to stratum, and from area to area in the North Sea.

Firstly, reservoirs that are stratigraphically close to the main source rock, appear to have lower charging risk. The Upper Jurassic Fulmar Formation in the Central North Sea is an example of this. The Fulmar is usually overlain, and also sealed by, the main regional source rock, the Upper Jurassic KCF (Richards et al., 1993). Among the 68 unsuccessful wells targeted in the Fulmar Formation, only 3 wells failed on migration issues (5 ± 4%, Figure 2.4a). In comparison, the Paleogene prospects in the Central and Northern North Sea, which also rely on the hydrocarbon source from the KCF, carry much higher hydrocarbon charging risk. 26 ± 13 % of the unsuccessful wells (11 in 43 wells) targeted at this stratigraphic level failed due to a lack of charge

(Figure 2.4a). Charging the Paleogene prospects generally requires a longer migration from the Upper Jurassic level through a thick sequence of Cretaceous chalks and shales, causing a high degree of complexity and uncertainty to the migration route. Hence, areas with thin Cretaceous sediments, well-developed high angle faults and/or salt piercements tend to have lower charging risk for Paleogene prospects (Isaksen and Ledje, 2001).

Similarly, the post-Permian reservoirs in the Southern North Sea have the same problem. The main source rock of the Southern North Sea Basin is the Upper Carboniferous Westphalian Coal Measures (Cornford, 1998). Upward hydrocarbon migration to fill post-Permian reservoirs must first cross the evaporites of the Permian Zechstein Group. The Zechstein evaporites can be up to 2500m thick in the basin centre (Johnson et al., 1994). Evaporites, especially halite, also have the capability to reseal after fracturing, which makes it a nearly perfect seal (Johnson et al., 1994). Hydrocarbon migration through the evaporites is therefore very difficult. Consequently, despite some good quality Triassic and Jurassic reservoir rocks being present in the Southern North Sea, these reservoirs are rarely seen as potential exploration targets (Balson et al., 2002). In the past, almost all the wells aimed at the Triassic targets were dry (Balson et al., 2002). Only in areas where the Zechstein evaporites are extremely thin, have the evaporites been breached and led to Triassic gas deposits, such as in the Esmond, Forbes and Gordon Fields (Ketter, 1991). Brown et al. (1994), however, proposed a new possible way of charging the Triassic reservoirs, which is by the piercement of Paleogene dykes through the evaporites. They identified the presence of Paleogene igneous dykes near the Bunter Field with seismic and magnetic data. Since there is no obvious salt ‘touchdown’ near the field, they suggested that the sediments fracturing during dyke intrusion is the mechanism that breached the Zechstein evaporites (Brown et al., 1994).

2.6.2 Reservoir

- **Poor/absence of reservoir development**

According to the results in Figure 2.3, approximately one fifth of the unsuccessful exploration wells in the UK offshore area were caused by not encountering their anticipated target reservoirs, because the reservoirs were either unexpectedly thin or missing. The ease of recognising reservoirs on seismic profiles, which is the primary method for illustrating subsurface structures, depends on the energy and frequency of the applied seismic waves (Chopra et al., 2006). It is traditionally considered that the vertical seismic resolution limit of a target interval is λ/8, where λ is the wavelength of the seismic wave in the target interval, computed from the frequency of the wave and the seismic velocity of the interval (Widess, 1973). The most widely applied seismic wave frequency is about 30 Hz, with which the seismic method is generally capable of resolving a target thicker than 25m (Chopra et al., 2006). Based on this resolution threshold, the cause of poor/absence of reservoir development can be divided into two types: 1) for reservoirs above the resolution, i.e. > 25m thick, false picking or false interpretation of seismic reflections; 2) and for those below the resolution, false prediction of reservoir presence due to the improper integration of seismic data and sedimentary models.

1) False interpretation of seismic reflections:

The Upper Jurassic shallow-marine sandstones, also known as the Fulmar Formation, is the most common example for which exploration wells missing the target reservoirs. Significantly, 49 ± 10 % of the unsuccessful wells searching for the Fulmar sandstones are caused by the issue of thin reservoir (Figure 2.4 b). For example, in Block 21/11 of the North Sea, the Dauntless Field was initially discovered with 186 ft oil-bearing Fulmar Sandstone by well 21/11-4 (Report P743-P883). However, the sandstones are found to be either missing or thin in all five following appraisal wells, causing the discovery to be re-interpreted as only a small oil-pool sealed by a stratigraphic trap (Report P743-P883). A similar case was seen in the Durward Field in Block 21/16. Four appraisal wells to assess the reservoir all missed the Fulmar Formation, leading

to the downgrading of all other close-by Jurassic prospects and the ultimate relinquishment of the whole area (Report P743-P883).

The Fulmar Formation sandstones typically present 100-400m thick (Richards et al., 1993), which is significantly above the minimum resolution of the seismic technique (25 m, see above). It is, however, somewhat contradictory that a large number of wells were still troubled with finding the reservoir. Two reasons for this learned from the relinquishment report are due to sudden replacement of sandstones by shales, and the low seismic impedance contrast between the shallow-marine sandstones and neighbouring deep-sea shales that causes this replacement not be aware of. For example, in the Northern North Sea, wells 3/23-1 and 3/28c-5 were drilled one after another looking for Upper Jurassic sandstone reservoirs (Report P1170). On the seismic image, the Upper Jurassic strata are seen to thicken from well 3/23-1 to well 3/28c-5. 3/28c-5 was therefore drilled into the thickest part of the Upper Jurassic strata. However, it was then discovered that this thickening was due to the occurrence of a Heather shale interval that had not previously been met in well 3/23-1. A similar situation also occurred for well 21/6a-7, in which the interpreted thick shallow-marine sands were found to be a deep-sea shale (Heather) which did not appear in nearby wells (Report P1048).

Well logs have a vertical resolution of 0.1 – 2m (Tittman, 1991) and are directly measured in the depth domain, as opposed to seismic where information is collected in the time domain. They are excellent calibrators for seismic data. To avoid false interpretation of seismically resolvable beds, before drilling, well-seismic ties must be done if there is any available well information, and also that regional sequence stratigraphy must be carefully reviewed (Mathieu, 2015).

The high rate of failure on predicintg the thickness of shallow-marine sandstones also reflects that the academia and industry currently lack a sufficient understanding on the sedimentary environment and distribution pattern of the sandstones. Tectonic activity, movement of the underlying Permian salt and the resulting bathymetry are the first-order controls upon the distribution of the shallow marine Fulmar sandstones (Howell et al., 1996; Stewart, 1986). Small-scale fault movement and sea-level fluctuation is the second-order control, which mainly influences the lateral thickness

variation and internal depositional fabrics of the sandstone (Howell et al., 1996). Under the co-control of these factors, the Fulmar Formation is distributed in a complex pattern of elongate and narrow belts, bounded by a series of graben faults (Figure 2.5, Howell et al., 1996; Stewart, 1986). Although the shallow marine sandstones can be locally up to 400m thick, their actual lateral extension may be more restricted and variable than in the applied sedimentary models. According to well location, it seems that the risk of reservoir presence for the Fulmar Formation is more significant in the Western Central Graben. 79% of the Fulmar reservoir missing cases were reported from the Block 21, Northern Block 29 and South-eastern Block 22. Special attention concerning reservoir presence should be paid when looking for Fulmar reservoirs in these areas.

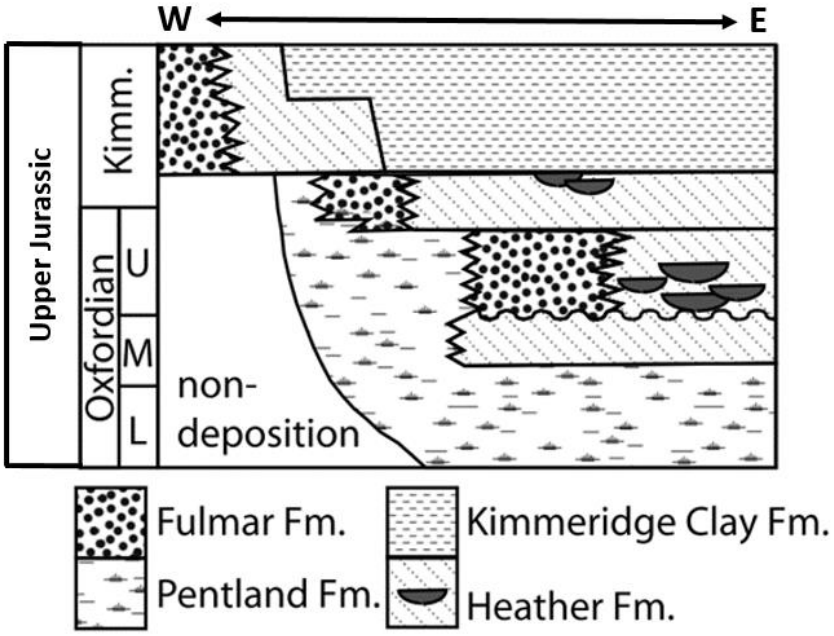

Figure 2.5 Upper Jurassic Lithostratigraphic diagram for the Eastern Central Graben, UK North Sea, showing the distribution of the Fulmar Formation as discrete sand packages (Jeremiah and Nicholson, 1999, redrawn by Wilkinson et al., 2014).

In some cases, false judgement of sand presence can be misled by misinterpreted positive AVO response (AVO: amplitude versus offset; Castagna, 2000). There are some unsuccessful well examples that encountered AVO anomaly shales rather than expected hydrocarbon-bearing sandstones. For instance, well 28/15-1 and -2 drilled into a shale unit that was predicted to be an oil-filled Palaeocene Forties Sandstone, causing the greater Forties play in the area to be re-considered to be shale-dominated

with low hydrocarbon potential (Report P2188). Presence of hydrocarbon in sandstone decreases the rock's P-wave velocity (Vp) value and gives a low Vp/Vs (Vs: S-wave velocity) value to show an AVO anomaly (Krol et al., 2000). Nevertheless, some low-density shales can also exhibit similar low Vp/Vs values due to a high Vs, causing a false-positive AVO response (Avseth et al., 2008). One way to avoid the false interpretation of AVO reponse due to a high Vs value of shales, may be to better understand the seismic properties of local shale, and take the risk of AVO response into consideration during prospect risk assessment.

2) False prediction of reservoir presence:

The failure to precisely map out the reservoir targets below or near the seismic resolution limit usually occurs in the exploration for stratigraphic traps, which are mostly deep-marine sandstone targets. This type of failure includes drilling beyond the pinch-out of a stratigraphic trap (e.g. well 20/07-3, Report P272) and encountering only a few sandstone stringers interbedded within shales (e.g. well 20/7b-5, Report P1047). The deep-marine petroleum system, in particularly that of the Paleogene, is perhaps the most well-understood interval in the North Sea given that its shallowest depth and clearest profiles on seismic images (Ahmadi et al., 2003). However, this advantage does not seem to have significantly mitigated the risk of reservoir presence for the Paleogene reservoirs, when referring to the reservoir presence risk of the Cretaceous-Jurassic deep-water sandstones (Figure 2.4b). It suggests the quality of seismic data is nor the reason for the difficulty of interpreting the presence of deep-marine sandstones. The deep marine facies is possibly the most studied, but the least understood sedimentary system (Shanmugam, 2016; Shanmugam and Moiola, 1985). One main reason for this is because the deep ocean is largely inaccessible. Another reason is due to the complexity of deep-marine sedimentation itself. Many factors control the composition, geometry, stratigraphy and distribution of deep marine sediments, such as: sediment composition and size, transport media (single or multiple channel or non-channelized spillover flow), transport mechanism (slide, slump, debris or turbiditic flow) and basin bathymetry (Shanmugam, 2016). As a result, deep marine sediments are highly variable (Shanmugam, 2016). Some of these variabilities are recognisable on seismic images, whereas some are not (Weimer and Slatt, 1999). To predict sandstone presence hence requires a good combination of

seismic data with sedimentary models. However, the deep water sandstone models tend to be too general to reflect the great variabilities in practice (Stow and Mayall, 2000), which makes the prediction difficult. The experience of exploration for deep-sea sandstone reservoirs in the Faroe-Shetland Basin has suggested that a reasonable trap model, a sedimentary model, acoustic impedance anomalies and the conformance of the three are the essentials for predicting the location of hydrocarbon-bearing deep water sandstone (Lamers and Carmichael, 1999).

- **Low-porosity/Low-permeability**

The problem of low-porosity/low-permeability is the most prominent in the sandstones of the Permian Rotliegend and Carboniferous reservoirs in the Southern North Sea (Figure 2.4c). The results show that 36 ± 10 % of the unsuccessful Rotliegend wells, and more significantly, 52 ± 12 % of the unsuccessful Carboniferous wells are due to the low-porosity or low-permeability problem.

For most Rotliegend sandstones, the porosity and permeability are mainly lost from the progressive growth of quartz cement and illite during burial (Gluyas and Leonard, 1995; Rossel, 1982). Even a small percentage of illite can severely damage the reservoir quality, impairing the permeability by several orders of magnitude, as a result of the fibrous mineral structure and large surface areas of illite minerals (Wilson, 1994). In addition, the porosity of the Rotliegend Sandstone may also be reduced by dolomite or siderite cement, which is precipitated from the invasion of highly saline pore fluids from the neighbouring Zechstein evaporites (Sullivan et al., 1994). However, despite the low matrix porosity and permeability, some Rotliegend fields can still produce gas at commercial rates through natural fractures, which formed during the Cretaceous and Paleogene inversion of the Southern North Sea basin (Gauthier et al. 2000; Winter & King 1991). This highlights the importance of enhanced porosity, e.g. by fracturing, in reservoirs of low matrix porosity and long burial history.

The Carboniferous sandstone reservoirs in the Southern North Sea have the similar diagenetic controls on porosity as the Rotliegend sandstones. Quartz cement and illite are the dominant porosity control factors for the Carboniferous reservoir sandstones in the same way as the Rotliegend sandstones (Corbin et al., 2005). But the problem of low reservoir quality are more severe in the Carboniferous reservoirs: Fraser et al. (1990) showed that the porosity of the Carboniferous reservoirs drop below 10% at depth > 2.5 km, due to the destruction of primary porosity by pervasive quartz and dolomite cementation (Fraser et al., 1990; Leeder and Hardman, 1990). The depth of 2.5 km can therefore be seen as the commercial cut-off depth for of Carboniferous targets in exploration.

Over half of the wells in this study were drilled for reservoirs associated with sealing fault boundaries (Table 2.9). It is important to be aware that faults may locally affect the occurrence of low-porosity reservoirs. This is because the migrations of basinal fluids along faults may lead to mineral precipitation or dissolution, and hence, reducing or increasing the porosity of nearby sandstones (Fisher et al., 2003). For example, Shell in 1991 drilled a well (well 49/24-3) to reach a Rotliegend reservoir. The well encountered strong gas shows, as expected, but the reservoir was tested to be a low-porosity, low-permeability reservoir due to a high degree of quartz cementation. This was not predicted in the pre-drill analysis. A post well study suggested the quartz cement is presumably precipitated by fluids travelling up a large nearby fault (namely the Dowsing fault in Report P007).

- **Reservoir compartmentalization**

28 wells in this study encountered the reservoir compartmentalization problem, accounting for 8 ± 2 % of the total failures. Among the 28 wells, 13 were targeted on Jurassic reservoirs, and in particular, 6 of the 13 wells were targeted on the Fulmar Formation. Another 9 wells were aimed at the Carboniferous reservoirs in the Southern North Sea. Most of the reservoir compartmentalization problems in the Fulmar Formation were caused by fractures or sub-seismic resolution faults formed during tectonic movement, or the flow of the Permian salt (e.g. Report P1427, P1125). Since there is a large number of wells targeted on the Fulmar Formation, the number does not mean that the Fulmar Formation carries a high risk of reservoir compartmentalization. Reservoir compartmentalization is also a common issue in the other North Sea reservoirs, such as the Paleogene, Triassic and Permian reservoirs (Jolley et al., 2010). The Carboniferous reservoirs, however, seem to have a high risk of being compartmentalized, as there are fewer wells drilled into the Carboniferous reservoirs, but the number of failure wells remains significant (Table A 2. 7). Because of the fluvial nature of the majority of Carboniferous reservoirs, permeability heterogeneity due to facies variation is perceived to be the main cause of reservoir compartmentalization (e.g. Well 42/10b-2, Report P1229; Well 44/16-1, Report P2102).

- **High uncertainty concerning the lateral variation of reservoir quality**

The high uncertainty with reservoir lateral variation of reservoir quality is responsible for 8 ± 2 % of the total failures. This uncertainty usually occurs when a target reservoir is found to be very different from in pre-drill reservoir model, even if the exploration well has discovered hydrocarbons. For example, well 13/24a-2A encountered an oil-bearing Cretaceous section which was primarily thought to be a deep-water sandstone (Report P1404 & 1459); but the drilling cuttings showed that the reservoir is in fact made of granite debris. Unfamiliarity with this type of reservoir caused great concern and uncertainty about the potential lateral variation of reservoir quality across the field, and finally, resulted in the abandonment of the discovery. In some other failure cases, exploration wells may be abandoned after finding a much more complex reservoir structure than the pre-drill geological model, for which the resolution of seismic data is insufficient to determine the actual lateral extent of the reservoir (e.g. Well 22/14b-5, Report P1114; Well 13/28-1, Report P1866; Well 22/22b-2Y, Report P233).

2.6.3 **Seal**

Having effective seals is equally important to having valid charge, reservoir and trap. None of these is optional, although the seal risk is often overlooked (Downey, 1984). Seal failure may be indicated in advance by the presence of hydrocarbon in shallow strata above a target. Shallow strata showing strong amplitudes on a seismic image (Figure 2.6) or encountering hydrocarbons during drilling (e.g. well 42/27a-3, Report P1054 - P1133) are the warning signals that the deeper target may be leaking.

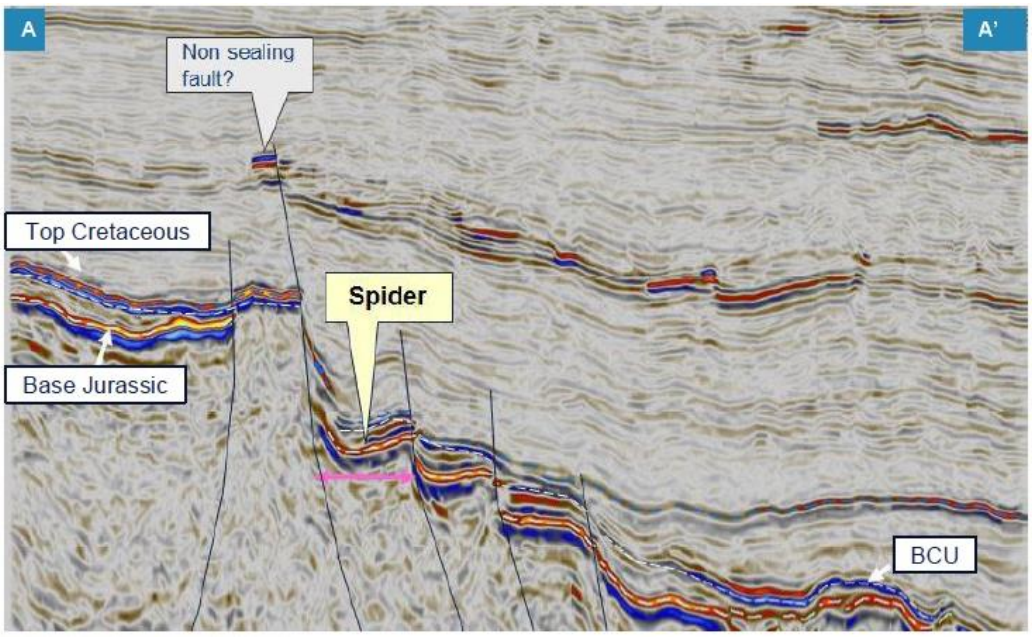

Figure 2.6 A high amplitude in the shallow strata in connection with the deep exploration target through a fault advises that the fault is not sealed. '*Spider*' is the name of the exploration target. (Report P1608)

The number of seals required for a trap depends on the style of the trap. A 4-way dip trap (anticlinal trap) only requires a top seal that is capable of preventing hydrocarbons from migrating upwards. A fault-bounding trap requires both a top seal and bounding-fault seal. The stratigraphic trap is most complicated in terms of the seal. In addition to the top and side seals, it also requires a bottom seal.

The degree of seal risk also varies with trap style. It has been reported that the risk of seal increases from 4-way dip trap to fault-bounding trap and further to stratigraphic

trap (Downey, 1984). In the results of the analysis here, 7 ± 2% of the total wells were unsuccessful on the caprock seal, 3 ± 2% on the bottom/lateral seal and 10 ± 3% on the bounding-fault seal (Figure 2.3). However, it should be aware that not all the traps included in this study need a bounding-fault or lateral/bottom lithological seal. A large proportion of the traps are 4-way dip traps that only call for a top seal. Table 2.10 is a modified result that has categorised the data based upon trap style, to compare the seal risk of each trap style. It shows that the risks of both fault seal (24 ± 6%) and side/bottom lithological seal (36 ± 14%) are high, and in general, fault-bounding traps and stratigraphic traps have higher seal risk than 4-way dip traps.

Table 2.10 The sealing risks of different trap styles estimated using the data of the unsuccessful wells in this study. Unsealed reservoirs are most likely to occur in stratigraphic traps (P_{occur} = 36%), followed by fault-bounding traps (P_{occur} = 24%), and then 4-way dip traps (P_{occur} = 14%).

	Failed sealing component	Frequency	P_{occur}	Uncertainty
4-way dip trap	Caprock	12.5	14%	6%
	Bottom/lateral seal	0	0	0
	Bounding-fault	0	0	0
	Total number of wells = 88			
Fault-bounding trap	Caprock	7.5	5%	3%
	Bottom/lateral seal	0	0	0
	Bounding-fault	33.5	24%	6%
	Total number of wells = 138			
Stratigraphic / structural-stratigraphic combination trap	Caprock	0.5	1%	3%
	Bottom/lateral seal	11.5	36%	14%
	Bounding-fault	1.5	5%	4%
	Total number of wells = 32			

It is, however, surprising that the P_{occur} of top seal failure reported from fault-bounding traps (5 ± 3%) and stratigraphic traps (1 ± 3%) are substantially lower than that of 4-way dip traps (14 ± 6%, Table 2.10). For stratigraphic traps, since the top, lateral and bottom seals usually rely on the same seal rock, it is difficult to tell which part actually fails in practice. In most cases for the analysis presented here, lateral/bottom seal failure is assumed. As for fault-bounding traps, there is no rational geological explanation why the top seal of 4-way dip traps should be riskier than that of fault-bounding traps. A possibility is that, when reservoir seals have failed, exploration

geologists tend to attribute the failure to the fault seal rather than the top seal. In other words, people may have some cognitive bias towards blaming faults for a leaking trap when we cannot figure out which seal part has actually failed.

- **Top seal**

The most important seal rocks in the North Sea are the Upper Jurassic KCF shales and the Lower Permian Zechstein evaporites (Glennie, 1998; Underhill, 1998). There are 10 wells in this study that encountered failed, or likely failed KCF caprock shales. This number is small given that there are 157 Jurassic wells in the dataset (Table 2.8). Notably, 3 of the failure cases are because of heavy erosion at the base Cretaceous Unconformity into the KCF (well 20/5b-12, -2, Report P1658; well 22/16a-2Z, P1421). One case is due to faulting over trap (9/28b-19a, report P1285) and one is related to underlying salt piercement (well 29/7-1, Report P457). The other 5 wells do not have clear reasons for failure in the relinquishment reports.

The deep Central North Sea Basin below the Cretaceous is overpressured (Holm, 1998). Some of the overpressures may leak-off at different points into the shallower basin, typically through the highest points of tilted-block structures (e.g. the structure drilled by well 22/30-1 in Wilkinson et al., 1997). Since these fault block structures are the main exploration targets in the North Sea, there has been concern that some of these structures may have been breached by overpressure leak-off (Gaarenstroom et al., 1993). This study, however, has not come cross any failures of this type, indicating that this issue may not be common.

The sealing capability of the Zechstein evaporites is robust in the vast majority of cases. Only 4 cases of Zechstein seal failure are on the record. The evaporites were breached during basin inversion in one of the cases (well 49/22b-16, Report P1544) and by faulting in another case (well 49/29-9, P1364). The flow of evaporites causing the touchdown of the overlying succession on the underlying reservoir also lead to one failure (well 48/11c-13, P1008). The last case did not give a failure mechanism in the relinquishment report.

The previous two paragraphs have summarised the variety of seal rock failures that have occurred to the two main UK offshore seal rocks. Another common failure situation which has not been seen in the two seal rocks is a sand-prone seal. This issue has occurred in the Paleogene and the Lower Permian (the Silverpit Formation) seal rocks (well 9/27a-4, Report P1284; well 42/27a-3, Report P1054 - P1133). A common top seal risk for a 4-way dip trap is the fracturing of the top seal during folding (Downey, 1984), yet this risk appears to be insignificant in the North Sea despite the extensional tectonic setting. The only few cases of seal rock fracturing in this study are related to the halokinesis of underlying salt (e.g. well 29/7-1, Report P457) or, in the Southern North Sea, due to basin inversion (e.g. well 49/22b-16, Report P1544). Non-deposition of seal rock is possible, but this case is rare in the North Sea and has never been reported in any of the relinquishment reports.

- **Fault seal**

150 in 380 wells in this study were drilled into the traps associated with faults (Table 2.9), indicating that around 40% of the hydrocarbon reservoirs on the UK continental shelf are within fault-seal traps. And there are 34 wells (24 ± 6%, Table 2.10) that are certain or very likely to be unsuccessful due to failed fault sealing. 12 of the wells were on the Rotliegend targets, revealing that the Rotliegend reservoirs have the riskiest bounding faults. 8 wells failed on Fulmar Formation targets. But given the large number of wells targeted on the Fulmar, the fault seal risk of Fulmar reservoirs is considered not outstanding. In addition to this, the Middle Jurassic Brent Group has 5 unsuccessful wells related to leaky fault seals, and the Triassic reservoirs have 4.

The Permian Zechstein evaporites are ideal seal rocks (Glennie, 1998). All the Rotliegend sandstones that are juxtaposed against the evaporites by faults are sealed (Knott, 1993). So why are the sandstones still so risky on fault seal? According to Knott's (1993) conclusions, the sealing ability of a fault is strongly related to the throw of the fault. All the Rotliegend sandstones faults that have throws greater than the sandstone thickness are sealed (Knott, 1993). Similarly, 90% of the Brent Group faults whose throws are greater than the reservoir thickness are sealed (Knott, 1993). The reason for having so many unsealed Rotliegend faults is possibly because these faults have not entirely offset the Rotliegend Group, i.e. fault displacement < reservoir

thickness. The Rotliegend Sandstone is one of the thickest sand units in the North Sea, with the bed thickness frequently exceeding 200-300m (Johnson et al., 1994). It, therefore, requires larger faults than other sandstones to move it apart, which may cause the lower fault sealing probability. The inversion in the Southern North Sea Basin and reactivation of faults during inversion might also pose some additional risks.

In the Moray Firth-Central North Sea post-well analysis project, lack of lateral seal was reported to account for 27.3% of the total failures (Mathieu, 2015). In the Norwegian sector, this number is 19% in 196 wildcat wells (Ofstad et al., 2000b). Both of these numbers are higher than the degree of fault risk suggested by this study (10 ± 3%). It is likely that this study has underestimated the chance of failure of fault seals. Many of the wells mentioned in the relinquishment reports were not drilled by the current licence holders, but by the oil companies that explored in the area before. Some of the wells were even drilled in the 1960s or 1970s. Accessing the full old data is difficult. The information regarding oil charge, reservoir presence and quality, trap robustness can be learned from well-logs and seismic data, whereas seal integrity is not evident from this primary exploration data. It is possible that many of the oil companies who write the relinquishment reports have little information about the seals of the prospects penetrated by old wells. This lack of sufficient information may have caused an underestimation of fault seal risk in this study.

- **Lateral/bottom lithological seal**

As of 2011, 12% of UK offshore hydrocarbon fields or significant discoveries are in structural-stratigraphic combination traps, and 6% in pure stratigraphic traps (DECC, 2012). More importantly, it has been suggested that 50% of the undiscovered hydrocarbon potential in the UK offshore water are in stratigraphic or combination traps (Stoker et al., 2006). Stratigraphic and the combination traps are mostly formed in Upper Jurassic, Cretaceous or Paleogene deep water sediments (DECC, 2012). Nearly half of the current Paleogene reservoirs rely on stratigraphic seals (DECC, 2012). 50-70% of remaining potentials in the Upper Jurassic, Cretaceous and Paleogene reservoirs are in stratigraphic traps (DECC, 2012). The other potential possibly remains in the Triassic and Middle Jurassic fluvial-deltaic sandstones, at the pinch-out of sandstones at basin margin and the sub-Permian unconformity. Carboniferous successions may also contain some reservoirs of stratigraphic traps.

Exploration for stratigraphic traps is challenging. Many of the North Sea stratigraphic discoveries were, in fact, made by chance while drilling for other targets (Stoker et al., 2006). What makes it so difficult is their lack of recognisable features on seismic images. Stratigraphic traps are usually small in size, or conformable to their surrounding lithologies, making them below the seismic resolution (Caldwell et al., 1997). Additionally, some stratigraphic traps may be associated with some surfaces of sharp contrast, such as unconformity planes (Figure 1.3), which can produce strong seismic noise blurring the trap (Caldwell et al., 1997). Most of the post-well analyses in the relinquishment reports do not explain explicitly why the sealing of stratigraphic traps are unsuccessful, possibly because the answers are not clear to the oil companies. It is possible that many of failures are due to the issue of trapping, i.e. they do not form closed space in 3D dimensions, instead of leaking seal rocks (e.g. well 22/13b-9, Report P1420 & P1801; 20/4a-10, Report P1100). Hence, some of the seal rocks failures in this study may actually be trap geometry definition problems.

2.6.4 Trap

Based on whether the errors in petroleum trap interpretation are on the vertical or lateral scale, the failures of trap definition are grouped into two categories in this study: 1) incorrect trap geometry definition and 2) incorrect trap depth prediction. Both can lead to a variety of failure reasons for dry wells, such as drilling off target structure, drilling the reservoir below the oil-water contact, the absence of the target trap, and the trap volume being much smaller than the pre-drill prognosis. In the last section, it has been discussed that the ability to predict reservoir presence is, to a great extent, related to the vertical resolution of the seismic technique. Here, on the other hand, defining the geometry of a trap relies on the horizontal resolution of seismic data. The optimum seismic horizontal resolution that can be achieved is typically between 10m and 50m, depending on the depth and other geological and technical factors (Sheriff, 1997). Incorrect target depth prediction, in contrast, is mainly a time-depth conversion problem rather than a seismic resolution problem.

In this study, 106 cases of trap definition failure have been documented (Table A 2. 1). There are 79 cases (23 ± 4 %) being caused by incorrect trap geometry definition and 22 cases (6 ± 2%) by incorrect target depth prediction (Table A 2. 1). The issue of trap definition seems to be significant for reservoirs of all the ages on the UK Continental Shelf (Table 2.11). The following sections will discuss the potential causes of the trap risk.

Table 2.11 The trap risk for each main reservoir level on the UK Continental Shelf. The data is compiled Table A 2. 2- Table A 2. 7.

	Incorrect trap geometry definition		Incorrect trap depth prediction	
	P_{occur}	Uncertainty	P_{occur}	Uncertainty
Paleogene	22%	12%	9%	9%
K-J* turbidites	26%	10%	0	0
Jurassic shallow marine sandstones	19%	8%	0	0
Triassic	26%	13%	19%	12%
Permian	20%	8%	13%	7%
Carboniferous	22%	10%	9%	7%

*K-J = Cretaceous-Jurassic

- **Challenge for trap definition 1 – complex basin history – examples from the Permian and Carboniferous reservoirs**

Most of the UK's Carboniferous and Permian hydrocarbon reservoirs are located in the Southern North Sea. The high risk of trap definition of the Carboniferous and Permian reservoirs, which are suggested by the high P_{occur} values in Table 2.11, is consistent with the past experience that seismic time-depth conversion is known to be problematic in many areas of the Southern North Sea (Corbin et al., 2005). In comparison with other regions of the North Sea, the Southern North Sea has a more complex basin history that was intermittently affected by multiple periods of basinal inversion (Oudmayer and de Jager, 1993). The regional uplift and erosion during the Cretaceous and Paleogene had a profound influence on the development of the Southern North Sea basin (Glennie and Underhill, 1998). As a result, the Permian and Carboniferous strata have been uplifted by up to 1.0 km (Glennie, 1998). They are more compacted than anticipated for their current depth of burial, and therefore, these reservoirs have faster seismic velocity than would be predicted from their current depth of burial (Glennie, 1998). The result is that the reservoirs are usually deeper than the prognosis based on the seismic data. Moreover, since the degree of the inversion is uneven across the basin, and seismic velocity is highly variable both vertically and laterally, the determination of the trap geometry of hydrocarbon reservoirs is also challenging.

The difficulty of exploration in the Southern North Sea can be, to some extent, reflected by the history of well 48/8-2. The well was designed to drill a time-high on the seismic image, but post well analysis suggested that the well has in fact drilled into a depth-low of the target structure (Report P1734). The 'real' structural high is located northwest of well 48/8-2, which was primarily shown as a time-low on the seismic image (Report P1734). The failure of the well is mainly due to the application of an improper velocity model. Well-seismic ties are important in controlling the high uncertainty of time-depth conversion in the Southern North Sea (Glennie, 1997). However, this control becomes less robust 50m away from wells (Corbin et al., 2005). In future, a better understanding of the tectonic framework, application of more sophisticated rock velocity models and seismic technique innovation will be the keys to combat the trap definition issues in the Southern North Sea.

- **Challenge for trap definition 2 – shallow salt and igneous rocks – examples from Triassic reservoirs**

In total, there are 9 Triassic wells in this study having the issues of trap definition. Notably, 6 of the wells are located in the Irish Sea (Block 110 and 113), indicating trap definition is of high risk for the local Triassic gas reservoirs. Altogether, 3 Triassic wells were unsuccessful due to unexpected presence of salt in shallow successions, and all the 3 wells are in the Irish Sea; 1 well is due to the presence of volcanics; 1 is due to higher than expected velocity in shallow chalks; and 1 is due to an incorrect rock velocity model but without further details. Salt and igneous rocks have much faster seismic velocity than sedimentary rocks. If they are not anticipated in pre-drill prognosis, these rocks will cause huge errors in the seismic time-depth conversion. For instance, well 110/14d-8 reached the target Triassic Sherwood Sandstone 700 ft deeper than the prognosis because of a presence of thick, injected salt layer in the overburden (Report P009). Well 110/3b-6a reached its target reservoir 500 ft deeper than prognosis due to an unexpected shallow volcanic unit (Report P1547). Target reservoirs of these wells are below the predicted oil-water contact in the pre-drill models, and therefore do not contain hydrocarbon. In the Faroe-Shetland Basin, exploration drilling has attempted to explore sub-basalt plays, such as well 6104/21-1, 6004/8a-1, 6005/13-1 and 6104/21-2 (Woodburn et al., 2014). The drilling results showed that basalt would greatly impair the quality of seismic data and make the seismic interpretation and trap definition of sub-basalt structures difficult (Woodburn et al., 2014). One common conclusion from these wells is that the basalts encountered are often thicker than expected, causing reservoirs target to be deeper than the pre-drill prognosis, and to have a lower porosity or to be below the oil-water contact (Woodburn et al., 2014).

- **Challenge for trap definition 3 - thin sandstones - examples from deep marine sandstones**

Similar to the Triassic, Permian and Carboniferous reservoirs, the risk of trap definition is also significant for Paleogene and Cretaceous-Jurassic deep-marine sandstone targets. 22 ± 12% of the unsuccessful wells aimed at Paleogene reservoirs, and 26 ± 10% at Cretaceous-Jurassic deep marine sandstone reservoirs, have encountered the trap issue. However, the cause of the high risk of trap definition in the Paleogene reservoirs is different from in the Carboniferous-Triassic reservoirs. It is mainly from the difficulty of predicting the thickness of the sandstones, and the position where the sands pinch out. The issue of predicting reservoir thickness has been discussed in *Section 2.6.2*; the determination for the edge of deep-marine sands is related to the horizontal resolution of seismic data, which is about 10-50m (Sheriff, 1997). One sedimentary characteristic of deep-marine sands is their frequent alternations with deep-sea shales. When the boundary between the sands and the surrounding shales are transitional, instead of sharp, it would be extremely difficult to recognise the edge and extent of the sands. This poses a great risk to the prediction of the geometry and the volume of a stratigraphic reservoir trap. Typically, the determination of reservoir boundary utilises the AVO anomalies on a prospect (Loizou, 2005). Nevertheless, this method has an additional risk that the AVO anomaly could be due to a lithological effect rather than hydrocarbon presence (e.g. well 205/9-2, Report P1838; well 21/29b-9, Report P1563).

Loizou (2014) reviewed 79 Palaeocene exploration wells in the Faroe-Shetland Basin completed since 1972. 23 of the wells achieved technical success whereas the remaining 56 wells were dry (success rate 29.1%, Loizou, 2014). It is noteworthy that 80% of the failures were caused by trap issues (Loizou, 2014). This number is much more significant than the one derived in this study. One reason for this discrepancy may be due to the location difference of the studied samples. Only 7 Palaeocene wells in this study are from the Faroe-Shetland Basin. The rest wells are located in the Central or Northern North Sea, where most of the Paleogene targets are 4-way dipping structural traps (Pegrum and Spencer, 1990), such as in the Forties (Wills, 1991), Monstrose (Hogg, 2003) and Frigg fields (Brewster, 1991). The definition of 4-

way dipping traps in most cases is not a problem, and therefore, the overall degree of trap risk for the local Paleogene targets are not as high as in the Faroe-Shetland Basin. Under the current exploration trend with stratigraphic reservoirs becoming more important (DECC, 2012), the greatest effort in the exploration for turbidite stratigraphic targets should be spent on trap definition. The Paleogene deep water successions are rarely affected by faulting and have no thick, complex overburden (Ahmadi et al., 2003). These attributes give them an innate advantage in seismic imaging (Ahmadi et al., 2003). The Paleogene reservoirs have benefited the most from the advance of the seismic technique compared to the other ages of reservoirs (Ahmadi et al., 2003). A sharp rise of Palaeocene target success rate in the Faroe-Shetland Basin from a historic 29% to 75% in the recent decade (9 success in 12 wells) has proven this notion (Loizou, 2014). To maintain or further improve this high rate of success, it is important to apply the best quality possible seismic data acquisition and processing, with the combination of other techniques to fully assess Paleogene prospects before drilling (Loizou, 2014).

- **Challenge for trap definition 4 – fault**

Over half of the unsuccessful wells in this project are targeted on fault-seal traps (Table 2.9). It is necessary to be aware of the risk in trap definition brought by faults. In Report P1559, there is a case in which an exploration well (15/23-3) tested a fault-bounding Jurassic turbidite sandstone prospect. However, after the acquisition and re-interpretation of a new seismic dataset, the dip angle of the main bounding fault of the trap was re-calculated to be different from the previous prediction. The new estimated volume of the trap was 30% smaller than the previous estimation, causing a large shrinkage in the economic value of the prospect and hence, the ultimate relinquishment of the exploration license. The volume of fault-bounding traps is, to a great extent, affected by the dip angles of fault planes. It is, therefore, important in prospect evaluation to consider the uncertainty of fault angles calculated and their variation across the reservoir. Faults used to be interpreted on a 2-D seismic profile by connecting the lateral discontinuities on seismic reflectors, and geological reasoning (Admasu and Tönnies, 2005). With the advent of the 3-D seismic technique and some advanced auto-interpretation software, the interpretation of faults now can be completed with high confidence when the quality of seismic data is good (Hale, 2013). But the risk about the dip angle of fault plane may remain significant when the data quality is poor (Admasu and Tönnies, 2005).

Another potential exploration risk related to faulting is that faults may impair the quality of seismic signals below fault planes. Fault planes have different seismic properties from the sedimentary rocks they cut through, so that they can form strong reflective planes for seismic waves (Hale, 2012). Penetration of seismic waves through fault planes, therefore, can be difficult, which may increase the uncertainty with the extent of the reservoir below a huge fault plane.

2.6.5 Hydrocarbon Quality

In the studied wells, 14 wells encountered low-quality hydrocarbons, and were then plugged and abandoned (Table 2.9). Nine of the wells are due to the presence of heavy oil, and two are caused by sulfur-rich oil, which is also often known as sour oil (Table 2.12).

A mature KCF source rock typically generates a medium-gravity oil (36-55 ^{o} API, 42 ± 5 ^{o} API on average; Cornford, 1998, p. 456). In previous studies (e.g. Ahsan et al., 1997; Cornford, 1998, p. 454), occurrences of heavy oil have been reported over much of the North Sea, but are mostly restricted to Paleogene reservoirs. The Paleogene reservoirs are buried at relatively shallow depth (<2 km) than the hydrocarbon reservoirs of other ages. The depth range indicates that the generation of heavy oil in the Paleogene reservoirs is related to micor-biological activities (Head et al., 2003). 80^{o}C is the maximum temperature threshold for living microorganism in the subsurface (Head et al., 2003). Under the average North Sea geothermal gradient of 34.6 ^{o}C /km (Kubala et al., 2003), the regime of biological activities is above 2.3km of depth. This is consistent with the traditional assumption that the reservoirs below 2km in the North Sea show little or no evidence of biodegradation (Ahsan et al., 1997; Barnard and Cooper.B.C, 1981). However, in the results of this study, the majority of the reservoirs containing heavy oil problems are, in fact, Jurassic reservoirs (Table 2.12). It suggests that, in addition to the Paleogene reservoirs, heavy oil still can be a risk for the further deeper and older oil reservoirs. The occurrence of heavy oil in Jurassic reservoirs may be due to the biodegradation occurred during the shallow burial of these reservoirs, or it may indicate that temperature is not the only control of oil biodegradation.

This study has only two reports of sour oil (well 14/18-1 and 15/26b-5). Both of the reports are from the Upper Jurassic deep-water sandstone reservoirs (Table 2.12). Similarly, the majority of the discoveries of sour oil in the North Sea are also from the Upper Jurassic oilfields near these two wells, around the area of the Witch Ground Graben (Cornford, 1998). These Upper Jurassic reservoirs are either deep-water sandstone reservoirs (e.g. the Miller, Claymore and Buzzard Fields; Doré and Robbins, 2005; Harker et al., 1991; Rooksby, 1991) or shallow marine sandstone

reservoirs (e.g. the Piper and Tartan Fields; Coward et al., 1991; Schmitt and Gordon, 1991). Regarding burial depth, the occurrence of H_2S in the Central and Northern North Sea has been suggested to be only significant at depths below 3.5 km (Worden et al., 2003). The depth suggests the origin of the H_2S is from the thermochemical sulphate reduction (Worden et al., 2003). Based on these observations and experience, it can be inferred that the exploration activities near the Witch Ground Graben, looking for Upper Jurassic prospects below 3.5km, have a high risk of encountering sour oil.

Table 2.12 A list of the the 14 unsuccessful wells caused by low hydrocarbon quality

Well	Reservoir target	Failure reason
2/3-1	Jurassic Brent Group	Heavily biodegraded oil (16^o API)
9/28b-19a	Jurassic, Brae Sandstone	Volatile hydrocarbon
13/24a-2A	Cretaceous, Chalks; Lower Cretaceous sand	Heavy oil
14/18-1	Jurassic Claymore Sandstone	Sour oil - presence of H_2S
14/24-1	Palaeocene and Cretaceous reservoirs	Heavy to dead oil due to biodegradation
15/21b-45	Jurassic Galley and Dirk Sandstones	Heavily biodegraded oil (12^o API)
15/26b-5	Jurassic, Ettrick Sandstone	Sour oil - presence of H_2S
15/26b-9	Jurassic, Sgiath Sandstone	Heavy oil: high wax content and asphaltene drop-out
16/8c-13	Jurassic, Brae Formation	Gas condensate
21/11-6	Jurassic, Fulmar Sandstone	Heavy oil - 17.5 API oil
21/27b-7	Eocene, Tay Formation	Heavy oil: reservoir modelling shows that the estimated recovery factor is no more than 30%
43/20b-2	Carboniferous, Namurian - Westphalian sand	CO_2 rich gas: contains 9 mol% of CO_2
206/10-1	Devono-Carboniferous, Clair Group and Cretaceous, Whiting sands	Heavy oil - 13^{o}API oil
210/29a-3	Jurassic, Brent Group	Heavy oil

2.6.6 **Reliability and application of the data**

The database of this study has covered all the hydrocarbon basins and all the petroleum systems on the UK Continental Shelf. Based on the historic drilling results documented in the relinquishment reports, it quantitatively demonstrates and compares the significance of each geological risk in the exploration drilling in UK offshore water. In spite of having made great efforts to ensure that the data are complete and representative, there are still some defects in the data. First of all, the risk of "no reservoir presence" may lead to an underestimation of the P_{occur} of the other risks. For example, if the target reservoir of a well is missing, then it is impossible to decide whether the quality of the reservoir is good, or whether the trap or seal is effective. This may lead to 0-2% of underestimation for the P_{occur} of other risks. Although the degrees of the underestimations are minor and covered within the uncertainty intervals of P_{occur}, these underestimations are still worth keeping in mind when reviewing past drilling data. The occurrence of each geological risk is independent, but this example shows that the occurrence of some risks may affect the assessment processes for other risks. Secondly, there have been significant difficulties in the well data collection process as the information in the relinquishment reports is often incomplete, or is inconsistent, or in different data format; some oil companies may not have shared some of the core exploration data. In order to minimize the error of the results, we have maximized the sample size by covering all the reports available. Each result is also assigned with a 90% confidence interval to indicate the reliability of the data.

Referring back and scrutinizing past exploration cases is useful when evaluating a new prospect. But before making use of the past statistics, oil exploration teams should understand in what circumstances and how to do this. For a new prospect that does not have adequate subsurface information, the past statistics can be applied to estimate the chance of success of the prospect as a whole, or probability of success of a particular geological component of the reservoir, such as the trap or seal. This estimation would be the most reliable when the undrilled prospect shares the same geological background with the referred past cases, or when they all belong to the same petroleum play (Peel and Brooks, 2016). As for the exploration in a frontier basin where geological information is scarce, the historical exploration data of the UK offshore basins may be useful in inferring the general geological risks of the new basin.

However, this inference requires the frontier basin to have a similar geological setting as the UK Continental Shelf. This is important as oil companies need to decide the exploration efforts and capital to be invested in the new basin on the basis of its economic potential. In the UK offshore area where there has been rich exploration experience, most new prospects have already been covered by high-quality seismic data. For these prospects with sufficient information, the past statistics can better be used as a risk check. But it should be aware that the risk analysis of new prospects must not be constrained by the past data, because in many cases, with sufficient information, oil exploration teams can confidently determine that a risk of the new prospect is lower than those tested in the past (Peel and Brooks, 2016). On the other hand, the risk of a prospect could increase after comparisons to old exploration cases. However, it should be noted that this increase of risk is not necessarily a bad thing. The real world has not changed and what changes are that the exploration teams now understand the prospect better. A smarter decision will be made upon this better understanding. To give up drilling is a wise option at many times, and it may save millions of pounds sterling.

When reading through the relinquishment reports, I noticed that many risk assessments assigned a success probability of 100% to a particular geological factor, signifying the success is certain. However, the truth is that nothing is certain in the subsurface before a well is drilled and the 100% is clearly an overestimation. If the oil exploration team is confident with the success of a geological factor, 95% may be a more appropriate probability. Using 100% instead of 95% may lead to an overestimation of a few percentage points in the final result. Even after a well has reached the subsurface, cautons are still needed to eliminate any risk by promoting its probability of success to 100%. For example, if a well found a thick, oil saturated, good quality reservoir as all expected in the pre-drill prognosis, there is still risks regarding the lateral variation of the sand, the edge of the reservoir and reservoir compartmentalization. Hence, the suggestion here is that ‘do not easily give out a 100% success probability’.

In practice, some exploration geoscientists may tend to simply equate the future chance of success to the past success rate (Peel and Brooks, 2016). For instance, if 10 wells have continuously discovered good quality reservoirs in a particular geological formation, some exploration teams may assume the 11th well would also

encounter a good quality reservoir in the same formation. But from a statistical point of view, this equivalence only works when the sample size of the past cases is large enough (Wilson, 1927). The fact is that the success of the past 10 wells cannot simply guarantee the 11th well will be 100% successful. Peel and Brooks (2016) proposed a more statistically reasonable method of using past data to predict the rate future success, through the equation of COS = (s + 1)/(n + 2), where 's' equals the number of successful case and 'n' the sample size (Peel and Brooks, 2016). Figure 2.7 is the application figure that is based on this equation. According to this equation, the chance of success of the 11 wells, given all the previous wells are successful, is 91.7%.

The oil industry's ability to manage exploration risk is ever growing as exploration techniques evolve and experience accumulates. Under this trend, the overall success rate of exploration is forecasted to be ever increasing in the future, and meanwhile, the significance of each exploration risks will also keep changing. The P_{occur} of the geological risks in current exploration or future exploration is almost certain to be lower than the P_{occur} inferred by the old drilling data. Combining the past statistics and experience with technology innovation is a way to enhance the exploration potential in the future.

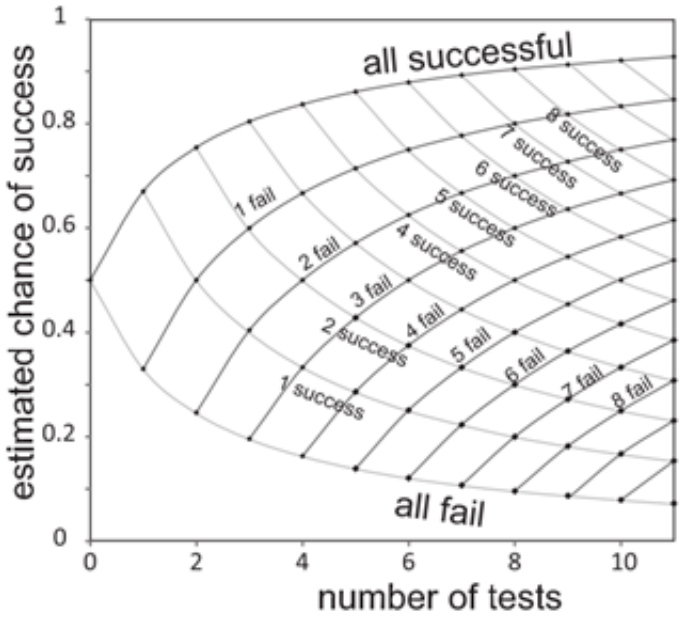

Figure 2.7 Estimation for the future chance of success based on a small number (<10) of past tests (Peel and Brooks, 2016). This diagram is constructed using the equation COS = (s + 1)/(n + 2).

2.7 Conclusion

Using the well data collected from the relinquishment reports, this study has quantitatively expressed and compared the geological risks of hydrocarbon exploration on the UK Continental Shelf. Six main conclusions are drawn:

1. Thin reservoir (27 ± 4%), low porosity (22 ± 4%) and incorrect definition for trap geometry (23 ± 4%) are the most significant geological risk in hydrocarbon exploration and have caused the most exploration failures.

2. Reservoirs close to source rocks have lower charging risk. In the Central and Northern North Sea, the Paleogene reservoirs have higher charging risk (26 ± 13 %) than the Cretaceous and Jurassic reservoirs, which are closer to the regional source rock on the stratigraphic framework. In the Southern North Sea, post-Permian reservoirs are rarely considered as exploration targets due to the long migration distance from Carboniferous source rock and the presence of thick Zechstein evaporites truncating the migration route.

3. The risk of encountering a thin reservoir, or no reservoir presence, occurs most frequently in the reservoirs of the Central and Northern North Sea, particularly the shallow marine sandstones (49 ± 10%), i.e. the Fulmar Formation.

4. The issue of incorrect definition for trap geometry is common, but in different geological formations, the main causes are different. In the Carboniferous and Rotliegend reservoirs in the Southern North Sea, it is due to the complex history of basin inversion. In the Triassic reservoirs of the Irish Sea, it is usually caused by the unexpected presence of salt and/or igneous rocks in the shallow strata. In turbidite reservoirs, the reason is that many of the turbidite sand bodies are below seismic resolution and difficult to depict on seismic images.

5. Fault-bounding (24 ± 6%) and stratigraphic traps (36 ± 14 %) are riskier on the reservoir seal than 4-way-dipping traps (7 ± 2%). Among the main reservoir units of the North Sea, the Rotliegend reservoirs are probably the riskiest on the fault seal, probably due to the great thickness of the sandstones.

6. Heavy oil and sour oil are the most common two types of hydrocarbon quality issues. Most of the heavy oil cases are found in the Jurassic reservoirs. The oil resources in the Witch Ground Graben tend to have a high degree of sulphur content.

Summary statement: this work designed a novel method for quantifying the geological risks in hydrocarbon exploration. It has built the largest dataset of unsuccessful wells in the existing literature, and used the dataset to demonstrate the significance of each geological risk, and how the significance varies in reservoirs of different ages and sedimentary environments.

Table A 2. 1 The general geological risks of exploration drilling on the UK Continental Shelf. The overall success probability for the studied well is assumed as 30%, according to the historical drilling data (see Section 2.3).

	Geological risks	Frequency	P_{occur}	Uncertainty	P_{avoid}	Uncertainty
Source	Migration route missed trap	47.5	14%	3%	90%	2%
	Migration event prior to trap formation	4	1%	1%	99%	1%
Reservoir	No/poor reservoir development	94.5	27%	4%	81%	3%
	Low-porosity and/or low-permeability	78	22%	4%	84%	3%
	Reservoir compartmentalization	27	8%	2%	95%	2%
	High uncertainty concerning the lateral variation of reservoir quality	7	2%	1%	99%	1%
Trap	Incorrect trap geometry and extent prediction	78.5	23%	4%	84%	3%
	Incorrect trap depth prediction	22	6%	2%	96%	2%
Seal	Failed caprock sealing	24	7%	2%	95%	2%
	Failed bottom/lateral lithological sealing	11	3%*	2%	98%	1%
	Failed bounding-fault sealing	36.5	10%†	3%	93%	2%
Hydrocar-bon	Low hydrocarbon quality	14	4%	2%	97%	1%

Total number of the wells = 348;
Assumed overall success rate for all the wells = 30%;
*number of wells containing fault-sealed targets = :
*number of twells containing target reservoirs with stratigraphic seals =:

Table A 2. 2 The geological risks of Paleogene deep-water sandstone reservoirs

Geological risks		Frequency	P_{occur}	Uncertainty	P_{avoid}	Uncertainty
Source	Migration route missed trap	11	26%	13%	83%	8%
	Migration event prior to trap formation	0	0%	0%	100%	0%
Reservoir	No/poor reservoir development	14.5	34%	14%	78%	9%
	Low-porosity and/or low-permeability	3	7%	8%	95%	5%
	Reservoir compartmentalization	0	0%	0%	100%	0%
	High uncertainty concerning the lateral variation of reservoir quality	0	0%	0%	100%	0%
Trap	Incorrect trap geometry and extent prediction	9.5	22%	12%	86%	8%
	Incorrect trap depth prediction	4	9%	9%	94%	6%
Seal	Failed caprock sealing	5	12%	10%	92%	6%
	Failed bottom/lateral lithological sealing	2.5	6%	7%	96%	5%
	Failed bounding-fault sealing	0.5	1%*	3%	99%	2%
Hydrocar-bon	Low hydrocarbon quality	3	7%	8%	95%	5%
Total number of the wells = 43 Assumed overall success rate for all the wells = **35%**						

Table A 2. 3 The geological risks of Cretaceous-Jurassic deep-water sandstone reservoirs

Geological risks		Frequency	P_{occur}	Uncertainty	P_{avoid}	Uncertainty
Source	Migration route missed trap	8	11%	7%	92%	5%
	Migration event prior to trap formation	0	0%	0%	100%	0%
Reservoir	No/poor reservoir development	25	34%	11%	74%	8%
	Low-porosity and/or low-permeability	13	18%	9%	87%	7%
	Reservoir compartmentalization	2	3%	4%	98%	3%
	High uncertainty concerning the lateral variation of reservoir quality	4	5%	5%	96%	4%
Trap	Incorrect trap geometry and extent prediction	19	26%	10%	80%	8%
	Incorrect trap depth prediction	0	0%	0%	100%	0%
Seal	Failed caprock sealing	5	7%	6%	95%	4%
	Failed bottom/lateral lithological sealing	4	5%	5%	96%	4%
	Failed bounding-fault sealing	5	7%	6%	95%	4%
Hydrocar-bon	Low hydrocarbon quality	7	10%	7%	93%	5%
Total number of the wells = 73; assumed overall success rate for all the wells = **25%**						

Table A 2. 4 The geological risks of Upper Jurassic shallow marine sandstone reservoirs (Fulmar Formation)

Geological risks		Frequency	P_{occur}	Uncertainty	P_{avoid}	Uncertainty
Source	Migration route missed trap	4.5	7%	5%	95%	4%
	Migration event prior to trap formation	0	0%	0%	100%	0%
Reservoir	No/poor reservoir development	33	49%	10%	66%	7%
	Low-porosity and/or low-permeability	4	6%	5%	96%	3%
	Reservoir compartmentalization	7	10%	6%	93%	4%
	High uncertainty concerning the lateral variation of reservoir quality	0	0%	0%	100%	0%
Trap	Incorrect trap geometry and extent prediction	12.5	19%	8%	87%	5%
	Incorrect trap depth prediction	0	0%	0%	100%	0%
Seal	Failed caprock sealing	6.5	10%	6%	93%	4%
	Failed bottom/lateral lithological sealing	3.5	5%	4%	96%	3%
	Failed bounding-fault sealing	8	12%	6%	92%	5%
Hydrocar-bon	Low hydrocarbon quality	1	1%	2%	99%	2%
Total number of the wells = 67; assumed overall success rate for all the wells = **30%**						

Table A 2. 5 The geological risks of Triassic reservoirs

Geological risks		Frequency	P_{occur}	Uncertainty	P_{avoid}	Uncertainty
Source	Migration route missed trap	7	23%	12%	84%	9%
	Migration event prior to trap formation	1	3%	5%	98%	4%
Reservoir	No/poor reservoir development	5	16%	11%	89%	8%
	Low-porosity and/or low-permeability	4	13%	10%	91%	7%
	Reservoir compartmentalization	2	6%	7%	95%	5%
	High uncertainty concerning the lateral variation of reservoir quality	0	0%	0%	100%	0%
Trap	Incorrect trap geometry and extent prediction	8	26%	13%	82%	9%
	Incorrect trap depth prediction	6	19%	12%	86%	8%
Seal	Failed caprock sealing	2	6%	7%	95%	5%
	Failed bottom/lateral lithological sealing	0	0%	0%	100%	0%
	Failed bounding-fault sealing	5	16%	11%	86%	8%
Hydrocar-bon	Low hydrocarbon quality	0	0%	0%	100%	0%
Total number of the wells = 31; assumed overall success rate for all the wells = **25%**						

Table A 2. 6 The geological risks of Lower Permian Rotliegend reservoirs

Geological risks		Frequency	P_{occur}	Uncertainty	P_{avoid}	Uncertainty
Source	Migration route missed trap	14.5	23%	9%	84%	6%
	Migration event prior to trap formation	3	5%	4%	97%	3%
Reservoir	No/poor reservoir development	4	6%	5%	95%	4%
	Low-porosity and/or low-permeability	22	35%	10%	75%	7%
	Reservoir compartmentalization	1	2%	3%	99%	2%
	High uncertainty concerning the lateral variation of reservoir quality	0	0%	0%	100%	0%
Trap	Incorrect trap geometry and extent prediction	12.5	20%	8%	86%	6%
	Incorrect trap depth prediction	8	13%	7%	91%	5%
Seal	Failed caprock sealing	5.5	9%	6%	94%	4%
	Failed bottom/lateral lithological sealing	0.5	1%	2%	99%	1%
	Failed bounding-fault sealing	12	19%	8%	86%	6%
Hydrocar-bon	Low hydrocarbon quality	0	0%	0%	100%	0%
Total number of the wells = 62; assumed overall success rate for all the wells = **30%**						

Table A 2. 7 The geological risks of Carboniferous reservoirs

Geological risks		Frequency	P_{occur}	Uncertainty	P_{avoid}	Uncertainty
Source	Migration route missed trap	7.5	16(%)	9%	89%	6%
	Migration event prior to trap formation	0	0%	0%	100%	0%
Reservoir	No/poor reservoir development	4	9%	7%	94%	5%
	Low-porosity and/or low-permeability	24	52%	12%	63%	8%
	Reservoir compartmentalization	8	17%	9%	88%	6%
	High uncertainty concerning the lateral variation of reservoir quality	2	4%	5%	97%	3%
Trap	Incorrect trap geometry and extent prediction	10	22%	10%	85%	7%
	Incorrect trap depth prediction	4	9%	7%	94%	5%
Seal	Failed caprock sealing	0.5	1%	3%	99%	2%
	Failed bottom/lateral lithological sealing	1	2%	4%	98%	2%
	Failed bounding-fault sealing	1	2%	4%	98%	2%
Hydrocar-bon	Low hydrocarbon quality	1	2%	4%	98%	2%
Total number of the wells = 46; assumed overall success rate for all the wells = **30%**						

Chapter 3

The geological risks of exploring for a CO_2 storage reservoir

Statement of Work

This chapter has been published on: Xia C, Wilkinson M. The geological risks of exploring for a CO_2 storage reservoir[J]. International Journal of Greenhouse Gas Control, 2017, 63: 272-280.

The content of this chaper is my own work. My supervisor Mark Wilkinson provided the research idea and aided with polishing the English writing.

Abstract

Experience of developing saline aquifers as CO_2 storage sites is limited. Drawing on the experience of hydrocarbon exploration, there are geological risks that may be encountered during the search for CO_2 storage sites, such as finding a reservoir of

insufficient thickness, of low porosity or lacking an adequate seal. This study uses drilling records of 382 hydrocarbon boreholes on the UK Continental Shelf to analyse the geological risks of exploring for a new CO_2 storage reservoir, on the assumption that the probability of occurrence of geological risks are similar. The most significant risks for a new borehole are the absence of the target reservoir (19 ± 3 % of cases), low reservoir quality (16 ± 5 %) and lack of trap (16 ± 3 %). Overall, 48 ± 8 % of subsurface structures, identified from seismic data, can potentially store CO_2. For saline aquifers that have already been penetrated by wells within the potential storage site, most of the geological risks are eliminated or at least reduced; reservoir compartmentalization is the major remaining geological risk. This study demonstrates a method to quantitatively apply drilling data from hydrocarbon exploration to the exploration for CO_2 storage reservoirs in analogous geological settings.

3.1 Introduction

One of the challenges of developing saline aquifers as CO_2 storage sites is the lack of pre-existing geological data, in contrast to developing storage in a depleted hydrocarbon field where legacy data should be available. A potential risk is hence drilling a target aquifer, and discovering, for example, that the expected reservoir unit is absent, or is of too low porosity to be useable. This is a surprisingly common result for hydrocarbon exploration wells, even when drilling in areas with relatively well-known geology such as the UK Continental Shelf (UKCS). Because CO_2 geological storage is a field with limited practical experience, in this study we use historical drilling records for hydrocarbon exploration on the UKCS to estimate the probability of finding a useable CO_2 storage site upon drilling a single borehole.

A borehole drilled in the exploration for conventional hydrocarbons can be unsuccessful because of an absence of any of the components of the conventional petroleum system: source, migration, reservoir, trap, seal and preservation. If any of these essential elements are absent, then a borehole will be unsuccessful – here we term these essential elements to be 'risk factors'. Potential CO_2 stores only require three of these fundamental elements: reservoir, seal and trap, and accordingly have 3 risk factors, or more correctly groups of risk factors as each can be subdivided (Table 1). The probability of finding an effective CO_2 storage reservoir (probability of success, POS) can be estimated by deriving the probability of an exploration borehole encountering a reservoir with integral reservoir, seal and trap (Equation 3.1).

Equation 3.1 POS = P (reservoir success) × P (seal success) × P (trap success)

The UKCS is an unusual hydrocarbon province in world terms due to the unusually wide stratigraphic distribution of hydrocarbon resources (Brennand et al., 1998). Commercially viable hydrocarbon reserves have been found in reservoirs of Paleogene, Cretaceous, Jurassic, Triassic, Permian and Carboniferous ages (Eriksen et al., 2003). Reservoirs were deposited in a wide range of sedimentary environments, and have had burial histories that vary from almost continuous burial to multiple periods of basin inversion. This study estimates the probability of success of locating storage sites for CO_2 in reservoirs of varying ages and sedimentary environments on the UKCS by using historical drilling for hydrocarbons as an analogue. Note that only

geological factors are considered, and not technical drilling issues which may result in the loss of the borehole, for example a stuck drill bit.

3.2 Method

For a CO_2 storage reservoir to be effective, all the geological risks concerning the seal, reservoir and trap must be avoided. Hence, the overall probability of finding an effective CO_2 storage location ($P_{success}$) is:

Equation 3.2 POS = P_{avoid} (reservoir presence) × P_{avoid} (reservoir quality) × P_{avoid} (reservoir non-compartmentalized) × P_{avoid} (reservoir lateral certainty) × P_{avoid} (trap geometry) × P_{avoid} (trap at prognosed depth) × P_{avoid} (caprock seal) × P_{avoid} (fault seal)* × P_{avoid} (lateral/bottom seal)**

(*only for fault-bounding traps; ** only for stratigraphic traps)

The P_{avoid} in the equation can be inferred from the historical data of hydrocarbon exploration wells targeted at the same geological unit. For each geological unit, the P_{avoid} have been listed in Table A 2. 2 - Table A 2. 7. The uncertainty for the POS in Equation 3.2 can be derived by Equation 3.3.

Equation 3.3 Assume $x=a\pm p$, $y=b\pm q$; then $x*y \approx a*b\pm (a*q+b*p)$, of which $a*q+b*p$ is the uncertainty of $x*y$

3.3 Results

Figure 3.1 illustrates the overall probability of avoiding each geological risk when exploring for hydrocarbon and potential CO_2 storage reservoirs (Raw data in Table A 2. 1). Figure 3.2 shows the POS of applying different age reservoirs in the UK offshore area as CO_2 storage reservoirs. The overall POS is 49 ± 8 %, and the data suggests the most potential storage reservoirs are in the Paleogene, Triassic and Rotliegend sandstones (Figure 3.2). Table 3.1 is the calculated POS for using different style traps as CO_2 storage reservoirs.

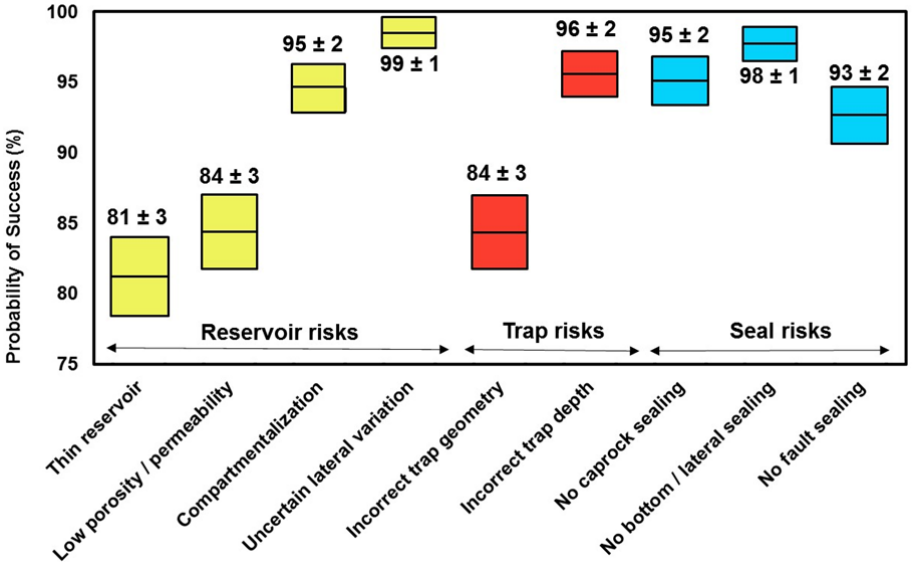

Figure 3.1 The probability of not encountering geological risks (P_{avoid}) in a borehole, i.e. the probability of success for each risk category.

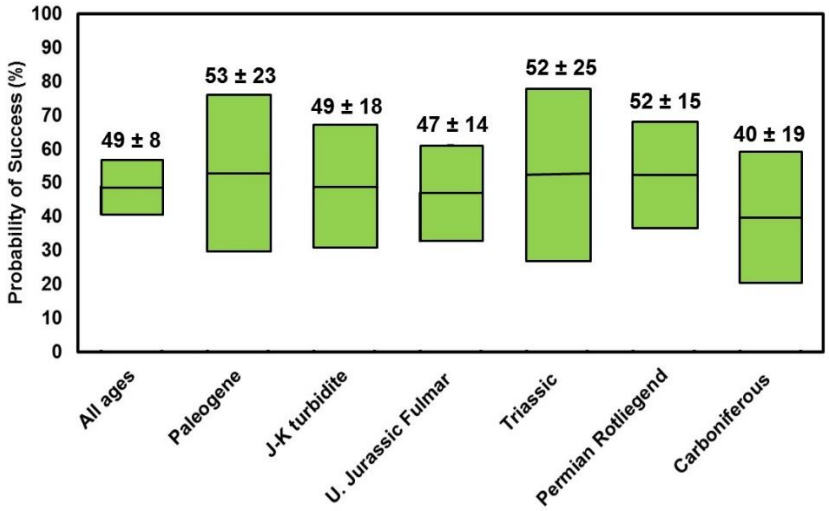

Figure 3.2 The POS of a borehole to encounter a suitable CO_2 storage reservoir in the North Sea by age of the reservoir (periclinal traps only). J-K is Jurassic-Cretaceous

Table 3.1 The POS of applying different styles of traps in the North Sea as storage reservoirs. The calculations of POS and its uncertainty follow Equation 3.2 and the data are from Table A 2. 1

	Failed sealing component	Frequency	P_{risk} (%)	Uncertainty (%)	P_{avoid} (%)	Uncertainty (%)	POS (%)	Uncertainty (%)
Periclinal trap (n = 88)	Caprock	12.5	14	6	**90**	**4**	49	8
	Bottom/lateral seal	0	0	0	100	0		
	Bounding-fault	0	0	0	100	0		
Fault-bounding trap (n = 137)	Caprock	7.5	5	3	96	2	45	8
	Bottom/lateral seal	0	0	0	100	0		
	Bounding-fault	33.5	24	6	**82**	**4**		
Stratigraphic / combination trap (n = 46)	Caprock	0.5	1	3	99	3	36	10
	Bottom/lateral seal	11.5	25	11	**74**	**10**		
	Bounding-fault	1.5	3	4	100	0		

3.4 Discussion

The most important risk factors for a new borehole drilled for CO_2 storage, as indicated by experience of drilling for hydrocarbons, are reservoir presence; reservoir quality; and trap definition (Figure 2.3). Absent, thin or low-porosity target reservoirs could cause a CO_2 storage project to fail after the drilling of a first well, at considerable expense. Incorrect trap definition could lead to erroneous estimates of storage volume or a failure to trap CO_2 in the target structure, leading ultimately to leakage.

3.4.1 Risk of reservoir absence or being too thin

From the hydrocarbon drilling records, 27 ± 4 % of the unsuccessful exploration wells have reservoirs whose thicknesses do not meet the pre-drill expectations (Figure 2.3). Assuming the overall success rate of hydrocarbon exploration wells is 30% (see *Section 2.4*), it suggests that 81 ± 3 % of CO_2 storage wells will find the target reservoir to be satisfactory. For a borehole drilled into a saline aquifers with few existing wells, there is hence a significant risk (approximately 1 in 5) that the target reservoirs will be absent or too thin. The risk of reservoir absence is highest among shallow marine sandstone, and decreases through turbidite sandstones and fluvial-deltaic sandstones, to aeolian sandstones (Figure 2.4). Hence, the depositional environment of the reservoir determines the risk of reservoir absence, presumably by controlling geometry especially lateral continuity.

3.4.2 Risks associated with poor reservoir quality

The chance of encountering a target reservoir with adequate porosity and permeability for CO_2 injection and storage is estimated at 84 ± 3% (Figure 3.1). Storing CO_2 in a low-porosity, low-permeability reservoir is costly and technically challenging. The In Salah project is a case in point where the reservoir has 10-15% porosity and 1-50 mD permeability (Eiken et al., 2011). To improve the injectivity of the reservoirs, three horizontal injection wells were drilled, at considerably higher cost than vertical wells (Ringrose et al., 2013). If large number of saline aquifers are to be drilled for

CO_2 storage in future, it is highly likely that some of them may encounter the problem of poor reservoir quality. However, the depth of burial for the majority of CO_2 storage reservoirs in future are expected to be in the range of 1 – 3 km, compared to the common depth of 2 – 6 km for the oil and gas fields on the UKCS. As depth is a strong control upon the porosity of sandstone reservoirs, an important question is whether the probability of encountering a low-porosity hydrocarbon reservoir is a good analogue for the CO_2 storage case. But one complicating factor for hydrocarbon reservoirs is the filling of hydrocarbons, which has been suggested to preserve porosity by halting or retarding quartz cementation (Wilkinson and Haszeldine, 2011; Worden et al., 1998). This is shown by higher porosity in oil-bearing sections than the water-bearing equivalents in many oilfields (e.g. Marchand et al., 2000). It is here considered that the effect of relatively shallow burial depth for CO_2 storage will at least partly offset the need for better reservoir quality, and the lack of porosity preservation by hydrocarbon charge in an aquifer. Thus, the probability of encountering a low porosity hydrocarbon reservoir is considered to be still applicable for estimating the probability of drilling into a low porosity aquifer sandstone, though with a degree of caution.

3.4.3 Risks associated with poor trap definition

A good evaluation of a trap requires its depth, relief, lowest-closing contour and geometry to be correctly described. Precise definition of traps is also required to quantify the storage capacity of a CO_2 storage site, and to predict the unwanted lateral migration of CO_2. The inherent uncertainty in defining tarps is determined by a combination of several factors, including reservoir depth, reservoir geometry, the lithology of reservoirs and their neighbouring units, geological background of basins and quality of seismic data. For reservoirs of different depths, sedimentary environments and tectonic histories, the cause of the risk of trap definition can be very different. This section focuses on Palaeogene and Cretaceous turbidite reservoirs in Central and Northern North Sea, and the Triassic - Permian reservoirs in the Southern North Sea, both of which have substantial potential for CO_2 storage (Heinemann et al., 2012; Senior, 2010).

The probability of correctly defining the trap geometry of Paleogene reservoirs is estimated to be 86 ± 9 % (Table A 2. 2), hence there is a 14 ± 9 % probability that the

trap will not be adequate. However, the risk of trap definition for Palaeogene targets has been estimated to be substantially higher in some other studies. For example, Loizou (2014) suggested that 80% of the unsuccessful wells in the Faroe-Shetland Basin are due to trap definition. This may be because the vast majority of exploration targets in the area are stratigraphic traps, where the definition of trap geometry is more challenging than conventional structural traps. This study, however, includes only 7 wells from the Faroe-Shetland Basin. Most of the study wells are from the Central and Northern North Sea, where many of the Paleogene targets are periclinal traps, such as in the Forties, Montrose and Frigg Fields. Definition of periclinal traps in most cases is not problematic and therefore the overall risk associated with trap definition for Paleogene targets in the North Sea is not as high as only for the Paleogene targets in the Faroe-Shetland Basin. One factor that makes trap definition of turbidite sandstone targets difficult are their small thicknesses, which are often below seismic resolution (Chopra et al., 2006).

Traps in the Southern North Sea have problems of definition that are not found in the Central and Northern North Sea. The Southern North Sea has undergone multiple periods of inversion with regional uplift and erosion from Cretaceous to Neogene (Glennie and Underhill, 1998). As a result, the basin has been uplifted by up to 1 km (Glennie, 1998). Many sedimentary rocks in the Southern North Sea are now more compacted than would be anticipated for their current depth of burial and therefore have higher seismic velocity than expected (Glennie, 1998). Moreover, as the degree of the inversion is uneven across the basin, so the seismic velocity is highly variable both vertically and laterally. To construct an accurate seismic velocity model and conduct accurate time-depth conversion is therefore very difficult in many areas. Hence, it is common to have high uncertainties in depth prognoses for Southern North Sea drilling targets, and these uncertainties must be thoroughly considered and assessed during the selection of a CO_2 storage site.

3.4.4 Risks factors associated with the seals

In traditional petroleum geology, seals have been neglected compared to reservoir rocks (Downey, 1984). In the field of CO_2 storage, in clear contrast, studying and assessing reservoir seals have been the aim of considerable research effort (e.g. Busch et al., 2010; Lu et al., 2009; Wilkinson et al., 2014). The important properties

of seals, for hydrocarbon reservoirs or CO_2 storage, are thickness, lateral variation, capillary entry pressure and degree of fracturing (Downey, 1984). Therefore, the probabilities of sealing success for hydrocarbon reservoirs and aquifer reservoirs can be seen as equivalent. However injecting CO_2 will increase reservoir pressure and therefore impose additional risks on the seals, at least locally. It is possible that the increased pressure can create or re-open fractures in seal rocks, or that the buoyancy of a CO_2 column breaches seal rocks (Busch et al., 2010). Furthermore, the CO_2 can potentially react with some of the minerals in the seal rocks, increasing the risk of leakage if flow paths are created (Smith et al., 2013). From the above, it is concluded that the risk associated with seal quality is higher for CO_2 reservoirs than for hydrocarbon fields.

3.5 The probability of success (POS) for new CO_2 storage boreholes

Based on the geographical location of CO_2 storage sites relative to existing hydrocarbon fields, CO_2 storage saline aquifer reservoirs can be divided into two groups:

- Saline aquifers associated with a hydrocarbon field. These saline aquifers can be directly above the hydrocarbon reservoir of the field, such as the Utsira Formation of the Sleipner project; below the hydrocarbon reservoir, such as the Tubåen Formation of the Snøhvit project; or downdip of the hydrocarbon reservoir, such as the in the In Salah project (Cooper et al., 2009). These potential CO_2 storage sites are henceforth referred to as 'proven reservoirs'.
- Saline aquifers that are distant from hydrocarbon fields. These reservoirs are henceforth referred to as 'unproven reservoirs'.

The experience of hydrocarbon exploration is applicable to both unproven and proven reservoirs, but has to be applied differently.

3.5.1 The geological risks of an unproven storage site – implications for regional storage capacity assessments

An unproven reservoir for CO_2 storage can be treated as an undrilled hydrocarbon prospect, as the methods of subsurface characterization of hydrocarbon reservoirs and saline aquifers are essentially the same. The probability of encountering any given geological risk during hydrocarbon exploration can be used to predict that of the same geological risk in developing unproven aquifer reservoirs, and ultimately the associated POS.

The fact that drilling into known reservoir horizons, on identifiable structures, carries a significant risk that the site will be unsuitable for CO_2 storage (Figure 3.2) has implications for regional assessments of CO_2 storage capacity. Currently, the vast majority of national/regional estimation of CO_2 storage capacity is only at a theoretical

level (Bachu et al., 2007; Holloway et al., 2006b; Senior, 2010). All the subsurface formations that appear to be capable of storing CO_2 based on available information are considered over their known geographical extent (e.g. Heinemann et al., 2012; Holloway et al., 2006). However, by analogy with hydrocarbon exploration, not all the geographical extent of potential reservoir formations will have all the geological factors required to be effective CO_2 stores. Over a significant proportion of the mapped geographical range of a formation, there will be either no (or only a thin) reservoir; no seal; or individual traps may be incorrectly defined. To generate more reliable estimates of CO_2 storage capacity, it is important to understand what percentage of the subsurface might in fact be suitable for CO_2 storage.

In this study, the overall probability of success for aquifer reservoirs in periclinal traps is estimated to be 49 ± 8 % and fault-bounded traps to be an indistinguishable 45 ± 8 % (Table 3.1). Hence only approximately 1 in 2 CO_2 storage structures, which appear to be competent storage locations in a preliminary regional assessment, are expected to be successful. This suggests that the early stage estimates of CO_2 storage capacity in many studies need to be reduced by a factor of 2 to get a more realistic CO_2 storage capacity. The newly generated estimates by this method is approximately at the effective level, based on the classification pyramid of storage capacity in Bachu (2008). If financial and regulatory factors are also taken into consideration, these storage capacity estimates will be further reduced. The POS estimated for stratigraphic traps is 36 ± 10% (Table 3.1), suggesting that in an area where many of the traps have a stratigraphic component, early stage estimates of CO_2 storage capacity may need to be reduced by a factor of 3.

3.5.2 The geological risks of a proven reservoir

To apply the data presented here to estimate the POS of boreholes targeted at proven reservoirs is more problematic than the unproven reservoirs above. There are less uncertainties than for unproven reservoirs as once a well is drilled, many geological risks are reduced. Reservoir thickness and quality can be measured; reservoir pressure can be tested; the depth of the reservoir can be accurately determined. However, proven reservoirs still have only limited well coverage and there are three geological risks remaining that are subject to varying degrees of uncertainty: the

degree of reservoir compartmentalization; the lateral variation in reservoir quality; and trap definition.

Reservoir compartmentalization is usually not apparent in the appraisal phase of a reservoir but gradually becomes evident in the operation phase as pressure and production data accumulate and can be compared with reservoir models (Jolley et al., 2010; Smalley et al., 1994). Understanding the degree and scale of reservoir compartmentalization is critical for CO_2 storage reservoirs, because it has a strong impact on the volume of reservoir available for CO_2 storage and for pressure dissipation. Furthermore, a compartmentalized reservoir may cause rapid pressure rise around injection wells and prevent further injection (Holloway et al., 2006).

The probability of encountering a reservoir with compartmentalization issues is here estimated as 5 ± 2 % (Figure 3.1), however, this is only reservoirs which are characterised by a rapid pressure decline during well testing. As most hydrocarbon reservoirs have some degrees of compartmentalization (Smalley and Hale, 1996), there might be a larger number of reservoirs whose issues of compartmentalization have not been identified during initial well testing and are hence not reported in the relinquishment reports upon which this study is based. The actual number of compartmentalised reservoirs cannot be assessed in the present study. In total, there are 28 boreholes in this study that were abandoned due to the compartmentalization of target reservoirs. 13 of the boreholes were targeted on Jurassic reservoirs and in particular 6 of them are within the Fulmar Formation. The failures in the Fulmar Formation are mostly due to fractures or sub-seismic faults that are related to fault movement or Permian salt haloakinesis. Since there is are large number of wells targeted on the Fulmar Formation, this does not mean that the Fulmar Formation carries a higher risk of reservoir compartmentalization than other units. Another 9 wells were drilled into the Carboniferous reservoirs in the Southern North Sea. The Carboniferous reservoirs, however, do seem to have a high risk of being compartmentalized as there are not many Carboniferous wells but the number of failed boreholes is high (Table A 2. 7). Permeability heterogeneity due to facies variation because of the fluvial-deltaic depositional environment is reported to be the main cause of reservoir compartmentalization.

Although this study has not identified any compartmentalized reservoir in turbidite sandstones, the risk of compartmentalization must not be overlooked. Some Paleogene oilfields in UK water have a complex architecture, formed by turbidite channels, sheet turbidite sandstones and sealing faults (Jolley et al., 2010). Examples include the Schiehallion Field and Pierce Field (Gainski et al., 2010; Scott et al., 2010). In the Southern North Sea, it has been reported that the Triassic Bunter Sandstone aquifer is more suitable for CO_2 storage reservoir than the Permian Rotliegend Sandstone because it has less compartmentalization problems (Holloway et al., 2006). This is demonstrated by good pressure communication between the gas fields of the Bunter Sandstone (Holloway et al., 2006b). However, a lack of pressure barriers within a reservoir does not mean there are no baffles to fluid flow. The Bunter Sandstone was primarily deposited as a fluvial system, which may result in complex compartmentalization caused by overlapping and superimposed channels separated by non-reservoir overbank sediments (Ketter, 1991). There are only a limited number of gas fields within the Bunter Sandstone, which means the reservoirs of these fields may not be representative of the Bunter Sandstone as a whole. When characterising a ‘proven structure’ within the Bunter Sandstone, a careful assessment of reservoir compartmentalization is necessary.

3.6 Limitations and possible applications of the method

This study uses data from hydrocarbon exploration to estimate the risk of exploring for a new CO_2 storage reservoir. An important question is the validity of the analogy between hydrocarbon reservoirs and CO_2 storage reservoirs. The geological criteria for a successful hydrocarbon reservoir are not precisely the same as those for a successful storage reservoir, although both require competent reservoir, seal and (probably) a trap. In the previous sections, it has been suggested that the overall risks associated with the seal for CO_2 storage reservoirs are likely to be higher than for hydrocarbon reservoirs, whereas the risks associated with reservoir quality are considered to be comparable for the two. Regarding trap definition, saline aquifers will invariably lack any direct hydrocarbon indicators in seismic data, which, in some cases, assist in the definition of structures with trapped hydrocarbons. In these cases, the risk associated with trap definition for CO_2 storage in aquifers may exceed that for at least some hydrocarbon fields.

Another significant difference between the two kinds of reservoirs is their spatial scales. To store a volume of CO_2 that is significant for climate change mitigation, a large size of aquifer rather than a pilot site is required, whose areal extent can be several or tens of times larger than a regular hydrocarbon field. Over 70-80% of North Sea oil and gas fields are too small for commercial CO_2 storage, i.e. their storage capacity is less than 50 Mt of CO_2 (Holloway et al., 2006b). The larger areal size of CO_2 storage reservoirs, compared to the average size of hydrocarbon fields, could increase some of the geological risks of locating a suitable reservoir. The risk of reservoir compartmentalisation, for example, may be higher for a large storage site simply because there is more probability of locating a sealing fault in a large area than in a smaller area. The risk of encountering lateral variation of seals or reservoirs is presumably also greater when a larger geographical area is being considered.

There is also the question of the overburden to the storage site, i.e. the stratigraphy between the top of the seal and the surface. In oil and gas exploration, this is of only secondary importance, while in CO_2 storage, it includes the location of any potential

natural leakage pathways (faults, gas chimneys), and is also the 'seal of last resort' in the event of vertical leakage from the reservoir. At least part of the overburden is likely to be contained in the 'storage complex' – again providing a requirement for an understanding of the overburden which exceeds that required by hydrocarbon exploration. Whether any potential CO_2 storage site will, in the future, be rejected on grounds of unsuitable overburden geology remains to be seen, but it should be noted that overburden geology adds to the geological risks of searching for a CO_2 storage site. Other aspects in which hydrocarbon and CO_2 storage reservoirs have differing criteria include the cut-off limit of reservoir permeability, and the tolerance of the reservoir rocks to variations in pressure. For the former, gas can be produced at commercial rates from reservoirs with permeabilities that would be prohibitively low for CO_2 injection; compare 1-50 mD permeability in the commercially viable In Salah gas field (Eiken et al., 2011) with a minimum permeability of 200 mD, and a desired 500 mD, suggested for CO_2 storage by Chadwick et al. (2008). From the above, it might be concluded that the geological criteria for a successful CO_2 storage reservoir are more rigorous than those for a hydrocarbon reservoir, and hence that the probability of success of a borehole, drilled to locate a CO_2 storage site, might be rather less than for a hydrocarbon exploration borehole drilled in a geologically comparable area. This may be partly countered by the generally shallower burial depth of CO_2 storage compared to hydrocarbon exploration in the UKCS, the influence of which upon reservoir quality was discussed in *Section 3.4.2*.

The results of this study are based upon data from the UKCS, and the results are hence most directly applicable to the search for CO_2 storage reservoirs in this geographical area. Caution must be exercised in applying the conclusions to other geographical areas, and judgement must be applied as to how comparable, from a geological perspective, an area is to the UKCS. In a rift basin with comparable age sediments, at comparable burial depths, then confidence may be quite high. However, for a better understanding of the geological risks of exploring for CO_2 storage sites worldwide, it would be useful to undertake comparable studies using legacy exploration data from other hydrocarbon provinces, especially those with a high likelihood of being used for CO_2 storage.

3.7 Conclusions

1. On the assumption that past drilling for hydrocarbons on the UKCS provides a good analogue for drilling for a CO_2 storage site, then for a subsurface location with limited geological information, the probability of a borehole encountering a reservoir suitable for CO_2 storage is only c. 41 – 57 % (P10 to P90), despite the well-known geology of the area. This has implications for regional assessments of CO_2 storage capacity.
2. For reservoirs with stratigraphic traps within the UKCS, the probability of success is slightly lower, at 36 ± 10%.
3. Most geological risks are much reduced after a borehole is drilled. The remaining most significant risk is probably reservoir compartmentalization.
4. CO_2 storage aquifers are expected to be larger than many hydrocarbon fields, and involve factors that are of only secondary importance in the case of hydrocarbon exploration. The geological risk of drilling to locate a CO_2 storage reservoir may hence be generally higher than estimated using data from hydrocarbon exploration.

Summary statement: The CO_2 geological storage is a new industry sector, and the operators generally have little experience of managing exploration risk. This work is the first study that systematically introduces the geological risks to the drilling for CO_2 storage reservoirs. It also demonstrated a new method of using the risk data of hydrocarbon exploration wells in the risk assessment for CO_2 storage reservoirs.

Chapter 4

Diagenesis of the Pentland Formation

ABSTRACT

The Pentland Formation is a Middle Jurassic unit of sandstones, shales and coals that form economic hydrocarbon reservoirs in the Central North Sea area. This chapter uses conventional core-analysis data, point-count, X-ray diffraction and X-ray fluorescence to study the controls on the porosity and quartz cement in the sandstone reservoirs of the Pentland Formation. The Pentland Formation is currently buried at a depth of 3-6 km. Core-analysis data show that the median helium porosity of the sandstones can be predicted with confidence by the formula of $\Phi = 30.9\% - 0.0039\% \times \text{depth}$ (R^2=0.69), and the median permeability by $k = 93179 \times e^{-0.002 \times \text{depth}}$ (R^2=0.64).

The Pentland Sandstone can be divided into three facies: very fine- to fine-grained clean sandstone (Facies 1), very fine- to fine-grained argillaceous sandstone (Facies 2) and medium-grained sandstone (Facies 3). Facies 2 had been compacted to be low-porosity (<10%) sandstones during early burial due to its high content of detrital

illite (>15%). Facies 1 is the most porous and dominant sand facies, and form the major oil-producing reservoirs within the Pentland Formation.

The Facies 1 sandstones contain an average of 10.3% of quartz cement. A plot of quartz cement abundance vs. depth indicates that the quartz cement grows at a rate of 2.3%/km below 2000 m of burial. The petrographic data, however, shows that the most abundant quartz cement occurs in the highest porosity Pentland Sandstone, which somewhat contradicts with the conventional impression that pervasive quartz cement severely damages the reservoir porosity. These best quality Pentland Sandstone is also associated with the least amount of quartz cement. The triadic relationship between quartz cement, reservoir porosity and illite content is interpreted to be that the illite content determines the remaining sandstone porosity after the course of mechanical compaction, which further determines the available maximum space for the growth of quartz cement in the following burial process.

The chemical data measured by X-ray fluorescence suggest that the Pentland Sandstones and Shale are isolated chemical systems during diagenesis. There is no detectable exchange of silica, potassium or other chemical elements between the sandstone and shale.The large amount of quartz cement in the Pentland Sandstone (5-15%) is inferred to be predominantly sourced from the local pressure dissolution of quartz grains, with 1% of quartz cement might be produced by the deep burial dissolution of a small amount of K-feldspar (>2 km). Kaolin does not transform into illite with progressive burial, due to a lack of K-feldspar and potassium source in the Pentland Formation.

4.1 Introduction

The North Sea is one of the largest oil-producing provinces in the world (Watkins, 2002). The Pentland Formation, however, is a relatively minor unit of hydrocarbon reservoir for the North Sea oil province (Wilkinson et al., 2014b). The importance of studying the Pentland Formation is because it demonstrates a unique diagenetic pathway that differs significantly from the other well-studied sandstone reservoirs of the North Sea, such as the Brent Group (Bjørlykke et al., 1992; Giles et al., 1992) or Fulmar Formation reservoirs (Stewart, 1986). The most notable diagenetic features of the Pentland Formation may be the precipitation of kaolin after K-feldspar dissolution and the preservation of kaolin to 6 km burial depth (Wilkinson et al., 2014b, 2006). Since it is a relatively minor reservoir, little effort has been made to describe the diagenesis of the Pentland Formation. The first literature that solely focuses on the Pentland Formation was only published in 2014 by Wilkinson et al. Even so, an integrated study on the diagenesis and the control of the reservoir quality of the Pentland Formation is yet to be fulfilled. This project is set to study and document the diagenetic properties of the Pentland Formation

An important aspect of this project is to understand the issue of mass transfer between sandstones and shales. It has been proposed that the diagenetic process of sediments may cause a substantial mass change in the sediments, with up to 10% addition or removal of the rock volume (Thyne, 2001). This means that a considerable volume of porosity can potentially be created, or blocked, during the burial process of sandstones. Although diagenetic mass transfer is likely to be crucial for forming commercial oil and gas reservoirs in the deep subsurface, the real significance and the driving mechanisms of the process have not been fully resolved (Bjørlykke, 2011). The dispute over this topic has lasted for about 40 years since the 1970s (Schmidt and Mcdonald, 1979). The Pentland Formation was chosen as the study object for two reasons. First, the Pentland Formation was deposited in a fluvial-deltaic environment and is typically characterised by alternations of shales and sandstones, potentially allowing the transfer of solutes between the two. Secondly, some geochemical data of the Pentland Formation have already been collected and published (Wilkinson et al., 2014b). The results suggested that the sandstones of

Pentland Formation may become continuously depleted in aluminium and potassium with increasing depth (see Figure 4.1). But the study of Wilkinson et al. (2014) lacked sufficient data to make a firm conclusion. Therefore, an objective of this project is to further investigate mass transfer between sandstones and shales in the Pentland Formation.

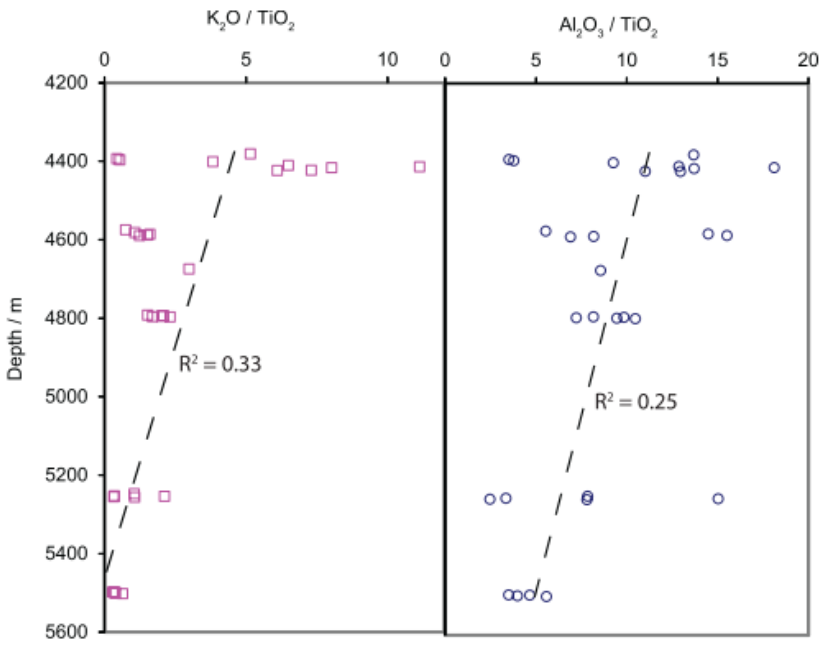

Figure 4.1 The figure in Wilkinson et al. (2014) showing potassium and aluminium (ratioed to Ti as an immobile element) decrease with depth within the Pentland Formation sandstones (n = 29). The chemical data were plotted as 'mobile'/'immobile' element ratios versus depth. This is because the diagenetic movement of one chemical element in sediments will at the same change the fraction percentage of other elements. Rationing one mobile element to an immobile element can avoid the fraction change of the mobile element due to the movement of other elements.

All of the previously studied samples of the Pentland Formation, i.e. those in Wilkinson et al. (2014), were from depths below 4 km. However, the process of mass transfer between sandstones and shales, if ever possible, may have started from 2 km (see review in Milliken, 2003). Hence, in order to make up the full picture of the diagenetic process and the mass transfer in the Pentland Formation, this study has intensively studied the sandstones of the Pentland Formation buried at 2-4 km. The results will reflect the full diagenetic history, the controlling factors upon the reservoir porosity, and the loss or gain of mass during the burial of the Pentland Formation.

The basic aim and method of this study are to investigate the textural, compositional and chemical evolution of the Pentland Formation in diagenesis by comparing the changes in rock samples at different depths. This approach is based on the assumption that all the Pentland Formation samples were the same upon deposition, which however is impossible in the natural environment. To minimize the variation in the original composition of sediments, this study has 1) sampled from an as small as possible geographical area to reduce the transition in sediment provenance; 2) divided the sandstones into different facies based on grain-size, clay content and sedimentary structures, and examined the petrography and diagenesis of each facies individually.

4.2 The sedimentology, stratigraphy and provenance of the Pentland Formation

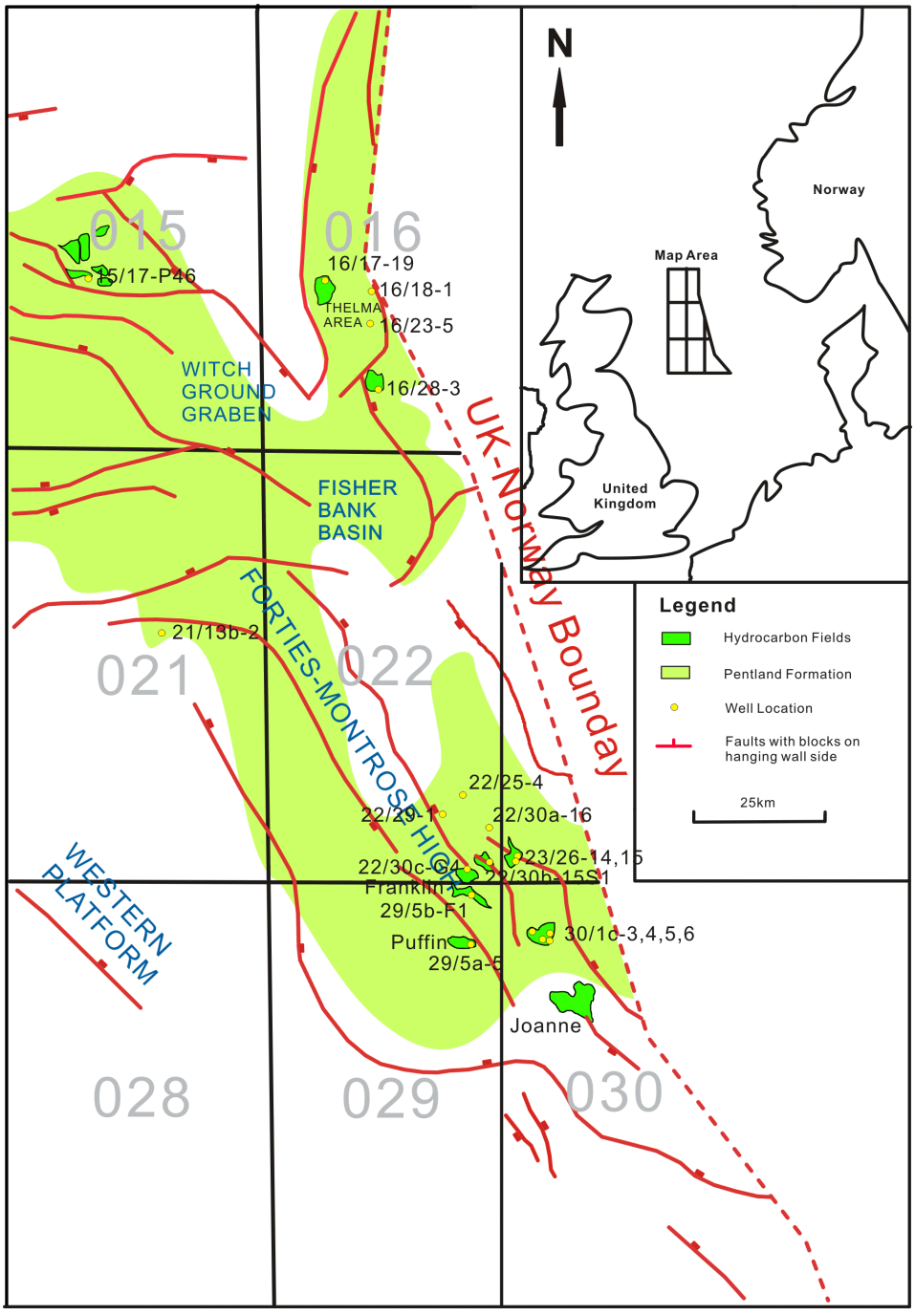

Figure 4.2 Distribution of the Pentland Formation in the North Sea (Richards et al., 1993), and locations of the wells from where the core samples of this study were obtained.

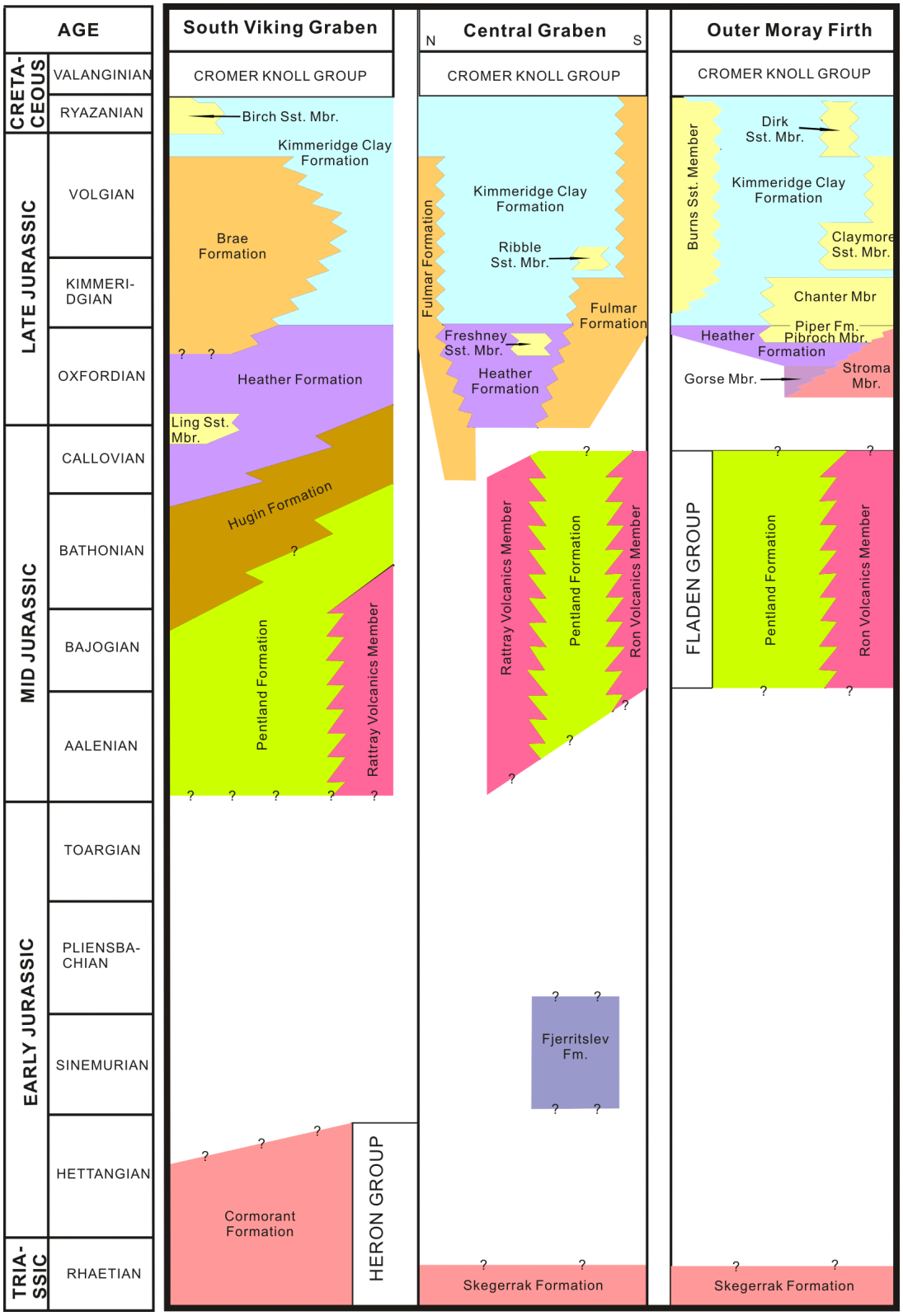

Figure 4.3 The position of the Pentland Formation within the Jurassic stratigraphic frameworks of the South Viking Graben, Central Graben and Outer Moray Firth (redrawn from Richards et al. 1993).

Table 4.1 Synonyms of the Pentland Formation adopted in other studies or in different oil companies (Richards et al., 1993)

Location	Name	Stratigraphic Group	User
Beryl Embayment/ South Viking Graben	Sleipner Formation	Vestland Group	(Vollset and Doré, 1984)
Beryl Embayment/ South Viking Graben	Sleipner Formation	Beryl Group	(Richards, 1989)
Beryl Embayment/ South Viking Graben	Middle Beryl Sandstone and Linnhe Formation		Mobil
Beryl Embayment/ South Viking Graben	'C' Sands		BP and Hamilton
Beryl Embayment/ South Viking Graben	'Coaly Unit'		Conoco
Central North Sea	Bryne Formation	Vestland Group	(Vollset and Doré, 1984)
Outer Moray Firth	Parry Sandstones		Ultramar

The term 'Pentland Formation' was initially introduced by Deegan and Scull (1977) to represent a heterolithic unit of sandstone, siltstone, shale and coal that lies between the Upper Jurassic marine Humber Group sediments and the Triassic non-marine Skagerrak Formation sediments in the Central North Sea. In some publications or internal reports of oil companies, the Pentland Formation may have a different name (Table 4.1), such as the Coaly Unit or Sleipner Formation. The Pentland Formation is confined to the deep part of the Central Graben, South Viking Graben and Outer Moray Firth (Figure 4.2). The Pentland Formation near the basin margins had been subjected to erosion during the Late Jurassic, which left an extensive Jurassic-Cretaceous unconformity across the Central North Sea (Gatliff et al., 1994).

The sediments of the Pentland Formation are comprised predominantly of sandstones with interbedded shales and coals deposited in a fluvial-deltaic or lagoonal environment on a coastal plain (Clark et al., 1993; Deegan and Scull, 1977). The formation is contemporaneous to the Brent Group reservoirs, which are the main oil-producing stratigraphic unit in the Northern North Sea (Underhill, 1998). The thickest Pentland Formation was encountered by the well 21/3-3, in which about 1500m thick Pentland Formation is present but with a high portion of volcanic rocks (Richards et al., 1993). The depocentre of the Pentland Formation was suggested to be located at the southern East Central Graben, southeast of the Forties-Montrose high, where up to 500m thickness was recorded (Gatliff et al., 1994). Locally, the Pentland Formation contain thick sections of igneous rocks that are in the form of tuffs, lavas and intrusives. These igneous rocks have been reported to be associated with the

three contemporaneous volcanic centres in the Central North Sea: the Glenn, Puffin and Fisher Bank Volcanos (Gatliff et al., 1994).

On the top of the Pentland Formation is the sandstone of the Fulmar Formation, or the shale of the Heather Formation (Figure 4.3). Where shale is present, either within the Pentland Formation or the Heather Formation, it isolates the Pentland reservoir from the overlying Fulmar reservoir. In most of the oilfields that have discovered oil within both the Fulmar and Pentland Formations, the Fulmar is the chief oil-bearing level, whereas the Pentland only contains small additional reserves (Wilkinson et al., 2006). Below the Pentland Formation are usually Permian or Triassic strata that have been deeply eroded (Richards et al., 1993). Lower Jurassic rocks are typically absent in the Central North Sea and a likely reason for this is the uplift in the northern Central Graben as a result of the intense volcanic activity at the time (Smith and Ritchie, 1993).

Precise age dating of the Pentland Formation is difficult due to the scarcity of biostratigraphic indicators in the non-marine sediments (Lasocki et al., 1999). Although the Pentland Formation was generally considered to be deposited during the Middle Jurassic, it is uncertain that if sedimentation extended into the Oxfordian (Jeremiah and Nicholson, 1999). Jeremiah & Nicholson (1999) suggested that the Pentland fluvial-deltaic system represents the transporting agent for the marine sandstones of the Fulmar Formation during the Oxfordian. If this is true, then the Pentland and Fulmar Formations should have the same provenance. The contact between the two formations at basin margins is difficult to determine due to substantial erosion at the Cretaceous-Jurassic boundary. However, supporting evidence for the suggestion was demonstrated recently by Wilkinson et al. (2014), in which they showed that both the Fulmar and Pentland sediments exhibit similar heavy mineral indices to the Triassic Skagerrak Formation sandstone. The Skagerrak Formation is a Triassic, fluvial or alluvial sandstone unit with subordinate mudstones (Cameron, 1993). The Skagerrak Formation is widespread across the Central Graben, and stratigraphically lies directly below the Jurassic sediments with a deeply eroded surface between the two. The Pentland Formation and the initial sedimentation of the Fulmar Formation were restricted to Mid-Jurassic topographic lows surrounded by a landmass comprising predominantly of the Skagerrak Sandstones (Jeremiah and Nicholson, 1999). Thus from the palaeogeography point of view, it is also reasonable

to speculate that the Skagerrak Formation has provided sediments to the two Jurassic formations.

4.3 Methodology

4.3.1 Data collection

The data supporting this study come from 21 hydrocarbon wells and overall there are four data sources:

(1) The majority of the petrographic data of the deeply buried Pentland Formation (> 4 km) originally came from some reports provided by a group of oil companies. A summary of the data has been published in Wilkinson et al. (2014). These data include the analytical results of point-counting, X-ray diffraction, X-ray fluorescence and SEM images. Systematic quality control has been applied to ensure the reliability of these data and the details for this have been described in Wilkinson & Haszeldine (2011) and Wilkinson et al. (2014).

(2) Well logs, as well as some conventional core analysis reports (with porosity and permeability data) for the study wells, were downloaded from the database 'Common Data Access' (CDA), where digital well and seismic information and reports from the UK oil and gas industry are available.
(CDA: https://www.ukoilandgasdata.com/dp/controller/PLEASE_LOGIN_PAGE)

According to the description of experiments in the core analysis reports, the permeability data were collected by measuring the flow rate of nitrogen gas through clean, dried core plug samples under a pressure of 400 psi in a micro-permeameter (Darcy's law). For obtaining the porosity data, a known volume of helium gas at a known pressure was expanded into a chamber containing core plug samples in a Boyle's Law porosimeter, whereby the grain volume in the samples can be measured. Then, the bulk volume of the sample was calculated by mercury displacement using a hand-operated mercury displacement pump at atmospheric pressure. The porosity is determined by dividing the grain volume to the bulk volume of the sample.

The core analysis was conducted by professional third-party core laboratories using established routine analysis method and the data are considered credible.

(3) Photos of the study borehole cores and their burial depth information can be found on the British Geological Survey Core Store website.
(URL: http://www.bgs.ac.uk/data/offshoreWells/wells.cfc?method=searchWells)

(4) 23 sandstone and 36 shale samples of the Pentland Formation were collected from the British Geological Survey Core Store at Keyworth, Nottingham for petrographic, X-ray diffraction and X-ray fluorescence analysis. The UK North Sea Blocks 15 and 16 are where most of the samples are primarily from, with a few from the Block 21 and 22 (Figure 4.2). Cores of the Pentland Formation are scarce as it is not a regular target of hydrocarbon exploration. The sampling wells were selected on the basis that they are located within an as small as possible geographical area, so that the variation of the samples regarding their provenances and sedimentary environments are controlled to the minimum.

In addition, there were 39 core samples of the Pentland Sandstone from the Kessog Field being particularly collected during the second time of sampling at the Core Store, for the purpose of studying the phenomenon of hydrocarbon emplacement preserving porosity in the Kessog Field (see Chapter 5). These sandstone samples were studied using the point-count method.

4.3.2 Study techniques

- **Thin-section and petrographic study**

After collection, the sandstone samples were cleaned in an ultrasonic bath for 30mins to remove any contaminations from drilling fluids. Then blue resin was added in to consolidate the rocks as some of the samples from depth have not been completely lithified. Consolidating the rock can avoid grain plucking and artificial new pores when sawing the sample. Moreover, the presence of resin blue helps to identify genuine pore area under the microscope.

Point-counts of thin-section were made with 300 counts per sample; the method of calculating the errors of the results was from Van der Plas & Tobi (1965). The point-

count result is reported as percentages of bulk volume. Grain size of the core samples (sandstone) was determined on microphotographs, by measuring and calculating the mean diameter of 100 quartz grains per sample. Since this mean grain size is measured on a 2D cross-section of quartz grains, it needs to be converted to the actual 3D mean grain size. The conversion is by multiplying the mean 2D grain size with a factor of 1.273 (Kong et al., 2005).

The grain size data was used to calculate the sorting factor. The units of grain size measures were converted from metric to the phi-scale, then the 5^{th}, 16^{th}, 84^{th} and 95^{th} percentiles of the phi-based grain size distribution were used to determine the sorting coefficient using equation (4.1).

Sorting coefficient = $(\Phi_{84} - \Phi_{16})/4 + (\Phi_{95} - \Phi_{5})/6.6$ (McManus, 1988) (4.1)

The point-count data of any Pentland Sandstone samples with over 20% (point-counted percentage) of carbonate cement were not included in the database for analysis, since the silicate diagenesis of highly carbonate-cemented sandstones is ceased or significantly retarded (Gluyas and Coleman, 1992). These samples will not follow the same diagenetic pathway as the normal Pentland sandstones, which contain <5% carbonate cement (Wilkinson et al., 2014b).

When assessing the variation of mineral proportions with depth, one drawback of point-count data is that the loss of porosity from compaction will significantly affect the percentage compositions of minerals. To eliminate this effect, the fractionation of minerals were normalized to 100% when comparing the relative abundance of each mineral at different depths. Hence, there are two formats of point-count data in this study: one is the percentage of minerals plus porosity equals 100% (Marked as ‘mineral%+ porosity%= 100%’); and the other is the percentage of minerals equals 100% (mineral%=100%).

The method of calculating the sandstone parameters of COPL (porosity loss due to compaction) and CEPL (porosity loss due to cementation) follows Equation 4.1 - Equation 4.4, which were suggested by Ehrenberg (1989). An original sandstone porosity of 40% upon deposition was assumed (Houseknecht, 1987).

Equation 4.1: Original Porosity (OP) = 40%

Equation 4.2: Intergranular Volume (IGV) = Porosity + Kaolin Cement + Carbonate Cement + Quartz Cement

Equation 4.3: COPL = OP – [(100 × IGV) - (OP × IGV)]/(100 - IGV)

Equation 4.4: CEPL = (OP - COPL) × CEM/IGV

- **X-ray diffraction (XRD)**

XRD analysis was conducted in the X-ray lab of the School of Geosciences, University of Edinburgh. Both the samples of the Pentland Sandstone and Shale were analysed.

The shale samples were first ground into powders in a high-speed spinning mill, and then further wet-ground in a McCrone micronising mill and spray-dried to make powders in the status of fully random crystal orientation (for detailed procedure, see Hillier, 1999). This spray drying process is for reducing the problem of preferred crystal orientation in XRD analysis (Hillier, 1999). In the next step, the spray-dried shale powders were analysed in a Panalytical X-ray diffractometer to generate X-ray diffraction spectra, which were then analysed using the software – Topaz 3.0 (Rietveld Method) to calculate mineralogical composition.

The procedure of XRD analysis for the sandstone samples are the same as that for shales, except that the sandstones did not go through the spray-drying process. This is because, after thin-section making, there is no sufficient sandstone sample left for the spray-drying process.

Eleven shale samples were additionally selected for XRD clay separates analysis, i.e. the analysis for the mineralogy of <2 μm particles in the samples. Details for the whole process of clay separation and analysis can be found in Hardy & Tucker (1988). In general, it follows the practice of:

1) Dispersion: powders of the shales were dissolved in beakers filled with distilled water, and then mixed and settled in an ultrasonic bath for 30mins. Afterwards, the materials remained suspended in the water are mostly clays (slurry). Sand- and silt-sized particles have accumulated in the bottom of the beakers.

2) Timed settling: the slurry was transferred to measuring cylinders, and left for settling for 4 hours. Then, the top 5 cm of the topmost solvent column, where clay-size particles concentrate, were extracted using burette.

3) Clay separation: The extracted clay slurry was then placed in a centrifuge to separate clays out of the solvent.

4) Analysis: The separated clays were plastered onto glass discs, and then treated with the procedure of air-drying, ethylene glycolation (6 hours), heating at 400^{o}C for 30min and heating at 550^{o}C for 30min. After each treatment, the glass discs with clay separates need to be scanned in the X-ray diffractometer. For each sample, a total of 4 scan patterns, corresponding to the 4 steps of treatment, were recorded for each sample.

Final quantification of the relative percentage of each clay mineral was based on the intensity of its representative peak on the diffraction pattern (Hardy and Tucker, 1988), by Equation 4.5. The peak selected for Kaolinite is the 001 peak, illite the 001 peak and chlorite the 001 peak (see Hillier, 2002). The peak intensity was measured using the software Topaz 3.0.

Equation 4.5 $I_{KAOLINITE}/2.5 + I_{ILLITE} + I_{SMECTITE} + I_{CHLORITE}/2.0 = 100\%$ (Weir et al., 1975)

I = intensity of the representative peak of a clay mineral on XRD spectrum

---

Two experiments were conducted to test the accuracy and precision of the XRD analysis of sandstones and shales:

In the first experiment, five samples were synthesised with three common components in clastic sediments: quartz, K-feldspar and illite (hectorite). High purity (> 99%) quartz was bought commercially (Table 4.2); the K-feldspar grains were hand-picked from the Norwegian granites; the hectorite is bought from a commercial mineral company (Table 4.2). The five synthesised samples contain different proportions of these components. The accuracy of the XRD method can be inferred by comparing the analysed compositions of the samples to the known compositions.

Table 4.2 The raw material ingredients for the synthesis of sandstone and shale samples

Minerals	Sources	Possible contaminants
Quartz	99.9% purity quartz	N/A
K-feldspar	Norwegian granite	Quartz, albite
Hectorite (illite)	Ward's Natural Science Establishment, Inc., California	Calcite

The principle of the second experiment is similar to that of the first experiment, which is by comparing the analysed compositions to the standard composition of the sample. The only difference is that the second experiment used a shale sample of more complex compositions. The shale is provided by Steve Hillier in the James Hutton Institute, Aberdeen. To assess both the accuracy and precision of the XRD method, the experiment measured the compositions of five samples that were prepared from the same piece of a shale sample (Table 4.4).

The results of the two experiments (Table 4.3 & Table 4.4) suggest the following indications:

1) For minor and trace mineral components, e.g. <3%, the errors in the results measured by XRD can be large, and the accuracy is low.

2) The accuracies of the measurements for different minerals vary greatly. For example, in Table 4.3, the percentages of K-feldspar and muscovite are similar, but the average relative error for the measured K-feldspar is 44.0%, whereas that of the muscovite is - 4.2%.

3) X-ray diffraction analysis is overall a semi-quantitative method. This might be because, in addition to the abundance of each mineral constituent, there are other factors affecting the intensity of diffracted X-rays, such as mineral crystallinity, slight variation in the chemistry of minerals, and preferred crystal orientation (Moore and Reynolds, 1997).

4) The precision of XRD can be referred from the repeated five analyses on the same sample (Table 4.4). For minerals of low abundance (< 10%), the precision is <0.5% (absolute percentage), and for minerals > 10% in mass percent, the precision is < 1-2% (absolute percentage).

One aim of this project is to study the mineralogical variation of sandstones and shales with depth in diagenesis. Due to the semi-quantitative nature of XRD analysis, conclusions that are solely based upon XRD may not be robust. However, in addition to XRD data, there are also point-count data in this study that reveals the mineralogy of each sample. If a conclusion from the XRD data is also supported by point-count data, then the conclusion can be considered as reliable. Chemical data, obtained by X-ray fluorescence, may also be used as a check for the conclusions from XRD and point-count data.

Table 4.3 The compositions of five synthetic samples (Wt% known) and the compositions measured by XRD (Wt% found).

		Quartz	K-feldspar	Hectorite	Total
Synthetic sample 1	Wt% known	50.03	19.92	30.50	100.45
	Wt% found	57.80	17.12	24.40	99.32
	Abs. error	7.77	-2.80	-6.10	
	Rel. error	15.53%	-14.06%	-20.00%	
Synthetic sample 2	Wt% known	70.01	14.89	15.09	99.99
	Wt% found	76.10	12.29	11.16	99.55
	Abs. error	6.09	-2.60	-3.93	
	Rel. error	8.70%	-17.46%	-26.04%	
Synthetic sample 3	Wt% known	89.66	5.05	5.29	100.00
	Wt% found	90.00	4.53	3.62	98.15
	Abs. error	0.34	-0.52	-1.67	
	Rel. error	0.38%	-10.30%	-31.57%	
Synthetic sample 4	Wt% known	70.00	0.00	30.00	100.00
	Wt% found	70.30	2.96	26.42	99.68
	Abs. error	0.30	2.96	-3.58	
	Rel. error	0.43%		-11.93%	
Synthetic sample 5	Wt% known	50.04	0.00	49.96	100.00
	Wt% found	56.60	3.80	39.13	99.53
	Abs. error	6.56	3.80	-10.83	
	Rel. error	13.11%		-21.68%	

Table 4.4 Test for the accuracy and precision of X-ray diffraction on shale analysis: five analyses on five samples made from the same piece of a shale with known compositions. The known compositions are highlighted in **bold font**. Sample number of the shale 1189795.

	Quartz	Plagioclase	K-feldspar	Siderite	Anatase	Pyrite	Chlorite	I+I/S-ML	Muscovite	Kaolinite
Percentage (%)	**21.0**	**0.3**	**3.4**	**6.0**	**0.4**	**0.0**	**1.7**	**22.8**	**3.8**	**40.6**
1st analysis (%)	22.4	2.3	4.7	2.9	3.4	0.2	3.8	22.2	3.3	34.8
*abs. error (%)	1.4	2.0	1.3	-3.1	3.0	0.2	2.1	-0.6	-0.5	-5.8
**rel. error	6.5%	666.7%	37.9%	-51.2%	755.0%		125.9%	-2.8%	-14.2%	-14.3%
2nd analysis (%)	21.7	2.2	4.5	3.0	3.4	0.1	3.4	21.7	3.9	36.1
*abs. error (%)	0.7	1.9	1.1	-3.0	3.0	0.1	1.7	-1.1	0.1	-4.5
**rel. error	3.2%	646.7%	31.5%	-50.2%	737.5%		100.0%	-4.8%	2.1%	-11.1%
3rd analysis (%)	23.8	1.5	4.8	3.3	3.5	0.3	3.6	19.9	3.9	35.6
*abs. error (%)	2.8	1.2	1.4	-2.7	3.1	0.3	1.9	-2.9	0.1	-5.0
**rel. error	13.1%	390.0%	40.9%	-45.2%	782.5%		111.2%	-12.9%	2.9%	-12.3%
4th analysis (%)	23.1	1.9	5.3	3.0	3.5	0.2	3.6	20.4	3.7	35.4
*abs. error (%)	2.1	1.6	1.9	-3.0	3.1	0.2	1.9	-2.4	-0.1	-5.2
**rel. error	9.8%	516.7%	55.0%	-49.5%	762.5%		110.0%	-10.4%	-1.8%	-12.8%
5th analysis (%)	22.8	2.3	5.3	2.9	3.3	0.3	3.2	20.5	3.8	35.7
*abs. error (%)	1.8	2.0	1.9	-3.1	2.9	0.3	1.5	-2.3	0	-4.9
**rel. error	8.6%	663.3%	54.7%	-51.0%	722.5%		88.8%	-10.2%	0	-12.1%
Average rel.error	8.2%	576.7%	44.0%	49.4%	752.0%		107.2%	8.2%	-4.2%	-12.5%

* abs. error (%) = absolute error, ** rel. error = relative error, *** I+I/S-ML = illite + illite/smectite – mixed layers

- **X-ray diffraction versus point-count**

Both XRD and point-count can quantify the mineralogy of a rock, the two techniques, however, do not provide the same information. XRD measures the mass percentage of each mineral phase within the sample powder crushed from a solid rock, whereas point-count measures the volume percentage of each mineral in the natural solid form of a rock. This can make a big difference to a clay-rich sandstone because of the high volume of micro-porosity within clay minerals. For example, the measurements of Hurst and Nadeau (1995) showed that there is 43% of micro-porosity on average in kaolinite, 50% in chlorite and approximately 90% in illite. As a result, XRD quantified percentages of clay minerals are supposed to be much lower than point-count quantified clay percentages. Because the distribution and geometries of clay minerals in a sandstone have a great impact on the reservoir quality, in particular on permeability, point-count data which is more sensitive to the clay distribution and geometry may be more useful in delineating the property of a reservoir rock.

- **X-ray fluorescence (XRF)**

Both major and trace chemical elements of the study samples have been analysed at the X-ray lab of the School of Geosciences, with the Panalytical PW2404 wavelength-dispersive sequential X-ray spectrometer. A 3kW rhodium-anode was used as the X-ray source.

For major element analysis, the sample powders left from XRD analysis were made into 40mm-diameter fused glass discs. To make the discs, about 0.9-1.0 g sample powder was mixed with 5 times the amount of borate (flux: sample = 5:1) and fused in a Pt-5%Au crucible at 1100°C for 20mins.

For trace elements analysis, the powders were pressed into 40mm-diameter pellets, which requires about 8g of sample powder to be compressed under 8 tons of pressure for 2 mins. The accuracy of the technique was ensured by running internal standards. The precision check was provided by running analysis on the same sample for 5 times and comparing the results (Table 4.5).

Some samples did not have enough powder (8g) for trace element analysis, which initially caused a worry that the insufficiency of powder would affect the reliability of the analysis. However, by analysing the pellets made with 4g, 5g, 6g, 7g, 8g of powder of the same sample (Table 4.6), it shows that the variation of powder amount within this range does not influence the reliability of the technique.

Table 4.5 Repeating five times of XRF major element analysis on the sandstone sample 23/26b-15, 16048 ft. The numbers are expressed in percent (%). For SiO_2, the precision is between 0.1-0.09%; for the other major elements, the precision is generally within 0.03 %.

SiO_2	Al_2O_3	Fe_2O_3	MgO	CaO	Na_2O	K_2O	TiO_2	MnO	P_2O_5	LOI	Total
75.39	10.34	1.70	1.25	1.41	2.33	2.027	0.594	0.023	0.153	4.49	99.70
75.38	10.35	1.70	1.24	1.41	2.35	2.028	0.596	0.025	0.153	4.49	99.71
75.39	10.32	1.70	1.25	1.41	2.34	2.029	0.597	0.024	0.153	4.49	99.69
75.45	10.34	1.70	1.25	1.41	2.37	2.027	0.594	0.024	0.154	4.49	99.80
75.36	10.34	1.70	1.25	1.41	2.35	2.025	0.595	0.024	0.154	4.49	99.70

Table 4.6 Trace element study of the Shale Sample 16/17-19,14036ft. Unit of the results is ppm. The two 8g sample analyses were made on the same sample but two powder pellets. The results show that the sample weight variation within the range of 4-8g does not affect the accuracy of the technique.

Wt.	*Zn*	*Cu*	*Ni*	*Cr*	*V*	*Ba*	*Sc*	*La*	*Ce*	*Nd*
8g (1)	8.5	2.2	n.d.	5.9	13.4	299	2.1	1.3	9.3	2.7
8g (2)	8.8	1.4	0.2	12.1	12.1	289.6	2.3	1.7	7.2	3.2
7g	8.7	1.2	n.d.	4.6	12	298.3	3	0.9	8	3.7
6g	8	1.6	n.d.	4	15.1	285.8	1.6	0.4	9.2	4.4
5g	8.5	1.1	n.d.	4.1	11.1	294.6	1.9	0.8	7.5	2.3
4g	10.3	1.8	n.d.	5.2	12.9	290.8	2.5	2.5	8.5	2.7

Wt.	*U*	*Th*	*Pb*	*Nb*	*Zr*	*Y*	*Sr*
8g (1)	0.3	1.6	2.8	3.8	55.5	4.5	55.7
8g (2)	0.2	1.8	2.8	3.9	54.7	4.4	45
7g	0.2	1.7	2.8	3.8	56.6	4.5	48.8
6g	0.3	1.8	2.8	3.8	55.8	4.2	51.3
5g	0.5	1.9	2.6	3.8	56.9	4.7	52.7
4g	0.2	1.6	3	3.8	56.6	4.7	51.4

Using XRF, this study has collected the chemical composition data of 40 Pentland Sandstone samples from 8 wells and 29 Pentland Shale samples from 9 wells (Table A 4.6 - Table A 4.9). Besides, the chemical data of 29 Pentland sandstones in Wilkinson et al. (2014) were also used. The information regarding the grain-size of the sandstones studied by Wilkinson et al. (2014) was obtained from borehole core descriptions in the geological reports and well logs of the sampling wells, and confirmed the observation on the high-resolution core photos in the British Geological Survey offshore borehole database (http://www.bgs.ac.uk/data/bmd.html).

4.4 Results

Figure 4.4 shows the burial history of the Pentland Formation in two studied wells of this project (16/28-3 and 16/18-1), modelled by *PetroMod*. The reservoirs in these two wells are currently buried at 3500 m and 4400m, and the figure shows that the Pentland Formation was shallowly buried at 0-1500m for a considerably long period of time (170-60 Ma), and then subjected to a rapid burial for over 2000 m during Paleogene to the present.

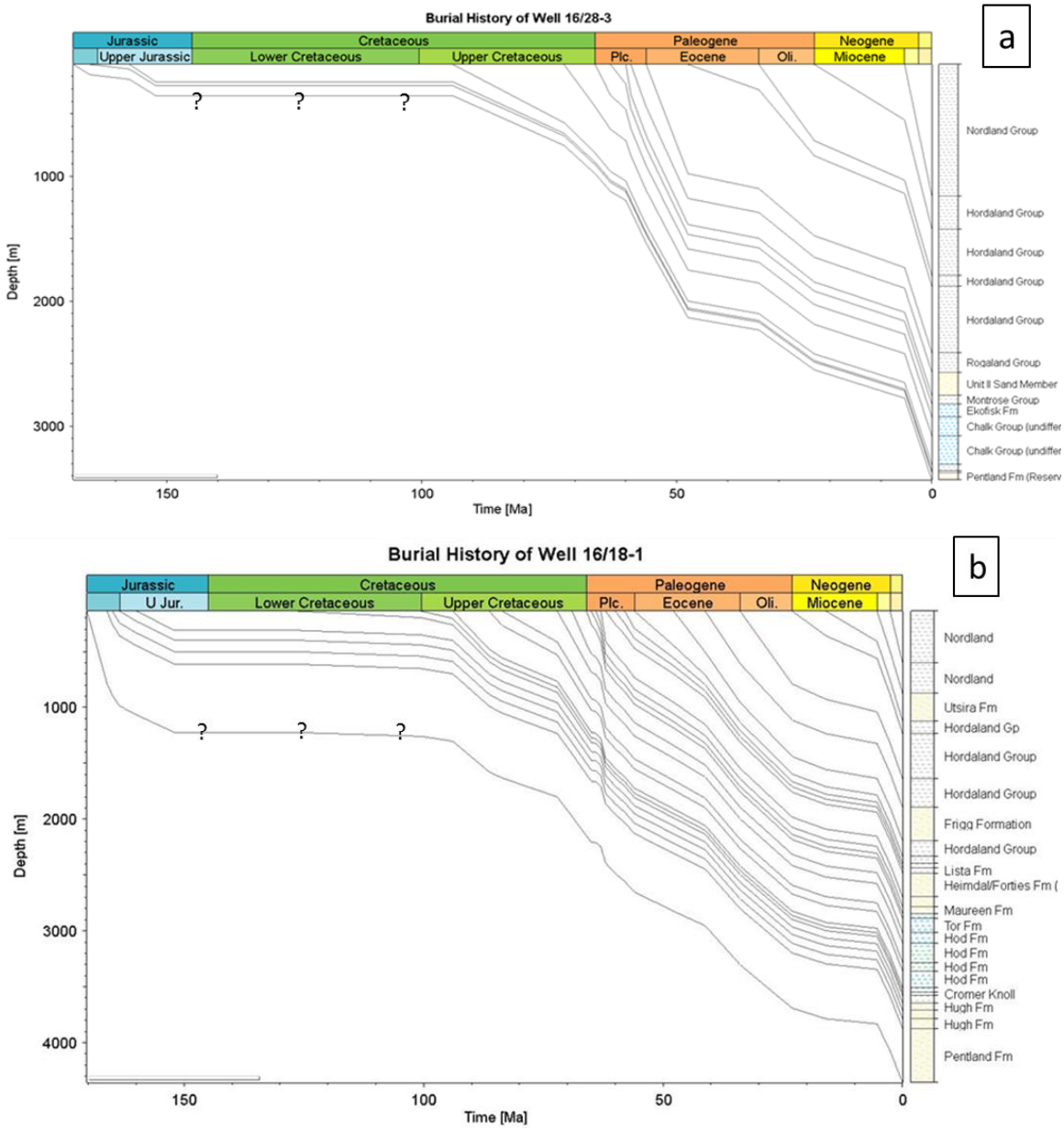

Figure 4.4 Burial curves of wells 16/28-3 and 16/18-1 modelled by PetroMode. The reservoirs of the Pentland Formation had been subjected to rapid burial during Paleogene – Present. Lower Cretaceous sediments are missing in the strata record; it is unclear whether this was due to non-deposition or erosion (marked by "?").

4.4.1 Reservoir porosity

The porosity data of the Pentland Sandstone has only been published recently in Wilkinson et al. (2014), and there has been no published permeability data. This study has enlarged the porosity dataset of Wilkinson et al. (2014) by adding the porosity of another 12 Pentland wells (Figure 4.5). Permeability data are also provided (Figure 4.6).

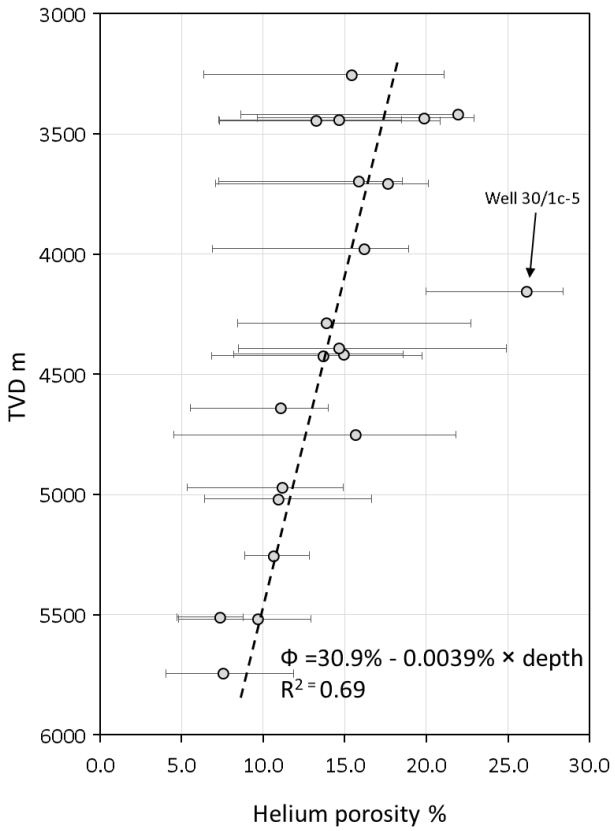

Figure 4.5 Median Porosity (P50) of the Pentland Sandstone in different wells as a function of burial depth (Error bar = P10-P90 range of the porosity). The porosity data come from wells (in order of increasing depth) 9/13-11, 9/13-12, 9/13-15, 9/19-7z, 16/18-1, 16/23-5, 16/28-3, 22/05b-A12, 22/20-1, 22/29-1S1, 22/30A-16, 22/30B-15S1, 22/30C-G4, 23/26b-14, 23/26b-15, 29/5A-5, 29/5B-F1, 30/1C-3, 30/1C-4, 30/1C-5, 30/1C-6. The sandstone porosity of well 30/1c-5 is anomalously high, which was interpreted to be affected by early hydrocarbon emplacement (see Chapter 5). Data of well 30/1c-5 was, therefore, not used to infer to median porosity trend. Porosity data of the shallowest well in this study, 15/17-P46, is not available.

Prediction for the porosity of the Pentland Sandstone is not difficult. The median porosity at each depth can be estimated, with certain confidence (R^2=0.69), using the equation of Φ = 30.9% - 0.0039% x depth (Figure 4.5). The porosity dataset includes the conventional core-analysis data from 21 Pentland wells and 2283 core samples.

The large dataset can ensure the wide applicability of the porosity prediction curve to the exploration targets of the Pentland Formation in future. The median porosity curve suggests the average porosity of the Pentland Sandstone decreases at a rate of 3.9%/km. The porosity decrease process is gradual without a sharp decline at any depth. However, there are cases where anonymously high-porosity sandstones may exist in the Pentland Formation, such as in well 30/1c-5, which potentially form high-valued hydrocarbon reservoirs at deep subsurface. Investigation into the high-porosity of the well 30/1c-5 suggests that these high-porosity sandstones were related to early hydrocarbon emplacement (see Chapter 5).

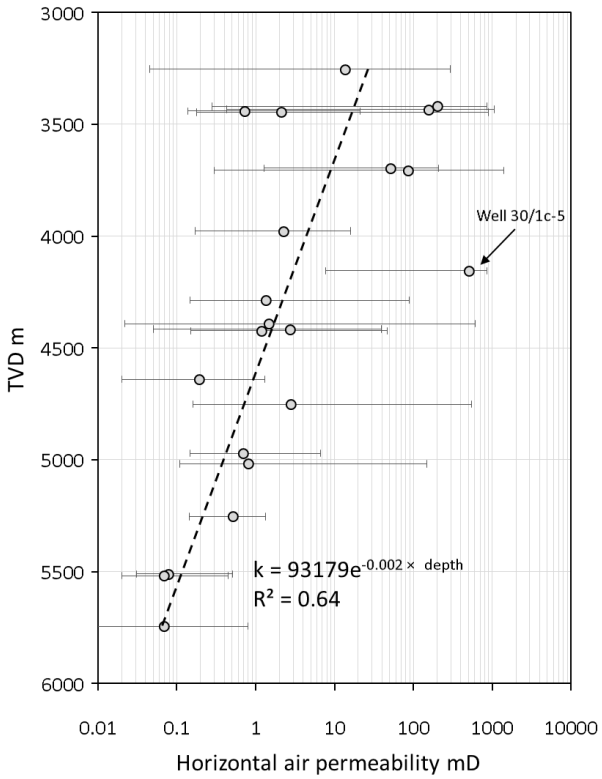

Figure 4.6 Median (P50) horizontal air permeability of the Pentland Sandstone as a function of depth (Error bar = P10-P90 range of the porosity). Data come from the same 21 wells as Figure 4.5. Permeability of well is anomalously high, which is considered to be related to early hydrocarbon emplacement in the reservoir (see Chapter 5). Permeability data of well 30/1c-5 was not used to infer the median permeability trend line.

The median permeability of the Pentland Sandstone can be predicted by the exponential equation of $k = 93179 \times e^{-0.002 \times depth}$ (Figure 4.6). In the same age (Middle Jurassic), fluvial-deltaic sandstones of the Brent Group in the Northern North Sea, a two-magnitude of permeability drop at 3500-4000 km depth was observed, which was interpreted to be caused by the growth of illite (Bjørlykke et al., 1992). Authigenic illite

is characterised by a fibrous structure, and once it appears, it will greatly reduce the permeability of sandstone reservoirs by orders of magnitude. However, Figure 4.6 suggests that the permeability decline of the Pentland Sandstone with depth is a gradual gradual process without of a sharp drop at any depth, which indicates that the large-scale illite growth occurred in the Brent Group sandstones has not occurred in the Pentland Sandstone.

4.4.2 Sandstone facies and detrital minerals

Sandstones of the Pentland Formation are generally light grey-brown in colour, and frequently alternate with black shales and coals. The thicknesses of the sandstones are highly variable, which can change from one metre to hundreds of metres (e.g. in well 9/13-12 and 15/17-P16). Grain-size measurement shows the sandstones are predominantly composed of very fine- to fine-grained sand grains (Figure 4.7). Based upon sedimentary structure, grain-size and detrital clay content, the Pentland Sandstone can be divided into three facies (Figure 4.7): very fine- to fine-grained clean sandstones (Facies 1), very fine- to fine-grained argillaceous sandstones (Facies 2) and medium-coarse grained sandstones (Facies 3).

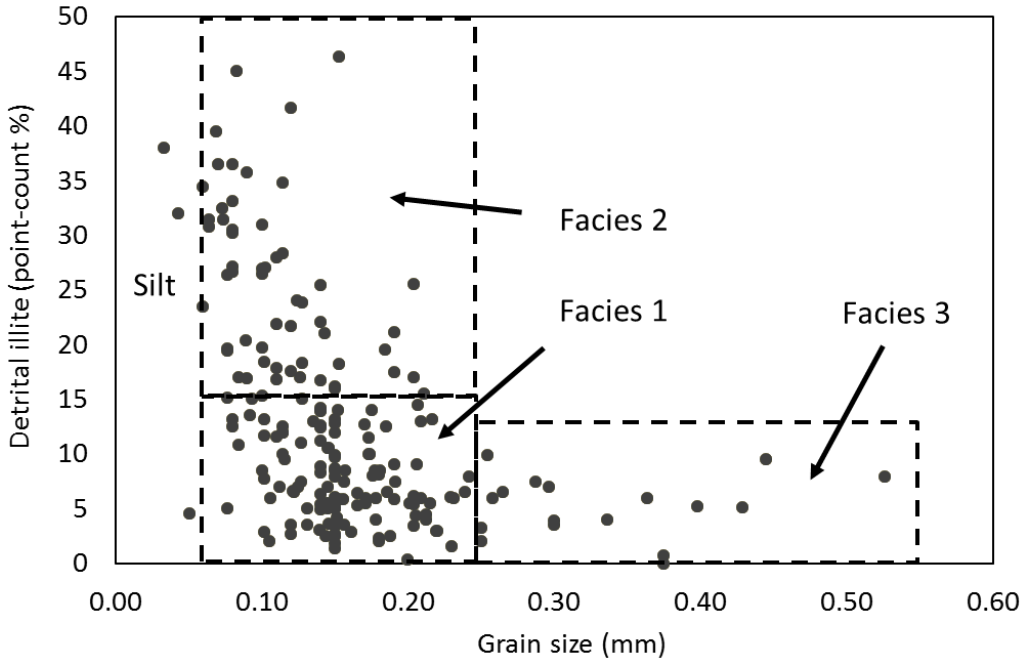

Figure 4.7 Grain-size distribution and detrital illite content within the Pentland Sandstone, and the associated facies division based upon these two parameters. Most of the Pentland sandstones (65%, Table 4.7) are Facies 1 sandstones.

Facies 1 is the most porous sandstones within the Pentland Formation (Table 4.7), and includes 65% of the studied samples. Since the sampling from the sandstone sections of the Pentland Formation did not especially discriminate the clay content and grain-size of sandstones, the obtained fractions of each sandstone facies in Figure 4.7 are, therefore, representative for the overall facies distribution of the Pentland Sandstone. The Facies 1 sandstone, due to its high porosity and large

proportion within the whole sandstone population, is the principal oil-producing reservoir facies within the Pentland Formation (Table 4.7). The importance of the Facies 2 sandstone is downgraded by its low porosity (3.0±0.4%, Table 4.7), and Facies 3 sandstone is by its low proportion (7%) within the formation.

Table 4.7 Average sandstone texture parameters (± standard error of the mean) of the Facies 1, 2 and 3 of the Pentland Sandstone. The porosity data are measured by point-counting. Facies 1 and 3 are high-porosity sandstones, whereas the porosity of Facies 2 is significantly lower than the Facies 1 and 3.

	n	Prop.*	Total porosity (%)	Primary porosity (%)	Secondary porosity (%)	Grain size (mm)	Sorting coefficient†
Facies 1	123	65%	10.8±0.5	5.9±0.4	4.9±0.3	0.16±0.0	0.56±0.01
Facies 2	53	28%	3.0±0.4	1.1±1.3	1.9±0.2	0.12±0.01	0.65±0.02
Facies 3	14	7%	9.1±1.9	4.8±1.3	4.3±0.9	0.35±0.02	0.60±0.04

* Prop.: the proportion of each sandstone facies within the total number of sandstones.
† Sorting coefficient 0.50-0.70 corresponds to moderately well-sorted sands.

Table 4.8 Average point-counted mineralogy of the Facies 1, 2 and 3 Sandstone. (mineral%=100%)

	Qtz (%)	QOG (%)	Kfs (%)	Pl (%)	Kln (%)	Ill (%)	Ms (%)	CC (%)
Facies 1	67.3±0.7	10.0±0.5	1.7±0.2	2.9±0.2	4.6±0.3	7.5±0.3	1.4±0.1	1.4±0.2
Facies 2	58.2±1.2	3.6±0.4	1.8±0.3	3.4±0.5	3.4±0.5	24.3±1.1	2.5±0.5	2.0±1.1
Facies 3	74.0±2.4	8.1±1.1	1.1±0.3	1.2±0.5	4.3±1.1	5.2±0.7	0.9±0.3	1.7±0.9

Note: the fractions of the minerals sum up to 100% with the fraction of point-counted porosity having been excluded.
Abbreviations: Qtz (quartz), QOG (quartz overgrowth), Kfs (K-feldspar), Pl (plagioclase), Kln (Kaolin), Ill (Illite), Ms (muscovite), CC (carbonate cement)

Rock samples of Facies 1 sandstone are characterised by massive structure as illustrated in Figure 4.8 (a). The sand grains are generally moderately well-sorted (Table 4.7). Detrital quartz is the predominant framework grain (67.3±0.7 %), with minor contents of K-feldspar (1.7±0.2%) and plagioclase (2.9±0.2%; Table 4.8). Quartz cement is the main porosity-occluding phase that occupies 10.0±0.5 % solid volume of the sandstones. The principal clay minerals are kaolin and illite (Table 4.8), which is typical for a sandstone deposited in a humid, fluvial-deltaic environment

(Bjørlykke, 2014). The kaolin in the sandstones occurs in the form of dense blocky and vermicular aggregates, which fills in oversized pores left presumably by the dissolution of feldspar grains. The mode of occurrence of illite is more diverse: it can be compacted clasts, grain rims or coats, primary porosity in-fill matrix or replacement of kaolin. The vast majority of illite in the Pentland Sandstone is considered to be detrital, as authigenic illite in the Pentland Formation is rare due to a lack of potassium source (Wilkinson et al., 2014b).

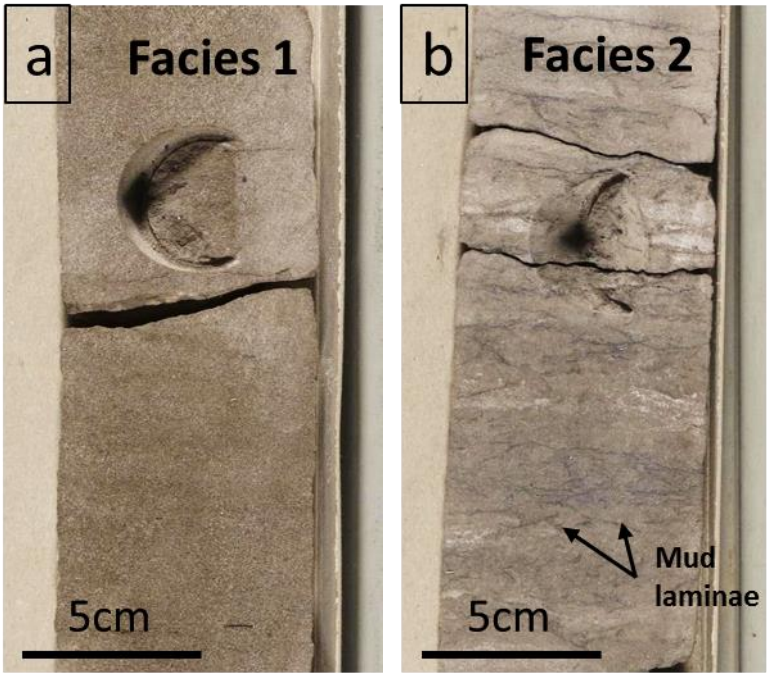

Figure 4.8 (a) Core photo of the Facies 1 very fine- to fine-grained, clean sandstone, which is characterised by massive rock structure. Well 23/26b-14, driller's depth 15860 ft, TVD 4757m (b) Core of the Facies 2 very fine- to fine-grained, argillaceous sandstones. Note the presence of contorted mud laminae. Well 23/26b-14, driller's depth 15678 ft, TVD 4756 m.

The bulk rock of Facies 2 sandstone is characterised by the presence of deformed mud laminae, which might be a result of sediments slumping down over-steepened channel margins in a fluvial-deltaic environment. The high content of clays in Facies 2 may be partly due to the frequent leaching of fresh muddy waters through the sediments in a humid deltaic environment that efficiently brings in clay minerals (Ajdukiewicz and Larese, 2012). The amounts of K-feldspar, plagioclase and kaolin in Facies 2 sandstone are close to the Facies 1 (Table 4.8). However, Facies 2 sandstone contains a significantly higher amount of illite (24.3±1.1%), which has a soft structure and will make the sandstone more prone to be compacted than the Facies 1 and 3 sandstones (Chuhan et al., 2003). The petrographic data shows that

Facies 2 sandstone only have 3.0±0.4% of point-counted porosity on average, which normally does not form valid reservoirs (Table 4.8). Quartz cement only constitutes 3.6±0.4% volume of the sandstone (Table 4.8).

Facies 3 are sandstones of good reservoir quality with 9.1±1.9 % of average point-counted porosity. The occurrence of the Facies 3 sandstones, however, is much less common than Facies 1 and Facies 2, which only constitutes 7% of the total studied samples (14 in 190 samples). But Facies 3 sandstone may be locally abundant as exhibited in well 16/17-19 where 5 among 6 collected samples are Facies 3 sandstones. The amount of porosity and mineral composition of Facies 3 are similar to Facies 1 sandstones (Table 4.8).

4.4.3 Sandstone paragenesis

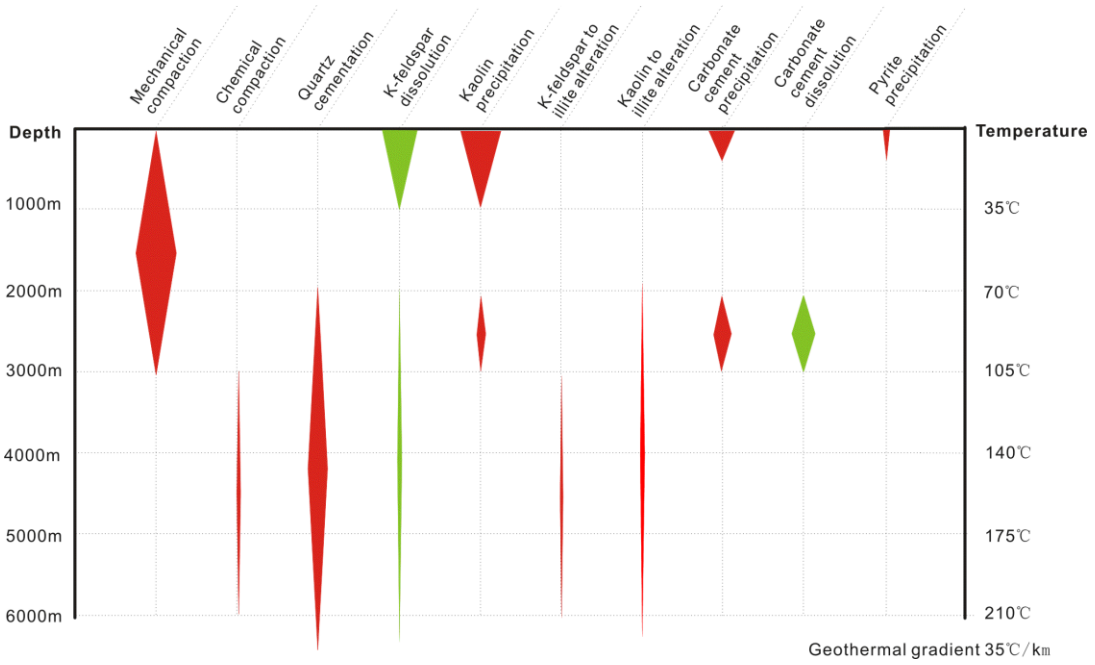

Figure 4.9 The general diagenetic sequence of the Pentland Sandstone inferred from the result and interpretation of this study. Red diamond symbols represent porosity loss processes; green diamonds represent porosity enhancement processes. Depth for the deep carbonate cement is inferred from the stable isotope data in Wilkinson et al. (2014b)

Figure 4.9 is a summary of the diagenetic progress of the Pentland Sandstone during burial. The corresponding evidence is described in the following paragraphs of this section.

Diagenesis of the Pentland Sandstone commenced near the earth surface with the leaching of meteoric water through the sediments. Precipitation of kaolin within the secondary pores left by dissolved feldspars is the most characteristic petrographic feature of the Pentland Sandstone, which suggests that the sandstones have been extensively leached by meteoric waters (Bjørlykke, 1994). The interaction between the sandstones and meteoric water most likely occurred at depth of 0-100m, where the meteoric water just entering the sediments was the most undersatuarted and corrosive for feldspar minerals (Bjørkum et al., 1990; Giles, 1987). On palaeogeography, the Pentland Formation represents the river system that connected the downstream Fulmar Formation and the upstream Triassic Skagerrak Formation (source area). However, it is notable that the contents of K-feldspar in the Fulmar

Formation (avg. 6.5% ± 0.2%, n=627, point-count data) and Skagerrak Formation (21 ± 1%, n=184) are significantly higher than in the sandstones of the Pentland Formation (1.6±0.1%, n=244), indicating 5-20% of K-feldspar has been removed from the latter (Wilkinson et al., 2014b). Framboidal pyrite associated with detrital illite was observed in the Pentland Sandstone from a shallow depth (Figure 4.10), and it is interpreted to be precipitated, also during early diagenesis, from the microbial reduction of detrital ferric iron (Worden and Burley, 2003).

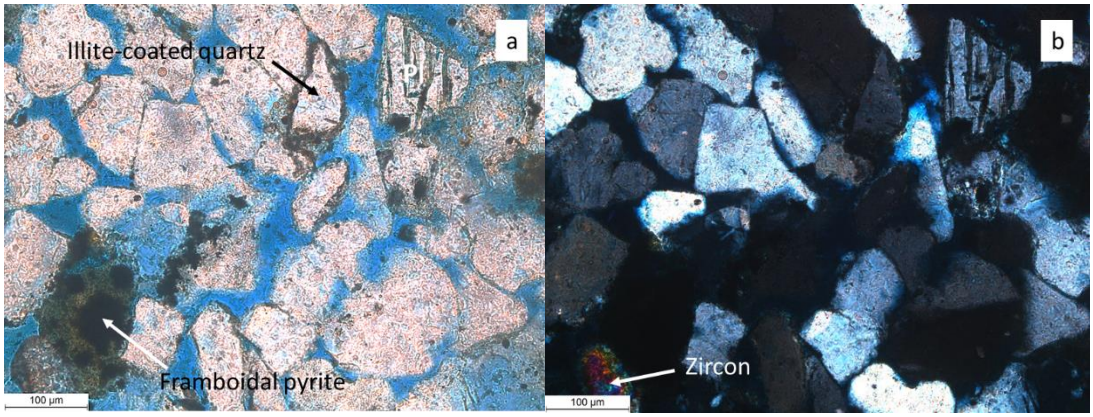

Figure 4.10 Photomicrographs of a Pentland Sandstone from the shallowest studied well (Well 15/17-P46, driller' depth 10419 ft, TVD 2390.9 m). A detrital clay clast associated with diagenetic framboidal pyrite is present; only a few grains are coated by clay coats. Pl= plagioclase

Mechanical compaction is the mechanism governing the loss of sandstone porosity at shallow depth (0-2 km), prior to the initiation of quartz cementation. By reference to the compaction experiments of clean sandstones, the porosities of Facies 1 and Facies 3 sandstone were reduced from 40-45% near the earth surface to 25-30% at 2 km by compaction (Ajdukiewicz and Lander, 2010; Chuhan et al., 2003). In comparison, Facies 2 sandstone, due to its high illite content, was more susceptible to compactional porosity loss and would have lost much of its porosity from compaction during shallow burial. Dissolution of calcite cement was observed in a Pentland sandstone at 2389m (Figure 4.11). This observation suggests two things: a) there was calcite precipitation in the sandstone at a shallow depth above 2.4 km; b) the early calcite was then dissolved at intermediate burial depth around 2.4 km.

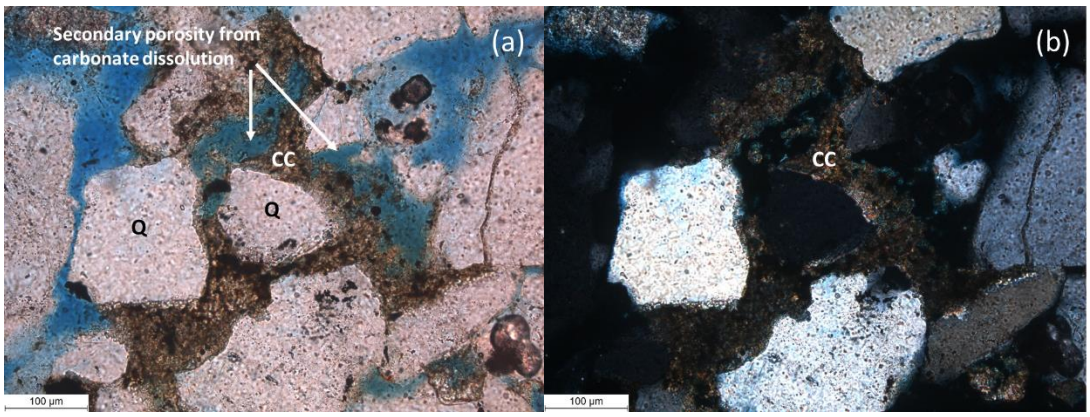

Figure 4.11 Calcite cement dissolution (2389.3 m TVD, well 15/17-P46). (a) and (b) are views under plane polarised light (PPL) and cross polarised light (XPL) of the optical microscope. Dissolution of the calcite cement seems to start from the central area of the cement and then gradually continues towards the edge. Q = quartz; CC = calcite cement.

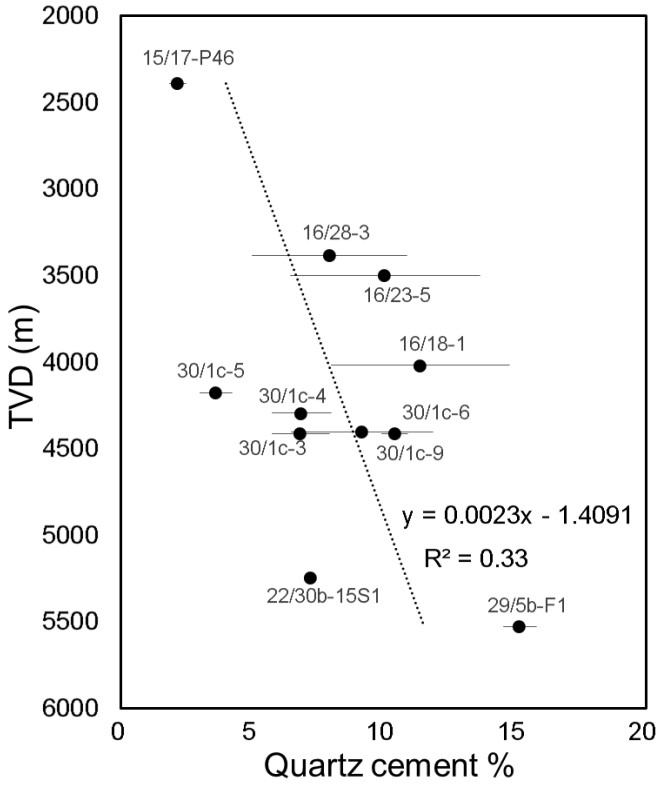

Figure 4.12 Variation of quartz cement versus depth in Facies 1 sandstones (plot from point-count data). Quartz cement in the Pentland Sandstone starts to develop from 2km and increases at an average rate of 2.3%/km with depth. (Mineral%=100%)

Point-count data of the shallowest buried samples (c. 2300 m, well 15/17-P46) suggest that quartz cement has already occupied c. 2 % of the rock volume by the depth (70-80ºC, Figure 4.12). The start of quartz cement in the Pentland Sandstone is projected by the data (Figure 4.12) to be at about 2000 m of burial. As depth

increases, the quartz cement in the Facies 1 sandstone, which is the chief reservoir of the Pentland Formation, forms at a rate of 2.3%/km on average (Figure 4.12). In some deeply buried Pentland Sandstone, the amount of quartz cement can locally account for up to 20% of volume of a sandstone, virtually occluding all the porosity (e.g. in well 22/30a-16, Table A 4.1). The majority of the quartz cement grows as syntaxial rims on detrital quartz grains, and occasionally, the cement can be in the form of long prisms sticking out from quartz grains.

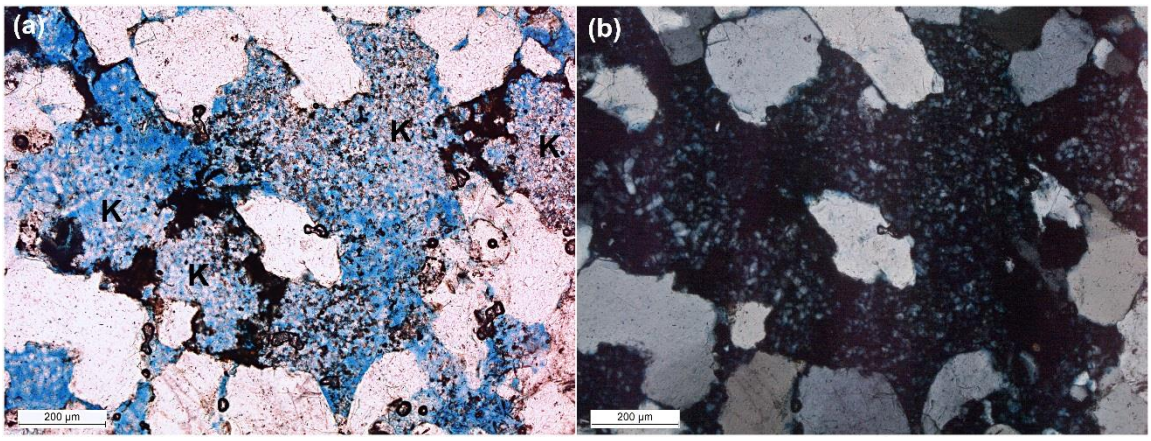

Figure 4.13 Anomalously large secondary pores (blue area in [a]) filled with kaolin (Well 16/28-3, 3384.8m TVD). The intact size of these large secondary pores suggests that they are formed at deep depth.). (a) PPL image, (b) XPL image; K = kaolin

Over-sized secondary pores filled with kaolin may also appear in some deep Pentland Sandstone (e.g. Figure 4.13). These secondary pores do not show any sign of compaction, suggesting that they were newly formed in the sandstones and that K-feldspar dissolution to precipitate kaolin has also occurred in some deep Pentland Sandstone. However, the point-count data do not indicate that a significant portion of K-feldspar or plagioclase has been dissolved in the Pentland Sandstone. Further discussion regarding the amount and timing of feldspar dissolution in the sandstone will be given in *Section 4.5.2 - K-Feldspar dissolution and secondary porosity*. Albeit the feature of kaolin transforming into illite can be occasionally observed under the microscope (e.g. Figure 4.16), it is much more common to see the preservation of kaolin until great burial depth (Figure 4.17). The point data (Figure 4.15) suggests that depth does not affect the amounts of kaolin and illite in the sandstones. Also, the permeability data of the Pentland reservoirs does not show a significant drop in permeability caused by the growth of authigenic fibrous illite at depth (Figure 4.6). The stability of kaolin in the Pentland Formation is attributed to the unusual lack of K-feldspar, which cannot provide the necessary potassium source for the proceeding of

the reaction (Wilkinson et al., 2006). Partly for this reason, the Pentland reservoir still can be productive even at a great burial depth; for example, the Franklin Field produces gas condensate from a Pentland Reservoir at 5.8 km (Lasocki et al., 1999).

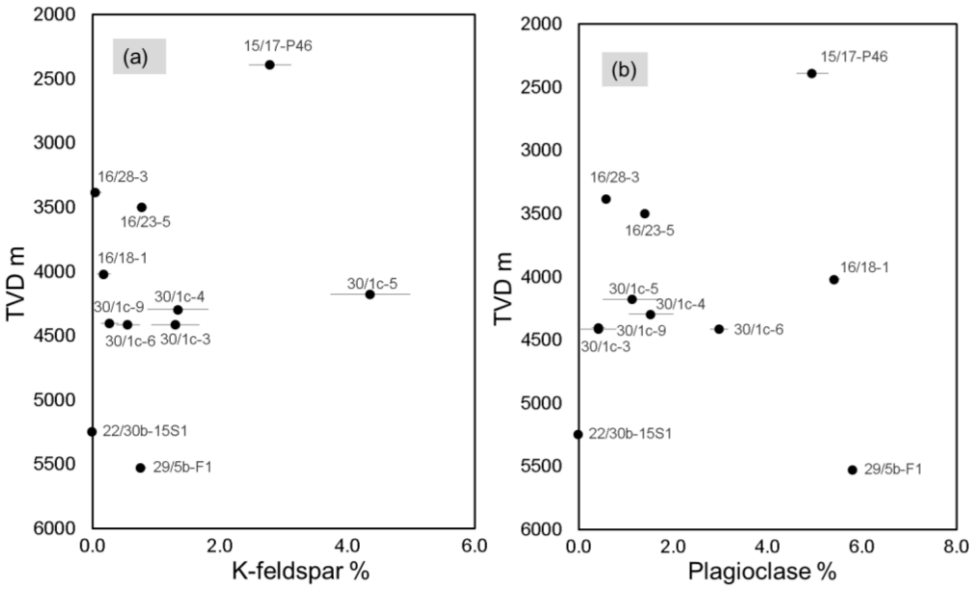

Figure 4.14 The contents of K-feldspar and plagioclase in Facies 1 sandstone as a function of depth (data measured by point-count). The contents of K-feldspar and plagioclase do not show clear correlation with depth. Most of the wells contain <2% of K-feldspar and plagioclase. (Mineral%=100%)

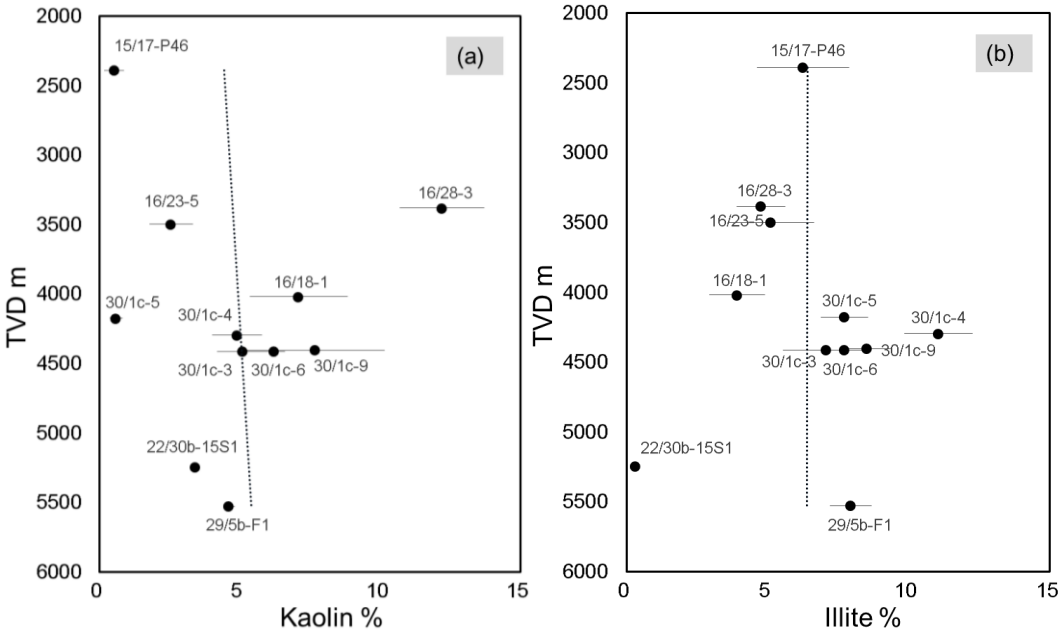

Figure 4.15 Variation of kaolin and illite in Facies 1 sandstone as a function of depth (data measured by point-count). The contents of kaolin and illite are not correlated with depth, suggesting there was no significant transformation of kaolin into illite. (Mineral%=100%)

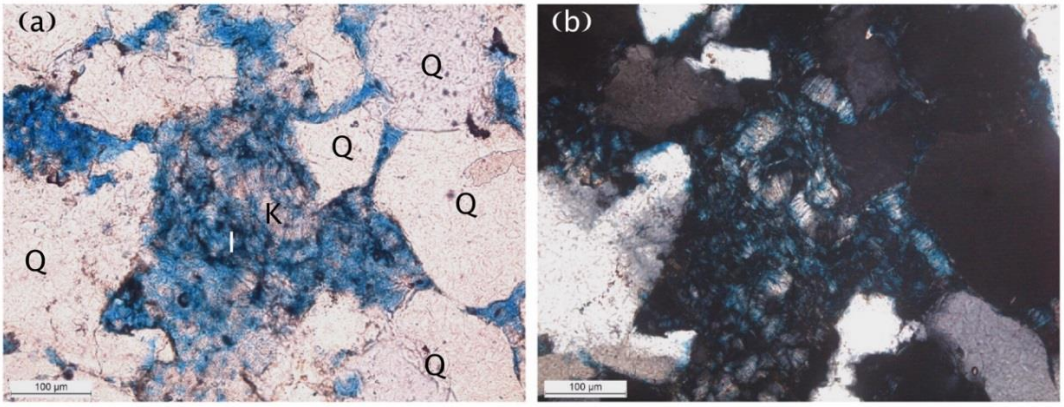

Figure 4.16 Vermiform kaolin and fibrous illite co-exist in the same pore. The kaolin is undergoing transformation into illite (3383.8 m TVD, well 16/28-3). (a) PPL image, (b) XPL image; Q = quartz, K = kaolin, I = illite.

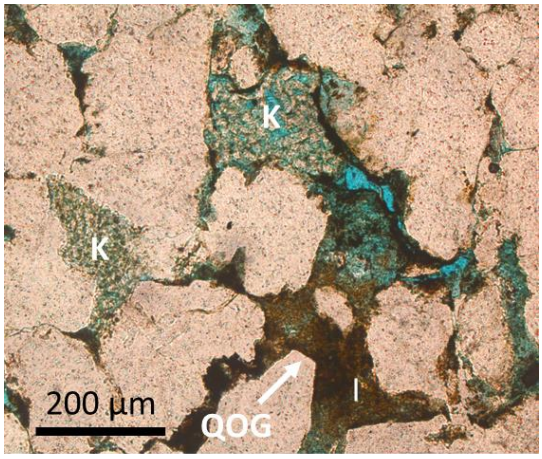

Figure 4.17 Preservation of kaolin in a deeply buried Pentland Sandstone (5247.41 m TVD, well 22/30b-15S1). The kaolin fills in secondary pores, as depicted by the clay coats, presumably left from K-feldspar dissolution. QOG = quartz overgrowth, K = kaolin, I = illite.

4.4.4 Shale composition

Table 4.9 XRD-measured mineralogy of Pentland Shale

Well	n	TVD (m)	Qtz (%)	Kfs (%)	Ab (%)	Kln (%)	Ill (%)	Mnt (%)	Chl (%)	Ms (%)	Py (%)	Cal (%)	Dol (%)	Ant (%)
15/17-P46	3	2381	34.1	4.0	4.2	19.9	21.6	1.5	1.9	5.0	3.7	1.4	0.0	1.7
16/17-19	5	4251	7.8	4.4	1.5	37.5	25.1	3.2	2.4	7.7	2.8	0.5	0.1	4.9
16/18-1	2	4024	18.2	3.1	2.2	27.4	32.6	1.9	2.2	6.5	0.2	0.3	0.1	4.0
16/23-5	5	3500	18.4	2.0	0.8	35.5	20.4	1.3	2.2	5.9	6.9	0.5	0.4	4.1
16/28-3	5	3387	10.2	3.1	1.7	44.0	19.5	3.4	2.7	7.3	0.7	0.6	0.2	4.9
22/25b-4S1	1	4788	25.0	1.8	0.5	30.3	29.6	0.5	2.0	5.9	0.1	0.4	0.0	2.6
22/29-1	1	4580	14.5	4.2	0.9	20.4	45.9	0.8	1.9	7.3	0.2	0.3	0.1	1.8
22/30a-16	3	5493	16.4	2.6	1.3	36.2	25.3	1.6	1.6	7.6	0.6	0.3	0.0	4.5
29/5a-5	1	4396	29.5	9.2	3.1	1.8	43.9	0.6	1.7	7.4	0.3	0.4	0.6	0.6
Average			19.3	3.8	1.8	28.1	29.3	1.6	2.1	6.7	1.7	0.5	0.2	3.2

Abbreviation of mineral: Qtz (quartz), Kfs (K-feldspar), Ab (ablite), Kln (kaolin), Ill (illite), Mnt (montmorillonite), Chl (chlorite), Ms (muscovite), Py (pyrite), Cal (calcite), Dol (dolomite), Ant (ankerite)

Mineralogy of the shales in the Pentland Formation has been analysed using XRD (Table 4.9). The major mineralogical constituents of Pentland Shale is the same as the Pentland Sandstone, but the proportions of the minerals are different. The shales are dominated by illite (avg. 29%, Table 4.9) and kaolin (avg. 28%). Quartz is the third most abundant mineral (19%), followed by muscovite (7%) and K-feldspar (4%). Anatase (3%) was also detected in the shales. Plots of Pentland Shale mineralogy versus burial depth (Figure 4.18) show that the deeper shales contain more Illite and muscovite, and less quartz and albite and the shallow shales. The contents of kaolin and K-feldspar in the shales do not show a linear relationship with depth. The result of the XRD analysis on the eleven clay separates from the Pentland Shale is displayed in Figure 4.19; it shows the relative abundance of kaolin and illite are not dependent on the burial depth.

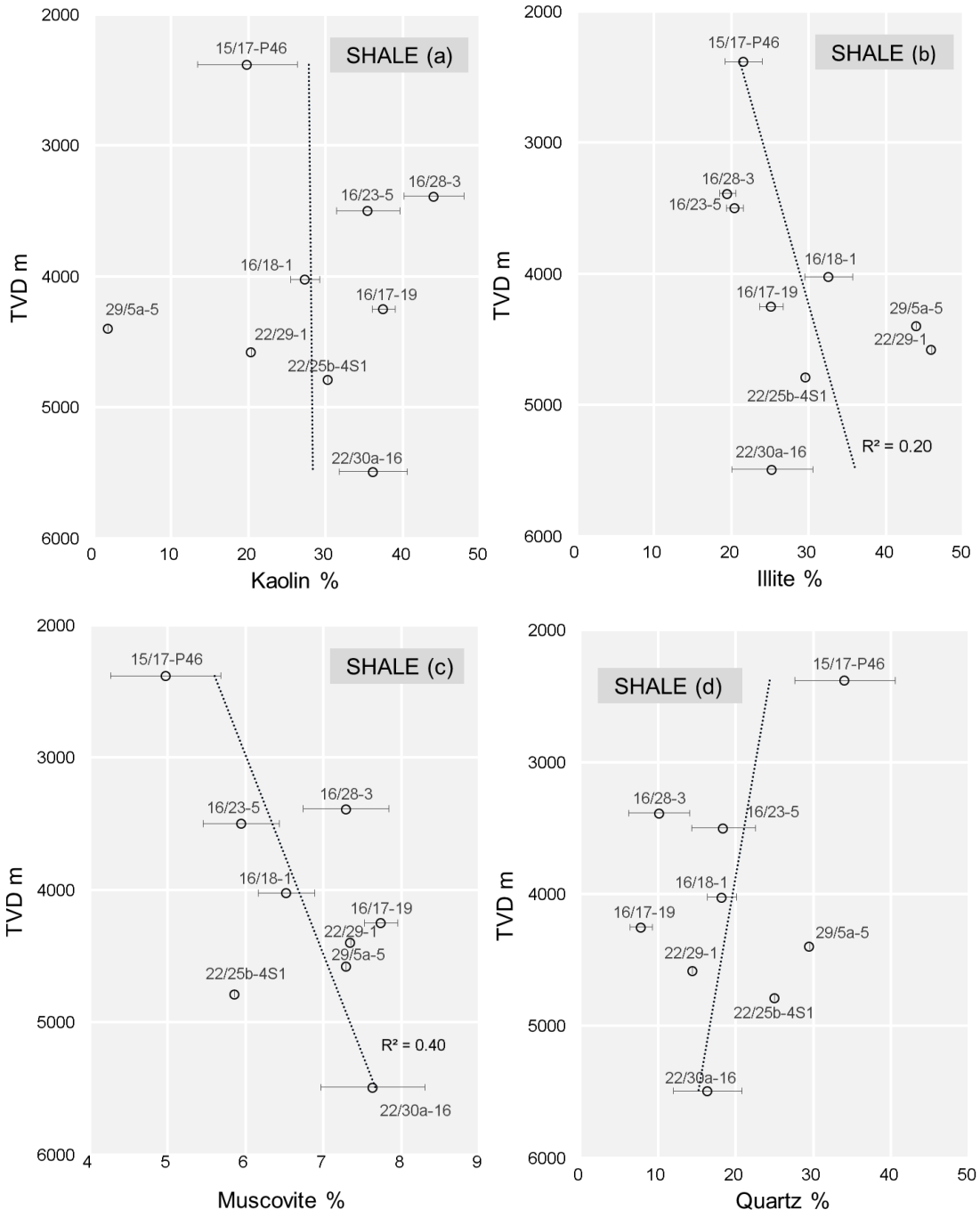

Figure 4.18 The XRD-measured contents of kaolin (a), illite (b), muscovite (c), quartz (d), K-feldspar (e) and ablite (f) in the shales of the Pentland Formation.

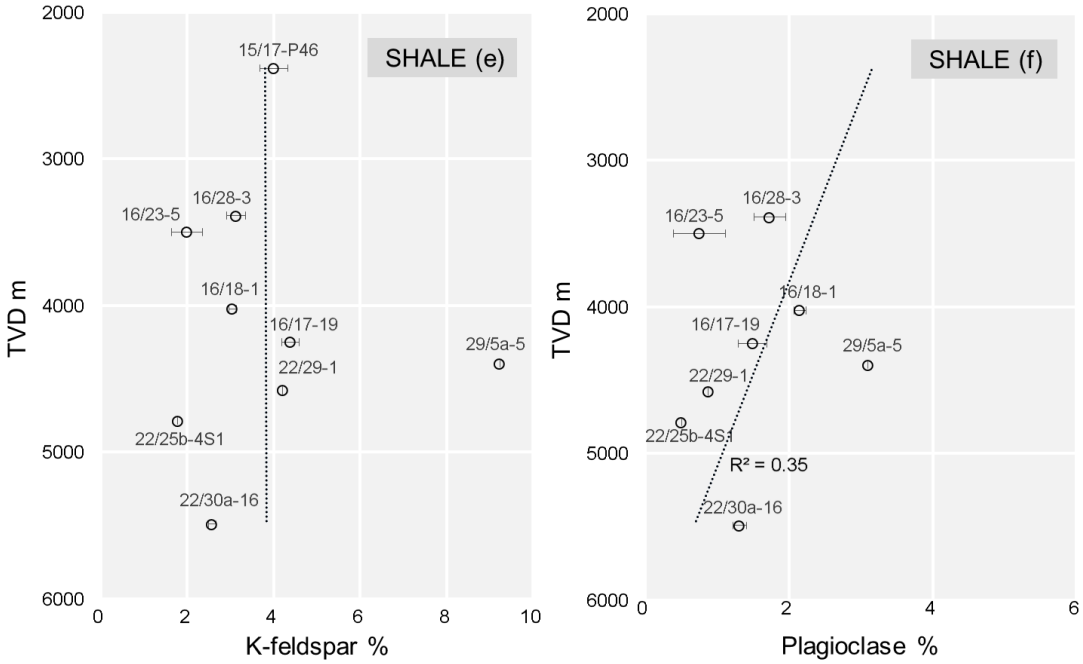

Figure 4.18 continued

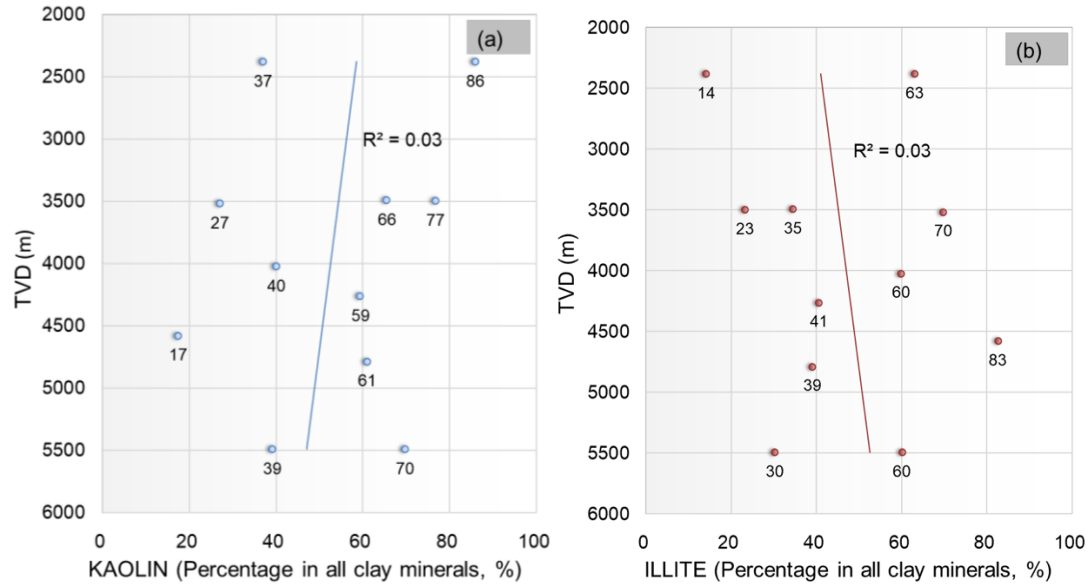

Figure 4.19 Results of XRD analysis of clay separates from the Pentland Shale. Kaolin and illite are the predominant clay minerals, but the relative abundance of illite over kaolin does not increase with depth, suggesting there was little kaolin being transformed into illite.

4.4.5 Geochemistry

Table 4.10 lists the main chemical composition of very fine- to fine-grained Pentland Sandstone, which is the principal reservoir lithological facies of the Pentland Formation (see *Section 4.4.2*). However, the chemical data in Table 4.10 cannot be further subdivided for Facies 1 and Facies 2 sandstone respectively since the chemical data from Wilkinson et al. (2014), which form part of the dataset, lacked the corresponding point-count data for differentiating the sedimentary facies. The XRF-measured concentrations of major and trace chemical elements, by the experiments in this study, are listed in Table A 4.6 - Table A 4.9.

The chemical data (Table 4.10) show that silica is the predominant rock-forming chemical element in the Pentland Sandstone, with SiO_2 comprising an average of 88.7% mass of the rock. Al_2O_3 and Fe_2O_3, respectively, constitute 4.5 % and 1% of the average rock mass. The average concentrations of other chemical elements are generally below 1%.

Table 4.10 Average chemical compositions of the Pentland SANDSTONE of different wells

Well	n	Avg. TVD (m)	SiO_2 (%)	Al_2O_3 (%)	Fe_2O_3 (%)	MgO (%)	CaO (%)	Na_2O (%)	K_2O (%)	TiO_2 (%)	MnO (%)	P_2O_5 (%)
15/17-P46	5	2391.1	86.3	3.5	1.3	0.3	0.3	0.3	1.0	0.5	0.0	0.1
16/23-5	3	3492.5	87.9	4.4	0.8	0.4	0.7	0.0	0.2	0.7	0.0	0.0
16/28-3	4	3383.2	91.4	4.1	0.4	0.2	0.2	0.0	0.3	0.5	0.0	0.1
16/18-1	3	4019.8	89.5	4.3	1.0	0.6	0.9	0.6	0.3	0.4	0.0	0.0
30/1C-5	5	4155.7	89.2	4.7	1.1	0.3	0.1	0.7	1.5	0.5	0.0	0.0
22/30c-G4	10	5736.6	88.8	5.1	1.3	0.4	0.3	0.9	0.6	0.3	0.0	0.0
22/25b-4S1	4	4795.5	83.9	7.9	1.7	0.7	0.1	0.1	1.7	0.9	0.0	0.0
22/29-1S1	6	4599.4	87.1	5.3	1.0	0.5	0.7	0.4	1.0	0.6	0.0	0.0
22/30B-15S1	5	5253.2	92.4	2.9	0.3	0.2	0.1	0.2	0.3	0.6	0.0	0.0
22/30A-16	4	5499.7	92.7	2.1	0.9	0.5	0.5	0.2	0.2	0.4	0.0	0.0
29/5A-5	6	4415.1	87.1	5.1	0.9	0.3	0.2	0.7	2.6	0.4	0.0	0.0
Average			88.7	4.5	1.0	0.4	0.4	0.4	0.9	0.5	0.0	0.0

In the Pentland Shale (Table 4.11), the main rock-forming chemical elements are the same as the Pentland Sandstone, but the relative importance of the elements are different. The shales contain less SiO_2 (52.9% vs. 88.7%) and much more Al_2O_3 (22.8% vs.4.5%) than the sandstones. Fe_2O_3 (4.1%), K_2O (3.3%) and TiO_2 (2.2%) are also important rock-forming chemical elements for the Pentland Shale.

Table 4.11 Average chemical compositions of the Pentland SHALE of different wells

Well	n	Avg. TVDSS (m)	SiO_2 (%)	Al_2O_3 (%)	Fe_2O_3 (%)	MgO (%)	CaO (%)	Na_2O (%)	K_2O (%)	TiO_2 (%)	MnO (%)	P_2O_5 (%)
15/17-P46	3	2381.4	58.2	16.6	6.5	1.0	0.2	0.3	3.1	1.5	0.0	0.1
16/17-19	5	4248.7	45.9	26.2	4.4	0.6	0.3	0.2	2.8	3.2	0.0	0.4
16/18-1	5	4023.1	52.5	24.5	5.4	1.6	0.3	0.4	3.5	2.9	0.1	0.3
16/23-5	5	3499.5	44.4	21.3	7.7	0.5	0.3	0.1	1.8	2.3	0.0	0.6
16/28-3	5	3387.3	47.0	26.7	2.0	0.5	0.2	0.3	2.1	2.8	0.0	0.2
22/25b-4S1	1	4788.4	62.1	24.6	1.3	0.7	0.1	0.0	3.6	2.0	0.0	0.1
22/29-1	1	4579.6	56.8	25.6	2.2	1.0	0.2	0.3	5.0	1.5	0.0	0.1
22/30a-16	3	5492.9	48.2	24.5	1.6	0.6	0.3	0.2	2.3	2.8	0.0	0.1
29/5a-5	1	4396.1	61.0	15.3	5.8	1.5	0.1	0.4	5.4	0.9	0.0	0.1
Average			52.9	22.8	4.1	0.9	0.2	0.2	3.3	2.2	0.0	0.2

4.5 Discussion

4.5.1 Reservoir quality control of the Pentland Sandstone

- **Illite Content**

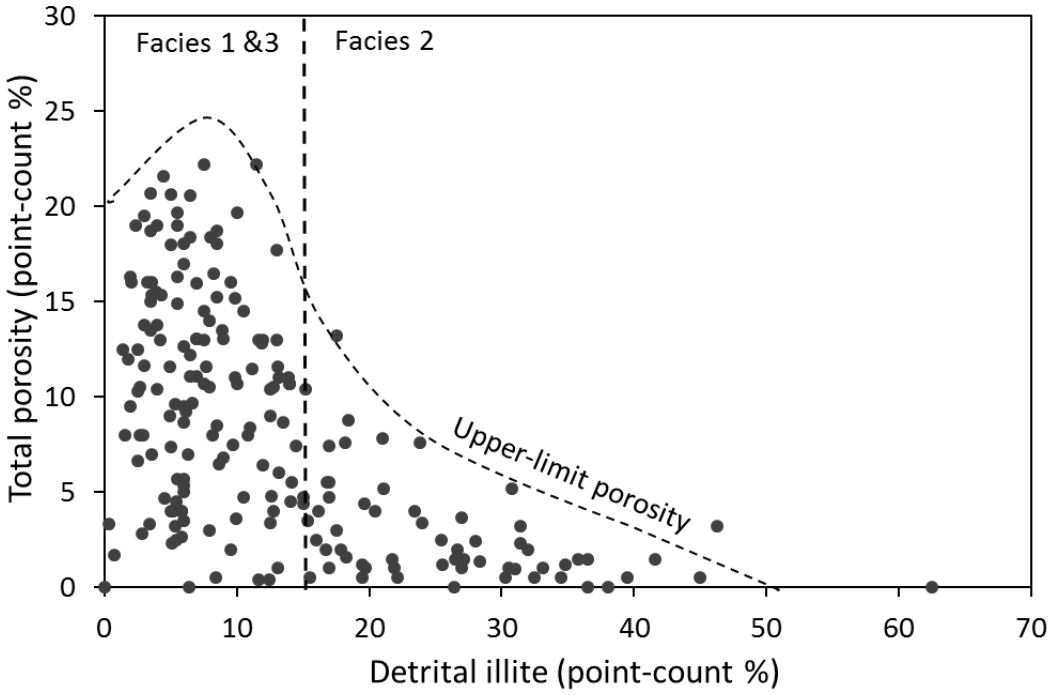

Figure 4.20 Point-counted detrital illite content vs. thin-section porosity. The content of illite defines the upper-limit porosity that a Pentland Sandstone may attain. Porosities of the sandstones with >15% of detrital illite (Facies 2 sandstone) are invariably low, capped by the low upper-limit porosity.

Figure 4.20 demonstrates the relationship between the content of detrital illite in the Pentland Sandstone and the reservoir porosity. Point-counted porosity of the sandstones containing >15% illite is generally below 10%, which means these sandstones are unlikely to form prolific hydrocarbon reservoirs. 15% of detrital illite is, therefore, the '*cut-off*' line for high-porosity sandstones. This suggests that any Pentland Sandstone with >15% of illite upon deposition will almost certain to become a low-porosity sandstone at depth. In contrast, the porosity of Facies 1 sandstone is highly variable, ranging from 0-23%, and high-porosity reservoirs (>10%) and low-porosity (<10%) reservoirs occur almost in the same frequency (Figure 4.20). The

content of detrital illite affects the upper-limit of the sandstone porosity, as indicated by the upper-limit porosity line in Figure 4.18. The further variation of sandstone porosity between the upper-limit porosity and 0% porosity is not clearly correlated to the illite content, suggesting that illite content has little influence on the porosity or that there are many factors, including illite, that are co-controlling the porosity which makes the data points widely scattered.

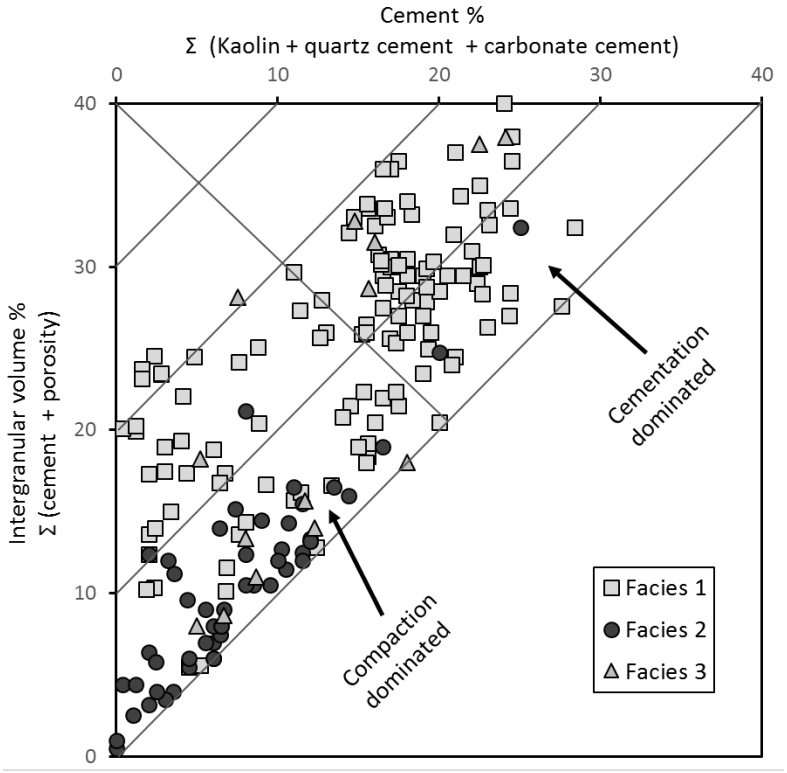

Figure 4.21 Diagram, based on point-count data, assessing the relative importance of compactional process and cementation to the porosity development in the Pentland Sandstone. It suggests that the porosity of Facies 2 Sandstone is lost predominantly from compaction, whereas for Facies 1 Sandstone, both compaction and cementation play important roles in the porosity loss.

Figure 4.21 compares the relative importance of compaction and cementation to the porosity loss of the Facies 1, 2 and 3 sandstones. It shows that the data points representing Facies 2 sandstone are clustered in the left-bottom corner of the diagram, where suggests the porosity loss is dominated solely by compaction. The significant porosity loss of Facie 2 sandstone from compaction is most likely owing to the compression, deformation and loss of micro-porosity within illite itself. No other mineral in the Pentland Sandstone is as soft and compactable as illite. The

mechanical compaction of sandstones happens at shallow depth (<1.5 km, Baldwin and Butler, 1985). It can be envisaged that the illite-rich Facies 2 sandstone will be compacted to a low-porosity sandstone at shallow depths (<1.5 km), soon from the beginning of burial. As for the Facies 1 sandstone, the situation of porosity loss is more complicated: Figure 4.21 suggests that in some sandstones, compaction is the dominant porosity-control mechanism, whereas in more of the sandstones, most porosity appear to be lost from cementation. The case of the Facies 3 sandstone is similar to Facies 1 sandstone, with data points being somewhat evenly distributed in the two sides of the diagram. Overall, both compaction and cementation are important process controlling the reservoir porosity of Facies 1 and 3 sandstones, but the relative significances of the two processes are highly variable from case to case.

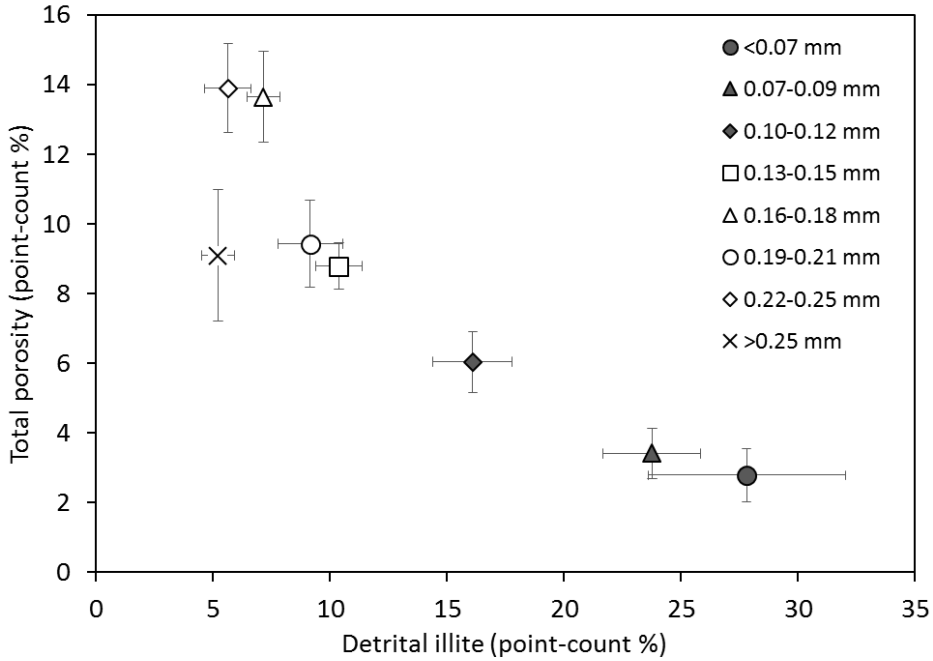

Figure 4.22 The detrital illite content and total porosity of sandstones of different grain-size. Sandstones of grain-size >0.13mm contain less detrital illite and higher porosity than the sandstones of grain-size <0.13mm.

Grain-size of a sandstone reflects the water energy of the depositional environment. Smaller sand grain-size corresponds to lower energy environment, which will generally incorporate more clay minerals in the sandstone. Figure 4.22 shows the porosity and illite content of the Pentland Sandstone in relationship to the sandstone grain size. It shows that within the interval of very fine- to fine-grained sandstones, the porosity generally increases with increasing grain-size; the porosity difference between fine-grained and medium-grained sandstones, however, is not obvious. The

whole figure suggests that the grain-size of a Pentland Sandstone can reflect the reservoir porosity as it partly indicates the illite content of the sandstone.

- **Quartz Cement**

Quartz cement is the most common authigenic phase in deep sandstones, and also the most significant porosity-occluding mechanism (McBride, 1989; Worden and Morad, 2000). Quartz cement started to develop in the Pentland Sandtone from the depth of 2000m (c.60-80^{o}C), and growed at an average rate of 2.3 km/% in the subsequent burial process (see *Section 4.4.3*). This section aims to reveal the factors that influence the growth of quartz cement and the effect of quartz cement on the porosity of the Pentland Sandstone.

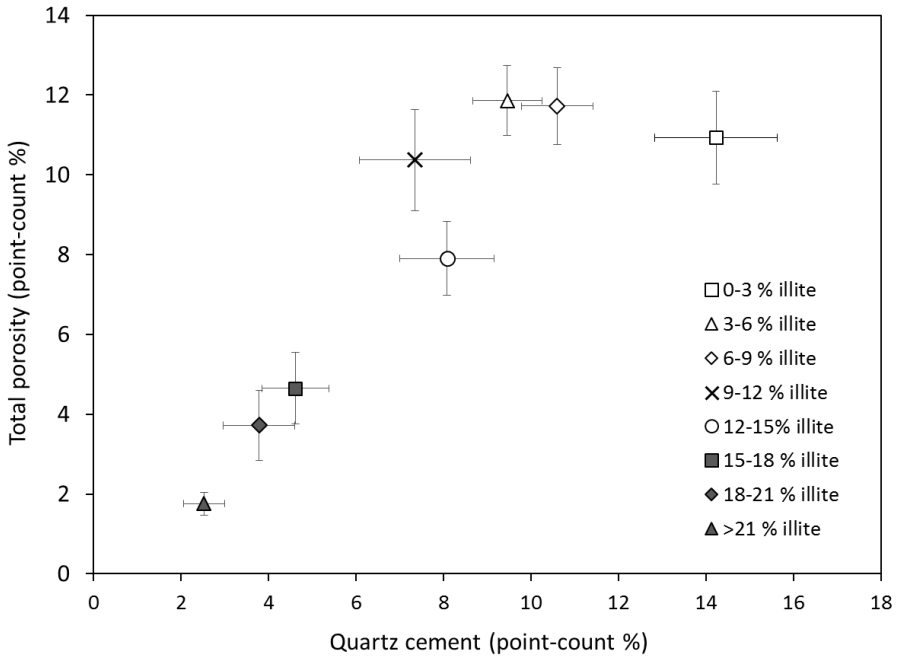

Figure 4.23 The relationships between the amounts of quartz cement, total porosity and illite content in the Pentland Sandstone (All Facies included). This figure shows that sandstones of higher porosity have more quartz cement; cleaner sandstones generally contain higher porosity and more quartz cement. Error bars = ± 1 × standard error of the mean

One notable petrographic feature related to the quartz cement in Pentland Sandstone is that the cement appears to be the most abundant in the sandstones of high porosity (see Figure 4.23), which is somewhat contradictive with the conventional impression that pervasive quartz cement severely damages the reservoir porosity. In the sandstones with 0-3% of illite, for example, the content of quartz cement reaches an average of 14%, yet the sandstones still remain highly porous with 11% of total porosity (Figure 4.23). In addition, Figure 4.23 indicates that an increasing content of

illite has a significant negative impact on both the amounts of porosity and quartz cement of sandstones. Illite may affect quartz cementation in four ways:

i. The fibrous morphology of illite can significantly decrease the permeability within the pore space of a sandstone (Lander and Bonnell, 2010), and thereby inhibiting quartz cement by retarding silica supply to the cement growth sites;
ii. Illite may also present as grain coats, which can potentially inhibit quartz cementation by reducing the free surface area that is available for the growth of quartz cement (Storvoll et al., 2002);
iii. Since illite enhances the compaction of the Pentland Sandstone (see *Section 4.5.1 – Illite content*), illite-rich sandstones are destined to have a low porosity at depth, and consequently, the lack of pore space would not allow much quartz cement to form.
iv. On contrary to the above three scenarios, illite may also lead to more quartz cement: the illite at the contacts of quartz grains may enhance pressure dissolution, causing an oversaturation of silica in pore-fluids relative to quartz cement, and ultimately result in the precipitation of new quartz cement (Bjørkum, 1996).

For Scenario i, the fibrous morphology is characteristic for authigenic illite that is developed during diagenesis. Fibrous illite that is formed from the alteration of kaolin can be found in the Pentland Sandstone (e.g. Figure 4.16), but due to a lack of K-feldspar, the total amount of authigenic illite in the Pentland Sandstone is negligible, whose abundance is below the level that can be quantified by the point-count method (Wilkinson et al., 2014b). The impact of authigenic fibrous illite on quartz cement by reducing the reservoir permeability is therefore considered to be insignificant (also see *Section 4.4.3 – Sandstone Paragenesis*).

Based on my experience of observing the Pentland Sandstone under the microscope, grain-coating illites are scarce in the sandstone. The percentage of grains with coats on their surface is generally less than 10%. Such a low abundance of illite coats is unlikely to effectively inhibit quartz cementation (Ajdukiewicz and Larese, 2012), and accordingly, Scenario ii can be dismissed.

After excluding the significances of Scenario i and ii, Scenario iii is the only possible mechanism that can account for the pattern in Figure 4.23, where quartz cement increases with decreasing illite. The elusive observation that high-porosity sandstones also contain a high volume of quartz cement can also be well explained by Scenario iii, which proves the scenario's validity (Figure 4.23). Another understanding of Scenario iii is that the content of illite generally decides the reservoir porosity after mechanical compaction, which will further affect the available maximum volume that quartz cement can reach. There is petrographic evidence manifesting this speculation from those most deeply buried Pentland Sandstone, where quartz cement has highly developed to approach to the maximum volume (Figure 4.24). Figure 4.24 shows that the amount of quartz cement has a negative linear correlation with the content of illite, indicating that the maximum volume of quartz cement in the sandstone may be restrained by the content of illite.

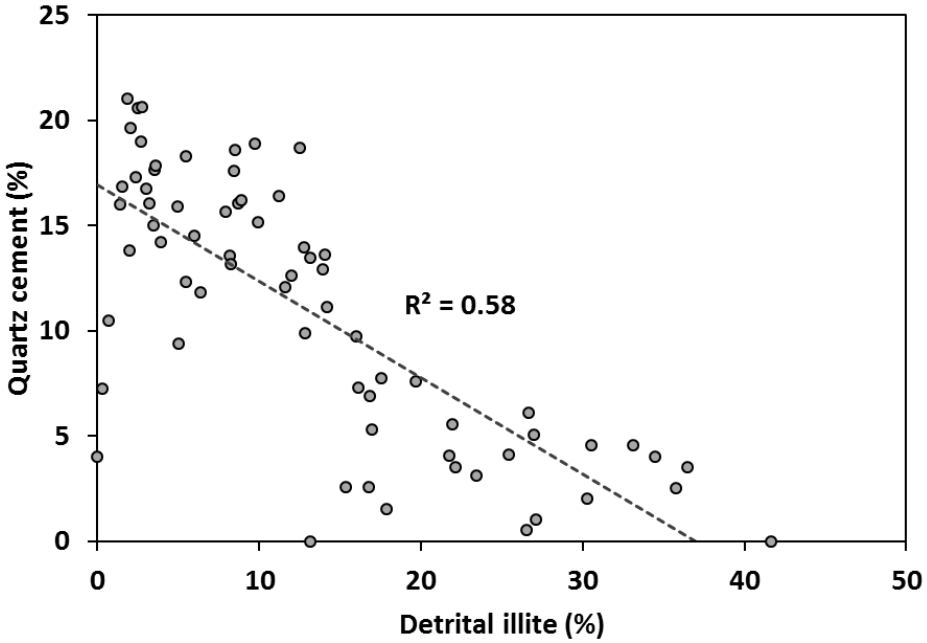

Figure 4.24 In the deepest Pentland Sandstone (5200-5600 m, c.180-200ºC), where quartz cement has developed closing to its full potential, the amount of quartz cement shows a negative correlation with illite content. Petrographic data from wells 29/5b-F1 and 22/30b-15S1.

The scale of influence of Scenario iv on quartz cement is difficult to assess. Bjørkum (1996) showed that even an extremely thin layer of illite (<1 μm) is able to enhance pressure dissolution at quartz-quartz contacts. Therefore, in theory, the trace amount of illite in the cleanest Pentland Sandstone (0-3% illite, Figure 4.23), which are usually distributed as clay seams between grains, is sufficient to facilitate pressure dissolution

and quartz cementation as a whole. The highest content of quartz cement in the cleanest sandstones (avg. 14%) may be partly related to the ‘catalytic’ effect of illites. However, as the amount of illite increases, the reservoir permeability will drop, which may inhibit pressure dissolution by restricting the export of silica from the dissolution sites. In addition, as the amount of illite increases, the thickness of illite platelets might also increase, which will then become ‘grain coats’ (>10 μm) that prevents quartz cementation and pressure dissolution (Storvoll et al., 2002). Therefore, the increasing amount of illite may turn illite from ‘catalytic’ to ‘inhibitive’ for pressure dissolution. This is consistent with the situation observed in Figure 4.23 that the increasing content of illite content in the sandstone is accompanied by decreasing quartz cement. It is possible that the ‘catalytic’ effect of illites on pressure dissolution is the most effective when the content of illite is low.

- **Overpressure**

The point-count data (Table 4.7) show that about half of the porosity within the Pentland Sandstone is primary porosity. A viable way of preserving primary porosity is to inhibit mechanical compaction at shallow depth (Bloch et al., 2002). Shallow development of reservoir overpressure inhibiting mechanical compaction can be a potential explanation for the high primary porosity in Pentland Sandstone (Holm, 1995; Osborne and Swarbrick, 1999). The development of the overpressure within the Central Graben has been reported to be caused by compaction disequilibrium due to the rapid basin subsidence during Paleogene and Neogene, and possibly also by the maturation of hydrocarbon source rocks (Holm, 1998). Pore fluids within the deep sediments, which are overlain by kilometres of low-permeability chalks and mudstones, cannot escape upwards easily, which resulted in the highly overpressured deep regime of the Central Graben (Haszeldine et al., 1999).

Pressures in the Pentland Formation follow the normal depth-pressure trend of the Central Graben (Holm, 1998), where the basin margin is normally pressured whereas the centre is highly overpressured (Figure 4.25). The Pentland Sandstone at the margin, which is currently buried at 3-4 km, have pressures that lie close to the basinal hydrostatic gradient. In strong contrast, the sandstones deeply buried to > 4km in the centre are significantly overpressured with many of the pressures approaching the lithostatic gradient (Figure 4.25). A model for the overpressure development within the Pentland Formation is lacking in the literature. But given that the Pentland Formation shares nearly the same burial history with the immediate overlying Fulmar Formation, it is reasonable to infer that its overpressure development history is also very similar to the Fulmar (Wilkinson et al., 2014). A number of pressure models of the Fulmar Formation suggest that the reservoir overpressure started to build up from the depth of 2.5-3.5 km during Paleogene (Holm, 1998; Wilkinson et al., 1997). For the Pentland Formation, the data show a similar estimation that the initiation depth of overpressure is 3.5 km during the (see the burial history in Figure 4.4;), and then from 3.5-4.5 km the pressure rapidly rises to an extremely high level, more than two times higher than the pressure at 3.5 km.

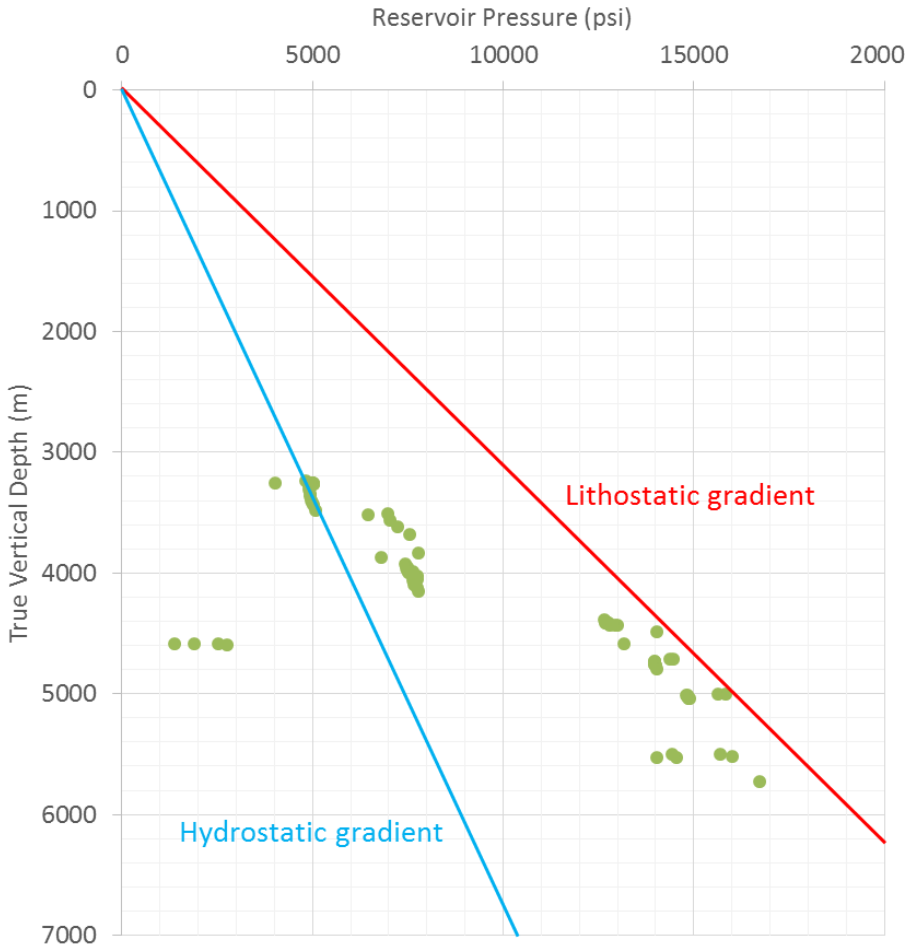

Figure 4.25 Reservoir pressure of the Pentland Formation. All the pressure data were obtained by repeat formation test from 9 wells, including 22/05b-A12, 16/23-5, 9/13-5, 16/18-1, 9/19-7z, 29/5a-5, 23/26b-14, 23/26b-15 (in the order of increasing depth). The data points which lay on the left side of the hydrostatic gradient are presumably due to poor quality measurement as underpressured reservoirs have not been reported in the North Sea (Moss et al., 2003). The North Sea hydrostatic and lithostatic gradients are from Moss et al. (2003).

Figure 4.26 shows that the mean porosity (by well) of the highly overpressured Pentland Sandstone is not, or even lower than that of the non-overpressured reservoirs. As such, the data does not suggest that overpressure has a considerable effect on the porosity of the Pentland Sandstone (Figure 4.26). The reason for the overpressure being insignificant may be because it developed too late. Present day overpressure starts at about 3.5km, but the process of mechanical compaction has almost completed above this depth.

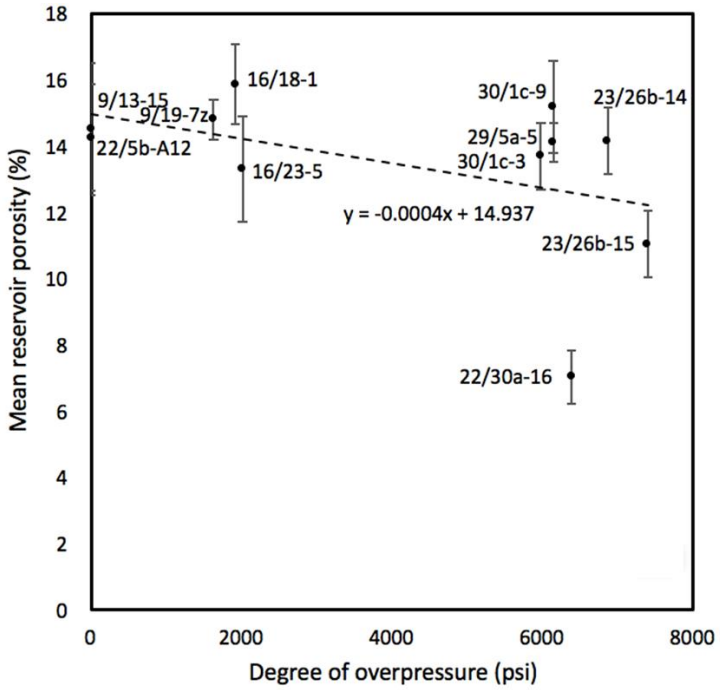

Figure 4.26 Average HELIUM porosity (by wells) as a function of the degree of overpressure, showing that the reservoirs of high overpressure degrees do not contain higher porosity than the reservoirs of low degree overpressure (porosity error bars = 2×standard error of the mean). Degree of overpressure = reservoir pressure – reservoir hydrostatic pressure. The labels of the data points record the wells where pressure data were collected.

- **Early Hydrocarbon emplacement**

Whether early hydrocarbon emplacement can preserve the porosity of sandstone reservoirs is a controversial topic (Worden et al., 1998). The Chapter 5 of this thesis will study the cause of the high-porosity in the Pentland Sandstone of the Kessog Field, Central North Sea. Analysis of the results indicates that the formation of these high porosities is due to the early emplacement of hydrocarbon in the reservoir, and that hydrocarbon emplacement can preserve up to 10% of porosity in the Pentland Sandstone (see Chapter 5). Figure 4.5 also shows that the porosity of well 30/1c-5 is significantly higher than the porosity of other wells. But the other wells of the Pentland Formation in Figure 4.5 do not exhibit high porosity that is indicative of an influence of early hydrocarbon emplacement on reservoir porosity. Therefore, the influence of hydrocarbon emplacement on the porosity of the Pentland Sandstone appears to be only locally significant.

4.5.2 K-Feldspar dissolution and secondary porosity

Figure 4.14 illustrated the variations of the amounts of K-feldspar and plagioclase in different Pentland wells as a function of depth. The content of K-feldspar in most of the wells is generally < 2% (except in wells 15/17-P46 and 30/1c-5) and the figure does not show a clear trend of K-feldspar decline with depth that is suggestive of K-feldspar dissolution with progressive burial. However, the deep-burial dissolution of K-feldspar in sandstones is usually reported at a depth of 2000-3500 m (c.80-120^{o}C; Wilkinson et al., 2014b), for which depth range there is only one well (15/17-P46) that supplied the petrographic data. The content of K-feldspar in the shallowest well 15/17-P46 is 1-2% higher than in the deeper wells (Figure 4.14), one likely scenario is that there has been a small amount of K-feldspar dissolution between the depth of well 15/17-P46 (c.2400 m) and the deeper Pentland wells (>3300 m), but this trend was not reflected in Figure 4.14 due to a lack of petrographic data in the depth interval. There is petrographic evidence supporting this scenario from well 16/28-3 (3384.8 m, see Figure 4.13), where anomalously large secondary pores filled by kaolin are present. These secondary pores do not show any sign of compaction, suggesting that they were newly formed in the sandstones, at a depth close to their current burial depth. Wilkinson et al. (2014) denied the possibility that the oversized pores in the Pentland Sandstone were preserved within the robust sandstone framework maintained by quartz cement and reservoir overpressure, as these mechanisms have not initiated until the depth of 2000 m. The presence of large secondary pores in deep Pentland Sandstone, therefore, suggests that there has been some recent K-feldspar dissolution, and the amount of dissolved K-feldspar indicated by the data from well 15/17-P46 is 1-2%.

Evidence that is indicative of K-feldspar dissolution also can be found in the Kessog Field. Point-count data show that the content of K-feldspar in the crestal well of the field, where firstly filled by hydrocarbons, is 2% higher than in the wells located at the field flanks. Meanwhile, the content of kaolin in the crestal well is correspondingly 3% lower, which suggests that the reaction of K-feldspar dissolution to precipitate has been inhibited in the crestal well, possibly by the emplaced hydrocarbons. The comparison between the crestal and flank wells of the Kessog Field indicates there has been 2% of deep K-feldspar dissolution in the sandstone, which is inconsistent with the estimation based on the petrographic data of well 15/17-P46.

4.5.3 Silica source of quartz cementation

According to whether the silica source for quartz cementation is within or outside of a sandstone body, there are external sources and internal sources that may provide the silica (Worden and Morad, 2000). A potential external source is the silica that migrates from neighbouring shales into a sandstone (van de Kamp, 2008), either by element diffusion or advection. In the case of the Pentland Formation, the chemistry data of the Pentland Shale, however, show that the amount of silica in the shale is not correlated to depth (Figure 4.27), suggesting that the shales do not lose any silica during burial. The geochemical evidence can exclude the possibility of the shales, regardless of above, below or enclosed within the Pentland Sandstone, as a silica source for the quartz cementation in the sandstone.

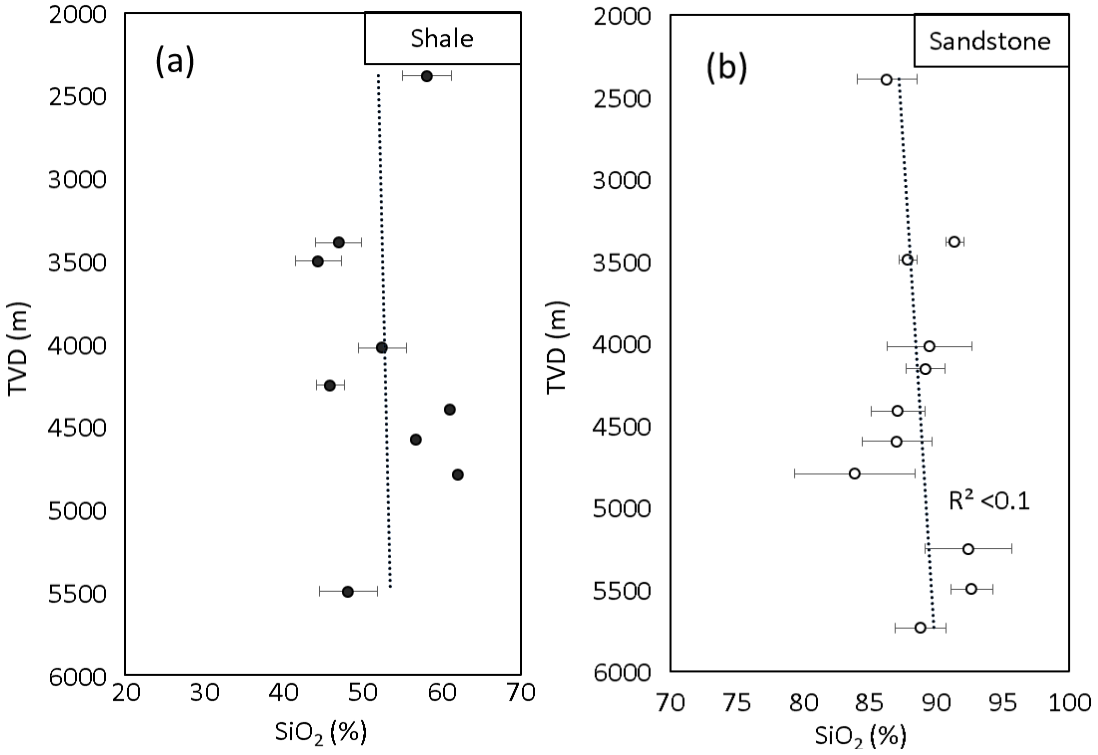

Figure 4.27 The variation of SiO_2 (wt %) in the Pentland Shale (a) and Sandstone (b) with depth. The chemical data show insignificant correlations with depth, indicating that the SiO_2 (wt %) of the sandstones and shales do not change with progressive burial and diagenetic process. The sandstones are very fine- to fine-grained Pentland Sandstone. The raw chemical data can be found in Table 4.10, Table 4.11, Table A 4.6 and Table A 4.8.

Another potential external silica source lies in those more deeply-buried sandstones of the same sedimentary basin. The scenario is that, since silica solubility in water is

positively correlated to temperature (Giles and de Boer, 1990), the upwards convectional flows of pore-fluid from deep sandstones, which are saturated with silica, may lead to the precipitation of quartz cement as temperature drops in shallow sandstones (Haszeldine et al., 1984). The potential upward fluid migration routes can be sub-vertical faults or titled sandstone beds that connect the deep and shallow sandstones. The overall direction of this basinal-scale silica transfer is generally from deep to shallow sandstones, and the expected chemical trend resulted from this silica transfer mechanism would be a decrease in sandstone SiO_2 (wt %) with increasing depth. Nevertheless, this scenario is refuted by the chemical data (Figure 4.27), which shows the SiO_2 (wt %) of the Pentland Sandstone is constant, if not increases, with depth. Another problem with the scenario of basinal-scale silica transfer is the low solubility of silica in pore-fluids (50-100 ppm, Giles and de Boer, 1990). Geochemical modelling suggests that to precipitate 1% of quartz cement in 1 unit of sandstone, 10^8 units of water flux from the deep basin is required (Bjorlykke, 1994). Such a large volume of water flux, however, is unrealistic to form in sedimentary basins (Bjørlykke and Jahren, 2012). Hence, an external source of silica from deeper sandstones seem to be improbable for the quartz cement in the Pentland Sandstone.

Silica can also be sourced from mineral reactions within a sandstone itself. There are four potential internal silica sources: biogenic silica dissolution, clay mineral transformation, feldspar dissolution and stylolite/pressure dissolution at quartz grain contacts (Worden and Morad, 2000). Biogenic silica is exclusive to marine sediments (Worden and Morad, 2000), and it is therefore not supposed to be present in the Pentland Formation, which is fluvial-deltaic in origin. Clay mineral transformation in the Pentland Sandstone refers particularly to the transformation of kaolin into illite. Nevertheless, this process appears to be almost ceased in the Pentland Sandstone, as suggested by the preservation of kaolin till great depth (see *Section 4.4.3 – Sandstone paragenesis*), owing to an extreme lack of potassium source. The amount of dissolved K-feldspar in the Pentland Sandstone at deep burial is estimated to be around 1-2% (*Section 4.5.2 – K-feldspar dissolution)*. According to mass balance calculation ($1cm^3$ K-feldspar→$0.5\ cm^3$quartz), the produced quartz cement from K-feldspar dissolution in the Pentland Sandstone will account for 0.5-1% volume of the sandstone. After excluding all other possible silica sources, the remaining amount of quartz cement in the Pentland Sandstone that is excess of 0.5-1% must be provided from the development of quartz stylolite/pressure dissolution. Figure 4.9 displays that

the average amount of quartz cement in the Facies 1 Pentland Sandstone typically vary between 5% and 15%. It is reasonable to speculate that stylolitization and pressure dissolution of detrital quartz grains has provided the silica ingredient for quartz cement that occupies 4-14% volume of the sandstone reservoirs.

4.5.4 Mass transfer between sandstones and shales

The occurrences of the diagenetic chemical reactions of K-feldspar dissolution, quartz cementation and illite growth indicate that chemical elements involved in these reactions are mobile within a certain scale. The size of this element mobility scale, however, is yet to be understood and remains highly controversial (Bjørlykke, 2011; Day-Stirrat et al., 2010). Scenarios ranging from a scale of millimetres to kilometres, from the size of a petrographic thin-section to a sedimentary formation have all been proposed (see review in Thyne, 2001; Wilkinson et al., 2003). This section will use the Pentland Formation as a case to investigate the issue of element mobility, and test the possibility of chemical exchange between sandstones and shales in diagenesis.

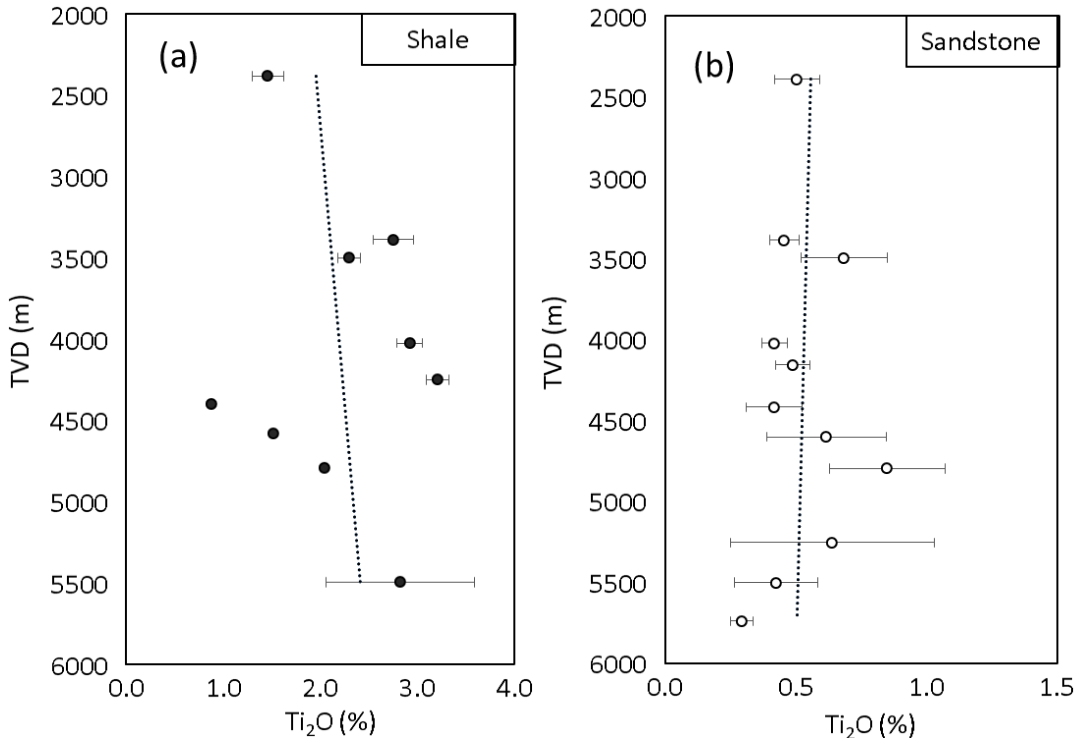

Figure 4.28 The variation of TiO_2 (wt %) in the Pentland Shale (a) and Sandstone (b) with depth, suggesting that burial depth and diagenetic process do not affect the concentration of titanium in the two rocks. The sandstones are very fine- to fine-grained Pentland Sandstone (same in Figure 4.29 and Figure 4.30).

Among the major elements of sedimentary rocks, titanium is the least disputed regarding its mobility in diagenetic systems. Treating titanium as a highly 'immobile'

element (mobility scale <1mm) has generally been a consensus among the diagenetic study community (Milliken et al., 1994; Wilkinson et al., 2003). The chemical data of the Pentland Formation also reflects an immobile attribute of titanium by showing that the amounts of TiO_2 (%) within the sandstones and shales are not depth-dependent (Figure 4.28).

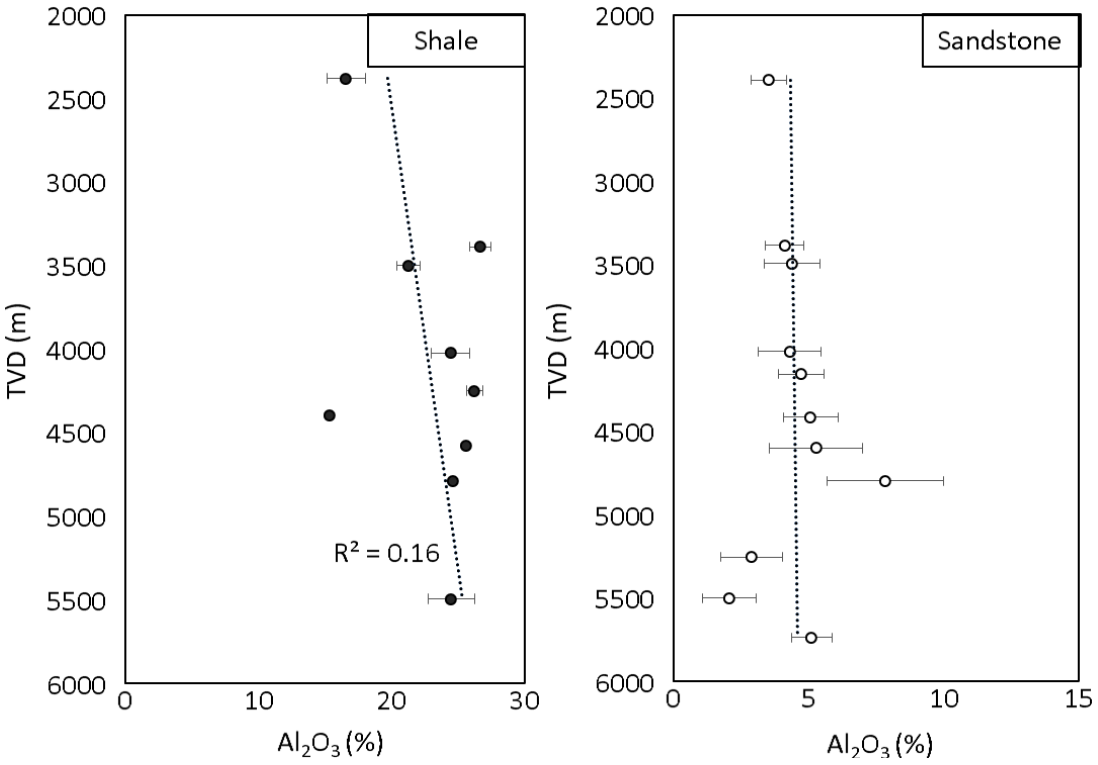

Figure 4.29 The variation of Al_2O_3 (wt %) in the Pentland Shale (a) and Sandstone (b) with depth. The amount of Al_2O_3 in Pentland Sandstone is not correlated to depth, indicating the sandstone have not lost any aluminium to Pentland Shale in diagenesis.

The mobility of aluminium in diagenesis, however, has been subject to intensive debation (Giles and de Boer, 1990; Surdam et al., 1984; Wilkinson and Haszeldine, 1996). Still, a number of studies assumed it to be a highly immobile element in diagenesis, due to its extremely low solubility in the pore-fluids (1ppm at 150^{o}C, Bjørlykke and Aagaard, 1992). Evidence from the sandstones of the Pentland Formation, which fits a vertical trendline to the variation of Al_2O_3 (%) with depth, suggests aluminium is conserved within the sandstones during burial. Albeit there is seemingly a subtle increase in Al_2O_3 (%) in the Pentland Shale, this increase of aluminium is more likely because of different depositional compositions of the shales, since there was no export of aluminium from the sandstone.

The solubility of potassium in pore-fluids is about 2-3 magnitudes higher than aluminium and therefore is expected to be more mobile than the latter (Kharaka and Hanor, 2003). The measured K_2O (%) content in the Pentland Sandstone is nearly constant with depth, indicating that the sandstone has not exported any potassium during deep burial (Figure 4.30). As such, the variation of potassium in the Pentland Shale is interpreted to be related to a variation in the original composition of the sediments.

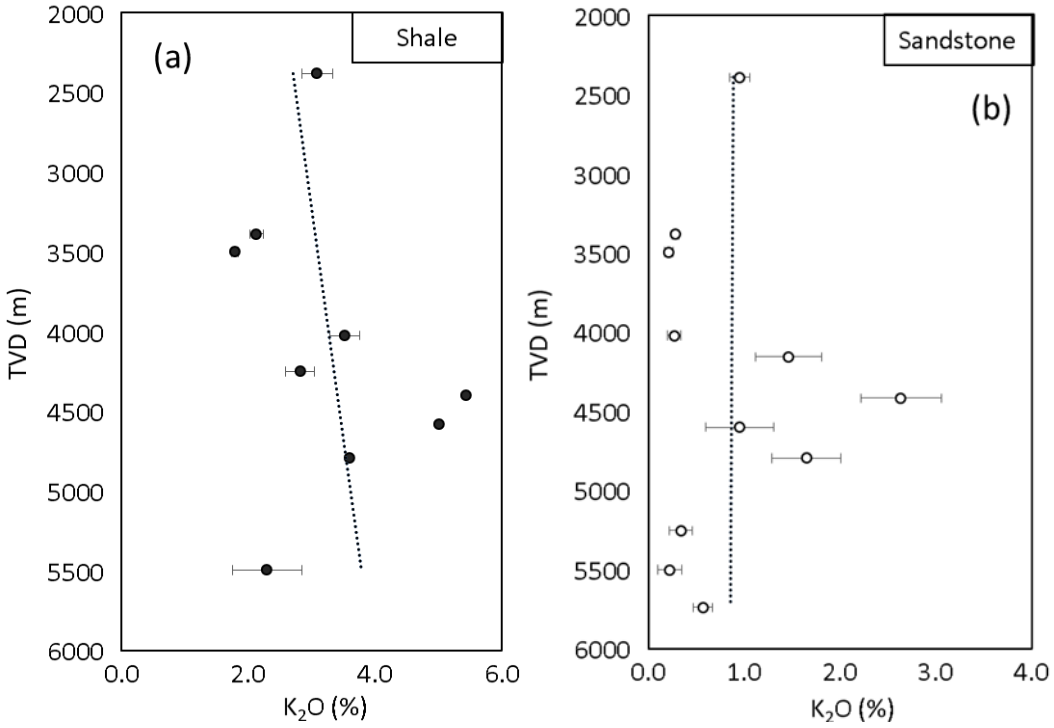

Figure 4.30 The variation of K_2O (wt %) in the Pentland Shale (a) and Sandstone (b) with depth. With increasing depth, K_2O (wt %) in the Pentland Sandstone shows no trend, which indicates there was no diagenetic transfer of potassium from the sandstone to the shale.

The trends with depth of other major chemical elements in Pentland Sandstone and Shale are presented in Appendix (Figure A 4.1 - Figure A 4.4). Similar to the results of titanium, aluminium and potassium, no significant transfer of other major elements has been discovered between the sandstone and shale.

The conclusion that there was no exchange of aluminium and potassium between the Pentland Sandstone and shale contradicts the conclusions of many other studies which yielded evidence for the mass transfer of the two chemical elements in diagenesis. The wider implication of the conclusion of this study should be carefully

scrutinised. In the literature, the majority of the evidence that supports the scenario of aluminium and potassium movement from sandstones to shales is from the Paleogene fluvial-deltaic sediments in the Gulf Coast (Awwiller, 1993; Day-Stirrat et al., 2010; Wilkinson et al., 2003). These sediments have two important common features: 1) the sandstones have a high abundance of K-feldspar (10-40%); 2) the shales are dominated by illite-smectite clays. The sandstones and shales of other basins which have reported the evidence for sandstone-shale mass transfer also have these features, such as the Fulmar Formation of the North Sea (Wilkinson and Haszeldine, 1996) and the Paleogene sediments of the Indonesian Mahkam Delta Basin (Furlan et al., 1996). The Pentland Formation, however, is different: the Pentland Sandstone is depleted in K-feldspar (Figure 4.14) and the shales are dominated by kaolin (Figure 4.18). Although a few percentages of K-feldspar still exist within the Pentland Sandstone, these K-feldspar grains may be the most stable species of K-feldspar that have survived through the meteoric water leaching process near earth surface. Because of the stability, their dissolution rates will be extremely slow and consequently, there is little K^+ and Al^{3+} being freed for diagenetic reactions in the Pentland Formation. Therefore, the reason for no significant mass transfer in the Pentland Formation is because there is no sufficient mass to transfer, rather than because the mass cannot be transferred. The case of the Pentland Formation cannot either prove or disprove the possibility of diagenetic mass transfer between sandstones and shales.

4.6 Conclusions

(1) The median (P50) helium porosity of the Pentland Formation reservoirs can be predicted with confidence using the formula $\Phi = 30.9\% - 0.0039\% \times \text{depth}$ (R^2=0.69), and the median (P50) permeability can be predicted by $k = 93179 \times e^{-0.002 \times \text{depth}}$ (R^2=0.64).

(2) The Pentland Sandstone can be divided into three facies:

- Facies 1: very fine- to fine-grained clean sandstones (0-15% detrital illite)
- Facies 2: very fine- to fine-grained argillaceous sandstones (>15% detrital illite)
- Facies 3: medium- to coarse-grained sandstones

(3) Facie 1 is the predominant oil-producing within the Pentland Formation, due to its high porosity and large fraction among the sandstones. Facies 1 and 3 sandstones are quartzose with minor amounts of K-feldspar, plagioclase, kaolin and illite.

(4) Compaction and cementation seem to have generally caused equal amounts of porosity loss to Facies 1 and 3 sandstones. Facies 2, due to its high illite content, has been compacted to a low-porosity sandstone (point-counted porosity <10%) above the burial depth of 2000 m, and does not form valid hydrocarbon reservoirs.

(5) Facies 1 sandstone on average contains 10.3% of quartz cement. Quartz cement is the most developed in high-porosity sandstones. The sandstone of the highest porosity normally contains the least amount of illite and the largest amount of quartz cement. This is considered to be because the content of illite mainly determines the sandstone porosity after compaction, which further determines the maximum space that quartz cement can reach in the following burial process.

(6) Silica source of quartz cement in the Pentland Sandstone is provided by the development of quartz styolitization and pressure dissolution. There might be a small amount of quartz cement, equivalent to 0.5-1% volume of the bulk rock, that is precipitated from the dissolution of K-feldspar

(7) The sandstones and shales of the Pentland Formation act as independent isochemical bodies in diagenesis, with no detectable exchange of chemical elements.

Summary statement: this study documented the diagenetic patterns in the Pentland Formation. The geochemical data, however, contradict many previous studies claiming that the diagenetic systems of sandstone and shale units are mutually affected (e.g. Day-Stirrat et al., 2010; Land, 1997; Milliken et al., 1994; Wilkinson et al., 2014b, 2003). The geochemical data of this study suggest that the sandstones and shales of the Pentland Formation do not have any significant exchange of chemical components.

4.7 Appendix

Table A 4.1 Average compositions of the Pentland sandstones determined by point-count. The data above the dashed-line is from this study, and the data below is from Wilkinson et al. (2014). The data error = standard deviation of the mean. (Mineral% + Porosity% = 100%)

Well	TVD (m)	n	Quartz (%)	K-feldspar (%)	Plagioclase (%)	Mica (%)	QOG (%)	Dolomite (%)	Illite (%)	Kaolin (%)	Porosity (%) Primary / Secondary	Grain-size (mm)	Sorting
15/17-P46	2389-2394	5	67±2	2.8±0.3	4.9±0.5	1.2±0.3	1.9±0.3	0.6±0.6	5.5±1.5	0.5±0.3	7.6±1.3 / 5.7±1.1	0.13±0.02	0.69±0.09
16/17-19	3382-3385	6	81±1	0.2±0.1	0.6±0.3	0.5±0.2	6.0±1.2	0.1±0.1	6.2±0.8	1.2±0.3	1.0±0.3 / 2.6±0.5	0.37±0.07	0.70±0.07
16/18-1	4018-4022	3	61±1	0.2±0.1	5.4±1.4	0.9±0.6	11.0±3.4	5.4±2.9	3.8±1.0	6.8±1.6	1.8±1.3 / 2.4±0.1	0.17±0.02	0.53±0.03
16/23-5	3490-3502	5	56±6	1.6±0.9	2.3±0.5	0.7±0.1	8.9±1.2	2.1±1.5	18.8±5.8	1.5±0.5	1.2±0.4 / 3.6±1.3	0.11±0.01	0.49±0.03
16/28-3	3382-3385	4	65±3	n.d	0.6±0.1	0.4±0.2	7.3±2.0	n.d	4.4±0.8	11.3±2.6	2.4±0.7 / 5.5±1.1	0.19±0.02	0.55±0.06
30/1c-3	4409-4423	8	68±2	1.3±0.3	0.5±0.2	0.4±0.1	6.4±1.0	4.4±2.3	8.2±1.9	5.5±1.0	2.0± 0.7 / 2.1±0.5	0.15±0.01	0.54±0.04
30/1c-4	4290-4302	8	61±2	2.3±0.4	0.8±0.2	1.3±0.4	3.5±1.2	0.4±0.2	19.3±4.5	2.4±0.8	2.3±0.5 / 6.3±1.1	0.15±0.02	0.77±0.06
30/1c-5	4151-4160	9	66±2	5.2±0.8	1.7±0.6	1.4±0.6	2.6±0.5	n.d	19.6±7.3	0.6±0.4	7.6±1.0 / 2.0±0.4	0.10±0.01	0.58±0.04
30/1c-6	4382-4391	6	65±3	2.7±0.5	2.1±1.4	1.1±0.5	2.7±0.6	1.2±0.5	19.5±11.8	2.9±1.2	1.6±0.6 / 2.3±1.5	0.15±0.02	0.60±0.04
30/1c-9	4400-4411	8	65±3	0.6±0.3	0.3±0.1	0.5±0.1	7.8±2.2	1.1±0.3	11.8±2.6	6.3±1.7	1.3±0.6 / 3.2±1.3	0.15±0.02	0.63±0.05
22/29-1S1	4559-4662	18	59±2	2.6±0.6	1.4±0.2	1.4±0.3	8.5±0.9	1.1 ±0.7	12.1±1.7	3.0±1.0	2.5±0.1 / 2.1±0.1	n.a	n.a
22/30a-16	5440-5482	7	59±2	n.d	1.8±0.7	2.7±1.0	14.8±3.9	0.4±0.4	8.2±2.0	5.3±1.4	0.1±0.1 / 0.2±0.1	n.a	n.a
22/30b-15S1	5242-5247	5	72±2	n.d	n.d	1.1±0.2	5.2±1.6	3.2±2.0	0.5±0.3	4.1±1.2	1.4±0.7 / 1.1±0.3	0.32±0.05	n.a

Well	TVD (m)	n	Quartz (%)	K-feldspar (%)	Plagioclase (%)	Mica (%)	QOG (%)	Dolomite (%)	Illite (%)	Kaolin (%)	Porosity (%) Primary / Secondary	Grain-size (mm)	Sorting
22/30c-G4	5705-5770	20	62±2	1.8±0.2	1.9±0.2	1.1±0.2	3.5±0.8	0.8±0.5	21.6±3.2	3.8±0.6	1.2±0.4 / 0.5±0.3	n.a	n.a
23/26a-2z	5149	2	63±3	n.d	0.5±0.5	0.5±0	6.4±0.3	n.d	11.0±5.0	9.4±1.4	2.8±1.4 / 2.9±1.0	n.a	n.a
23/26b-14	4742-4790	23	71±1	0.8±0.2	0.5±0.1	0.8±0.2	2.6±0.5	n.d	7.8±1.3	5.1±0.7	6.7±0.8 / 2.3±0.3	n.a	n.a
23/26b-15	5014-5040	10	78±2	0.1±0.1	0.4±0.2	0.6±0.3	3.4±0.8	0.6±0.6	5.9±1.0	2.9±0.6	4.5±1.2 / 1.5±0.5	n.a	n.a
29/5b-F1	5501-5594	66	57±1	0.8±0.1	5.7±0.3	n.d	10.0±0.7	0.3±0.1	13.2±1.3	4.0±0.2	2.2±0.3 / 4.8±0.4	0.14±0.01	n.a
29/5a-5	4412-4421	2	43±10	6.2±1.5	2.0±2.0	0.6±0.4	5.3±4.6	n.d	15.1±12.1	n.d	4.1±4.1 / 2.2±2.2	n.a	n.a
30/1c-4	4284-4327	5	59±2	1.2±0.6	1.5±0.5	0.9±0.2	4.8±1.1	0.7±0.4	13.4±2.6	3.6±0.9	5.9±2.5 / 3.0±0.4	0.19±0.02	0.63±0.04
30/1c-5	4177-4186	19	60±1	3.4±0.5	0.5±0.1	3.4±1.0	2.9±0.6	n.d	6.7±0.9	0.8±0.3	11.6±1.1 / 5.0±0.5	0.16±0.01	0.58±0.02
30/1c-6	4388-4421	44	52±1	0.3±0.1	2.3±0.2	2.1±0.3	6.9±0.6	4.1±1.3	14.1±2.1	5.1±0.5	6.1±0.7 / 3.3±0.3	0.15±0.01	0.56±0.02
Average	4770	265	61.0	6.6	1.5	2.2	3.9	11.8	1.4	1.2	3.9 / 3.3	0.16	0.59

TVD = true vertical depth; QOG = quartz overgrowth; n.d = not detected; n.a = data not available

Table A 4.2 Point-count data

Well	*TVD (m)	**n	Quartz (%)	K-feldspar (%)	Plagioclase (%)	Mica (%)	QOG (%)	Dolomite (%)	Illite (%)	Kaolin (%)	Primary porosity (%)	Secondary porosity (%)	Grain-size (mm)	Sorting coefficient
15/17-P46	2389.33	300	81	2	5	2	1	4	4	0	11	4	0.21	0.95
15/17-P46	2389.94	300	83	4	3	1	2	0	3	2	9	3	0.14	0.72
15/17-P46	2390.85	300	81	3	6	0	2	0	4	0	7	9	0.12	0.46
15/17-P46	2391.61	300	77	2	5	1	3	0	10	0	8	8	0.12	0.53
15/17-P46	2393.90	300	66	4	6	3	2	0	11	0	3	5	0.08	0.79
16/17-19	4242.8	300	81	0	1	1	3	0	8	2	2	1	0.53	0.52
16/17-19	4249.2	300	79	0	0	0	9	1	5	2	0	4	0.40	0.71
16/17-19	4250.7	300	82	0	0	0	6	0	9	0	1	1	0.44	0.98
16/17-19	4251.7	300	83	1	1	1	2	0	4	2	2	3	0.51	0.71
16/17-19	4253.8	300	79	0	1	0	7	0	6	1	1	4	0.36	0.68
16/17-19	4261.1	300	82	0	0	0	8	0	5	1	0	2	0.43	0.57
16/18-1	4018.10	300	63	0	8	2	5	9	3	10	4	2	0.14	0.50
16/18-1	4019.40	300	65	0	5	0	12	8	3	4	1	3	0.20	0.60
16/18-1	4021.76	300	64	0	3	1	17	0	6	8	0	2	0.16	0.50
16/23-5	3489.96	300	54	1	3	1	10	0	27	1	1	3	0.10	0.58
16/23-5	3491.33	300	55	0	2	1	10	0	28	2	0	1	0.11	0.51
16/23-5	3491.94	300	37	5	4	1	7	0	31	0	1	1	0.07	0.50
16/23-5	3496.21	300	77	1	1	0	6	8	4	2	3	4	0.15	0.41
16/23-5	3502.30	300	69	1	2	0	14	3	7	3	1	8	0.12	0.45
16/28-3	3381.59	300	76	0	0	1	3	0	3	16	3	5	0.16	0.50
16/28-3	3382.75	300	74	0	1	0	13	0	4	6	4	9	0.15	0.62
16/28-3	3383.75	300	73	0	1	0	9	0	6	9	1	4	0.21	0.40
16/28-3	3384.75	300	61	0	1	0	7	0	6	17	1	4	0.23	0.66
21/13b-2	3647.8	300	41	8	0	1	5	26	18	0	0	0	n.a	n.a
30/1c-3	4408.84	250	73	3	1	0	2	0	13	6	2	4	0.10	0.47
30/1c-3	4409.90	250	78	2	0	0	7	2	3	7	2	1	0.10	0.46
30/1c-3	4410.55	250	64	0	0	0	9	18	6	3	2	2	0.15	0.53

Well	*TVD (m)	**n	Quartz (%)	K-feldspar (%)	Plagioclase (%)	Mica (%)	QOG (%)	Dolomite (%)	Illite (%)	Kaolin (%)	Primary porosity (%)	Secondary porosity (%)	Grain-size (mm)	Sorting coefficient
30/1c-3	4414.86	250	70	1	1	0	11	6	5	4	1	2	0.20	0.42
30/1c-3	4415.87	250	67	1	0	1	7	11	6	8	1	3	0.19	0.54
30/1c-3	4416.91	250	64	1	1	0	5	0	18	10	0	1	0.13	0.67
30/1c-3	4418.72	250	80	0	0	0	6	0	4	1	7	4	0.18	0.46
30/1c-3	4422.60	250	73	1	0	0	6	0	12	6	0	0	0.14	0.75
30/1c-4	4289.72	250	72	1	0	0	12	1	5	8	2	8	0.17	0.69
30/1c-4	4292.43	250	69	4	1	3	3	0	18	1	4	5	0.10	0.73
30/1c-4	4295.30	250	63	2	0	3	0	0	31	0	0	5	0.06	0.96
30/1c-4	4296.50	250	70	1	2	1	5	1	10	2	2	13	0.25	0.56
30/1c-4	4297.53	250	50	2	0	0	0	0	46	1	0	3	0.15	1.02
30/1c-4	4300.88	250	72	3	1	0	2	0	18	1	2	5	0.15	0.70
30/1c-4	4300.95	250	61	2	1	3	3	0	24	3	3	5	0.13	0.61
30/1c-4	4301.67	250	72	4	0	0	5	0	13	5	4	7	0.22	0.87
30/1c-5	4150.50	250	59	4	1	2	1	0	31	1	2	2	0.06	0.76
30/1c-5	4151.10	250	66	6	2	3	0	0	20	0	4	0	0.09	0.54
30/1c-5	4151.30	250	77	2	0	0	6	0	12	1	11	2	0.11	0.56
30/1c-5	4151.60	250	70	4	0	0	5	0	18	4	10	4	0.19	0.80
30/1c-5	4157.32	250	67	6	1	3	2	0	20	0	3	2	0.08	0.43
30/1c-5	4157.60	250	73	8	0	1	2	0	15	0	9	2	0.08	0.44
30/1c-5	4158.00	250	81	6	6	0	2	0	5	0	11	1	0.08	0.47
30/1c-5	4159.00	250	80	3	2	0	2	0	13	0	9	1	0.11	0.58
30/1c-5	4159.90	250	81	5	3	1	3	0	8	0	8	3	0.10	0.65
30/1c-6	4381.50	250	77	2	0	0	5	1	13	1	3	2	0.14	0.50
30/1c-6	4382.53	250	60	2	0	1	0	0	35	1	0	1	0.11	0.78
30/1c-6	4385.49	250	72	2	0	0	2	0	21	3	1	4	0.19	0.53
30/1c-6	4393.32	250	54	4	2	1	2	1	26	9	0	1	0.20	0.55
30/1c-6	4398.35	250	69	3	1	3	4	4	15	1	2	2	0.13	0.64
30/1c-6	4391.25	250	72	5	1	1	4	2	12	3	4	3	0.11	0.57

Well	*TVD (m)	**n	Quartz (%)	K-feldspar (%)	Plagioclase (%)	Mica (%)	QOG (%)	Dolomite (%)	Illite (%)	Kaolin (%)	Primary porosity (%)	Secondary porosity (%)	Grain-size (mm)	Sorting coefficient
30/1c-9	4400.42	250	72	0	0	0	11	2	10	3	0	3	0.11	0.57
30/1c-9	4400.88	250	64	1	0	0	21	2	6	4	0	0	0.17	0.50
30/1c-9	4404.03	250	72	0	1	0	6	0	9	9	3	4	0.19	0.59
30/1c-9	4404.11	250	66	0	1	0	7	1	6	18	3	6	0.20	0.46
30/1c-9	4404.65	250	72	0	0	1	8	0	8	10	4	10	0.24	0.61
30/1c-9	4406.35	250	67	0	0	1	9	0	19	2	0	1	0.08	0.67
30/1c-9	4406.95	250	62	2	0	1	1	0	26	5	0	0	0.08	0.74
30/1c-9	4411.16	250	70	0	0	1	1	2	12	2	0	0	0.10	0.92

*TVD = true vertical depth; **n = number of point count

Table A 4.3 XRD results of the Pentland Sandstone

Well	TVD (m)	Quartz (%)	K-feldspar (%)	Plagioclase (%)	Kaolinite (%)	Illite (%)	Montmorillonite (%)	Chlorite (%)	Muscovite (%)	Pyrite (%)	Calcite (%)	Dolomite (%)	Ankerite (%)	Siderite (%)	Anatase (%)	Brookite (%)	Total (%)
15/17-P46	2389.33	91	1	3	0	2	0	0	0	0	1	0	0	0	0	0	100
15/17-P46	2389.94	88	3	3	1	2	0	0	0	0	1	0	0	0	0	0	100
15/17-P46	2390.85	87	3	6	1	1	0	1	0	1	1	0	0	0	0	0	100
15/17-P46	2391.61	86	2	5	2	3	0	0	1	1	0	0	0	0	0	0	100
15/17-P46	2393.90	74	4	6	6	4	0	1	2	1	0	0	0	0	1	0	100
16/28-3	3381.59	79	0	1	13	2	0	2	1	0	0	0	0	0	0	0	100
16/28-3	3382.75	91	0	2	3	2	0	1	0	0	1	0	0	0	0	0	100
16/28-3	3383.75	90	0	2	3	3	0	0	0	0	0	0	0	0	0	0	100
16/28-3	3384.75	85	1	2	8	1	0	1	0	0	0	0	0	0	1	0	100
16/23-5	3489.96	86	1	2	4	3	0	1	2	0	0	0	0	0	0	1	100
16/23-5	3491.33	85	0	1	5	4	1	1	2	0	0	0	0	0	0	1	100
16/23-5	3491.94	64	3	2	21	4	0	1	2	1	0	0	0	0	2	0	100
16/23-5	3496.21	88	1	2	1	1	0	0	1	0	0	2	2	0	0	0	100
21/13b-2	3631.39	45	1	0	7	35	1	1	5	2	1	0	0	0	1	1	99
21/13b-2	3632.00	50	0	0	5	34	0	1	4	2	1	0	0	0	1	1	99
21/13b-2	3634.97	43	1	0	7	27	0	2	4	2	0	11	2	0	1	0	100
21/13b-2	3641.75	55	1	2	6	21	1	1	4	1	0	5	1	0	1	0	100
21/13b-2	3647.85	51	0	2	8	6	1	2	2	0	0	22	4	0	0	1	100
16/18-1	4018.10	76	0	10	5	3	0	1	1	0	0	1	2	1	1	0	100
16/18-1	4019.40	87	0	7	1	1	0	0	0	0	0	1	2	0	0	0	100
16/18-1	4021.53	87	1	7	2	1	0	0	0	0	0	0	0	0	0	0	100

Well	TVD (m)	Quartz (%)	K-feldspar (%)	Plagioclase (%)	Kaolinite (%)	Illite (%)	Montmorillonite (%)	Chlorite (%)	Muscovite (%)	Pyrite (%)	Calcite (%)	Dolomite (%)	Ankerite (%)	Siderite (%)	Anatase (%)	Brookite (%)	Total (%)
30/1c-5	4150.50	71	1	11	1	12	0	1	0	0	1	0	0	0	1	1	100
30/1c-5	4151.30	83	0	10	0	3	0	1	1	0	0	0	0	0	1	0	100
30/1c-5	4157.60	68	10	16	0	3	0	0	1	0	0	0	0	0	1	0	100
30/1c-5	4159.00	80	7	9	0	2	0	0	1	0	0	0	0	0	0	0	100
30/1c-5	4159.90	88	2	2	0	4	0	0	2	0	0	0	0	0	1	0	100
16/17-19	4242.82	92	0	2	1	3	0	0	1	0	0	0	0	0	0	0	100
16/17-19	4250.74	93	0	1	0	3	0	0	1	0	0	0	0	0	0	0	100
16/17-19	4251.66	88	1	2	1	5	0	0	1	0	0	0	0	0	0	0	100
16/17-19	4261.10	94	0	2	0	2	0	0	0	0	0	0	0	0	0	0	100
22/30C-G4	5704.00	91	0	2	3	2	0	0	1	0	0	0	0	0	0	0	100
22/30C-G4	5708.28	88	0	7	1	3	0	0	0	0	0	0	0	0	0	0	100
22/30C-G4	5715.40	69	1	12	7	6	0	1	3	0	0	0	0	0	0	0	100
22/30C-G4	5739.45	85	1	8	4	1	0	1	0	0	0	0	0	0	0	0	100
22/30C-G4	5743.30	81	0	7	1	6	0	0	2	0	0	1	0	0	0	0	100
22/30C-G4	5748.02	79	0	14	1	4	0	0	1	0	0	0	0	0	0	0	100
22/30C-G4	5756.45	63	4	11	4	6	1	1	3	0	0	2	3	1	0	0	100
22/30C-G4	5763.25	67	1	11	1	10	1	1	1	0	0	0	0	5	1	0	100
22/30C-G4	5768.45	82	1	10	2	3	0	0	1	0	1	0	0	0	0	0	100

Table A 4.4 XRD results of the Pentland Shale

Well	TVD (m)	Quartz (%)	K-feldspar (%)	Plagioclase (%)	Kaolinite (%)	Illite (%)	Montmorillonite (%)	Chlorite (%)	Muscovite (%)	Pyrite (%)	Calcite (%)	Dolomite (%)	Ankerite (%)	Siderite (%)	Anatase (%)	Brookite (%)	Total (%)
15/17-P46	2380.8	25	4	4	24	25	2	2	6	4	1	0	0	0	2	0	99
15/17-P46	2381.4	31	5	5	20	23	1	2	6	4	2	0	0	0	2	0	99
15/17-P46	2382.0	47	3	4	16	17	1	2	4	3	1	0	0	0	1	0	99
16/17-19	4243.1	8	5	1	37	26	5	4	8	0	0	0	0	0	4	0	99
16/17-19	4244.8	9	4	1	36	30	4	2	8	1	0	0	0	0	5	0	99
16/17-19	4252.0	13	5	2	30	27	1	2	8	3	0	0	0	4	6	0	99
16/17-19	4253.2	4	4	2	46	21	4	2	7	3	1	0	0	0	6	0	99
16/17-19	4262.5	6	4	2	39	22	3	3	7	7	1	0	0	0	5	0	100
16/18-1	4023.1	16	3	2	27	36	1	2	7	0	0	0	0	0	5	0	99
16/18-1	4024.6	20	3	3	28	30	3	2	6	0	1	0	0	0	3	0	99
16/23-5	3494.4	31	3	2	33	18	1	2	5	1	0	0	0	0	4	0	99
16/23-5	3498.3	7	1	0	40	24	1	2	7	10	1	1	0	0	5	0	100
16/23-5	3500.2	21	3	1	35	21	1	2	7	3	1	1	0	0	4	0	99
16/23-5	3501.3	21	2	1	35	19	2	2	5	6	0	0	0	1	4	0	99
16/23-5	3503.4	12	2	0	35	20	2	3	6	15	1	0	0	0	4	1	99
16/28-3	3385.0	10	3	2	42	19	3	4	8	2	1	0	0	0	5	0	100
16/28-3	3386.5	2	4	2	52	16	5	3	9	0	1	0	0	0	4	1	99
16/28-3	3387.2	25	3	2	34	20	2	2	6	0	0	0	0	0	5	1	99
16/28-3	3388.2	10	3	2	42	21	4	3	7	0	1	0	0	0	5	0	99
16/28-3	3389.8	5	3	1	50	22	4	1	7	0	0	0	0	0	5	1	99

Well	TVD (m)	Quartz (%)	K-feldspar (%)	Plagioclase (%)	Kaolinite (%)	Illite (%)	Montmorillonite (%)	Chlorite (%)	Muscovite (%)	Pyrite (%)	Calcite (%)	Dolomite (%)	Ankerite (%)	Siderite (%)	Anatase (%)	Brookite (%)	Total (%)
21/13b-2	3516.8	11	3	1	8	19	2	2	6	0	2	23	22	0	0	1	100
21/13b-2	3517.8	12	2	1	10	24	0	2	6	0	1	23	17	0	1	0	99
21/13b-2	3519.0	16	2	1	12	27	2	1	7	0	1	17	12	0	0	0	100
21/13b-2	3519.5	14	2	2	11	24	4	2	7	0	1	17	13	0	1	0	99
22/25b-4S1	4788.4	25	2	1	30	30	0	2	6	0	0	0	0	0	3	0	99
22/29-1	4579.6	14	4	1	20	46	1	2	7	0	0	0	0	0	2	0	99
22/30a-16	5492.1	19	3	2	38	21	2	1	7	1	0	0	0	0	5	1	99
22/30a-16	5492.7	23	3	1	36	20	2	2	6	0	0	0	0	0	6	0	99
22/30a-16	5493.9	8	2	1	35	35	1	1	10	1	0	0	0	0	3	1	98
29/5a-5	4396.1	30	9	3	2	44	1	2	7	0	0	1	0	0	1	0	100

Table A 4.5 Mineralogy of the clay separates from Pentland Shale measured by XRD analysis

Well	Depth (m)	Kaolin %	Illite %	Chlorite %
15/17-P46	2381.4	37	63	n.d.
15/17-P46	2382.0	86	14	n.d.
16/23-5	3494.44	66	35	n.d.
16/23-5	3498.37	77	23	n.d.
21/13b-2	3519.0	27	70	3
16/18-1	4023.1	40	60	n.d.
16/17-19	4262.5	59	41	n.d.
22/25b-4S1	4788.4	61	39	n.d.
22/29-1	4579.6	17	83	n.d.
22/30a-16	5492.7	70	30	n.d.
22/30a-16	5493.9	39	60	n.d.

n.d. = not detected

Table A 4.6 XRF major element analysis results of the Pentland Sandstone. LOI = Loss on ignition.

Well	TVD (m)	SiO_2 (%)	Al_2O_3 (%)	Fe_2O_3 (%)	MgO (%)	CaO (%)	Na_2O (%)	K_2O (%)	TiO_2 (%)	MnO (%)	P_2O_5 (%)	LOI (%)	Total (%)
15/17-P46	2389.30	92.38	2.30	0.56	0.37	0.68	0.22	0.66	0.27	0.02	0.04	2.52	100.01
15/17-P46	2389.90	88.56	2.81	0.74	0.24	0.24	0.18	0.91	0.38	0.01	0.04	5.89	99.99
15/17-P46	2390.90	87.75	2.71	1.19	0.22	0.21	0.28	0.88	0.63	0.01	0.06	6.07	100.00
15/17-P46	2391.60	83.50	3.89	1.33	0.26	0.13	0.27	0.99	0.50	0.01	0.05	9.07	99.99
15/17-P46	2393.90	79.27	5.95	2.53	0.36	0.18	0.34	1.32	0.76	0.01	0.08	9.20	100.00
16/23-5	3490.00	86.76	5.41	0.55	0.18	0.13	0.06	0.23	0.85	0.00	0.05	5.78	99.99
16/23-5	3491.30	87.70	5.45	0.57	0.20	0.11	0.11	0.28	0.85	0.00	0.05	4.67	99.99
16/23-5	3496.20	89.16	2.34	1.14	0.79	1.92	-0.06	0.13	0.35	0.02	0.03	4.19	100.01
21/13b-2	3631.40	64.29	14.24	6.01	2.23	0.69	0.22	3.36	0.76	0.03	0.43	7.73	100.00
21/13b-2	3632.10	61.64	13.96	6.34	2.10	0.43	0.22	3.47	0.76	0.05	0.23	10.81	100.01
21/13b-2	3635.00	56.93	13.24	5.28	4.38	4.20	0.13	3.03	0.71	0.05	0.20	11.86	100.01
21/13b-2	3641.80	65.88	12.27	4.39	3.38	2.38	0.05	2.67	0.74	0.04	0.19	8.03	100.01
21/13b-2	3647.80	58.98	7.91	2.20	6.89	7.94	-0.01	0.96	0.14	0.09	0.05	14.85	99.99
16/17-19	4250.70	96.16	1.83	0.15	0.21	0.16	-0.07	0.42	0.15	0.00	0.05	0.95	100.01
16/17-19	4251.70	92.17	3.85	0.48	0.21	0.13	-0.04	0.83	0.35	0.00	0.07	1.94	99.99
16/17-19	4242.80	96.04	1.86	0.17	0.14	0.22	NA	0.34	0.15	NA	0.17	0.99	100.09
16/17-19	4253.80	96.89	1.61	0.13	0.11	0.00	NA	0.34	0.11	NA	0.01	0.85	100.06
16/17-19	4288.50	96.30	1.72	0.32	0.13	0.06	NA	0.32	0.07	0.00	0.02	1.00	99.93
16/28-3	3381.59	89.90	5.63	0.46	0.18	0.09	0.03	0.36	0.52	0.00	0.08	2.75	100.00
16/28-3	3382.75	92.03	2.78	0.49	0.19	0.24	0.10	0.31	0.50	0.00	0.05	3.30	99.99
16/28-3	3383.75	92.97	3.05	0.19	0.17	0.31	0.04	0.24	0.29	0.00	0.14	2.61	100.01
16/28-3	3384.75	90.69	5.01	0.29	0.17	0.22	-0.07	0.22	0.51	0.00	0.15	2.81	100.00
16/18-1	4018.10	83.19	6.64	1.82	0.83	1.40	0.76	0.40	0.51	0.02	0.06	4.39	100.01

Well	TVD (m)	SiO_2 (%)	Al_2O_3 (%)	Fe_2O_3 (%)	MgO (%)	CaO (%)	Na_2O (%)	K_2O (%)	TiO_2 (%)	MnO (%)	P_2O_5 (%)	LOI (%)	Total (%)
16/18-1	4019.40	91.87	2.91	0.75	0.60	1.01	0.52	0.18	0.34	0.01	0.04	1.79	100.01
16/18-1	4021.80	93.40	3.38	0.49	0.28	0.18	0.59	0.23	0.41	0.00	0.03	1.01	100.00
30/1c-5	4150.50	84.72	7.19	2.30	0.58	0.04	0.94	1.40	0.67	0.00	0.02	2.12	99.98
30/1c-5	4151.30	90.48	3.77	2.23	0.43	0.05	0.62	0.53	0.38	0.00	0.06	1.37	99.93
30/1c-5	4157.60	87.06	5.95	0.47	0.27	0.18	1.24	2.49	0.60	0.01	0.01	1.51	99.80
30/1c-5	4159.00	90.89	4.31	0.26	0.22	0.00	0.61	1.90	0.31	NA	0.01	1.34	99.87
30/1c-5	4159.90	92.86	2.38	0.48	0.22	0.12	0.18	0.97	0.48	0.01	0.01	2.14	99.84
22/30c-G4	5704.00	94.24	2.38	0.79	0.29	0.02	0.09	0.33	0.29	0.00	0.01	1.31	99.75
22/30c-G4	5707.68	95.77	1.83	0.16	0.18	0.04	0.22	0.17	0.30	NA	0.01	0.93	99.61
22/30c-G4	5715.40	86.13	8.42	0.45	0.24	0.13	1.06	0.87	0.34	NA	0.01	2.29	99.96
22/30c-G4	5719.80	91.28	4.21	0.35	0.22	0.14	0.73	0.45	0.26	NA	0.02	1.99	99.64
22/30c-G4	5748.02	91.14	4.14	0.85	0.32	0.12	1.12	0.40	0.16	0.00	0.02	1.60	99.87
22/30c-G4	5768.45	90.94	4.73	0.50	0.25	0.10	1.22	0.48	0.20	NA	0.02	1.32	99.76
22/30c-G4	5743.30	87.37	6.28	0.67	0.60	0.32	1.34	0.80	0.35	0.00	0.05	1.88	99.66
22/30c-G4	5739.45	93.59	3.55	0.33	0.20	0.08	0.75	0.22	0.09	NA	0.01	1.12	99.94
22/30c-G4	5756.45	78.67	8.60	2.77	1.05	1.46	1.51	0.96	0.39	0.03	0.02	4.31	99.77
22/30c-G4	5763.25	78.84	7.04	5.69	1.04	0.18	1.08	1.01	0.58	0.05	0.02	4.11	99.64

Table A 4.7 XRF trace element analysis results of the Pentland Sandstone. Units of the trace elements: ppm.

Well	TVD (m)	Zn	Cu	Ni	Cr	V	Ba	Sc	La	Ce	Nd	U	Th	Pb	Nb	Zr	Y	Sr	Rb
15/17-P46	2389.30	4.7	3.1	NA	25.8	8.5	184.6	1.1	5.0	22.5	8.3	0.8	2.1	4.4	6.4	283.7	5.3	41.3	13.1
15/17-P46	2389.90	13.1	4.7	2.4	37.3	11.2	247.6	1.9	9.5	31.7	11.7	1.9	3.4	6.1	8.3	352.8	7.8	47.6	18.1
15/17-P46	2390.90	8.4	9.2	2.1	80.5	13.1	232.1	2.8	19.2	61.0	24.2	2.8	8.1	7.8	13.5	1057.2	16.0	46.9	16.6
15/17-P46	2391.60	65.1	16.9	20.5	45.7	27.1	230.2	3.7	15.9	45.1	19.5	1.5	4.5	8.5	11.5	362.8	9.8	62.8	22.7
15/17-P46	2393.90	48.2	7.1	18.4	80.2	36.9	266.1	6.6	20.0	54.5	23.1	2.0	6.2	10.1	18.9	597.4	17.7	69.6	34.2
16/23-5	3490.00	25.0	4.9	8.1	94.1	32.2	1054.4	6.3	7.0	21.4	7.6	0.7	2.7	4.5	23.0	279.5	7.3	153.4	7.0
16/23-5	3491.30	14.0	7.0	7.2	99.7	28.5	2373.9	5.5	7.9	16.9	2.8	0.9	3.2	4.1	21.5	333.2	7.3	152.4	8.1
16/23-5	3496.20	55.2	4.1	5.4	47.6	10.8	1090.8	2.9	1.3	7.8	0.7	0.4	1.5	2.2	8.5	186.6	6.6	72.8	3.9
21/13b-2	3631.40	24.7	22.2	42.9	108.8	100.4	4201.7	19.4	31.9	56.1	20.7	2.5	9.8	17.0	20.3	233.1	31.0	232.3	94.0
21/13b-2	3632.10	38.0	45.0	45.7	106.1	98.6	9117.9	18.8	32.1	29.5	-1.1	3.2	10.0	19.5	20.5	244.8	27.6	238.8	98.4
21/13b-2	3635.00	22.4	18.6	36.7	106.2	90.0	1175.7	14.7	38.5	78.9	31.2	1.8	9.9	13.3	19.6	215.6	25.7	182.1	85.4
21/13b-2	3641.80	20.5	20.5	33.9	145.3	89.3	571.5	13.4	30.3	67.0	28.9	2.8	8.5	15.4	18.3	213.8	23.1	116.9	75.4
21/13b-2	3647.80	13.8	10.3	13.8	35.9	39.8	749.9	8.7	6.4	12.3	6.2	0.4	1.8	6.3	4.7	47.0	8.0	45.2	25.0
16/17-19	4250.70	8.5	2.2	NA	5.9	13.4	299.0	2.1	1.3	9.3	2.7	0.3	1.6	2.8	3.8	55.5	4.5	55.7	10.5
16/17-19	4251.70	22.7	3.8	0.4	18.3	29.6	336.8	3.3	5.3	19.1	7.0	1.0	2.9	5.5	9.3	107.9	7.9	60.9	22.2
16/17-19	4242.80	12.1	1.5	NA	4.2	14.4	248.7	2.8	2.9	10.3	4.2	0.5	1.9	2.6	4.7	52.9	9.2	35.2	8.7
16/17-19	4253.80	14.7	0.2	0.8	2.7	7.6	101.5	1.7	0.6	7.3	2.9	0.0	1.2	3.5	4.2	46.8	3.1	24.2	8.3
16/17-19	4288.50	17.0	NA	NA	2.8	5.7	592.2	2.3	2.6	8.2	2.8	0.3	0.7	5.0	3.1	40.6	2.6	39.0	7.4
16/28-3	3381.59	16.6	10.1	0.4	57.0	41.3	959.3	6.9	29.4	58.6	22.6	0.6	1.4	24.2	15.3	81.7	4.7	145.8	6.6
16/28-3	3382.75	65.5	6.7	2.0	81.3	15.0	4722.8	1.7	41.9	74.5	24.4	0.7	21.5	68.3	10.8	278.1	7.7	114.2	4.8
16/28-3	3383.75	41.3	7.7	0.2	41.3	18.3	3496.9	2.5	15.6	23.9	5.4	0.0	3.3	57.3	9.5	72.5	9.7	130.5	3.8
16/28-3	3384.75	14.6	11.1	1.5	63.2	47.2	1190.8	7.8	53.4	104.3	37.9	0.4	2.0	19.1	17.3	116.4	10.0	270.0	5.2
16/18-1	4018.10	32.0	7.8	20.3	98.8	31.1	573.3	6.1	8.0	23.9	8.5	0.6	2.1	12.0	12.4	250.0	7.2	63.0	12.5

16/18-1	4019.40	38.7	6.6	5.2	109.9	18.3	447.2	4.8	1.8	13.8	3.7	0.5	1.2	4.6	7.0	317.1	3.9	40.5	5.1
16/18-1	4021.80	114.2	10.2	11.0	117.9	19.1	278.1	2.2	4.2	18.4	6.8	0.3	1.6	8.9	8.4	326.2	4.8	38.5	6.9
30/1c-5	4150.50	21.4	8.3	13.8	71.5	41.9	1119.9	8.1	10.9	36.1	15.0	1.2	2.8	11.7	11.3	378.7	15.4	64.1	30.5
30/1c-5	4151.30	NA	NA	NA	NA	NA	NA	NA	NA	NA	NA	NA	NA	NA	NA	NA	NA	NA	NA
30/1c-5	4157.60	NA	NA	NA	NA	NA	NA	NA	NA	NA	NA	NA	NA	NA	NA	NA	NA	NA	NA
30/1c-5	4159.00	NA	NA	NA	NA	NA	NA	NA	NA	NA	NA	NA	NA	NA	NA	NA	NA	NA	NA
30/1c-5	4159.90	NA	NA	NA	NA	NA	NA	NA	NA	NA	NA	NA	NA	NA	NA	NA	NA	NA	NA
22/30c-G4	5704.00	1.7	4.5	2.5	35.2	6.4	81.3	2.8	1.4	13.1	4.8	0.7	1.4	3.3	5.0	229.8	7.6	24.0	8.8
22/30c-G4	5707.68	2.2	3.4	2.1	159.7	6.4	193.2	3.8	2.5	36.5	12.1	1.1	3.1	6.7	5.5	1296.5	11.8	39.5	4.5
22/30c-G4	5715.40	NA	NA	NA	NA	NA	NA	NA	NA	NA	NA	NA	NA	NA	NA	NA	NA	NA	NA
22/30c-G4	5719.80	5.6	5.5	9.1	59.8	18.9	190.3	2.7	7.1	23.7	9.4	0.4	1.4	11.8	5.0	240.3	5.2	51.0	11.7
22/30c-G4	5748.02	533.2	5.0	5.8	29.1	10.9	160.0	2.3	4.5	19.1	9.7	0.1	1.0	8.1	3.3	90.4	6.6	57.2	11.2
22/30c-G4	5768.45	40.0	5.6	7.1	32.8	15.9	187.4	2.4	8.0	26.4	11.7	0.1	1.0	9.3	4.9	91.6	5.7	54.7	13.2
22/30c-G4	5743.30	23.3	8.3	7.7	79.6	19.3	194.7	4.4	9.2	27.4	11.6	0.7	2.1	9.6	7.3	251.5	7.5	65.9	20.8
22/30c-G4	5739.45	NA	4.6	2.6	16.0	8.0	95.0	2.1	3.1	13.0	5.6	NA	0.9	5.6	1.9	47.2	2.5	46.1	6.2
22/30c-G4	5756.45	15.4	7.8	17.5	86.9	32.6	287.5	4.6	20.7	45.5	23.2	0.7	2.1	9.7	7.4	187.1	10.4	89.3	24.4
22/30c-G4	5763.25	21.5	10.6	18.6	137.6	26.2	184.0	7.5	7.5	32.3	14.5	1.0	3.7	8.3	11.2	617.0	16.1	57.4	27.6

Table A 4.8 XRF major element analysis of the Pentland Shale. LOI = Loss on ignition.

Well	TVDSS (m)	SiO_2 (%)	Al_2O_3 (%)	Fe_2O_3 (%)	MgO (%)	CaO (%)	Na_2O (%)	K_2O (%)	TiO_2 (%)	MnO (%)	P_2O_5 (%)	LOI (%)	Total (%)
15/17-P46	2380.8	53.7	18.4	7.0	1.1	0.3	0.3	3.3	1.6	0.1	0.1	14.1	100.0
15/17-P46	2381.4	56.7	17.7	7.1	1.1	0.2	0.3	3.3	1.6	0.1	0.1	11.7	100.0
15/17-P46	2382.0	64.2	13.8	5.3	0.8	0.2	0.1	2.6	1.1	0.0	0.1	11.8	100.0
16/17-19	4231.1	48.0	27.4	2.1	0.5	0.1	0.2	3.1	3.0	0.0	0.2	15.3	100.0
16/17-19	4244.8	49.9	27.9	2.0	0.6	0.2	0.2	3.4	3.0	0.0	0.2	12.7	100.0
16/17-19	4252.0	48.5	24.9	6.7	0.5	0.6	0.1	3.0	3.6	0.1	1.0	10.9	100.0
16/17-19	4253.2	40.8	25.0	3.4	0.8	0.5	0.5	2.2	3.2	0.0	0.6	23.1	100.0
16/17-19	4262.5	42.6	26.1	7.6	0.4	0.1	0.1	2.3	3.2	0.0	0.2	17.4	100.0
16/18-1	4020.2	54.8	25.3	2.8	1.5	0.8	0.5	4.0	3.0	0.0	0.6	6.7	100.0
16/18-1	4023.1	55.4	25.9	2.3	1.4	0.1	0.4	3.7	3.3	0.0	0.2	7.4	100.0
16/18-1	4023.6	41.0	18.9	17.0	2.3	0.6	0.3	2.6	2.6	0.2	0.2	14.2	100.0
16/18-1	4024.0	52.6	27.4	3.1	1.7	0.1	0.3	3.9	2.9	0.0	0.2	7.8	100.0
16/18-1	4024.6	58.9	24.8	1.6	1.0	0.1	0.4	3.4	2.7	0.0	0.1	7.0	100.0
16/23-5	3498.4	45.3	20.5	9.5	0.7	0.4	0.2	1.8	2.4	0.0	0.4	18.9	100.0
16/23-5	3494.4	53.3	18.6	2.2	0.4	0.1	0.1	1.9	2.4	0.0	0.1	20.9	100.0
16/23-5	3500.2	38.8	24.1	9.4	0.5	0.3	0.1	1.9	2.6	0.0	0.5	21.8	100.0
16/23-5	3501.3	47.2	21.8	4.4	0.5	0.3	0.2	1.8	2.2	0.0	0.6	20.9	100.0
16/23-5	3503.4	37.3	21.4	12.9	0.5	0.4	0.2	1.6	1.9	0.0	1.2	22.7	100.0
16/28-3	3385.0	48.2	27.3	3.5	0.5	0.2	0.2	2.1	3.2	0.0	0.2	14.6	100.0
16/28-3	3386.5	38.2	26.2	1.5	0.6	0.2	0.3	1.9	2.1	0.0	0.1	28.9	100.0
16/28-3	3387.2	55.1	24.0	1.6	0.5	0.2	0.2	2.1	3.1	0.0	0.2	13.2	100.0
16/28-3	3388.2	50.2	28.9	1.9	0.6	0.2	0.2	2.5	3.0	0.0	0.2	12.2	100.0
16/28-3	3389.8	43.1	26.9	1.5	0.6	0.3	0.4	2.0	2.4	0.0	0.3	22.4	100.0
22/25b-4S1	4788.4	62.1	24.6	1.3	0.7	0.1	0.0	3.6	2.0	0.0	0.1	5.4	100.0

22/29-1	4579.6	56.8	25.6	2.2	1.0	0.2	0.3	5.0	1.5	0.0	0.1	7.4	100.0
22/30a-16	5492.1	43.1	21.6	1.4	0.5	0.3	0.2	1.6	3.2	0.0	0.2	28.0	100.0
22/30a-16	5492.7	55.2	24.4	1.2	0.4	0.2	0.2	1.9	3.9	0.0	0.1	12.5	100.0
22/30a-16	5493.9	46.4	27.6	2.3	0.9	0.3	0.3	3.4	1.4	0.0	0.1	17.4	100.0
29/5a-5	4396.1	61.0	15.3	5.8	1.5	0.1	0.4	5.4	0.9	0.0	0.1	9.1	99.6

Table A 4.9 XRF TRACE element analysis of the Pentland Shale. Units of the trace elements: ppm.

Well	TVD (m)	Zn	Cu	Ni	Cr	V	Ba	Sc	La	Ce	Nd	U	Th	Pb	Nb	Zr	Y	Sr	Rb
15/17-P46	2389.30	112.3	22.1	37.1	103.4	124.2	339.1	22.3	53.8	110.6	50.2	2.8	13.1	35.6	50.1	345.4	33.1	123.0	103.6
15/17-P46	2389.90	NA	NA	NA	NA	NA	NA	NA	NA	NA	NA	NA	NA	NA	NA	NA	NA	NA	NA
15/17-P46	2390.90	81.7	19.6	31.7	89.5	87.6	284.3	17.2	44.7	94.6	42.9	6.7	11.1	28.5	37.3	287.5	29.4	89.2	75.1
16/17-19	4231.1	101.3	28.9	41.8	143.8	319.1	806.1	32.3	109.1	194.6	86.5	3.8	12.4	37.5	90.3	344.7	34.9	514.1	157.6
16/17-19	4244.8	85.8	23.3	31.0	131.3	330.7	1347.8	29.5	106.1	183.4	83.7	4.5	13.3	35.2	90.0	342.9	34.2	523.5	159.4
16/17-19	4252.0	60.0	33.7	35.4	148.8	336.3	910.6	30.5	86.3	177.9	80.7	2.6	12.7	42.5	105.4	357.2	42.2	2746.3	121.2
16/17-19	4253.2	112.9	54.4	90.4	170.0	334.7	985.8	33.4	121.8	258.5	128.0	3.9	10.0	117.1	88.3	336.3	36.4	1608.6	98.0
16/17-19	4262.5	56.8	51.4	45.4	186.7	238.2	603.9	30.9	97.0	167.1	72.5	3.7	15.9	23.0	112.1	276.1	25.2	436.8	133.7
16/18-1	4020.2	88.8	26.0	79.7	181.1	245.6	727.4	21.1	70.6	150.5	68.1	2.5	10.5	27.1	73.3	308.6	34.6	849.6	62.4
16/18-1	4023.1	57.3	35.4	63.6	296.9	333.0	818.1	37.2	99.4	189.0	84.8	3.5	15.8	21.7	107.2	383.2	38.0	252.6	141.8
16/18-1	4023.6	59.0	42.1	118.5	244.8	263.7	744.1	42.0	74.0	156.4	70.2	3.2	13.0	20.7	82.4	304.4	44.4	191.8	103.7
16/18-1	4024.0	57.0	40.5	88.4	261.7	255.2	1011.2	41.8	111.6	206.4	89.8	3.7	15.9	20.8	96.4	344.6	38.1	280.8	159.8
16/18-1	4024.6	18.1	35.3	52.9	256.6	268.0	748.5	45.3	73.8	142.8	60.5	3.7	13.7	19.6	86.0	351.2	31.7	197.9	139.3
16/23-5	3498.4	90.7	25.6	80.2	181.1	239.5	731.2	26.7	65.2	147.9	68.2	2.1	10.5	27.1	72.6	307.8	34.2	845.7	61.6
16/23-5	3494.4	57.4	19.3	92.7	176.5	128.9	750.0	18.0	43.8	84.6	35.5	2.3	8.0	28.8	71.9	322.8	21.5	183.0	65.7
16/23-5	3500.2	91.7	32.4	126.1	181.0	230.6	854.3	18.8	86.6	168.7	72.3	2.4	13.5	38.6	88.8	295.1	29.7	1395.9	72.3
16/23-5	3501.3	102.7	27.2	91.2	245.0	212.3	745.7	14.2	121.4	251.7	109.6	1.8	15.6	19.2	66.3	408.4	28.7	1896.0	65.4
16/23-5	3503.4	194.6	39.9	135.1	164.9	233.7	980.1	18.3	132.5	297.8	126.7	n.d	11.6	61.7	61.0	258.3	36.2	3647.6	60.8
16/28-3	3385.0	51.6	41.6	121.6	224.0	267.1	531.8	29.0	75.3	153.0	63.6	4.3	14.5	23.2	103.3	424.4	27.9	295.7	77.4
16/28-3	3386.5	37.2	112.0	38.5	206.6	291.3	420.0	33.9	109.5	202.7	86.0	4.9	14.8	14.4	69.6	188.1	23.3	286.1	87.4
16/28-3	3387.2	40.6	35.3	129.4	226.5	254.1	529.2	33.8	65.2	139.2	58.5	3.0	12.6	16.7	92.9	360.8	27.6	300.3	81.7
16/28-3	3388.2	NA	NA	NA	NA	NA	NA	NA	NA	NA	NA	NA	NA	NA	NA	NA	NA	NA	NA
16/28-3	3389.8	138.0	67.9	43.2	187.9	289.8	3556.0	41.6	98.4	192.8	82.2	3.4	11.6	47.1	79.3	226.2	32.2	885.0	84.9

22/25b-4S1	4788.4	21.4	108.1	63.4	225.6	234.3	506.2	28.4	74.4	138.6	48.8	4.4	14.6	25.4	56.4	317.1	27.1	89.5	96.1
22/29-1	4579.6	19.1	68.3	22.7	199.9	198.8	750.7	24.7	61.7	115.4	36.4	2.6	11.3	21.4	35.3	250.9	29.2	116.1	158.3
22/30a-16	5492.1	95.4	43.3	43.7	280.2	375.3	7238.8	34.0	106.4	158.1	45.5	2.4	10.5	54.8	99.4	513.7	35.6	373.2	47.9
22/30a-16	5492.7	19.0	37.9	29.3	189.6	281.2	817.3	27.8	71.8	113.0	44.7	2.9	14.3	12.5	138.3	485.8	27.3	179.8	54.0
22/30a-16	5493.9	82.0	47.0	176.5	206.9	209.2	11334.1	25.5	60.8	57.4	8.3	3.6	14.3	56.5	34.2	206.7	37.9	366.4	113.1
29/5a-5	4396.1	95.9	10.7	49.3	141.0	147.0	375.7	25.4	77.3	157.1	62.6	2.8	9.1	58.0	24.9	325.5	33.1	156.3	126.2

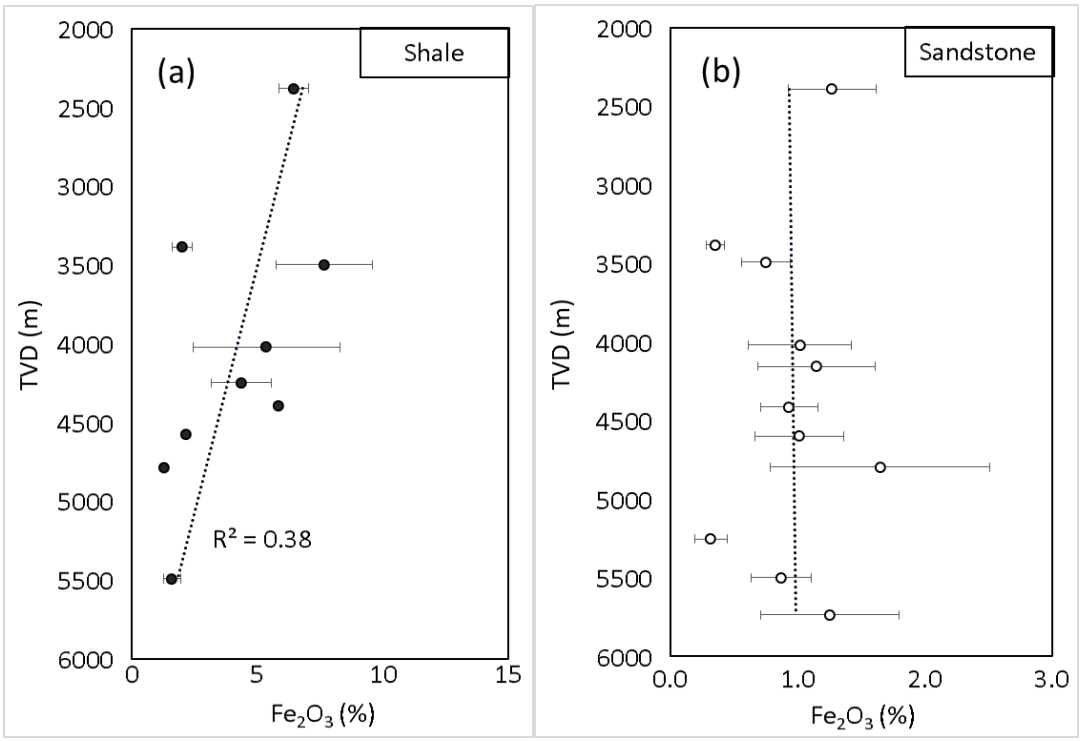

Figure A 4.1 Fe_2O_3 vs. depth in the Pentland Shale (a) and Sandstone (b). Fe_2O_3 (%) in the sandstone is constant with depth, indicating there was no movement of iron from the sandstone to the shale. The sandstones are very fine- to fine-grained Pentland Sandstone (same in Figure A 4.2 - Figure A 4.4).

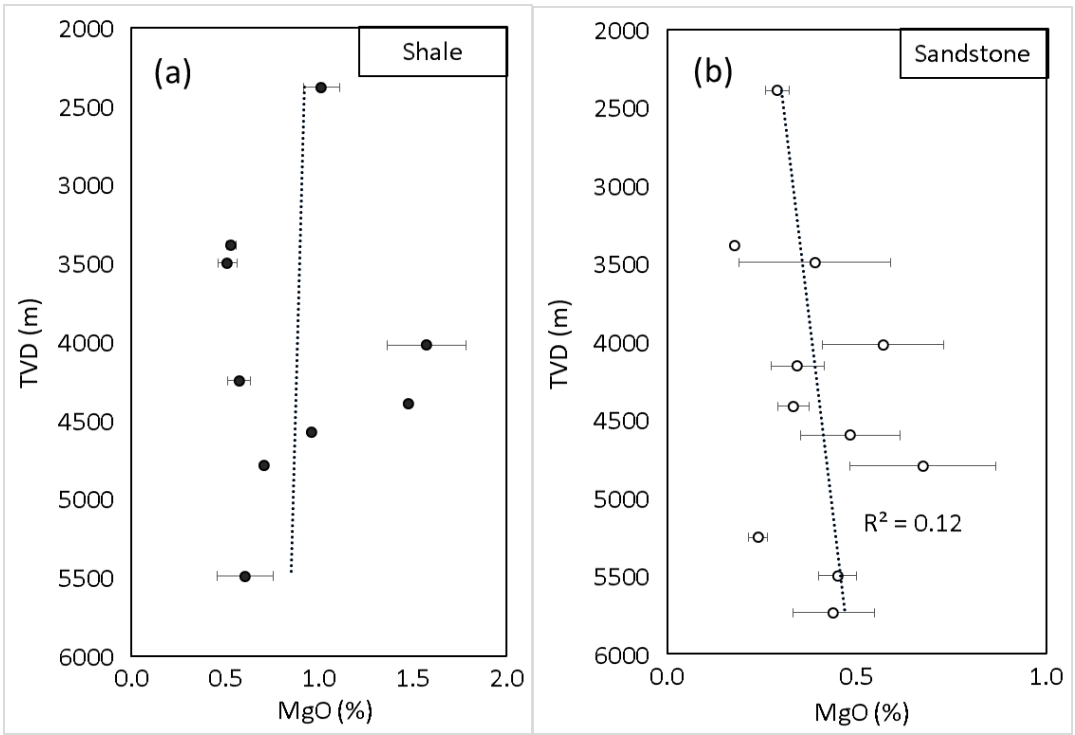

Figure A 4.2 MgO vs. depth in the Pentland Shale (a) and Sandstone (b). There is no robust trend that reflects the exchange of magnesium between the two lithologies.

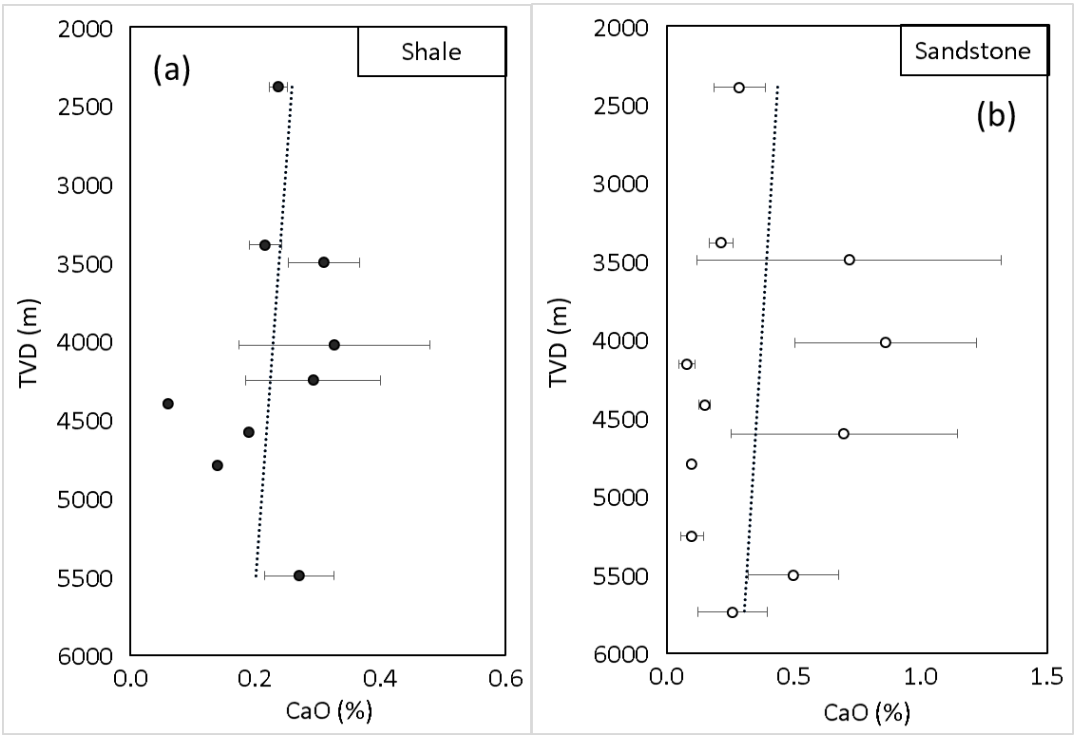

Figure A 4.3 CaO vs. depth in the Pentland Shale (a) and Sandstone (b). No mass transfer of CaO between the two lithologies was identified.

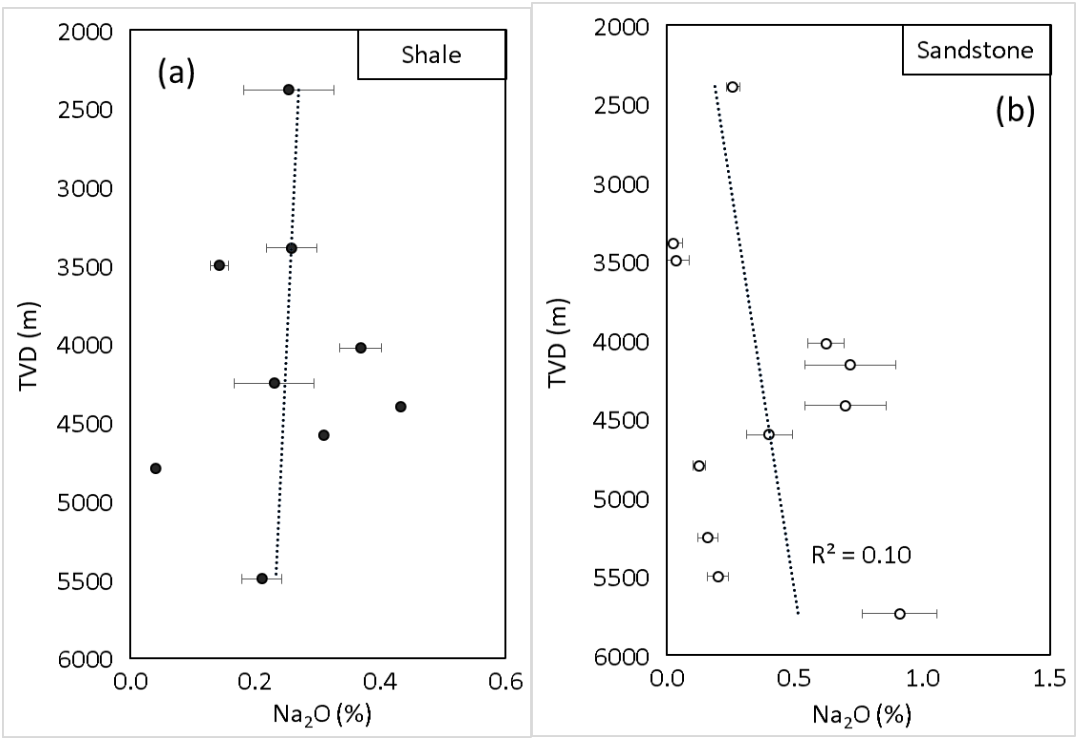

Figure A 4.4 Na_2O vs. depth in the Pentland Shale (a) and Sandstone (b). No mass transfer of Na_2O between the two lithologies was identified.

Chapter 5

Hydrocarbon Emplacement Preserves Porosity in the Pentland Formation of the Kessog Field, North Sea

ABSTRACT

The Kessog Field in the Central North Sea is one of the few oilfields whose main hydrocarbon reserve is held in the Mid Jurassic Pentland Formation. The reservoir of the field is located at about 4 km below the seabed. The porosity of some parts of the reservoir, in particular the top, is substantially higher than the other sandstones of the Pentland Formation at the similar depth. For example, the sandstones in well 30/1c-5, which was drilled through the crest of the reservoir structure, has an average porosity of 25%. In comparison, the empirically predicted average porosity for the Pentland Sandstone at this depth is only about 15%.

These relatively high-porosity sandstones exhibit some characteristic features: 1) sandstones of the highest porosity occur at the crest of the reservoir where hydrocarbon first accumulated; 2) the porosity show good correlations with the level of hydrocarbon saturation in two wells; 3) porosity-loss of these sandstones are mostly from compaction; 4) the type of porosity in the high-porosity sandstone are predominantly primary. All of these characteristics of the sandstones can be explained by the concept of hydrocarbon emplacement preserving porosity, which strongly indicates that hydrocarbon emplacement has had a strong influence upon these high-porosity sandstones. On the other hand, petrographic and porosity data do not show any relationship between the high porosities of the sandstones and the sandstone texture, grain coats, reservoir overpressure and mineral dissolution (secondary porosity). Early hydrocarbon emplacement is the only possible mechanism that could explain the formation of the high-porosity sandstones in the Kessog Field.

These relatively high-porosity sandstones also contain a significantly higher amount of K-feldspar, but less kaolin, than the low-porosity sandstones. Petrographic data combined with the structural information of the reservoir suggest the different contents of K-feldspar in between the high-porosity and low-porosity sandstones were generated in diagenetic processes, possibly due to the inhibition of K-feldspar dissolution by the emplacement of hydrocarbon. As the continuous dissolution of K-feldspar requires the removal of silicon, the mechanism by which hydrocarbon inhibiting K-feldspar dissolution is probably similar to how hydrocarbon reduces quartz cementation.

5.1 Introduction

The effect of early hydrocarbon emplacement on reservoir porosity is controversial. Some studies have recorded higher porosity and less quartz cement in the reservoirs where formational waters have been replaced by hydrocarbon, thereby invoking hydrocarbon emplacement as a mechanism of porosity preservation (e.g. Gluyas et al., 1993; Wilkinson and Haszeldine, 2011). However, at least an equal number of studies have reached the opposite conclusion. These studies observed continuous quartz cementation in oil-filled reservoirs and also that the porosity of these reservoirs does not appear to be higher than the water-filled counterparts. Hence, they suggest hydrocarbon has no effect on reservoir porosity (e.g. Giles et al., 1992; Midtbø et al., 2000; Walderhaug, 1990). A thorough summary of the evidence held by the two sides of the controversy can be found in (Worden et al., 2018, 1998; Worden and Morad, 2000).

The answer to this disputed question has both scientific and commercial significance. If hydrocarbon is indeed capable of preserving porosity, it means the porosity of hydrocarbon reservoirs can be maintained down to great depths (>5km) once hydrocarbon is emplaced. As a result, the lower limit of depth of exploration targets can be extended to a deeper regime and the number of high-quality deep reservoirs may be larger than previous estimates. This knowledge can also be of great importance for oilfield production, as it provides the possibility of predicting the distribution pattern of porosity-permeability within an oilfield by simply modelling the history of hydrocarbon filling, reducing the need to collect expensive core data (Worden et al., 1998).

The debate as to the effect of hydrocarbon on sandstone porosity has lasted for nearly a century since Johnson first raised the issue in 1920, and today, it remains highly contentious (e.g. Worden et al., 2018). The reason can be attributed to the constant presence of conflicting evidence from different oilfields: the oil zones of some oilfields clearly show higher porosity and less quartz cement than the water zones, while in some other fields such a trend is not observed. Based on this evidence, geoscientists can ask the answer of whether or not hydrocarbon can preserve porosity; or instead, we can treat the evidence as the result of the varying effect of hydrocarbon on porosity

preservation under different conditions. Hence, an alternative way to reconcile the debate is to think about the question ‘what is the potential amount of porosity that hydrocarbon can preserve within various time intervals, or at various temperatures and depths?’. The answer to this question has great value both in theory and practice: it will solve the controversy, and provide direct guidance to porosity prediction and reservoir quality risk assessment. The main barrier to obtaining this answer is that, in practice, it is usually difficult to quantify the amount of the preserved porosity as there are many other variables also affecting the porosity, such as sandstone composition, texture, grain coats and secondary porosity. The factors of grain wettability, hydrocarbon type and the timing of hydrocarbon emplacement are also crucial. It is nearly impossible to precisely determine the significance of each of the variables to porosity preservation or enhancement. However, this issue can possibly be solved if the data of an adequate number of oilfields are available. The principle is the same in mathematics that more equations (data of more oilfields) can deal with more unknowns (the variables).

Table 5.1 summaries the previous studies that have documented the effect of hydrocarbon on reservoir porosity. The aim of this study is to present more evidence to demonstrate the effect of hydrocarbon preserving porosity. The research target is the Pentland Formation reservoir in the Kessog Field of the Central North Sea. Part of the Kessog reservoir exhibits anomalously high porosity, which is 10% higher than the porosity that would be predicted for a Pentland Formation sandstone at the given depth (Figure 5.1). Importantly, these high porosity sandstones are characterized by high oil saturation. Conventional core data, petrographic data and hydrocarbon saturation data will be used to test the hypothesis that the preservation of the high porosity in the Kessog Field is related to hydrocarbon emplacement.

Table 5.1 Previous studies on the effect of hydrocarbon emplacement preserving sandstone porosity

Reservoir Name	Excess porosity	Hydrocarbon type	Rock type	Facies	Depth	Age	Reference
Norphlet Formation, Alabama, USA	4.5% preserved by oil and reservoir overpressure; 10.5% by chlorite coats	Gas	Arkosic to subarkosic sandstones	Eolian	6000m	J3	(Dixon et al., 1989)
Magnus Sandstone, North Sea	7%: 17-24% in oil zone 17% in water zone	Oil	Quartz arenite to sub-litharenite	Turbidite	2800 - 3300m	J3	(Emery et al., 1993)
(**?**) Brae Sandstone, North Sea	10%: 12-22% in oil zone 12% in water zone	Oil and gas condensate	Quartz arenite	Turbidite	4000 - 4200m	J3	(Marchand et al., 2001)
Brewster gas accumulation, Australia	8.5% (thin-section porosity): 9% by actual measurement 0.5% by model prediction	Gas	Quartz arenite to sub-litharenite	n.a	n.a	J3-K1	(Bloch et al., 2002)
An anonymous sandstone, Outer Moray Firth, North Sea	5%: 12-17% in oil zone 12% in water zone	n.a	Quartz arenite	Shallow marine	3500m	J3	(England et al., 2003)
Fulmar Formation, North Sea	10%: 16-25% in oil zone 16% in water zone	Oil and gas condensate	Quartz arenite	Shallow marine	5000 - 5150m	J3	(Wilkinson and Haszeldine, 2011)
Ula Formation, North Sea	10%: 10-20% in oil zone 10% in water zone	Oil and gas condensate	Quartz arenite	Shallow marine	3350 - 3800m	J3	(Worden et al., 2018)

Exceptional porosity = highest porosity in oil-zone minus highest porosity in water-zone. J3 = Upper Jurassic; K1=Lower Cretaceous. (?) Whether the high porosity in this case is preserved by hydrocarbon is controversial (see Aase and Walderhaug, 2005; Marchand et al., 2002, 2001, 2000).

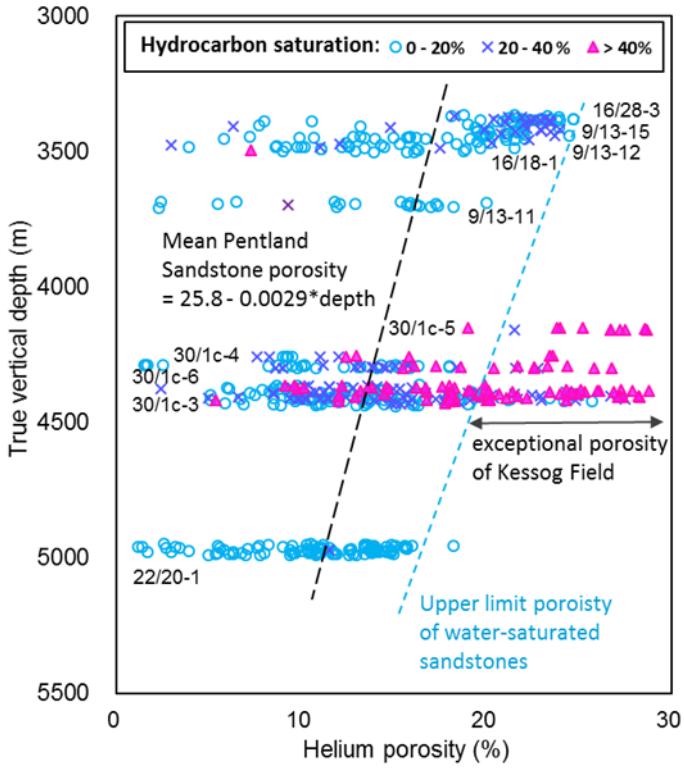

Figure 5.1 Porosity of the hydrocarbon-saturated sandstones at the Kessog Field (wells 30/1c-3, -4, -5 and -6) can be 10% higher than the porosity of water-saturated sandstones. The trend line of Mean Pentland Sandstone porosity is inferred from the porosity of 2283 core samples collected from 20 wells (Wilkinson et al., 2014b); the 'Upper-limit porosity of water-saturated Pentland Sandstone' trend line is inferred from the porosity data of wells 9/13-12, -13 and -15, 16/18-1, 16/28-3, 22/20-1, which are water-saturated. The figure has illustrated the porosity of all Pentland wells with available hydrocarbon saturation data.

5.2 Geology of the Kessog Field

The Pentland Formation has been frequently encountered by hydrocarbon wells in the Central North Sea, but for most oilfields, it is only a minor reservoir. Reserves in the reservoirs of the Pentland Formation are usually much smaller than in the Fulmar or Skagerrak Formation (Gluyas and Hichens, 2003). The Kessog Field, however, is an exception, for which the principal reservoir is the Pentland Formation.

The Kessog Field is a high-pressure, high-temperature gas condensate field discovered by BP in 1985. The reserves are equivalent to 100 million barrels of oil (Offshore Europe, 2001). Developing the field, however, was a great technical challenge due to a combination of extreme pressures and temperatures and a complex, compartmentalized reservoir.

The north edge of the field is bounded by a NW-SE trending fault, and the structure of the whole field is a tilted fault block (Figure 5.2 and Figure 5.3). The western part of the field is sealed by shales, where the Pentland Formation is unconformably overlain by the Upper Jurassic Kimmeridge Clay Formation (Figure 5.3). In comparison, the eastern part is sealed by Cretaceous carbonate sediments, possibly because the Kimmeridgian shales have been eroded during the Late Jurassic or Early Cretaceous. The hydrocarbon source for the field is most likely the overlying Kimmeridge Clay Formation.

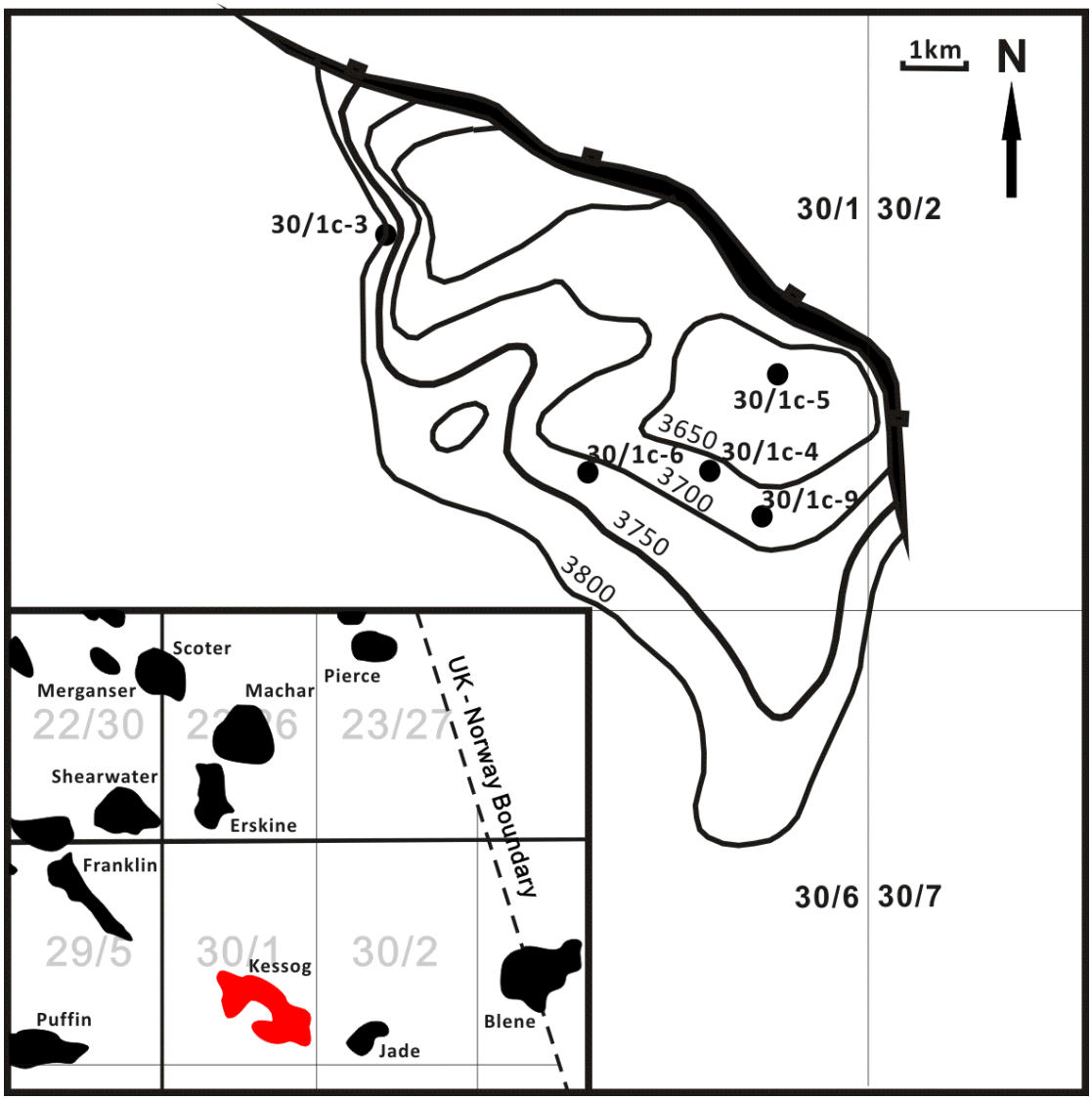

Figure 5.2 Structural map of the Kessog Field. The Kessog Field is a half-graben structure. Redrawn from the geological report of well 30/1c-9 (Total UK Ltd).

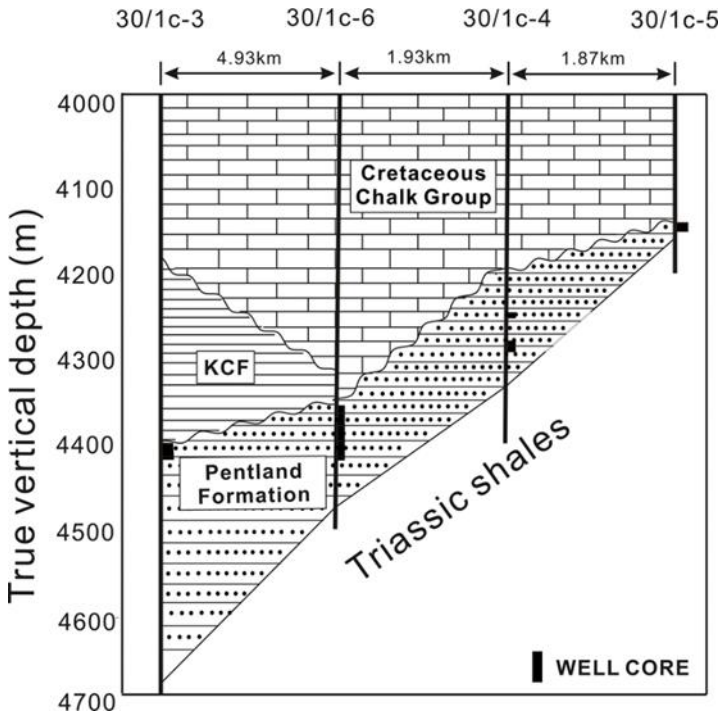

Figure 5.3 A Cross-section of the Kessog Field based on the logs of well 30/1c-3, -4, -5 & -6. Note the distances between the wells are unequal. KCF = Kimmeridge Clay Formation

5.3 Method

There are five wells in the Kessog Field for study: wells 30/1c -3, -4, -5, -6 & -9. Porosity, permeability, pressure, oil saturation and well-log data of these wells are available in the UK Common Data Access database (CDA: https://cdal.com/). Additionally, 39 core samples from the five wells were collected for thin-section petrographic study from the corestore of the British Geological Survey. The methodology and result have been present in Chapter 4.

Additional data used in this chapter are the hydrocarbon saturation values of core samples gathered from the conventional core analysis reports of 10 Pentland Wells. Names of the wells have been listed in Figure 5.1. The hydrocarbon saturation values were determined by the retord method. The method first injects mercury into the gas filled pore of a sample using a mercury pump, and the injected volume of mercury is equivalent to the volume of gas. Then, the method heats the sample and measures the volumes of water and oil driven off. The oil saturation value is the ratio of the volume of oil to the total pore volume, which is the sum of the volumes of gas, oil and water. These core analysis works were conducted by professional third-party laboratories for oil companies, and the results are considered credible.

A kinetic model based on thermal history was used to simulate and predict the amount of quartz cement in the sandstone of the Kessog Field. The model uses the algorithm from Lander and Walderhaug (1999), which has now been commercialized as a software named Touchstone.

5.4 Results

5.4.1 Porosity of the Kessog Field

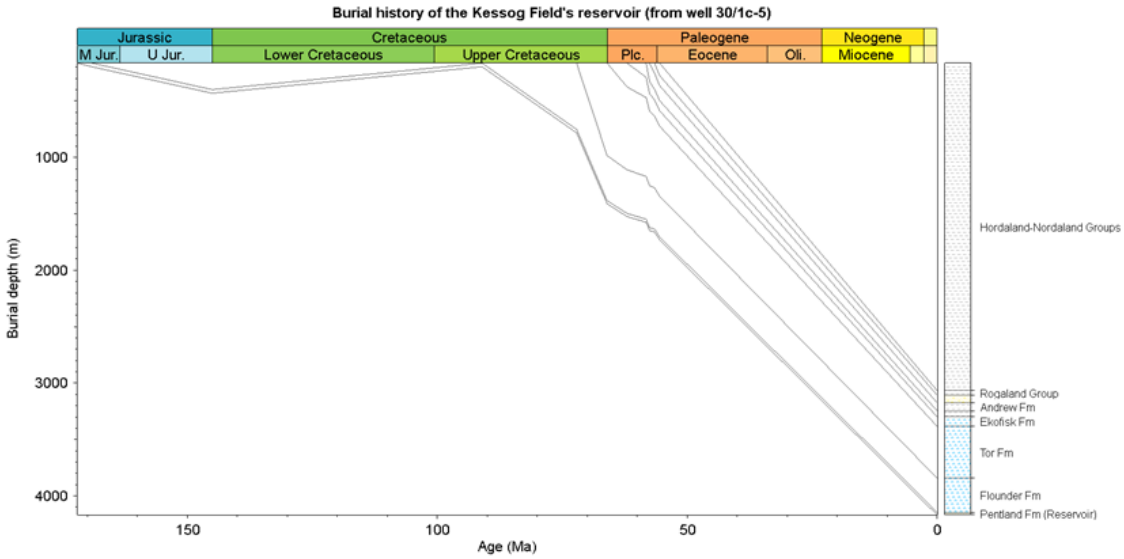

Figure 5.4 Burial curve of well 30/1c-5. The reservoir of the Kessog Field has been buried near to the surface during 170-70 Ma (<1000m), and it was rapidly buried to > 4100 m during 70 Ma- present.

The reservoir of the Kessog Field is buried at a depth of 4.1 – 4.5 km (Figure 5.4). The porosity of wells 30/1c-3, -4, -5, -6 and -9 is illustrated in Figure 4.5 and Figure 5.1. The data from well 30/1c-9 lacks hydrocarbon saturation measurements and hence is not plotted in Figure 5.1.

The porosity of well 30/1c-5, which is located at the crest of the Kessog reservoir (Figure 4.5), is apparently abnormally high. It averages 24.7% (Table 5.2), whereas at the given depth, the porosity predicted by the porosity trend line for the Pentland sandstones is only about 15% (Figure 4.5). In contrast, the porosities of well 30/1c-3, -4, -6 and -9 are significantly lower, but follow the prediction by the trend line (Figure 4.5). The predicted porosity for the depths of these wells is around 14 % (Figure 4.5); the actual average porosity of the reservoirs of well 30/1c-3, -4, -6 and -9 are respectively 13.7%, 14.1%, 15.8% and 15.2%, all of which are close to the predicted value of 14 % (Table 5.2).

Hydrocarbon has filled in all the reservoirs of well 30/1c-3, -4, -5 and -6. But the level of hydrocarbon saturation displays three different patterns in relation to the porosity in these reservoirs:

(1) The shallowest well 30/1c-5 contains a high porosity, high oil saturation reservoir. In all the measured samples, both porosity and the level of hydrocarbon saturation are consistently high, generally with porosity > 20% and hydrocarbon saturation > 40% (Figure 5.5 a). Nevertheless, the porosity does not appear to have a linear relationship with hydrocarbon saturation.

(2) The reservoirs of well 30/1c-4 and -6 are different from that of well 30/1c -5 by showing linear relationships to the level of hydrocarbon saturation (Figure 5.5 b and c). The higher the saturation, the better the porosity. The reservoirs of these two wells also show large variation in porosity and hydrocarbon saturation. In well 30/1c-6 for example, the porosity varies between 0-30% and the hydrocarbon saturation 0-80%.

(3) In the deepest well 30/1c-3, the level of hydrocarbon saturation is much lower than in the other wells (Figure 5.5 d). Correspondingly, it also has an overall lower porosity. However, as in well 30/1c-5, there is no clear linear relationship between the porosity and hydrocarbon saturation in well 30/1c-3

Table 5.2 Average depth, porosity and oil saturation of the reservoirs of well 30/1c-3, -4, -5, -6 and -9 (in order of increasing depth)

Well	Avg. depth* (m)	Avg. porosity (%)	Avg. hydrocarbon saturation (%)	Reservoir thickness (m)
30/1c-5	4155	24.7	57	23.5
30/1c-4	4288	14.1	27	138
30/1c-6	4392	15.8	35	117.5
30/1c-9	4412	15.2	n.a†	203
30/1c-3	4423	13.7	14	280
Whole field average	4376	15.3	29	152

Note: data of the wells are listed in the order of increasing depth.

†n.a = data not available

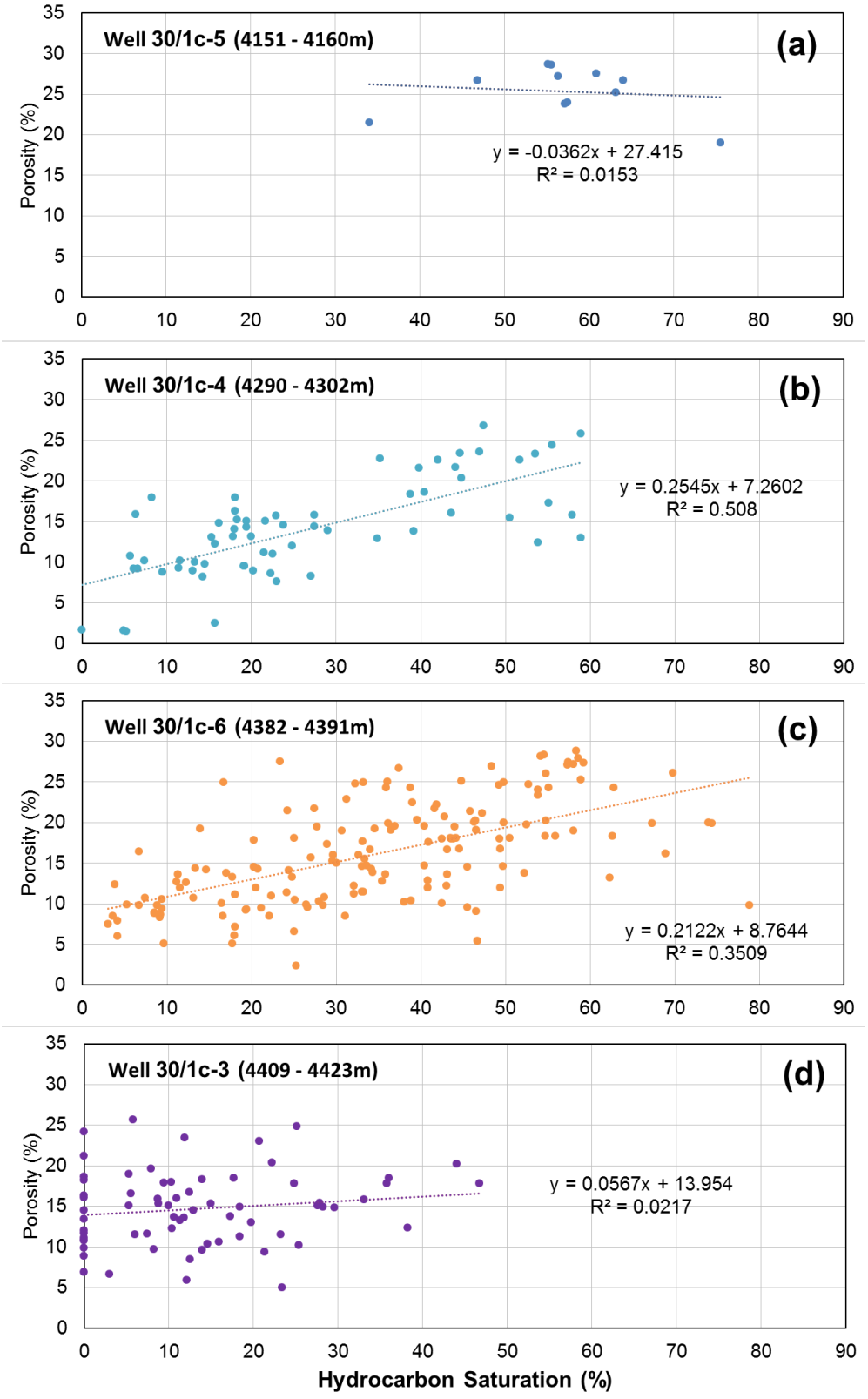

Figure 5.5 Hydrocarbon saturation vs porosity for the reservoirs of well 30/1c-3, -4, -5 and -6 (in the order of depth). The porosity of the reservoirs of well 30/1c-3 and -6 generally increases with increasing hydrocarbon saturation. Whereas, the porosity in well 30/1c-5 and -3 are not correlated to the degree of hydrocarbon saturation.

5.4.2 Petrography of the Kessog reservoir sandstones

This section aims at describing the texture, composition and porosity of the reservoir sandstones of the Kessog Field, and comparing them to other Pentland Sandstone encountered elsewhere around the North Sea. The raw data of point-count and grain-size measurement for individual samples are compiled in Table A 4.2, and the average sandstone composition and grain-size for different wells are in Table A 4.1.

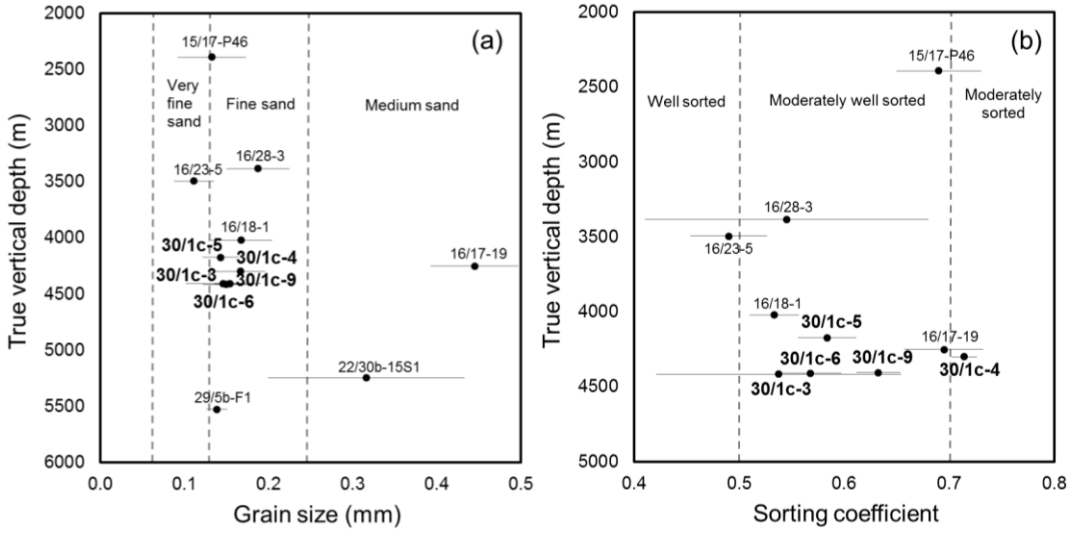

Figure 5.6 (a) Grain–size and (b) sorting of the Pentland Formation sandstones. The wells from the Kessog Field are highlighted in **bold font**.

In general, sandstones of the Pentland Formation are mostly composed of fine-grained, moderately well-sorted sands (Figure 5.6). Figure 5.7 presents how the Pentland sandstones in the Kessog Field appear under the microscope. For more straightforward comparison, Figure 5.7 selected five sandstone samples with similar grain-size and sorting from each of the five wells of the Kessog Field. The petrography data of the sandstones show that the average grain-sizes of the sandstones in different wells are nearly uniform, all falling in a narrow range of 0.14-0.17 mm (fine-grained; Figure 5.6). The sandstones of wells 30/1c-3, -5, -6 and -9 also exhibit similar degrees of sorting, with the sorting coefficients confined within the range of 0.54-0.63 (Figure 5.6). These numbers of sorting coefficient correspond to moderately well-sorted sands. The sandstones in well 30/1c-4 are slightly less well sorted (sorting coefficient: 0.77), which is made of moderately sorted sands.

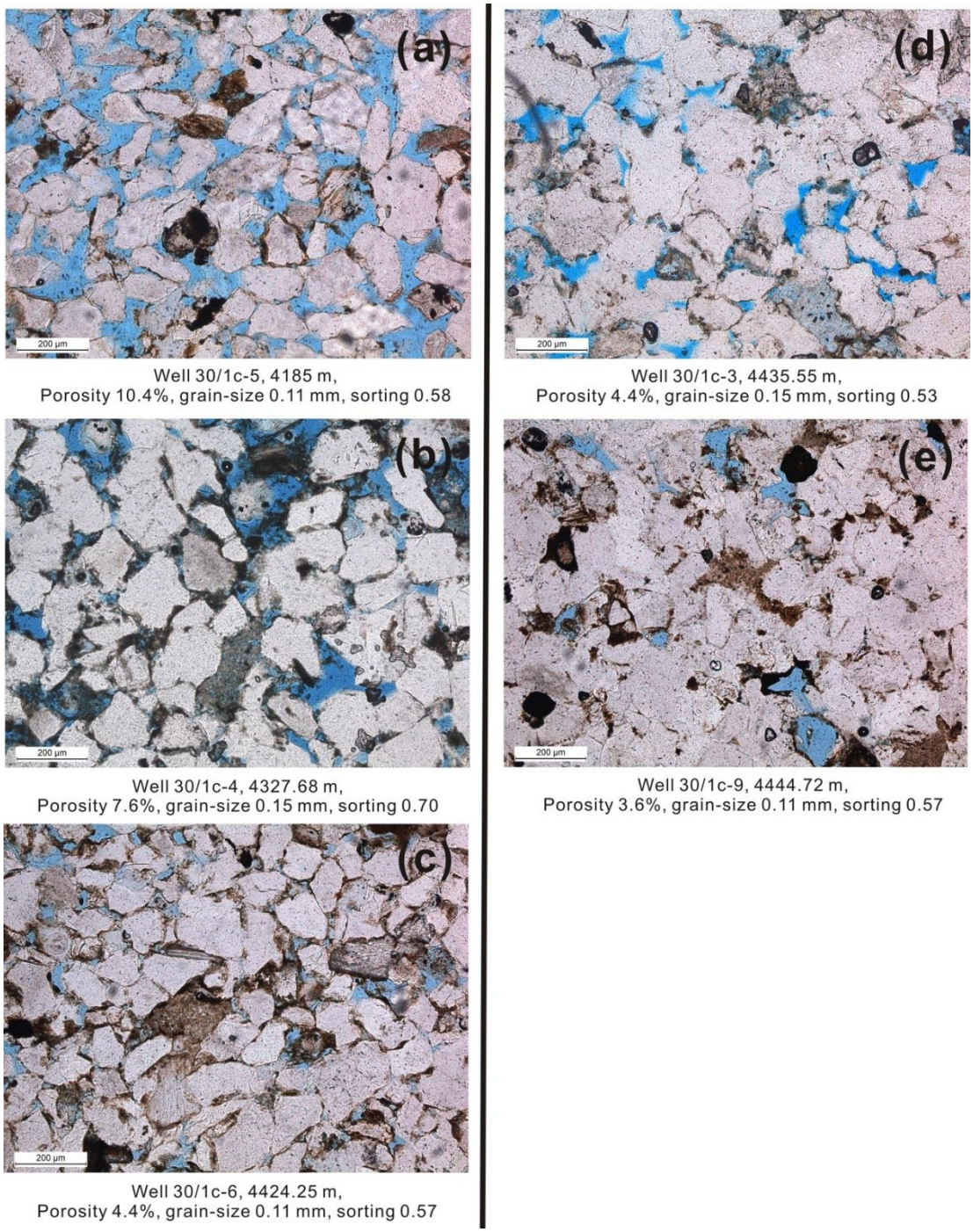

Figure 5.7 Microphotographs showing how the reservoir sandstones like in different wells of the Kessog Field. The photos are in the order of from shallow to deep depth. All sandstones are of the similar grain-size and sorting, and all the photos are on the same scale. In the shallowest well 30/1c-5, the sandstones are porous; whereas in the deepest well 30/1c-9, the sandstones have been well cemented.

The framework grains of the Pentland sandstones are invariably dominated by quartz. Feldspar in most cases is present in only small or trace amounts (<2%). The content of K-feldspar in the reservoir of the Kessog Field appears to show a decline with depth (Figure 5.8). In the shallowest well 30/1c-5, the point-counted percentage of K-feldspar averages at 3.8±0.4% (Table 5.3). In the second shallowest well 30/1c-4, the number decreases to 1.8±0.3%. In the further deeper wells of 30/1c-3, -6 and -9, the reservoir, respectively, contains 1.3±0.3%, 0.6±0.1% and 0.6±0.3% of K-feldspar. It is worthwhile considering whether this trend was formed in the diagenetic process or during the deposition of the sandstones, and the discussion about this question is in *Section 5.5.2 - hydrocarbon emplacement and K-feldspar dissolution*.

The clay minerals in the Pentland Formation are either kaolin or illite (see *Section 4.4.3*). The bulk of the reservoir of the Kessog Field typically contains 3-8% of kaolin, which is close to other Pentland Sandstone (Figure 4.15); the notable exception is the reservoir of well 30/1c-5 whose content of kaolin is < 1%, significantly lower than in the other reservoirs. The amount of illite in most Pentland sandstones is between 5 and 15%, though in a few wells the number can reach 20% (Figure 4.15). Sandstones of the Kessog Field are also rich in illite (8-15%, Table 5.3), which is similar to other Pentland sandstones.

An unusual diagenetic feature of the Pentland Formation is that the kaolin in the formation does not transform into illite under increasing temperature and depth of burial. Previous studies have attributed the reason to a lack of potassium source (K-feldspar) in the formation (See Chapter 4; or Bjørlykke and Aagaard, 1992; Wilkinson et al., 2006). In Figure 5.9, the ratio of kaolin/(kaolin + illite) was used to represent the relative abundance of kaolin and illite in the Kessog Field reservoir. The figure shows that this ratio does not appear to correlate with depth. However, within the reservoir of Kessog Field, there is a sharp rise of this ratio with depth. It increases from 0.08 in well 30/1c-5, through 0.17 in well 30/1c-4, to around 0.5 in wells 30/1c-3, 6 and -9, reflecting that kaolin gets less and illite becomes more abundant with increasing depth in the Kessog Field.

During diagenesis, quartz cement is the dominant porosity occluding phase in the Pentland sandstones. Below the depth of 4km, over 10% volume of the sandstones can be occupied by quartz cement (Figure 4.9). Meanwhile, the amount of quartz

cement is highly variable between different wells. For example, at a depth of 5.5 km, quartz cement can account for up to 14.8 ± 3.9 % volume of a sandstone (well 22/30a – 16), or can be as little as 3.5 ± 0.8 % as in the reservoir of well 22/30c-G4. Generally, the sandstones of the Kessog Field contains 3-8% of quartz cement. Still, there are considerable variations between the wells. The amount of quartz cement is the least in the shallowest well 30/1c-5 (2.8±0.4 %) and shows a trend of increasing with depth. In the second shallowest well 30/1c-4, the amount is 4.0±0.9 %. In the deepest wells of 30/1c-3, -6 and -9, the amounts are 6.4±1.0%, 6.4±0.6% and 7.8±0.2%, respectively (Table 5.3). Using the *Touchstone* algorithm, the predicted amount of quartz cement, according to the thermal history and sandstone texture data of well 30/1c-5, is about 18%, in contrast to actual measured 2.8±0.4 % of quartz cement, indicating that quartz cementation has been effectively inhibited in well 30/1c-5.

Primary porosity appears to be especially important for the quality of the Kessog reservoir. Figure 5.10 (a) shows that the number of primary porosity has a positive correlation with the total porosity. In the high porosity reservoirs (Figure 5.10 a; point-counted porosity >10%), the porosity is predominantly primary porosity. In contrast, the percentage of secondary porosity is widely scattered in high-porosity sandstones, with no correlation with the amount of total porosity (Figure 5.10 b). Sandstones that are rich in primary porosity are the most frequently found in the high-porosity reservoirs of well 30/1c-5 and -6 (Figure 5.10 a).

Table 5.3 Summary of the Kessog Field's petrographic data from this study and Wilkinson et al. (2014)

Well	TVD (m)	n	Quartz (%)	K-feldspar (%)	Plagioclase (%)	Mica (%)	QOG (%)	Dolomite (%)	Illite (%)	Kaolin (%)	Porosity (%) Primary / Secondary	Grain-size (mm)	Sorting
30/1c-3	4409-4423	8	68±2	1.3±0.3	0.5±0.2	0.4±0.1	6.4±1.0	4.4±2.3	8.2±1.9	5.5±1.0	2.0± 0.7 / 2.1±0.5	0.15±0.01	0.54±0.04
30/1c-4	4290-4302	13	60±1	1.8±0.3	1.1±0.2	1.1±0.3	4.0±0.9	0.5±0.2	17.0±3.0	2.9±0.6	3.7±1.1 / 5.0±0.8	0.17±0.01	0.71±0.04
30/1c-5	4151-4160	28	62±1	3.8±0.4	0.8±0.2	2.6±0.7	2.8±0.4	n.d	9.2±1.2	0.7±0.2	10.3±0.9 / 3.9±0.5	0.14±0.01	0.58±0.02
30/1c-6	4382-4391	50	54±1	0.6±0.1	2.1±0.2	2.0±0.3	6.4±0.6	3.7±1.1	14.7±1.9	4.8±0.5	5.5±0.7 / 3.1±0.3	0.15±0.01	0.57±0.02
30/1c-9	4400-4411	8	65±1	0.6±0.3	0.3±0.1	0.5±0.1	7.8±2.2	1.1±0.3	11.8±2.6	6.3±1.7	1.3±0.6 / 3.2±1.3	0.15±0.02	0.63±0.05

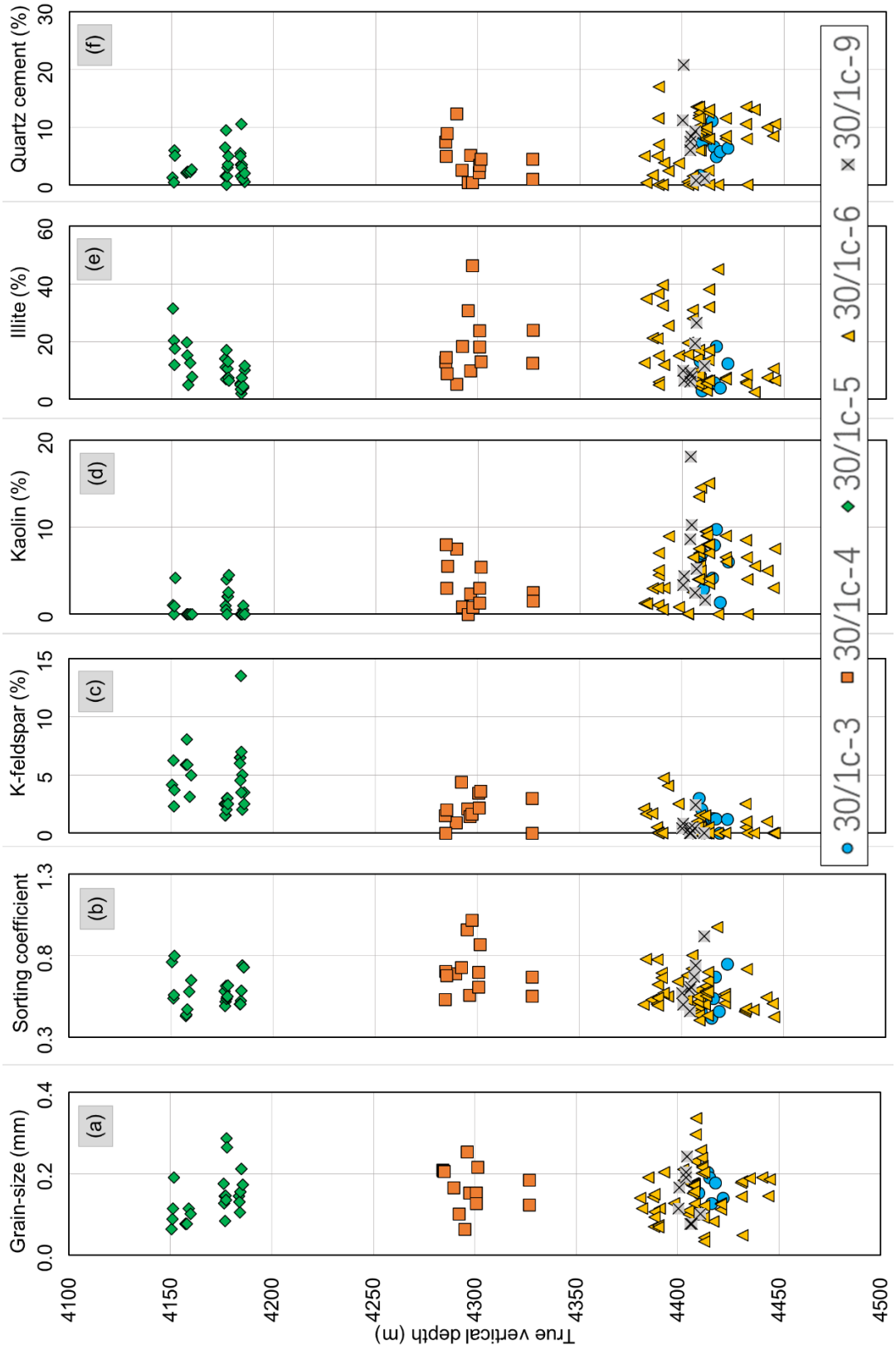

Figure 5.8 Sandstone petrography vs depth at the Kessog Field. Sandstones of between different wells do not show little difference regarding the range of grain-size and sorting. The sandstones of well 30/1c-5, however, contain more K-feldspar and less kaolin, illite and quartz cement than the sandstones of the other Kessog wells.

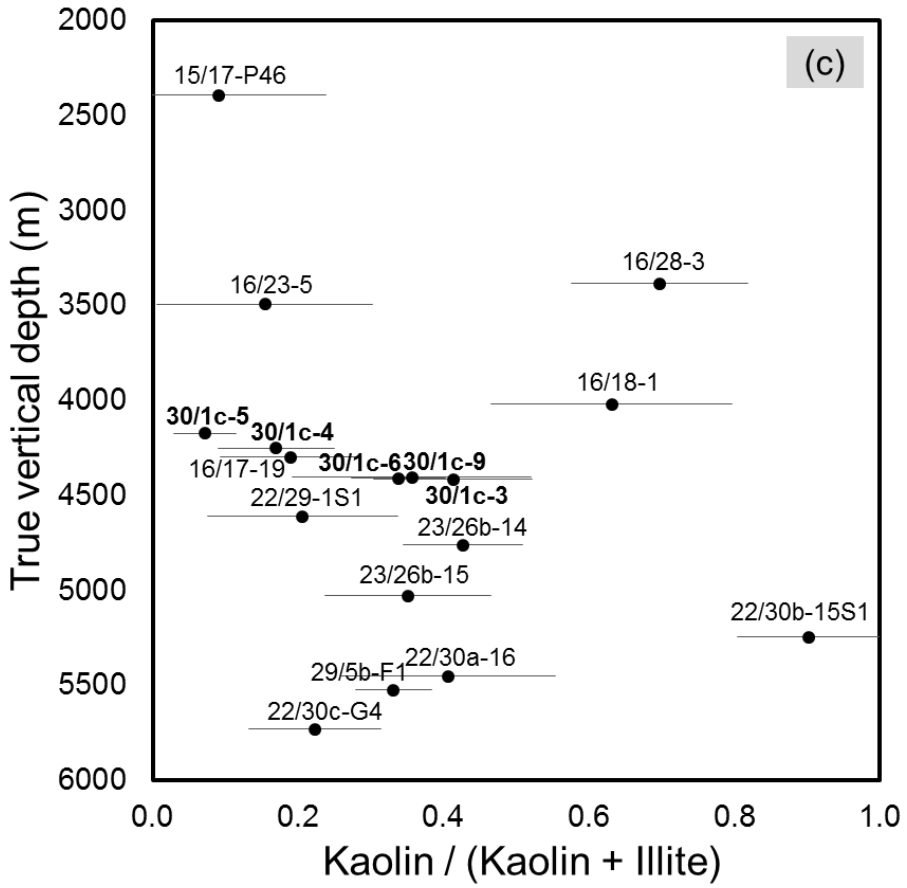

Figure 5.9 The content of (a) kaolin and (b) illite in the Pentland Formation. (c) shows the relative abundance between kaolin and illite versus depth.

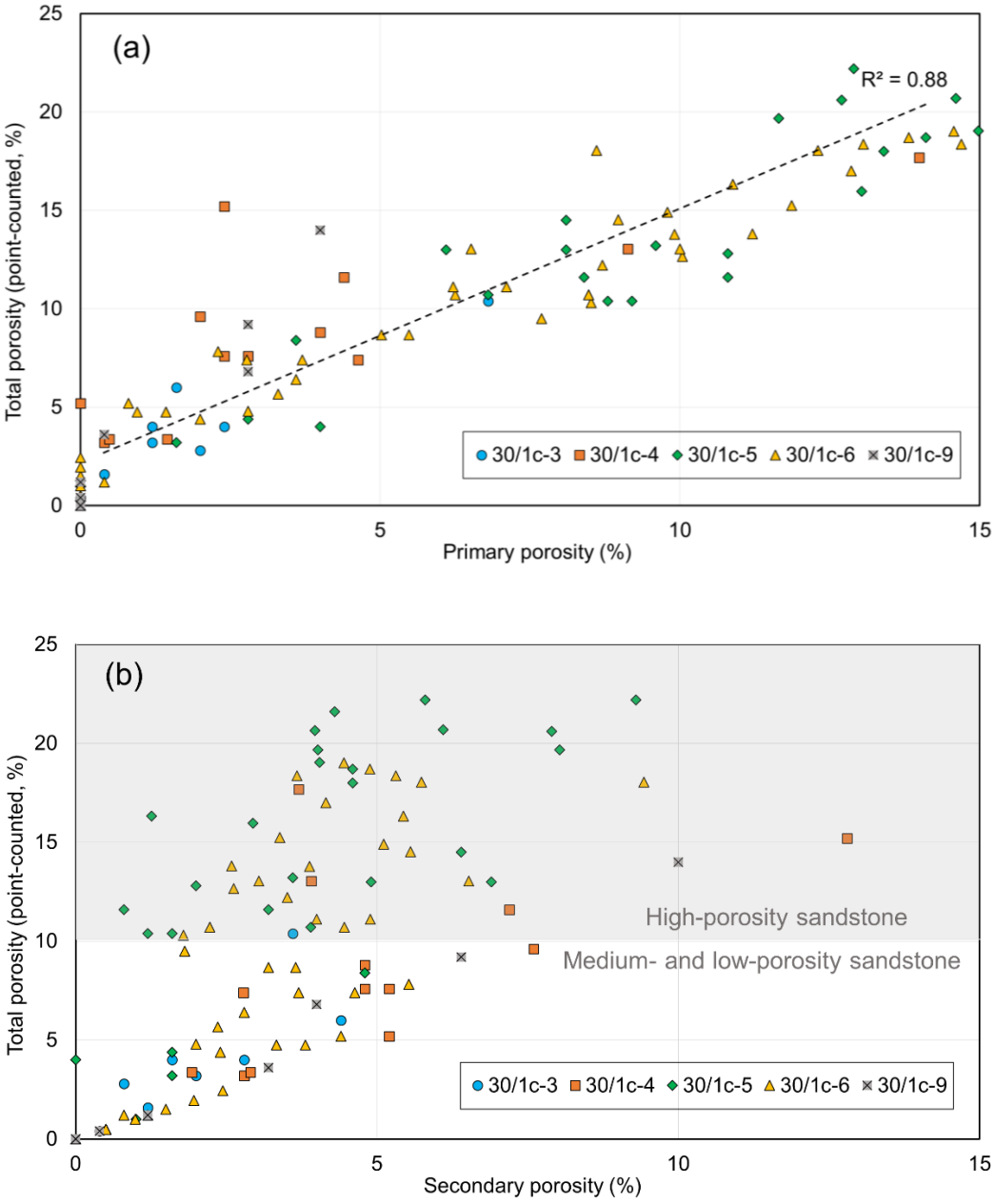

Figure 5.10 The point-counted total porosity of the Kessog Field's reservoir as a function of (a) primary porosity, (b) secondary porosity, (c) Primary porosity/ Total porosity.

5.5 Discussion

5.5.1 Porosity preservation in the Kessog Field

How does a sandstone, or what kind of sandstone would, form high-porosity reservoirs at depth? The most critical factor in deciding the porosity of a sandstone during burial is its depositional composition and texture (Bjørlykke and Jahren, 2015). For example, clean, fine-grained and well-sorted sandstones are more likely to become high-porosity reservoirs (Chuhan et al., 2003). Besides, there are other four commonly evoked mechanisms that can explain the occurrence of high-porosity sandstone reservoirs: grain-coats (microquartz and chlorite), overpressure, mineral dissolution (secondary porosity) and early hydrocarbon emplacement (Bloch et al., 2002). In addition, bitumen coating on quartz grains (Maast et al., 2011), phosphate poisoning (Warren and Pulham, 2001) and thermal anomalies near salt (Taylor et al., 2010), which are relatively less common, are also potential mechanisms of forming high porosity reservoirs. This section is going to assess which of the mechanisms is responsible for the causing of high porosity in the Kessog Field.

(a) Sandstone texture

Grain size, sorting and content of detrital quartz are the most indicative parameters of the texture and composition of a sandstone upon deposition. K-feldspar, kaolin and illite, although common in the Pentland Formation, may have been subjected to substantial modifications during diagenesis (Giles and de Boer, 1990; Worden and Burley, 2003). Hence, the contents of these minerals are possibly not reliable for indicating the detrital composition of a sandstone.

Figure 5.6 (a) and (b) compare the grain-size, sorting and quartz content between the Pentland sandstones in different wells around the North Sea. On none of the parameters do the sandstones of wells 30/1c-3, -4, -5, -6 and -9 appear to be significantly different from the Pentland sandstones elsewhere. Figure 5.8 is particularly focused on the variation of sandstone petrography within the Kessog Field, between the sandstones of wells 30/1c-3, -4, -5, -6 and -9. In the *Results* Section (5.4.2), it has been mentioned that there are only minor differences regarding the

average grain-sizes and sorting coefficiency of the sandstones within the Kessog Field. For example, the average grain sizes of the sandstones are in the narrow range of 0.14-0.17 mm. The average porosity of well 30/1c-5 is about 10% higher than the average porosities of the other wells. This minor difference on grain-size is unlikely to cause the large difference of porosity between well 30/1c-5 and wells 30/1c-3, -4, -6 and -9.

Figure 5.7 illustrates the images of five reservoir samples from the five wells in the Kessog Field. These sandstones are similar to each other on grain size and sorting, but they exhibit distinctly different reservoir properties. It strongly suggests that sandstone texture is not the deciding factor of porosity in this case. The texture of a high porosity sandstone can equally form a low porosity reservoir in the same oilfield.

(b) Grain coats

The generation of high porosity in many deep sandstone reservoirs is often attributed to the occurrence of grain coats (Bloch et al., 2002). Grain coats covering the surface of detrital quartz reduce the free surface for the growth of quartz cement, leading to less quartz cementation and hence preservation of higher porosity. In North Sea oilfields, three types of grain coats are commonly reported: microquartz, chlorite and illite. The importance of grain coats, however, is prone to be overlooked, as they are often not readily identifiable under microscope (Aase and Walderhaug, 2005; Wilson, 1992). This section examines the possibility of porosity preservation by microquartz and grain-coating chlorite and illite for the reservoir of the Kessog Field.

Microquartz: Microquartz is a type of quartz cement. It differs from the conventional pore-filling quartz cement in crystal size: diameters of microquartz crystals are mostly in the range of 0.1-1 μm, whereas the diameters of ordinary quartz cement can be of two magnitudes larger, around 20-100 μm (Aase et al., 1996). Microquartz occurs as compact clusters of tiny crystals that cover a large area on the surface of quartz grains. Ordinary quartz cement cannot grow on the surface covered by microquartz, and hence porosity can be preserved. Studies on microquartz and reservoir quality have indicated that at temperatures of 100-150^{o}C, sandstones with microquartz may contain 10% more porosity than the sandstones that are without microquartz (e.g.

Aase et al., 1996; Aase and Walderhaug, 2005; Ramm et al., 1997; Wilkinson and Haszeldine, 2011).

The source of silica for the precipitation of microquartz has been reported to be provided by the fossils of a marine sponge — *Rhaxella* (Vagle et al., 1994). Sponge spicules need to be incorporated into sediments upon deposition, and during later burial as temperature increases, they dissolve and are re-precipitated as microquartz cement (Aase et al., 1996). There is, however, a strict environment control over the occurrence of *Rhaxella*: it only lives in the marine environment (Haslett, 1992). This means sediments deposited in a non-marine setting, such as the Pentland Formation, should not contain *Rhaxella* and the associated microquartz cement.

Nonetheless, there have been few exceptional cases in which microquartz does occur in fluvial-deltaic sandstones, and the causes are interpreted not related to siliceous fossils. The examples include the fluvial Skagerrak Formation in the North Sea (Nguyen et al., 2013) and the Safaniya Sandstone in Saudi Arabia (Çağatay et al., 1996). Nguyen et al. (2013) did not quantify the exact amount of microquartz in their samples of the Skagerrak Formation; the amount reported by Çağatay et al. (1996) in the Safaniya Sandstone is 1-2%. The authors interpreted the microquartz cement in these sandstones as having being precipitated from fluvial waters.

This paragraph is for examining the possibility of microquartz precipitation from fluvial waters. The solubility data of chalcedony, which is the early-form of microquartz (Williams et al., 1985; Worden et al., 2012), is used to represent the solubility of microquartz. Silica saturation relative to microquartz (chalcedony) at a likely Jurassic surface temperature (20 ^{o}C) is about 8 ppm (Walther and Helgeson, 1977). The silica content of fluvial waters can vary between 13-32 ppm (Blatt, 1979). A mass balance calculation by Blatt (1979) showed that if fluvial waters circulated through a sand body at a rate of 20 m/year, and all the over-saturated silica precipitated, then it is possible to precipitate 1-2% of microquartz within several million years. This calculation assumes the supply of silica is the rate-limiting process for microquartz precipitation at low temperature. However, this may not be true. The chemical data of formation waters in sedimentary basins have shown that most of the waters at shallow depth are saturated in silica with respect to microquartz (Giles and de Boer, 1990). But microquartz is rarely observed, indicating that it is precipitation rate (Walderhaug,

1996) or nucleation rate (Wilkinson, 2015) of microquartz cement, rather than silica supply, that is the rate-limiting process for microquartz growth at low temperatures. A much more likely scenario is that although fluvial waters are saturated in silica, no microquartz can be precipitated because of the extreme low precipitation rate at low temperatures. The microquartz cement in the Skagerrak and Safaniya sandstones must have another cause, maybe due to intense evaporation under hot conditions that result in a high concentration of silica in the pore waters of sediments. The Pentland Formation was deposited in a humid environment which did not have high rates of evaporation.

Chlorite coats: Grain-coating chlorite is another type of grain coat that is important for porosity preservation in some sandstone reservoirs. Previous studies indicated that the effectiveness of chlorite coats preventing quartz cementation is comparable to that of microquartz: for similar sandstones, those containing chlorite coats sometimes can have 10-15% higher porosity than the sandstones free of chlorite coats (Dixon et al., 1989; Ehrenberg, 1993).

Chlorite coats can form through multiple ways and in a wide range of depositional environments, but they occur most frequently in fluvial-deltaic sediments (Dowey et al., 2012). Including the Pentland Formation, there were large areas of fluvial-deltaic sediments being deposited in the North Sea area during the Middle Jurassic. The distribution of chlorite within these Middle Jurassic sediments, however, is uneven and shows a regional pattern. A considerable amount of chlorite coats have been reported in some sandstones of the Northern North Sea and the Haltenbanken area (Ehrenberg, 1993). These sandstones are usually characterised by high porosity. The frequency of occurrence of chlorite seems to decrease southwards in the North Sea. In the Brent Group which is located more southerly, chlorite presents only in minimal amount, and its effect on the porosity of the reservoir is negligible (Bjørlykke et al., 1992; Giles et al., 1992). In the farther south Pentland Formation, chlorite has not been reported (Wilkinson et al., 2014b, 2006).

The regional distribution pattern of chlorite in the North Sea is very likely related to the change of paleoenvironment, or sediment supply, from the north to the south of the North Sea in Middle Jurassic. The paleo-environment becomes arider towards the north (Underhill, 1998), which would aid the formation of iron-oxide grain coats

(precursor of chlorite minerals; Dowey et al., 2017). Whereas the Central North Sea in the Middle Jurassic was under a humid environment, which is suggested by the presence of extensive coals and kaolin minerals in the Pentland Formation (Richards et al., 1993). Hence, the Pentland Formation is expected not to contain many iron-oxide minerals which would form chlorites in diagenesis.

This study has only occasionally observed trace amount of chlorite in the Pentland Formation (see *Section 4.4 - Results*). It is therefore considered that chlorite coats are not important for the porosity and permeability of the Pentland sandstones. Chapter 4 also includes some XRD data of the sandstone samples from well 30/1c-5 Formation (represented below, Table 4.12), which drilled the best porosity reservoir in the Kessog Field. The data show the sandstones only contain minor chlorite. Hence, the high porosity of the sandstones of well 30/1c-5 cannot be related to chlorite coats.

Table 4.12 XRD data of five sandstone samples from well 30/1c-5. Raw data is in Table A 4.3

TVDSS (m)	Quartz (%)	K-feldspar (%)	Plagioclase (%)	Kaolinite (%)	Illite (%)	Smectite (%)	**Chlorite (%)**	Muscovite (%)	Carbonate (%)
4150.5	71.4	1.0	10.9	0.9	11.7	0.3	**1.1**	0.4	0.7
4151.3	82.6	0.1	9.6	0.3	3.2	0.4	**1.5**	1.2	0.1
4157.6	67.5	10.0	15.9	0	3.2	0.	**0.4**	0.9	0.7
4159	80.0	6.6	8.6	0	2.2	0.2	**0.2**	1.2	0.5
4159.9	87.7	1.8	2.1	0	4.2	0.2	**0.2**	1.7	0.6

Illite coats: Illite also commonly occurs as grain coats, and in the Pentland Formation it is the dominant type of clay minerals (Table 5.3). The effectiveness of illite coats for preserving porosity, however, is uncertain, but it is generally agreed to be less significant than chlorite coats (Bloch et al., 2002; Pittman et al., 1992). On the one hand, only a few studies (e.g. Heald and Larese, 1974; Storvoll et al., 2002) have asserted that sandstones with illite coats contain less quartz cement and higher porosity. On the other hand, many more studies indicate that illite coats seem to have enhanced the pressure solution between quartz grains, causing more porosity loss (e.g. Bjørkum, 1996; Oelkers et al., 1996; Thomson and Stancliffe, 1990; Walderhaug,

1994). Hence, the effect of illite coats on reservoir quality can be either positive or negative.

Figure 5.11 (a, b) shows a microphotograph of a porous sandstone from well 30/1c-5. In the photo, the surface of quartz grains with illite coats and without illite coats exhibits clear shape difference. The surface covered by illite (marked by red lines) can be described as uneven and irregular, while the surface without illite covers is more smooth and euhedral, indicating a better development of quartz overgrowth on the surface. In this case, the shape difference suggests that illite coats have, to some extent, inhibited quartz cementation.

The exact mechanism by which clay coats preventing quartz cementation is not yet well understood (Worden and Morad, 2003). To efficiently preserve porosity, two aspects of clay coats seem important (Wilson, 1992):

- Thickness of the coats: if the coats are not sufficiently thick, quartz cement may overgrow on or through the grain coats, as shown in Figure 5.11 (c, d).
- Coverage of clay coats on the quartz surface. For point counting, it is important to make sure that only the thick clay coats (> 5μm) are counted. Thin clay coats should be omitted as they are unable to prevent quartz overgrowth.

Here, the influence of illite coats on the porosity of the Kessog Field's sandstones are considered from the two aspects of clay coats listed above. Figure 5.11 (c, d) shown that many of the clay coats in the sandstones are too thin to inhibit the growth of quartz cement. If assuming only the illite coats with the thickness of the coats in Figure 5.11 (a, b; marked by red lines) can successfully restrict quartz cementation, then the amount of the illite coats with such thickness in the sandstones can be roughly estimated. According to visual estimation, only about less than 10% of quartz surface are covered by thick clay coats. It is unlikely that such a small amount of clay coats can be significant for porosity preservation of a sandstone in general. Figure 5.11 (e, f) is a microphotograph of a well-cemented sandstone from well 30/1c-9, which typically contains about 10% clay coat with the 'adequate thickness' assumed, as the sandstone in Figure 5.11 (a, b). Illite coats in the sandstone appear as brown or black, curved strips between creamy white quartz grains. Given the high grade of quartz cementation which has virtually occluded all the porosity in this sandstone, it is clear

that the illite coats of this abundance did not have any significant inhibiting effect on quartz cementation. The reason is probably because pore space is usually bounded by several quartz grains. Quartz cement can grow from any of the surfaces of the quartz grains to fill the pore space. Only when most of the quartz grains are covered by illite coats would the porosity loss by quartz cementation be restricted.

Summary: Microscopic study did not observe microquartz and chlorite coats in the sandstone thin-sections from the Kessog Field. However, this does not necessarily mean the sandstones do not contain these two minerals at all. It could be due to the small number of samples counted, only sandstones free of microquartz and chlorite were collected, or because the volumes of these grain coats are too small to be point-counted. Therefore, in this section on *grain coats*, we have, from the formation mechanism point of view, discussed why the presence of microquartz and chlorite are unlikely in the reservoirs, and hence concluded that microquartz and chlorite cannot be the cause of the high-porosity sandstones in the Kessog Field. Illite coats are present in the sandstones. But the number of thick clay coats, which can potentially prevent quartz cementation, is limited, appearing to cover only less than 10% of the surface of quartz grains. Figure 5.11 (e, f) suggests Figure 5.11this level of thick clay coats cannot effectively prevent quartz overgrowth.

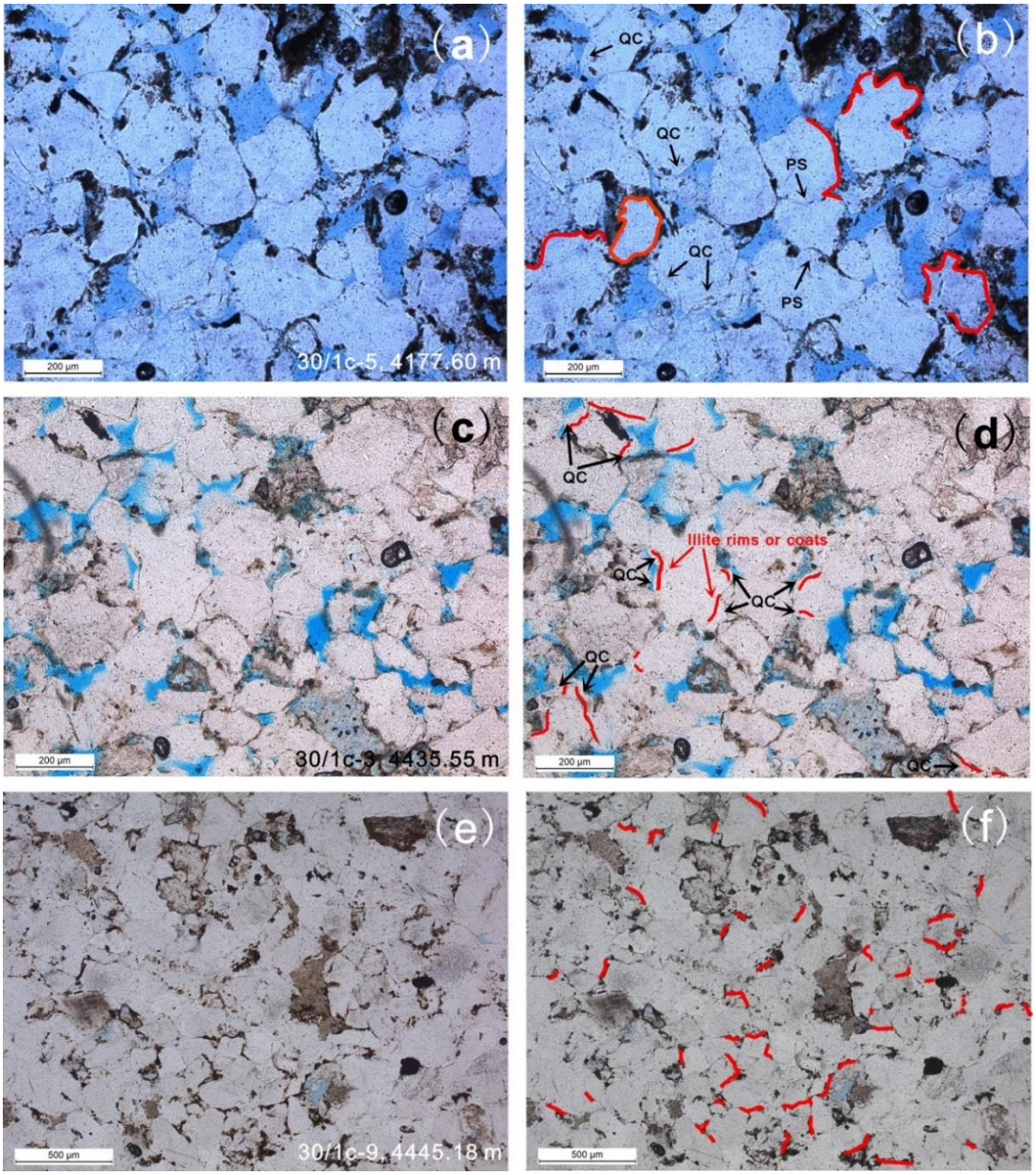

Figure 5.11 Photomicrographs of three thin-sections to show the relationship between illite coats and quartz cementation. Illite coats are highlighted in red in the photos on the right; on the left are the original photos. Detailed descriptions and significances of these photos are given in the context of the section about 'illite coats'.QC = quartz cement; PS = pressure solution.

(c) Overpressure

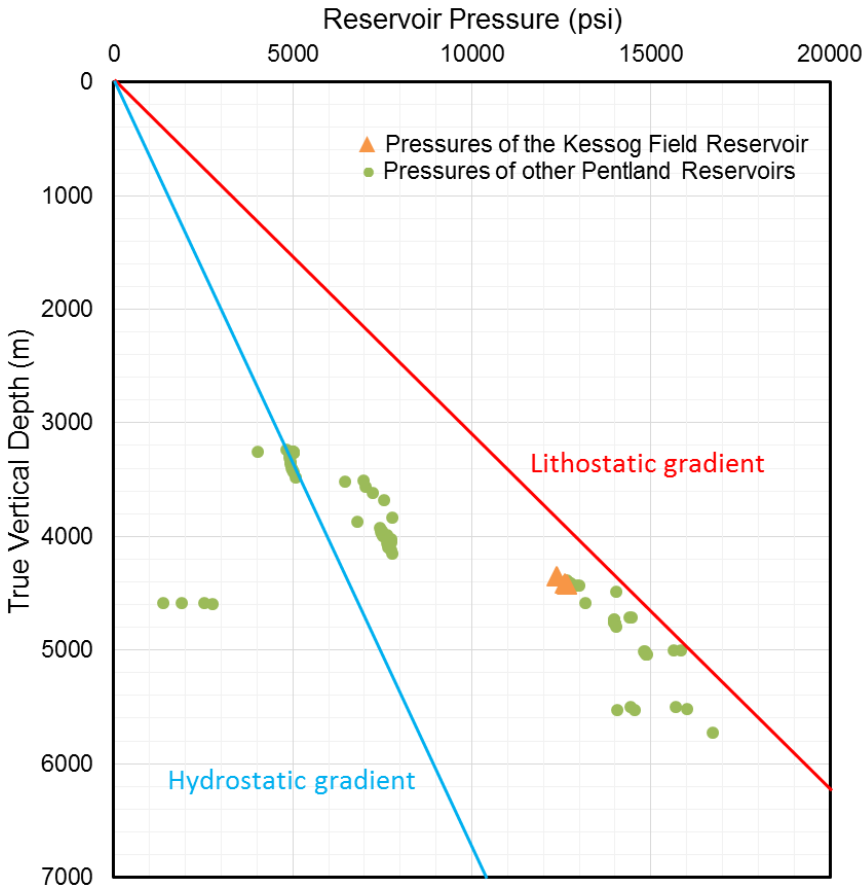

Figure 5.12 Reservoir pressure of the Pentland Formation. The triangles represent the data from the Kessog Field. All the pressure data were obtained by repeat formation test from 9 wells, including 22/05b-A12, 16/23-5, 9/13-5, 16/18-1, 9/19-7z, 29/5a-5, 23/26b-14, 23/26b-15 (in the order of increasing depth). The data points which lay on the left side of the hydrostatic gradient are presumably due to poor quality measurement as underpressured reservoirs have not been reported in the North Sea (Moss et al., 2003). The North Sea hydrostatic and lithostatic gradients are from Moss et al. (2003).

The porefluid pressure information of the Pentland Formation is presented in Figure 5.12. The degree of overpressure in the Pentland Formation varies with depth, and can be broadly divided into three levels: (a) normally pressured at the depth above 3.3 km; (b) slightly overpressured between 3.3 km and 4.2 km; (c) and highly overpressured below 4.2 km. The reservoir of the Kessog Field is highly overpressured, with the reservoir pressure close to the lithostatic pressure (Figure 5.12).

Overpressure in hydrocarbon reservoirs can offset the stress imposed by the weight of overburden sediments and thereby inhibit mechanical compaction and preserve porosity (Nguyen et al., 2013). In general, the shallower the onset of overpressure, the greater the potential for preserving high porosity (Stricker and Jones, 2016). The depth at which the overpressure starts is critical. The build-up of overpressure in the deep Central North Sea is considered to result from the rapid deposition of 2-3 km thick Paleogene sediments and the maturation of source rocks in the deep basin (Holm, 1998). It can be envisaged that, after the deposition of the Paleogene sediments and the maturation of the source rock, the Pentland Formation in the basin centre had already been buried to a considerable depth, at least below 2 km. The present-day data pressure data (Figure 5.12) suggests the onset of overpressure is from 3.2 km. This late build-up of overpressure means it is unlikely that overpressure can preserve porosity by reducing mechanical compaction in the Pentland Formation. The process of mechanical compaction has mostly completed before the depth of 2 km (Baldwin and Butler, 1985).

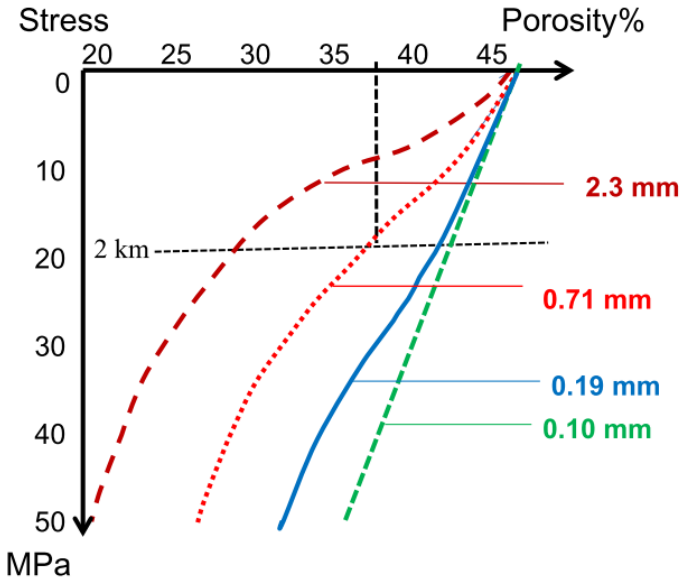

Figure 5.13 Porosity loss of well-sorted sands from mechanical compaction (Bjørlykke, 2014). The numbers (e.g. 2.3 mm) are grain sizes. The reservoir of the Kessog Field is made of 0.15 mm, very well-sorted sands. The compactional curve of the sands would fall in between the curves of 0.19 and 0.10 mm sands.

On the other hand, the sands forming the reservoir of the Kessog Field, as have shown by the petrographic data (Figure 5.6), are fine-grained and moderately well-sorted sands. The ability of this kind of sands to resist mechanical compaction has

been tested by experimental studies (e.g. Chuhan et al., 2003; Fawad et al., 2010). The experimental result (Figure 5.13) suggests that the kind of sands which form the reservoir of the Kessog Field, would only lose 3% of porosity by mechanical compaction during shallow burial (0- 2km). In other words, the sands of the Kessog Field are inherently resistant to compaction. This speculation is in accordance with the petrographic characteristic of the sandstones, which shows the compactional features such as bent mica grains, fractured grains, pressure dissolution and sutured grain contacts are rare in the sandstones. Hence, the total amount of porosity that could be preserved through inhibiting mechanical compaction from overpressure is limited.

Below the depth of 2 km, the porosity loss of sandstones begins to be dominated by the processes of pressure dissolution and quartz cementation. Osborne and Swarbrick (1999) showed a figure in which the volume of quartz cement in highly overpressured reservoirs is 3 % less than in slightly overpressured reservoirs. This suggests that overpressure can also inhibit quartz cementation through reducing pressure solution. While evidence for overpressure preventing quartz cementation is rare in the literature, and Osborne and Swarbrick (1999) have stated that that the mechanism behind the phenomenon is unclear, this process still sounds likely if pressure solution is indeed controlled by pressure (there is a discussion on this topic in Bjørkum, 1996). If overpressure can prevent 3 % of quartz cement as suggested by Osborne and Swarbrick (1999), it can reduce the porosity loss of a sandstone by about 6 %, which is significant (3 % cement + 3 % pressure solution, if briefly overlooking the minor volume change of sediments).

So what is the significance of overpressure inhibiting pressure dissolution in the Pentland sandstones? The pressure data shows the Pentland Formation at 4.2-5.8 km are invariably highly overpressured (Figure 5.12); the effective stress in all the wells only varies in a minimal range of 2000-3000 psi (Figure 5.12). The reservoir of the Kessog Field is not more highly pressured than the other reservoirs of the similar depth. Hence, there is no correlation between the degree of overpressure and porosity. Also, the pressure difference within the reservoir of the Kessog Field is anticipated to be small, i.e. less than the difference between the pressures of different oilfields. The minor difference of pressure within the Kessog Field cannot match and explain the large variation in porosity within the field. Hence, no evidence in the

Pentland Formation suggests that overpressures have an influence on the porosity of the sandstones.

(d) Secondary porosity

Wilkinson et al. (2014) suggested the amount of K-feldspar dissolved during the deep burial of the Pentland Formation is 5%. But after collecting more data, the study on the diagenesis of the Pentland Formation in Chapter 4 indicates there is only about 1-2% of K-feldspar dissolution during the burial of the sandstones. This newly created amount of secondary porosity is too small to be significant for the reservoirs of the Pentland Formation.

On the other hand, the petrographic data (Table 5.3) shows that in the sandstones of well 30/1c-5, which are the most porous sandstones in the Kessog Field, the amount of primary porosity is 10.3 ± 0.9 % whereas that of secondary porosity is 3.9±0.5 %. Secondary porosity is apparently less important than primary porosity in these high porosity sandstones. Figure 5.10 also shows this, in which the porosity of the high-porosity sandstones of the Kessog Field is predominantly primary. These lines of evidence suggest that high porosity sandstones in the Kessog Field are mainly formed by the preservation of primary porosity, rather than from the creation of secondary porosity.

(e) Other porosity preservation mechanisms

Maast et al. (2011) noticed a highly porous section of sandstones between the oil-leg and water-leg of the reservoir of the Miller Field, UK Central North Sea (well 16/3b-5). This section of sandstones is about 15m thick, containing porosity that is approximately 10% higher than both the oil- and water-legs of the reservoir. Through observations under the microscope, Maast et al. (2011) concluded that this high porosity is preserved by grain-coating bitumens on quartz grains. The high porosity sandstones in the Kessog Field, however, mostly occur in the top of the reservoir where it is hydrocarbon-saturated. The area is not where bitumen would necessarily be expected to form.

Two other mechanisms — phosphate poisoning (Warren and Pulham, 2001) and thermal anomalies near salt (Taylor et al., 2010) are unlikely to happen in the Kessog Field as it is not known close to any phosphate or salt beds.

(f) Hydrocarbon emplacement

The reservoirs of wells 30/1c-3, -6 & -9 are buried approximately 250m deeper than the reservoir of well 30/1c-5 (Figure 5.8). Modelling (Touchstone©) showed that 250m of deeper burial could result in 2.5% more quartz cement (Aase and Walderhaug, 2005; Lander and Walderhaug, 1999). But this amount of quartz cement is insufficient to account for the large difference in porosity between the reservoirs of well 30/1c-5 and 30/1c-3, -6 & -9 (Figure 5.8). There must be some mechanism that caused the high porosity in well 30/1c-5. Hydrocarbon emplacement is now the only remaining potential mechanism, after all other likely mechanisms have been excluded in the discussions above.

In general, hydrocarbon fills a reservoir from the top to the bottom of the reservoir. As a result, the exceptional porosity preserved due to hydrocarbon emplacement is expected to exhibit a typical pattern: the highest porosity should be at the top of the reservoir where hydrocarbon first accumulated. And then, the porosity is expected to systematically decrease downwards from the oil-zone into the water-zone (Wilkinson and Haszeldine, 2011). This is consistent with the pattern of porosity variation between different wells in the Kessog Field, where the highest porosity occurs in the well (30/1c-5) located at the crest of the field, indicating that the high porosity can be a result of local hydrocarbon emplacement at a relatively early time.

One difficulty in studying the influence of hydrocarbon on porosity in the Kessog Field is that the hydrocarbon saturation data do not indicate the existence of a clear oil-water contact, so that a direct comparison between the sandstones of oil-zone and water-zone cannot be made. But alternatively, the data of porosity as a function of hydrocarbon saturation (Figure 5.5) can be used to deal with the problem. In *Section 5.4.1* (*Porosity of the Kessog Field),* three distinct patterns of relationship between porosity and hydrocarbon saturation in the Kessog Field were described. The reservoir of well 30/1c-5 (the crestal well) shows the first pattern, in which both the porosity and hydrocarbon saturation are invariably high. Considering the process of hydrocarbon migration, it is not difficult to explain why these reservoir characteristics would form as the reservoir of well 30/1c-5 was the first to receive hydrocarbon charge in the field, presumably at a shallow depth when the sandstone was still uncompacted. In this circumstance, hydrocarbon was able to access most of the pore space,

reaching a high level of hydrocarbon saturation. Also because of the early timing of hydrocarbon emplacement, the high oil saturation has effectively inhibited quartz overgrowth. Therefore, the sandstone we see today has both high porosity and hydrocarbon saturation. Hydrocarbon filling a reservoir is a long process even on the geological scale, which may take tens of Ma (Gluyas et al., 1993b; Haszeldine et al., 2003). When hydrocarbon filled to the depth of wells 30/1c-4 and -6, the sandstones may have already been compacted and partly cemented. Hydrocarbon can only access the remaining large pore space, causing a high variation in oil saturation among the core samples. At places where hydrocarbon saturation was high, quartz overgrowth has since been inhibited. The result is that these sandstones show wide variation in porosity and hydrocarbon saturation, and these two parameters would also show close correlations, as we see today in wells 30/1c-4 and -6 in Figure 5.5 (b and c).

30/1c-3 is the deepest well, and hydrocarbon presumably filled the reservoir of 30/1c-3 last. By that time the quartz cement had fully grown, and the effect of hydrocarbon has been negligible for the porosity of the sandstone. Therefore, the concept of hydrocarbon emplacement preserving porosity can in fact well explain the characteristics of porosity and hydrocarbon saturation in the Kessog Field. The characteristics of the reservoir of well 30/1c-5 may be representative of reservoirs that were filled by hydrocarbon at shallow depth (< 2 km). And the reservoirs of well 30/1c-4 & -6 and well 30/1c-3 could be examples of reservoirs filled at intermediate depth (2-3.5 km) and deep depths (> 3.5km) respectively.

In terms of petrography, the high-porosity sandstones of the Kessog Field have two distinct features. The first one has been illustrated in Figure 5.10 that primary porosity is the dominant type of porosity in these sandstones. The second feature is shown in Figure 5.14, which demonstrates compaction is the main mechanism of porosity loss for the high porosity sandstones of well 30/1c-5 (crestal well); whereas in the sandstones of other wells, the porosity was lost mostly through cementation.

In a sandstone whose diagenesis has been affected by the emplacement of hydrocarbon, what petrographic features might be expected? The assumption is that hydrocarbon emplacement could inhibit quartz cementation. Hence, the sandstones affected by hydrocarbon should be less cemented and consolidated, and more

compressible. The sandstone would, therefore, lose more porosity from compaction than from cementation, as shown in Figure 5.14. Also, because primary porosity is smaller than secondary porosity, given a constant rate of quartz overgrowth, quartz cement will occlude primary porosity faster than secondary porosity. The result is that as the cementation process proceeds, the proportion of secondary porosity among total porosity will increase. However, in a case that quartz cement is inhibited, primary porosity would, in turn, be the main type of porosity (Figure 5.10). This is possibly the reason for why there are the high porosity sandstones in the Kessog Field whose porosity is dominated by primary porosity.

In summary, the high porosity sandstones of the Kessog Field have a combination of four characteristic features. Two of them are illustrated by core porosity data and two are by petrographic data, as follows:

- Porosity feature (I): highest porosity occurs in the top of the reservoir;
- Porosity feature (II): both porosity and hydrocarbon saturation are the highest in the top of the reservoir (well 30/1c-5); in well 30/1c-4 and -6, levels of hydrocarbon saturation show clear correlations to porosity; however, in the deepest well 30/1c-3, hydrocarbon saturation does not show any correlation with porosity;
- Petrographic feature (I): primary porosity is the dominant type of porosity in the high porosity sandstones;
- Petrographic feature (II): compaction is the primary mechanism of porosity loss.

All those features of porosity and petrography above can be explained by the concept of early hydrocarbon emplacement preserving porosity. It strongly suggests that early hydrocarbon emplacement is the cause of the high porosity in the sandstones. Also, in the discussions above, all other potential mechanisms capable of preserving or enhancing porosity are considered to be unlikely to occur in the sandstones, or to be insignificant for the formation of high porosity. Therefore, it can be concluded that the high porosity sandstones in the Kessog Field are preserved due to early hydrocarbon emplacement.

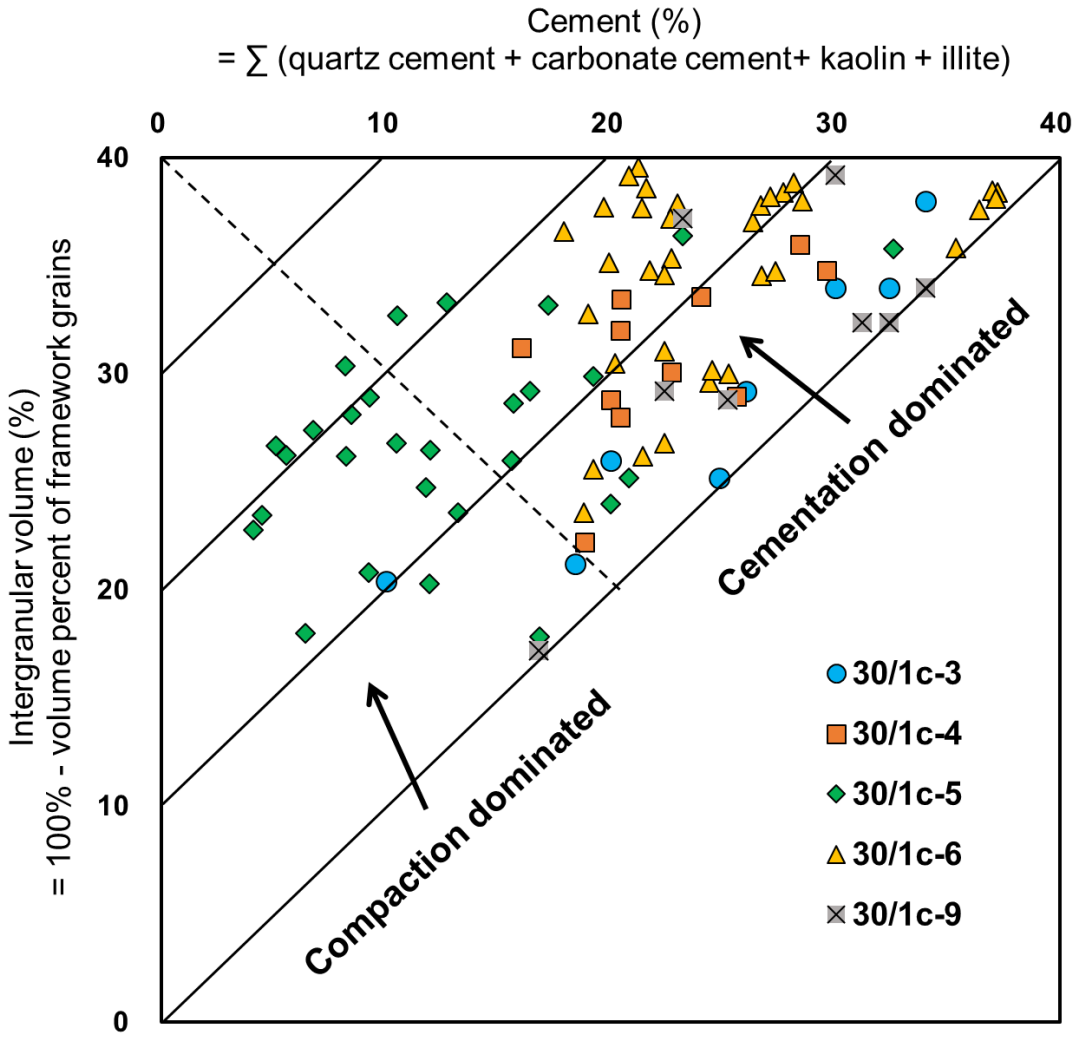

Figure 5.14 Diagram showing the relative importance of compactional processes and cementation to the porosity development of the reservoir sandstones in the Kessog Field (Ehrenberg, 1989; Houseknecht, 1987). Compaction is the dominant porosity loss mechanism for the sandstones of well 30/1c-5, whereas cementation has caused more porosity loss to the sandstones of the other Kessog wells.

5.5.2 Hydrocarbon emplacement retard K-feldspar dissolution and diagenesis

The last section has concluded that the emplacement of hydrocarbon has effectively preserved porosity in some sandstones of the Kessog Field, in particular in the sandstones of the crestal well 30/1c-5. However, in the same reservoir compartment (well 30/1c-5), we also noticed that the content of K-feldspar is significantly higher than the other parts of the reservoir, i.e. in wells 30/1c-3, -4, -6 and -9 (Table 5.3). The Pentland Formation as a whole has only small quantities of K-feldspar (1.5 ± 0.1 %, Wilkinson et al., 2014b), and the average of the Kessog Reservoir is no different in this regard (1.6 ± 0.2 %, Table 5.3). In contrast, the percentage of K-feldspar in well 30/1c-5 is more than twice as high (3.8 ± 0.4 %, Table 5.3). Meanwhile, the amount of kaolin, which is a common product of K-feldspar dissolution (Bjørlykke and Aagaard, 1992), is minimal in the reservoir of 30/1c-5 (0.7 ± 0.2 %, Table 5.3). For comparison, the average content of kaolin in the Kessog Field is 3.7 ± 0.3 %, and the whole Pentland Formation sandstones 3.8 ± 0.2 % (Table A 4.1). The high content of K-feldspar and the low abundance of kaolin in well 30/1c-5 are apparently exceptional among the Pentland sandstones, and this section attempts to identify the cause of this phenomenon.

In total, there are three reasons that can explain the difference in the content of K-feldspar between the reservoirs of well 30/1c-5 and wells 30/1c-3, -4, -6 and -9. We write them in the format of hypotheses:

i. These sandstones were deposited from different sources, and thereby contained different initial compositions;
ii. These sandstones had the same initial compositions, but the sandstone in well 30/1c-5 is less leached by meteoric water near the surface, which resulted in less K-feldspar dissolution;
iii. These sandstones were of uniform sedimentology and had been leached by the same degree of meteoric water flow. The different K-feldspar contents were caused at depth, through the inhibition of K-feldspar dissolution in well 30/1c-5 by the presence of hydrocarbon.

The discussions on the sandstone's petrography in the last section *(5.5.1)* have concluded that the variations in the original composition and texture of sandstones are minimal across the Kessog Field. It is unlikely for sandstones of well 30/1c-5 to have contained a significantly higher amount of K-feldspar than the sandstones of the other wells upon deposition. Thinking from another angle, supposing hypothesis (i) were correct and the sandstone of 30/1c-5 was indeed richer in K-feldspar upon deposition, it cannot explain why the sandstone would become kaolin-poor at depth comparing to the other reservoir sandstones. Therefore, hypothesis (i) is not valid.

As the Pentland Formation was deposited in a fluvial-deltaic setting, it is reasonable to assume that some parts of it have been leached by meteoric water. The degree of leaching, however, can vary from site to site. Areas that were subjected to more erosion are generally where exposed to more meteoric water flushing in the past (Bjørlykke, 1994). The reservoir of the Kessog Field was once exposed on land and affected by erosion during the Late Jurassic/Early Cretaceous, as evidenced by the unconformity surface below the Cretaceous strata (Figure 5.3). The degree of meteoric water leaching across the field can be inferred from the degree of erosion, which is represented by the remaining thickness of Jurassic sediments after erosion. In the western part of the field (Figure 5.3), thick Upper Jurassic sediments of the Kimmeridge Clay Formation are present, and the Middle Jurassic reservoir rock is fully preserved (280m thick in well 30/1c-3). In sharp contrast, Upper Jurassic sediments in the eastern part of the field are absent, probably having been entirely eroded, and the Middle Jurassic reservoir has also been heavily eroded and reduced to a small thickness. In well 30/1c-5 particularly, the reservoir is only 24.5m thick, compared to the thickness of 280m in well 30/1c-3. Hence, in the Kessog Field, the degree of meteoric water leaching is expected to be the greatest where well 30/1c-5 is located. The hypothesis (ii) that the preservation of K-feldspar in 30/1c-5 is due to less meteoric water leaching can be rejected.

According to Formula 5.1, the dissolution of K-feldspar producing kaolin would also release silica and potassium at the same time. For the reaction to proceed, the silica needs to be efficiently removed from the dissolution site, by either diffusion or advection through aqueous phase. In the oil phase, however, silica and potassium are insoluble. As a result, the replacement of water by oil would reduce the transport rate of potassium and silica within the pore space (Wilkinson and Haszeldine, 2011;

Worden et al., 1998). If K-feldspar dissolution at high temperatures (>70ºC) is controlled by the transport rate of products, rather than by the kinetics of the reaction, the whole process would be significantly slowed down after the emplacement of hydrocarbon. Therefore, early hydrocarbon emplacement preserving K-feldspar in sandstone reservoirs is sensible in theory. The preservation of K-feldspar in the reservoir of well 30/1c-5 could be an example of this process. The possibilities of other mechanisms (hypotheses i & ii) to account for this phenomenon have been excluded.

Formula 5.1 (Bjørlykke and Jahren, 2015)

$2KAlSi_3O_8$	$+ 2H^+ + 9H_2O =$	$Al_2Si_2O_5(OH)_4$	$+ 4H_4SiO_4$	$+ 2K^+$
K-feldspar		kaolin	dissolved silica	dissolved potassium

If the high content of K-feldspar in the sandstones of well 30/1c-5 is owing to the preservation of K-feldspar, we would expect that dissolving some K-feldspars in the sandstones of well 30/1c-5 would produce a sandstone that is similar to those in wells 30/1c-3, 4, 6 and 9. Table 5.4 and Table 5.5 are the calculation process of mass balance between these two groups of sandstones. The proportions of porosity and carbonate cement were taken out in the calculation (Table 5.4). Note that the microporosity within authigenic kaolin and illite were assumed to be 40% and 90% respectively, according to the measurement of Hurst and Nadeau (1995). The calculation of mass balance takes into account the diagenetic processes of quartz cementation, K-feldspar dissolution and mica dissolution. The result shows that by dissolving 3.5 cm^3 detrital quartz for quartz cementation, 1.0 cm^3 K-feldspar for the precipitation of kaolin and quartz, 1.3 cm^3 K-feldspar for illite and quartz, 1.3 cm^3 mica for kaolin, the sandstones of well 30/1c-5 will end up with a composition that is close to the average composition of the sandstones of wells 30/1c-3, -4, -6 &-9 (Table 5.5). This suggests that the sandstones of well 30/1c-5 and well 30/1c-3, -4, -6 and -9 could, in fact, be equivalent in terms of mineralogical composition. It is possible that the sandstones of well 30/1c-5 are just at an earlier stage of diagenesis than the sandstones of well 30/1c-3, -4, -6 and -9. The implication of this mass balance calculation is that in addition to quartz cementation, the diagenetic processes such as the dissolution of K-feldspar and mica have all been inhibited in the reservoir of well 30/1c-5. The most likely reason is the early emplacement of hydrocarbon. On the other hand, the calculation indicates that the sandstones of 30/1c-5 and well 30/1c-3,

-4, -6 and -9 could have had the same composition during shallow burial, which again refutes hypotheses (i) and (ii) that the sandstones already were different at shallow depth (< 2km).

Table 5.4 The mineralogical compositions, excluding carbonate cement and porosity, of the sandstones in the Kessog Field

	n	Quartz (%)	QOG (%)	K-feldspars (%)	Plagioclase (%)	Kaolin (%)	Illite (%)	Mica (%)	Sum (%)
30/1c-3	8	75.6	7.0	1.4	0.5	6.0	9.0	0.4	100
30/1c-4	13	68.3	4.6	2.1	1.3	3.3	19.1	1.3	100
30/1c-6	50	64.1	7.8	0.7	2.6	5.9	16.8	2.2	100
30/1c-9	8	70.6	8.5	0.6	0.3	7.0	12.6	0.5	100
Averages of the above 4 wells	79	66.7	7.3	1.0	1.9	5.6	16.0	1.7	100
30/1c-5	28	76.0	3.4	4.6	1.0	0.9	10.9	3.1	100

Table 5.5 A mass balance calculation showing how the sandstones of 30/1c-5 become the sandstones of 30/1c-3, -4, -6 & -9 through diagenetic reactions. More details of the calculation are in Appendix 4.

Sandstone of well 30/1c-5	Mineral dissolution and re-precipitation	Composition of the product sandstone		Average sandstone composition of wells 30/1c-3, -4, -6 & -9
		Mineral Volume	Percentage	Percentage
Original Composition: 76.0 cm^3 Quartz 3.4 cm^3 QOG 4.6 cm^3 K-feldspar 1.0 cm^3 Plagioclase 0.9 cm^3 Kaolin 10.9 cm^3 Illite 3.1 cm^3 mica Total Volume: 100 cm^3	Dissolution of 3.0 cm^3 detrital quartz → 3.0 cm^3 quartz cement Dissolution of 2.5 cm^3 K-feldspar → 1.9 cm^3 Kaolin + 1.05 cm^3 quartz cement Dissolution of 1.0 cm^3 K-feldspar → 6.6 cm^3 Illite + 0.6 cm^3 quartz cement Dissolution 1.3 cm^3 mica → 2.3 cm^3 kaolin	Quartz: 73.0 cm^3 QOG: 3.4 + 3.0 + 1.05 + 0.6 = 8.05 cm^3 K-feldspar: 4.6 - 2.5 - 1.0 = 1.1 cm^3 Plagioclase: 1.0 cm^3 Kaolin: 0.9 + 1.9 +2.3 = 5.1 cm^3 Illite: 10.9+6.6=17.5 cm^3 Mica: 3.1-1.3=1.8 cm^3 Total volume of the new sandstone: 107.4 cm^3	**68.0 % Quartz** **7.4 % QOG** **1.0 % K-feldspar** **0.9 % Plagioclase** **4.8 % Kaolin** **16.3 % Illite** **1.7 % mica** **Total: 100%**	**66.7 % Quartz** **7.3% QOG** **1.0% K-feldspar** **1.9% Plagioclase** **5.6% Kaolin** **16 % Illite** **1.7% mica** **Total: 100%**

5.5.3 Why is predicting the effect of hydrocarbon emplacement difficult?

This and the next section (*5.5.4*) contain some of the author's speculation on the general issue of predicting the effect of hydrocarbon on reservoir porosity.

The process of hydrocarbon emplacement affecting reservoir diagenesis undoubtedly deserves great attention, as every exploratory target is, or is at least thought to be, hydrocarbon-filled; and some studies (Bloch et al., 2002; Emery et al., 1993; Marchand et al., 2001; Wilkinson and Haszeldine, 2011; Worden et al., 2018), including this one, have suggested hydrocarbon is capable of preserving up to 10% extra porosity. However, it should be realised that such an effect of porosity preservation by hydrocarbon will not happen in every oilfield. These conclusions are more probabilistic. Geoscientists have mostly understood and proven the phenomenon of hydrocarbon preserving porosity, but we still do not know the probability of its occurrence. The issue of determining the probability is the main challenge to applying this knowledge in practical hydrocarbon exploration.

In general, there are two ways to obtain the probability: empirical data analysis and modelling. Empirical data analysis needs to be based on a large amount of oilfield data. The larger the dataset, the better the prediction accuracy. But to collect a large set of data requires researchers to interpret the porosity data of a large number of oilfields in detail, identifying the presence of anomalous porosity and its cause. This would be a very labour- and time-consuming work. Moreover, the predictive ability of this method may sometimes be low: for reservoirs with few drilling records or highly variable geology, the accuracy of prediction might be low. Hence, empirical data analysis does not seem to be a promising method for estimating the probability of hydrocarbon emplacement preserving porosity.

Predictive models for reservoir quality have been evolving rapidly in the past few decades (Ajdukiewicz and Lander, 2010). Nonetheless, there is yet to be any practical model that has been proven to be widely applicable to address the issue of hydrocarbon emplacement preserving porosity. In fact, actual oilfield data rarely support any predictive models that are based upon the mechanism of hydrocarbon

inhibiting quartz cementation (Taylor et al., 2010). This is very likely due to the great difficulty in understanding how hydrocarbon are distributed within the reservoir. Taking the Kessog Field as an example, it was difficult to decide whether to describe the reservoir as filled or underfilled. For example, fluid saturation data in Figure 5.5 shows the oil saturation of the majority of measured samples are lower than 50%. From this point of view, the reservoir can be seen as underfilled. But the whole oilfield has contained 100 million barrels of oil equivalent hydrocarbons, which is already a huge reserve. Although the porosity of some reservoir sections can be anomalously high, e.g. 25%, the average porosity of the whole field is only 15.3%, which is not exceptional. Hydrocarbon emplacement in the Kessog Field might have started at an early time, as is indicated by the preservation of high porosity in the crest of the reservoir. But, maybe due to complex reservoir structures, hydrocarbon were only able to fill a small portion of pore space and the average hydrocarbon saturation of the whole field is only 29% (Figure 5.2). This could reflect the situation in many hydrocarbon reservoirs where early hydrocarbon emplacement did not necessarily lead to the preservation of high porosity. The effect of hydrocarbon emplacement preserving porosity is also highly depending on how the hydrocarbon are distributed in the pore scale and reservoir scale. But these points are extremely difficult to model or predict.

The timing of hydrocarbon emplacement is important not only for inhibiting early quartz cementation, but also for allowing hydrocarbon to charge a reservoir to a high saturation level. Pore water in loose sands (>20% helium porosity) might be easily replaced by hydrocarbon fluids, and the difficulty of replacing pore water may increase exponentially as the porosity of sandstones decreases. For each type of sandstone, there might be a corresponding cut-off depth for hydrocarbon emplacement to effectively preserve on porosity. But this cut-off depth is, further, a function of a sandstone's grain-size, sorting and mineralogy (particularly clay content), which again makes the question complicated. However, it might be useful to determine an average or general cut-off depth of hydrocarbon charge that is applicable for most sandstones.

5.5.4 Stratigraphy and hydrocarbon emplacement preserving porosity

Hydrocarbon reservoirs of different stratigraphic levels have their own unique spatial relationships to the source rocks. These reservoirs will have different histories of burial and hydrocarbon filling in general, which may further produce a significant influence on the reservoir quality. This section includes some speculations on this aspect.

Both the processes of quartz cementation and source rock maturation are highly temperature-sensitive. However, the temperatures from which the two processes start are different: quartz cementation starts at 70-80 ^{o}C (Bjørlykke and Egeberg, 1993; Gluyas et al., 1993a), whereas the main hydrocarbon generation window for source rocks is at 110 – 140 ^{o}C (Brooks et al., 1987). This means for a sandstone reservoir to have received hydrocarbon prior to the start of quartz cementation, there must be a much deeper maturing source rock providing the hydrocarbon. Assuming in a basin with a geothermal gradient of 35 ^{o}C/km, the source rock needs to be approximately 1 km deeper than the sandstone reservoir. After realizing this point, the structural and stratigraphic information of a basin could help us analyse what kind of reservoirs is more likely to be charged with hydrocarbons at shallow depth.

Take the Upper Jurassic petroleum system of the Central North Sea as an example (Figure 5.15). Source rock is the Kimmeridge Clay Formation (KCF). There are two main types of sandstone reservoirs: (1) the turbidite sandstones encased in the KCF (e.g. the Burns and Claymore Sandstone Members); (2) and the widespread shallow marine Fulmar Formation sandstones. The turbidite sand bodies might be locally thick but are laterally restricted (Fraser et al., 2002; Richards et al., 1993). Charging these reservoirs is almost solely dependent on the source rocks surrounding the turbidites (Figure 5.16a). When the source rocks become mature and start to generate hydrocarbons (110-140 ^{o}C), quartz may have already well cemented the reservoirs. In this case, hydrocarbon emplacement would be too late to inhibit quartz cementation. The Fulmar Formation, in comparison, is laterally extensive, highly homogenous and lacks internal barriers to fluid flow (Howell et al., 1996; Wilkinson and Haszeldine, 2011). When tectonic movements tilted the strata, the excellent lateral connectivity

and homogeneity of the Fulmar sandstones can readily connect the shallow reservoir with the deep source rock (Figure 5.16b). For this process to work, the body of the Fulmar sands only needs to be of several kilometres of good lateral continuity, which is not difficult to achieve for a shallow marine sandstone. The consequence is that comparing to other reservoirs of the same age, including the Pentland Formation, the Fulmar Formation is more likely to be charged during early burial.

These two contrasting models can explain why many shallow marine sandstone reservoirs in the Central North Sea contain anomalously high porosity, with the process of quartz cementation seems to have been repressed by hydrocarbons (e.g. Wilkinson and Haszeldine, 2011; Worden et al., 2018); whereas the cases are rare and contentious for the turbidite reservoirs (e.g Aase and Walderhaug, 2005; Maast et al., 2011; Marchand et al., 2000).

These two models (Figure 5.16) demonstrate the importance of the spatial relationship between reservoirs and source rocks. They show some reservoir units inherently have a better chance than others to be filled at shallow depth. The most important characteristic of these reservoirs is lateral continuity and internal homogeneity, which provides passageways for the upward migration of hydrocarbons from deep basin to shallow reservoirs. Proximity to source rocks, however, is not necessarily an advantage for a reservoir. Despite that it is more likely to be hydrocarbon-charged, the timing of this charge tends to be relatively late, after the main time period of quartz cementation. Some other reservoirs, which although may be several kilometers away from the source rock, are on the contrary more likely to be filled with hydrocarbon at an early time, and form high-quality reservoirs as a result of early hydrocarbon emplacement inhibiting quartz cementation.

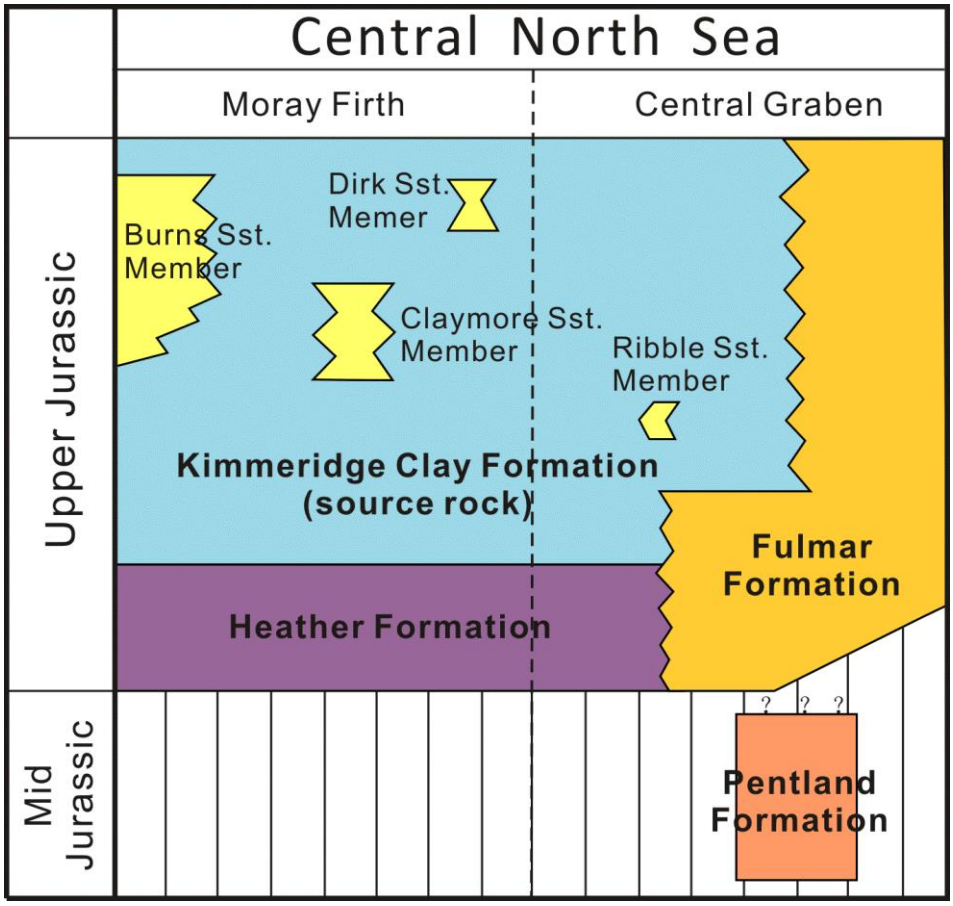

Figure 5.15 The Upper Jurassic stratigraphy of the Central North Sea (modified from Richards et al., 1993). The Pentland Formation of this study is also marked; but its boundary with the Fulmar Formation is uncertain (conformal or unconformal?; Richards et al., 1993).

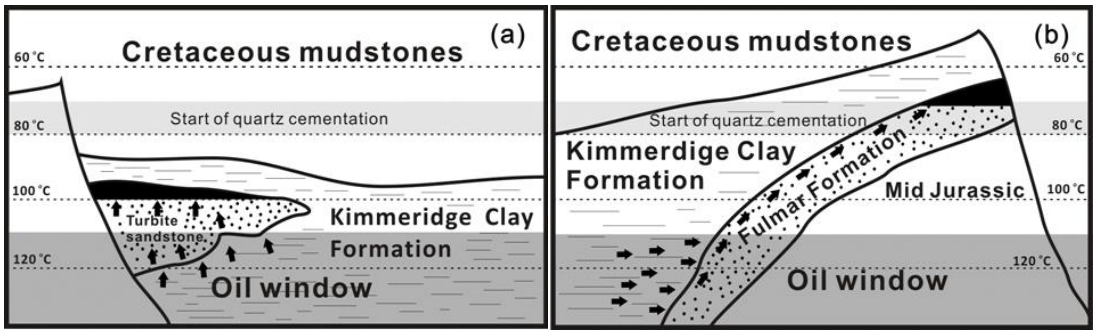

Figure 5.16 Hydrocarbon charging models for the Upper Jurassic turbidite and shallow marine sandstones of the Central North Sea. The Fulmar Formation tends to be charged at a shallower depth than the same age turbidite sandstone reservoirs.

5.6 Conclusion

1. Some of the reservoir sandstones of the Kessog Field are highly porous, even though they are now buried to below 4km. Most of the high-porosity sandstones are found within the top of the reservoir that is drilled by well 30/1c-5. The porosity of these sandstones averages at about 25%, which is 10% higher than the porosity of a similar sandstone at the same depth. Meanwhile, some sandstones in the other wells of the Kessog Field, 30/1c-3, -4 -6 and -9, also exhibit similar high-porosity characteristics. This study investigated the cause of the high porosity in the Kessog Field.

2. The high-porosity sandstones of the Kessog Field are similar to the low-porosity sandstones in the same field regarding sandstone texture and original composition. The texture and composition of these sandstones also do not appear to be different from other Pentland Sandstones elsewhere. Therefore, the high-porosity of the Kessog sandstones is not considered to be related to the texture and original composition of the sandstones.

3. Microquartz and chlorite coats do not occur in the Pentland Formation, so that they cannot be the cause of the high porosity. Grain-coating illite is present on only less than 10% of the surface of the quartz grains of the sandstones. Such a small amount of illite coats are incapable of effectively inhibiting quartz cementation.

4. The dominant type of porosity in the reservoir is primary porosity, and hence the possibility that the high-porosity results from mineral dissolution (secondary porosity) can be refuted. Also, all the Pentland sandstones in the deep basin are overpressured at similar levels. The minor differences in the degree of overpressure between wells cannot explain the substantial differences in porosity between the wells. There is no correlation between porosity and the level of overpressure.

5. Hydrocarbon emplacement is the only possible mechanism that can explain the occurrence of the high porosity sandstone in the Kessog Field.

6. The reservoir of the Kessog Field displays some distinct porosity and petrographic features. For example, the high-porosity sandstones mostly occur in the crestal part of the reservoir; the reservoirs in well 30/1c-4 and -6 showing strong correlations between the porosity and the level of hydrocarbon saturation. Regarding the petrography of the high-porosity sandstones, primary porosity is the dominant type of porosity, whereas the amount of secondary porosity in the high-porosity sandstones does not appear to be higher than in the low-porosity sandstones. Compaction is the main mechanism of porosity loss for the high-porosity sandstones. In comparison, for the medium to low-porosity sandstones, porosity loss is mainly from cementation. All of these characteristics of the high porosity sandstones can be explained by the scenario of early hydrocarbon emplacement preserving porosity, which strongly suggests the high-porosity sandstones of the Kessog Field is formed by the early emplacement of hydrocarbon.

7. The high-porosity sandstones also contain more K-feldspar and less kaolin. Hydrocarbon emplacement inhibiting the diagenetic dissolution of K-feldspar is very likely to be the cause of the phenomenon. The possibilities that this was due to a difference in the depositional processes or due to the leaching of meteoric water through the reservoirs are considered to be low. A mass balance calculation showed that the high-porosity sandstones, which is also richer in K-feldspar, can evolve to become the low-porosity sandstones with some pressure dissolution; quartz cementation; the dissolution of some of the K-feldspar; and also the transformation of some mica. It suggests that the high-porosity sandstones and low-porosity sandstones could have been identical at the time of deposition. The current difference between the two sandstones is because they are at different stages of diagenesis. Diagenetic processes in the high-porosity sandstones have been inhibited by hydrocarbon emplacement.

Summary statement: This study delivers a clear answer to the controversy of whether oil can prevent quartz cementation. It demonstrated that hydrocarbon emplacement has preserved up to 10% of reservoir porosity in the Kessog Field. Also, it shows the evidence indicating that hydrocarbon emplacement can also retard other diagenetic reactions, such as the dissolution of K-feldspar and mica and the precipitation of kaolin.

Chapter 6

The Mass Transfer of Silica, Aluminium and Potassium at Sandstone-Shale Contacts

ABSTRACT

After the study in Chapter 4, this project will continue to search for the evidence of mass transfer in sediments during diagenesis. The samples of this study are collected from five hydrocarbon reservoirs comprised of interbedded sandstones and shales. The sandstone samples are mostly turbidite sandstones. The shales are Kimmeridge Clay shales, which are the source rocks of the oilfields where the samples collected. The contacts between the sandstones and the shales are expected to be dynamic areas of pore fluid flow during the maturation of the shales.

A total of 9 groups of sandstone and 3 groups of shale were collected from the sandstone-shale contacts in the reservoirs of the five oilfields. Within each group, the space interval between samples is 1 cm. These samples have been used to study the mass transfer on the scale of 0-10 cm. Another three groups of sandstones and three groups of shales with larger interval space between samples varing from decimeters to meters, were also collected. The aim is to study the potential mass transfer on the corresponding scale. Petrographic data (point-count), mineralogical data (X-ray diffraction) and chemical data (X-ray fluorescence) were utilised for the study.

On the scale of 0-10cm, the chemistry of the sandstone samples appears to be largely controlled by the 'upwards-fining' sedimentary sequence of turbidite deposits. But on the larger scale of decimeter to meters, the composition of sediments become more variable. The mineralogical and chemical data of the studied samples do not show any evidence that suggests the process of mass transfer by diffusion.

To study the mass transfer by pore fluid flow is more difficult. First, it needs to determine the direction of pore fluid flow in a reservoir. Two reservoirs, which only comprised of a thick sandstone bed and a thick shale bed, were chosen for stud, assuming the direction of pore fluid flow is from the shale to the sandstone. The reservoir of well 21/1a-20 is the most likely case in this study where a considerable scale of mass transfer has occurred. A thin layer of shale enclosed within the sandstone reservoir of well 21/1a-20 shows depleted content of quartz (c.3%) when compared to the shale that is below the sandstone reservoir (c.32%). It suggests the shale within the sandstone has lost silica during diagenesis. Also, the trends of SiO_2 (%) and SiO_2/TiO_2 in the sandstone increases towards the sandstone-shale contact; and meanwhile, the shale also shows decreasing trends of SiO_2 (%) and SiO_2/TiO_2 towards the sandstone. These patterns of chemical variation indicate that there might be some exchange of silica between the sandstone and shale. However, the point-count data of the sandstone do not prove there is a substantial difference in the contents of quartz cement between the sandstones close to the shale and the sandstones more distant from the shale. Thus, the hypothesis of the mass transfer of silica in the reservoir of well 21/1a-20 cannot be confidently verified to be correct.

Similarly, the study for the diagenetic mobility of iron, magnesium and calcium, using the same method, also did not find any chemical trend or evidence that indicates there was significant transfer of these element across the studied sandstone-shale contact.

Overall, this study has not found any indisputable evidence that suggests the mass transfer has occurred in any of the studied samples. It suggests the mobility of chemical elements in the deep subsurface is limited, probably below the scale of the detection of the study method, i.e. <5 cm. Sandstones and shales are closed systems in diagenesis.

6.1 Introduction

K-feldspar is a main mineralogical component in clastic sediments. It is composed of the chemical elements of silica, aluminium, potassium and oxygen (chemical formula: $KAlSi_3O_8$). The presence of dissolved K-feldspar grains is a common phenomenon in sandstone reservoirs during diagenesis (Wilkinson et al., 2001). However, the timing of the dissolution and the re-distribution of the dissolution products are matters of debate (e.g. Bjørlykke, 2011; Day-Stirrat et al., 2010). It is highly controversial as to how far the products, i.e. the ions of silica, aluminium and potassium, can be re-distributed to after the K-feldspar dissolution (Giles, 1987; Wilkinson et al., 2003). This issue is of great importance to reservoir quality prediction. If the products are confined within a reservoir, then the creation of new porosity (secondary porosity) due to K-feldspar dissolution will be offset by the occlusion of old porosity by the growth of authigenic minerals (Giles and de Boer, 1990). There will be no net porosity increase for the reservoir. If this is the case, then the prediction of reservoir quality can be primarily based upon the assumption about the original composition of sediment at the surface. However, if the silica, aluminium and potassium can be transferred out of a sandstone reservoir, for example, to a neighbouring shale, then an increase in the reservoir porosity would be expected. This process can potentially create high-porosity reservoirs at depth but will make the prediction of reservoir quality more challenging, as we need to understand further the scale of any mass transfer processes that have occurred.

Perry and Hower (1970) studied the mineralogical and chemical variations within the Pleistocene-Eocene shales in the Gulf of Mexico, and they observed a potassium increase in the clay-size fraction of the shales with depth. This was the first time that the movement of chemical elements during sediment diagenesis was systematically studied. In the following decades after 1970, a large volume of literature on the topic has been published, but the question of how far chemical elements can migrate in the subsurface remains unsolved (Bjørlykke, 2011). Generally, there are two schools of thoughts: '*open system*' and '*closed system*'. Supporters of the *'open system'* theory claim that the solutes released from mineral dissolution in sandstones can be exported to adjacent shales, creating new porosity in the original reservoirs (e.g. Day-Stirrat et al., 2010). Opponents of this point of view ('*closed system*'), however, argue that the mobilisation of solutes in deep sandstones is highly restricted and that any

movements of solutes are extremely limited, even at a thin-section scale (Bjørlykke and Jahren, 2012; Hayes and Boles, 1992). The chemical elements usually considered are silica, aluminium and potassium, as they are key constituents of the common authigenic minerals in diagenesis, such as quartz cement and illite (Giles and de Boer, 1990). The diagenetic mobility of these elements has a profound influence on the quality of sandstone reservoirs.

Evidence supporting the '*open system*' scenario in the literature can be broadly divided into five types:

1. The volumetric relationship between the reactive and product minerals in a reservoir (e.g. Sullivan and McBride, 1991; Wilkinson and Haszeldine, 1996): for example, Wilkinson and Haszeldine (1996) noted that the amount of dissolved K-feldspar in the Fulmar Formation sandstone of the North Sea is not matched by the volume of newly-precipitated illite, thus indicating an export of mass from the reservoirs.
2. Comparisons between the sandstones inside and outside carbonate concretions: Gluyas and Coleman (1992) analysed the chemistry of these two types of sandstones from four different geological formations in the North Sea, and they concluded that the silica content of the sandstones has increased from 220 to 350 kg m^{-3} through burial (silica import), whereas the content of Al, K and Na remains constant.
3. Comparisons between thin and thick sandstone/shale beds: in the North Sea Miller Field, for instance, Gluyas et al. (2000) found that thin shales interbedded within the main sandstone reservoir have higher contents of aluminium and potassium and lower silica when compared with the thick shales above the reservoir, suggesting that the interbedded shales have gained Al and K and lost Si in diagenesis.
4. Observations of increased amounts of kaolin-to-illite alteration (Ehrenberg, 1991) and quartz cement (Thyne, 2001) near sandstone-shale contacts.
5. The correlation between the chemistry of sediments and depth: the majority of the supporting evidence belongs to this type. In particular in the Gulf of Mexico, many studies have documented an increase in potassium (e.g. Awwiller, 1993; Berger et al., 1999; Day-Stirrat et al., 2010; Land, 1997; Milliken et al., 1994), and a few studies aluminium enrichment (e.g. Lynch et al., 1997; Wilkinson et al., 2003), in the local Eocene-Paleocene shales as depth increases. Similar

chemical trends have also been observed in Cenozoic sandstones and shales in the Mahakam Delta Basin, Indonesia (Furlan et al., 1996).

In addition, the scenario of mass transport between sandstones and shales is also favoured by the coincidence that the main chemical (diagenetic) reactions in the two sedimentary rocks occur at similar depths, and right produce the required solutes for the exchange of mass (Thyne, 2001).

Sceptics of the 'open system' theory, citing reservoir and fluid flow modelling evidence, argue that there is no viable mechanism that would allow a significant transfer of silica, aluminium and potassium to occur in the deep basin (Bjørlykke and Jahren, 2012). Mass transfer by diffusion is restricted by a lack of high concentration gradients of elements in the reservoir pore fluids, as the fluids, after a long period of burial, have been in close equilibrium with the minerals present (Egeberg and Aagaard, 1989; Giles, 1987). The mass transfer by fluid flow (advection) is also restricted since modelling shows that the actual rate of fluid flow in the subsurface is 2-3 orders of magnitude lower than the required rate of fluid flow to transport a considerable amount of silica, aluminium and potassium (Bjørlykke, 1994).

To envisage a possible mechanism of mobilising elements, advocates of the 'open system' theory appeal to the organic acids or CO_2 generated during the maturation of source rocks (e.g. Lundegard and Land, 1986; MacGowan and Surdam, 1988; Stoessell and Pittman, 1990). Experimental evidence suggests that the solubility of aluminium can be increased by up to three orders of magnitude in the presence of organic acids (Surdam et al., 1984). Nevertheless, the debate on the topic of organic acids is as complex as the issue of the mass transfer itself and is also highly controversial (see Giles et al., 1994; Surdam et al., 1984). This study will not investigate the mechanism by which organic acids enhance the solubility of Al, nor measure the concentration of organic acids under real reservoir conditions. Rather, this study is designed to search for the geological evidence that can support or refute any of the potential mechanisms for mass transfer, and if possible, to measure the possible scale of mobility of silica, aluminium and potassium.

A novel method is employed in this study. Sandstone and shale samples were collected at sandstone-shale contacts. The samples are cut along the length of the

core (i.e. perpendicular to bedding, see Figure 6.1). These samples are bar-shaped, 10 – 15 cm in length. Then, they were cut by a rock saw into regular pieces, as inFigure 6.2. Analysing the chemical variation through the samples may reveal the potential mass transfer process at the sandstone-shale contact. The sandstones are reservoir rocks of some North Sea oilfields. The shales, except for those from well 16/17-19, are from the Kimmeridge Clay Formation, which is the main source rock in the North Sea. The pore fluids at the contacts between the sandstones and shales are expected to be dynamic during the time of source rock maturation, when large volumes of pore fluids and hydrocarbon were migrating out of the shales.

The compositions of sandstones and shales are controlled by sediment provenance, depositional environment and diagenetic processes (Bjørlykke, 2014). One major problem in the study of mass transfer is distinguishing the chemical variation of samples caused by diagenesis from that caused by the variations in sedimentary environment or provenance (Day-Stirrat et al., 2011). In some cases, it is possible that all the three factors have strong influences on the chemistry of sandstones and shales, which makes chemical data difficult to interpret. The method of this study has two advantages in minimising the effect of provenance and depositional process. The first advantage is sampling from turbidite sandstones, which are largely uniform and tend to have minimal variation in the lateral and vertical extent (Gluyas et al., 2000; Worden and Barclay, 2003). The second advantage is the close spacing between samples. The sample pieces cut from the same bar sample (Figure 6.1) can be considered to be sampled from the same location, which can ensure a minimum change in the original composition of the sediments.

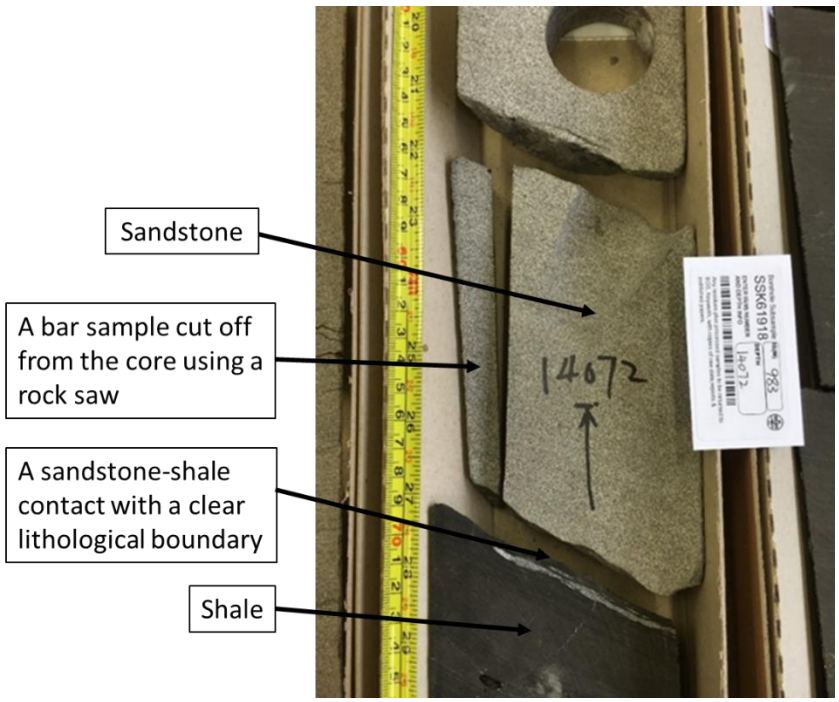

Figure 6.1 A sandstone bar sample cut at a sandstone-shale contact in the core from well 21/1a-20. The black rock in the bottom of the core box is a shale.

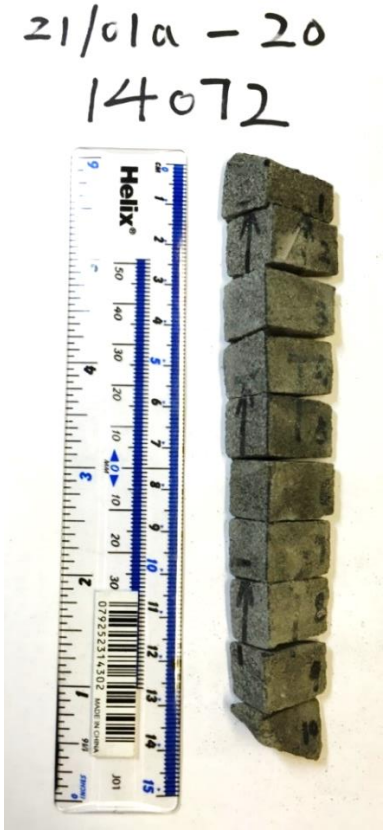

Figure 6.2 The same bar sample in Figure 6.1 after being cut by a rock saw into regular pieces. Our aim is to analyse the change of chemical composition in the sandstone as approaching the shale in the bottom of Figure 6.1.

6.2 Geological setting

The samples in this study are collected from 5 hydrocarbon wells that belong to four North Sea oilfields: the Miller (wells 16/8b-5 and 16/8b-A1), Thelma (well 16/17-19), Tweedsmuir South (well 21/1a-20) and Magnus Fields (well 211/12a-18). This section introduces the geological background of these four oilfields.

6.2.1 The Miller Field

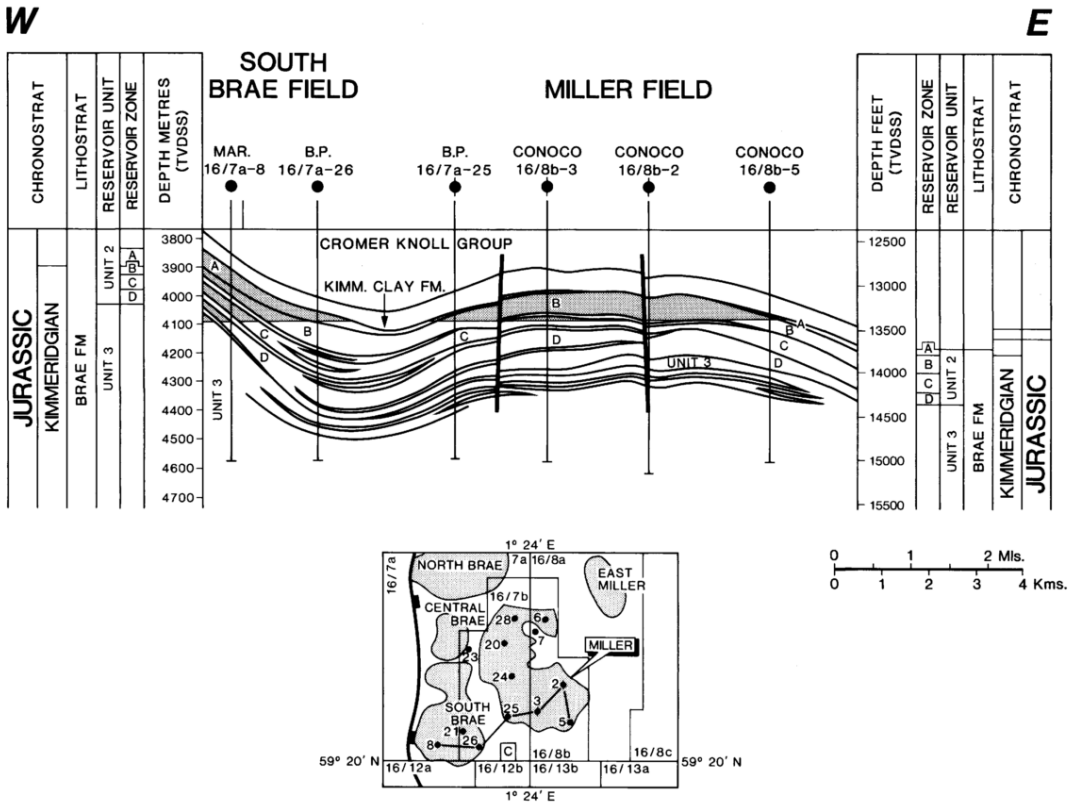

Figure 6.3 Structural cross-section of the Miller Field (Rooksby, 1991)

The Miller Field is producing from an Upper Jurassic turbidite sandstone named the Brae Formation (Figure 6.3; Turner et al., 1987). Stratigraphically, the Brae Formation is enclosed within the Kimmeridge Clay Formation, which provides the hydrocarbon source to the field (Marchand et al., 2000). The main reservoir comprises fine- to coarse-grained sandstones deposited from turbidity currents in a mid-fan channel setting (Prosser et al., 1995). Sedimentary facies and reservoir properties of the reservoir are largely constant across the field (Gluyas et al., 2000; Rooksby, 1991).

Several studies have investigated the petrology of the Miller reservoir sandstones, and the results are listed in Table 6.1. Quartz overgrowths are the dominant cement in the sandstones, constituting 0-10% of the reservoir (Table 6.2). Carbonate minerals are another common type of cement in the reservoir, typically occurring in the form of concretions or disseminated patches (Gluyas et al., 2000). The carbonate concretions are thought to have been precipitated at a shallow depth close to the sediment-water interface as the earliest cement in the reservoir (Gluyas et al., 1985).

The porosity of the Miller reservoir lies in the range of 12-23% with an average of 16% (Rooksby, 1991). The porosity is the highest (23%) at the crest of the reservoir, which is significantly higher than in the flanks of the field, and also higher (about 8%) than the porosity that would be expected from the empirical porosity-depth relationship of normal sandstones (Marchand et al., 2000). Corresponding to the porosity trend, there is less quartz cement in the upper-most part of the reservoir than the lower reservoir (Marchand et al., 2000). There are two possible explanations for this: early filling of hydrocarbons inhibited quartz cementation in the reservoir crest (Marchand et al., 2000), or the quartz cementation was inhibited by the presence of abundant microquartz cement (Aase and Walderhaug, 2005).

The process of mass transfer between the sandstones and shales in the Miller reservoir has been studied by Gluyas et al. (2000). They suggested migrations of silica from shales to sandstones, and potassium and aluminium from sandstones to shales. These conclusions are primarily based on the observations that the shales interbedded by the reservoir sandstones are less rich in silica but are more enriched in potassium and aluminium than the shales overlying the sandstones (Figure 6.4).

Table 6.1 The detrital mineralogy of the main reservoir of Miller Field determined in different studies.

Reference	(Prosser et al., 1995)	(Gluyas et al., 2000)	(Marchand et al., 2000)	(Aase and Walderhaug, 2005)
Detrital Quartz	Form >90% of the framework grains	Form > 90% of the fabric grains	60.3-87.1%	52-72%, average 66%
Feldspar	1-2% K-feldspar, minor plagioclase	1–2 vol.% K-feldspar, rare plagioclase	4.7-16.5%, K-feldspar dominates	Average 1-2%, maximum <4%, K-feldspar dominates
Detrital clays	<3%	< 3%	trace	3-10%, average 5%
Rock fragments	minor	minor	trace	0-5%

Table 6.2 The amount of quartz cement (point-counted) in the reservoir sandstones of the Miller Field from various studies.

	(Prosser et al., 1995)	(Gluyas et al., 2000)	(Marchand et al., 2000)	(Aase and Walderhaug, 2005)
Quartz cement	0-10%, up to 15%	5.8 ± 1.6 (2σ) vol.%	3.2-16.8%	8.8% in the oil zone; 8.7% in the water zone

Table 6.3 The average percentages of silica and aluminium in mudstones within and above the Brae Formation (Gluyas et al., 2000). The corresponding plot is in Figure 6.4

	SiO_2 (wt %)	**Al_2O_3 (wt %)**
Mudstones within the Brae Fm.	75.38 ± 2.10	14.74 ± 1.88
Mudstones above the Brae Fm.	79.95 ± 2.02	11.00 ± 1.77

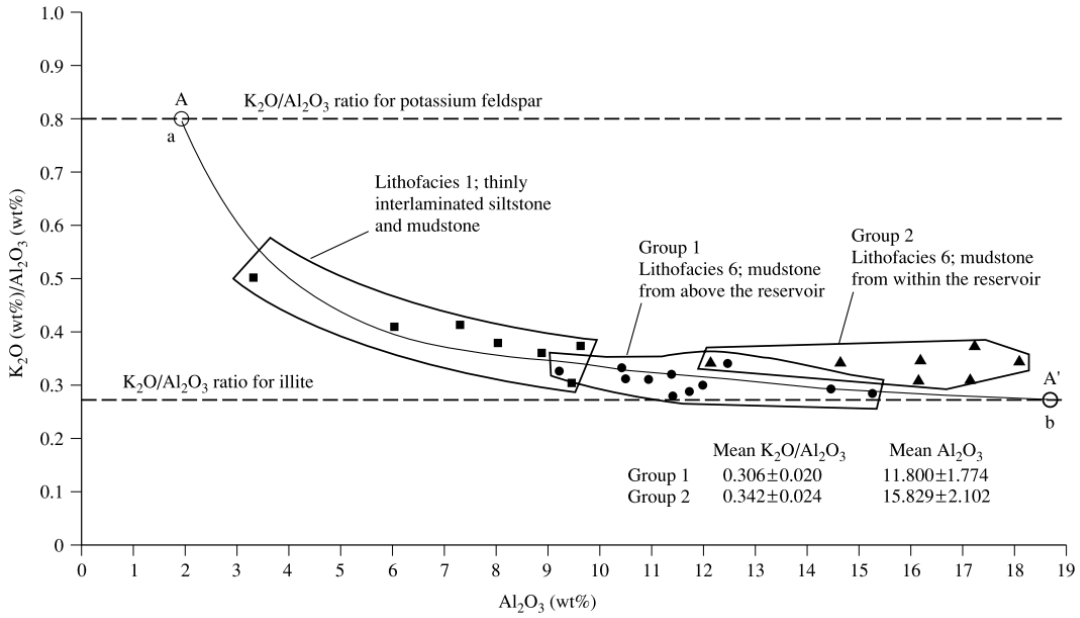

Figure 6.4 The relationship between K_2O/Al_2O_3 and Al_2O_3 (%) for the mudstones of different lithofacies in the Miller Field (Gluyas et al., 2000). The Group 1 mudstone, which is above the reservoir, contains less potassium and aluminium than the Group 2 mudstone which is interbedded with the sandstones of the reservoir.

6.2.2 The Thelma Field

Well 16/17-19 is a production well of the Thelma Field in the southern Viking Graben. The core for this study was taken from a coal-bearing paralic Middle Jurassic sequence, which is attributed to the Sleipner Formation by the field operator (Gambaro and Donagemma, 2003). It is broadly equivalent to the Pentland Formation in the Central North Sea (Richards et al., 1993; Underhill, 1998).

6.2.3 The Tweedsmuir South Field

Well 21/1a -20 is the discovery well of the Tweedsmuir South Field. The reservoir of the field is the Burns Sandstone within the Kimmeridge Clay Formation. There is no published information about the field.

6.2.4 The Magnus Field

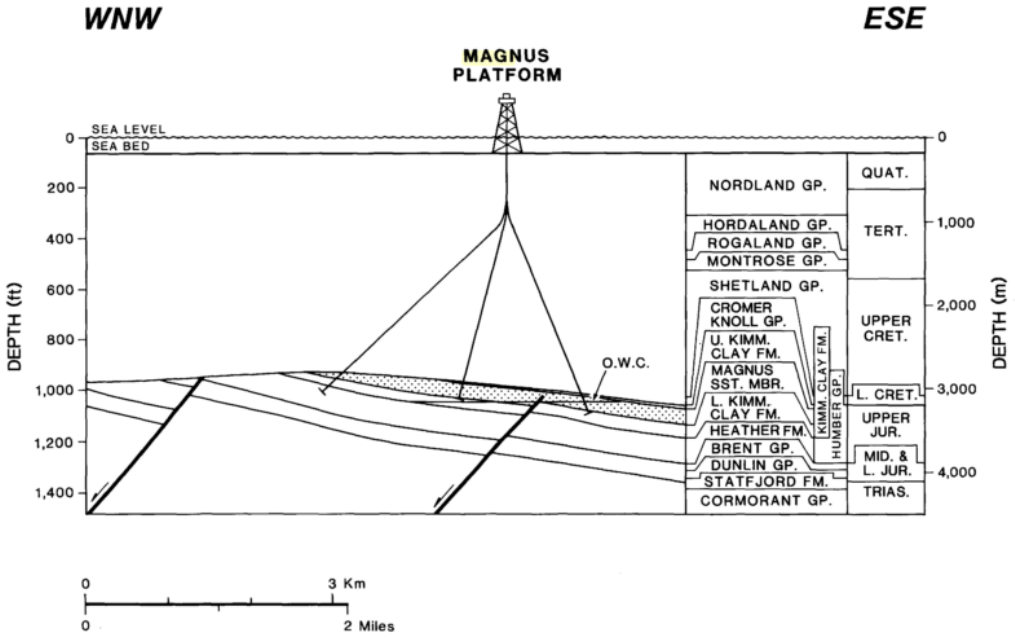

Figure 6.5 Schematic geological cross-section of the Magnus Field (Shepherd, 1991)

The Magnus Field is in a tilted fault block sealed by Cretaceous mudstones on top (Figure 6.5). The reservoir, the Magnus Sand Member (MSM), is composed of Upper Jurassic turbidite sandstones enclosed within the Kimmeridge Clay Formation (De'Ath and Schuyleman, 1981). The sandstones are thickly bedded (2-7 m) but are separated by shale beds into different pressure compartments (Shepherd, 1991).

The MSM was deposited in a submarine fan setting and is dominantly stacked turbidite channel sandstones (De'Ath and Schuyleman, 1981; Worden and Barclay, 2003). The sandstone is highly homogenous without clear cross-bedding structures and grading or bioturbation features (De'Ath and Schuyleman, 1981; Shepherd, 1991). High-density turbidity currents have thoroughly mixed the sands during sediment transportation, leaving little variation in the original composition of the sands (Shepherd, 1991; Worden and Barclay, 2003).

The MSM sandstone is a feldspathic sandstone (De'Ath and Schuyleman, 1981). K-feldspar is more abundant than plagioclase (De'Ath and Schuyleman, 1981). Detrital illite, kaolin and muscovite are rare (Worden and Barclay, 2003). The sandstone was once exposed on land, due to inversion during the early Cretaceous, and had fresh

water infiltrated through the reservoir. As a result, the formation water in the Magnus Field is now brackish, fresher than seawater (De'Ath and Schuyleman, 1981). The infiltration of meteoric water also dissolved some K-feldspar grains and precipitated kaolin in the reservoir (Emery et al., 1990). But this phenomenon seems to have only affected the top 8m section of the reservoir (Emery et al., 1990). In deep burial, authigenic minerals become pervasive in the Magnus Field reservoir. The main authigenic minerals include quartz, ankerite, kaolin and illite, whereas K-feldspar has been gradually decomposed and dissolved through burial (Worden and Barclay, 2003).

6.3 Samples and method

There are five sampling wells in this study. The logs of the cores of these five wells, where the study samples were taken, are displayed in Figure 6.6 - Figure 6.10. The original positions of the samples in the cores are also marked in the figures. All the logs are created based on the core images on the website of the British Geological Survey Core Store (http://www.bgs.ac.uk/data/bmd.html).

There are two types of samples for analysis: bar samples and discrete samples. The bar samples are 10 – 15 cm long and were cut by a rock saw from the edge of cores, which have been shown in Figure 6.1 and Figure 6.2. They are sampled from the contacts between sandstones and shales. The discrete samples are individual samples that are collected from a thick sandstone or shale bed (represented by star symbols in Figure 6.6 - Figure 6.10). Each sample is labelled after the driller's depth.

The samples' chemical compositions are analysed by X-ray fluorescence (XRF). The details of the sample preparation and analysis procedure for XRF have been given in the Methodology Section of Chapter 4, page 130.

Two indexes were used to infer the mobility of silica, aluminium and potassium. One is the absolute weight percentage of their oxides, i.e. SiO_2 (%), Al_2O_3 (%) and K_2O (%), which are directly measured by XRF. The other one is their ratios to an immobile element, i.e. *'mobile /immobile'*. Titanium (Ti) was chosen as the immobile element (see discussion in Wilkinson et al., 2003). The ratio of 'mobile /immobile' can eliminate the change in the percentage composition of an element caused by the import or export of other elements. For example, if a sandstone containing 70% of SiO_2, 4% K_2O, 1% TiO_2 and 25% other elements losses 10% of SiO_2, the percentage of K_2O will be passively increased to 4.4%, even if K_2O is immobile. However, the ratio of K_2O/TiO_2 will remain constant at 4 and hence it is a useful indicator of elemental mobility.

Using the chemical data of the samples, this project will take four approaches to study the mass transfer:

(1) Compare the chemical compositions of concretion sandstone samples to those of the adjacent normal sandstone samples.

(2) Analyse the chemical variations within sandstone/shale bars sample versus the distance to the closest sandstone-shale contact. This approach is designed to study the mass transfer process near sandstone-shale contacts on a scale of 0 – 15 cm.

(3) Compare the chemical variations between the discrete samples within a same sedimentary bed. The basic mechanism of this approach is the same of the last one. The only difference is that the interval space between the discrete samples is wider than the bar samples. This approach is for studying the mass transfer at a scale of 10 – 500 cm.

(4) Compare the difference in the average chemical compositions between the samples at sandstone-shale contacts and the samples within the middle of thick sandstone/shale units. If there were chemical interactions between sandstones and shales, those close to the contacts might have become enriched or depleted in some chemical elements.

The chemistry of sandstones and shales is controlled by both the processes of deposition and diagenesis (Bjørlykke, 2014). To assess the degree of controlling of the two processes, a simple statistical idea is used in data interpretation. Deposition and diagenesis may produce different trends of chemical variations within the samples, and therefore the method is to count the number of bar samples (or groups of discrete samples) that show trends consistent with what would be anticipated under the control of deposition or diagenesis. Then, the size of numbers and their ratios to the total number of studied samples can indicate the relative significance of deposition and diagenesis in controlling the chemical composition of samples. In addition, the robustness of each chemical trend was further classified into two levels: strong and weak. A chemical trend is valued as ‘strong’ when both the R^2 of the trend lines of the absolute percentage of an element and the ratio of it to TiO_2 are higher than 0.5.

All the bar samples were collected at the boundaries between sandstones and shales (except for one from well 16/17-19), but the discrete samples are usually from inside

a sandstone or shale bed. Therefore, comparing the compositions of these two types of samples is equivalent to comparing the samples inside and at the edge of a sedimentary bed. The compositions of these two groups of samples are expected to be different if the mass transfer between sandstones and shales had occurred. The Student's t-test statistical method is applied to determine if the two sets of data are significantly different from each other (Student, 1908).

Some of the samples were also analysed by point-count and X-ray diffraction (XRD) to study the mineralogy of the samples. The procedures of the methods are the same as the ones described in the Methodology section of Chapter 4.

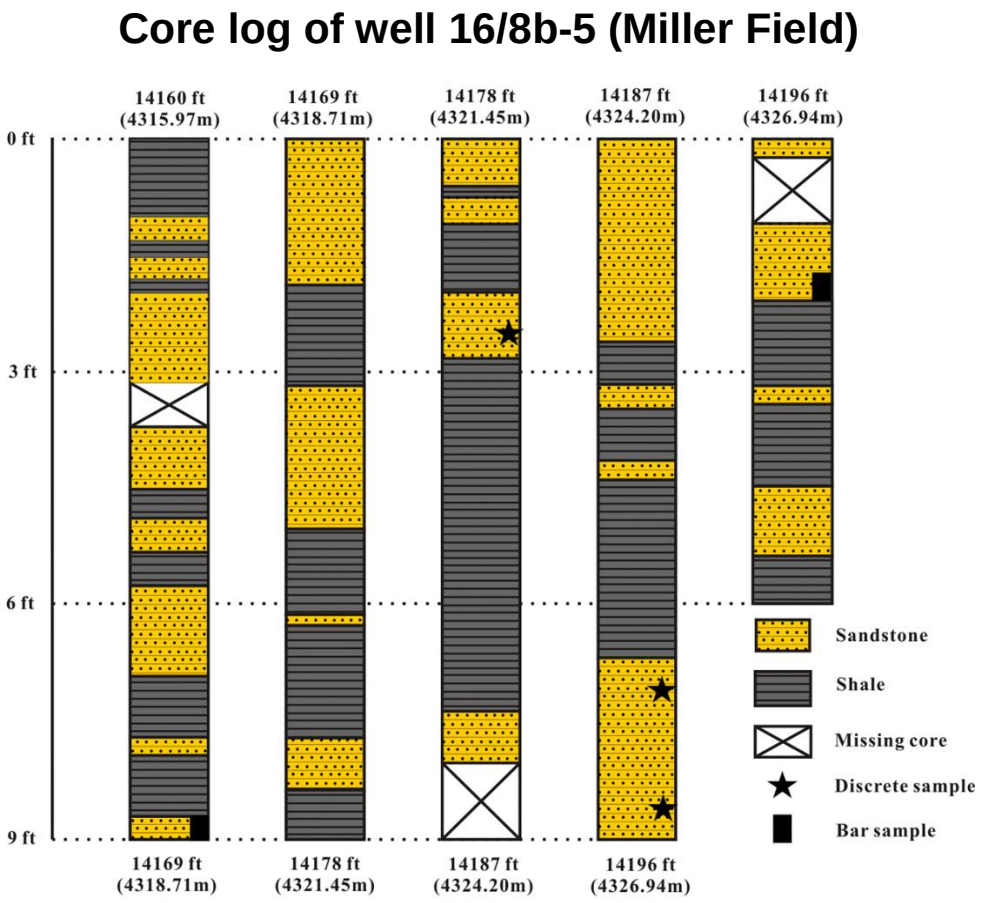

Figure 6.6 Core log of well 16/8b-5 and the positions of the studied samples

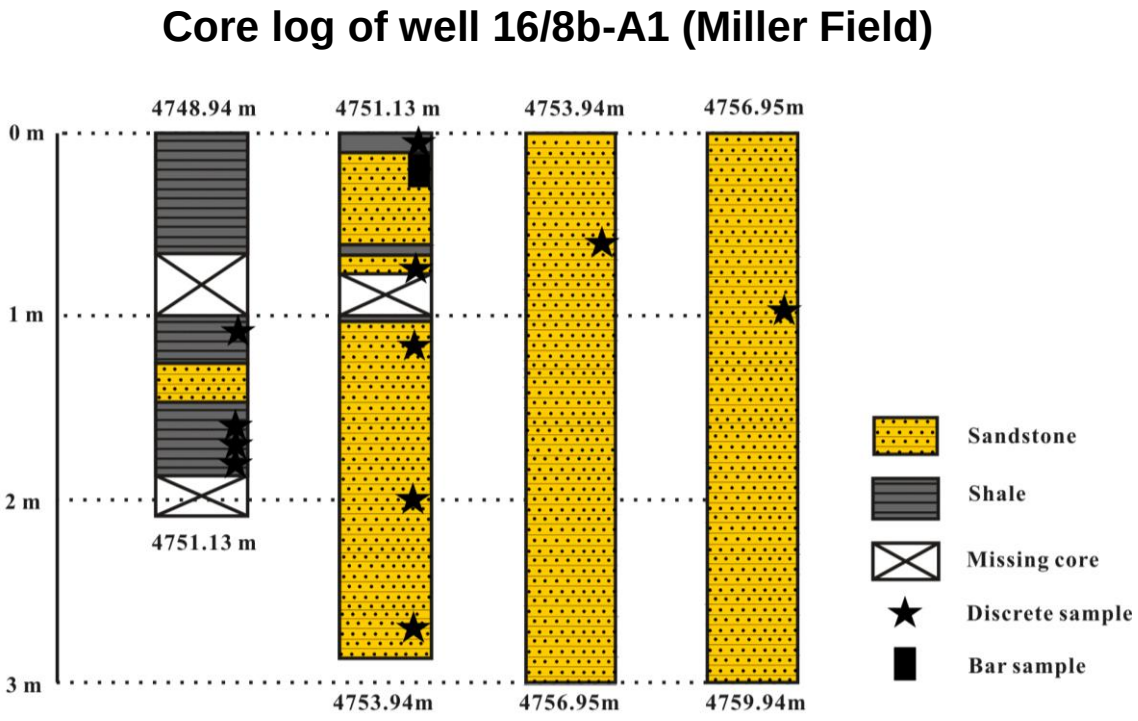

Figure 6.7 Core log of well 16/8b-A1 and the positions of the studied samples

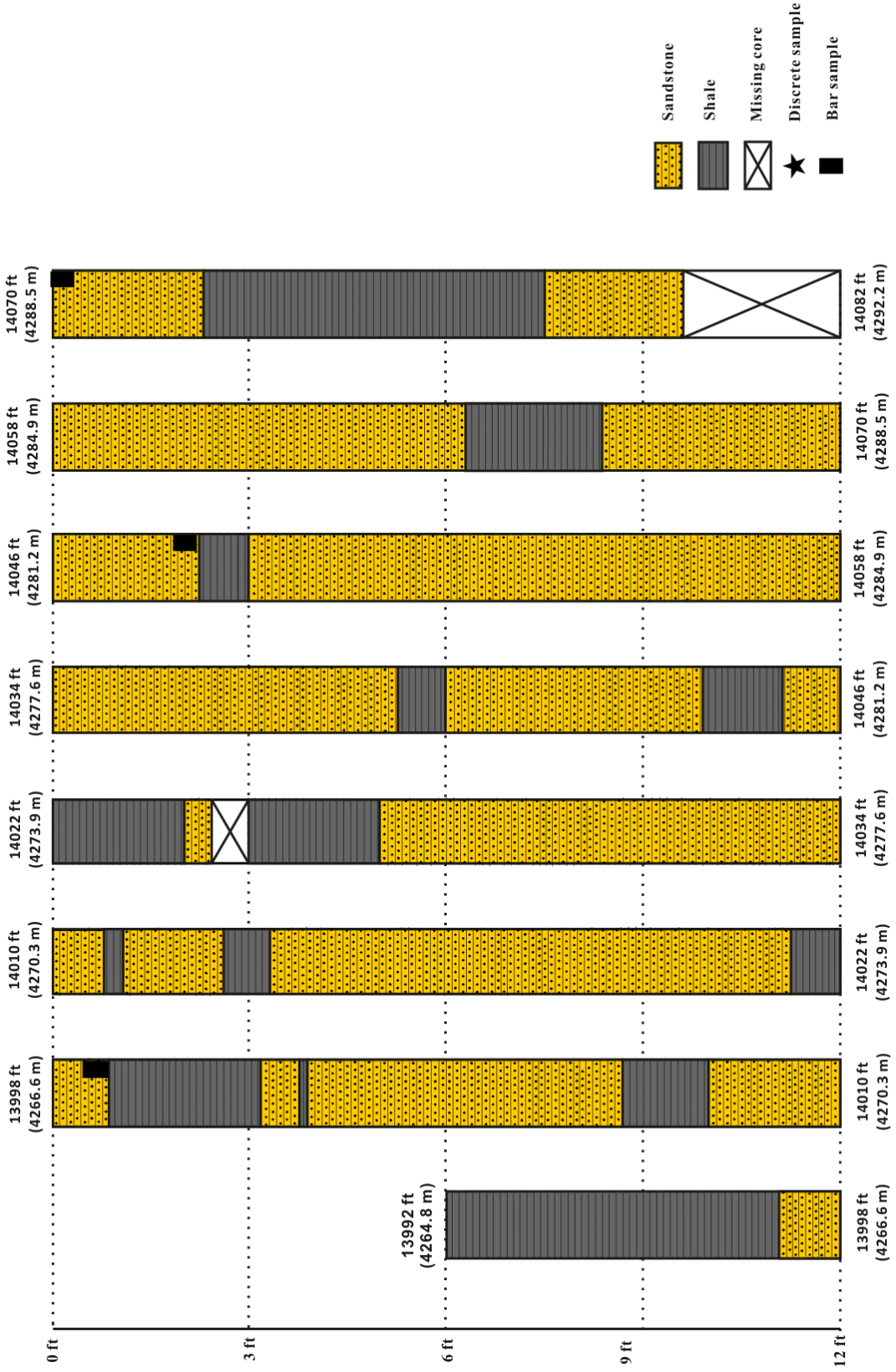

Figure 6.8 Core log of well 16/17-19 and the positions of the studied samples

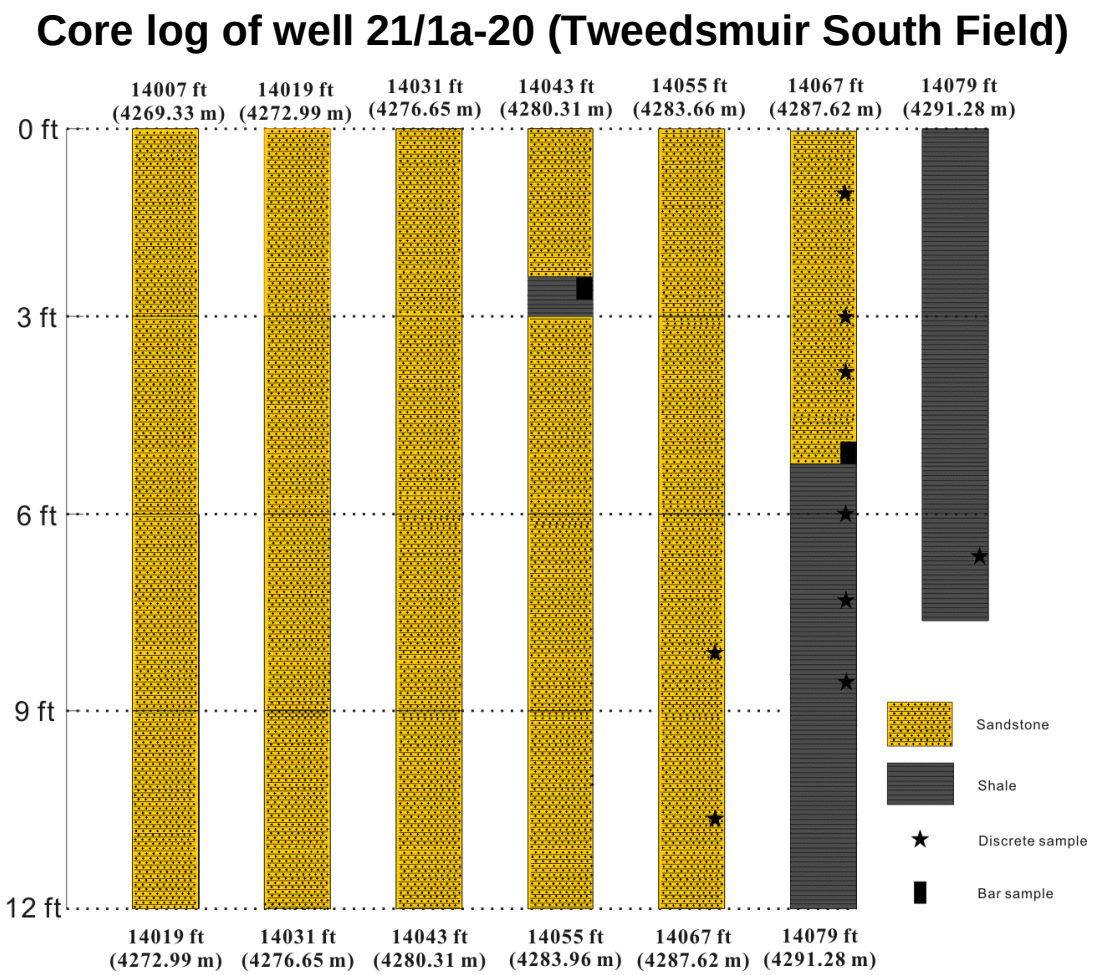

Figure 6.9 Core log of well 21/1a-20 and the positions of the studied samples

Core log of well 211/12a-18 (Magnus Field)

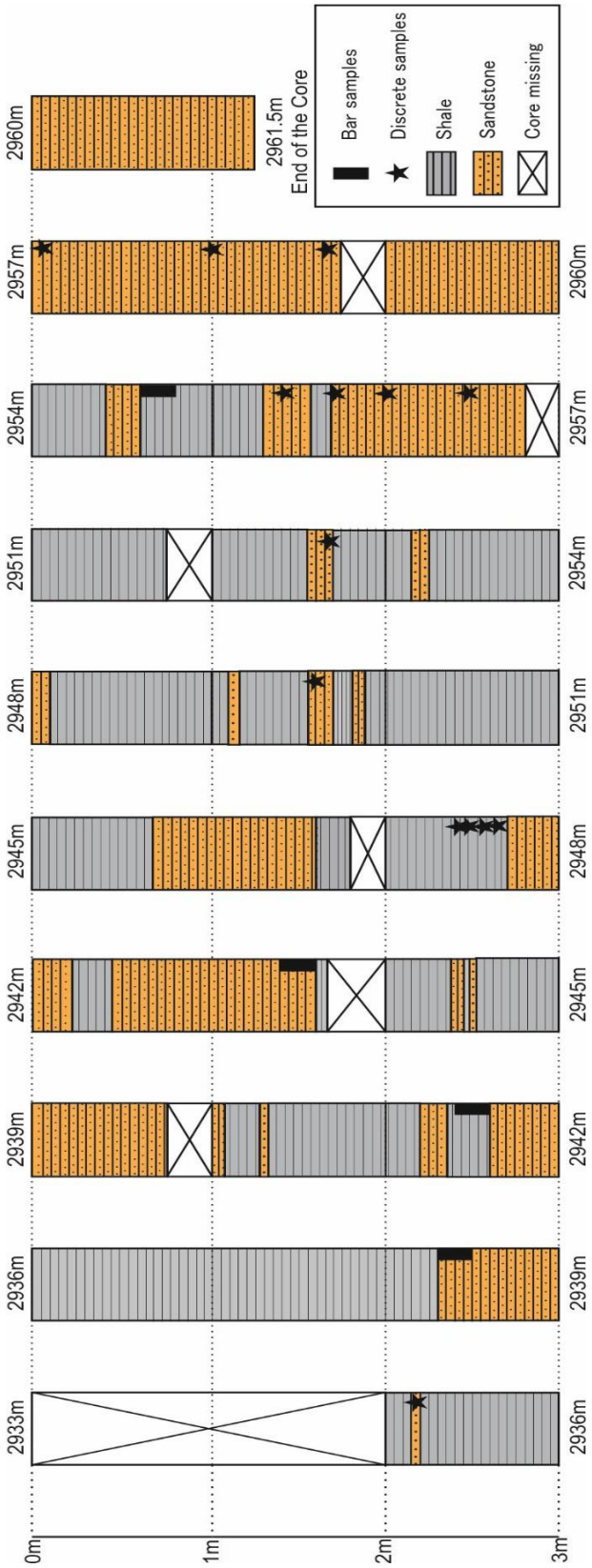

Figure 6.10 Core log of well 211/12a-18 and the positions of the studied sample

6.4 Results

Borehole cores of the study reservoirs are generally complete, although a few sections are missing. The boundaries between sandstones and shales are mostly sharp and well-defined, rather than of gradual transition. During sampling, it can be determined whether the sandstones are oil-saturated according to their colour (dark-brown) and the characteristic odour of petroleum. The shales interbedded within the reservoirs are also soaked with hydrocarbons, as they have been observed to have oil seeping out during the process of sample cleaning and cutting in the laboratory, suggesting that these shales are possibly mature or post-mature as hydrocarbon source rocks.

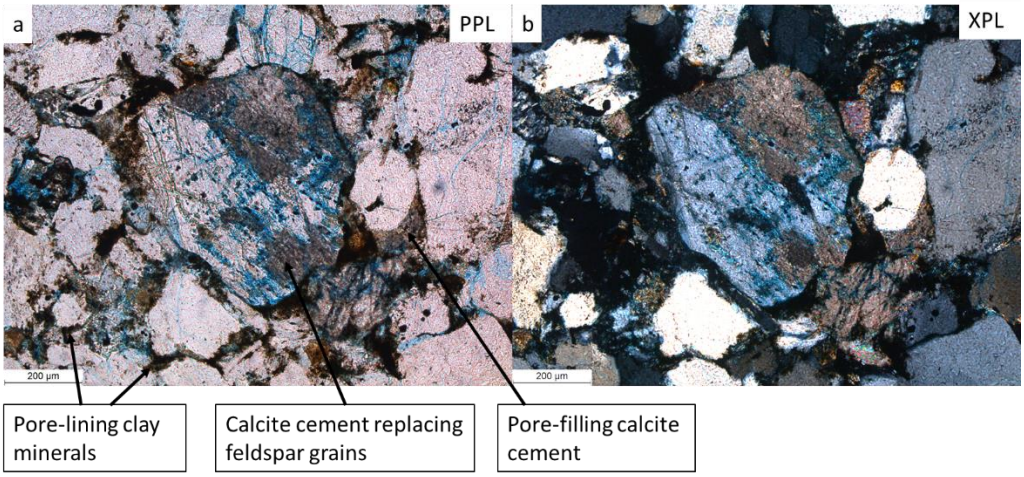

Figure 6.11 A Miller sandstone showing the diagenetic features of feldspar dissolution and calcite cement replacing detrital feldspars. (a) PPL image, (b) XPL image of the same view. Sample 14180.7, Well 16/8b-5.

Observations under the microscope and point-counting (Table 6.4) suggest the sandstones of wells 16/8b-5 and 16/8b-A1 (Miller Field) are quartz arenites, with quartz overgrowth being the dominant authigenic phase (2-10%). There is a minor content of K-feldspar (1-2%) in the reservoir, and some of the feldspars show features of dissolution (Figure 6.11). Black-coloured clay, most likely illite, is the only type of clay mineral observed (Figure 6.11). Sandstones of well 16/8b-5 contain a small amount of calcite cement; the calcite cemet occurs as pore-filled cement or a replacement of dissolved feldspar grains (Figure 6.11). The XRD data agree well with the point-count data (Table 6.4). The mineralogical compositions of the sandstones measured by XRD are 80-95% quartz, 0-3% K-feldspar, 0-3% plagioclase, <1% kaolin and 0-5% illite (Table A 6.1). The XRD-determined mineralogy of the shales in the

Miller Field contains 30-40% illite, 12-18% kaolin, 20-40% quartz, 4-8% K-feldspar and 5-11% pyrite (Table A 6.1).

The reservoir of well 16/17-19 belongs to the Pentland Formation, and it has been studied in Chapter 4. According to the point-count data of Chapter 4 (Table A 4.1 and Table A 4.2), the sandstones consist of 79-83% quartz, 0-2% K-feldspar, 1-2% kaolin, 4-9% illite and 3-9% quartz overgrowth. The sandstones have been cemented by an average of 6.0±1.2% quartz overgrowth at a high degree (Table A 4.1). The surface of the majority of the quartz grains lacks grain-rimming clays, which sometimes makes the differentiation between detrital quartz and quartz overgrowth difficult. It is possible that point-count data have underestimated the amount of quartz cement. The bar samples of the sandstones of well 16/17-19 have been analysed by XRD. Fifteen rock pieces of the bar samples show highly uniform compositions; they are made of 93-95% quartz, 0-1% K-feldspar, 1-2% plagioclase and 0-2% illite (Table A 6.1). The only exception is the Sample 13199.13, whose composition is very different from the other samples. It is comprised of 68% quartz, 11% kaolin and 11% illite (XRD data, Table A 6.1). This sample probably contains a high portion of shale as it was sampled at a sandstone-shale boundary.

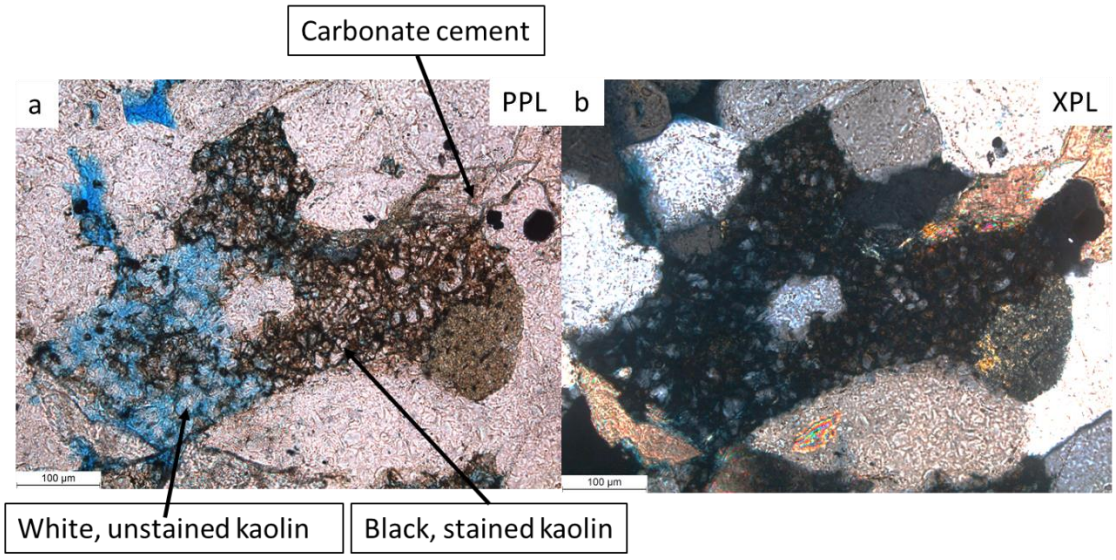

Figure 6.12 Black, oil-stained kaolins contrasting with white, unstained kaolins in two secondary pores next to each other. The white kaolin is interpreted to be newly formed in the reservoir after oil emplacement (Wilkinson et al., 2014b). Sample 14063.3, Well 21/1a-20.

The sandstones of well 21/1a-20 is also a quartz arenite; feldspar and lithic are rare in the reservoir (<1%, Table 6.4). Both quartz cement and kaolin are present in large

quantities, each accounting for around or over 10% of the total rock volume (Table 6.4). There are two types of kaolin the reservoir: one is black, presumably oil-stained and smaller in size, and the other is clean and seems to be better-crystallised (Figure 6.12). These two types of kaolin can sometimes be mixed in one pore or distributed separately in two adjacent pores. XRD data suggest the sandstones are made of 85-92% quartz, 0-1% K-feldspar, 1-2% plagioclase, 1-4% kaolin and 1-3% illite. The shales are of 20-40% illite, 10-30% kaolin, 0-40% quartz, 0-5% K-feldspar and 1-3% plagioclase. It is notable that the discrete shale samples are much richer in quartz (10-40%) than the bar shale samples (0-6%, Table A 6.1).

The sandstone of well 211/12a-18 (Magnus Field) contains 3-5% of point-counted K-feldspar and 6-10% plagioclase (Table 6.4). It is a feldspathic sandstone, which is different from the sandstones of the above-mentioned four wells. The contents of feldspars in the sandstone measured by XRD are even higher, which show 0-10% K-feldspar and 11-19% plagioclase (Table 6.4). Kaolin (0-3%) and illite (0-4%), same as in the other wells, are the main types of clay mineral (XRD data). Some thin sandstone beds (10-20 cm) enclosed within the shales of well 211/12a-18 have been cemented by carbonate minerals or by micro-quartz (Figure 6.13). The high degree of cementation may have preserved the early fabrics and mineralogy of the sandstones. These sandstones will be compared to the normal sandstones in the same reservoir in Section *6.5.1*, to infer the diagenetic changes that have occurred to the normal sandstones during burial. Figure 6.13 (a - d) show microphotographs for each of the three concretion samples and one photo of the normal sandstone.

The table recording the results of XRF analysis is in Table A 6.2. The variations of SiO_2, Al_2O_3 and K_2O within each of the bar samples, versus the distance to the nearest sandstone-shale contact, is plotted in Figure A 6.1 - Figure A 6.12(12 bar samples and hence 12 figures in total). The corresponding interpretation and discussion for the 12 figures are in Section *6.5.2*. The plots of SiO_2, Al_2O_3 and K_2O for the discrete samples are in Figure A 6.13 - Figure A 6.18 (6 groups of discrete samples with 6 figures), and the corresponding discussion is in Section *6.5.3*.

Table 6.4 Point-count result of the sandstone thin-sections. The uncertainties are at 90% confidence limit according to the reliability chart of point-count data in Van der Plas and Tobi (1965).

	Sample number (Depth)	Quartz	Marco-quartz cement	Micro-quartz cement	K-feldspar	Plagioclase	Kaolin	Illite	Calcite	Mica	Primary porosity	Secondary porosity	Lithic	Others /Unknown
16/8b -5 (Miller)	14180.7	70 ± 5	2 ± 2	0	1 ± 1	0	0	20 ± 5	6 ± 3	1 ± 1	1 ± 1	0	0	1 ± 1
	14195.5	73 ± 5	6 ± 3	0	1 ± 1	0	0	11 ± 4	3 ± 2	0	3 ± 2	3 ± 2	0	1 ± 1
16/8b-A1 (Miller)	4753	74 ± 5	9 ± 3	0	1 ± 1	0	0	7 ± 3	1 ± 1	1 ± 1	5 ± 2	2 ± 2	0	0
	4753.8	73 ± 5	8 ± 3	0	2 ± 2	0	0	6 ± 3	1 ± 1	1 ± 1	6 ± 3	3 ± 2	1 ± 1	0
	4754.6	77 ± 5	10 ± 3	0	1 ± 1	1 ± 1	0	5 ± 3	0	0	5 ± 2	2 ± 2	0	1 ± 1
	4758	81 ± 5	5 ± 2	0	1 ± 1	1 ± 1	0	8 ± 3	1 ± 1	0	3 ± 2	1 ± 1	1 ± 1	1 ± 1
21/1a-20 (Tweedsmuir)	14063.3	60 ± 6	20 ± 5	0	0	0	8 ± 3	4 ± 2	1 ± 1	2 ± 2	2 ± 2	3 ± 2	0	2 ± 2
	14065.8	68 ± 5	8 ± 3	0	0	0	3 ± 2	5 ± 3	5 ± 3	1 ± 1	3 ± 2	5 ± 3	0	1 ± 1
	14071	67 ± 5	12 ± 4	0	1 ± 1	0	9 ± 3	3 ± 2	4 ± 2	1 ± 1	3 ± 2	1 ± 1	0	1 ± 1

	Sample number (Depth)	Quartz	Marco-quartz cement	Micro-quartz cement	K-feldspar	Plagioclase	Kaolin	Illite	Calcite	Mica	Primary porosity	Secondary porosity	Lithic	Others /Unknown
	14071.89	64 ± 6	17 ± 4	0	1 ± 1	0	4 ± 2	4 ± 2	0	1 ± 1	1 ± 1	6 ± 3	0	0
	14071.96	64 ± 6	20 ± 5	0	1 ± 1	0	1 ± 1	7 ± 3	1 ± 1	0	3 ± 2	2 ± 2	0	1 ± 1
211/12a-18 (Magnus)	2935.38 concretion	60 ± 6	0	24 ± 5	3 ± 2	7 ± 3	0	4 ± 2	0	2 ± 2	0	0	1 ± 1	2 ± 2
	2949.57 concretion	48 ± 6	3 ± 2	13 ± 4	3 ± 2	6 ± 3	0	3 ± 2	22 ± 5	1 ± 1	0	0.0	1 ± 1	1 ± 1
	2952.68 concretion	49 ± 6	1 ± 1	0	3 ± 2	8 ± 3	0	1 ± 1	36 ± 6	1 ± 1	0	0.0	0	3 ± 2
	2955.43	60 ± 6	8 ± 3	0	2 ± 2	6 ± 3	7 ± 3	5 ± 3	1 ± 1	1 ± 1	4 ± 2	4 ± 2	1 ± 1	2 ± 2
	2956.00	50 ± 6	6 ± 3	0	5 ± 3	10 ± 3	4 ± 2	10 ± 4	1 ± 1	0	6 ± 3	9 ± 3	0	1 ± 1

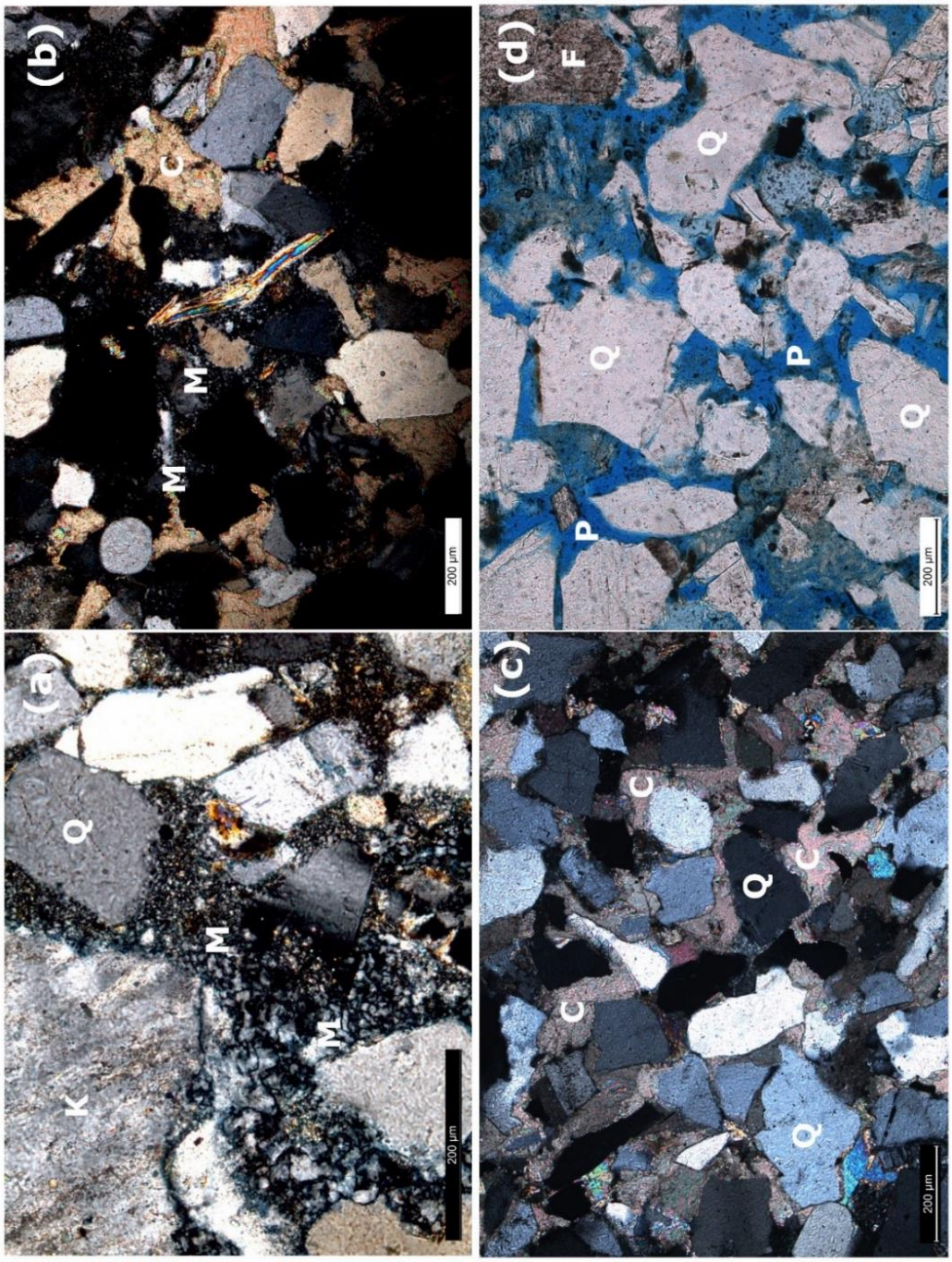

Figure 6.13 (a) Micro-quartz cement filling the matrix between detrital grains; note the variation of size in the cement, Sample 2935.38, Well 211/12a-18; (b) the matrix is partly filled by carbonate cement and partly by micro-quartz cement, Sample 2949.57, well 211/12a-18; (c) a carbonate concretion sandstone, Sample 2952.68, well 211/12a-28; (d) a normal sandstone in the reservoir of well 211/12a-18 for comparisons with the cemented sandstones, Sample 2956. C = carbonate cement, M= micro-quartz cement, K= K-feldspar, P= porosity, Q = quartz.

6.5 Discussion

6.5.1 Comparison between concretion sandstones and normal sandstones (Magnus Field)

Concretions in a sandstone, if formed near the sediment surface, potentially preserve the original fabric and composition of the sandstone upon deposition (Gluyas and Coleman, 1992). A freshly-deposited sandstone contains 30 - 40 % of porosity (Beard and Weyl, 1973), and hence if it is cemented at a shallow depth (<1 km), the volume of the cementing mineral can occupy ~40% of the sandstone (Pettijohn, 1975, pp. 76–77). The volumetric percentage of a cementing mineral in a sandstone is, therefore, an indication of the precipitation depth of the cement (Gluyas and Coleman, 1992). In the Magnus Field, among the three concretion samples of well 211/12a-18, one (sample No. 2952.68) contains 36 ± 6 % of calcite (point-count data); one (No. 2935.38) is quartz- rather than carbonate-cemented (24 ± 5 % of quartz cement); one (No. 2949.57) contains 13 ± 4 % of quartz cement and 22 ± 5 % carbonate cement, which are summed to c. 35% of matrix-filling cement (Table 6.4). Based on the volumes of cement, Sample 2952.68 and Sample 2949.57 are presumably cemented at an early time and thus may well preserve the early composition of the sandstones.

To study the compositional change of sandstones during burial by comparing sandstones outside concretions to the sandstones inside, it needs to assume that the compositions of the two groups of the sandstones at deposition were the same (Gluyas and Coleman, 1992). In this study, however, the concretion Sample 2935.38 and 2949.57 appear to have different original compositions as they contain a high abundance of micro-quartz cement (Figure 6.13 a and b), which is possibly related to the incorporation of large amounts of sponge spicules into the sandstones upon deposition (Vagle et al., 1994). Therefore, these two samples should not be considered in the comparison. This leaves Sample 2952.68 the only valid one for the comparison.

Table 6.5 compares the mineralogical composition of the concretion sandstone (Sample 2952.68) and the normal sandstones that are not cemented by carbonate minerals. The data are XRD data, and the proportion of carbonate cement in the data

has been removed, with the proportions of the rest minerals being re-calibrated to be summed to 100%. Student's t-test was applied to determine if the compositions of the two groups of sandstones are significantly different. The comparison of the result suggests the concretion sandstone contains more K-feldspar and less quartz, which implies there was an input of quartz into the normal sandstones, and an output of K-feldspar during diagenesis. This conclusion, however, is not firm since there is only one sample in the concretion sandstone group for the comparison. It is highly uncertain whether this sample is representative for the original sandstone upon deposition. More concretion samples are needed to support the conclusion.

Quartz and carbonate cement does not contain potassium, aluminium or titanium. Hence, the addition of silica or carbon into sandstones to form cement will not change the relative abundance between potassium, aluminium and titanium. Early cementation, regardless of whether quartz or carbonate, can therefore preserve the original ratio of K_2O/Al_2O_3, K_2O/TiO_2 and Al_2O_3/TiO_2 of the cemented sandstones. Table 6.6 shows the comparison of these ratios between the normal sandstones and the concretion sample. The t-test suggests there no significant difference in the ratio of K_2O/Al_2O_3, K_2O/TiO_2 and Al_2O_3/TiO_2 between the two types of sandstones. It indicates there is no or no substantial K_2O and Al_2O_3 loss or gain for the normal sandstones during diagenesis.

Table 6.5 A comparison of mineralogical composition (XRD data) between sandstones outside and inside carbonate concretions. In the t-test, if - t Critical < t Stat < t Critical, it means that, from a statistical point of view, the data available are not able to disprove that the mean values of two sample groups are equal. On the contrary, if t Stat < - t Critical or t Stat > t Critical, it suggests the mean values are significantly different. The confidence level of the t-test is set at 95%.

	Quartz (%)	K-feldspar (%)	Plagioclase (%)	Kaolinite (%)	Illite (%)	Muscovite (%)	Chlorite (%)	Montmorillonite (%)	Pyrite (%)	Anatase (%)	Total (%)
Group **A**: Sandstone outside concretion (average, n=8)	72.2	6.9	15.1	0.8	2.5	0.8	0.3	0.2	0.1	0.3	99.3
Standard error of the mean	1.2	0.6	0.8	0.2	0.4	0.2	0.1	0.0	0.0	0.0	
Group **B**: Concretion sandstone (Sample 2952.68)	60.5	11.2	17.5	0.8	4.0	2.4	0.8	0.3	0.3	0.4	98.1
t Stat (two-tail t Critical=2.4)	10.5	- 6.9	- 3.0	0.2	- 3.5	- 9.0	- 4.3	- 0.8	- 7.7	- 2.8	
Conclusion	A > B	A < B	A < B	A ? B	A < B	A < B	A < B	A ? B	A < B	A < B	

A ? B: data does not show a significant difference between Group A and Group B for the specific mineral.

Table 6.6 The comparison of K_2O/Al_2O_3, K_2O/TiO_2 and Al_2O_3/TiO_2 between the normal sandstones and concretion sandstones. Concretion sandstones and sandstones free of concretionary cement do not show significant difference on the chemical indexes of K_2O/Al_2O_3, K_2O/TiO_2 and Al_2O_3/TiO_2.

	Sample no. / depth (m)	K_2O/Al_2O_3	K_2O/TiO_2	Al_2O_3/TiO_2
Group A: Sandstones outside concretions	2955.73	0.25	10.88	43.94
	2956	0.27	11.00	40.65
	2956.5	0.30	8.22	27.57
	2957	0.28	10.28	36.50
	2958	0.30	10.22	34.33
	2958.75	0.27	10.00	37.06
	2943.56	0.24	7.36	30.41
	2943.58	0.24	7.36	30.27
	2943.6	0.25	8.84	35.37
	2943.61	0.25	8.40	33.85
	2943.62	0.27	8.52	31.00
	2938.48	0.21	12.07	56.71
	2938.49	0.24	13.58	56.00
	2938.5	0.25	13.00	51.33
	2938.52	0.27	13.00	47.83
	2938.54	0.27	12.83	48.42
	2938.56	0.28	14.45	51.36
	Average	0.26	10.59	40.74
	SEM	0.01	0.55	2.32
Group B: Concretions	2935.38	0.23	12.44	53.13
	2949.57	0.30	16.67	55.42
	2952.68	0.33	11.29	34.06
	Average	0.29	13.47	47.53
	SEM*	0.03	1.63	6.77
t Stat (two-tail t Critical=2.4)		- 0.8	- 2.0	- 1.1
Conclusion		A ? B†	A ? B	A ? B

*SEM = standard error of the mean.
†A ? B: data does not show a significant difference between Group A and Group B for the specific mineral.

6.5.2 Chemical variations along the sandstone/shale bar samples.

The bar samples were studied to investigate potential mass transfer process at the scale of 10 – 15 cm. The variation of chemical compositions across the bar samples have been plotted versus the distance to the nearest sandstone-shale contacts (Figure A 6.1 - Figure A 6.12). Three processes have or may have the ability to control the variation of chemical compositions: the sedimentary process, mass transfer by pore fluid flow and mass transfer by element diffusion. Each of the processes will produce different patterns of chemical variations at sandstone-shale contacts. The following section will summarise the models of the chemical variations that are produced by each of the processes. Then, the importance of each of the three processes in controlling the chemical variations in the bar samples is assessed by weighing how many of the actual observations can be explained by the models.

An upwards decrease in grain-size across the sedimentary bed, due to reducing water energy during deposition, is a common observation in turbidite sandstone deposits (Bouma, 1962; Lowe, 1982). Accordingly, turbidite sandstones will generally have an upwards decreasing content of quartz (silica) and increasing clay minerals (potassium and aluminium). This is the model of the chemical variation in sediments when the sedimentation process is controlling the composition of sediments. There are 12 bar samples altogether in this study. 3 of them are turbidite shales, 6 are turbidite sandstones and 3 are fluvial-deltaic sandstones (all from well 16/17-19). Only the 6 turbidite sandstone bar samples are considered in assessing the influence of turbidite sedimentation on sandstone composition. Within the 6 bar samples, the result demonstrates that 4 trends of silica (67% of all cases), 3 trends of potassium (50%) and 2 trends of aluminium (33%) are consistent with what would be expected from the upwards-finning feature of turbidite sandstones (Table 6.7). This suggests that the sedimentation process had a strong control over the composition of sediments in the scale of centimetres.

Diffusion is a process through which atoms or molecules migrate spontaneously from areas of high concentration to low concentration. Mineral dissolution in sandstone diagenesis will release ions into the pore water, and then the ions may diffuse to other

areas as the ingredients for new mineral growth (Giles, 1987; Thyne, 2001). For silica diffusion between sandstones and shales, several studies have suggested that the area of high silica concentration is on the shale side, due to a restriction on quartz cementation and the presence of numerous silica sources in shales (e.g. Day-Stirrat et al., 2010; Gluyas et al., 2000; Land, 1997). Potential silica sources in shales include detrital quartz dissolution, the breakdown of feldspars and illitization of smectites (van de Kamp, 2008; Worden and Barclay, 2003). If the assumption of silica diffusing from shales to sandstones is correct, it would be expected that the sandstones closer to shales receive more silica and as a result, gain more quartz cement (Thyne, 2001). As for the diffusions of potassium and aluminium, the majority of literature reports that the direction is the other way around, which is from sandstones to shales (see Day-Stirrat et al., 2010; Wilkinson et al., 2003; Wilkinson and Haszeldine, 1996). Therefore, the model of the variation of sandstone's composition under the control of diffusion is increasing silica but decreasing aluminium and potassium towards sandstone-shale boundaries. The model for shales is the opposite: decreasing silica but increasing aluminium and potassium towards sandstones. All of the 12 bar samples are suitable for the evaluation of the hypothesis of elemental diffusion controlling sediment's chemistry. In the result (Table 6.7), it shows that within the 12 samples, 5 trends of silica (42%), 2 trends of potassium (17%) and 1 trend of aluminium (8%) match the model. The numbers are insignificant; they suggest the control of diffusion on sediment's composition is weak or does not exist.

In the deep basin, the direction of fluid flow is generally from sandstones to shales (Bjørlykke, 1993). This is because shales are rapidly compacted during shallow burial with the porosity being reduced from 80% to 15% (Magara, 1976). A large volume of pore fluids in shales will be expelled and channelled into neighbouring sandstones. Hence, the chemical model of sandstone for mass transfer by pore fluid flow is increasing silica, aluminium and potassium towards sandstone-shale boundaries from inside a sandstone bed. However, a complexity is that most reservoirs in this study are composed of sandstones and shales that are interbedded with each other. Many of the shales are organic-rich and will produce extra fluid pressure during maturation to mobilise pore fluids within the reservoirs. In this case, the pattern of pore-fluid flow can be complex. For this reason, only the reservoirs of simple stratigraphy, preferably with just one shale bed and one thick sandstone bed, were selected to study the mass transfer process related to pore fluid flow. The reservoirs of wells 16/8b-A1 and 21/1a-

20 match this criterion (see the reservoir stratigraphy in Figure A 6.7 and Figure A 6.9). From these two wells, there are two sandstone bar samples in total, of which 2 aluminium trends (100%) and 1 potassium trend (50%) support this model (Table 6.7). It appears that pore fluid flow may have had some degrees of influence on the chemistry of the sandstone samples. But because of a lack of sufficient study cases, this conclusion is not robust.

In summary, this section has applied three simple chemical models of sediments that are associated with sedimentation process, mass transfer by element diffusion and transfer by pore fluid flow. The result suggests that, in the scale of centimetres, the sedimentation process appears to be the most influential controlling factor of sandstones' compositions. The model of turbidite sedimentation can explain nearly half the chemical trends. This sedimentary model assumes the sedimentary environment was stable during the deposition of sediments. The inconsistent observations of sediment's compositions can be caused by fluctuations in the sedimentary environments. Only a small fraction of the chemical variations can be explained by the model of element diffusion, suggesting diffusion has little impact upon sediments' chemistry. To evaluate the effect of pore fluid flow on sediments' compositions is more difficult as the pattern of pore fluid flow in reservoirs is complex. There are only two reservoirs (wells 16/8b-A1 and 21/1a-20) in this study within which the direction of fluid flow can be determined. The data from these two reservoirs indicate fluid flow may have certain degrees of influence upon sediments' compositions.

Table 6.7 The potential processes affecting the chemistry of a sandstone and the corresponding supporting chemical trends. The fitting goodness is valued as 'strong' when both the R^2 of the trendlines of the absolute percentage of an element and the ratio of it to titanium is higher than 0.5.

	Potential controlling processes of sediments' compositions					
	Sedimentation of turbidite		**Mass transfer by diffusion**		**Mass transfer by fluid flow**	
Number of samples available for study	n = 6		n = 12		n = 2	
Silica	Expected chemical trends: In sandstones, upward decreasing SiO_2 (%) and SiO_2/TiO_2 along the sedimentary sequence.		Expected chemical trends: In sandstones, increasing SiO_2 (%) and SiO_2/TiO_2 towards a shale. In shales, decreasing SiO_2 (%) and SiO_2/TiO_2 towards a sandstone.		Expected chemical trends: In sandstones, increasing SiO_2 (%) and SiO_2/TiO_2 towards a shale.	
	Sample	Fitting goodness	Sample	Fitting goodness	Sample	Fitting goodness
	16/8b-5, 14168.80-14169.07 ft (Figure A 6.1)	Weak	16/17-19, 14069.87 - 14070.13 ft (Figure A 6.6)	Weak		
	16/8b-A1, 4750.94-4751.04 m (Figure A 6.3)	Strong	211/12a-18, 2943.56 - 2943.62 m (Figure A 6.10)	Weak		
	211/12a-18, 2938.48-2938.56 m (Figure A 6.9)	Strong	#21/1a-20, 14044.87-14045.13 ft (Figure A 6.8)	Weak		
	211/12a-18, 2943.56-2943.62 m (Figure A 6.10)	Weak	#211/12a-18, 2941.51-2941.59 m (Figure A 6.11)	Strong		
Aluminium	Expected chemical trends: In sandstones, upward increasing Al_2O_3 (%) and Al_2O_3/TiO_2 along the sedimentary sequence.		Expected chemical trends: In sandstones, decreasing Al_2O_3 (%) and Al_2O_3/TiO_2 decreases towards a shale. In shales, increasing Al_2O_3 (%) and Al_2O_3/TiO_2 towards a sandstone.		Expected chemical trends: In sandstones, increasing Al_2O_3 (%) and Al_2O_3/TiO_2 decreases towards a shale. In shales, decreasing Al_2O_3 (%) and Al_2O_3/TiO_2 towards a sandstone.	
	16/8b-A1, 4750.94-4751.04 m (Figure A 6.3)	Strong	16/8b-5, 14168.80-14169.07 ft (Figure A 6.1)	Weak	*21/1a-20, 14071.87-14072.13 ft (Figure A 6.7)	Strong

	211/12a–18, 2938.48-2938.56 m (Figure A 6.9)	Weak			16/8b-A1, 4750.94-4751.04 m (Figure A 6.3)	Strong
Potassium	Expected chemical trends: In sandstones, upward increasing K_2O (%) and $K2O/TiO_2$ along the sedimentary sequence.		Expected chemical trends: In sandstones, decreasing K_2O (%) and K_2O/TiO_2 towards a shale. In shales, increasing K_2O (%) and K_2O/TiO_2 towards a sandstone.		Expected chemical trends: In sandstones, increasing K_2O (%) and K_2O/TiO_2 decreases towards a shale. In shales, decreasing K_2O (%) and K_2O/TiO_2 towards a sandstone.	
	16/8b-5, 14168.80–14169.07 ft (Figure A 6.1)	Weak	*21/1a-20, 14071.87-14072.13 ft (Figure A 6.7)	Weak	16/8b-A1, 4750.94 -4751.04 m (Figure A 6.3)	Strong
	16/8b-A1, 4750.94–4751.04 m (Figure A 6.3)	Strong	#211/12a-18, 2941.51-2941.59 m (Figure A 6.11)	Weak		
	*21/1a-20, 14071.87–14072.13 ft (Figure A 6.7)	Weak	#211/12a-18, 2954.66-2954.76 m (Figure A 6.12)	Weak		

'#' marks shale bar samples, otherwise are sandstones; '* 'reminds that the same chemical trend can be produced by two different processes, e.g. the silica trend of the samples of 21/1a - 20, 14071.87 - 14072.13 ft can be a result of elemental diffusion or mass transfer by fluid flow.

6.5.3 Chemical variations between the discrete samples of sandstone and shale

The last section studied the chemical variations of sediments in the scale of 0-10 cm. This section is aimed at studying the variations at a larger scale, from decimetres to meters, by using the discrete samples which were collected across a sandstone or shale bed. The method of analysis is the same as in the last section. The same influences of the sedimentary processes, mass transfer by diffusion and by pore fluid flow on the chemistry of sediments are considered.

There are 3 groups of discrete sandstones available for evaluating the influence of the sedimentary process on the sandstones' compositions (Table 6.8). All the three groups of sandstones are turbidite sandstones. One group shows a weak trend of silica (33% of all cases) that is consistent with the expected chemical trend controlled by sedimentation; two groups show weak trends of aluminium (67%) in support, and there is no suppor for a potassium trend. Comparing to the strong control of sedimentation on the compositions of turbidite sandstones in the scale of 0-10 cm, as shown in the last section, it appears that the control of sedimentation on the sandstones' compositions is much less significant over the scale of decimetres to meters.

For the control of diffusion over the composition of sediments, 4 in 6 groups of samples show silica trends that could be caused by element diffusion (Table 6.8). The number is significant which implies the effect of diffusion may be important. But it should be noted that there are two groups of samples from well 21/1a-20 whose silica trends also can be caused by the other two mechanisms (Table 6.8). When taking this factor into account, it is hard to firmly conclude whether the effect of element diffusion on the content of silica is substantial, given the small number of studied sample groups, and that the supportive silica trends are somewhat ambiguous (Figure A 6.15 and Figure A 6.16). For the aluminium and potassium trends, there are 2 and 1 trends, respectively, that fit the expected chemical trends under the control of element diffusion (Table 6.8). It does not provide strong evidence suggesting that diffusion controls the contents of aluminium and potassium in the sediments.

The reservoir of well 21/1a-20 is made of a thick Kimmeridge shale and a thick sandstone, and also, there is a thin layer of shale interbedded within the sandstone (Figure 6.9). The Kimmeridge shale is mature and was observed to be oil-bearing during the cleaning of the sample. The reservoir of well 21/1a-20 is ideal to test the effect of pore water flow on the mass transfer in sediments. There are three lines of evidence that indicate the occurrence of mass transfer in the reservoir:

1) In Figure A 6.15, all indexes of SiO_2/TiO_2, K_2O/TiO_2 and Al_2O_3/TiO_2 of the sandstone increase towards the Kimmeridge shale. It can be a result of migrations of Si, Al and K from the shale to the sandstone carried by fluid flow.

2) According to the XRD data (Table A 6.1), the average content of quartz in the thin shales interbedded within the sandstones is about 3%. This shale is exceptionally depleted in quartz comparing to the thick shale shales of the Kimmeridge Clay Formation (32%). It indicates there was a flux of silica, driven possibly by pore fluid flow, from the shale to the sandstone reservoir.

3) In the underlying shale (Figure A 6.16), the SiO_2 (%) and SiO_2/TiO_2 decline towards the sandstone, suggesting there possibly was a loss of silica from the shale to the sandstone.

Firstly, the question of whether the increases of K_2O/TiO_2 and Al_2O_3/TiO_2 towards the sandstone-shale boundary in Figure A 6.15, are due to the migrations of K and Al was investigated. Table A 6.1 lists the XRD-measured amounts of kaolin and illite in the discrete sandstones and the bar sandstones. Feldspar growth was not observed in the reservoir of 21/1a-20, and hence, the authigenic growths of kaolin and illite are the only sink of mobile Al. In Table 6.9, the bar samples, which are closer to the shales, do not show higher contents of kaolin and illite than the discrete samples. This does not suggest that there was a migration of Al from the shale to the sandstone and that the bar samples have absorbed more aluminium. For the migration of K, the chemical reaction of kaolin transformation to illite is where the K would be absorbed. If K were moving from the shale to the sandstone, we would expect to see the bar samples contains more illite, or have a lower ratio of kaolin/(kaolin+illite). However, the analysis results suggest there is no statistically discernible difference between the two types of sandstones, indicating there was no significant movement of K and Al from the

shale to the sandstone by pore fluid flow. Therefore, the increasing ratios of K_2O/TiO_2 and Al_2O_3/TiO_2 towards the sandstone-shale boundary in Figure A 6.15 is more likely a result of decreasing TiO_2 (%) from the sandstone to the shale.

Similarly, the migration of silica from shales to sandstones would lead to more quartz cement in the bar sandstones, which are closer to the shales, than in the discrete samples. We also applied t-test to determine if the amounts of quartz cement are different in the two types of sandstone, and the results do not suggest there any significant difference (see Table 6.10). This could imply three things:

1) There is no migration of silica between sandstones and shales.

2) The route of silica migration aid by fluid flow is not straight and perpendicular to the sandstone-shale boundary. It can be tortuous that follows the high-permeability zones in sandstones. If so, our method of comparing the sandstones near a shale to the sandstones more distant from the shale might not be able to reflect the migration of silica.

3) We only have five thin-sections for the comparison of quartz cement (Table 6.10). The number of thin-sections is too small to demonstrate a statistically significant difference in the amount of quartz cement between the bar sandstones and discrete sandstones.

Table 6.8 The potential processes affecting the chemistry of a sandstone and the corresponding supporting chemical trends in the discrete samples

	Potential controlling processes of sediments' compositions					
	Sedimentation of turbidite		**Mass transfer by diffusion**		**Mass transfer by fluid flow**	
Number of samples available for study	**n = 3**		**n = 6**		**n = 4**	
Silica	Expected chemical trends: In sandstones, upward decreasing SiO_2 (%) and SiO_2/TiO_2 along the sedimentary sequence.		Expected chemical trends: In sandstones, increasing SiO_2 (%) and SiO_2/TiO_2 towards a shale. In shales, decreasing SiO_2 (%) and SiO_2/TiO_2 towards a sandstone.		Expected chemical trends: In sandstones, increasing SiO_2 (%) and SiO_2/TiO_2 towards a shale.	
	Sample	Fitting goodness	Sample	Fitting goodness	Sample	Fitting goodness
	*21/1a-20, 14063.20-14071.00 ft (Figure A 6.15)	Weak	*21/1a-20, 14063.20–14071.00 ft (Figure A 6.15)	Weak	*21/1a-20, 14063.20-14071.00 ft (Figure A 6.15)	Weak
			211/12a-18, 2955.73–2958.75 m (Figure A 6.17)	Weak	*#21/1a-20, 14073-14085.6 ft (Figure A 6.16)	Weak
			*#21/1a–20, 14073–14085.6 ft (Figure A 6.16)	Weak		
			#211/12a-18, 2947.46–2947.69 m (Figure A 6.18)	Weak		
Aluminium	Expected chemical trends: In sandstones, upward decreasing Al_2O_3 (%) and Al_2O_3/TiO_2 along the sedimentary sequence.		Expected chemical trends: In sandstones, decreasing Al_2O_3 (%) and Al_2O_3/TiO_2 decreases towards a shale. In shales, increasing Al_2O_3 (%) and Al_2O_3/TiO_2 towards a sandstone.		Expected chemical trends: In sandstones, increasing Al_2O_3 (%) and Al_2O_3/TiO_2 decreases towards a shale. In shales, decreasing Al_2O_3 (%) and Al_2O_3/TiO_2 towards a sandstone.	
	*16/8b-A1, 4752. 29-4758.00 m (Figure A 6.13)	Weak	#16/8b-A1, 4750.3-4751.2 m (Figure A 6.14)	Weak	*16/8b-A1, 4752.29-4758.00 m (Figure A 6.13)	Weak
	211/12a-18, 2955.73-2958.75 m (Figure A 6.17)	Weak	#21/1a-20, 14073-14085.6 ft (Figure A 6.16)	Weak		
Potassium	Expected chemical trends: In sandstones, upward decreasing K_2O (%) and $K2O/TiO_2$ along the sedimentary sequence.		Expected chemical trends:		Expected chemical trends: In sandstones, increasing K_2O (%) and K_2O/TiO_2 decreases towards a shale. In shales,	

			In sandstones, increasing K_2O (%) and K_2O/TiO_2 towards a shale. In shales, decreasing K_2O (%) and K_2O/TiO_2 towards a sandstone.		decreasing K_2O (%) and K_2O/TiO_2 towards a sandstone.	
			#16/8b-A1, 4750.3-4751.2 m (Figure A 6.14)	Strong	16/8b-A1, 4752.29-4758.00 m (Figure A 6.13)	Weak

'#' marks shale bar samples, otherwise are sandstones; ' * ' reminds that the same chemical trend can be produced by two different processes, e.g. the silica trend of the samples of 21/1a - 20, 14071.87 - 14072.13 ft can be a result of elemental diffusion or mass transfer by fluid flow.

Table 6.9 The amount of kaolin and illite measured by XRD in the discrete and bar sandstone samples of well 21/1a-20. SEM = standard error of the mean

	Sample number/ depth	Kaolin	Illite	Kaolin/(kaolin+illite)
Discrete sandstone sample	14063.2	1.6	2.9	0.36
	14065.8	4.2	2.8	0.60
	14068.3	3.6	2	0.64
	14070.1	2.2	2.1	0.51
	14071	1.4	0.9	0.61
	average	2.6	2.1	0.54
	SEM	0.6	0.4	0.05
Bar sandstone sample	14071.87	1.2	2.9	0.29
	14071.9	1.5	1.2	0.56
	14071.93	2.1	1	0.68
	14072	1.8	1.1	0.62
	14072.13	2.7	1.4	0.66
	average	1.9	1.5	0.56
	SEM	0.3	0.4	0.07
t-test for kaolin/(kaolin+illite)		t Stat = - 0.20 two-tail t Critical = 2.3		
Conclusion		The data does not suggest the two type of sandstone samples data are significantly different		

Table 6.10 The amount of quartz overgrowth in the discrete and bar sandstone samples of well 21/1a-20

	Sample number/ depth	Quartz cement (%)
Discrete sandstone sample	14063.3	20 ± 5
	14065.8	8 ± 3
	14071	12 ± 4
	average	13
	SEM	4
Bar sandstone sample	14071.89	17 ± 4
	14071.96	20 ± 5
	average	19
	SEM	6
t-test	T Stat = -1.1, two-tail t Critial = 3.2	
Conclusion	The data does not suggest the contents of quartz in the two sandstones are different	

6.5.4 Comparing the chemical difference between the samples from sandstone-shale contacts and the samples within thick sandstone or shale units

Besides the three methods discussed in the last three sections, there is another way of applying the chemical data to test the hypothesis of the mass transfer between sandstones and shales. The approach is based on the theoretical idea that if the chemical interplay between sandstones and shales exists, chemical differences should be observed between the samples at sandstone-shale contacts (bar samples in this study) and samples in the middle of thick sandstone/shale beds (discrete samples).

For each element, there are two types of chemical indexes that can be applied to analyse their redistribution in diagenesis - the absolute percentage of the elements and their ratio to an immobile element (e.g. SiO_2 (%) and SiO_2/TiO_2 for silica). However, both the indexes have defects. Taking silica as an example, the problem of the index SiO_2 (%) is that even if there is no silica movement, the value of it may still change when there is a movement of other elements. The index of SiO_2/TiO_2 could avoid this problem, but it has other two drawbacks. First, the comparison of SiO_2/TiO_2 between samples is grounded on the assumption that the TiO_2 contents of the samples are the same upon deposition, which is not likely in the real situation. Second, the difference between the normal percentage of SiO_2 in a sandstone (80-95%) and that of TiO_2 (0-0.2%) is nearly of two magnitudes wide. This means that a small variation in TiO_2 (%) could cause large variation in SiO_2/TiO_2, which will make data interpretation to be difficult in some cases. Therefore, a more reasonable way of analysing the chemical data is taking into account both SiO_2 (%) and SiO_2/TiO_2, as the two can make up for the defects of each other. This is also applicable for the mobility study of other elements.

The contents of TiO_2 (%) in the study sandstones varies from 0.1% to 0.2% (Table 6.11). Considering an extreme condition of diagenetic mass transfer under which 10% of the mass of a sandstone has been changed (Thyne, 2001), that will lead to a maximum of 0.02% variation in TiO_2 (%). But the differences of TiO_2 (%) between some sandstone sample groups are even larger than that (Table 6.11), such as in

well 16/8b-5, 16/8b-A1 and 21/1a-20. These great differences are most likely due to the difference in the original compositions of the sediments. For these sample groups, titanium is not a robust reference element for the indication of element mobility. The indexes of SiO_2/TiO_2, K_2O/TiO_2 and Al_2O_3/TiO_2 of those samples are marked with grey colour fonts in Table 6.12 - Table 6.14. They are considered with caution as indicators for element mobility.

T-tests have been conducted for SiO_2 (%), SiO_2/TiO_2, K_2O (%), K_2O/TiO_2, Al_2O_3 (%) and Al_2O_3/TiO_2 of all sample groups (Table 6.12 - Table 6.14). The t-tests suggest that all the samples, except for those from well 21/1a-20, do not show significant difference in silica content between the sediments inside and the sediments at the edge of a sedimentary bed. The mobility of silica between the sandstones and shales of well 21/1a-20 has been discussed in detail in the last section.

As for aluminium and potassium, the situation is similar, that most of the sandstone groups do not show significant differences in the contents of aluminium and potassium. The exceptions are the sandstones from the Miller Field. Data from both the two Miller wells (16/8b-5 and 16/8b-A1) show that the sandstones at the edge are richer in aluminium, and in addition, in well 16/8b-A1 the sandstones at the edge are also significantly richer in potassium.

This paragraph further investigate the reasons for the different contents of Al and K in the reservoirs of the Miller Field using XRD data (Table 6.15). In well 16/8b-5, the amounts of K-feldspar, plagioclase and kaolin in the bar sandstones and discrete sandstones are similar (Table 6.15); the large difference in the content of Al is due to the amount of illite. But t-test suggests the measured numbers of illite cannot prove that these two types of sandstones contain substantially different amounts of illite. Hence, it lacks further evidence to suggest a movement of Al from the shale to the sandstone. In the reservoir of well 16/8b-A1, the high contents of Al and K in the sandstones at the sandstone-shale contact, as shown by XRD data, are because of larger amounts of K-feldspar and illite in the sandstones (Table 6.16). And the t-test suggests the differences in the amounts of K-feldspar and illite are significant (Table 6.16). There are two possible reasons for this: 1) the sandstones were primarily rich in K-feldspar and illite; 2) or there was a transfer of Al and K from the shales to the sandstones. We looked at the variation of Al and K within the bar sandstones (Table

6.16); they both show clear trends of increasing Al_2O_3(%), Al_2O_3/TiO_2, K_2O (%) and K_2O/TiO_2(%) towards the sandstone-shale contact. In Section *6.5.2*, the chemical trends were initially interpreted as a result of the gradual finning sedimentary sequence in turbidite sandstones. But could these trends be caused by mass transfer? As Table 6.18 shows, there are also the shale samples right on the top of the sandstones above the sandstone-shale contact being collected. The number of the Al- and K-bearings minerals in the shales measured by XRD are listed in Table 6.17. K-feldspar, kaolin and illite are abundant in the shales. The dissolution of K-feldspar can be the source of Al and K. If there were mobile Al and K moving from the shales to the sandstones, it would be perplexing why the mobile Al and K were not absorbed by the large amounts of kaolin and illite in the shales. Hence, based on all the information considered, it is more likely that the variation in the amounts of Al and K in the sandstones of well 16/8b-A1 at the sandstone-shale contact is due to the depositional characteristics of turbidite sandstones. However, the possibility that this is a sign of mass transfer cannot be totally excluded.

It is notable that the chemistry of the shales in well 21/1a-20 and 211/12a-12 show opposite trends in the variation of the contents of Al and K. In well 21/1a-20, the shales at the sandstone-shale contacts are richer in Al and K than the shales inside the sedimentary bed. While the trends in 211/12-12 are the other way around.

For the reservoir of 21/1a-20, the trends of Al_2O_3(%) and Al_2O_3/TiO_2, K_2O (%) and K_2O/TiO_2(%) do not show systematic variations, either in the sandstones or the shales, that can be supporting evidence for the mass transfer of Al and K between the sandstones and shales (Figure A 6.7, Figure A 6.8, Figure A 6.15, Figure A 6.16). The observation that the shale samples near the sandstone-shale contact are richer in Al and K than the shale samples distant from the contact is not sufficient to prove a mass transfer of Al and K between the sandstones and shales.

In the reservoir of well 211/12a-12, the situation is the same as in the reservoir of 21/1a-20 that the chemical trends of Al and K in the sandstones and shales do not show clear evidence that suggests migrations of Al and K from the shales to the sandstones (Figure A 6.9 - Figure A 6.12, Figure A 6.17, Figure A 6.18)

Table 6.11 The comparison of TiO_2 (%) between samples inside and at the edge of sedimentary beds. In the t-test, if - t Critical < t Stat < t Critical, it means that, from a statistical point of view, the data available is not able to disprove that the mean values of two sample groups are equal. On the contrary, if t Stat < - t Critical or t Stat > t Critical, it suggests the mean values are significantly different. The confidence level of the t-test is set at 95%.

Well	Sample location	TiO_2 (%)	t - test for TiO_2 (%)			Conclusion
			t Stat	t Critical (two tail)	Result	
16/8b-5 (Miller Field)	Inside (n = 3)	0.15 ± 0.00	- 4.6	2.2	∵ - 4.6 < - 2.2 ∴ TiO_2 (%) $_{Inside}$ < TiO_2 (%) $_{Edge}$	Ti is **NOT** a reliable reference element to indicate element movement for this group.
	Edge (n = 10)	0.20 ± 0.01				
16/8b-A1 (Miller)	Inside (n = 6)	0.13 ± 0.00	- 2.9	2.4	∵ - 2.9 < - 2.4 ∴ TiO_2 (%) $_{Inside}$ < TiO_2 (%) $_{Edge}$	Ti is **NOT** a reliable reference element to indicate element movement for this group.
	Edge (n = 6)	0.16 ± 0.01				
16/17-19 (Thelma)	Inside (n = 11)	0.11 ± 0.03	- 0.4	2.2	∵ - 2.2 < - 0.4 < 2.2 ∴ The data cannot reject TiO_2 (%) $_{Inside}$ = TiO_2 (%) $_{Edge}$	Titanium is a good reference element for this group.
	Edge (n = 15)	0.12 ± 0.01				
21/1a-20 (Tweedsmu-ir South)	Inside (n = 5)	0.23 ± 0.02	2.9	2.8	∵ 2.9 > 2.8 ∴ TiO_2 (%) $_{Inside}$ > TiO_2 (%) $_{Edge}$	Ti is **NOT** a reliable reference element to indicate element movement for this group.
	Edge (n = 6)	0.16 ± 0.00				
211/12a-18 (Magnus)	Inside (n = 6)	0.18 ± 0.01	1.2	2.1	∵ - 2.2 < 1.2 < 2.2 ∴ The data cannot reject TiO_2 (%) $_{Inside}$ = TiO_2 (%) $_{Edge}$	Titanium is a good reference element for this group.
	Edge (n = 11)	0.16 ± 0.01				
21/1a-20 (SHALE, Tweedsmuir South)	Inside (n = 4)	1.02 ± 0.15	-4.3	3.2	∵ - 4.3 < -3.2 ∴ TiO_2 (%) $_{Inside}$ < TiO_2 (%) $_{Edge}$	Ti is **NOT** a reliable reference element to indicate element movement for this group.
	Edge (n = 6)	1.77 ± 0.04				
211/12a-18 (SHALE, Magnus)	Inside (n = 4)	0.69 ± 0.02	1.6	2.5	∵ -2.5 < 1.6 < 2.5 ∴ The data cannot reject TiO_2 (%) $_{Inside}$ = TiO_2 (%) $_{Edge}$	TiO_2 is a good reference element for this group.
	Edge (n = 6)	0.63 ± 0.02				

'∵' is the mathematical symbol standing for 'because' and the symbol '∴' represents for 'therefore'; 'Inside' = inside a sedimentary bed; 'Edge' = at the edge of a sedimentary bed

Table 6.12 The comparison of SiO_2 (%) and SiO_2/TiO_2 between samples inside and at the edge of sedimentary beds. The index of SiO_2/TiO_2 in grey colour means the index might not be a reliable indicator for element mobility and should be considered with caution (for details see **Error! Reference source not found.**)

Well	Sample location	SiO_2 (%)	t-test for SiO_2 (%)		SiO_2/TiO_2	t-test for SiO_2/TiO_2		Conclusion
			t Stat / t Critical	Result		t Stat / t Critical	Result	
16/8b-5 (Miller)	Inside (n=3)	92.0 ± 1.0	0.8 / 2.2	∵ - 2.2 < 0.8 < 2.2 ∴ The data cannot reject SiO_2 (%)$_{Inside}$ = SiO_2 (%)$_{Edge}$	621 ± 25	4.0 / 2.6	∵ 4.0 > 2.6 ∴ SiO_2/TiO_2 (Inside) > SiO_2/TiO_2 (Edge)	Data do not show significant difference in silica content between the two sample groups.
	Edge (n=10)	91.0 ± 0.5			466 ± 23			
16/8b-A1 (Miller)	Inside (n=6)	95.3 ± 0.2	1.9 / 2.3	∵ - 2.3 < 1.9 < 2.3 ∴ The data cannot reject SiO_2 (%)$_{Inside}$ = SiO_2 (%)$_{Edge}$	765 ± 26	3.0 / 2.3	∵ 3.0 > 2.3, ∴ SiO_2/TiO_2 (Inside) > SiO_2/TiO_2 (Edge)	Data do not show significant difference in silica content between the two sample groups.
	Edge (n=6)	94.4 ± 0.4			608 ± 40			
16/17-19 (Thelma)	Inside (n=11)	96.4 ± 0.4	1.7 / 2.1	∵ - 2.1 < 1.7 < 2.1 ∴ The data cannot reject SiO_2 (%)$_{Inside}$ = SiO_2 (%)$_{Edge}$	1335 ± 191	2.1 / 2.2	∵ 2.2 < 2.1 < 2.4, ∴ The data cannot reject SiO_2/TiO_2 (Inside) = SiO_2/TiO_2 (Edge)	Data do not show significant difference in silica content between the two sample groups.
	Edge (n=15)	95.5 ± 0.2			891 ± 56			
21/1a-20 (Tweedsmuir South)	Inside (n=5)	91.6 ± 1.2	-2.4 / 2.3	∵ - 2.4 < - 2.3, ∴ SiO_2 (%)$_{Inside}$ < SiO_2 (%)$_{Edge}$	414 ± 40	- 4.1 / 2.3	∵ - 4.1 < - 2.3, ∴ SiO_2/TiO_2 (Inside) < SiO_2/TiO_2 (Edge)	The sandstones at the edge contain more silica.
	Edge (n=6)	94.4 ± 0.1			605 ± 19			
211/12a-18 (Magnus)	Inside (n=6)	83.2 ± 0.8	- 1.7 / 2.1	∵- 2.1 < - 1.7 < 2.1, ∴ The data cannot reject SiO_2 (%)$_{Inside}$ = SiO_2 (%)$_{Edge}$	464 ± 22	- 1.5 / 2.1	∵- 2.1 < - 1.5 < 2.1 ∴ data cannot reject SiO_2/TiO_2 (Inside) = SiO_2/TiO_2 (Edge)	Data do not show significant difference in silica content between the two sample groups.
	Edge (n=11)	84.6 ± 0.4			566 ± 45			
21/1a-20 (SHALE, Tweedsmuir South)	Inside (n=4)	46.1 ± 2.0	5.5 / 3.2	∵ 5.5 > 3.2 ∴ SiO_2 (%)$_{Inside}$ > SiO_2 (%)$_{Edge}$	49 ± 7	3.9 / 3.2	∵ 3.9 > 3.2 ∴SiO_2/TiO_2 (Inside) > SiO_2/TiO_2 (Edge)	The shales at the edge contain less silica.
	Edge (n=6)	32.9 ± 0.5			19 ± 1			

Well	Sample location	SiO_2 (%)	t-test for SiO_2 (%)		SiO_2/TiO_2	t-test for SiO_2/TiO_2		Conclusion
			t Stat / t Critical	Result		t Stat / t Critical	Result	
211/12a-18 (SHALE, Magnus)	Inside (n=4)	43.1 ± 0.2	- 1.8 / 2.1	∵ -2.1 < - 1.8 < 2.1 ∴ The data cannot reject SiO_2 (%)$_{Inside}$ = SiO_2 (%)$_{Edge}$	63 ±3	- 3.0 / 2.3	∵ - 3.0 < - 2.3 ∴ SiO_2/TiO_2 (Inside) < SiO_2/TiO_2 (Edge)	Data do not show significant difference in silica content between the two sample groups.
	Edge (n=6)	47.2 ± 1.2			75 ± 3			

Table 6.13 The comparison of Al_2O_3 and Al_2O_3/TiO_2 between discrete samples and bar samples.

Well	Sample location	Al_2O_3 (%)	t-test for Al_2O_3 (%)		Al_2O_3/TiO_2	t-test for Al_2O_3/TiO_2		Final conclusion
			t Stat / t Critical	Result		t Stat / t Critical	Result	
16/8b-5 (Miller)	Inside (n=3)	2.4 ± 0.2	- 2.4 / 2.3	∵ - 2.4 < - 2.3 ∴ $Al_2O_3(\%)_{Inside} < Al_2O_3(\%)_{Edge}$	16.0 ± 0.8	0.2 / 2.6	∵ - 2.6 < 0.2 < 2.6 ∴ The data cannot reject Al_2O_3/TiO_2 (Inside) = Al_2O_3/TiO_2 (Edge)	The sandstones at the edge contain more aluminium.
	Edge (n=10)	3.2 ± 0.2			15.7 ± 0.7			
16/8b-A1 (Miller)	Inside (n=6)	1.7 ± 0.1	- 2.6 / 2.2	∵ - 2.6 < - 2.2 ∴ $Al_2O_3(\%)_{Inside} < Al_2O_3(\%)_{Edge}$	13.8 ± 0.3	-1.6 / 2.2	∵ - 2.2 < -1.6 < 2.2, ∴ The data cannot reject Al_2O_3/TiO_2 (Inside) = Al_2O_3/TiO_2 (Edge)	The sandstones at the edge contain more aluminium.
	Edge (n=6)	2.4 ± 0.2			14.9 ± 0.6			
16/17-19 (Thelma)	Inside (n=11)	1.6 ± 0.2	- 1.9 / 2.1	∵ - 2.1 < - 1.9 < 2.1 ∴ The data cannot reject $Al_2O_3(\%)_{Inside} = Al_2O_3(\%)_{Edge}$	17.7 ± 1.3	- 0.7 / 2.1	∵ - 2.1 < 0.7 < 2.1, ∴ The data cannot reject Al_2O_3/TiO_2 (Inside) = Al_2O_3/TiO_2 (Edge)	Data do not show significant difference in aluminium content between the two sample groups.
	Edge (n=15)	2.2 ± 0.1			19.2 ± 1.2			
21/1a-20 (Tweeds-muir South)	Inside (n=5)	3.1 ± 0.3	2.0 / 2.6	∵- 2.6 < 2.0 < 2.6 ∴ The data cannot reject $Al_2O_3(\%)_{Inside} = Al_2O_3(\%)_{Edge}$	13.5 ± 0.4	- 1.5 / 2.4	∵ - 2.4 < -1.5 < 2.4 ∴ The data cannot reject Al_2O_3/TiO_2 (Inside) = Al_2O_3/TiO_2 (Edge)	Data do not show significant difference in aluminium content between the two sample groups.
	Edge (n=6)	2.4 ± 0.1			15.3 ± 1.0			
211/12a-18 (Magnus)	Inside (n=6)	6.6 ± 0.1	0.5 / 2.1	∵ - 2.1 < 0.5 < 2.1 ∴ The data cannot reject $Al_2O_3(\%)_{Inside} = Al_2O_3(\%)_{Edge}$	37.0 ± 2.2	- 1.5 / 2.1	∵ - 2.1< -1.5 < 2.1 ∴ The data cannot reject Al_2O_3/TiO_2 (Inside) = Al_2O_3/TiO_2 (Edge)	Data do not show significant difference in aluminium content between the two sample groups.
	Edge (n=11)	6.5 ± 0.2			42.9 ± 3.0			
21/1a-20 (SHALE, Tweedsm-uir South)	Inside (n=4)	14.4 ± 1.7	- 4.5 / 3.2	∵ - 4.5 < - 3.2 ∴ $Al_2O_3(\%)_{Inside} < Al_2O_3(\%)_{Edge}$	14.3 ± 0.5	1.4 / 2.4	∵ - 2.4 < 1.4 < 2.4 ∴ The data cannot reject Al_2O_3/TiO_2 (Inside) = Al_2O_3/TiO_2 (Edge)	The shales at the edge contain more aluminium.
	Edge (n=6)	23.3 ± 0.4			13.2 ± 0.5			
	Inside (n=4)	17.4 ± 0.3	3.3 / 2.1	∵ 3.3 > 2.1 ∴ $Al_2O_3(\%)_{Inside} > Al_2O_3(\%)_{Edge}$	25.4 ± 1.0	2.5 / 2.4	∵ 2.5 > 2.4	

Well	Sample location	Al_2O_3 (%)	t-test for Al_2O_3 (%)		Al_2O_3/TiO_2	t-test for Al_2O_3/TiO_2		Final conclusion
			t Stat / t Critical	Result		t Stat / t Critical	Result	
211/12a-18 (SHALE, Magnus)	Edge (n=6)	13.7 ± 0.6			21.6 ± 0.9		∴ Al_2O_3/TiO_2 (Inside) > Al_2O_3/TiO_2 (Edge)	The shales within the bed contain more aluminium.

Table 6.14 The comparison of K_2O (%), K_2O/TiO_2 and Al_2O_3/TiO_2 between discrete samples and bar samples.

Well	Sample location	K_2O (%)	t-test for K_2O (%)		K_2O/TiO_2	t-test for K_2O/TiO_2		K_2O/Al_2O_3	t-test for K_2O/Al_2O_3		Final conclusion
			t Stat/ t Critical	Result		t Stat/ t Critical	Result		t Stat/ t Critical	Result	
16/8b-5 (Miller)	Inside (n=3)	0.69 ± 0.07	- 2.0/2.4	∵ -2.4 <- 2.0 < 2.4 ∴ The data cannot reject $K_2O(\%)_{Inside} = K_2O(\%)_{Edge}$	4.62 ± 0.36	-0.1/2.8	∵ -2.8 <-0.1<2.8 ∴ The data cannot reject K_2O/TiO_2 (Inside) = K_2O/TiO_2 (Edge)	0.29 ± 0.01	-0.4/2.6	∵ - 2.6 <-0.4 < 2.6 ∴ The data cannot reject K_2O/Al_2O_3 (Inside) = K_2O/Al_2O_3 (Edge)	Data do not show significant difference in potassium content between the two sample groups.
	Edge (n=10)	0.95 ± 0.09			4.67 ± 0.28			0.29 ± 0.01			
16/8b-A1 (Miller)	Inside (n=6)	0.59 ± 0.03	-3.0/2.4	∵ - 3.0 < 2.4 ∴ $K_2O(\%)_{Inside} < K_2O(\%)_{Edge}$	4.65 ± 0.13	-2.33/2.31	∵ - 2.33 < - 2.31 ∴K_2O/TiO_2(Inside) < K_2O/TiO_2 (Edge)	0.34 ± 0.00	-3.1/2.2	∵ - 3.1 < 2.2 ∴ K_2O/Al_2O_3 (Inside) < K_2O/Al_2O_3 (Edge)	The sandstone at the edge contains more potassium.
	Edge (n=6)	0.85 ± 0.07			5.31 ± 0.22			0.36 ± 0.00			
16/17-19 (Thelma)	Inside (n=11)	0.34 ± 0.05	- 0.8/2.1	∵ -2.1<-0.8 < 2.1 ∴ The data cannot reject $K_2O(\%)_{Inside} = K_2O(\%)_{Edge}$	3.80 ± 0.29	1.0/2.1	∵ - 2.1< 1.0 < 2.1 ∴ The data cannot reject K_2O/TiO_2 (Inside) = K_2O/TiO_2 (Edge)	0.21 ± 0.01	4.0/2.1	∵ 4.0 > 2.1 ∴K_2O/Al_2O_3(Inside) > K_2O/Al_2O_3 (Edge)	Data do not show significant difference in potassium content between the two groups.
	Edge (n=15)	0.39 ± 0.03			3.41 ± 0.18			0.18 ± 0.00			
21/1a-20 (Tweedsmuir South)	Inside (n=5)	0.27 ± 0.02	2.4/2.6	∵ -2.6 < 2.4 < 2.6 ∴The data cannot reject $K_2O(\%)_{Inside} = K_2O(\%)_{Edge}$	1.18 ± 0.06	-2.9/2.3	∵ - 2.9 < 2.3 ∴K_2O/TiO_2(Inside) < K_2O/TiO_2 (Edge)	0.09 ± 0.00	-0.6/2.3	∵ - 2.3 < -0.6 < 2.3 ∴ The data cannot reject K_2O/Al_2O_3 (Inside) = K_2O/Al_2O_3 (Edge)	Data do not show significant difference in potassium content between the two sample groups.
	Edge (n=6)	0.22 ± 0.01			1.38 ± 0.03			0.09 ± 0.01			
211/12a-18 (Magnus)	Inside (n=6)	1.83 ± 0.02	1.8/2.2	∵ -2.2 < 1.8 < 2.2	10.2 ± 0.4	-0.5/2.1	∵ - 2.1 < -0.5 < 2.1 ∴ The data cannot reject	0.28 ± 0.01	2.5/2.2	∵ 2.5 > 2.2 ∴K_2O/Al_2O_3(Inside) > K_2O/Al_2O_3 (Edge))	Data do not show significant difference in

Well	Sample location	K_2O (%)	t-test for K_2O (%)		K_2O/TiO_2	t-test for K_2O/TiO_2		K_2O/Al_2O_3	t-test for K_2O/Al_2O_3		Final conclusion
			t Stat/ t Critical	Result		t Stat/ t Critical	Result		t Stat/ t Critical	Result	
	Edge (n=11)	1.63 ± 0.02		∴ The data cannot reject $K_2O(\%)_{Inside} = K_2O(\%)_{Edge}$	10.8 ± 0.8		K_2O/TiO_2 (Inside) = K_2O/TiO_2 (Edge)	0.25 ± 0.01			potassium content between the two sample groups.
21/1a-20 (SHALE, Tweedsmuir South)	Inside (n=4)	1.93 ± 0.21	-3.1/3.2	∵ -3.2 < -3.1 < 3.2 ∴ The data cannot reject $K_2O(\%)_{Inside} = K_2O(\%)_{Edge}$	1.9 ± 0.1	4.1/2.3	∵ 4.1 > 2.3 ∴ The data cannot reject K_2O/TiO_2 (Inside) = K_2O/TiO_2 (Edge)	0.13 ± 0.00	5.0/2.3	∵ 5.0 > 2.3 ∴K_2O/Al_2O_3(Inside) > K_2O/Al_2O_3 (Edge)	The shales at the edge contains more potassium.
	Edge (n=6)	2.71 ± 0.06			1.5 ± 0.1			0.12 ± 0.00			
211/12a-18 (SHALE, Magnus)	Inside (n=4)	2.18 ± 0.03	3.2/2.1	∵ 3.3 > 2.1, ∴ $K_2O(\%)_{Inside} < K_2O(\%)_{Edge}$	3.2 ± 0.1	2.52/2.45	∵ 2.52 > 2.45 ∴K_2O/TiO_2(Inside) > K_2O/TiO_2 (Edge)	0.13 ± 0.00	-0.1/2.1	∵ -2.1 < - 0.1 < 2.1 ∴ The data cannot reject K_2O/Al_2O_3 (Inside) = K_2O/Al_2O_3 (Edge)	The shales within the bed contain more potassium.
	Edge (n=6)	1.72 ± 0.08			2.7 ± 0.1			0.13 ± 0.00			

Table 6.15 The number of Al- and K-bearing minerals in the sandstones of well 16/8b-5. Raw data in Table A 6.1.

Sample type	Sample number/ depth (ft)	K-feldspar %	Plagioclase %	Kaolin %	Illite %
Discrete sandstone (samples within a thick sandstone bed)	14180.6	1.4	1.6	0	4.3
	14194	0.7	1.8	0	3.4
	14195.3	1	1.8	0	1.2
	Average	1.0	1.7	0.0	3.0
	SEM	0.2	0.1	0.0	0.9
Bar sandstone (samples near a sandstone-shale contact)	14168.8	2	1.6	1.3	3.6
	14168.9	1.2	1.9	0	6.8
	14169	1.8	1.5	0	4.7
	14169.03	2.4	2.3	0	5.7
	14169.07	2.8	2.6	0	4.5
	14197.8	0.4	1.8	0	3.5
	14197.87	0.7	1.6	0	2.2
	14197.93	0.6	2	0	3.6
	14198	0.8	2.1	0	3.2
	14198.07	0.9	1.8	0	3.3
	14198.13	0.8	1.8	0	8.1
	Average	1.3	1.9	0.1	4.5
	SEM	0.2	0.1	0.1	0.5
t-test for illite % between the two sandstones		t Stat = -1.3, t Critical = 2.2			
Conclusion		The data does not suggest the amount of illite in the sandstones are significantly different			

Table 6.16 The number of Al- and K-bearing minerals in the sandstones of well 16/8b-A1.

Sample type	Sample number/ depth (m)	K-feldspar %	Plagioclase %	Kaolin %	Illite %
Discrete sandstone (samples within a thick sandstone bed)	4751.9	0.5	2.0	0	3.5
	4752.3	0.3	1.7	0	0.6
	4753	0.5	1.0	0	1.0
	4753.8	1.3	1.1	0	1.9
	4754.6	1.3	1.5	0	1.3
	4758	1.4	2.2	0	0.9
	Average	0.9	1.6	0.0	1.5
	SEM	0.2	0.2	0.0	0.4
Bar sandstone (samples near a sandstone-shale contact)	4750.94	3.0	2.4	0	5.0
	4750.96	1.6	1.8	0	2.9
	4750.98	2.0	1.7	1.0	1.8
	4751	1.6	1.8	0	3.7
	4751.02	1.1	1.4	0	2.3
	4751.04	1.6	1.3	0	3.0
	Average	1.8	1.7	0.2	3.1
	SEM	0.3	0.2	0.2	0.5
t-test for K-feldspar % between the two sandstones		t Stat = -2.8, t Critial = 2.2			
Conclusions		The data suggests the discrete sandstones contain less K-feldspar than the bar sandstones			
t-test for illite % between the two sandstones		t Stat = -2.5, t Critial = 2.2			
Conclusions		The data suggests the discrete sandstones contain less illite than the bar sandstones			

Table 6.17 The main mineralogy of the shales above the bar sandstones of well 16/8b-A1 (the bar sandstones in Table 6.16. Raw data in Table A 6.1.

Sample type	Sample number/ depth (m)	Quartz %	K-feldspar %	Plagioclase %	Kaolinite %	Illite %
Discrete Shale sample	4750.3	40.4	7.4	1.8	12	29.7
	4751	39.3	4.4	1.4	12.8	31.5
	4751.05	40.1	3.9	0.7	13.4	32.8
	4751.1	38.6	6.5	0	14.1	31.2
	4751.2	21.2	6.7	na	18.4	38.9

6.5.5 Mass transfer of iron, magnesium and calcium

The cross-formational transfers of iron, magnesium and calcium are also of great importance to reservoir quality study as these chemical elements are related to the precipitation of carbonate cement in sandstones. Hendry et al. (2000) studied ankerite cement in the Upper Jurassic shallow marine sandstones of Central North Sea, and interpreted the cement to be precipitated from imported Mg^{2+} and Fe^{2+} from adjacent shales. A possible source of iron, magnesium and calcium in shales can be produced from the dissolution of Fe- and Mg-bearing carbonate cement induced by CO_2 and carboxylic acids during the thermal maturation of organic matters (Surdam et al., 1989). The organic-rich shales of the Kimmeridge Clay Formation (KCF) have been reported to contain a considerable amount of ferroan calcites and dolomites, which could possibly serve as a source of iron, magnesium and calcium (Irwin et al., 1977; Scotchman, 1989). This section is going to test the hypothesis that iron, magnesium and calcium had been released in the KCF during diagenesis and exported to contiguous sandstone reservoirs for diagenetic reactions. Reservoirs of the Miller, Tweedsmuir South and Magnus Fields, whose reservoirs are in contact with the KCF, were selected to test the hypothesis.

The variations of Fe_2O_3, MgO, CaO in the sandstones that are in direct contact with the KCF are presented in Figure X to Y. There were 6 sites of sandstone-shale contacts being investigated, among which 4 sites show increasing concentrations of Fe_2O_3 towards the shales (Table 6.18). The concentrations of magnesium and calcium, however, seldom show a clear correlation with the distance to shales (Table 6.18). Then, the question is that as approaching the KCF, is the common increase of Fe_2O_3 in sandstones a result of the diagenetic transfer of iron from the shales into the sandstones? The comparison between the chemistry of sandstones at sandstone-shale contacts and sandstones within thick sedimentary beds, however, suggests that in all the studied reservoirs, there is no significant difference in the content of Fe_2O_3 between these two groups of sandstone (Table 6.19). This indicates that proximity to shales does not have a significant effect on the Fe_2O_3 content of sandstones, and the variation of Fe_2O_3 in the sandstone samples is not likely to be related to a flux of Fe_2O_3 from shales into sandstones. Similarly, the contents of MgO and CaO in sandstones also do show clear variation as a function of the distance to the KCF, suggesting there was no detectable amount of magnesium and calcium being transferred from the KCF into the sandstones (Table 6.20 and Table 6.21). The hypothesis of iron, magnesium

and calcium migrating from shales into sandstones during diagenesis is therefore not supported by the chemical data.

The lack of geochemical evidence for the diagenetic transfer of iron, magnesium and calcium between sandstones and shales may be due to three reasons: (1) carbonate cement are not precipitated upon the first entry into sandstones; the cement may be precipitated in association with pre-existing carbonate minerals, or until the solutes have migrated to the sandstone section with designated pH conditions. (2) XRD data indicate that the KCF near the studied reservoirs generally contain small amounts of calcite and dolomite cement (<3%) and trace ankerite and siderite cement (<1%; Table A 6.1), and there were little ions of iron, magnesium and calcium being freed for diagenetic mass transfer. In addition to carbonate minerals, feldspars and clay minerals may also buffer the acid and CO_2 generated by the maturation of organic matter (Giles and Marshall, 1986).(3) The solubilities of iron (1-100 ppm), Mg (1-100 ppm) in pore waters under the subsurface conditions are typically low, which are on the same magnitude as potassium (Kharaka and Hanor, 2003). Low solubility constrains the diagenetic mobilization of iron and magnesium in diagenesis.

Table 6.18 The groups of samples showing chemical trends that are consistent with the hypothesis of iron, magnesium and calcium migrating from shales into sandstones during diagenesis.

		Increasing Fe_2O_3 toward shales	Increasing MgO toward shales	Increasing CaO toward shales
Sandstone	Bar samples n=6 scale: 0-10 cm	(1) Well 16/8b -5, 14168.80 – 14169.07 ft (2) Well 16/8b-5, 14197.80 – 14198.13 ft (3) Well 16/8b-A1 4750.94 – 4751.04 m (4) Well 211/12a-18 2938.48 – 2938.56 m	(1) Well 16/8b -5, 14168.80 – 14169.07 ft (2) Well 16/8b-5, 14197.80 – 14198.13 ft	(1) Well 16/8b-A1, 4750.94 – 4751.04 m
	Discrete samples n=2 scale: 0-200 cm			
		Decreasing Fe_2O_3 toward sandstones	Decreasing MgO toward sandstones	Decreasing CaO toward sandstones
Shale	Bar samples n=2 scale: 0-10 cm			
	Discrete samples n =2 scale: 0-200 cm		(1) Well 16/8b-A1, 4750.3 – 4751.2 m	(1) Well 16/8b-A1, 4750.3 – 4751.2 m (2) Well 21/1a-20, 14073 – 14086.6 ft

Table 6.19 Comparison of Fe2O3 (%) and t-test results between samples inside and at the edge of a sandstone or shale bed.

Well	Sample location	Fe_2O_3 (%)	t Stat / t Critical	Conclusion of t-test
16/8b-5 (Miller)	Inside (n=3)	0.69±0.05	- 1.96 / 2.18	No significant difference
	Edge (n=10)	1.13±0.11		
16/8b-A1 (Miller)	Inside (n=6)	0.42±0.03	0.40 / 2.57	No significant difference
	Edge (n=6)	0.39±0.01		
21/1a-20 (Tweeds-muir)	Inside (n=5)	0.57±0.13	2.2 / 2.8	No significant difference
	Edge (n=6)	0.25±0.01		
211/12a-18 (Magnus)	Inside (n=6)	0.55±0.03	-0.4 / 2.1	No significant difference
	Edge (n=11)	0.57±0.02		
21/1a-20 (SHALE, Tweeds-muir)	Inside (n=4)	8.88±0.86	1.86 / 2.31	No significant difference
	Edge (n=6)	9.88±0.56		
211/12a-18 (SHALE, Magnus)	Inside (n=4)	8.11±0.56	0.30 / 2.13	No significant difference
	Edge (n=6)	7.74±0.63		

Table 6.20 Comparison of MgO (%) and t-test results between samples inside and at the edge of a sandstone or shale bed.

Well	Sample location	MgO (%)	t Stat / t Critical	Conclusion of t-test
16/8b-5 (Miller)	Inside (n=3)	0.26±0.01	- 1.22 / 2.18	No significant difference
	Edge (n=10)	0.29±0.01		
16/8b-A1 (Miller)	Inside (n=6)	0.18±0.01	-2.52 / 2.23	$Sandstone_{(edge)}$ contains more Mg
	Edge (n=6)	0.20±0.00		
21/1a-20 (Tweeds-muir)	Inside (n=5)	0.32±0.07	2.4 / 2.8	No significant difference
	Edge (n=6)	0.14±0.00		
211/12a-18 (Magnus)	Inside (n=6)	0.30±0.01	-2.06 / 2.20	No significant difference
	Edge (n=11)	0.41±0.05		
21/1a-20 (SHALE, Tweeds-muir)	Inside (n=4)	1.04±0.07	-1.87 / 2.31	No significant difference
	Edge (n=6)	1.21±0.05		
211/12a-18 (SHALE, Magnus)	Inside (n=4)	0.84±0.02	3.03 / 2.13	$Shale_{(inside)}$ contains more Mg
	Edge (n=6)	0.68±0.03		

Table 6.21 Comparison of CaO (%) and t-test results between samples inside and at the edge of a sandstone or shale bed.

Well	Sample location	CaO (%)	t Stat / t Critical	Conclusion of t-test
16/8b-5 (Miller)	Inside (n=3)	1.07±0.38	1.30 / 4.30	No significant difference
	Edge (n=10)	0.46±0.09		
16/8b-A1 (Miller)	Inside (n=6)	0.13±0.03	2.74 / 2.36	$Sandstone_{(inside)}$ contains more Ca
	Edge (n=6)	0.03±0.01		
21/1a-20 (Tweeds-muir)	Inside (n=5)	0.64±0.20	1.64 / 2.78	No significant difference
	Edge (n=6)	0.26±0.01		
211/12a-18 (Magnus)	Inside (n=6)	0.74±0.08	-1.47 / 2.13	No significant difference
	Edge (n=11)	1.00±0.14		
21/1a-20 (SHALE, Tweeds-muir)	Inside (n=4)	3.17±0.54	2.38 / 3.18	No significant difference
	Edge (n=6)	1.64±0.15		
211/12a-18 (SHALE, Magnus)	Inside (n=4)	0.41±0.01	-1.26 / 2.18	$Shale_{(inside)}$ contains more Ca
	Edge (n=6)	0.48±0.05		

6.5.6 The limit of detection of the method

How much transfer of mass can the analytical technique and statistical method of a study detect? This question is as important as the question of the mass transfer itself, but it is often overlooked and no previous study has discussed this issue in detail. For instance, if a method is only sensitive to over 0.5% change in potassium, which equals to the removal of 3.3% of K-feldspar, then its application may be limited in some situations as such an amount of K-feldspar dissolution may not have occurred in some sandstones. Therefore, in order to understand the significance and also the limitation of a study, it is important to consider the limit of detection.

The fundamental principle of the method in this study is to compare the relative abundance of each chemical element between samples to reveal any chemical change during diagenesis and any potential mass transfer processes. The difference between chemical compositions is essential. Hence, the precision of the XRF instrument and the method, which refers to the degree of scattering of data, is critical in determining the detection limit. When preparing samples for XRF major element analysis, the powder of rock samples needs to be made into glass discs first, before being sent to the XRF instrument for analysis. One approach to estimate the precision is by analysing and comparing two glass discs made from the same sample, and this study has selected 5 samples for this practice (Table 6.22).

From the results (Table 6.22), it can be reckoned that the uncertainty for the measurement of Al_2O_3 (%) is generally within 0.2%; that of K_2O (%) is within 0.02%; and for the ratio of K_2O/Al_2O_3, it is within 0.01. This means any changes in K_2O/Al_2O_3 that are greater than 0.01 can be detected by the method of this study. So how much K-feldspar dissolution does this number correspond to? In the sandstone samples (Table A 6.2), the contents of Al_2O_3 (%) are between 1 - 6%, which means to change 0.01 of K_2O/Al_2O_3, 0.01 – 0.06% K_2O needs to be moved. Given that the concentration of potassium in K-feldspar ($KAlSi_3O_8$) is 14.0%, 0.06 – 0.36% of K-feldspar is required to provide 0.01 – 0.06% K_2O. Therefore, so long as there is 0.06 – 0.36% of K-feldspar dissolution in a sample and the products have been exported, it can potentially be detected in this study. In the traditional methods of studying mass transfer, i.e. by plotting potassium versus depth, at least 2-3% change of an element is required to present an argument that this element is mobile in diagenesis (e.g. Milliken et al.,

1994; Wilkinson et al., 2003). In comparison, the detection ability of the method of this study is about of one magnitude higher.

The grade of uncertainty for the ratios related to TiO_2 is dependent on the percentage of TiO_2. When the percentage is high (TiO_2 > 0.5%), the uncertainties are well-controlled: for SiO_2/TiO_2, it is < 0.2; for K_2O/TiO_2, it is < 0.02. However, when the percentage of TiO_2 is less than 0.1%, the uncertainties will increase greatly. For example, the Sample 13999 in Table 6.22 has a factor of 92 in SiO_2/TiO_2 between two repeat analyses. Therefore, cautions should be paid to the validity of data when the content of TiO_2 is low (<0.1%).

The above-mentioned is the technical detection limit of the method of this study. In practice, there is natural variability in samples that needs to be considered. The uncertainty in the samples' natural variability is a function of the sedimentary environment and the number of the samples collected. In a sedimentary environment with constantly changing water energy and sediment supply, the variation and uncertainty in the composition of sediments would relatively high. On the other hand, the uncertainty can be better managed by collecting a larger number of study samples.

Table 6.22 Repeated analysis on two glass discs made from the same sample.

Well	Sample number		Lithology		SiO_2	Al_2O_3	Fe_2O_3	MgO	CaO	Na_2O	K_2O	TiO_2	P_2O_5	LOI	Total
	Depth/ft	Depth/m			%	%	%	%	%	%	%	%	%	%	%
211/12a-18		2947.46	Shale	1st	43.60	17.74	7.28	0.90	0.41	0.61	2.187	0.674	0.178	26.12	99.52
				2nd	43.70	17.73	7.21	0.82	0.40	0.67	2.199	0.674	0.184	25.92	99.32
211/12a-18		2947.66	Shale	1st	42.86	16.57	7.76	0.78	0.42	0.63	2.085	0.735	0.185	27.39	99.23
				2nd	42.99	16.55	7.68	0.75	0.41	0.74	2.085	0.735	0.191	27.42	99.37
211/12a-18		2947.69	Shale	1st	42.54	17.90	10.02	0.87	0.42	0.67	2.245	0.726	0.218	23.93	99.33
				2nd	42.76	18.02	9.96	0.82	0.41	0.75	2.269	0.732	0.225	23.89	99.61
21/1a- 20	14073		Shale	1st	39.28	20.03	8.75	1.22	1.44	0.12	2.649	1.527	0.596	24.03	99.04
				2nd	39.06	19.82	8.79	1.28	1.44	0.11	2.630	1.520	0.59	24.22	98.86
16/17-19	13999		Sandstone	1st	96.06	1.89	0.24	0.13	0.00	n.d.	0.315	0.081	0.029	1.19	99.90
				2nd	95.83	1.89	0.24	0.12	0.00	n.d.	0.313	0.075	0.028	1.11	99.58

Table 6.22 continued

Well	Sample number		Lithology		SiO_2/ TiO_2	K_2O/ TiO_2	K_2O/ Al_2O_3
	Depth/ft	Depth/m					
211/12a-18		2947.46	Shale	1st	64.69	3.24	0.12
				2nd	64.80	3.26	0.12
211/12a-18		2947.66	Shale	1st	58.31	2.84	0.13
				2nd	58.52	2.84	0.13
211/12a-18		2947.69	Shale	1st	58.63	3.09	0.13
				2nd	58.42	3.10	0.13
21/1a- 20	14073		Shale	1st	25.73	1.74	0.13
				2nd	25.78	1.73	0.13
16/17-19	13999		Sandstone	1st	1185.87	3.89	0.17
				2nd	1277.73	4.17	0.17

6.6 Conclusion

This study was designed to investigate the potential mass transfer process between sandstones and shales during diagenesis. It examined the reservoirs of five oilfields which are characterized by alternating sandstone and shale beds. The scope of the search varies from centimetres to meters, depending on the interval space between samples (discrete or bar samples). Petrographic (point-count), mineralogical (XRD) and chemical data (XRF) were combined to verify if the mass transfer has occurred in any of the reservoirs. The technical limit of detection of the study method is excellent, which can detect the import and export of the mass produced by 0.06 – 0.36% of K-feldspar dissolution. The majority of the sandstones are turbidite sandstones whose variation in the original composition is expected to be limited. The shales in the study are mostly mature hydrocarbon source rocks, which may have released a considerable volume of fluids due to maturation of organic matters. The contacts between the sandstones and shales are possibly the most dynamic areas for the transfer of mass in the deep basin. The conclusions of this study are:

(1) The comparing results of the concretion sandstones and the normal sandstones in well 211/12a-18 show that the normal sandstones contain less K-feldspar and more quartz than the concretion sandstones. However, because there is only one concretion sandstone, it is uncertain whether the different compostions were caused by depositional process or diagenetic process.

(2) The chemical data showed the chemical variation of sandstones and shales within the range of 0-10cm. Most of the chemical trends in turbidite sandstones are consistent with the characteristic upwards-fining sequence of turbidite, indicating an influence of the depositional process on the sediment’s compositions. But on a large scale, i.e. decimeters to meters, the chemistry of the sediments are more variable, and cannot simply be explained by the pattern of the upwards-fining sequence. It may indicate more fluctuations in the sedimentary environment.

(3) Among the 12 bar samples and 6 groups of discrete studied, only a few show chemical trends that can be possibly explained by diffusion. However, the mineralogical and petrographic data of those samples and the related sandstones or

shales in the same reservoir do not suggest the chemical trends are caused by the mass transfer. Therefore, the studied samples do not show any evidence for any process of mass transfer by diffusion in diagenesis.

(4) Studying the mass transfer by pore fluid flow needs to first confirm the direction of the flow. Reservoirs within multiple layers of thick shales are not appropriate for the study, because each of the shale beds can produce the driving force for the fluid flow and consequently, the pattern of flow is complicated. Only the reservoirs of wells 16/8b-A1 (Miller) and 21/1a-20 (Tweedsmiur), which only contains a single thick shale bed, are selected to study the mass transfer by pore fluid flow. The reservoir of well 21/1a-20 is the most likely case where the mass transfer has occurred. The potentially transferred solute is silica; the transfer scale is 0-3 m, and the mechanism is by the pore water flow from the shale into the sandstone. The supportive evidence include: 1) the shale interbedded in the sandstone is depleted in quartz (c.3%) comparing to the thick shales below the sandstone (c.32%), indicating a loss of quartz from the shale into the sandstone; 2) the systematic increase of SiO_2 (%) and SiO_2/TiO_2 in the sandstone towards the sandstone-shale contact; 3) the corresponding decrease of SiO_2 (%) and SiO_2/TiO_2 in the shale towards the sandstone. If there were a movement of silica from the shale to the sandstone, the sandstone near the sandstone-shale contact would receive more silica and develop more quartz cement. However, the point-count data does not prove that there is a significant difference in the amount of quartz cement between the sandstones at the contact and the sandstones inside the sedimentary bed. Therefore, the hypothesis of silica transfer by pore fluid flow in the reservoir of well 21/1a-20 cannot be confidently verified to be correct.

(5) On the other hand, the results of this study show the chemical and mineralogical variation within turbidite sandstones are small. For instance, in the comparison between the samples on the edge of a sandstone bed and the samples inside the sandstone bed, only 20-40% of all cases showed that there are statistically significant differences in the contents of Si, Al or K.

(6) The chemical data also indicate that there were no transfer of iron, magnesium and calcium across the sandstone-shale boundaries in the studied oilfields.

(6) The lack of firm evidence in this study to prove the occurrence of any mass transfer process suggests that sandstones and shales are ‘closed’ systems in diagenesis, and the scale of element mobility is highly limited. One possible reason for this study does not find any evidence of the mass transfer is because the actual scale of element movement may be below the minimum scope of detection of this study, i.e. of 5-10 cm. The chemical elements in sediments may only migrate from pores to the next pores during diagenesis, and the scale is less than 1-2 cm. The chemistry of sandstone is subjected to little modefication in the deep basin.

Summary statement: Some studies claimed that the organic acids and CO_2 generated from the maturation of organic matters can enhance the solubility and therefore the mobility of some metallic elements, particularly aluminium and potassium (MacGowan and Surdam, 1990, 1988; Surdam et al., 1984). In addition, many papers have suggested an ‘open’ diagenetic system between sandstones and shales, with the exchange of chemical elements between the two in diagenesis (Awwiller, 1993; Day-Stirrat et al., 2010; Land, 1997; Milliken et al., 1994, 1989; Thyne, 2001; Wilkinson et al., 2014b, 2003, 1997). This study, however, drew the opposite conclusions. The geochemical data indicates that sandstones and shales do not exchange chemical elements during diagenesis. This reflects that the main rock-forming minerals of sediments - Si, Al, K, Fe, Mg and Ca are all highly immobile elements in the subsurface.

6.7 Appendix

Table A 6.1 XRD mineralogy analysis results of both the discrete and bar samples

Well	Lithology	Sample type	Sample number		Quartz (%)	K-feldspar (%)	Plagioclase (%)	Kaolinite (%)	Illite (%)	Muscovite (%)	Chlorite (%)	Smectite (%)	Calcite (%)	Dolomite (%)	Siderite (%)	Ankerite (%)	Pyrite (%)	Anatase (%)	Total (%)
			Driller's depth/ft	Driller'sdepth/m															
16/8b-5	Sandstone	Discrete	14180.6		88.5	1.4	1.6	0.0	4.3	1.1	0.0	0.0	1.5	0.0	0.0	0.1	0.3	0.1	98.9
16/8b-5	Sandstone	Discrete	14194		90.3	0.7	1.8	0.0	3.4	1.2	0.6	0.2	0.4	0.1	0.1	0.1	0.3	0.3	99.4
16/8b-5	Sandstone	Discrete	14195.3		91.6	1.0	1.8	0.0	1.2	1.8	0.7	0.0	0.5	0.0	0.2	0.1	0.2	0.3	99.4
16/8b-5	Sandstone	Bar	14168.8		88.3	2.0	1.6	1.3	3.6	1.3	0.5	0.2	0.2	0.0	0.0	0.2	0.3	0.2	99.6
16/8b-5	Sandstone	Bar	14168.9		86.4	1.2	1.9	0.0	6.8	1.2	0.5	0.3	0.4	0.1	0.0	0.1	0.7	0.1	99.7
16/8b-5	Sandstone	Bar	14169		88.2	1.8	1.5	0.0	4.7	2.1	0.0	0.0	0.4	0.0	0.0	0.1	0.5	0.2	99.7
16/8b-5	Sandstone	Bar	14169.03		86.1	2.4	2.3	0.0	5.7	1.7	0.1	0.0	0.4	0.0	0.1	0.1	0.5	0.1	99.7
16/8b-5	Sandstone	Bar	14169.07		85.9	2.8	2.6	0.0	4.5	1.7	0.5	0.3	0.4	0.0	0.0	0.0	0.6	0.2	99.5
16/8b-5	Sandstone	Bar	14197.8		91.1	0.4	1.8	0.0	3.5	1.3	0.0	0.1	0.5	0.1	0.0	0.2	0.3	0.2	99.5
16/8b-5	Sandstone	Bar	14197.87		90.9	0.7	1.6	0.0	2.2	2.0	0.3	0.1	0.4	0.2	0.0	0.2	0.3	0.2	99.1
16/8b-5	Sandstone	Bar	14197.93		90.3	0.6	2.0	0.0	3.6	1.4	0.2	0.0	0.7	0.2	0.0	0.2	0.3	0.1	99.4
16/8b-5	Sandstone	Bar	14198		91.1	0.8	2.1	0.0	3.2	1.0	0.2	0.0	0.5	0.0	0.0	0.2	0.3	0.2	99.6
16/8b-5	Sandstone	Bar	14198.07		89.1	0.9	1.8	0.0	3.3	1.6	0.9	0.4	0.5	0.2	0.0	0.2	0.5	0.2	99.4
16/8b-5	Sandstone	Bar	14198.13		83.6	0.8	1.8	0.0	8.1	2.1	0.3	0.7	0.3	0.4	0.0	0.3	1.1	0.0	99.5
16/8b-A1	Sandstone	Discrete		4751.9	90.7	0.5	2.0	0.0	3.5	1.2	0.3	0.2	0.3	0.0	0.1	0.0	0.1	0.5	99.3

Well	Lithology	Sample type	Sample number		Quartz (%)	K-feldspar (%)	Plagioclase (%)	Kaolinite (%)	Illite (%)	Muscovite (%)	Chlorite (%)	Smectite (%)	Calcite (%)	Dolomite (%)	Siderite (%)	Ankerite (%)	Pyrite (%)	Anatase (%)	Total (%)
			Driller's depth/ft	Driller'sdepth/m															
16/8b-A1	Sandstone	Discrete		4752.3	94.6	0.3	1.7	0.0	0.6	1.1	0.5	0.2	0.2	0.1	0.0	0.0	0.1	0.3	99.7
16/8b-A1	Sandstone	Discrete		4753	95.1	0.5	1.0	0.0	1.0	1.4	0.0	0.0	0.2	0.0	0.0	0.0	0.2	0.3	99.8
16/8b-A1	Sandstone	Discrete		4753.8	93.7	1.3	1.1	0.0	1.9	0.2	0.5	0.0	0.4	0.0	0.0	0.0	0.1	0.3	99.4
16/8b-A1	Sandstone	Discrete		4754.6	94.0	1.3	1.5	0.0	1.3	0.7	0.2	0.0	0.3	0.0	0.0	0.0	0.2	0.3	99.8
16/8b-A1	Sandstone	Discrete		4758	93.1	1.4	2.2	0.0	0.9	1.1	0.2	0.0	0.2	0.0	0.0	0.0	0.2	0.4	99.7
16/8b-A1	Sandstone	Bar		4750.94	87.0	3.0	2.4	0.0	5.0	1.2	0.2	0.2	0.2	0.1	0.0	0.1	0.2	0.2	99.7
16/8b-A1	Sandstone	Bar		4750.96	91.1	1.6	1.8	0.0	2.9	1.3	0.1	0.2	0.2	0.0	0.0	0.0	0.2	0.3	99.7
16/8b-A1	Sandstone	Bar		4750.98	91.7	2.0	1.7	1.0	1.8	1.7	0.1	0.0	0.1	0.0	0.0	0.0	0.2	0.2	100.5
16/8b-A1	Sandstone	Bar		4751.00	90.4	1.6	1.8	0.0	3.7	1.2	0.3	0.1	0.2	0.0	0.0	0.0	0.1	0.3	99.7
16/8b-A1	Sandstone	Bar		4751.02	92.6	1.1	1.4	0.0	2.3	1.6	0.2	0.0	0.3	0.0	0.0	0.0	0.1	0.2	99.7
16/8b-A1	Sandstone	Bar		4751.04	93.3	1.6	1.3	0.0	3.0	0.2	0.0	0.0	0.1	0.0	0.0	0.0	0.0	0.2	99.7
16/8b-A1	Shale	Discrete		4750.30	40.4	7.4	1.8	12.0	29.7	n.a	n.a	n.a	n.a	0.2	n.a	1.3	5.3	1.7	99.7
16/8b-A1	Shale	Discrete		4751.00	39.3	4.4	1.4	12.8	31.5	n.a	n.a	n.a	n.a	0.2	n.a	1.3	7.5	1.1	99.4
16/8b-A1	Shale	Discrete		4751.05	40.1	3.9	0.7	13.4	32.8	n.a	n.a	n.a	n.a	1.2	n.a	n.a	6.5	1.1	99.7
16/8b-A1	Shale	Discrete		4751.10	38.6	6.5	0.0	14.1	31.2	n.a	n.a	n.a	n.a	1.5	n.a	n.a	6.4	1.4	99.7
16/8b-A1	Shale	Discrete		4751.20	21.2	6.7	na	18.4	38.9	n.a	n.a	n.a	n.a	1.3	n.a	n.a	11.0	2.2	99.7
16/17-19	Sandstone	Bar	13998.84		94.4	0.2	1.3	0.6	1.8	0.8	0.2	0.0	0.1	0.0	0.0	0.0	0.1	0.3	99.4
16/17-19	Sandstone	Bar	13998.87		94.9	0.9	1.5	0.6	0.6	0.5	0.4	0.0	0.1	0.0	0.0	0.0	0.1	0.2	99.6

Well	Lithology	Sample type	Sample number		Quartz (%)	K-feldspar (%)	Plagioclase (%)	Kaolinite (%)	Illite (%)	Muscovite (%)	Chlorite (%)	Smectite (%)	Calcite (%)	Dolomite (%)	Siderite (%)	Ankerite (%)	Pyrite (%)	Anatase (%)	Total (%)
			Driller's depth/ft	Driller'sdepth/m															
16/17-19	Sandstone	Bar	13998.9		94.7	0.4	1.5	0.9	1.3	0.4	0.0	0.0	0.1	0.0	0.0	0.0	0.1	0.3	99.5
16/17-19	Sandstone	Bar	13998.93		93.8	0.5	1.9	0.5	1.6	0.2	0.3	0.3	0.2	0.0	0.0	0.0	0.1	0.4	99.5
16/17-19	Sandstone	Bar	13998.97		94.8	0.1	1.4	0.5	1.1	0.9	0.3	0.2	0.2	0.0	0.0	0.2	0.1	0.3	99.7
16/17-19	Sandstone	Bar	13999		92.8	0.5	1.3	0.3	2.9	0.9	0.3	0.2	0.2	0.0	0.0	0.0	0.1	0.3	99.6
16/17-19	Sandstone	Bar	13999.03		92.6	0.7	1.9	0.5	2.1	0.9	0.4	0.2	0.2	0.0	0.0	0.0	0.1	0.2	99.6
16/17-19	Sandstone	Bar	13999.07		93.3	0.5	1.9	1.1	1.1	0.6	0.4	0.3	0.2	0.0	0.0	0.0	0.1	0.3	99.5
16/17-19	Sandstone	Bar	13999.1		91.1	0.1	1.6	3.1	1.4	0.8	0.8	0.2	0.1	0.0	0.0	0.0	0.2	0.2	99.4
16/17-19	Sandstone	Bar	13999.13		67.6	1.8	1.5	10.9	11.5	2.5	0.7	0.5	0.0	0.0	0.1	0.0	0.4	1.9	97.3
16/17-19	Sandstone	Bar	14069.87		94.3	0.3	1.7	0.0	1.5	0.5	0.4	0.3	0.3	0.0	0.0	0.0	0.2	0.3	99.4
16/17-19	Sandstone	Bar	14069.93		94.8	0.2	1.6	0.2	1.3	0.4	0.4	0.3	0.2	0.0	0.0	0.0	0.1	0.3	99.5
16/17-19	Sandstone	Bar	14070		95.0	0.8	1.6	0.0	0.8	0.3	0.3	0.2	0.2	0.0	0.0	0.0	0.1	0.2	99.3
16/17-19	Sandstone	Bar	14070.07		94.8	0.2	1.6	0.2	1.3	0.5	0.2	0.3	0.2	0.0	0.0	0.0	0.1	0.3	99.4
16/17-19	Sandstone	Bar	14070.13		95.5	0.3	1.1	0.0	1.4	0.6	0.1	0.3	0.1	0.0	0.0	0.0	0.1	0.2	99.5
16/17-19	Sandstone	Bar	14070.2		94.9	0.1	1.4	0.0	1.5	0.8	0.3	0.1	0.2	0.0	0.0	0.0	0.1	0.2	99.4
21/1a-20	Sandstone	Discrete	14063.2		90.2	0.3	1.6	1.6	2.9	0.2	0.3	0.3	0.3	0.3	0.1	0.7	0.2	0.3	99.2
21/1a-20	Sandstone	Discrete	14065.8		85.1	0.9	0.9	4.2	2.8	1.2	0.6	0.2	0.5	0.7	0.0	1.2	0.7	0.4	99.5
21/1a-20	Sandstone	Discrete	14068.3		88.9	0.9	1.2	3.6	2.0	0.8	0.4	0.1	0.4	0.3	0.1	0.3	0.3	0.3	99.5
21/1a-20	Sandstone	Discrete	14070.1		91.4	0.7	1.2	2.2	2.1	0.9	0.3	0.0	0.3	0.0	0.1	0.0	0.2	0.3	99.6

Well	Lithology	Sample type	Sample number		Quartz (%)	K-feldspar (%)	Plagioclase (%)	Kaolinite (%)	Illite (%)	Muscovite (%)	Chlorite (%)	Smectite (%)	Calcite (%)	Dolomite (%)	Siderite (%)	Ankerite (%)	Pyrite (%)	Anatase (%)	Total (%)
			Driller's depth/ft	Driller'sdepth/m															
21/1a-20	Sandstone	Discrete	14071		94.4	0.4	1.0	1.4	0.9	0.6	0.4	0.1	0.2	0.0	0.0	0.0	0.1	0.3	99.8
21/1a-20	Shale	Discrete	14073		12.8	2.7	1.1	26.6	32.0	5.6	2.5	0.2	0.5	1.9	0.2	0.3	9.3	2.4	98.2
21/1a-20	Shale	Discrete	14074.4		38.7	2.2	1.8	15.7	18.1	4.2	1.0	0.9	3.8	1.9	0.1	1.7	7.9	1.2	99.0
21/1a-20	Shale	Discrete	14075.6		37.1	0.4	2.6	14.0	17.7	2.5	1.2	1.2	3.8	1.2	0.3	1.1	14.3	1.1	98.4
21/1a-20	Shale	Discrete	14085.6		40.8	0.1	1.9	11.1	20.8	3.4	0.9	0.3	6.0	1.0	0.0	0.7	10.1	0.5	97.7
21/1a-20	Sandstone	Bar	14071.87		91.4	0.0	1.4	1.2	2.9	1.0	0.5	0.7	0.3	0.0	0.0	0.0	0.1	0.2	99.7
21/1a-20	Sandstone	Bar	14071.9		91.5	1.0	2.0	1.5	1.2	0.5	0.4	0.4	0.4	0.0	0.1	0.0	0.1	0.5	99.6
21/1a-20	Sandstone	Bar	14071.93		92.1	1.1	1.5	2.1	1.0	0.3	0.5	0.0	0.4	0.0	0.0	0.0	0.1	0.3	99.3
21/1a-20	Sandstone	Bar	14072		92.0	0.7	1.7	1.8	1.1	0.8	0.4	0.2	0.5	0.0	0.1	0.0	0.1	0.3	99.7
21/1a-20	Sandstone	Bar	14072.13		91.4	0.9	1.4	2.7	1.4	0.5	0.4	0.0	0.2	0.0	0.0	0.0	0.2	0.5	99.6
21/1a-20	Shale	Bar	14044.87		0.3	4.4	0.0	19.2	38.5	8.3	3.3	0.0	0.0	3.3	0.2	1.1	14.1	4.9	97.6
21/1a-20	Shale	Bar	14044.93		1.7	5.1	0.0	21.3	39.0	6.6	3.6	0.6	0.0	3.4	0.2	0.0	10.6	4.6	96.7
21/1a-20	Shale	Bar	14045		3.2	2.7	2.3	20.0	23.7	9.1	6.8	3.2	0.2	2.7	0.9	0.0	15.4	4.7	94.9
21/1a-20	Shale	Bar	14045.07		5.7	2.2	0.0	19.3	39.6	7.4	4.2	1.1	0.1	2.0	0.0	0.0	12.3	5.0	98.9
21/1a-20	Shale	Bar	14045.13		5.4	4.4	0.0	19.6	38.0	2.9	5.9	0.7	0.5	1.4	0.2	0.0	13.1	4.8	96.8
211/12a-18	Shale	Discrete		2947.46	24.7	3.7	8.9	12.5	30.9	3.8	4.0	2.5	1.7	0.0	0.2	0.0	6.1	0.3	98.9
211/12a-18	Shale	Discrete		2947.55	31.7	0.0	11.7	13.5	14.5	9.1	4.3	4.2	1.9	0.0	0.1	0.0	7.4	1.0	98.5
211/12a-18	Shale	Discrete		2947.66	30.1	1.0	8.1	9.4	30.0	7.2	2.2	0.7	1.1	0.0	0.0	0.0	8.9	0.2	98.7

Well	Lithology	Sample type	Sample number		Quartz (%)	K-feldspar (%)	Plagioclase (%)	Kaolinite (%)	Illite (%)	Muscovite (%)	Chlorite (%)	Smectite (%)	Calcite (%)	Dolomite (%)	Siderite (%)	Ankerite (%)	Pyrite (%)	Anatase (%)	Total (%)
			Driller's depth/ft	Driller'sdepth/m															
211/12a-18	Shale	Discrete		2947.69	22.4	3.8	4.6	12.2	33.6	8.0	3.0	0.4	1.0	0.0	0.1	0.0	9.5	0.5	98.6
211/12a-18	Shale	Bar		2941.51	44.9	0.8	8.0	7.6	18.9	6.4	2.4	2.3	1.3	0.0	0.1	0.0	5.5	1.8	98.2
211/12a-18	Shale	Bar		2954.76	53.2	0.0	5.6	7.1	21.1	3.4	1.7	1.5	1.5	0.0	0.2	0.0	3.7	0.5	98.8
211/12a-18	Sandstone	Discrete		2955.73	71.0	7.1	14.6	0.6	3.0	1.0	0.3	0.2	0.3	0.0	0.1	0.3	0.2	0.4	98.7
211/12a-18	Sandstone	Discrete		2956	65.6	9.9	19.0	1.3	0.8	1.3	0.6	0.2	0.4	0.2	0.0	0.4	0.1	0.2	99.8
211/12a-18	Sandstone	Discrete		2956.5	69.8	4.9	15.9	0.3	3.8	0.4	0.1	0.1	0.7	1.4	0.1	1.3	0.1	0.3	98.8
211/12a-18	Sandstone	Discrete		2957	68.3	7.4	15.1	1.1	2.4	1.0	0.0	0.2	0.4	1.6	0.2	0.6	0.2	0.4	98.4
211/12a-18	Sandstone	Discrete		2958	75.9	4.6	11.1	0.5	3.7	1.4	0.0	0.2	0.4	0.2	0.1	0.2	0.1	0.3	98.5
211/12a-18	Sandstone	Discrete		2958.75	73.0	8.0	13.3	1.0	1.4	1.0	0.3	0.0	0.4	0.3	0.1	0.5	0.1	0.1	99.4
211/12a-18	Concretion	Discrete		2935.38	66.0	7.7	14.8	3.0	2.8	1.5	1.7	0.6	0.5	0.0	0.2	0.2	0.7	0.0	99.5
211/12a-18	Concretion	Discrete		2949.57	54.7	8.8	15.8	0.6	0.7	1.3	1.3	0.7	12.1	1.3	0.1	1.2	0.2	0.4	98.9
211/12a-18	Concretion	Discrete		2952.68	47.4	8.8	13.7	0.6	3.1	1.9	0.6	0.2	20.1	0.6	0.1	0.9	0.2	0.3	98.2
211/12a-18	Sandstone	Bar		2938.56	69.4	7.0	14.5	0.1	3.1	0.0	0.8	0.4	1.2	0.8	0.1	1.4	0.1	0.2	98.9
211/12a-18	Sandstone	Bar		2943.62	74.0	5.3	14.8	1.4	1.4	0.3	0.4	0.4	0.7	0.3	0.1	0.3	0.1	0.3	99.4

Table A 6.2 XRF analysis results of both the discrete and bar samples. LOI = Loss on ignition.

Well	Lithology	Sample type	Sample number		SiO_2 %	Al_2O_3 %	Fe_2O_3 %	MgO %	CaO %	Na_2O %	K_2O %	TiO_2 %	MnO %	P_2O_5 %	LOI %	Total %
			Depth/ft	Depth/m												
16/8b-5	Sandstone	Discrete sample	14180.60		89.66	2.71	0.79	0.24	1.99	0.00	0.85	0.16	0.01	0.04	3.37	99.82
16/8b-5	Sandstone	Discrete sample	14194.00		92.88	2.49	0.66	0.24	0.57	0.00	0.70	0.15	0.00	0.04	1.93	99.67
16/8b-5	Sandstone	Discrete sample	14195.30		93.45	1.96	0.61	0.28	0.64	0.00	0.53	0.14	0.01	0.03	1.90	99.54
16/8b-5	Sandstone	Bar sample	14168.80		91.33	3.91	0.90	0.23	0.16	0.00	1.07	0.20	0.00	0.03	2.01	99.84
16/8b-5	Sandstone	Bar sample	14168.90		89.32	4.01	1.41	0.28	0.14	0.00	1.30	0.23	0.00	0.05	2.87	99.61
16/8b-5	Sandstone	Bar sample	14169.00		90.59	3.53	1.30	0.27	0.15	0.00	1.18	0.21	0.00	0.05	2.46	99.74
16/8b-5	Sandstone	Bar sample	14169.03		90.26	3.66	1.38	0.27	0.15	0.00	1.22	0.22	0.00	0.05	2.63	99.84
16/8b-5	Sandstone	Bar sample	14169.07		88.96	3.74	1.38	0.28	0.15	0.00	1.24	0.22	0.00	0.05	3.77	99.81
16/8b-5	Sandstone	Bar sample	14197.80		92.91	2.29	0.79	0.29	0.69	0.00	0.59	0.17	0.00	0.03	1.94	99.70
16/8b-5	Sandstone	Bar sample	14197.87		92.45	2.41	0.77	0.28	0.82	0.00	0.66	0.19	0.01	0.03	2.10	99.72
16/8b-5	Sandstone	Bar sample	14197.93		92.54	2.19	0.79	0.29	0.84	0.00	0.60	0.17	0.01	0.03	2.25	99.71
16/8b-5	Sandstone	Bar sample	14198.00		93.39	2.20	0.77	0.26	0.59	0.00	0.62	0.16	0.00	0.03	1.86	99.88
16/8b-5	Sandstone	Bar sample	14198.07		91.72	2.68	0.99	0.35	0.75	0.00	0.76	0.17	0.01	0.03	2.45	99.90
16/8b-5	Sandstone	Bar sample	14198.13		87.49	4.49	1.91	0.42	0.58	0.00	1.21	0.27	0.01	0.04	3.56	99.97
16/8b-A1	Sandstone	Discrete sample		4752.29	95.52	1.56	0.38	0.15	0.09	n.d.	0.51	0.12	0.00	0.02	1.52	99.76
16/8b-A1	Sandstone	Discrete sample		4751.88	94.14	2.12	0.37	0.16	0.22	n.d.	0.74	0.15	0.00	0.02	2.05	99.87
16/8b-A1	Sandstone	Discrete sample		4753.00	95.35	1.61	0.54	0.19	0.10	0.00	0.53	0.12	0.00	0.02	1.24	99.69
16/8b-A1	Sandstone	Discrete sample		4753.80	95.78	1.77	0.30	0.18	0.19	0.00	0.62	0.12	0.00	0.02	1.15	100.13
16/8b-A1	Sandstone	Discrete sample		4754.60	95.60	1.56	0.45	0.18	0.18	0.00	0.52	0.12	0.00	0.02	0.98	99.61
16/8b-A1	Sandstone	Discrete sample		4758.00	95.69	1.77	0.47	0.19	0.00	0.00	0.60	0.13	0.00	0.02	0.95	99.82
16/8b-A1	Sandstone	Bar sample		4750.94	92.79	3.37	0.45	0.22	0.10	0.00	1.19	0.19	0.00	0.03	1.61	99.96
16/8b-A1	Sandstone	Bar sample		4750.96	93.93	2.54	0.41	0.19	0.02	0.00	0.91	0.15	0.00	0.03	1.34	99.52

Well	Lithology	Sample type	Sample number		SiO_2 %	Al_2O_3 %	Fe_2O_3 %	MgO %	CaO %	Na_2O %	K_2O %	TiO_2 %	MnO %	P_2O_5 %	LOI %	Total %
			Depth/ft	Depth/m												
16/8b-A1	Sandstone	Bar sample		4750.98	94.46	2.38	0.39	0.20	0.02	0.00	0.87	0.17	0.00	0.03	1.28	99.80
16/8b-A1	Sandstone	Bar sample		4751.00	94.53	2.44	0.39	0.21	0.02	0.00	0.83	0.18	0.00	0.03	1.14	99.76
16/8b-A1	Sandstone	Bar sample		4751.02	95.30	1.89	0.36	0.18	0.01	0.00	0.68	0.14	0.00	0.02	1.17	99.75
16/8b-A1	Sandstone	Bar sample		4751.04	95.52	1.74	0.35	0.19	0.01	0.00	0.63	0.12	0.00	0.02	1.33	99.91
16/8b-A1	Shale	Discrete sample		4750.30	49.66	13.49	6.67	1.14	3.70	0.19	1.74	0.86	0.05	0.40	21.58	99.47
16/8b-A1	Shale	Discrete sample		4751.00	55.86	14.05	5.26	0.87	0.38	0.20	3.28	0.60	0.01	0.16	17.77	98.45
16/8b-A1	Shale	Discrete sample		4751.05	56.70	14.29	4.63	0.86	0.39	0.19	3.32	0.60	0.01	0.19	17.64	98.82
16/8b-A1	Shale	Discrete sample		4751.10	58.00	15.00	4.68	0.89	0.47	0.21	3.46	0.64	0.02	0.19	16.39	99.95
16/8b-A1	Shale	Discrete sample		4751.20	46.42	18.30	7.46	0.90	0.31	0.28	3.87	0.87	0.02	0.16	21.07	99.67
16/17-19	Sandstone	Bar sample	13998.84		95.42	1.93	0.32	0.14	0.06	n.d.	0.34	0.15	n.d.	0.06	1.33	99.64
16/17-19	Sandstone	Bar sample	13998.87		97.11	1.57	0.27	0.10	0.02	n.d.	0.26	0.10	n.d.	0.04	1.04	100.37
16/17-19	Sandstone	Bar sample	13998.90		96.36	1.52	0.31	0.10	0.02	n.d.	0.25	0.09	n.d.	0.04	1.01	99.53
16/17-19	Sandstone	Bar sample	13998.93		96.21	1.66	0.36	0.11	0.03	n.d.	0.29	0.11	n.d.	0.05	1.12	99.79
16/17-19	Sandstone	Bar sample	13998.97		96.23	1.72	0.28	0.10	0.02	n.d.	0.33	0.12	n.d.	0.05	1.07	99.74
16/17-19	Sandstone	Bar sample	13999.00		95.48	2.04	0.29	0.11	0.02	n.d.	0.40	0.20	n.d.	0.05	1.34	99.79
16/17-19	Sandstone	Bar sample	13999.03		95.23	1.98	0.26	0.11	0.01	n.d.	0.38	0.14	0.00	0.04	1.89	99.88
16/17-19	Sandstone	Bar sample	13999.07		95.83	1.89	0.24	0.12	0.00	n.d.	0.31	0.08	n.d.	0.03	1.11	99.43
16/17-19	Sandstone	Bar sample	13999.10		94.63	2.60	0.25	0.09	0.01	n.d.	0.33	0.09	n.d.	0.03	1.99	99.87
16/17-19	Sandstone	Bar sample	13999.13		70.77	7.99	0.80	0.24	0.12	n.d.	1.27	1.51	0.00	0.24	17.14	100.00
16/17-19	Sandstone	Bar sample	14047.93		92.73	4.18	0.22	0.19	0.03	0.00	0.88	0.21	0.00	0.01	1.54	99.99
16/17-19	Sandstone	Bar sample	14047.97		94.18	3.05	0.25	0.18	0.01	0.00	0.59	0.13	0.00	0.01	1.36	99.76
16/17-19	Sandstone	Bar sample	14048.00		95.38	2.40	0.25	0.16	0.01	0.00	0.46	0.11	0.00	0.02	1.06	99.85
16/17-19	Sandstone	Bar sample	14048.07		95.96	1.96	0.15	0.17	0.01	0.00	0.40	0.10	0.00	0.01	0.90	99.66

Well	Lithology	Sample type	Sample number		SiO_2 %	Al_2O_3 %	Fe_2O_3 %	MgO %	CaO %	Na_2O %	K_2O %	TiO_2 %	MnO %	P_2O_5 %	LOI %	Total %
			Depth/ft	Depth/m												
16/17-19	Sandstone	Bar sample	14048.13		96.27	1.79	0.13	0.17	0.04	0.00	0.35	0.08	0.00	0.01	0.92	99.77
16/17-19	Sandstone	Bar sample	14048.16		96.05	2.00	0.14	0.16	0.01	0.00	0.31	0.08	0.00	0.01	0.98	99.73
16/17-19	Sandstone	Bar sample	14069.87		96.62	1.32	0.45	0.17	0.06	0.00	0.27	0.07	0.00	0.01	0.87	99.84
16/17-19	Sandstone	Bar sample	14069.93		96.92	1.20	0.45	0.15	-0.01	0.00	0.25	0.06	0.00	0.01	0.90	99.93
16/17-19	Sandstone	Bar sample	14070.00		97.49	0.92	0.37	0.15	-0.02	0.00	0.20	0.04	0.00	0.01	0.71	99.87
16/17-19	Sandstone	Bar sample	14070.07		97.03	1.08	0.36	0.15	0.01	0.00	0.23	0.05	0.00	0.01	0.86	99.79
16/17-19	Sandstone	Bar sample	14070.10		97.28	0.90	0.31	0.14	-0.02	0.00	0.21	0.04	0.00	0.01	0.67	99.54
16/17-19	Sandstone	Bar sample	14070.13		97.22	1.20	0.37	0.15	-0.02	0.00	0.31	0.06	0.00	0.01	0.76	100.07
21/1a-20	Sandstone	Discrete sample	14063.20		91.89	2.57	0.61	0.40	0.87	0.00	0.23	0.22	0.01	0.04	3.17	100.00
21/1a-20	Sandstone	Discrete sample	14065.80		86.89	4.34	1.10	0.56	1.38	n.d.	0.35	0.33	0.01	0.05	4.64	99.55
21/1a-20	Sandstone	Discrete sample	14068.30		91.32	3.47	0.51	0.31	0.62	n.d.	0.25	0.23	0.00	0.04	2.94	99.60
21/1a-20	Sandstone	Discrete sample	14070.10		93.80	2.82	0.31	0.16	0.20	n.d.	0.27	0.21	n.d.	0.04	1.93	99.69
21/1a-20	Sandstone	Discrete sample	14071.00		94.16	2.40	0.30	0.15	0.13	0.00	0.24	0.17	0.00	0.03	2.10	99.69
21/1a-20	Sandstone	Bar sample	14071.87		94.17	2.24	0.30	0.14	0.26	0.00	0.25	0.17	0.00	0.03	2.00	99.56
21/1a-20	Sandstone	Bar sample	14071.90		94.86	2.17	0.25	0.14	0.28	0.00	0.22	0.15	0.00	0.03	1.87	99.98
21/1a-20	Sandstone	Bar sample	14071.93		94.51	2.21	0.25	0.14	0.29	0.00	0.21	0.17	0.00	0.03	1.83	99.64
21/1a-20	Sandstone	Bar sample	14072.00		94.30	2.45	0.26	0.13	0.28	0.00	0.22	0.16	0.00	0.03	2.08	99.92
21/1a-20	Sandstone	Bar sample	14072.07		94.39	2.38	0.24	0.13	0.24	0.00	0.21	0.15	0.00	0.03	1.86	99.63
21/1a-20	Sandstone	Bar sample	14072.13		94.23	2.77	0.20	0.13	0.22	0.00	0.20	0.14	0.00	0.03	1.83	99.74
21/1a-20	Shale	Discrete sample	14073.00		39.28	20.03	8.75	1.22	1.44	0.12	2.65	1.53	0.06	0.60	24.03	99.70
21/1a-20	Shale	Discrete sample	14074.40		49.79	13.57	6.72	1.14	3.71	0.21	1.75	0.87	0.05	0.40	21.63	99.83
21/1a-20	Shale	Discrete sample	14075.60		46.80	12.29	11.51	0.92	3.20	0.19	1.64	0.82	0.04	0.25	21.96	99.62
21/1a-20	Shale	Discrete sample	14085.60		48.42	11.67	8.54	0.89	4.32	0.19	1.68	0.86	0.05	0.24	22.74	99.59

Well	Lithology	Sample type	Sample number		SiO_2 %	Al_2O_3 %	Fe_2O_3 %	MgO %	CaO %	Na_2O %	K_2O %	TiO_2 %	MnO %	P_2O_5 %	LOI %	Total %
			Depth/ft	Depth/m												
21/1a-20	Shale	Bar sample	14044.87		31.16	22.27	10.98	1.35	2.16	0.11	2.75	1.87	0.08	0.99	25.77	99.49
21/1a-20	Shale	Bar sample	14044.90		33.05	23.83	8.91	1.31	1.76	0.11	2.78	1.72	0.07	0.77	25.41	99.73
21/1a-20	Shale	Bar sample	14044.93		33.73	23.90	8.31	1.27	1.60	0.12	2.89	1.71	0.07	0.62	25.13	99.34
21/1a-20	Shale	Bar sample	14045.00		31.17	21.82	12.36	1.20	1.96	0.08	2.39	1.95	0.08	1.27	25.12	99.39
21/1a-20	Shale	Bar sample	14045.07		34.48	24.06	9.08	1.08	1.20	0.12	2.74	1.69	0.06	0.54	24.81	99.87
21/1a-20	Shale	Bar sample	14045.13		33.83	23.85	9.65	1.05	1.16	0.14	2.70	1.67	0.06	0.53	25.02	99.65
211/12a-18	Sandstone	Discrete sample		2935.38	83.23	8.50	1.18	0.21	0.48	0.58	1.99	0.16	0.01	0.05	3.43	99.82
211/12a-18	Sandstone	Discrete sample		2949.57	73.69	6.65	0.75	0.65	7.44	1.02	2.00	0.12	0.03	0.07	7.32	99.74
211/12a-18	Sandstone	Discrete sample		2952.68	65.25	5.79	1.12	0.55	13.03	0.90	1.92	0.17	0.08	0.04	10.92	99.78
211/12a-18	Sandstone	Discrete sample		2955.73	83.66	7.03	0.47	0.29	0.69	1.63	1.74	0.16	0.00	0.05	4.12	99.84
211/12a-18	Sandstone	Discrete sample		2956.00	86.95	6.91	0.49	0.26	0.44	1.49	1.87	0.17	0.01	0.04	1.32	99.96
211/12a-18	Sandstone	Discrete sample		2956.50	83.39	6.34	0.68	0.33	0.61	1.18	1.89	0.23	0.01	0.05	4.91	99.63
211/12a-18	Sandstone	Discrete sample		2957.00	82.35	6.57	0.54	0.30	0.76	1.47	1.85	0.18	0.01	0.05	5.84	99.91
211/12a-18	Sandstone	Discrete sample		2958.00	80.74	6.18	0.61	0.33	1.01	1.26	1.84	0.18	0.01	0.04	7.60	99.82
211/12a-18	Sandstone	Discrete sample		2958.75	82.29	6.67	0.53	0.30	0.94	1.52	1.80	0.18	0.01	0.05	5.33	99.62
211/12a-18	Sandstone	Bar sample		2943.56	85.36	6.69	0.55	0.25	0.43	1.36	1.62	0.22	0.01	0.04	2.94	99.48
211/12a-18	Sandstone	Bar sample		2943.58	83.77	6.66	0.60	0.28	0.64	1.32	1.62	0.22	0.01	0.04	4.57	99.72
211/12a-18	Sandstone	Bar sample		2943.60	85.20	6.72	0.54	0.24	0.39	1.29	1.68	0.19	0.01	0.04	2.97	99.27
211/12a-18	Sandstone	Bar sample		2943.61	84.91	6.77	0.61	0.25	0.71	1.22	1.68	0.20	0.01	0.04	3.20	99.59
211/12a-18	Sandstone	Bar sample		2943.62	86.84	6.51	0.58	0.23	0.34	1.29	1.79	0.21	0.01	0.04	2.57	100.40
211/12a-18	Sandstone	Bar sample		2938.48	82.16	7.94	0.59	0.41	1.20	1.35	1.69	0.14	0.01	0.04	4.05	99.58
211/12a-18	Sandstone	Bar sample		2938.49	83.42	6.72	0.68	0.47	1.29	1.28	1.63	0.12	0.01	0.04	3.93	99.60
211/12a-18	Sandstone	Bar sample		2938.50	83.66	6.16	0.60	0.55	1.47	1.23	1.56	0.12	0.02	0.03	4.27	99.67

Well	Lithology	Sample type	Sample number		SiO_2 %	Al_2O_3 %	Fe_2O_3 %	MgO %	CaO %	Na_2O %	K_2O %	TiO_2 %	MnO %	P_2O_5 %	LOI %	Total %
			Depth/ft	Depth/m												
211/12a-18	Sandstone	Bar sample		2938.52	85.30	5.74	0.53	0.59	1.45	1.20	1.56	0.12	0.02	0.03	3.32	99.86
211/12a-18	Sandstone	Bar sample		2938.54	84.52	5.81	0.55	0.63	1.57	1.24	1.54	0.12	0.02	0.03	3.52	99.55
211/12a-18	Sandstone	Bar sample		2938.56	85.46	5.65	0.42	0.59	1.46	1.35	1.59	0.11	0.01	0.03	3.12	99.79
211/12a-18	Shale	Discrete sample		2947.46	43.60	17.74	7.28	0.90	0.41	0.61	2.19	0.67	0.02	0.18	26.12	99.72
211/12a-18	Shale	Discrete sample		2947.55	43.51	17.33	7.39	0.82	0.39	0.55	2.20	0.61	0.01	0.16	26.50	99.48
211/12a-18	Shale	Discrete sample		2947.66	42.86	16.57	7.76	0.78	0.42	0.63	2.09	0.74	0.03	0.19	27.39	99.44
211/12a-18	Shale	Discrete sample		2947.69	42.54	17.90	10.02	0.87	0.42	0.67	2.25	0.73	0.11	0.22	23.93	99.66
211/12a-18	Shale	Bar sample		2954.66	52.65	13.14	6.47	0.78	0.60	0.56	1.86	0.66	0.03	0.11	22.65	99.52
211/12a-18	Shale	Bar sample		2954.67	49.00	14.36	7.02	0.77	0.51	0.54	1.89	0.63	0.03	0.12	24.78	99.66
211/12a-18	Shale	Bar sample		2954.68	53.69	8.75	6.76	0.49	0.75	0.24	1.12	0.60	0.04	0.38	27.09	99.91
211/12a-18	Shale	Bar sample		2954.70	46.94	15.50	6.72	0.75	0.62	0.56	1.89	0.62	0.02	0.15	25.83	99.59
211/12a-18	Shale	Bar sample		2954.72	43.43	13.65	8.05	0.68	0.49	0.47	1.72	0.53	0.02	0.18	28.99	98.21
211/12a-18	Shale	Bar sample		2954.74	40.41	11.54	14.85	0.59	0.48	0.28	1.38	0.53	0.03	0.21	29.32	99.62
211/12a-18	Shale	Bar sample		2954.76	52.85	12.11	5.17	0.54	0.83	0.35	1.50	0.61	0.03	0.42	24.98	99.40
211/12a-18	Shale	Bar sample		2941.51	50.51	12.66	6.79	0.59	0.41	0.42	1.49	0.63	0.03	0.19	26.34	100.05
211/12a-18	Shale	Bar sample		2941.53	48.35	14.06	6.79	0.64	0.36	0.44	1.68	0.66	0.03	0.17	26.02	99.21
211/12a-18	Shale	Bar sample		2941.55	42.25	15.31	8.99	0.71	0.24	0.54	1.86	0.61	0.02	0.09	28.84	99.47
211/12a-18	Shale	Bar sample		2941.57	45.37	17.59	6.57	0.81	0.24	0.51	2.16	0.69	0.02	0.09	25.71	99.76
211/12a-18	Shale	Bar sample		2941.58	45.97	13.75	7.37	0.67	0.36	0.44	1.68	0.67	0.02	0.16	28.71	99.80
211/12a-18	Shale	Bar sample		2941.59	41.59	15.01	9.05	0.79	0.30	0.58	2.07	0.79	0.02	0.11	29.24	99.55

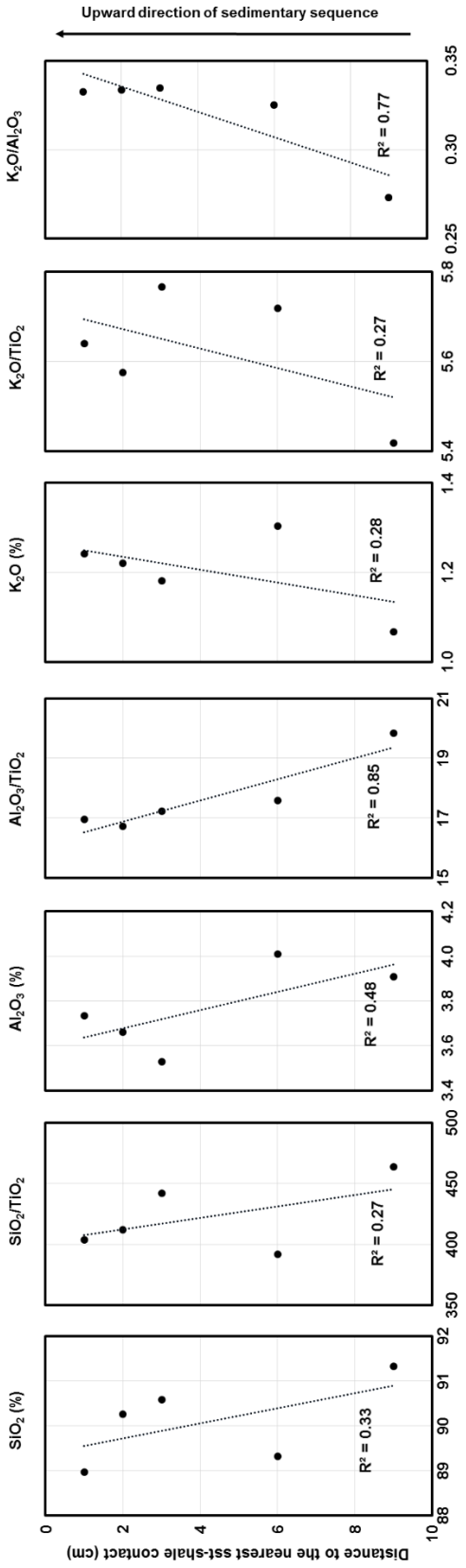

Figure A 6.1 Well 16/8b-5, **SANDSTONE BAR** sample, 14168.80 – 14169.07 ft. The sandstones show decreasing silica and aluminium, and increasing potassium towards shales (Scale: 0-10 cm).

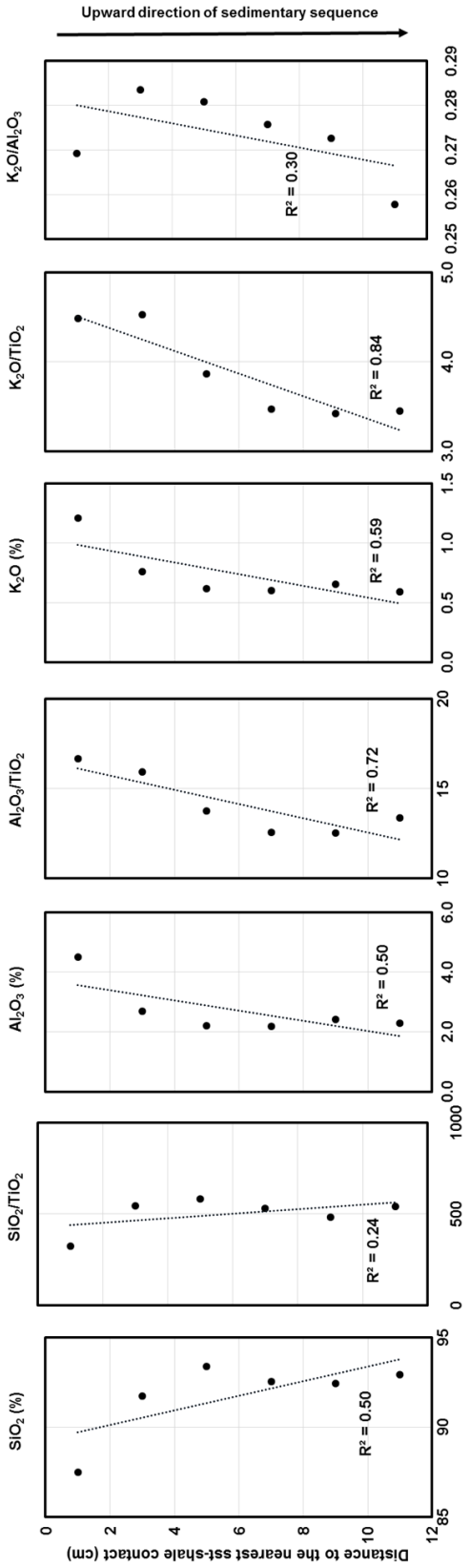

Figure A 6.2 Well 16/8b-5, **SANDSTONE BAR** sample, 14197.80 – 14198.13 ft. The sandstones show decreasing silica, and increasing aluminium and potassium towards shales (Scale: 0-10 cm).

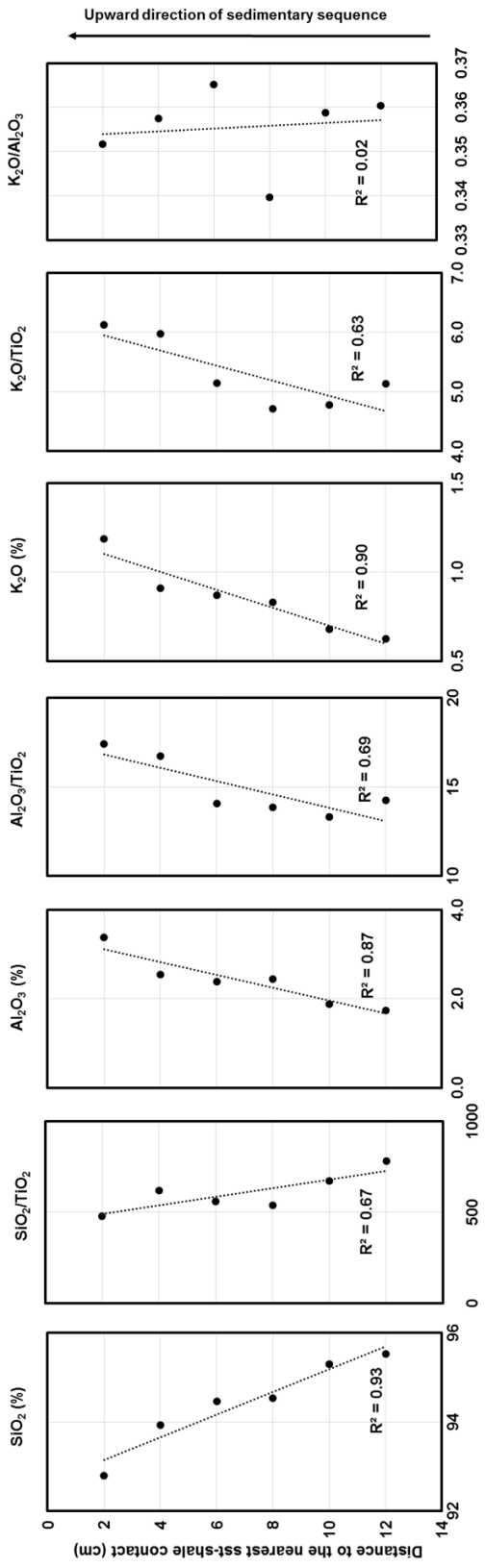

Figure A 6.3 Well 16/8b-A1, **SANDSTONE BAR** sample, 4750.94 – 4751.04 m. Silica decreases, and aluminium and potassium increases when approach the shale.

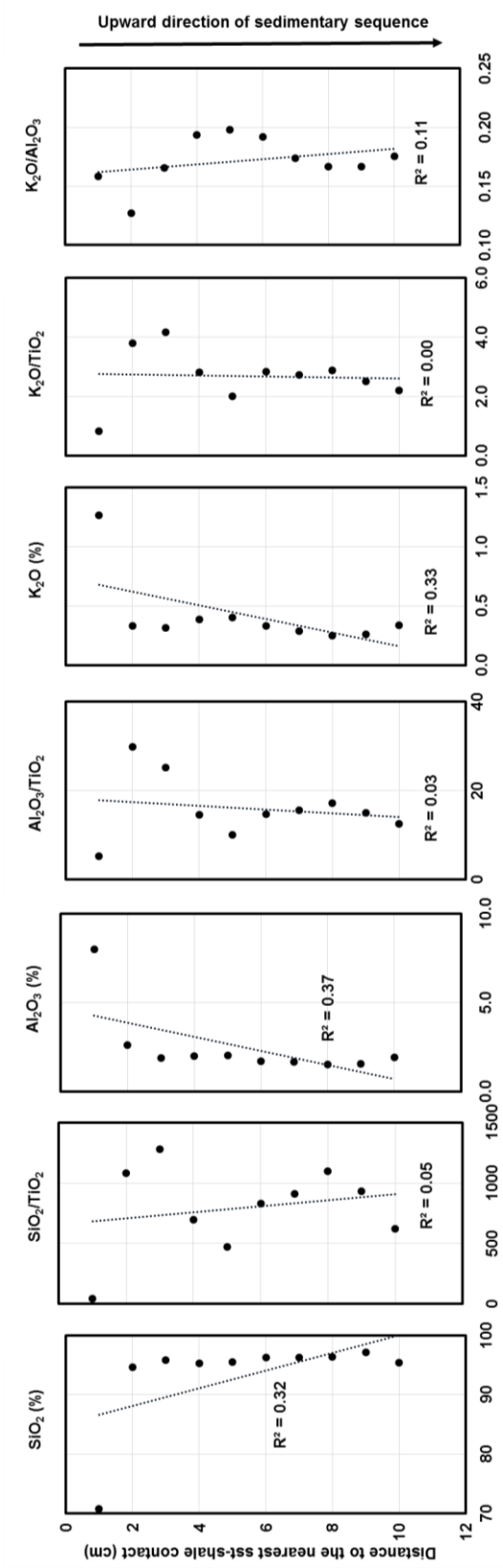

Figure A 6.4 Well 16/17-19, **SANDSTONE BAR** sample, 13998.84 – 13999.13 ft. Silica, aluminium and potassium do not show clear trends with the distance to shales.

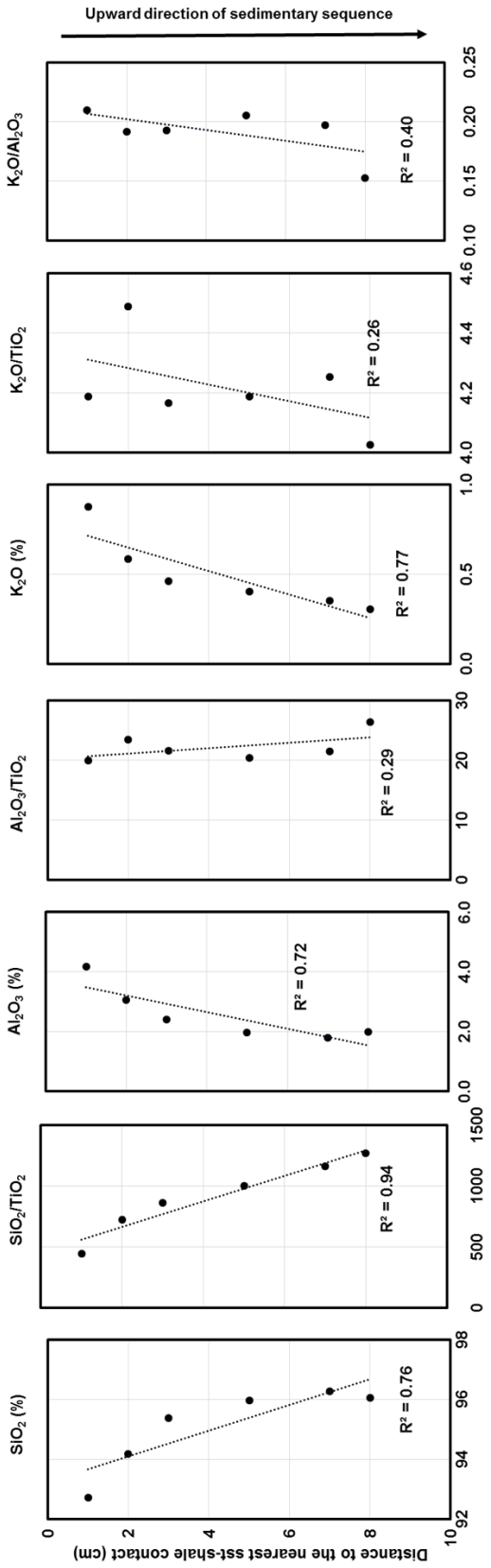

Figure A 6.5 Well 16/17-19, **SANDSTONE BAR** sample, 14047.93 – 14048.16 ft. The sandstones show decreasing silica, and increasing aluminium and potassium towards shales.

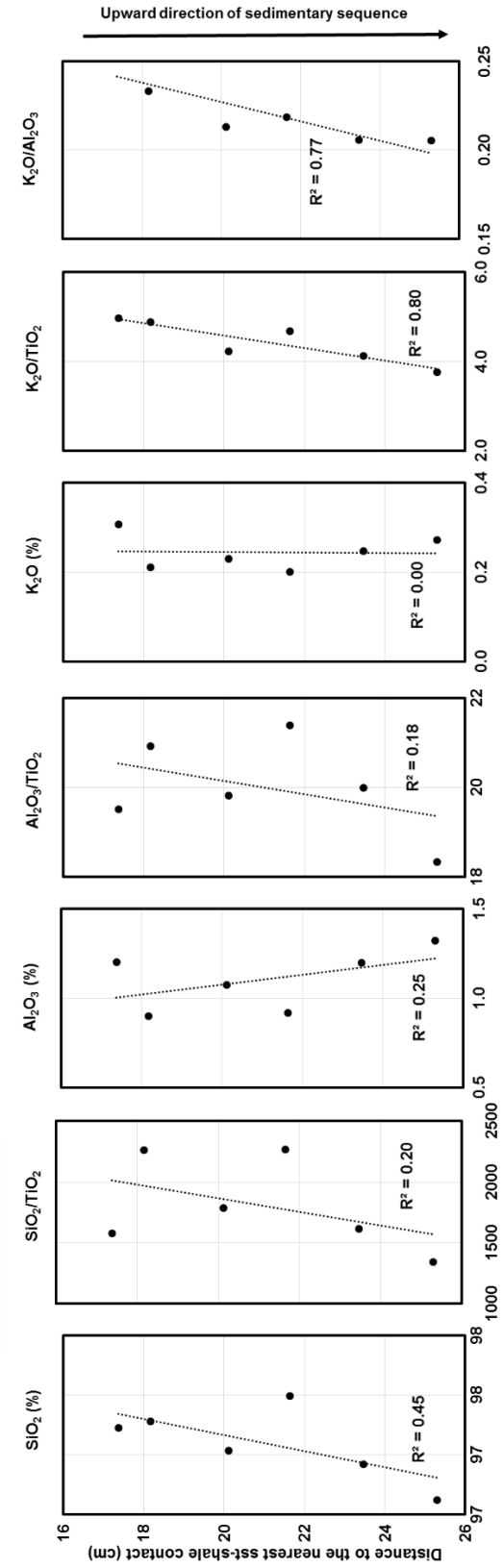

Figure A 6.6 Well 16/17-19, **SANDSTONE BAR** sample, 14069.87 – 14070.13 ft. Silica in the sandstones increase towards shales; aluminium decreases towards shales; potassium does not show a variation trend.

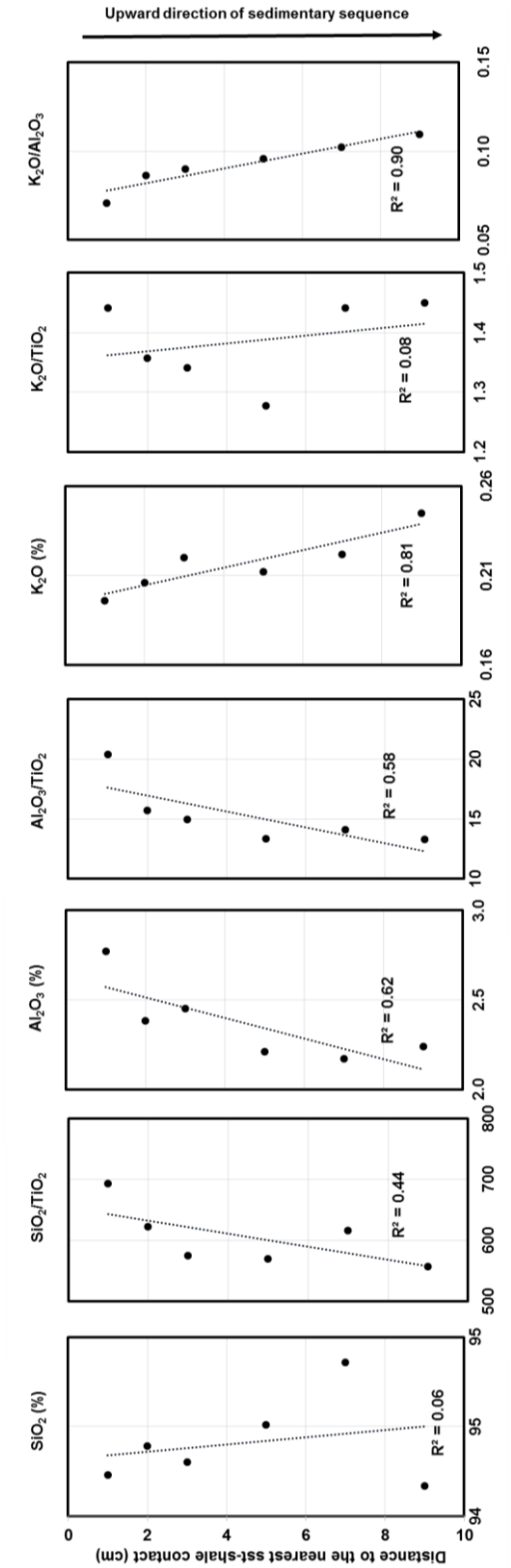

Figure A 6.7 Well 21/1a-20, **SANDSTONE BAR** sample, 14071.87 – 14072.13 ft. Aluminium increases and potassium decreases towards shales; silica does not show a clear trend.

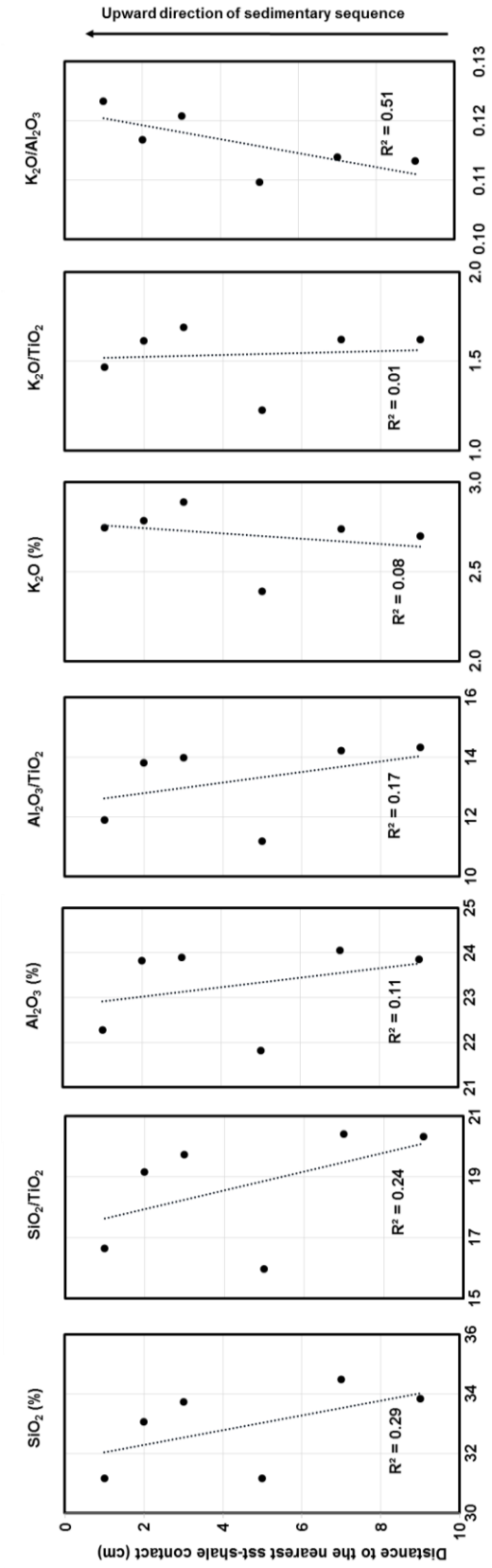

Figure A 6.8 Well 21/1a-20, **SHALE BAR** sample, 14044.87 – 14045.13 ft. Silica and aluminium in the shales show weak, increasing trends towards sandstones; potassium does not show a clear variation trend.

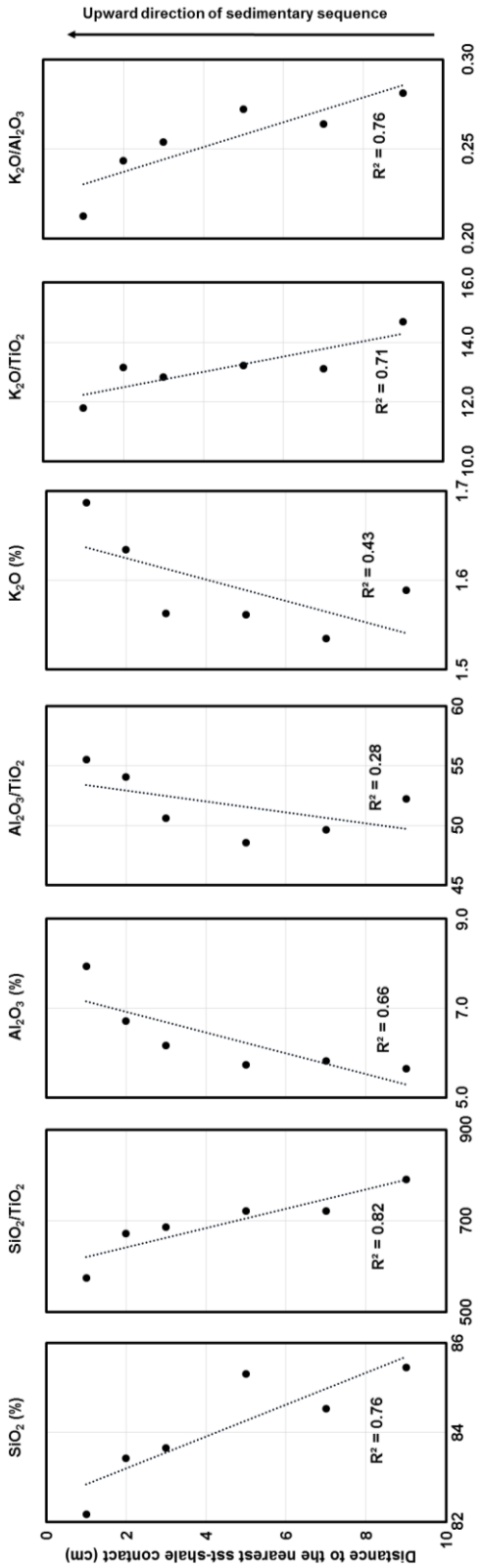

Figure A 6.9 Well 211/12a-18, **SANDSTONE BAR** sample, 2938.48 – 2938.56 m. The sandstones show decreasing silica, and increasing aluminium and potassium towards shales.

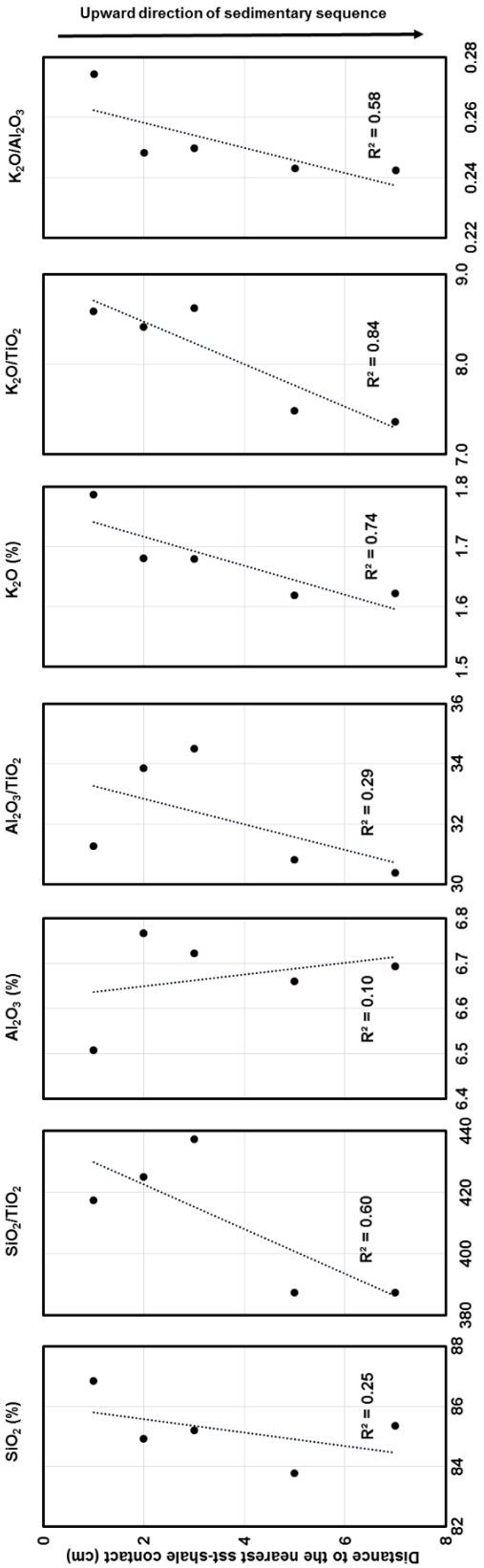

Figure A 6.10 Well 211/12a-18, **SANDSTONE BAR** sample, 2943.56 – 2943.62 m. Potassium in the sandstones increases towards shales, whereas silica and aluminium do not show clear variation trends.

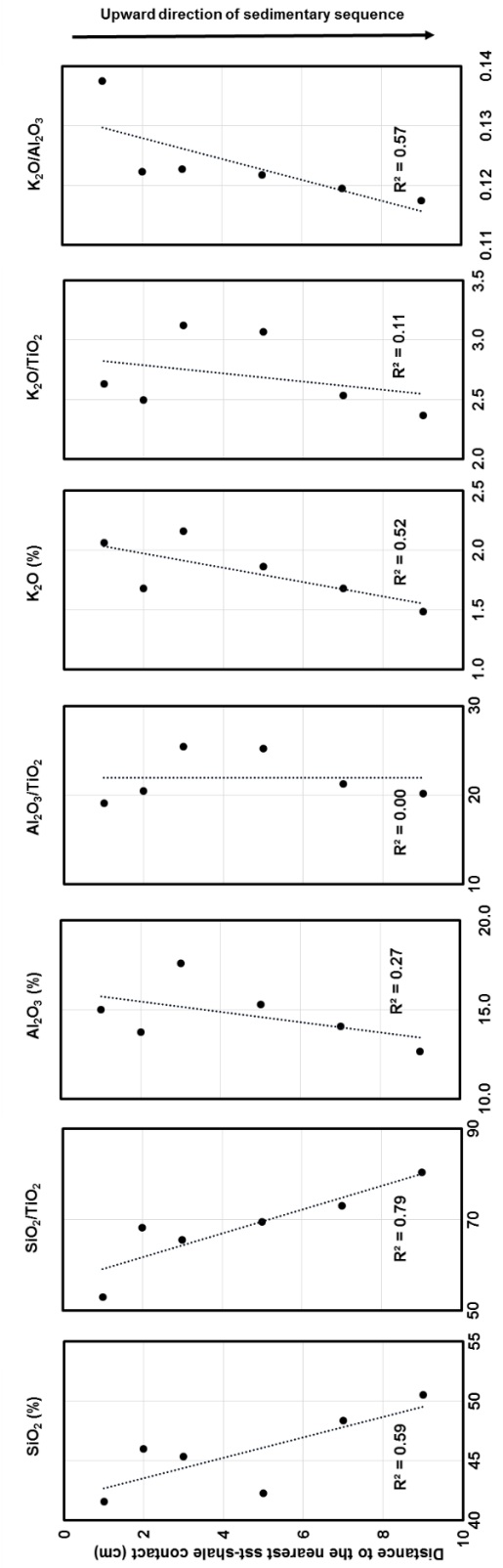

Figure A 6.11 Well 211/12a-18, **SHALE BAR** sample, 2941.51 – 2941.59 m. The shales show decreasing silica, and increasing potassium towards sandstones. Aluminium does not show a clear trend.

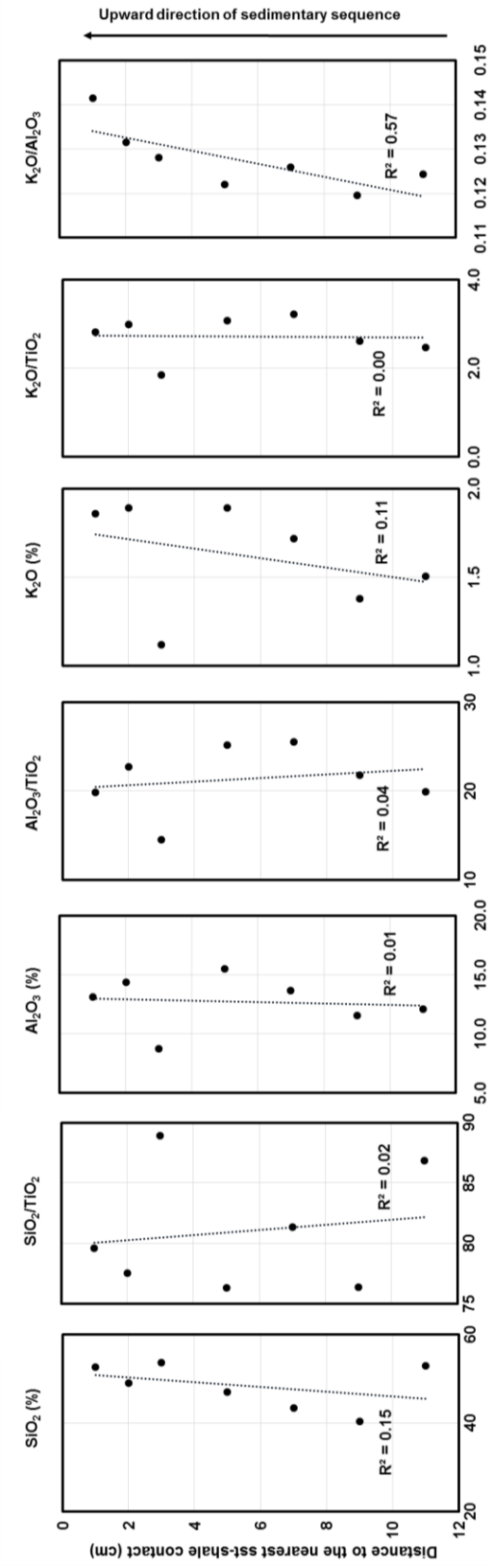

Figure A 6.12 Well 211/12a-18, **SHALE BAR** sample, 2954.66 – 2954.76 m. Silica, aluminium and potassium, all do not show consistents trends towards sandstones.

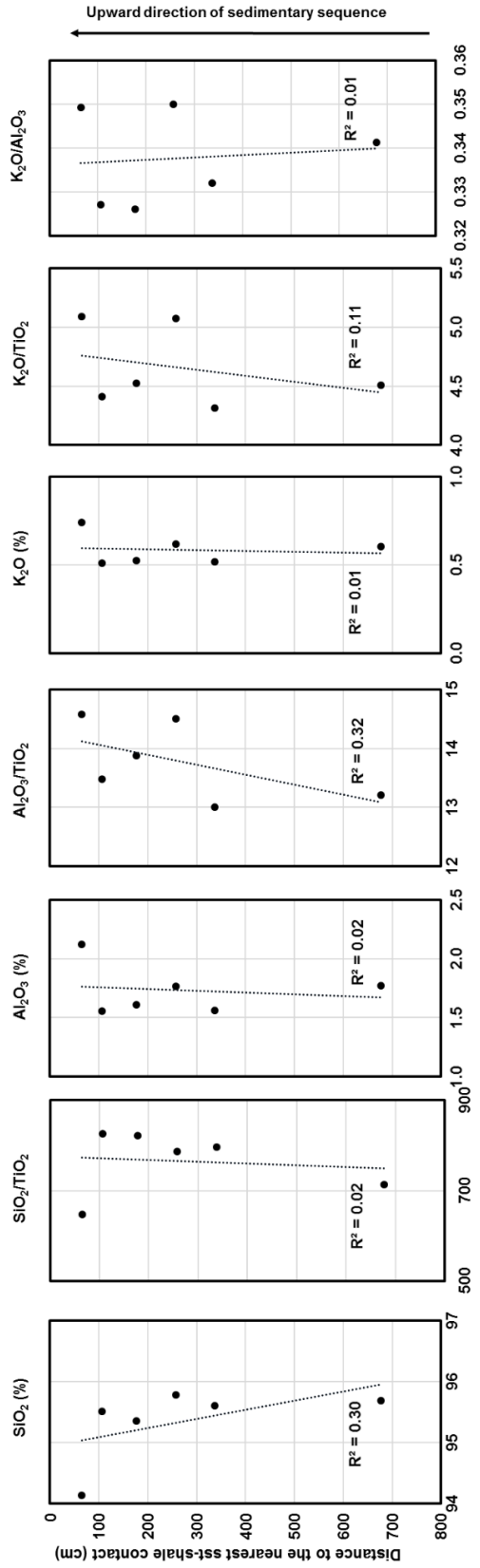

Figure A 6.13 Well 16/8b-A1, **SANDSTONE DISCRETE** samples 4752.29 – 4758.00 m. Silica, aluminium and potassium do not vary as a function of the distances to shales.

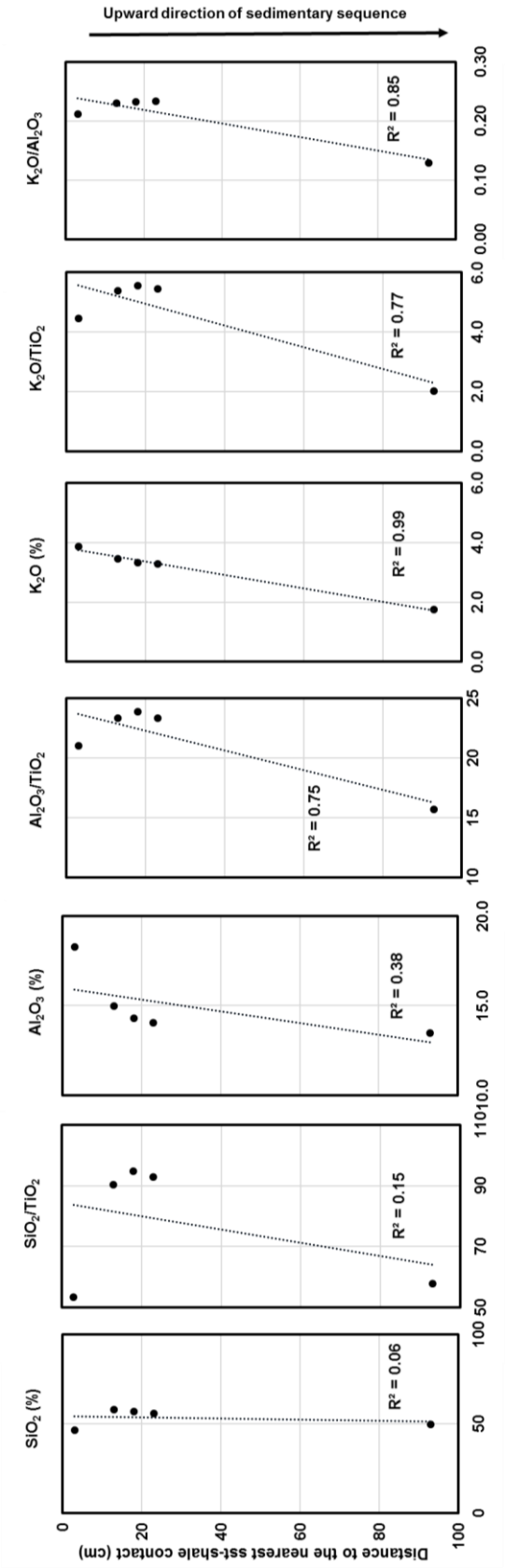

Figure A 6.14 Well 16/8b-A1, **SHALE DISCRETE** samples, 4750.3 – 4751.2 m. Aluminium and potassium appear to increase towards sandstones, while silica remains constant.

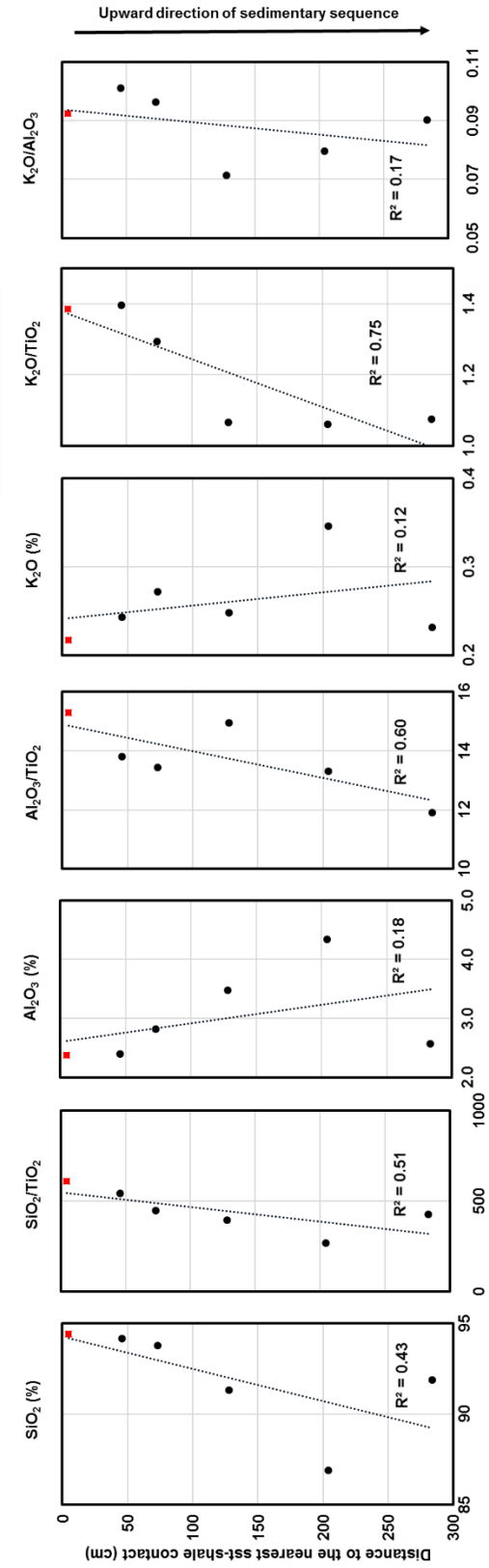

Figure A 6.15 Well 21/1a-20, **SANDSTONE DISCRETE** samples, 14063.20 - 14071.00 ft. The square symbols (red) represent the averages of the bar samples 14071.87 - 14072.13 ft, which is on the boundary of sandstone - shale contact. The sandstones show increasing silica towards shales. Aluminium and potassium do not show clear trends of variation.

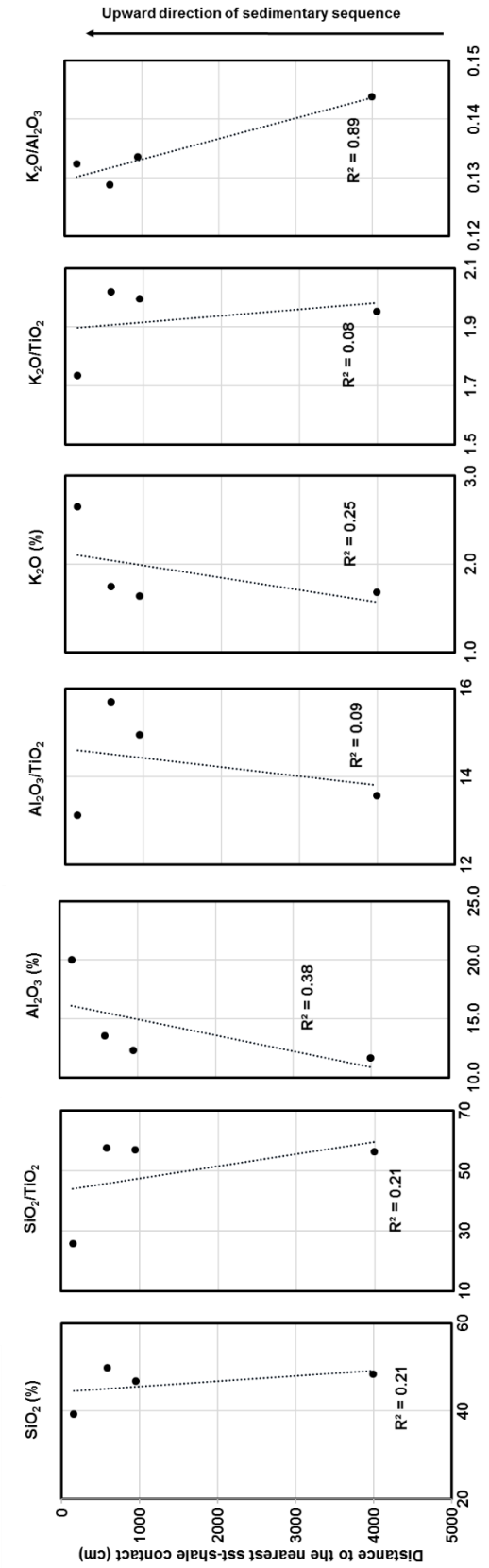

Figure A 6.16 Well 21/1a-20, **SHALE DISCRETE** samples, 14073 – 14085.6 ft. Between these shale samples, silica, aluminium and potassium lack clear trend of variation with the distance.

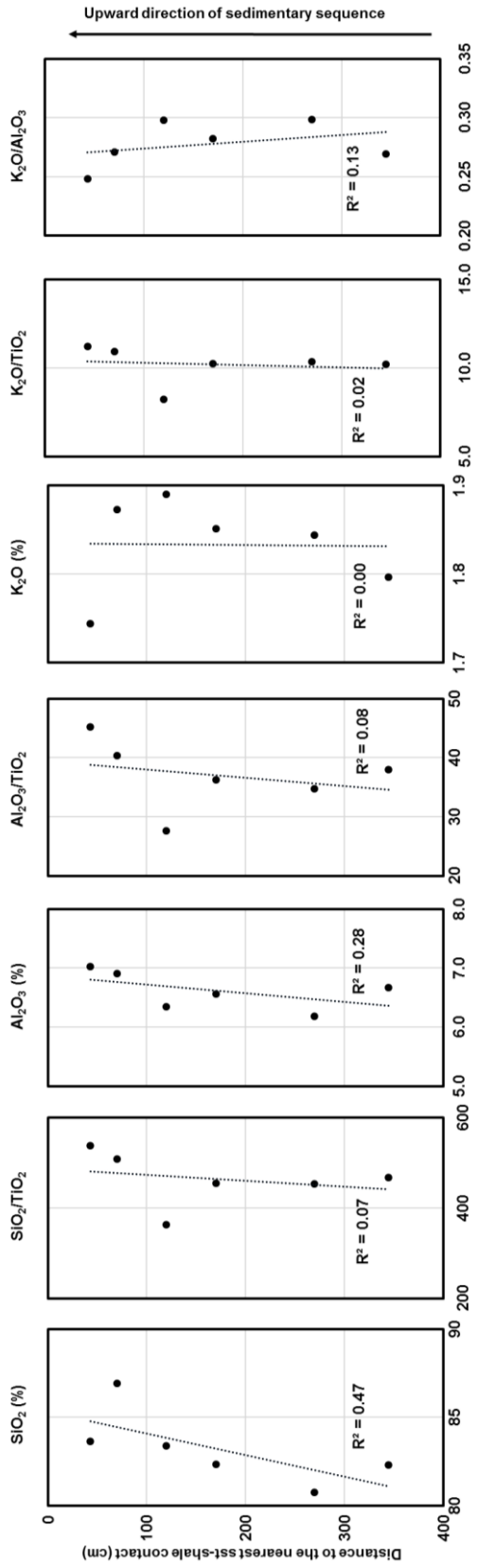

Figure A 6.17 Well 211/12a-18, **SANDSTONE DISCRETE** samples, 2955.73 – 2958.75 m. There are subtle increases in silica and aluminium towards shales; potassium is nearly constant.

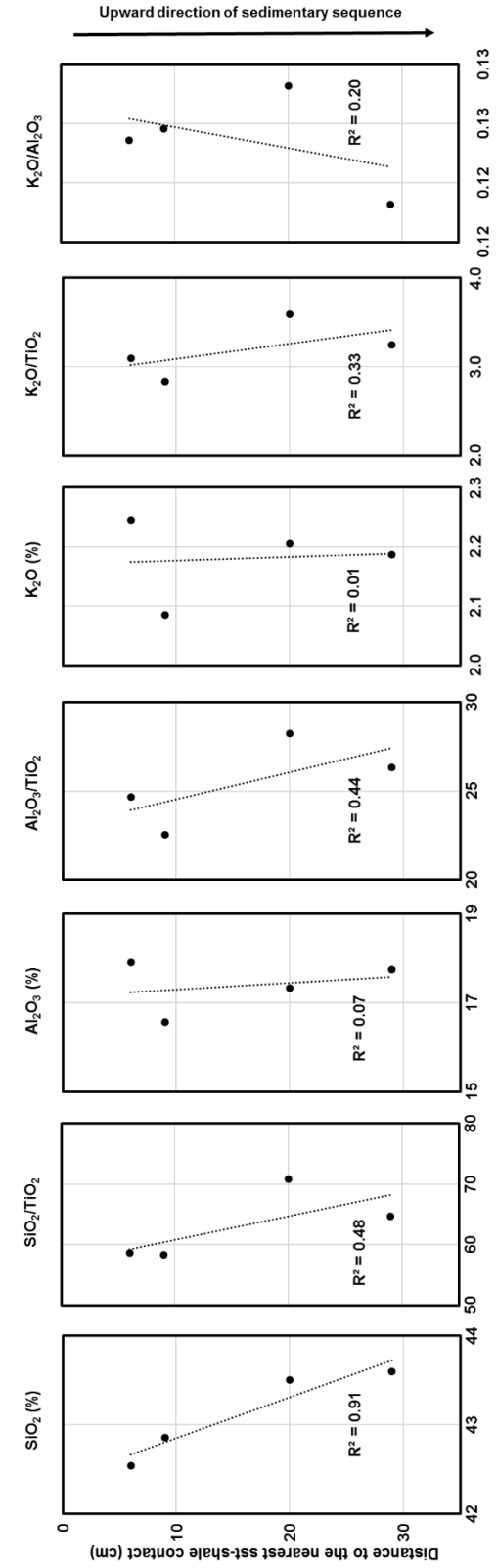

Figure A 6.18 Well 211/12a-18, **SHALE DISCRETE** samples, 2947.46 – 2947.69 m. Silica in the shales increases towards sandstones, whereas there is no clear trend for aluminium and potassium.

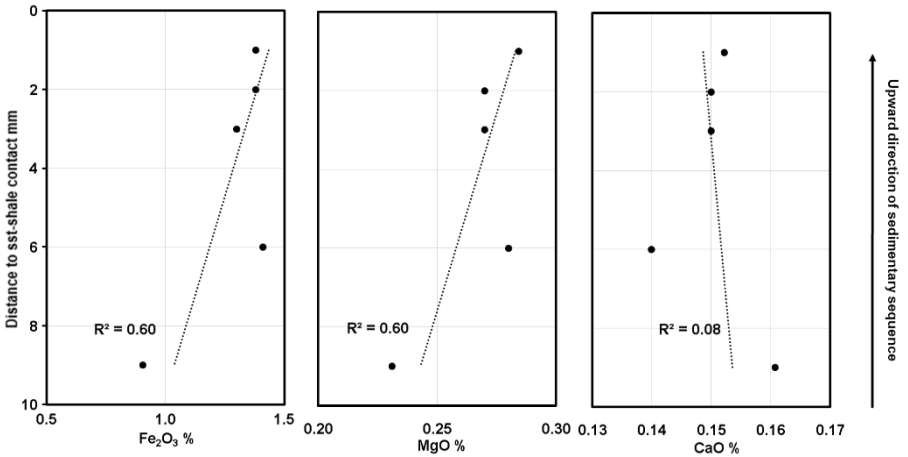

Figure A 6.19 Well 16/8b-5, SANDSTONE BAR sample, 14168.80 – 14169.07 ft, Miller Field.The sandstones show increasing Fe_2O_3 (%) and MgO (%) towards shales. CaO (%) does not show a clear trend.

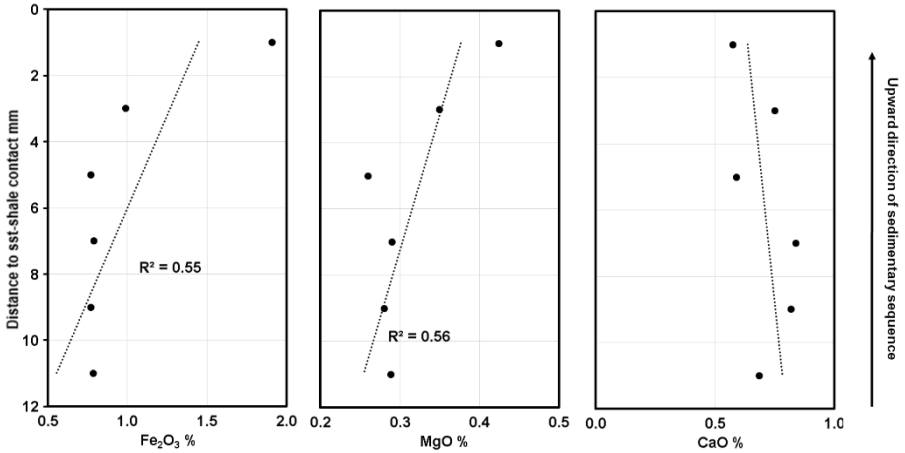

Figure A 6.20 Well 16/8b-5, SANDSTONE BAR sample, 14197.80 – 14198.13 ft, Miller Field. The sandstones show increasing Fe_2O_3 (%) and MgO (%) towards shales. No clear trend for CaO (%).

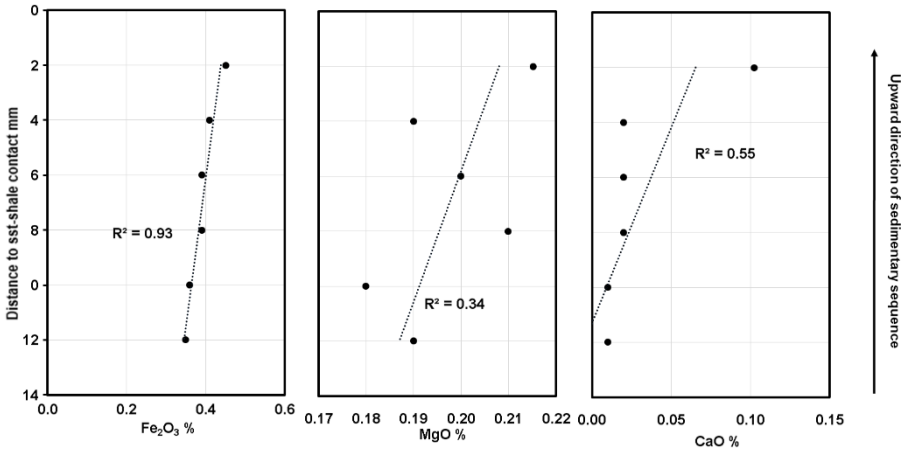

Figure A 6.21 Well 16/8b-A1, SANDSTONE BAR sample, 4750.94 – 4751.04 m, Miller Field. Fe_2O_3 (%) and CaO (%) in the sandstones increase towards shales. MgO (%) does not show a clear trend.

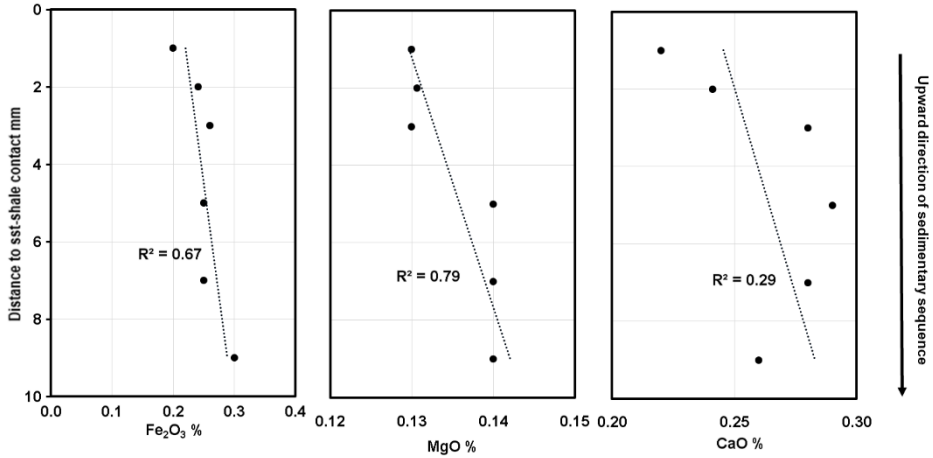

Figure A 6.22 Well 21/1a-20, SANDSTONE BAR sample, 14071.87 – 14072.13 ft. The sandstones show decreasing iron and magnesium towards shales. Calcium does not show a clear trend.

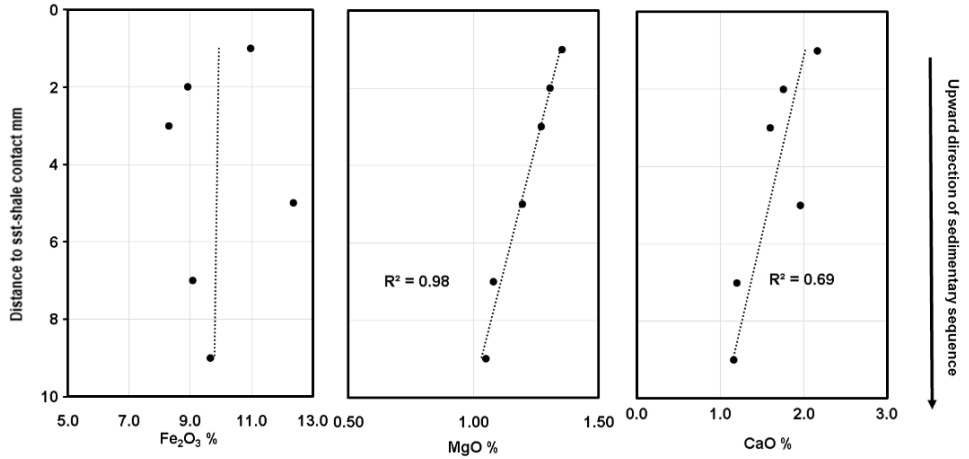

Figure A 6.23 Well 21/1a-20, SHALE BAR sample, 14044.87 – 14045.13 ft. The shales show increasing MgO and CaO towards the sandstones. Fe_2O_3 is constant with the distance.

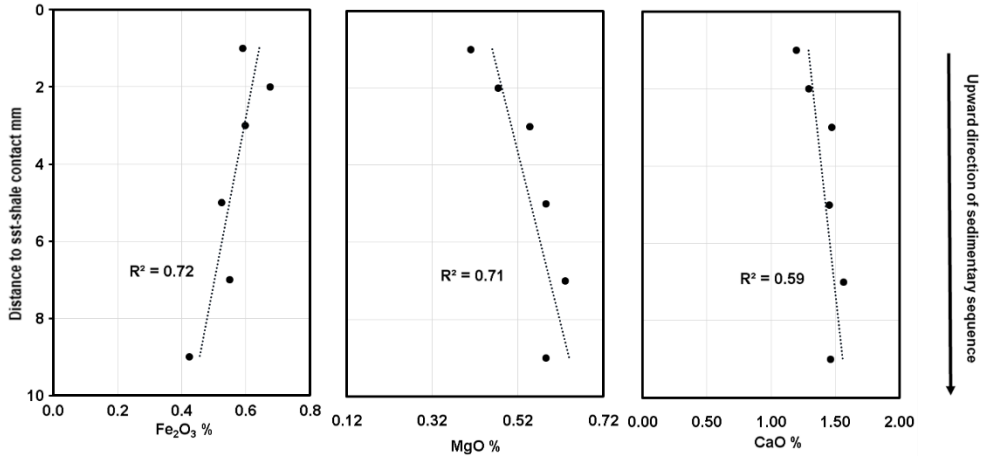

Figure A 6.24 Well 211/12a-18, SANDSTONE BAR sample, 2938.48 – 2938.56 m. Fe_2O_3 and CaO of the sandstones increase, whereas MgO decreases, towards shales.

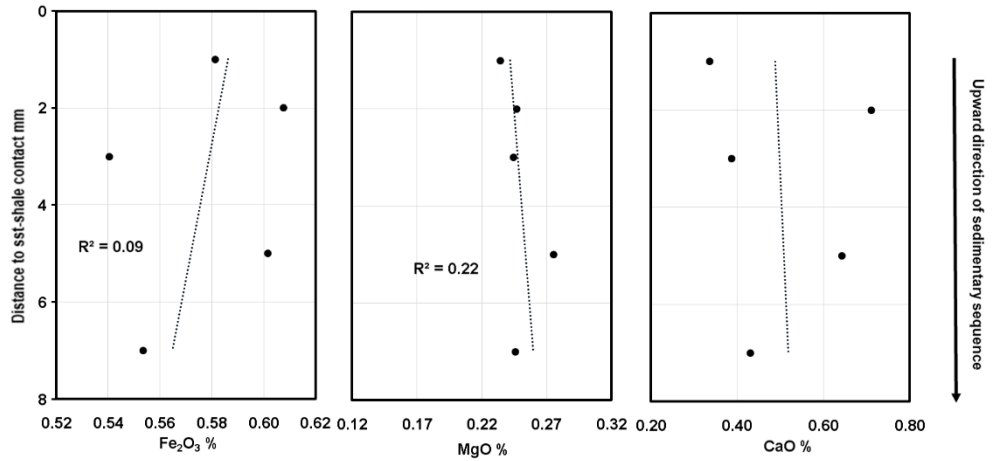

Figure A 6.25 Well 211/12a-18, SANDSTONE BAR sample, 2943.56 – 2943.62 m. The variations of Fe_2O_3, MgO and CaO between the sandstone samples do not show clear trend of variation.

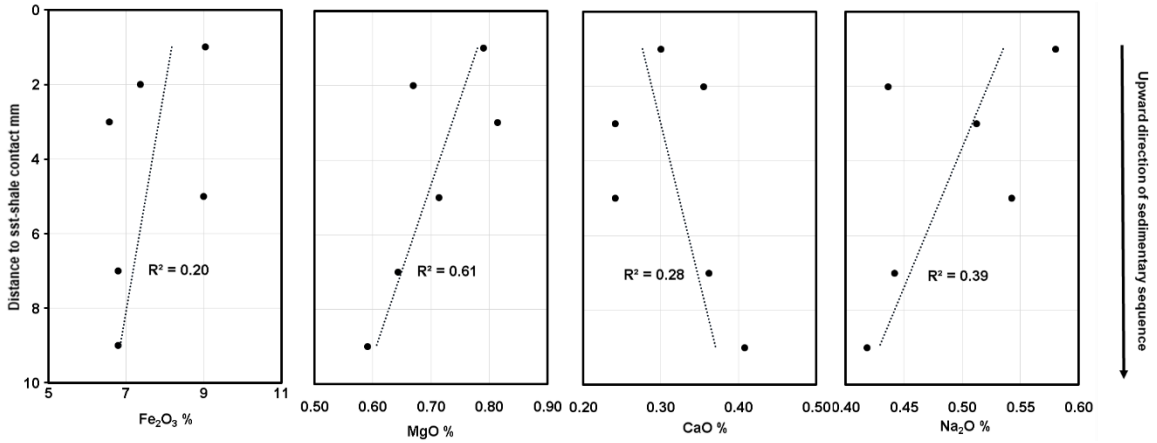

Figure A 6.26 Well 211/12a-18, SHALE BAR sample, 2941.51 – 2941.59 m. MgO in the shales generally increases towards sandstones-shale contact, Fe_2O_3 and CaO do not show clear variation with the distance.

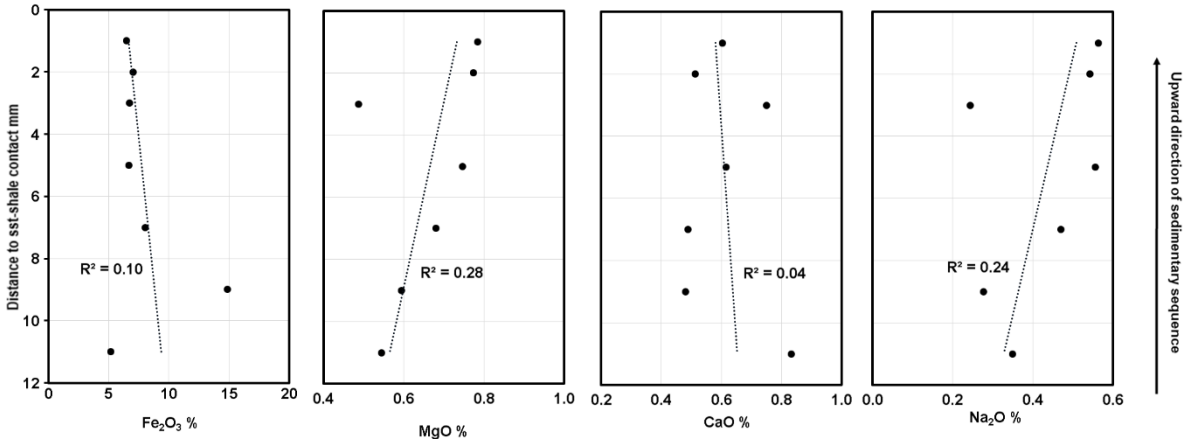

Figure A 6.27 Well 211/12a-18, SHALE BAR sample, 2954.66 – 2954.76 m. MgO in the shales generally increases towards sandstones-shale contact, Fe_2O_3 and CaO do not show clear variation with the distance.

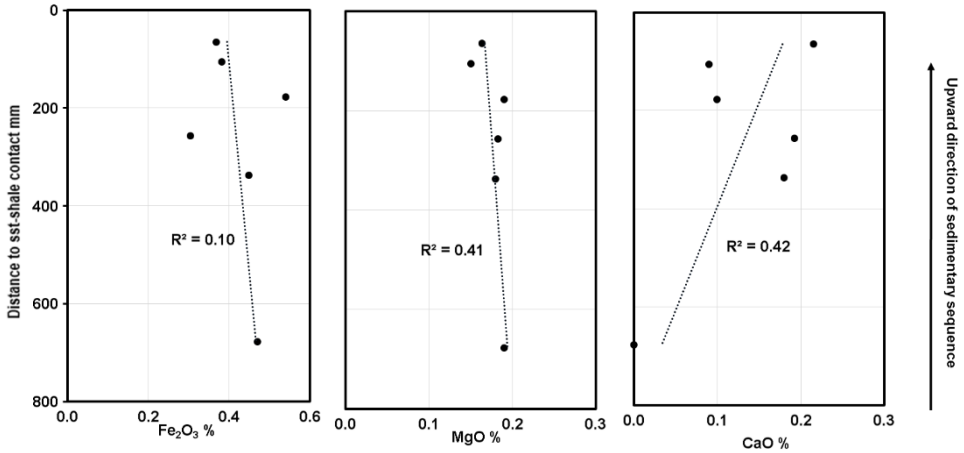

Figure A 6.28 Well 16/8b-A1, SANDSTONE DISCRETE samples 4752.29 – 4758.00 m. The variations of Fe_2O_3, MgO and CaO between the sandstone samples do not show clear trend of variation.

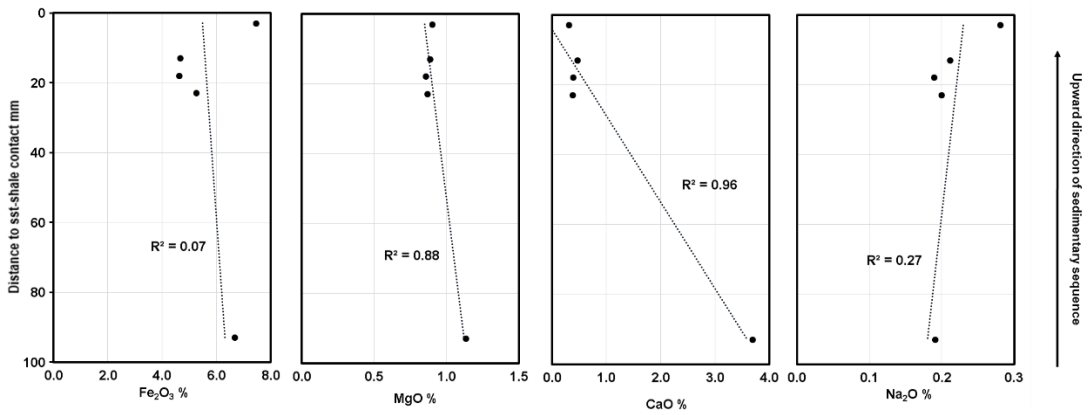

Figure A 6.29 Well 16/8b-A1, SHALE DISCRETE samples, 4750.3 – 4751.2 m. Fe_2O_3 and MgO do not show clear variation with the distance; the shales 10-20 mm distant from the sandstone contain much less CaO than the shales about 90 mm away from the sandstone.

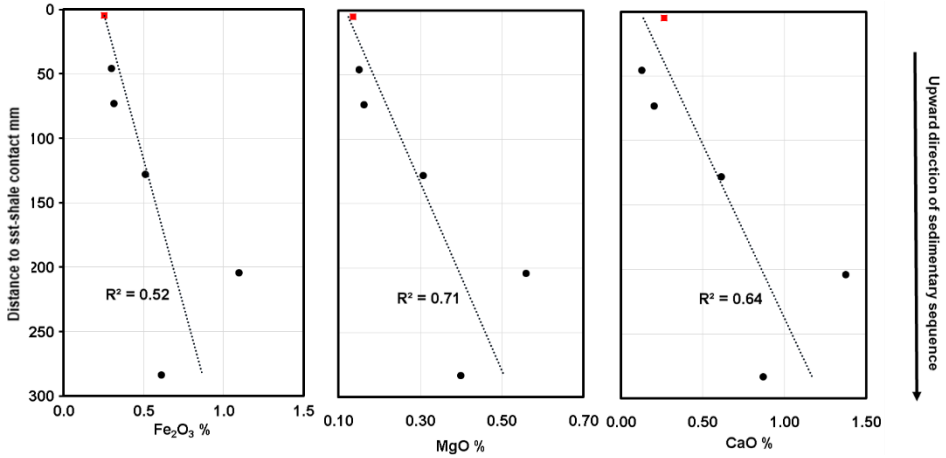

Figure A 6.30 Well 21/1a-20, SANDSTONE DISCRETE samples, 14063.20 - 14071.00 ft. The square symbols (red) represent the averages of the bar samples 14071.87 - 14072.13 ft, which is on the boundary between the sandstone and shale. Fe_2O_3, MgO and CaO in the sandstones generally increase towards the shale.

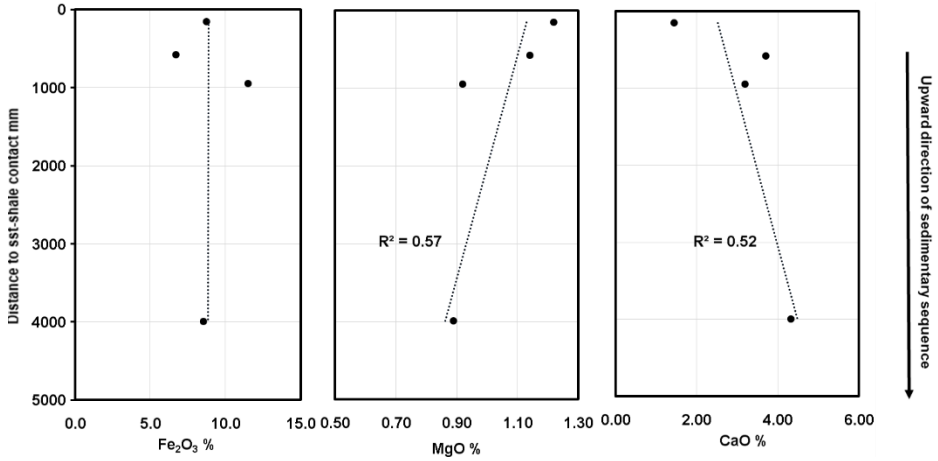

Figure A 6.31 Well 21/1a-20, SHALE DISCRETE samples, 14073 – 14085.6 ft. MgO appears to increase toward sandstones; CaO appears to decreases toward sandstones; Fe_2O_3 is constant with the distance.

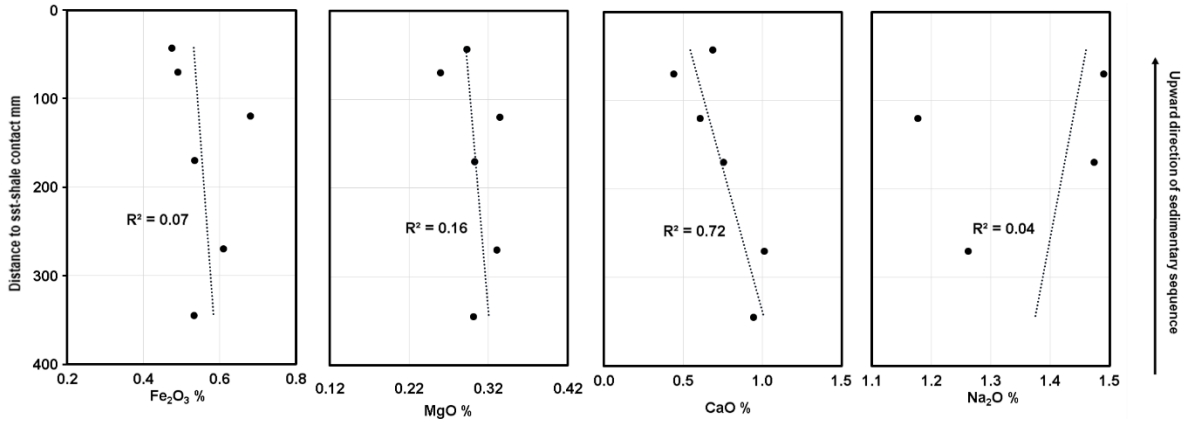

Figure A 6.32 Well 211/12a-18, SANDSTONE DISCRETE samples, 2955.73 – 2958.75 m. CaO decreases towards the shales; whereas Fe_2O_3 and MgO lack clear variation trend with the distance.

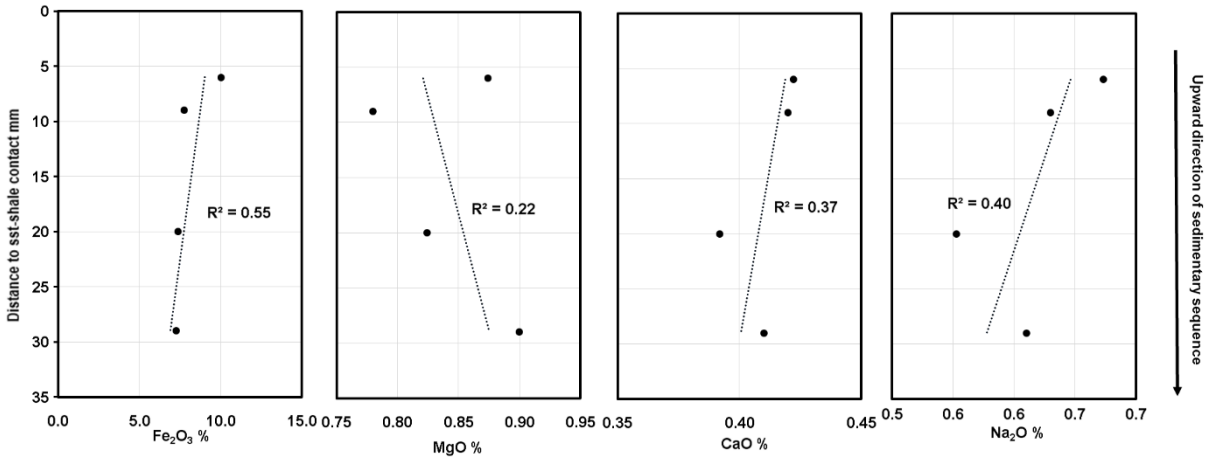

Figure A 6.33 Well 211/12a-18, SHALE DISCRETE samples, 2947.46 – 2947.69 m. Fe_2O_3 and CaO appear to increases towards sandstones; the trend of MgO is unclear.

Chapter 7

Conclusions and Future Work

7.1 Work summary, main conclusions and contribution to current literature

This PhD project covers several aspects of hydrocarbon exploration. It starts with quantifying the geological risks in exploration, to a focus on the reservoir properties of a specific sandstone unit – the Pentland Formation. The project then goes deeper by studying the phenomenon of hydrocarbon emplacement preserving sandstone porosity in the Pentland Sandstone of the Kessog Field. Finally, it included an investigation into the possibility of cross-formational transfer of chemical elements at sandstone-shale contacts. The time length of the whole PhD work, including thesis writing, is 3 years and 7 months.

Prior to this PhD project, there was little literature that had systematically summarised or quantified the geological risk of hydrocarbon exploration. This is most likely due to the lack of a large compiled dataset of unsuccessful wells. The information of

unsuccessful wells was kept separately by individual oil companies, with limited sharing or publishing of the data. The annual publication of North Sea relinquishment reports by the UK Oil and Gas Authority, however, provides an opportunity to fill in the data gap. After browsing through 651 relinquishment reports and collecting the data from 382 dry wells, this PhD study has presented an overview of the geological risks to exploration in the UK offshore area. And more importantly, this study has designed a novel method to manage and analyse the data from unsuccessful wells, and then used this method to estimate the probability of occurrence of each geological risk in exploration as a guide for future exploration activities. Notable conclusions of the study include:

(1) Reservoir absence, low porosity and a lack of a trap were identified to be the most significant risks for new exploration prospects. Among the studied unsuccessful wells, 27 ± 4% of them failed due to thin / absent target reservoirs, 22 ± 4% were because of low-porosity reservoirs, and 23 ± 4% were caused by a lack of trap.

(2) The risk of having a leaky seal was estimated to increase from periclinal traps, through fault-seal traps, to stratigraphic traps. Leaky top seals are not frequently present (7 ± 2% of drilled dry traps), but the risk of encountering leaky fault seals (24 ± 6%) and stratigraphic seals (36 ± 14 %) are significant.

The study of Chapter 2 has also, for the first time, illustrated how the significance of the risk associated with each component of the petroleum system, such as trap and seal, varies in reservoirs of different ages, sedimentary environments and burial histories, providing a practical guide for the future exploration risk assessment in the UK offshore area.

The dataset of geological risk built in this PhD project is not only significant for the oil industry, but also for the power and environmental sectors who are on track to utilise the subsurface space as CO_2 storage sites and achieve clean and sustainable energy production. Chapter 3 demonstrates an example of how to apply the drilling data from hydrocarbon exploration to the exploration for CO_2 storage reservoirs, which to date has limited practical experience to draw on. The key implications of the hydrocarbon drilling experience to the CO_2 storage practice are that:

(1) In general, 49 ± 8% of subsurface structures on the UK Continental Shelf, identified from seismic data, can potentially store CO_2 with long-term safety.

(2) For saline aquifers that have already been penetrated by wells within the potential storage site, most of the geological risks are eliminated or at least reduced; reservoir compartmentalization is the major remaining geological risk.

Predicting the porosity of an undrilled hydrocarbon reservoir is one of the most challenging work in hydrocarbon exploration. As suggested by the statistic risk data in Chapter 2, the chance for a new exploration well to encounter a low-porosity reservoir is 16 ± 5%, which reflects that the porosity prediction results in 16 ± 5% of all exploration cases are erroneous. Porosity prediction ahead of drilling can be improved through gaining a better understanding of the diagenetic process of sediments during burial. Chapter 4 is a study of the diagenesis of the Pentland Formation in the North Sea area, whose aim is to advance the future porosity prediction of this geological unit and other sandstone units with a similar sedimentary background. Techniques of point-counting, X-ray diffraction and X-ray fluorescence were applied to study the petrography, mineralogy and geochemistry of 62 Pentland sandstone samples and 36 shale samples, which are collected from 11 wells penetrated the Pentland Formation. Additionally, there are conventional core analysis data (helium porosity, horizontal air permeability) of 2283 core samples from 21 Pentland wells, pore fluid pressure data of 9 wells and hydrocarbon saturation data of 10 wells for aiding the reservoir quality analysis. Six key conclusions regarding the porosity of the Pentland Formation reservoirs were drawn:

(1) The conventional core analysis data suggest that the median (P50) helium porosity of the Pentland Formation reservoirs at a given depth can be predicted using the formula Φ = 30.9% - 0.0039% x depth (R^2=0.69), and the median (P50) permeability can be predicted by k (mD) = 93179 × $e^{-0.002 \times depth}$ (R^2=0.64).

(2) The Pentland Sandstone can be divided into three facies:

- Facies 1: very fine- to fine-grained clean sandstones (0-15% detrital illite)
- Facies 2: very fine- to fine-grained argillaceous sandstones (>15% detrital illite)
- Facies 3: medium- to coarse-grained sandstones

(3) The porosity of the Facies 2 sandstone, due to its high content of detrital illite, is invariably low below the depth of 2 km, and does not form economic reservoirs. Facies 1 constitute 65% of the Pentland Sandstone and it is the dominant oil-producing facies. The importance of Facies 3 is limited by its small fraction among the sandstones (c. 7%).

(4) Facies 1 sandstone on average contains 10.3% of quartz cement, which is the main porosity-occluding phase for the sandstone. Geochemical data show that the silica content in both the Pentland Sandstone and Shale are independent of burial depth, indicating the silica source for quartz cementation is within the sandstone itself, with no import of silica, and with no evidence for exchange of silica from shale to sand or *vice-versa*. Hence, the majority of silica inferred to be derived from stylolite-pressure dissolution, as there is little K-feldspar dissolution (0.5-1%, point-count data) or kaolin-illite transformation (<1%) in the sandstone to supply silica.

(5) The variation of the geochemical composition of the Pentland Sandstone and Shale also do not show any pattern that is suggestive of mass exchange and chemical interaction between the sandstone and shale during burial. The two lithologies behaved most likely as isochemical bodies in the subsurface, and the diagenesis of the shale did not affect the porosity of the sandstone.

This study has documented the diagenetic process and porosity evolution of the Pentland Sandstone at the burial depth of 2-6 km. The data are important for the exploration and porosity prediction of the Pentland hydrocarbon reservoirs. The established diagenetic pattern and porosity trend of the sandstone are also representative of, and can be widely applied to, feldspathic sandstones deposited in a humid, fluvial-deltaic environment worldwide.

Among the 21 Pentland wells whose helium porosity data are available, the median porosities of 20 wells can be well predicted using the empirical porosity-depth curve. However, there is one exceptional well, in which the porosity is about 10% higher than predicted. Understanding the cause of the high porosity in this well has substantial significance for hydrocarbon exploration as it may reveal the distribution pattern of high-value, high-porosity sandstone in the surface. The exceptional well (30/1c-5) was drilled at the structural crest of the Kessog Field. There are four other wells in the field

located in the reservoir structure flanks (wells 30/1c-3, -4, -6 and -9), but the average porosity of these wells are close to the predicted value by the porosity-depth curve, which is much lower than the porosity of well 30/1c-5. Point-count data, helium porosity data and hydrocarbon saturation data were used in Chapter 5 to investigate the cause of high porosity in well 30/1c-5 and found that:

(1) The grain-size, sorting and mineralogical composition of the high-porosity sandstones are similar to the *'normal-porosity'* Pentland Sandstone, indicating that the high sandstone porosity is not related to the texture and original composition of the sandstones.

(2) Porosity-preserving microquartz and chlorite coats do not occur in the Pentland Formation. Grain-coating illite presents only on the surface of less than 10% of quartz grains, which is insufficient to effectively inhibit quartz cementation. The dominant type of porosity in the high-porosity sandstone is primary porosity, and hence the possibility of mineral dissolution causing the high porosity can be refuted. Also, all the Pentland sandstones in the deep basin (>4km) are overpressured at similar levels, so that the minor differences in the degree of overpressure between wells cannot explain the substantial differences in porosity between the wells.

(3) Hydrocarbon emplacement inhibiting quartz cementation is considered to be the only possible mechanism that can explain the occurrence of high-porosity in the Kessog Field. High-porosity sandstones of the Kessog Field affected by hydrocarbon emplacement exhibit four characteristics:

- they occur at the crest of the reservoir;
- primary porosity is the main type of porosity;
- there is 2 - 5% less quartz cement than the water-saturated sandstones.
- there are 2 - 3% more K-feldspar and 2 - 6% less kaolin than the water-saturated sandstone, indicating that hydrocarbon emplacement also has the inhibited K-feldspar dissolution.

The scale of element mobility has been debated in the diagenesis research community for nearly half a century, and it is still continuing today (Bjørlykke and Jahren, 2012). This research question is related to whether the porosity of sandstone

reservoirs can be enhanced by mass export of solutes, or not (Giles and de Boer, 1990). This is studied in Chapter 4 by plotting the chemical composition of sandstones and shales against depth, to see if there is any coupled variation in the chemistry of these two types of rock as burial depth increases. This method can generally detect a gain or loss of over 2-3% of mass for a geological formation (see *Section 6.5.6*). Chapter 6, however, used a different method to study mass transfer. The rock samples were collected from sandstone-shale contacts, or inside a thick sandstone or shale bed. The intervals between the samples vary from centimetres to metres, which allowed the chemical variation of these samples to be studied over the scale of 0-10 cm and decimetres to metres. The principle of the method is to demonstrate whether there is systematic enrichment or depletion of a chemical element when approaching sandstone-shale contacts, as a clue to infer the potential transfer of any chemical solute between sandstones and shales. This method is sensitive to a transfer of the mass equivalent to the amount of solutes generated by 0.06 – 0.36% of dissolved K-feldspar, which is of one- to two-magnitudes higher than the method of Chapter 4 (see *Section 6.5.6*).

After studying the geochemistry of 18 groups of sandstones and shales from five North Sea oilfields (each group has 4 - 6 samples), no evidence was found that indicates there was a diagenetic mass transfer of SiO_2, Al_2O_3, K_2O, Fe_2O_3, MgO or CaO across sandstone-shale boundaries. As with Chapter 4, the work of Chapter 6 also suggests that sandstone and shale are isochemical during diagenesis. The implication for the oil industry is that when predicting sandstone porosity, the factor of mass transfer does not need to be considered, and neighbouring shales do not affect the chemistry of a sandstone.

7.2 Future work

(1) The unsuccessful wells in Chapter 2 were targeted primarily on sandstone reservoirs. The geological risk data derived from these wells are, therefore, the most applicable to the exploration of sandstone targets. However, the statistical method of the exploration risk can be universally applied to reservoirs of all types of rock. In future, similar studies focused on the other important types of hydrocarbon reservoirs, such as carbonate reservoirs and shale gas reservoirs, will provide useful practical guides for the risk assessment of these hydrocarbon reservoirs. It will also be interesting to see how the risks of these reservoirs differ from sandstone reservoirs, as they generally have different reservoir properties and trap styles.

(2) The risk data were collected from the exploration wells in the North Sea area. It is expected that exploration risks will differ greatly in sedimentary basins of different tectonic environments, with different stratigraphic frameworks and petroleum systems. Similar studies can be carried out in the other petroleum basins worldwide.

(3) As the UK Oil and Gas Authority continues to publish new relinquishment reports annually, it is important and worthwhile to update the risk database of exploration wells at regular intervals. With the addition of more data, statistical uncertainty will decrease. Therefore, the predicted probability of occurrence for a geological risk, based on the risk database, will become more accurate and instructive as the database contains more unsuccessful wells year after year.

(4) The type of hydrocarbon in the Kessog Field is gas condensate. It is unclear whether gas condensate is more effective than liquid hydrocarbons in inhibiting quartz cementation. Experimental studies could be designed to measure the wettability of quartz grains to gas condensate and liquid oil, as this controls how effectively the non-aqueous fluid covers grain surfaces and hence disrupts pore-scale transport pathways within the reservoir.

(5) Cathodoluminescence imaging can reveal any zonation in quartz cement. With an ion microprobe it is possible to measure the variation of oxygen isotopes (^{16}O and ^{18}O) across the zones from inside to the edge of quartz cement (Kelly et al., 2007). A

combination of these two techniques could be applied to reconstruct and compare the quartz cementation history in the oil-leg and water-leg sandstones of the Kessog Field.

(6) The controversy about the effect of hydrocarbon emplacement inhibiting quartz cementation can never be settled by a single one study. It has been reported in one relinquishment report that a gas-filled Triassic Bunter Sandstone was more porous than the water-bearing counterpart, and calcareous and evaporitic cement were observed to be inhibited in the reservoir, presumably by gas charge (Relinquishment Report P1332). This could be another good case for studying the phenomenon of hydrocarbon preserving reservoir porosity. Details for the oilfield and wells can be found in the Relinquishment Report P1332 that is downloadable from the Oil and Gas Authority website.

(7) The same research method of Chapter 6 for studying mass transfer could be applied to the Paleogene sandstones and shales in the Gulf of Mexico, United States, where a number of studies have claimed that potassium was transferred from the sandstones into the shales during diagenesis (Awwiller, 1993; Day-Stirrat et al., 2010; Land, 1997; Milliken et al., 1994; Wilkinson et al., 2003).

References

Aase, N.E., Bjørkum, P.A., Nadeau, P.H., 1996. The effect of grain-coating microquartz on preservation of reservoir porosity. AAPG Bull. Assoc. Pet. Geol. 80, 1654–1673.

Aase, N.E., Walderhaug, O., 2005. The effect of hydrocarbons on quartz cementation: diagenesis in the Upper Jurassic sandstones of the Miller Field, North Sea, revisited. Pet. Geosci. 11, 215–223. doi:10.1144/1354-079304-648

Admasu, F., Tönnies, K., 2005. An Approach towards Automated Fault Interpretations in Seismic Data. SimVis.

Ahmadi, Z.M., Sawyers, M., Kenyon-Roberts, S., Stanworth, C.W., Kugler, K.A., Kristensen, J., Fugelli, E.M.G., 2003. Palaeocene, in: Evans, D., Graham, C., Armour, A., Bathurst, P. (Eds.), The Millennium Atlas: Petroleum Geology of the Central and Northern North Sea. The Geological Society of London, London, pp. 235–259.

Ahsan, A., Karlsen, D.A., Patience, R.L., 1997. Petroleum biodegradation in the Tertiary reservoirs of the North Sea. Mar. Pet. Geol. 14, 55–64. doi:10.1016/S0264-8172(96)00046-3

Ajdukiewicz, J., Lander, R., 2010. Sandstone reservoir quality prediction: The state of the art. Am. Assoc. Pet. Geol. Bull.

Ajdukiewicz, J.M., Larese, R.E., 2012. How clay grain coats inhibit quartz cement and preserve porosity in deeply buried sandstones: Observations and experiments. Am. Assoc. Pet. Geol. Bull. 96, 2091–2119. doi:10.1306/02211211075

Al-Hajeri, M.M., Al Saeed, M., Derks, J., Fuchs, T., Hantschel, T., Kauerauf, A., Neumaier, M., Schenk, O., Swientek, O., Tessen, N., others, 2009. Basin and petroleum system modeling. Oilf. Rev. 21, 14–29.

Avseth, P., Dræge, A., van Wijngaarden, A.-J., Johansen, T.A., Jørstad, A., 2008. Shale rock physics and implications for AVO analysis: A North Sea demonstration. Lead. Edge 27, 788. doi:10.1190/1.2944166

Awwiller, D.N., 1993. Illite/smectite formation and potassium mass transfer during burial diagenesis of mudrocks: A study from the Texas Gulf Coast Paleocene-Eocene. Am. Assoc. Pet. Geol. Bull. 63, 501–512. doi:10.1306/D4267B3B-2B26-11D7-8648000102C1865D

Bachu, S., Bonijoly, D., Bradshaw, J., Burruss, R., Holloway, S., Christensen, N.P., Mathiassen, O.M., 2007. CO2 storage capacity estimation: Methodology and gaps. Int. J. Greenh. Gas Control 1, 430–443. doi:10.1016/S1750-5836(07)00086-2

Bailey, J.B., Arbin, P., Daffinoti, O., Gibson, P., Ritchie, J.S., 1993. Permo-Carboniferous plays of the Silver Pit Basin, in: Petroleum Geology of Northwest Europe: Proceedings of the 4th Conference. pp. 707–715. doi:10.1144/0040707

Bailey, N.J.L., Walko, P., Sauer, M.J., 1987. Geochemistry and source rock potential of the west of Shetlands. Pet. Geol. North West Eur. Graham Trotman, London 711–721.

Baldwin, B., Butler, C.O., 1985. Compaction Curves. Am. Assoc. Pet. Geol. Bull. 69, 622–626.

Balson, P., Butcher, A., Holmes, R., Johnson, H., Lewis, M., Musson, R., Henni, D.P., Jones, S., Leppage, P., Tuggey, G., 2002. North Sea Geology, Technical report produced for Strategic Environmental Assessment. doi:10.1002/hast.316

Barnard, P.C., Bastow, M. a., 1991. Hydrocarbon generation, migration, alteration, entrapment and mixing in the Central and Northern North Sea. Geol. Soc. London, Spec. Publ. 59, 167–190. doi:10.1144/GSL.SP.1991.059.01.12

Barnard, P.C., Cooper.B.C, 1981. Oils and source rocks of the North Sea area. Pet. Geol. Cont. shelf North West Eur. 169.

Beard, D.C., Weyl, P.K., 1973. Influence of texture on porosity of unconsolidated sands. Am. Assoc. Pet. Geol. Bull. 57, 349–369. doi:10.1306/819A4272-16C5-11D7-8645000102C1865D

Berger, G., Velde, B., Aigouy, T., 1999. Potassium sources and illitization in Texas Gulf Coast shale diagenesis. J. Sediment. Res. 69, 151–157. doi:10.2110/jsr.69.151

Besly, B.., 1998. Carboniferous, in: Glennie, K.W. (Ed.), Petroleum Geology of the North

Sea: Basic Concepts and Recent Advances, Fourth Edition. Blackwell Science Ltd, pp. 104–136.
Bjørkum, P.A., 1996. How important is pressure in causing dissolution of quartz in sandstones? J. Sediment. Res. 66, 147–154. doi:10.1306/D42682DE-2B26-11D7-8648000102C1865D
Bjørkum, P.A., Mjøs, R., Walderhaug, O., Hurst, A., 1990. The role of the late Cimmerian unconformity for the distribution of kaolinite in the Gullfaks Field, northern North Sea. Sedimentology 37, 395–406.
Bjørlykke, K., 2014. Relationships between depositional environments, burial history and rock properties. Some principal aspects of diagenetic process in sedimentary basins. Sediment. Geol. 301, 1–14. doi:10.1016/j.sedgeo.2013.12.002
Bjørlykke, K., 2011. Open-system chemical behaviour of Wilcox Group mudstones. How is large scale mass transfer at great burial depth in sedimentary basins possible? A discussion. Mar. Pet. Geol. 28, 1381–1382. doi:10.1016/j.marpetgeo.2011.01.009
Bjørlykke, K., 2010. Source Rocks and Petroleum Geochemistry, in: Petroleum Geoscience. Springer Berlin Heidelberg, Berlin, Heidelberg, pp. 339–348. doi:10.1007/978-3-642-34132-8_14
Bjørlykke, K., 1994. Fluid-flow processes and diagenesis in sedimentary basins. Geol. Soc. London, Spec. Publ. 78, 127–140. doi:10.1144/GSL.SP.1994.078.01.11
Bjørlykke, K., 1993. Fluid flow in sedimentary basins. Sediment. Geol. 86, 137–158. doi:10.1016/0037-0738(93)90137-T
Bjørlykke, K., Aagaard, P., 1992. Clay Minerals in North Sea Sandstones.
Bjørlykke, K., Egeberg, P.K., 1993. Quartz cementation in sedimentary basins. Am. Assoc. Pet. Geol. Bull. doi:10.1306/BDFF8EE8-1718-11D7-8645000102C1865D
Bjørlykke, K., Jahren, J., 2015. Sandstones and Sandstone Reservoirs, in: Petroleum Geoscience: From Sedimentary Environments to Rock Physics, Second Edition. pp. 119–149. doi:10.1007/978-3-642-34132-8
Bjørlykke, K., Jahren, J., 2012. Open or closed geochemical systems during diagenesis in sedimentary basins: Constraints on mass transfer during diagenesis and the prediction of porosity in sandstone and carbonate reservoirs. Am. Assoc. Pet. Geol. Bull. 96, 2193–2214.
Bjørlykke, K., Jahren, J., 2010. Sandstones and Sandstone Reservoirs, in: Bjørlykke, K. (Ed.), Petroleum Geoscience. pp. 113–140. doi:10.1007/978-3-642-02332-3
Bjørlykke, K., Nedkvitne, T., Ramm, M., Saigal, G.C., 1992. Diagenetic processes in the Brent Group (Middle Jurassic) reservoirs of the North Sea: an overview. Geol. Soc. London, Spec. Publ. 61, 263–287. doi:10.1144/GSL.SP.1992.061.01.15
Blatt, H., 1979. Diagenetic processes in sandstones. 26, 141–157.
Bloch, S., Lander, R.H., Bonnell, L., 2002. Anomalously high porosity and permeability in deeply buried sandstone reservoirs: Origin and predictability. Am. Assoc. Pet. Geol. Bull. 86, 301–328.
Bouma, A., 1962. Sedimentology of some Flysch deposits a graphic approach to facies interpretation.
BP, 2017. BP Energy Outlook Energy 2017. BP Stat. Rev. World Energy 52. doi:10.1017/CBO9781107415324.004
Brennand, T.P., Van Hoorn, B., James, K.H., Glennie, K.W., 1998. Historical review of north sea exploration, in: Petroleum Geology of the North Sea: Basic Concepts and Recent Advances: Fourth Edition. pp. 1–41. doi:10.1002/9781444313413.ch1
Brewster, J., 1991. The Frigg Field, Block 10/1 UK North Sea and 25/1, Norwegian North Sea. Geol. Soc. London, Mem. 14, 117–126. doi:10.1144/GSL.MEM.1991.014.01.15
Brindley, G.W., 1980. Quantitative X-ray mineral analysis of clays. Cryst. Struct. clay Miner. their X-ray Identif. 5, 411–438.
Brooks, J., Cornford, C., Archer, R., 1987. The role of hydrocarbon source rocks in petroleum exploration. Geol. Soc. London, Spec. Publ. 26, 17–46. doi:10.1144/GSL.SP.1987.026.01.02
Brown, G., Platt, N., McGrandle, A., 1994. The geophysical expression of Tertiary dykes in the southern North Sea. First Break.
Brzozowska, J., Eriksen, S., Holm, L., Olsen, S., 2003. Exploration history, in: Evans, D., Graham, C., Armour, A., Bathurst, P. (Eds.), The Millennium Atlas: Petroleum

Geology of the Central and Northern North Sea. The Geological Society of London, London, pp. 341–343.
Burnham, A.K., Sweeney, J.J., 1991. Modeling the Maturation and Migration of Petroleum: Chapter 5: PETROLEUM GENERATION AND MIGRATION 37, 55–63.
Busch, A., Amann-Hildenbrand, A., Bertier, P., Waschbuesch, M., Krooss, B.M., 2010. The Significance of Caprock Sealing Integrity for CO2 Storage, in: SPE International Conference on CO2 Capture, Storage, and Utilization. Society of Petroleum Engineers. doi:10.2118/139588-MS
Bush, J., Johnston, D., 1998. International oil company financial management in nontechnical language.
Çağatay, M.N., Saner, S., Al-Saiyed, I., Carrigan, W.J., 1996. Diagenesis of the Safaniya Sandstone Member (mid-Cretaceous) in Saudi Arabia. Sediment. Geol. 105, 221–239. doi:10.1016/0037-0738(95)00140-9
Caldwell, J., Sonneland, L., Neidell, N., 1997. Exploring for Stratigraphic Traps. Oilf. Rev. 9, 48–61.
Cameron, T.D.J., 1993. Triassic, Permian and Pre-Permian of the Central and Northern North Sea. British Geological Survey.
Castagna, J., 2000. An introduction to this special section: AVO: The Next Step. Lead. Edge 19, 1187. doi:10.1190/1.1438502
Chopra, S., Castagna, J., Portniaguine, O., 2006. Seismic resolution and thin-bed reflectivity inversion. CSEG Rec. 31, 19–25. doi:doi:10.1190/1.2369941
Chuhan, F.A., Kjeldstad, A., Bjørlykke, K., Høeg, K., 2003. Experimental compression of loose sands: relevance to porosity reduction during burial in sedimentary basins. Can. Geotech. J. 40, 995–1011. doi:10.1139/t03-050
Chung, F., 1999. Risk analysis and decision making software package. Tulsa, Oklahoma.
Clark, D.N., Riley, L.A., Ainsworth, N.R., 1993. Stratigraphic, structural and depositional history of the Jurassic in the Fisher Bank Basin, UK North Sea. Geol. Soc. London, Pet. Geol. Conf. Ser. 4, 415–424. doi:10.1144/0040415
Cooper, C., Wright, I., Ringrose, P., Simone, A., Crow, W., Gardner, C., Williams, C., Limb, H.G., Nevels, H., Young, A., Dodds, K., McKnight, R., Imbus, S., Rennie, S., 2009. A Technical Basis for Carbon Dioxide Storage, CPL Press.
Corbin, S., Gorringe, S., Torr, D., 2005. Challenges of developing Carboniferous gas fields in the UK Southern North Sea, in: Petroleum Geology: North-West Europe and Global Perspectives - Proceedings of the 6th Petroleum Geology Conference. Geological Society of London, pp. 587–594. doi:10.1144/0060587
Cornford, C., 1998. Source rocks and hydrocarbons of the North Sea, Petroleum Geology of the North Sea: Basic Concepts and Recent Advances: Fourth Edition. doi:10.1002/9781444313413.ch11
Coward, R.N., Clark, N.M., Pinnock, S.J., 1991. The Tartan Field, Block 15/16, UK. North Sea, in: United Kingdom Oil and Gas Fields 25 Years Commemorative Volume. Geological Society of London, pp. 377–386. doi:10.1144/GSL.MEM.1991.014.01.47
Day-Stirrat, R.J., Milliken, K.L., Dutton, S.P., Loucks, R.G., Hillier, S., Aplin, A.C., Schleicher, A.M., 2011. Discussion in response to Knut Bjørlykke regarding JMPG_1376 "Open-System Chemical Behavior In Deep Wilcox Group Mudstones, Texas Gulf Coast, USA" Mar. Pet. Geol. 28, 1383–1384. doi:10.1016/j.marpetgeo.2011.01.010
Day-Stirrat, R.J., Milliken, K.L., Dutton, S.P., Loucks, R.G., Hillier, S., Aplin, A.C., Schleicher, A.M., 2010. Open-system chemical behavior in deep Wilcox Group mudstones, Texas Gulf Coast, USA. Mar. Pet. Geol. 27, 1804–1818. doi:10.1016/j.marpetgeo.2010.08.006
De'Ath, N.G., Schuyleman, S.F., 1981. The geology of the Magnus oilfield. Pet. Geol. Cont. shelf north-west Eur. 342–351.
DECC, 2012. Stratigraphic plays of the UKCS.
Deegan, C.E. t, Scull, B.J., 1977. A standard lithostratigraphic nomenclature for the Central and Northern North Sea. HMSO.
Demaison, G., 1984. The generative basin concept.
Dix, C., 1955. Seismic velocities from surface measurements. Geophysics.

Dixon, S.A., Summers, D.M., Surdam, R.C., 1989. Diagenesis and preservation of porosity in Norphlet Formation (Upper Jurassic), southern Alabama. Am. Assoc. Pet. Geol. Bull. doi:10.1306/44B4A24E-170A-11D7-8645000102C1865D

Doré, G., Robbins, J., 2005. The Buzzard Field. Geol. Soc. London, Pet.

Dowey, P.J., Hodgson, D.M., Worden, R.H., 2012. Pre-requisites, processes, and prediction of chlorite grain coatings in petroleum reservoirs: A review of subsurface examples. Mar. Pet. Geol. 32, 63–75. doi:10.1016/j.marpetgeo.2011.11.007

Dowey, P.J., Worden, R.H., Utley, J., Hodgson, D.M., 2017. Sedimentary controls on modern sand grain coat formation. Sediment. Geol. 353, 46–63. doi:10.1016/j.sedgeo.2017.03.001

Downey, M.W., 1984. Evaluating Seals for Hydrocarbon Accumulations. Am. Assoc. Pet. Geol. Bull. 68, 1752–1763.

Egeberg, P.K., Aagaard, P., 1989. Origin and evolution of formation waters from oil fields on the Norwegian shelf. Appl. Geochemistry 4, 131–142. doi:10.1016/0883-2927(89)90044-9

Ehrenberg, S.N., 1993. Preservation of anomalously high porosity in deeply buried sandstones by grain-coating chlorite:Examples from the Norwegian continental shelf. Amer. Ass. Pet. Geol. Bull. 77, 1260–1286.

Ehrenberg, S.N., 1991. Kaolinized, potassium-leached zones at the contacts of the Garn Formation, Haltenbanken, mid-Norwegian continental shelf. Mar. Pet. Geol. 8, 250–269. doi:10.1016/0264-8172(91)90080-K

Ehrenberg, S.N., 1989. Assessing the Relative Importance of Compaction Processes and Cementation to Reduction of Porosity in Sandstones: Discussion; Compaction and Porosity Evolution of Pliocene Sandstones, Ventura Basin, California: DISCUSSION. Am. Assoc. Pet. Geol. Bull. 73, 1274–1276.

Ehrenberg, S.N., Nadeau, P.H., 2005. Sandstone vs. carbonate petroleum reservoirs: A global perspective on porosity-depth and porosity-permeability relationships. Am. Assoc. Pet. Geol. Bull. 89, 435–445.

EIA, 2017. International Energy Outlook 2017 Overview. U.S. Energy Inf. Adm. IEO2017, 143. doi:www.eia.gov/forecasts/ieo/pdf/0484(2016).pdf

Eiken, O., Ringrose, P., Hermanrud, C., Nazarian, B., Torp, T.A., Høier, L., 2011. Lessons learned from 14 years of CCS operations: Sleipner, In Salah and Snøhvit. Energy Procedia 4, 5541–5548. doi:10.1016/j.egypro.2011.02.541

Emery, D., Myers, K.J., Young, R., 1990. Ancient subaerial exposure and freshwater leaching in sandstones. Geology 18, 1178–1181. doi:10.1130/0091-7613(1990)018<1178:ASEAFL>2.3.CO;2

Emery, D., Smalley, P.C., Oxtoby, N.H., Ragnarsdottir, K. V., Aagaard, P., Halliday, a., Coleman, M.L., Petrovich, R., 1993. Synchronous Oil Migration and Cementation in Sandstone Reservoirs Demonstrated by Quantitative Description of Diagenesis [and Discussion]. Philos. Trans. R. Soc. A Math. Phys. Eng. Sci. 344, 115–125. doi:10.1098/rsta.1993.0080

England, G., Haszelding, S., Cleverley, J., Barclay, S., Bruce, Y., Fisher, Q., Graham, C., Fallick, T., 2003. Applying Ion-Microprobe Technology in Reconstructing Quartz Cement History in an Upper Jurassic Sandstone Reservoir of the Outer Moray Firth Basin, North Sea, United Kingdom, in: AAPG Annual Meeting, Salt Lake City, Utah.

Eriksen, S.H., Anderson, J.H., Grist, M., Stoker, S., Brzozowska, J., 2003. Oil and gas resources, in: Evans, D., Graham, C., Armour, A., Bathurst, P. (Eds.), The Millennium Atlas: Petroleum Geology of the Central and Northern North Sea. The Geological Society of London, London, pp. 345–358.

Etris, E., Crabtree, N., Dewar, J., 2001. True depth conversion: More than a pretty picture. CSEG Rec. 11–21.

ExxonMobil, 2017. 2017 Outlook for Energy 1–50.

Faust, L., 1951. Seismic velocity as a function of depth and geologic time. Geophysics.

Fawad, M., Mondol, N.H., Bjørlykke, K., 2010. Microfabric and rock properties of experimentally compressed silt-clay mixtures. Mar. Pet. Geol. 27, 1698–1712. doi:10.1016/J.MARPETGEO.2009.10.002

Fisher, M.., Mudge, D.., 1998. Triassic, in: Glennie, K.W. (Ed.), Petroleum Geology of the North Sea: Basic Concepts and Recent Advances, Fourth Edition. pp. 212–244.

Fisher, Q.J., Casey, M., Harris, S.D., Knipe, R.J., 2003. Fluid-flow properties of faults in sandstone: The importance of temperature history. Geology 31, 965. doi:10.1130/G19823.1

Fraser, A.J., Nash, D.F., Steele, R.P., Ebdon, C.C., Fraser, A.J., 1990. A regional assessment of the intra-Carboniferous play of Northern England. Geol. Soc. London, Spec. Publ. 50, 417–440. doi:10.1144/GSL.SP.1990.050.01.26

Fraser, S., Robinson, A., Johnson, H., Underhill, J., Kadolsky, D., 2002. Upper Jurassic, in: Evans, D., Graham, C., Armour, A., Bathurst, P. (Eds.), The Millennium Atlas: Petroleum Geology of the Central and Northern North Sea. The Geological Society of London, London, pp. 157–189.

Furlan, S., Clauer, N., Chaudhuri, S., Sommer, F., 1996. K transfer during burial diagenesis in the Mahakam Delta Basin (Kalimantan, Indonesia). Clays Clay Miner. 44, 157–169.

Fyfe, J.A., Gregersen, U., Jordt, H., Rundberg, Y., Eidvin, T., Evans, D., Stewart, D., Hovland, M., Andresen, P., 2003. Oligocene to Holocene, in: Evans, D., Graham, C., Armour, A., Bathurst, P. (Eds.), The Millennium Atlas: Petroleum Geology of the Central and Northern North Sea. The Geological Society of London, London, pp. 279–287.

Gaarenstroom, L., TROMP, R.A.J., de Jong, M.C., BRANDENBURG, A.M., 1993. Overpressures in the Central North Sea: implications for trap integrity and drilling safety. Pet. Geol. Northwest Eur. Proc. 4th Conf. 2, 1305–1313. doi:10.1144/0041305

Gainski, M., Macgregor, A.G., Freeman, P.J., Nieuwland, H.F., 2010. Turbidite reservoir compartmentalization and well targeting with 4D seismic and production data: Schiehallion Field, UK. Reserv. Compart. 347, 89–102. doi:10.1144/sp347.7

Gambaro, M., Donagemma, V., 2003. The T-Block Fields, Block 16/17, UK North Sea. Geol. Soc. London, Mem. 20, 369–382. doi:10.1144/GSL.MEM.2003.020.01.31

Garrett, S.W., Atherton, T., Hurst, A., 2000. Lower Cretaceous deep-water sandstone reservoirs of the UK Central North Sea. Pet. Geosci. 6, 231–240. doi:10.1144/petgeo.6.3.231

Gatliff, R.W., Richards, P.C., Smith, K., Graham, C.C., McCormac, M., Smith, N.J.P., Long, D., Cameron, T.D.J., Evans, D., Stevenson, A.G., 1994. United Kingdom offshore regional report: The geology of the central North Sea. Br. Geol. Surv. HMSO.

Gautier, D.L.D., 2005. Kimmeridgian shales total petroleum system of the North Sea graben province. Geological Survey (US).

Giles, M.R., 1987. Mass transfer and problems of secondary porosity creation in deeply buried hydrocarbon reservoirs. Mar. Pet. Geol. 4, 188–204. doi:10.1016/0264-8172(87)90044-4

Giles, M.R., de Boer, R.B., 1990. Origin and significance of redistributional secondary porosity. Mar. Pet. Geol. 7, 378–397. doi:10.1016/0264-8172(90)90016-A

Giles, M.R., Deboer, R.B., Marshall, J.D., 1994. How important are organic acids in generating secondary porosity in the subsurface, Organic Acids in Geological Processes. Springer Berlin Heidelberg, Berlin, Heidelberg. doi:10.1007/978-3-642-78356-2_14

Giles, M.R., Marshall, J.D., 1986. Constraints on the development of secondary porosity in the subsurface: Re-evaluation of processes. Mar. Pet. Geol. 3, 243–255. doi:10.1016/0264-8172(86)90048-6

Giles, M.R., Stevenson, S., Martin, S. V, Cannon, S.J.C., Hamilton, P.J., Marshall, J.D., Samways, G.M., 1992. The reservoir properties and diagenesis of the Brent Group: a regional perspective. Geol. Soc. London, Spec. Publ. 61, 289–327. doi:10.1144/GSL.SP.1992.061.01.16

Glennie, K.W., 1998. Lower Permian - Rotliegend, in: Petroleum Geology of the North Sea: Basic Concepts and Recent Advances: Fourth Edition. pp. 137–173. doi:10.1002/9781444313413.ch5

Glennie, K.W., 1997. Recent advances in understanding the southern North Sea basin: a summary, in: Petroleum Geology of the Southern North Sea: Future Potential, Geol. Soc. Sp. Publ. No. 123. pp. 17–30.

Glennie, K.W., 1986. Development of N.W. Europe's Southern Permian Gas Basin. Geol. Soc. London, Spec. Publ. 23, 3–22. doi:10.1144/GSL.SP.1986.023.01.01

Glennie, K.W., Provan, D.M.J., 1990. Lower Permian Rotliegend reservoir of the Southern North Sea gas province. Geol. Soc. London, Spec. Publ. 50, 399–416. doi:10.1144/gsl.sp.1990.050.01.25

Glennie, K.W., Underhill, J.R., 1998. Origin, development and evolution of structural styles, in: Petroleum Geology of the North Sea: Basic Concepts and Recent Advances, Fourth Edition. pp. 42–84.

Gluyas, J., Coleman, M., 1992. Material flux and porosity changes during sediment diagenesis. Nature 356, 52–54. doi:10.1038/356052a0

Gluyas, J., Garland, C., Oxtoby, N.H., Hogg, A.J.C., 2000. Quartz Cement: The Miller's Tale, in: Worden, R.H., Morad, S. (Eds.), Quartz Cementation in Sandstones. Blackwell Publishing Ltd., pp. 199–218.

Gluyas, J., Hichens, H., 2003. United Kingdom oil and gas fields: commemorative millennium volume, Appendix 1. Geol. Soc. London, Mem. 20, 947–977.

Gluyas, J., Leonard, A., 1995. Diagenesis of the Rotliegend sandstone: the answer ain't blowin' in the wind. Mar. Pet. Geol. 12, 491–497. doi:10.1016/0264-8172(95)91504-I

Gluyas, J., Swarbrick, R., 2003. Petroleum Geoscience.

Gluyas, J.G., Grant, S.M., Robinson, A.G., 1993a. Geochemical evidence for a temporal control on sandstone cementation. Diagenes. basin Dev. 36, 23–33.

Gluyas, J.G., Robinson, a G., Emery, D., Grant, S.M., Oxtoby, N.H., 1993b. The link between petroleum emplacement and sandstone cementation. Pet. Geol. Northwest Eur. Proc. 4th Conf. Pet. Geol. NW. Eur. Barbican Centre, London 2, 1395–1404. doi:10.1144/0041395

Gluyas, J.G., Spiro, B., Raiswell, R., Berner, R.A., Lowrey, C.J., Coleman, M.L., Mason, R., Whitaker, J.H.M., Saigal, G.C., Curtis, C.D., 1985. Reduction and Prediction of Sandstone Reservoir Potential, Jurassic, North Sea [and Discussion]. Philos. Trans. R. Soc. London A Math. Phys. Eng. Sci. 315.

Gray, J., 2013. Petroleum prospectivity of the principal sedimentary basins on the United Kingdom Continental Shelf Petroleum prospectivity of the principal sedimentary basins on the United Kingdom Continental Shelf 41.

Grunau, H.R., 1987. A worldwide look at the cap rock problem. J. Pet. Geol. 10, 245–266. doi:10.1111/j.1747-5457.1987.tb00945.x

Hale, D., 2013. Methods to compute fault images , extract fault surfaces , and estimate fault throws from 3D seismic images. Geophysics 78, O33–O43. doi:10.1190/GEO2012-0331.1

Hale, D., 2012. Fault surfaces and fault throws from 3D seismic images. SEG Tech. Progr. Expand. Abstr. 2012 1–6. doi:10.1190/segam2012-0734.1

Hardy, R., Tucker, M., 1988. X-ray powder diffraction of sediments. Tech. Sedimentol. 191–228.

Harker, S.D., Green, S.C.H., Romani, R.S., 1991. The Claymore Field, Block 14/19, UK North Sea. United Kingdom Oil Gas Fields 25 years Commem. Vol. 269–278.

Haslett, S.K., 1992. Rhaxellid sponge microscleres from the Portlandian of Dorset, UK. Geol. J. 27, 339–347. doi:10.1002/gj.3350270404

Haszeldine, R.S., Cavanagh, A.J., England, G.L., 2003. Effects of oil charge on illite dates and stopping quartz cement: Calibration of basin models. J. Geochemical Explor. 78–79, 373–376. doi:10.1016/S0375-6742(03)00151-1

Haszeldine, R.S., Samson, I.M., Cornford, C., 1984. Quartz diagenesis and convective fluid movement: Beatrice Oilfield, UK. North Sea. Clay Miner. 19, 391–402. doi:10.1180/claymin.1984.019.3.10

Haszeldine, R.S., Wilkinson, M., Darby, D., Macaulay, C.I., Couples, G.D., Fallick, A.E., Fleming, C.G., Stewart, R.N.T., McAULAY, G., 1999. Diagenetic porosity creation in an overpressured graben. Geol. Soc. London, Pet. Geol. Conf. Ser. 5, 1339–1350. doi:10.1144/0051339

Hayes, M.J., Boles, J.R., 1992. Volumetric Relations Between Dissolved Plagioclase and Kaolinite in Sandstones: Implications for Aluminum Mass Transfer in the San Joaquin Basin, California.

Head, I.M., Jones, D.M., Larter, S.R., 2003. Biological activity in the deep subsurface and the origin of heavy oil. Nature 426, 344–352. doi:10.1038/nature02134

Heald, M.T., Larese, R.E., 1974. Influence of coatings on quarzt cementation. J. Sediment. Petrol. 44, 1269–1274.

Heinemann, N., Wilkinson, M., Pickup, G.E., Haszeldine, R.S., Cutler, N.A., 2012. CO2 storage in the offshore UK Bunter Sandstone Formation. Int. J. Greenh. Gas Control 6, 210–219. doi:10.1016/j.ijggc.2011.11.002

Hendry, J.P., Wilkinson, M., Fallick, A.E., Haszeldine, R.S., 2000. Ankerite cementation in deeply buried Jurassic sandstone reservoirs of the central North Sea. J. Sediment. Res. 70, 227–239. doi:10.1306/2DC4090D-0E47-11D7-8643000102C1865D

Hill, P.J., Palfrey, A.J., 2003. The Britannia Field, Blocks 15/29a, 15/30, 16/26, 16/27a, 16/27b, UK North Sea. Geol. Soc. London, Mem. 20, 415–429. doi:10.1144/gsl.mem.2003.020.01.34

Hillier, S., 2002. Quantitative analysis of clay and other minerals in sandstones by X-ray powder diffraction (XRPD). Int. Assoc. Sedimentol. Spec. Publ. 34, 213–251.

Hillier, S., 1999. Use of an air brush to spray dry samples for X-ray powder diffraction. Clay Miner. 34, 127–135. doi:10.1180/claymin.1999.034.1.14

Hindle, A.D., 1997. Petroleum migration pathways and charge concentration: a three-dimensional model. Am. Assoc. Pet. Geol. Bull. 81, 1451–1481.

Hogg, A.J.C., 2003. The Montrose, Arbroath and Arkwright Fields, Blocks 22/17, 22/18, 22/23a, UK North Sea, in: United Kingdom Oil and Gas Fields. Commemorative Millennium Volume. pp. 611–616. doi:10.1144/GSL.MEM.2003.020.01.49

Holloway, S., Knox, R., 1992. Paleogene Of The Central and Northern North Sea. In: Lithostratigr. Nomencl. UK North Sea 1–160.

Holloway, S., Vincent, C.J., Bentham, M.B., Kirk, K.L., 2006a. Top-down and bottom-up estimates of CO2 storage capacity in the United Kingdom sector of the southern North Sea basin. Environ. Geosci. 13, 71–84. doi:10.1306/eg.11080505015

Holloway, S., Vincent, C.J., Kirk, K.L., 2006b. Industrial carbon dioxide emissions and carbon dioxide storage potential in the UK, Sustainable and renewable eneergy programme commercial report. Keyworth, Norttingham.

Holm, G.M., 1998. Distribution and Origin of Overpressure in the Central Graben of the North Sea 123–144.

Houseknecht, D.W., 1987. Assessing the Relative Importance of Compaction Processes and Cementation to Reduction of Porosity in Sandstones. Am. Assoc. Pet. Geol. Bull. 71, 633–642.

Howell, J.A., Flint, S.S., Hunt, C., 1996. Sedimentological aspects of the Humber Group (Upper Jurassic) of the South Central Graben, UK North Sea. Sedimentology 43, 89–114. doi:10.1111/j.1365-3091.1996.tb01462.x

Hurst, A., Nadeau, P.H., 1995. Clay microporosity in reservoir sandstones: an application of quantitative electron microscopy in petrophysical evaluation. Am. Assoc. Pet. Geol. Bull. 79, 563–573. doi:10.1306/8D2B1598-171E-11D7-8645000102C1865D

Irwin, H., Curtis, C., Coleman, M., 1977. Isotopic evidence for source of diagenetic carbonates formed during burial of organic-rich sediments. Nature 269, 209–213. doi:10.1038/269209a0

Isaksen, G.H., 2004. Central North Sea hydrocarbon systems: Generation, migration, entrapment, and thermal degradation of oil and gas. Am. Assoc. Pet. Geol. Bull. 88, 1545–1572.

Isaksen, G.H., Curry, D.J., Yeakel, J.D., Jenssen, A.I., 1998. Controls on the oil and gas potential of humic coals. Org. Geochem. 29, 23–44. doi:10.1016/S0146-6380(98)00042-4

Isaksen, G.H., Ledje, K.H.I., 2001. Source rock quality and hydrocarbon migration pathways within the greater Utsira High area, Viking Graben, Norwegian North Sea. Am. Assoc. Pet. Geol. Bull. 85, 861–884.

Jahn, F., Cook, M., Graham, M., 2008. Risk Analysis, in: Hydrocarbon Exploration and Production. pp. 1237–1240. doi:10.1016/B978-075067294-8/50003-8

Jeremiah, J.M., Nicholson, P.H., 1999. Middle Oxfordian to Volgian sequence stratigraphy of the Greater Shearwater area. Geol. Soc. London, Pet. Geol. Conf. Ser. 5, 153–170. doi:10.1144/0050153

Johnson, H., Warrington, G., Stoker, S.J., 1994. Permian and Triassic of the southern North Sea. Lithostratigraphic nomenclature of the UK North Sea. Lithostratigr. Nomencl. UK North Sea 1–141.

Johnson, R., 1920. The Cementation Process in Sandstone. Am. Assoc. Pet. Geol. Bull.

4, 33–35.
Jolley, S.J., Fisher, Q.J., Ainsworth, R.B., 2010. Reservoir compartmentalization: an introduction. Reserv. Compart. 347, NP. doi:10.1144/sp347.0\r10.1144/sp347.1
Kaiser, M., 2009. Modeling the time and cost to drill an offshore well. Energy.
Karasek, R.M., Vaughan, R.L., Masuda, T.T., 2003. The Beryl Field, Block 9/13, UK North Sea. Geol. Soc. London, Mem. 20, 153–166. doi:10.1144/GSL.MEM.2003.020.01.13
Kelly, J.L., Fu, B., Kita, N.T., Valley, J.W., 2007. Optically continuous silcrete quartz cements of the St. Peter Sandstone: High precision oxygen isotope analysis by ion microprobe. Geochim. Cosmochim. Acta 71, 3812–3832. doi:10.1016/j.gca.2007.05.014
Ketter, F.J., 1991. The Esmond, Forbes and Gordon Fields, Block 43/8a, 48/13a, 48/15a, 48/20a, UK. North Sea, in: United Kingdom Oil and Gas Fields 25 Years Commemorative Volume. pp. 425–432.
Kevin T. Biddle, C.C.W., 1994. Hydrocarbon Traps: Chapter 13: Part III. Processes 77, 219–235.
Kharaka, Y.K., Hanor, J.S., 2003. Deep fluids in the continents: I. Sedimentary basins. Treatise on geochemistry 5, 499–540.
Klemme, H.D., Ulmishek, G.F., 1991. Effective petroleum source rocks of the world: stratigraphic distribution and controlling depositional factors. Am. Assoc. Pet. Geol. Bull. 75, 1809–1851. doi:10.1306/BDFF8A88-1718-11D7-8645000102C1865D
Knott, S.D., 1993. Fault seal analysis in the North Sea. Am. Assoc. Pet. Geol. Bull. doi:10.1306/BDFF8D58-1718-11D7-8645000102C1865D
Kong, M., Bhattacharya, R.N., James, C., Basu, A., 2005. A statistical approach to estimate the 3D size distribution of spheres from 2D size distributions. Geol. Soc. Am. Bull. 117, 244. doi:10.1130/B25000.1
Krol, D.E., Noual, V., van Maren, P.J.T., 2000. Exploring mature areas: the role of technology. Nor. Pet. Soc. Spec. Publ. 9, 231–249. doi:10.1016/S0928-8937(00)80019-3
Kubala, M., Bastow, M., Thompson, S., Scotchman, I., Oygard, K., 2003. Geothermal regime, petroleum generation and migration, in: Evans, D., Graham, C., Armour, A., Bathurst, P. (Eds.), The Millennium Atlas: Petroleum Geology of the Central and Northern North Sea. The Geological Society of London, London, pp. 289–315.
Lamers, E., Carmichael, S.M.M., 1999. The Paleocene deepwater sandstone play West of Shetland. Pet. Geol. Northwest Eur. Proc. 5th Conf. Pet. Geol. Northwest Eur. 1, 645–660. doi:10.1144/0050645
Land, L.S., 1997. Mass Transfer During Burial Diagenesis in the Gulf of Mexico Sedimentary Basin: An Overview.
Lander, R.H., Bonnell, L.M., 2010. A model for fibrous illite nucleation and growth in sandstones. Am. Assoc. Pet. Geol. Bull. 94, 1161–1187. doi:10.1306/04211009121
Lander, R.H., Walderhaug, O., 1999. Predicting porosity through simulating sandstone compaction and quartz cementation. AAPG Bull. (American Assoc. Pet. Geol. 83, 433–449. doi:10.1306/00AA9BC4-1730-11D7-8645000102C1865D
Lapedes, D., 1978. McGraw-Hill encyclopedia of the geological sciences. McGraw-Hill.
Lasocki, J., Guemene, J.M., Hedayati, A., Legorjus, C., Page, W.M., 1999. The Elgin and Franklin fields: UK Blocks 22/30c, 22/30b and 29/5b, in: Geological Society, London, Petroleum Geology Conference Series. pp. 1007–1020.
Leeder, M.R., Hardman, M., 1990. Carboniferous geology of the Southern North Sea Basin and controls on hydrocarbon prospectivity. Geol. Soc. London, Spec. Publ. 55, 87–105. doi:10.1144/GSL.SP.1990.055.01.04
Loizou, N., 2014. Success in exploring for reliable, robust Paleocene traps west of Shetland. Geol. Soc. London, Spec. Publ. 397, 59–79. doi:10.1144/SP397.9
Loizou, N., 2005. West of Shetland exploration unravelled-an indication of what the future may hold. First Break 23, 53–59.
Lowe, D.R., 1982. Sediment Gravity Flows: II Depositional Models with Special Reference to the Deposits of High-Density Turbidity Currents. J. Sediment. Res. 52.
Lu, J., Wilkinson, M., Haszeldine, R.S., Fallick, A.E., 2009. Long-term performance of a mudrock seal in natural CO2 storage. Geology 37, 35–38. doi:10.1130/G25412A.1

Lundegard, P.D., 1992. Sandstone Porosity Loss--A Big Picture"View of the Importance of Compaction". J. Sediment. Res. 62, 250–260. doi:10.1306/D42678D4-2B26-11D7-8648000102C1865D

Lundegard, P.D., Land, L.S., 1986. Carbon dioxide and organic acids: their role in porosity enhancement and cementation, Paleogene of the Texas Gulf Coast. Roles Org. Matter Sediment Diagenes. 38, 129–146. doi:10.2110/pec.86.38.0129

Lutz, M., Kaasschieter, P.H., van Wijhe, H., others, 1975. Geological factors controlling Rotliegend gas accumulations in the Mid-European Basin, in: 9th World Petroleum Congress. World Petroleum Congress.

Lynch, F.L., Mack, L.E., Land, L.S., 1997. Burial diagenesis of illite/smectite in shales and the origins of authigenic quartz and secondary porosity in sandstones. Geochim. Cosmochim. Acta 61, 1995–2006. doi:10.1016/S0016-7037(97)00066-5

Ma, Y.Z., 2011. Uncertainty Analysis in Reservoir Characterization and Management: How Much Should We Know About What We Don't Know?, in: MA, Y.Z., Pointe, R.R.L. (Eds.), Uncertainty Analysis and Reservoir Modeling. AAPG Special Volumes, pp. 1–16. doi:10.1306/13301404M963458

Maast, T.E., Jahren, J., Bjørlykke, K., 2011. Diagenetic controls on reservoir quality in middle to upper Jurassic sandstones in the South Viking Graben, North Sea. Am. Assoc. Pet. Geol. Bull. 95, 1937–1958. doi:10.1306/03071110122

MacGowan, D.B., Surdam, R.C., 1990. Carboxylic acid anions in formation waters, San Joaquin Basin and Louisiana Gulf Coast, U.S.A.—Implications for clastic diagenesis. Appl. Geochemistry, Water-Rock Interactions Special Memorial Issue Ivan Barnes (1931–1989) 5, 687–701. doi:10.1016/0883-2927(90)90065-D

MacGowan, D.B., Surdam, R.C., 1988. Difunctional carboxylic acid anions in oilfield waters. Org. Geochem. 12, 245–259. doi:10.1016/0146-6380(88)90262-8

Magara, K., 1976. Water Expulsion from Clastic Sediments during Compaction--Directions and Volumes. Am. Assoc. Pet. Geol. Bull. 60, 543–553.

Marchand, A.M.E., Haszeldine, R.S., Macaulay, C.I., Swennen, R., Fallick, A.E., 2000. Quartz cementation inhibited by crestal oil charge: Miller deep water sandstone, UK North Sea. Clay Miner. 35, 201–210.

Marchand, A.M.E., Haszeldine, R.S., Smalley, P.C., Macaulay, C.I., Fallick, A.E., 2001. Evidence for reduced quartz-cementation rates in oil-filled sandstones. Geology 29, 915–918. doi:10.1130/0091-7613(2001)029<0915:EFRQCR>2.0.CO;2

Marchand, A.M.E., Smalley, P.C., Haszeldine, R.S., Fallick, A.E., 2002. Note on the importance of hydrocarbon fill for reservoir quality prediction in sandstones. Am. Assoc. Pet. Geol. Bull. 86, 1561–1571. doi:10.1306/61EEDD00-173E-11D7-8645000102C1865D

Mathieu, C., 2015. Moray Firth – Central North Sea Post Well Analysis.

McBride, E.F., 1989. Quartz cement in sandstones: a review. Earth-Science Rev. 26, 69–112. doi:10.1016/0012-8252(89)90019-6

McCarthy, K., Rojas, K., Niemann, M., Palmowski, D., Peters, K., Stankiewicz, A., 2011. Basic Petroleum Geochemistry for Source Rock Evaluation. Oilf. Rev. 23, 32–43.

McManus, J., 1988. Grain size determination and interpretation, in: Tucker, M. (Ed.), Techniques in Sedimentology. Blackwell Scientific Publications, pp. 63–85.

Megill, R., 1979. Introduction to exploration economics.

Midtbø, R.E.A., Rykkje, J.M., Ramm, M., 2000. Deep burial diagenesis and reservoir quality along the eastern flank of the Viking Graben. Evidence for illitization and quartz cementation after hydrocarbon emplacement. Clay Miner. 35, 227–237. doi:10.1180/000985500546602

Milliken, K.L., 2003. Late diagenesis and mass transfer in sandstone shale sequences. Treatise on geochemistry 7, 159–190.

Milliken, K.L., Mack, L.E., Land, L.S., 1994. Elemental Mobility in Sandstones during Burial - Whole-Rock Chemical and Isotopic Data, Frio Formation, South Texas. J. Sediment. Res. Sect. a-Sedimentary Petrol. Process. 64, 788–796. doi:10.1306/D4267EC4-2B26-11D7-8648000102C1865D

Milliken, K.L., McBride, E.F., Land, L.S., 1989. Numerical assessment of dissolution versus replacement in the subsurface destruction of detrital feldspars, Oligocene Frio Formation, South Texas. J. Sediment. Res. 59, 740–757. doi:10.1306/212F9061-2B24-11D7-8648000102C1865D

Moore, D.M., Reynolds, R.C., 1997. X-Ray diffraction and the identification and analysis of clay minerals,. Oxford Univ. Press. Oxford, New York 373.

Moss, B., Barson, D., Rakhit, K., Dennis, H., Swarbrick, R., 2003. Formation pore pressures and formation waters. Millenn. atlas Pet. Geol. Cent. North. North Sea Geol. Soc. 317–329.

Munns, J.W., Gray, J.C., Stoker, S.J., Andrews, I.J., Cameron, T.D.J., 2005. The remaining hydrocarbon potential of the UK Continental Shelf. Pet. Geol. North-West Eur. Glob. Perspect. – Proc. 6th Pet. Geol. Conf. 41–54. doi:10.1144/0060041

Nguyen, B.T.T., Jones, S.J., Goulty, N.R., Middleton, A.J., Grant, N., Ferguson, A., Bowen, L., 2013. The role of fluid pressure and diagenetic cements for porosity preservation in Triassic fluvial reservoirs of the Central Graben, North Sea. Am. Assoc. Pet. Geol. Bull. 97, 1273–1302. doi:10.130e/01151311163

Oakman, C.., 2014. The Lower Cretaceous plays of the Central and Northern North Sea: Atlantean drainage models and enhanced hydrocarbon potential. Pet. Geol. North-West Eur. Glob. Perspect. - Proc. 6th Pet. Geol. Conf. 6, 187–198. doi:10.1144/0060187

Oelkers, E.H., Bjorkum, P.A., Murphy, W.M., 1996. A petrographic and computational investigation of quartz cementation and porosity reduction in North Sea sandstones. Am. J. Sci. 296, 420–452. doi:10.2475/ajs.296.4.420

Offshore Europe, 2001. Offshore Europe [WWW Document]. URL http://www.offshore-mag.com/articles/print/volume-61/issue-2/departments/offshore-europe.html (accessed 2.7.18).

Ofstad, K., Kullerud, L., Helliksen, D., 2000a. Evaluation of Norwegian Wildcat Wells (Article 1). Nor. Pet. Soc. Spec. Publ. 9, 23–31. doi:10.1016/S0928-8937(00)80006-5

Ofstad, K., Øvretveit, A., Kullerud, L., Heggland, K., 2000b. Probability of discovery and the reasons for dry wells: results from the project: Evaluation of Norwegian Wildcat Wells (Article 3). Nor. Pet. Soc. Spec. Publ. 9, 47–55. doi:10.1016/S0928-8937(00)80008-9

Osborne, M.J., Swarbrick, R.E., 1999. Diagenesis in North Sea HPHT clastic reservoirs — consequences for porosity and overpressure prediction. Mar. Pet. Geol. 16, 337–353. doi:10.1016/S0264-8172(98)00043-9

Osborne, M.J., Swarbrick, R.E., 1997. Mechanisms for generating overpressure in sedimentary basins; a reevaluation. Am. Assoc. Pet. Geol. Bull. 81, 1023–1041.

Otis, R.M., Schneidermann, N., 1997. A process for evaluating exploration prospect. Am. Assoc. Pet. Geol. Bull. 81, 1087–1109. doi:10.1306/522B49F1-1727-11D7-8645000102C1865D

Oudmayer, B.C., de Jager, J., 1993. Fault reactivation and oblique slip in the Southern North Sea. Pet. Geol. Northwest Eur. Proc. 4th Conf. Pet. Geol. NW. Eur. Barbican Centre, London 1281–1290.

Peel, F.J., Brooks, J.R.V., 2016. A practical guide to the use of success versus failure statistics in the estimation of prospect risk. Am. Assoc. Pet. Geol. Bull. 100, 137–150. doi:10.1306/08101515059

Peel, F.J., Brooks, J.R. V, 2015. What to expect when you are prospecting: How new information changes our estimate of the chance of success of a prospect. Am. Assoc. Pet. Geol. Bull. 99, 2159–2171. doi:10.1306/070615045

Pegrum, R.M., Spencer, A.M., 1990. Hydrocarbon plays in the northern North Sea. Geol. Soc. London, Spec. Publ. 50, 441–470. doi:10.1144/GSL.SP.1990.050.01.27

Pepper, A.S., Corvi, P.J., 1995. Simple kinetic models of petroleum formation. Part I: oil and gas generation from kerogen. Mar. Pet. Geol. 12, 291–319. doi:10.1016/0264-8172(95)98381-E

Perry, E., Hower, J., 1970. Burial Diagenesis in Gulf Coast Pelitic Sediments. Clays Clay Miner. 18, 165–177. doi:10.1346/CCMN.1970.0180306

Pettijohn, F.J., 1975. Sedimentary Rocks. Springer-Verlag.

Pevear, D.R., 1999. Illite and hydrocarbon exploration. Proc. Natl. Acad. Sci. 96, 3440–3446. doi:10.1073/pnas.96.7.3440

Pittman, E.D., Larese, R.E., Heald, M.T., 1992. Clay coats occurrence and relevance to preservation of porosity in sandstones.

Primmer, T., Cade, C., Evans, J., Gluyas, J., 1997. Global patterns in sandstone

diagenesis: their application to reservoir quality prediction for petroleum exploration.
Prosser, D.J., McKeever, M.E., Hogg, A.J.C., Hurst, A., 1995. Permeability heterogeneity within massive Jurassic submarine fan sandstones from the Miller Field, northern North Sea, UK. Charact. Deep Mar. Clastic Syst. 94, 201–219. doi:10.1144/GSL.SP.1995.094.01.14
Ramm, M., Forsberg, A.W., Jahren, J.S., 1997. Porosity-depth trends in deeply buried Upper Jurassic reservoirs in the Norwegian Central Graben; an example of porosity preservation beneath the normal economic basement by grain-coating microquartz. Reserv. Qual. Predict. sandstones carbonates. 69, 177–199.
Richards, P.C., 1989. Lower and Middle Jurassic sedimentology of the Beryl Embayment, and implications for the evolution of the northern North Sea. University of Strathclyde.
Richards, P.C., Lott, G.K., Johnson, H., Knox, R.W., 1993. Jurassic of the central and northern North Sea. Lithostratigr. Nomencl. UK North Sea 3, 219.
Ringrose, P.S., Mathieson, A.S., Wright, I.W., Selama, F., Hansen, O., Bissell, R., Saoula, N., Midgley, J., 2013. The In Salah CO2 Storage Project: Lessons Learned and Knowledge Transfer. Energy Procedia 37, 6226–6236. doi:10.1016/j.egypro.2013.06.551
Rittenhouse, G., 1972. Stratigraphic-trap classification, in: Stratigraphic Oil and Gas Fields - Classification, Exploration Methods, and Case Histories. pp. 14–28.
Rooksby, S.K., 1991. The Miller Field, Blocks 16/7b, 16/8b, UK. North Sea. United Kingdom Oil Gas Fields 25 years Commem. Vol. 14, 159–164. doi:10.1144/GSL.MEM.1991.014.01.20
Rose, P., 2001. Risk analysis and management of petroleum exploration ventures.
Rose, P.R., 1999. Taking the risk out of petroleum exploration; the adoption of systematic risk analysis by international corporations during the 1990s. Lead. Edge 18, 192. doi:10.1190/1.1438250
Rose, P.R., 1992. Chance of success and its use in petroleum exploration, in: TR - The Business of Petroleum Exploration. AAPG Special Volumes, pp. 71–86.
Rose, P.R., 1987. Dealing with risk and uncertainty in exploration: how can we improve? Am. Assoc. Pet. Geol. Bull. doi:10.1017/CBO9781107415324.004
Ross, J.G., 2004. Risk and uncertainty in portfolio characterisation. J. Pet. Sci. Eng. 44, 41–53. doi:10.1016/j.petrol.2004.02.004
Rossel, N., 1982. Clay mineral diagenesis in Rotliegend aeolian sandstones of the southern North Sea. Clay Miner.
Schlömer, S., Krooss, B.M., 1997. Experimental characterisation of the hydrocarbon sealing efficiency of cap rocks. Mar. Pet. Geol. 14, 565–580. doi:10.1016/S0264-8172(97)00022-6
Schmidt, V., Mcdonald, D., 1979. The Role of Secondary Porosity in the Course of Sandstone Diagenesis.
Schmitt, H.R.H., Gordon, A.F., 1991. The Piper Field, Block 15/17, UK. North Sea, in: United Kingdom Oil and Gas Fields 25 Years Commemorative Volume. Geological Society of London, pp. 361–368. doi:10.1144/GSL.MEM.1991.014.01.32
Scotchman, I.C., 1989. Diagenesis of the Kimmeridge Clay Formation, onshore UK. J. Geol. Soc. London. 146, 285–303. doi:10.1144/gsjgs.146.2.0283
Scott, E.D., Gelin, F., Jolley, S.J., Leenaarts, E., Sadler, S.P., Elsinger, R.J., 2010. Sedimentological control of fluid flow in deep marine turbidite reservoirs: Pierce Field, UK Central North Sea. Geol. Soc. London, Spec. Publ. 347, 113–132. doi:10.1144/SP347.9
Senior, B., 2010. CO2 Storage in the UK - Industry Potential, UK Department of Energy and Climate Change. London.
Shanmugam, G., 2016. Submarine fans: A critical retrospective (1950–2015), Journal of Palaeogeography. Elsevier Ltd. doi:http://dx.doi.org/10.1016/j.jop.2015.08.011
Shanmugam, G., Moiola, R.J.R., 1985. Submarine fan models; problems and solutions, in: Submarine Fans and Related Turbidite Systems. Springer New York, pp. 29–33. doi:-
Shepherd, M., 1991. The Magnus Field, Block 211/7a, 12a, UK North Sea. Geol. Soc. London, Mem. 14, 153–157. doi:10.1144/GSL.MEM.1991.014.01.19
Sheriff, R.E., 1997. Seismic Resolution a key element. AAPG Explor.

Smalley, P., England, W., Rabaa, A.W.M., 1994. Reservoir Compartmentalization Assessed With Fluid Compositional Data. SPE Reserv. Eng. 9, 175–180. doi:10.2118/25005-PA

Smalley, P.C., Begg, S.H., Naylor, M., Johnsen, S., Godi, A., 2008. Handling risk and uncertainty in petroleum exploration and asset management: An overview. Am. Assoc. Pet. Geol. Bull. doi:10.1306/06040808063

Smalley, P.C., Hale, N.A., 1996. Early Identification of Reservoir Compartmentalization by Combining a Range of Conventional and Novel Data Types. SPE Form. Eval. 11, 163–170. doi:10.2118/30533-PA

Smith, D.A., 1966. Theoretical Considerations of Sealing and Non-Sealing Faults. Am. Assoc. Pet. Geol. Bull. 50, 363–374. doi:10.1306/5D25B48F-16C1-11D7-8645000102C1865D

Smith, K., Ritchie, J.D., 1993. Jurassic volcanic centres in the Central North Sea. Geol. Soc. London, Pet. Geol. Conf. Ser. 4, 519–531. doi:10.1144/0040519

Smith, M.M., Sholokhova, Y., Hao, Y., Carroll, S.A., 2013. Evaporite caprock integrity: An experimental study of reactive mineralogy and pore-scale heterogeneity during brine-CO2 exposure. Environ. Sci. Technol. 47, 262–268. doi:10.1021/es3012723

Spencer, A.M., Birkeland, Ø., Knag, G.Ø., Fredsted, R., 1999. Petroleum systems of the Atlantic margin of northwest Europe. Geol. Soc. London, Pet. Geol. Conf. Ser. 5, 231–246. doi:10.1144/0050231

Sperrevik, S., Gillespie, P.A., Fisher, Q.J., Halvorsen, T., Knipe, R.J., 2002. Empirical estimation of fault rock properties, in: Hunsdale, A.G.K. and R. (Ed.), Norwegian Petroleum Society Special Publications. Elsevier, pp. 109–125.

Statoil, 2017. Long-term macro and market outlook 2017.

Stewart, D.J., 1986. Diagenesis of the shallow marine Fulmar Formation in the central North Sea. Clay Miner. 21, 537–564.

Stoessell, R. K., and Pittman, E.D., 1990. Secondary Porosity Revisited: The Chemistry of Feldspar Dissolution by Carboxylic Acids and Anions. Am. Assoc. Pet. Geol. Bull. 74, 1795–1805.

Stoker, S.J., Gray, J.C., Haile, J., Andrews, I.J., Cameron, T.D.J., 2006. The importance of stratigraphic plays in the undiscovered resources of the UK Continental Shelf. Geol. Soc. London, Spec. Publ. 254, 153–167. doi:10.1144/gsl.sp.2006.254.01.08

Storvoll, V., Bjørlykke, K., Karlsen, D., Saigal, G., 2002. Porosity preservation in reservoir sandstones due to grain-coating illite: A study of the Jurassic Garn Formation from the Kristin and Lavrans fields, offshore Mid-Norway. Mar. Pet. Geol. 19, 767–781. doi:10.1016/S0264-8172(02)00035-1

Stow, D.A. V, Mayall, M., 2000. Deep-water sedimentary systems: New models for the 21st century, in: Marine and Petroleum Geology. pp. 125–135. doi:10.1016/S0264-8172(99)00064-1

Stricker, S., Jones, S.J., 2016. Enhanced porosity preservation by pore fluid overpressure and chlorite grain coatings in the Triassic Skagerrak, Central Graben, North Sea, UK. Geol. Soc. London, Spec. Publ. 435. doi:10.1144/SP435.4

Student, 1908. the Probable Error of a Mean. Biometrika 6, 1–25. doi:10.1093/biomet/6.1.1

Sullivan, K.B., McBride, E.F., 1991. Diagenesis of sandstones at shale contacts and diagenetic heterogeneity, Frio Formation, Texas. Am. Assoc. Pet. Geol. Bull. doi:10.1306/0C9B2759-1710-11D7-8645000102C1865D

Sullivan, M.D., Haszeldine, R.S., Boyce, A.J., Rogers, G., Fallick, A.E., 1994. Late anhydrite cements mark basin inversion: isotopic and formation water evidence, Rotliegend Sandstone, North Sea. Mar. Pet. Geol. 11, 46–54. doi:10.1016/0264-8172(94)90008-6

Surdam, R.C., Boese, S.W., Crossey, L.J., 1984. The Chemistry of Secondary Porosity: Part 2. Aspects of Porosity Modification 59, 127–149.

Surdam, R.C., Crossey, L.J., Hagen, E.S., Heasler, H.P., 1989. Organic-inorganic interactions and sandstone diagenesis. Am. Assoc. Pet. Geol. Bull. 73, 1–23.

Sylta, Ø., Pedersen, J.I., Hamborg, M., 1998. On the vertical and lateral distribution of hydrocarbon migration velocities during secondary migration. Geol. Soc. London, Spec. Publ. 144, 221–232. doi:10.1144/GSL.SP.1998.144.01.17

Taylor, S.R., Almond, J., Arnott, S., Kemshell, D., Taylor, D., 2003. The Brent Field, Block 211/29, UK North Sea. Geol. Soc. London, Mem. 20, 233–250.

doi:10.1144/gsl.mem.2003.020.01.20
Taylor, T., Giles, M., Hathon, L., Diggs, T., 2010. Sandstone diagenesis and reservoir quality prediction: Models, myths, and reality. AAPG.
Thomson, A., Stancliffe, R.J., 1990. Diagenetic controls on reservoir quality, eolian Norphlet Formation, South State Line Field, Mississippi, in: Sandstone Petroleum Reservoirs. pp. 205–224.
Thyne, G., 2001. A model for diagenetic mass transfer between adjacent sandstone and shale. Mar. Pet. Geol. 18, 743–755. doi:10.1016/S0264-8172(01)00025-3
Tissot, B.P., 1984. Recent Advances in Petroleum Geochemistry Applied To Hydrocarbon Exploration. Am. Assoc. Pet. Geol. Bull. 68, 545–563. doi:10.1306/AD461336-16F7-11D7-8645000102C1865D
Tittman, J., 1991. Vertical Resolution of Well Logs: Recent Development. Oilf. Rev. 3, 24–28.
Turner, C.C., Cohen, J.M., Connell, E.R., Cooper, D.M., 1987. A depositional model for the South Brae oilfield. Pet. Geol. Northwest Eur. Graham Trotman, London. 853–864.
UK DECC, 2015. Significant Offshore Discoveries. UK Department of Energy and Climate Change.
UK DECC, 2014. Drilling activity by year.
Underhill, J.., 1998. Jurassic, in: Glennie, K.W. (Ed.), Petroleum Geology of the North Sea: Basic Concepts and Recent Advances, Fourth Edition. pp. 245–293.
Vagle, G.B., Hurst, A., Dypvik, H., 1994. Origin of quartz cements in some sandstones from the Jurassic of the Inner Moray Firth (UK). Sedimentology 41, 363–377. doi:10.1111/j.1365-3091.1994.tb01411.x
van de Kamp, P.C., 2008. Smectite-Illite-Muscovite Transformations, Quartz Dissolution, and Silica Release in Shales. Clays Clay Miner. 56, 66–81. doi:10.1346/CCMN.2008.0560106
Van der Plas, L., Tobi, A.C., 1965. A chart for judging the reliability of point counting results. Am. J. Sci. 263, 87–90.
Vollset, J., Doré, A.G., 1984. A revised Triassic and Jurassic lithostratigraphic nomenclature for the Norwegian North Sea. Oljedirektoratet.
Walderhaug, O., 1996. Kinetic modeling of quartz cementation and porosity loss in deeply buried sandstone reservoirs. Am. Assoc. Pet. Geol. Bull. 80, 731–745. doi:10.1306/64ED88A4-1724-11D7-8645000102C1865D
Walderhaug, O., 1994. Precipitation rates for quartz cement in sandstones determined by fluid inclusion microthermometry and temperature-history modelling. J. Sediment. Res. 64A, 324–333. doi:10.2110/jsr.64.324
Walderhaug, O., 1990. A fluid inclusion study of quartz-cemented sandstones from offshore mid-Norway; possible evidence for continued quartz cementation during oil emplacement. J. Sediment. Res. 60, 203–210. doi:10.1306/212F9151-2B24-11D7-8648000102C1865D
Wallis, S., 2013. Binomial Confidence Intervals and Contingency Tests: Mathematical Fundamentals and the Evaluation of Alternative Methods. Dx.Doi.Org 20, 178–208. doi:10.1080/09296174.2013.799918
Walther, J. V., Helgeson, H.C., 1977. Calculation of the thermodynamic properties of aqueous silica and the solubility of quartz and its polymorphs at high pressures and temperatures. Am. J. Sci. 277, 1315–1351. doi:10.2475/ajs.277.10.1315
Warren, E.A., Pulham, A.J., 2001. Anomalous Porosity and Permeability Preservation in Deeply Buried Tertiary and Mesozoic Sandstones in the Cusiana Field, Llanos Foothills, Colombia. J. Sediment. Res. 71, 2–14. doi:10.1306/081799710002
Watkins, G.C., 2002. Characteristics of North Sea oil reserve appreciation. Q. Rev. Econ. Financ. 42, 335–372.
Weimer, P., Slatt, R.M., 1999. Turbidite systems, Part 1: Sequence and seismic stratigraphy. Lead. Edge 18, 454–463. doi:-
Weir, A.H., Ormerod, E.C., El Mansey, I.M.I., 1975. Clay mineralogy of sediments of the western Nile Delta. Clay Miner. 10, 369–386.
Widess, M.B., 1973. How thin is a thin bed? GEOPHYSICS 38, 1176–1180. doi:10.1190/1.1440403
Wilkinson, M., 2015. Does the nucleation of clay minerals control the rate of diagenesis in sandstones? Clay Miner. 50, 275–281. doi:10.1180/claymin.2015.050.3.01

Wilkinson, M., Darby, D., Haszeldine, R., 1997. Secondary porosity generation during deep burial associated with overpressure leak-off: Fulmar Formation, United Kingdom Central Graben. AAPG.

Wilkinson, M., Haszeldine, R.S., 2011. Oil charge preserves exceptional porosity in deeply buried, overpressured, sandstones: Central North Sea, UK. J. Geol. Soc. London. 168, 1285–1295. doi:10.1144/0016-76492011-007

Wilkinson, M., Haszeldine, R.S., Fallick, A.E., 2014a. Authigenic illite within northern and central North Sea oilfield sandstones: evidence for post-growth alteration. Clay Miner. 49, 229–246. doi:10.1180/claymin.2014.049.2.06

Wilkinson, M., Haszeldine, R.S., Fallick, A.E., 2006. Jurassic and Cretaceous clays of the northern and central North Sea hydrocarbon reservoirs reviewed. Clay Miner. 41, 151–186.

Wilkinson, M., Haszeldine, R.S., Milliken, K.L., 2003. Cross-Formational Flux of Aluminium and Potassium in Gulf Coast (USA) Sediments. Clay Miner. Cem. Sandstones 147–160.

Wilkinson, M., Haszeldine, R.S., Morton, A., Fallick, A.E., 2014b. Deep burial dissolution of K-feldspars in a fluvial sandstone, Pentland Formation, UK Central North Sea. J. Geol. Soc. London. 171, 635–647. doi:10.1144/jgs2013-144

Wilkinson, M., Haszeldine, S., 1996. Aluminium loss during sandstone diagenesis. J. Geol. Soc. London. 153, 657–660.

Wilkinson, M., Milliken, K.L., Haszeldine, R.S., 2001. Systematic destruction of K-feldspar in deeply buried rift and passive margin sandstones. J. Geol. Soc. London. 158, 675–683. doi:10.1144/jgs.158.4.675

Williams, L.A.N.N., Parks, G.A., Crerar, D.A., 1985. Silica diagenesis: I. Solubility controls. Deep Sea Res. Part B. Oceanogr. Lit. Rev. 32, 1021. doi:10.1016/0198-0254(85)93828-2

Wills, J.M., 1991. The Forties Field, Block 21/10, 22/6a, UK North Sea. Geol. Soc. London, Mem. 14, 301–308. doi:10.1144/GSL.MEM.1991.014.01.37

Wilson, E., 1927. Probable inference, the law of succession, and statistical inference. J. Am. Stat. Assoc.

Wilson, M.D., 1994. Diagenetic Mechanisms of Porosity and Permeability Reduction and Enhancement.

Wilson, M.D., 1992. Inherited grain-rimming clays in sandstones from eolian and shelf environments: their origin and control on reservoir properties. Soc. Sediment. Geol.

Woodburn, N., Hardwick, A., Masoomzadeh, H., Travis, T., 2014. Improved signal processing for sub-basalt imaging. Geol. Soc. London, Spec. Publ. 397, 163–171. doi:10.1144/SP397.6

Worden, R., Barclay, S., 2003. The Effect of Oil Emplacement on Diagenetic Clay Mineralogy: the Upper Jurassic Magnus Sandstone Member, North Sea, in: Worden, R.H., Morad, S. (Eds.), Clay Mineral Cements in Sandstones. International Association of Sedimentologists.

Worden, R.H., Bukar, M., Shell, P., 2018. The effect of oil emplacement on quartz cementation in a deeply buried sandstone reservoir. Am. Assoc. Pet. Geol. Bull. 102, 49–75. doi:10.1306/02071716001

Worden, R.H., Burley, S.D., 2003. Sandstone Diagenesis: The Evolution of Sand to Stone, in: Burley, S.D., Worden, R.H. (Eds.), Sandstone Diagenesis. Blackwell Publishing Ltd., pp. 1–44. doi:10.1002/9781444304459.ch

Worden, R.H., French, M.W., Mariani, E., 2012. Amorphous silica nanofilms result in growth of misoriented microcrystalline quartz cement maintaining porosity in deeply buried sandstones. Geology 40, 179–182. doi:10.1130/G32661.1

Worden, R.H., Morad, S., 2003. Clay minerals in sandstones: controls on formation, distribution and evolution, Clay Mineral Cements in Sandstones. Wiley Online Library, Oxford, UK. doi:10.1002/9781444304336.ch1

Worden, R.H., Morad, S., 2000. Quartz cementation in oil field sandstones: a review of the key controversies. Quartz Cem. sandstones 29, 1–20.

Worden, R.H., Oxtoby, N.H., Smalley, P.C., 1998. Can oil emplacement prevent quartz cementation in sandstones? Pet. Geosci. 4, 129–137. doi:10.1144/petgeo.4.2.129

Worden, R.H., Smalley, P.C., Barclay, S.A., 2003. H2S and diagenetic pyrite in North Sea sandstones: Due to TSR or organic sulphur compound cracking? J. Geochemical Explor. 78–79, 487–491. doi:10.1016/S0375-6742(03)00072-4

Xia, C., Wilkinson, M., 2017. The geological risks of exploring for a CO2 storage reservoir. Int. J. Greenh. Gas Control 63, 272–280. doi:10.1016/j.ijggc.2017.05.016

Yielding, G., Freeman, B., Needham, and D.T., 1997. Quantitative Fault Seal Prediction. Am. Assoc. Pet. Geol. Bull. 81, 897–917.